Optimal Propeller Selection when Accounting for a Ship's Manœuvring Response due to Environmental Loading.

by

David George Trodden

A thesis submitted for the degree of Doctor of Philosophy

29th August 2014

Newcastle University

School of Marine Science and Technology

Faculty of Science, Agriculture and Engineering

Armstrong Building,

Newcastle upon Tyne,

NE1 7RU

UK

Abstract

Carbon Dioxide (CO_2) is considered to be the most detrimental of all the Green House Gases on global warming (IMO, 2009). In an attempt to reduce the amount of CO_2 emissions from ships, this research approaches the problem from the perspective of more efficient design through superior estimation of design points.

Conventionally, a propeller is selected from the viewpoint that a ship travels at a constant design speed, with zero drift angle. However, a ship is subjected to the motions imposed on her from the environment. These motions tend to push a ship off her intended course, resulting in helm correction, speed correction (if the ship is to arrive at her intended destination on time) and consequently, altered inflow velocity to the propeller.

It is the novel aim of this research to determine if accounting for a ship's manœuvring motion will result in a propeller selection that has an overall higher efficiency, compared to one selected which neglects the manœuvring motion.

To achieve this aim, a ship manœuvring simulator has been developed which incorporates a modified mathematical propeller model that accounts for the unsteady manœuvring response of a ship subjected to an environment in which she is expected to sail.

The developed simulator has an iterative routine which enables it to select a propeller from a standard series that has the highest efficiency for the route in question.

Case studies are constructed which highlight how the efficiency of a propeller fairs when using the newly proposed propeller selection method, compared to the conventional propeller selection perspective.

The newly proposed propeller selection method is most suited to ships which are susceptible to relatively large drift angles and/or relatively high installed power requirements.

Results from the case studies are encouraging, with a gain of 2.34% in open water propeller efficiency for a 3600 Twenty foot Equivalent Unit container ship, equating to a saving of 3.22% in Carbon Dioxide emissions.

Acknowledgements

The author would like to thank a number of people who made the experience of working as a research student an enjoyable and personally rewarding one.

I would firstly like to thank my supervisors, Professor Mehmet Atlar and Doctor Michael Woodward of the School of Marine Science and Technology, Newcastle University. Their expertise and breadth of knowledge and experience provided invaluable assistance to this study. They have also both been of great support to me outside of the academic environment.

My office mates, Kawthar, Stavros, Alla, and Eren have been a great aid in bouncing around ideas, and in their turn I have learned of concepts outside of my particular field.

My wife, Maryam, has been another benefit of PhD research! She came into my life and heart, as a PhD student herself, in my first year of study, and has filled me with joy ever since.

My father, William and sister, Mary have provided endless encouragement and support throughout the study, and have helped make the experience a most enjoyable one.

Thanks go to Andrew and Brenden, the Computing Support staff who very willingly put up with, and indeed support, my unconventional views on computing.

Christine, the office cleaner, has my gratitude. She does a great job and thankfully leaves my messy desk and well-worn tea cup alone!

A special thanks go to the School secretaries, Vicky, Carol, Helen, Clare and Lisa who have provided great amusement with their interesting anecdotes whilst I try to operate the photocopier, not to mention all the help they provide behind-the-scenes.

The author gratefully acknowledges the Engineering and Physical Sciences Research Council (EPSRC) for sponsoring this research.

Contents

Abstract **i**

Acknowledgements **ii**

Nomenclature **xix**

Abbreviations **xxiv**

1 Introduction **1**

1.1 Motivation - Environmental Pollution from Ships. 1

1.2 Methodology, Research Contribution and Novelty 4

1.3 Structure of Thesis 6

1.3.1 Chapter 1: Introduction 6

1.3.2 Chapter 2: Ship Performance at Sea 6

1.3.3 Chapter 3: Simulation of Manœuvring Motion 7

1.3.4 Chapter 4: Propeller Flow Modelling in Steady and Unsteady Flow 12

1.3.5 Chapter 5: Validation of Simulation Modules 15

1.3.6 Chapter 6: Simulation Methodology and Results 15

1.3.7 Chapter 7: Conclusions, Further Work and Recommendations 15

1.4 Basis Ships 15

1.5 Practical Usage: The How-To Guide 17

1.6 Summary 17

2 Ship Performance at Sea **19**

2.1 Trial Conditions 20

2.2 In-Service Conditions 20

2.2.1 Speed Loss in a Seaway 21

2.2.2 Wind 22

2.2.3 Waves . . . 25
2.2.4 Current . . . 25
2.2.5 Leeway . . . 25
2.2.6 Passive Rudder . . . 27
2.3 A Method for Accurate Sea-Margin Prediction. . . . 27
2.4 Engine-Propeller Matching . . . 30
2.5 Summary . . . 34

3 Simulation of Manœuvring Motion 35
3.1 Coordinate System . . . 36
3.2 Equations of Motion . . . 36
3.3 Hydrodynamic Models for Time-Domain Simulation . . . 38
3.4 Hull . . . 38
3.4.1 Dynamic Stability . . . 39
3.5 Rudder . . . 41
3.5.1 Rudder Forces . . . 41
3.5.2 Hull - Rudder Interaction Coefficients . . . 43
3.5.3 Rudder Normal Force . . . 44
3.5.4 Effective Rudder Inflow Velocity . . . 44
3.5.5 Effective Rudder Inflow Angle . . . 45
3.5.6 Rudder Dynamics . . . 46
3.6 Propeller . . . 46
3.6.1 Wake and Thrust Deduction Factor . . . 47
3.7 Main Engine Machinery Model . . . 48
3.7.1 Engine & Propeller Dynamics . . . 48
3.8 Environment . . . 49
3.8.1 Wind . . . 50
3.8.2 Waves . . . 51
3.8.3 Current . . . 53
3.9 Automatic Pilot . . . 53
3.9.1 Tuning the Automatic Pilot . . . 55
3.9.2 Automatic Pilot Review . . . 56
3.10 Numerical Integration of Ordinary Differential Equations . . . 57

3.10.1 Conversion of Second Order Ordinary Differential Equations Into System of First Order Ordinary Differential Equations . . 58
3.11 Summary 58

4 Propeller Flow Modelling in Steady and Unsteady Flow 59
4.1 The Wageningen B-Screw Series 60
4.2 The General Conservation of Momentum Theory 60
4.2.1 Accounting for Changes in Angular Momentum 62
4.2.2 Glauert's Thrust Hypothesis 64
4.2.3 Momentum Theory Accounting for Finite Blade Number . . . 65
4.3 Blade-Element Theory 66
4.3.1 Blade-Element Theory Accounting for Wake-Skew Effects . . . 67
4.4 Combined Blade-Element Momentum Theory 70
4.5 Lift and Drag 74
4.5.1 Effects of Unsteady Inflow Velocity on Lift and Drag 75
4.5.2 Static Lift 86
4.5.3 Static Drag 87
4.5.4 Dynamic Lift 89
4.5.5 Dynamic Drag 91
4.5.6 Effects of Aspect Ratio 92
4.6 Prediction of Stall Angles 92
4.7 The Variation in Inflow Velocity Due to the Ship's Wake 93
4.8 Calculation Scheme 94
4.9 Calibration of Lift and Drag Coefficients. 96
4.9.1 Calibration of Quasi-Static $MBEMT$ Propeller Model 97
4.9.2 Calibration of Unsteady $MBEMT$ Propeller Model 98
4.9.3 Comparison between Quasi-Static and Unsteady Propeller Models at Non-Zero Drift Angles 102
4.10 Summary 105

5 Validation of Simulation Modules 106
5.1 Turning Circle Manœuvre 107
5.2 Zig-Zag Manœuvre 119
5.3 Standard Manœuvres for the KCS 121

5.3.1 Turning Circle Manœuvre . . . 122
5.3.2 10-10 Zig-Zag Manœuvre . . . 122
5.4 Summary . . . 130

6 Simulation Methodology and Results 131
6.1 The Optimisation Strategy . . . 132
6.1.1 The Process of Optimised Propeller Selection . . . 133
6.2 Methodology of Simulations with Different Propeller Models . . . 135
6.3 Results . . . 137
6.4 Fuel and CO_2 Emissions Savings . . . 140
6.4.1 *Esso Osaka* . . . 140
6.4.2 *KCS* . . . 141
6.5 Discussion of Results . . . 143
6.5.1 The Performance of the Newly Proposed Propellers in Calm Water, Trial Conditions . . . 145
6.5.2 Estimation of Sea-Margin using the *SiS* Simulator . . . 146
6.5.3 A Note on Computing Time . . . 147
6.6 Summary . . . 148

7 Conclusions, Further Work and Recommendations 150
7.1 Suggested Further Work and Recommendations . . . 157

References 160

Appendix A SiS User Manual 167
A.1 Introduction . . . 167
A.2 Example Input Files . . . 167
A.2.1 Example Input File for the *Esso Osaka* . . . 170
A.2.2 Example Input File for the *KCS* . . . 171
A.3 *SiS* Subprogram Descriptions . . . 172

Appendix B Miscellaneous Calculations 177
B.1 Non-Linear Manœuvring Coefficients . . . 177
B.1.1 Non Dimensionalising Factors . . . 177
B.2 Linear Manœuvring Coefficients . . . 178
B.2.1 Non Dimensionalising Factors . . . 178

B.3 Added Mass and Added Mass Moment of Inertia Terms 178
B.4 Calm Water Ship Calculations 179
B.4.1 Calm Water Ship Resistance Calculations 179
B.4.2 Calm Water Propeller Wake Fraction, w_P Calculation 180
B.4.3 Calm Water Thrust Deduction Factor, t Calculation 181
B.4.4 Parameters and Coefficients Used in Calm Water Calculations 181
B.5 Formulae used for the Wageningen B-Screw Series Calculations 185
B.5.1 Geometry of the Wageningen B-Screw Series Propellers 186
B.6 Coefficients for use in Blendermann's Wind Force Model 190
B.7 The Beaufort Scale 190

Appendix C Simulation Results **195**

C.1 Case 1. Esso Osaka, 20 Knot Wind (Fresh Breeze), oovoo Propulsion Model, Automatic Control, Propeller Optimisation 195
C.2 Case 2. Esso Osaka, 20 Knot Wind (Fresh Breeze), Unsteady MBEMT Propulsion Model, Automatic Control, Propeller Optimisation 204
C.3 Case 3. *Esso Osaka*, 20 Knot Wind (Fresh Breeze), Unsteady $MBEMT$ Propulsion Model, Automatic Control, with Propeller Selected from $OOBOO$ Model 213
C.4 Case 4. KCS, 20 Knot Wind (Fresh Breeze), Unsteady MBEMT Propulsion Model, Automatic Control, Propeller Optimisation 222
C.5 Case 5. KCS, 20 Knot Wind (Fresh Breeze), Unsteady MBEMT Propulsion Model, Automatic Control, Propeller Optimisation 231
C.6 Case 6. *KCS*, 20 Knot Wind (Fresh Breeze), Unsteady $MBEMT$ Propulsion Model, Automatic Control, with Propeller Selected from $OOBOO$ Model 240
C.7 The *Esso Osaka* with the Newly Proposed Propeller, Run in Calm Water, with the Unsteady $MBEMT$ Propulsion Model. 249
C.8 The *KCS* with the Newly Proposed Propeller, Run in Calm Water, with the Unsteady $MBEMT$ Propulsion Model. 258

List of Figures

1.1 Key components of Research. 18

2.1 Davenport Power Spectral Density Function 23
2.2 Time history of wind speed from Davenport PSD with $\bar{U}_W = 13.41 m/s$ 24
2.3 Leeway due to Wind 27
2.4 Propeller Efficiency Vs. Wind Probability 29
2.5 Wärtsilä 10 Cylinder RT-flex82C Main Engine & Propeller Demand Curve for KCS. 32
2.6 Impact on specific fuel consumption from operating engine away from optimum design point. 33

3.1 Coordinate System. 37
3.2 Velocity Vectors at the Rudder During a Steady Turn to Port . . 42
3.3 Schematic of longitudinal inflow velocity across a rudder. 44
3.4 Relative Wind Velocity and Direction 51
3.5 A block diagram of a PID controller in a feedback loop. 54
3.6 Calculation of Course Error. 55

4.1 Example output from `b_screw_geom.f90` for propeller with $a_E = 0.8$, $P/D = 1.0$ 61
4.2 Axial Momentum Model of an Actuator Disc. 62
4.3 Concept of the Annular Streamtube 63
4.4 Glauert's concept of an helicopter rotor in oblique flow. 65
4.5 Oblique Flow into a Propeller 67
4.6 Oblique Flow Velocity Vectors at a Propeller Blade Element . . . 68
4.7 Wake Skew Angle 69
4.8 Velocity Vectors to Calculate Wake Skew Angle. 71

4.9 Angle of attack vs azimuth (position "around the clock") angle at a drift angle of 0.00° 75
4.10 Angle of attack vs azimuth angle at a drift angle of 8.89° 76
4.11 Angle of attack vs azimuth angle at a drift angle of 13.33° 76
4.12 Angle of attack vs azimuth angle at a drift angle of 26.67° 77
4.13 Maximum change in Angle of Attack vs. drift angle 77
4.14 Lift and drag coefficients vs. angle of attack for symmetrical foil, when $\eta = 0.35$ 79
4.15 Lift and drag coefficients vs. angle of attack for symmetrical foil, when $\eta = 0.95$ 79
4.16 Lift coefficient vs. angle of attack over various non-dimensionalised pitch rate, when $\eta = 0.35$ 80
4.17 Lift coefficient vs. angle of attack over various non-dimensionalised pitch rate, when $\eta = 0.95$ 80
4.18 Drag coefficient vs. angle of attack over various non-dimensionalised pitch rate, when $\eta = 0.35$ 81
4.19 Drag coefficient vs. angle of attack over various non-dimensionalised pitch rate, when $\eta = 0.95$ 81
4.20 Non-dimensionalised Pitch Rate vs azimuth angle at a drift angle of 0.00° 83
4.21 Non-dimensionalised Pitch Rate vs azimuth angle at a drift angle of 8.89° 83
4.22 Non-dimensionalised Pitch Rate vs azimuth angle at a drift angle of 13.33° 84
4.23 Non-dimensionalised Pitch Rate vs azimuth angle at a drift angle of 26.67° 84
4.24 Absolute maximum value of non-dimensional pitch rate vs. drift angle 85
4.25 Effect of camber on lift coefficient. 87
4.26 Method to estimate zero lift angle. 88
4.27 Effect of aspect ratio on lift coefficient. 93
4.28 Blade-Element Momentum Theory Algorithm 95

4.29 Comparison plot of $OOVOO$ and calibrated quasi-static $MBEMT$ propeller models for *Esso Osaka* stock propeller 98
4.30 Comparison plot of $OOVOO$ and calibrated quasi-static $MBEMT$ propeller models for KCS stock propeller 99
4.31 Comparison plot of $OOVOO$ and uncalibrated unsteady $MBEMT$ propeller models when $\frac{P}{D} = 1.0$ and $a_E = 0.6$. 99
4.32 Comparison plot of $OOVOO$ and calibrated unsteady $MBEMT$ propeller models for *Esso Osaka* stock propeller 101
4.33 Comparison plot of $OOVOO$ and calibrated unsteady $MBEMT$ propeller models for KCS stock propeller 102
4.34 Comparison plot of calibrated quasi-static and unsteady $MBEMT$ propeller models when drift angle = 0.0° 103
4.35 Comparison plot of calibrated quasi-static and unsteady $MBEMT$ propeller models when drift angle = 5.0° 103
4.36 Comparison plot of calibrated quasi-static and unsteady $MBEMT$ propeller models when drift angle = 10.0° 104

5.1 $OOVOO$ and unsteady $MBEMT$ comparison for propeller used in the turning circle manœuvre. 108
5.2 Variation of advance ratio at the propeller during turning circle manœuvre 108
5.3 Track of 35^o starboard turning circle (V = 10.0 knots). 110
5.4 Drift Angle Time History of 35^o starboard turning circle (V = 10.0 knots) 111
5.5 Speed Time History of 35^o starboard turning circle (V = 10.0 knots) 111
5.6 Yaw Angle Time History of 35^o starboard turning circle (V = 10.0 knots) 112
5.7 Track of 35^o starboard turning circle (V = 10.0 knots) without influence of sway and yaw from propeller. 113
5.8 Drift Angle Time History of 35^o starboard turning circle (V = 10.0 knots) without influence of sway and yaw from propeller. . .114
5.9 Speed Time History of 35^o starboard turning circle (V = 10.0 knots) without influence of sway and yaw from propeller. 114

5.10 Yaw Angle Time History of 35^o starboard turning circle (V = 10.0 knots) without influence of sway and yaw from propeller. 115
5.11 Comparison of Tactical Diameter* and Advance* of different institutions and propeller models, (refer to main text for definition of Tactical Diameter* and Advance*). 115
5.12 Track of 35^o port turning circle (V = 7.7 knots). 116
5.13 Drift Angle Time History of 35^o port turning circle (V = 7.7 knots). 117
5.14 Speed Time History of 35^o port turning circle (V = 7.7 knots). . .117
5.15 Yaw Rate Time History of 35^o port turning circle (V = 7.7 knots).118
5.16 Heading Angle Time History of 10-10 ZigZag (V = 7.5 knots) . .119
5.17 Speed Time History of 10-10 ZigZag (V = 7.5 knots) 120
5.18 Yaw Rate Time History of 10-10 ZigZag (V = 7.5 knots). 120
5.19 Comparison of 1st and 2nd Overshoot Angles from different institutions and propeller models. 121
5.20 Local drift angle at propeller of *Esso Osaka* during 10-10 Zig-Zag Manœuvre 122
5.21 Track of 35^o starboard turning circle (V = 15.0 knots). 123
5.22 Drift Angle Time History of 35^o starboard turning circle (V = 15.0 knots) 124
5.23 Speed Time History of 35^o starboard turning circle (V = 15.0 knots) 124
5.24 Yaw Angle Time History of 35^o starboard turning circle (V = 15.0 knots) 125
5.25 Track of 35^o port turning circle (V = 15.0 knots) 125
5.26 Drift Angle Time History of 35^o port turning circle (V = 15.0 knots) 126
5.27 Speed Time History of 35^o port turning circle (V = 15.0 knots) . .126
5.28 Yaw Angle Time History of 35^o port turning circle (V = 15.0 knots) 127
5.29 Track of 10-10 Zig-Zag manœuvre (V = 15.0 knots) 127
5.30 Drift Angle Time History of 10-10 Zig-Zag manœuvre (V = 15.0 knots) 128

5.31 Speed Time History of 10-10 Zig-Zag manœuvre (V = 15.0 knots). 128
5.32 Yaw Angle Time History of 10-10 Zig-Zag manœuvre (V = 15.0 knots) 129

6.1 Propeller Optimization Algorithm 135
6.2 Brake specific fuel consumption for 6 cylinder RTA82T, suitable for the *Esso Osaka* (obtained from Wärtsilä (2013b)). 141
6.3 Brake specific fuel consumption for 10 cylinder RTA82C, suitable for the *KCS* (obtained from Wärtsilä (2013b)). 142
6.4 Comparison of optimised open-water propeller efficiency from accounting for, and neglecting a ship's drift angle in propeller selection. 143
6.5 Comparison of required brake power from accounting for, and neglecting a ship's drift angle in propeller selection. 144
6.6 Comparison of fuel consumption and CO_2 emissions from accounting for, and neglecting a ship's drift angle in propeller selection. 144

A.1 Directory structure of *SiS* simulator. 168
A.2 *SiS* Programme Flow. 169

B.1 Geometry of B-Screw Propeller (Oosterveld and van Oossanen, 1975). 189

C.1 Case 1: Ship Track. 197
C.2 Case 1: Speed vs. Time. 197
C.3 Case 1: Hull Forces vs. Time 198
C.4 Case 1: Rudder Force vs. Time 198
C.5 Case 1: Propeller Force vs. Time. 199
C.6 Case 1: Seaway Force vs. Time 199
C.7 Case 1: Wind Force vs. Time 200
C.8 Case 1: Yaw Rate vs. Time 200
C.9 Case 1: Rudder Command and Heading vs. Time. 201
C.10 Case 1: Drift Angle vs. Time 201
C.11 Case 1: Engine Power vs. Time 202
C.12 Case 1: Propeller Revolutions vs. Time 202

C.13 Case 1: Engine Torque vs. Time 203
C.14 Case 1: Open Water Propeller Efficiency vs. Time 203
C.15 Case 2: Ship Track 206
C.16 Case 2: Speed vs. Time 206
C.17 Case 2: Hull Forces vs. Time 207
C.18 Case 2: Rudder Force vs. Time 207
C.19 Case 2: Propeller Force vs. Time 208
C.20 Case 2: Seaway Force vs. Time 208
C.21 Case 2: Wind Force vs. Time 209
C.22 Case 2: Yaw Rate vs. Time 209
C.23 Case 2: Rudder Command and Heading vs. Time. 210
C.24 Case 2: Drift Angle vs. Time 210
C.25 Case 2: Engine Power vs. Time 211
C.26 Case 2: Propeller Revolutions vs. Time 211
C.27 Case 2: Engine Torque vs. Time 212
C.28 Case 2: Open Water Propeller Efficiency vs. Time 212
C.29 Case 3: Ship Track 215
C.30 Case 3: Speed vs. Time 215
C.31 Case 3: Hull Forces vs. Time 216
C.32 Case 3: Rudder Force vs. Time 216
C.33 Case 3: Propeller Force vs. Time 217
C.34 Case 3: Seaway Force vs. Time 217
C.35 Case 3: Wind Force vs. Time 218
C.36 Case 3: Yaw Rate vs. Time 218
C.37 Case 3: Rudder Command and Heading vs. Time. 219
C.38 Case 3: Drift Angle vs. Time 219
C.39 Case 3: Engine Power vs. Time 220
C.40 Case 3: Propeller Revolutions vs. Time 220
C.41 Case 3: Engine Torque vs. Time 221
C.42 Case 3: Open Water Propeller Efficiency vs. Time 221
C.43 Case 4: Ship Track 224
C.44 Case 4: Speed vs. Time 224
C.45 Case 4: Hull Forces vs. Time 225

C.46 Case 4: Rudder Force vs. Time 225
C.47 Case 4: Propeller Force vs. Time 226
C.48 Case 4: Seaway Force vs. Time 226
C.49 Case 4: Wind Force vs. Time 227
C.50 Case 4: Yaw Rate vs. Time 227
C.51 Case 4: Rudder Command and Heading vs. Time. 228
C.52 Case 4: Drift Angle vs. Time 228
C.53 Case 4: Engine Power vs. Time 229
C.54 Case 4: Propeller Revolutions vs. Time 229
C.55 Case 4: Engine Torque vs. Time 230
C.56 Case 4: Open Water Propeller Efficiency vs. Time 230
C.57 Case 5: Ship Track 233
C.58 Case 5: Speed vs. Time 233
C.59 Case 5: Hull Forces vs. Time 234
C.60 Case 5: Rudder Force vs. Time 234
C.61 Case 5: Propeller Force vs. Time 235
C.62 Case 5: Seaway Force vs. Time 235
C.63 Case 5: Wind Force vs. Time 236
C.64 Case 5: Yaw Rate vs. Time 236
C.65 Case 5: Rudder Command and Heading vs. Time. 237
C.66 Case 5: Drift Angle vs. Time 237
C.67 Case 5: Engine Power vs. Time 238
C.68 Case 5: Propeller Revolutions vs. Time 238
C.69 Case 5: Engine Torque vs. Time 239
C.70 Case 5: Open Water Propeller Efficiency vs. Time 239
C.71 Case 6: Ship Track 242
C.72 Case 6: Speed vs. Time 242
C.73 Case 6: Hull Forces vs. Time 243
C.74 Case 6: Rudder Force vs. Time 243
C.75 Case 6: Propeller Force vs. Time 244
C.76 Case 6: Seaway Force vs. Time 244
C.77 Case 6: Wind Force vs. Time 245
C.78 Case 6: Yaw Rate vs. Time 245

C.79 Case 6: Rudder Command and Heading vs. Time. 246
C.80 Case 6: Drift Angle vs. Time 246
C.81 Case 6: Engine Power vs. Time 247
C.82 Case 6: Propeller Revolutions vs. Time 247
C.83 Case 6: Engine Torque vs. Time 248
C.84 Case 6: Open Water Propeller Efficiency vs. Time 248
C.85 *Esso Osaka* in Calm Water: Ship Track 251
C.86 *Esso Osaka* in Calm Water: Speed vs. Time 251
C.87 *Esso Osaka* in Calm Water: Hull Forces vs. Time 252
C.88 *Esso Osaka* in Calm Water: Rudder Force vs. Time. 252
C.89 *Esso Osaka* in Calm Water: Propeller Force vs. Time 253
C.90 *Esso Osaka* in Calm Water: Seaway Force vs. Time. 253
C.91 *Esso Osaka* in Calm Water: Wind Force vs. Time 254
C.92 *Esso Osaka* in Calm Water: Yaw Rate vs. Time 254
C.93 *Esso Osaka* in Calm Water: Rudder Command and Heading vs. Time. 255
C.94 *Esso Osaka* in Calm Water: Drift Angle vs. Time 255
C.95 *Esso Osaka* in Calm Water: Engine Power vs. Time 256
C.96 *Esso Osaka* in Calm Water: Propeller Revolutions vs. Time . . .256
C.97 *Esso Osaka* in Calm Water: Engine Torque vs. Time 257
C.98 *Esso Osaka* in Calm Water: Open Water Propeller Efficiency vs. Time. 257
C.99 *KCS* in Calm Water: Ship Track 260
C.100 *KCS* in Calm Water: Speed vs. Time. 260
C.101 *KCS* in Calm Water: Hull Forces vs. Time 261
C.102 *KCS* in Calm Water: Rudder Force vs. Time 261
C.103 *KCS* in Calm Water: Propeller Force vs. Time. 262
C.104 *KCS* in Calm Water: Seaway Force vs. Time 262
C.105 *KCS* in Calm Water: Wind Force vs. Time 263
C.106 *KCS* in Calm Water: Yaw Rate vs. Time 263
C.107 *KCS* in Calm Water: Rudder Command and Heading vs. Time. .264
C.108 *KCS* in Calm Water: Drift Angle vs. Time 264
C.109 *KCS* in Calm Water: Engine Power vs. Time 265

C.110 *KCS* in Calm Water: Propeller Revolutions vs. Time 265
C.111 *KCS* in Calm Water: Engine Torque vs. Time 266
C.112 *KCS* in Calm Water: Open Water Propeller Efficiency vs. Time .266

List of Tables

1.1 Main particulars of the *Esso Osaka* and the *KCS*. 16

3.1 Coefficients for use in Townsin et al. (1992) method for added wave resistance. 52

3.2 μ coefficient for use in Townsin et al. (1992) method for added wave resistance. 52

4.1 Parameters used in the calibration of the lift and drag coefficients for the quasi-static $MBEMT$ propeller model. 97

4.2 Parameters used in the calibration of the lift and drag coefficients for the unsteady $MBEMT$ propeller model. 100

6.1 Case studies for propeller selection analysis. 136

6.2 Results from running the *SiS* simulator on the *Esso Osaka* for different case studies. 138

6.3 Results from running the *SiS* simulator on the *KCS* for different case studies. 139

6.4 Fuel Consumption and CO_2 Emissions for the *Esso Osaka* 141

6.5 Fuel Consumption and CO_2 Emissions for the *KCS* 142

6.6 % gain in Efficiency and % reduction in fuel consumption and CO_2 emissions from the newly proposed propeller selection methodology. . 148

A.1 Ship type designation as used in the input file for the *SiS* simulator . 170

A.2 FORTRAN modules and main subprograms used in propeller modelling calculations. 176

B.1 Stern Shape Factors 182

B.2 Approximate $(1 + k_2)$ values 182

B.3 Coefficients for K_T polynomials 187

B.4 Coefficients for K_Q polynomials 188
B.5 B-Screw Dimensions for Four, Five, Six and Seven-Bladed Propellers 189
B.6 B-Screw Dimensions for Three-Bladed Propellers 190
B.7 Values for V_1 as used in equations B.4 and B.5 191
B.8 Values for V_2 as used in equations B.4 and B.5 192
B.9 Blendermann's Coefficients 193
B.10 The Beaufort Scale 194

Nomenclature

Generally, throughout this Thesis, text written in a `teletype` font refer to FORTRAN modules or subprogrammes.

α Angle of incidence [rad]

α_{ss} Angle of static stall [rad]

β Drift angle. [rad]

β Hydrodynamic pitch angle [rad]

γ_{RA} Wind angle relative to ship's centreline. [°]

γ_{TA} Angle of where the true wind is blowing from. North is 0 or 360. [°]

γ_{rw} Wind angle relative to ship's direction of travel. [°]

δ_R Rudder angle. [°]

δ Wind cross-force parameter. [-]

η_H Hull efficiency. [-]

η_{p_o} Propeller open water efficiency. [-]

η_R Relative rotative efficiency. [-]

η_s Shaft efficiency. [-]

ρ_{sw} Density of salt water. $[Kgm^{-3}]$

ρ_{air} Density of air. $[Kgm^{-3}]$

τ Trim, positive by the stern. $[m]$

χ Wake skew angle [rad]

ψ Ship's heading with respect to the world coordinate system. [°]

ω Angular velocity [rad/s]

A_R Rudder area. [m^2]

a_E Expanded Blade Area Ratio [-]

A_{L_w} Lateral projected above-water area of ship [m^2]

A_{F_w} Frontal projected above-water area of ship [m^2]

B Characteristic Beam, usually taken to be moulded beam. [m]

C_D Drag coefficient [-]

C_L Lift coefficient [-]

CD_l Head-wind drag coefficient [-]

CD_t Beam-wind drag coefficient [-]

c Chord length [m]

C_{X_w} Wind force coefficient in pure surge direction [-]

C_{Y_w} Wind force coefficient in pure sway direction [-]

C_{N_w} Wind moment coefficient in pure yaw direction [-]

D Propeller diameter. [m]

I_{pp} Mass moment of inertia of propeller shaft system about its axis. [Kgm^2]

I_{zz} Mass moment of inertia about the Z axis. [Kgm^2]

J_{pp} Added mass moment of inertia of propeller about its axis. [Kgm^2]

J_{zz} Yaw added mass moment of inertia. [Kgm^2]

K Goldstein factor. [-]

K_Q Propeller torque coefficient. [-]

K_T Propeller thrust coefficient. [-]

L Characteristic Length, usually taken to be length along the waterline. $[m]$

L_{oa} Length overall. $[m]$

L_{pp} Length between perpendiculars. $[m]$

L_{wl} Length along the waterline. $[m]$

m Mass. $[Kg]$

m_x Surge added mass. $[Kg]$

m_y Sway added mass. $[Kg]$

$\dot{m}$ Mass flux $[kgs^{-1}m^{-2}]$

n Propeller revolutions. [usually rpm]

N_H Moment due to the ship hull's interaction with the water. $[Nm]$

N_R Moment due to the action of the rudder. $[Nm]$

N_P Moment due to action of the propeller. $[Nm]$

N_A Moment due to the wind. $[Nm]$

R Non-dimensional pitch rate [-]

R Radius of propeller $[m]$

R_H Radius of propeller hub $[m]$

r Yaw rate. [rad s^{-1}]

R_{app} Appendage resistance [N]

R_W Wave making resistance [N]

R_B Bulbous bow resistance [N]

R_{tr} Resistance due to immersed transom stern [N]

T Mean draught. $[m]$

T_a Draught at after perpendicular. $[m]$

T_f Draught at forward perpendicular. $[m]$

u Surge velocity. $[ms^{-1}]$

v_o Sway velocity at midship. $[ms^{-1}]$

V Resultant ship velocity. $[ms^{-1}$ or knots]

V_v Resultant ship velocity. $[ms^{-1}$ or knots]

V_s Service speed of ship. $[ms^{-1}$ or knots]

v Sway velocity. $[ms^{-1}]$

V_a Speed of advance. $[ms^{-1}]$.

V_i Induced velocity $[ms^{-1}]$

V_p Flow velocity across blade element $[ms^{-1}]$

$V_{\theta i}$ Tangential component of induced velocity $[ms^{-1}]$

V_{ai} Axial component of induced velocity $[ms^{-1}]$

V_{i0} Mean induced velocity $[ms^{-1}]$

$\bar{V}_{Ai}$ Disc averaged axial induced velocity $[ms^{-1}]$

$\bar{V}_{Ti}$ Disc averaged in-plane transverse induced velocity $[ms^{-1}]$

V_{RA} Velocity of wind relative to the ship (apparent wind speed). $[ms^{-1}]$

V_{TA} Velocity of the wind (true wind speed). $[ms^{-1}]$

V_{rw} Velocity of the wind, relative to the ship's resultant speed. $[ms^{-1}]$

x_G Distance of ship's centre of gravity from midships. Positive values fwd. $[m]$

X_H Force in the X direction due to the ship hull's interaction with the water. $[N]$

X_R Force in the X direction due to the action of the rudder. $[N]$

X_P Force in the X direction due to action of the propeller. $[N]$

X_A Force in the X direction due to the wind. $[N]$

Y_H Force in the Y direction due to the ship hull's interaction with the water. $[N]$

Y_R Force in the Y direction due to the action of the rudder. $[N]$

Y_P Force in the Y direction due to action of the propeller. $[N]$

Y_A Force in the Y direction due to the wind. $[N]$

Z Number of blades on a propeller [-]

Abbreviations

BEMT Blade Element Momentum Theory.

BN Beaufort Number.

CO_2 Carbon Dioxide.

DWT Deadweight - a measure of how much weight (tonnes) a ship can safely carry.

GHG Green-House Gas.

HFO Heavy Fuel Oil.

IMO International Maritime Organisation.

MARPOL International Convention for the Prevention of Pollution from Ships.

MBEMT Modified Blade Element Momentum Theory.

NO_x Oxides of Nitrogen.

OOVOO Propeller model based on the work of Oosterveld and van Oossanen (1975).

PID Proportional Integral Derivative.

PSD Power Spectral Density.

SFC Specific Fuel Consumption

g/kWhr

SO_x Oxides of Sulphur.

TEU Twenty-Foot Equivalent Unit.

USD United States of America Dollars [$].

VLCC Very Large Crude Carrier.

Chapter 1. Introduction

The aim of this introductory Chapter is to give the reader an overview of the entire research study. This aim is met via addressing the following objectives:

Problem Definition This is covered in Section 1.1 and provides the motivation behind this research, describing problems associated with environmental damage as a direct result of ship operations, and how various technologies are presently used to address this issue. A brief statement is made as to how this research aims at addressing this issue.

Methodology Overview This is the subject of Section 1.2 and explains what makes this study a novel approach to the problem, and outlines the broad methodology used in this study.

Structure of Thesis Section 1.3 describes how the thesis is laid out, why, and perhaps how to read it. It provides a synopsis of the main Chapters of this thesis, and why the methods used in the main Chapters were chosen.

Basis Ships A description of two basis ships is provided in Section 1.4. These ships are used as case studies for analysis in this research. The basis ships are referred to regularly throughout this thesis.

How-To Guide A practical usage example is given to demonstrate, in a nutshell, how the proposed methods can be applied.

1.1 Motivation - Environmental Pollution from Ships.

A ship, by its very nature, produces various by-products which, when not properly treated, can lead to damage to the environment. For example, untreated grey/black-water (sewage) contains nutrients such as Nitrogen and Phosphorus, which when discharged from a ship, promote excessive algal-blooms which in turn

consume an excessive amount of Oxygen in the water, leading to destruction of aquatic life.

Other examples of by-products produced by ships in their normal day-to-day operation (that is, intact, and undamaged) include introduction of foreign species from ballast water, oil pollution from bilge water, sound pollution from machinery, and exhaust gas emissions from main and auxiliary engines.

There are mechanisms to treat many of these by-products so that they become harmless. For example grey/black water is required to be treated to MARPOL Annex IV standard (MEPC, 2006), of which various solutions exist, one example being the Wärtsilä Hamworthy Membrane Bio-Reactor (MBR) (Wärtsilä, 2013a). Similar regulations and associated solutions exist for other shipping by-products.

Treating the by-product so that it becomes relatively harmless is one solution, however, for certain by-products like exhaust gas emissions, treatment is more challenging. Various technologies are able to treat certain types of "species", (pollutants) found in exhaust gases, for example scrubbers can reduce the amount of oxides of Sulphur (SO_x) released into the environment, and catalytic reduction systems can reduce the amount of oxides of Nitrogen (NO_x) emitted. Incidentally, whilst SO_x and NO_x are considered harmful to the environment, they are not considered to contribute to global warming. According to DNV and PSE (2013), Carbon dioxide (CO_2) is a gas that is known to contribute to global warming. The production of CO_2 is an inevitable consequence of burning fossil fuels. It is possible to capture and store CO_2, but this poses the question of what next to do with the CO_2.

According to the current IMO Greenhouse Gas Study (IMO, 2009), international shipping was estimated to have emitted 870 million tonnes, or about 2.7% of the global man-made emissions of CO_2 in 2007. This estimate is thought to be under predicted, and at the 65th Session of the IMO's MEPC (May 2013), it was agreed to research and update these figures. The report claims that exhaust gases are the primary source of greenhouse gas (GHG) emissions from ships and Carbon Dioxide is the most important GHG, both in terms of quantity and of global warming potential.

IMO's Marine Environment Protection Committee (MEPC) has thoroughly investigated the control of GHG emissions from ships, and in July 2009 formulated specific technical and operational measures to reduce these emissions. These

adopted measures have been incorporated into the International Convention for the Prevention of Pollution from Ships (MARPOL) as a new chapter in Annex VI entitled "Regulations on energy efficiency for ships". This makes it mandatory for all existing bulk carriers, gas carriers, tankers, container ships, general cargo ships, refrigerated cargo ships and combination carriers (other ship types are currently being analysed for future inclusion) over 400 gross tonnage to comply with the Ship Energy Efficiency Management Plan (SEEMP), and the Energy Efficiency Design Index (EEDI) for new ships. These regulations came into force on the 1st January 2013.

The SEEMP establishes a mechanism to improve the energy efficiency of a ship from improved operations, and incorporates best practices for fuel efficient ship operation, as well as guidelines for voluntary use of the Energy Efficiency Operational Indicator (EEOI). The EEOI enables operators to measure the fuel efficiency of a ship in operation and to gauge the effect of any changes in operation, e.g. more frequent propeller cleaning, or maintaining an even speed profile.

The EEDI is a technical measure, and aims at promoting the use of more energy efficient (less polluting) equipment and engines. The EEDI requires a minimum energy efficiency level per tonne mile for different ship type and size categories. The EEDI is non-prescriptive, meaning that the designers and builders are free to use whatever technology they wish in order for the ship to attain the required energy efficiency level and comply with the regulations. The required EEDI is calculated by a formula based on the technical design parameters for a given ship, the value for the EEDI is then verified during the ship's sea trials.

The IMO are also developing Market Based Measures (MBM) that may provide a financial incentive for ship owners to invest in new technology or trade Carbon.

Aim: It is the intent of this research to focus on minimising the production of CO_2 (the most prolific and damaging GHG) from ship's exhausts via a philosophy of improved efficiency by design for *in-service* conditions. This aim is achieved by taking into account, at the early design stage, the primary effects of the environmental conditions experienced by a ship sailing in realistic, real-world conditions.

1.2 Methodology, Research Contribution and Novelty

Ships are commonly hydrodynamically tuned for a specific design point, but are frequently operated away from this optimum design point (Hochkirch and Bertram, 2010). This can be for numerous reasons, for example the propeller may be running on the heavy side due to fouling on the underwater part of the ship, or from operating procedure as dictated from the shipping company. Operating the ship away from her design point results in an increase in fuel consumption (and therefore exhaust emissions). This is largely a question of awareness that requires addressing throughout the whole industry.

If a more realistic operating profile can be obtained at the design stage of the ship, then the more potential there is for efficiency gains. To attain greater efficiency, all aspects of ship design should be optimised around a design point for which the ship is expected to operate, and not an artificial one, for example, devoid of weather. The closer a designer can estimate and optimise for the behaviour of a ship operating in her day-to-day environment, then the higher the efficiency a ship attains when sailing in that environment. It is of the author's opinion, that the EEDI in its present implementation discourages design for *in-service* conditions. The value for the EEDI that the ship attains is verified from sea trials (id est calm water). A ship optimised for service conditions will not be optimal when run in trial conditions, and thus may even fail the EEDI requirement, however in real working conditions the design may surpass the EEDI requirement.

The resistance and powering aspects of ship design is conventionally conducted on the basis of performance in calm water (ITTC, 2008). The reasoning behind this is that a new (or modified) ship is required to undergo sea trials to ensure that she will meet both the owners requirements and IMO regulations. These trials need to be standardised and thus take place in deep, calm water. The ship's designers will factor in a *sea margin* which will ensure that the ship will operate adequately in *service* conditions. This sea margin is conventionally a rough estimate, either based upon rule of thumb or experience of similar ships in similar weather conditions. The ship's resistance in service conditions is estimated as the calm water resistance times the sea margin.

The day-to-day operation of a ship takes place in *service* conditions, id est, she will be subjected to the influence of the environment in which she is sailing. Not

only will the resistance (and powering) of the ship be different in service conditions compared to trial, but the ship's motions will be different too due to the dynamic response of the ship to her environment. The same sea-state will affect different ships in different ways. It is not only the environment itself, but also the motion response of the ship in the seaway that will affect the added resistance.

It is the intent of this research to focus on selecting an optimised propeller which has a higher efficiency when operated in service conditions, compared to one that has been optimised neglecting the manœuvring motion of a ship. This concept is novel, as propeller design is conventionally performed from assuming the flow to be steady and from directly in front of the propeller plane (albeit, the flow becomes non-uniform due to the presence of the hull).

In order to obtain a representation of how a ship behaves when operating in real life conditions, a non-linear time-domain ship simulator has been developed for this research. The simulator is written in Fortran (2008 standard), is known to compile on POSIX compliant UNIX clones, using either the Intel Fortran Compiler (`ifort`) or the GNU fortran compiler (`gfortran`) and makes use of the OpenMP (OpenMP, 2013) specification for parallel programming. The simulator computer programme is called the Ship in Service (*SiS*) simulator.

The simulator calculates the manœuvring motions (surge, sway and yaw) of a ship when subjected to weather. The simulator can be used to obtain an estimate for the sea-margin, when given as input appropriate wind, wave and current statistics for the area(s) of service. It is the author's impression that the idea of obtaining an accurate estimate of sea-margin from a ship simulator is not implemented in practice, however, the simulator, as will become apparent, could become a valuable initial design tool.

A ship's motions, as predicted by the simulator, can be used to obtain the thrust and torque on the propeller, as well as a ship's drift angle at the propeller, at an instance of time. Knowing the thrust that the propeller is required to provide means that an optimised basis propeller (which can be further optimised later on in the design spiral) can be selected for the conditions that the ship is actually expected to operate in. The thrust and torque on the propeller may be calculated using numerous methods, but now that the simulator provides an estimate of inflow angle at the propeller, the designer has an added degree of fidelity to the mathematical propeller model. The author believes that this concept is also novel.

Section 1.3 outlines in more detail the methodology and implementation of this research.

1.3 Structure of Thesis

This Section aims at not just providing a synopsis of the Chapters that comprise this Thesis, but also provides a justification as to why the author chose certain methods over others.

Whilst not completely necessary, the Chapters of this thesis should be read in order, as following Chapters are usually a development from the previous one.

1.3.1 Chapter 1: Introduction

This Chapter provides a broad understanding of the entire research work to the reader, lays out the thesis structure, and shows motivation, it also describes why particular methods were chosen to be used in preference to others.

1.3.2 Chapter 2: Ship Performance at Sea

Chapter 2 outlines the differences between the calm water scenario found in *trial* conditions, and the more realistic *in-service* conditions. These differences occur from the environment in which a ship is sailing. An exposition is given as to how the environmental forces of wind, waves and currents occur. These external forces tend to alter a ship's speed and course, so if the ship is to arrive at her intended destination on time, then the ship's controls need to respond appropriately. A narrative of the ship's response to her environment is given.

This Chapter also gives an example of how a time-history of wind (which is also applicable to wave) velocity can be obtained from a Power Spectral Density (PSD) function.

An example is shown of how propeller performance varies when accounting for environmental conditions, and describes in detail how a ship simulator can be used, in combination with weather statistics, to predict a sea margin which can be used for design purposes.

An account is given of how the propeller loading must be matched to the engine to ensure optimum efficiency of the propulsion system as a whole. This also shows

that when the ship is operated away from her design point, the engine burns a proportionately greater amount of fuel.

1.3.3 Chapter 3: Simulation of Manœuvring Motion

Having described the external forces from the environment, this Chapter aims at modeling them mathematically, along with the ship's response to the environment.

Calculating the motion response of a ship in a seaway can be obtained from model tests, semi-empirical or empirical methods (from numerical models which mimic a ship's behaviour), or with the use of Computational Fluid Dynamics (CFD). Physical model tests, whilst perhaps the most accurate method, require an initial design already, are time consuming and expensive to implement. CFD attempts to model the actual flow physics of the subject in question. For the subject of a ship under control, with a rotating propeller, in the influence of a seaway, a huge amount of time and computing power is required, with the end result being no better than other methods. The Unsteady Reynolds-Averaged Navier Stokes Equations (URANSE) and continuity equations sufficient to describe all features of the fluid flow around the ship hull are still considered as a subject of research rather than the state of the art in industry, i.e. engineering practice. (Peric and Bertram, 2011), (ITTC, 2011). CFD can only model the physics which are known, whereas model tests account for all flow physics (albeit, there may be some scaling errors).

Of course, as CFD technology increases and computers become more powerful, the choice of using CFD as a design and analysis tool for marine simulation is likely to become more widely used.

The method for estimating a ship's motion response to her environment in this research is based upon semi-empirical numerical models, as this method, once developed, provides a fast execution time, is suitable for initial design purposes, and is readily extensible for further development.

To provide a basis model to build upon, and provide a suitable proof of concept for further work, the sea-keeping motions of roll, pitch and heave are neglected in this study, and only the manœuvring motions of surge, sway and yaw are considered. It is assumed that the predominant factor in an altered flow field will be drift angle, as when the ship has attained a quasi-steady state in a seaway, the

averaged drift angle will be non-zero, whereas the other motions, with the exception of roll, can be assumed to have averaged values of near-zero.

A Review of Manœuvring Simulation Methods

There are two models that are distinguished in hydrodynamic modelling of ship manœuvring. The Whole Ship Model, sometimes referred to as the Abkowitz type model, considers the forces on the hull, rudder and propeller, including their interactions, as one entity. The Modular Model, as the name suggests, takes a modular approach, considering hull, rudder and propulsion separately. This model is sometimes referred to as the Manœuvring Mathematical Modeling Group (MMG) model.

The Whole Ship Model

One of the earliest manœuvring models is attributed to Abkowitz (1964). The forces are formulated as equation 1.1.

$$X, Y, N = f\left(u, du, v, r, \dot{u}, \dot{v}, \dot{r}, \dot{\delta}\right) \tag{1.1}$$

The formulae for ship motions are derived from a third order Taylor series expansion. The coefficients of the Taylor expansion are called hydrodynamic, or manœuvring derivatives, and, for the Abkowitz model, are obtained by regression analysis on experimental data of scale models.

An inconvenience with this type of model is that if, for example, the dimensions of the rudder are altered, then this change influences the entire model. Also, the value of a coefficient has no direct physical meaning.

Norrbin (1971) developed a manœuvring model which uses only terms of first and second order. Norrbin's model also includes thrust and torque on a propeller, and flow velocity over the rudder, making it suitable for representing manœuvres of the engine. Another advantage of Norrbin's model is that in takes into account finite water depth.

The Modular Model

The Japanese research group Manœuvring Mathematical Modeling Group (MMG) developed a concept for modeling the manœuvring motion of a ship (Ogawa and Kasai, 1978), (Kose et al., 1981). These models are based upon

physical considerations, and as such the hull, rudder and propulsion system are considered as separate entities. In considering these elements as separate entities, terms need to be formulated for any interactions that occur between them.

An example of a modular model is the one developed by Oltmann and Sharma (1984), where the hydrodynamic forces are split into ideal fluid effects, hull lifting effects, hull cross-flow, hull resistance, propeller thrust and torque and rudder forces, including interactions between hull, propeller and rudder.

This modular approach makes it possible to change a particular element without affecting other parts of the model, enabling researchers to develop and refine parts of the model that are particularly important for them. (For example, Eloot et al. (2006) are interested in ship manœuvrability in confined waters, and have adapted modules to suit their particular purpose). It is for this reason that the modular model type is used in this research.

Obtaining the Manœuvring Coefficients

The manœuvring coefficients can be obtained from experiments with model tests, full scale sea trials together with system identification, regression analysis results from similar designs or theoretical prediction methods. One needs to exercise caution when dealing with dimensionless manœuvring derivatives, as there is no uniformity between authors as to how they were non-dimensionalised. The disadvantage of the model tests and full scale trials for use in this study, is that the results are only applicable to that particular ship and are unavailable at the initial design stage.

Although there have been numerous models developed to predict the manœuvring motion of a ship, the one based on the modular approach of Inoue et al. (1981a), Inoue et al. (1981b) is chosen for use in this research. This is a practical, widely used and proven method which is applicable to a wide range of ship types. Although not implemented in this research, Inoue et al.'s method also considers the sea-keeping motion of roll.

Propeller Model

There are numerous standard series propellers that are in existence today. The principle aim of a propeller series is to provide insight into how a propeller will operate in certain conditions, and to provide design diagrams which will assist in

selecting the most efficient geometry of the actual (full size) propeller.

The Wageningen B-Screw standard series (sometimes referred to as the Troost series, from its original presenter Troost (1938a), Troost (1938b), Troost (1938c)) was chosen as a basis propeller series for this research. This is a fixed pitch, non-ducted propeller, and is perhaps the most widely used series with the most extensive range of research conducted on (Carlton, 2007). The original series suffered from certain unfairness between various design diagrams which were attributed to scale effects resulting from the different model tests. This was addressed by Lammeren et al. (1969), and the series was completely re-appraised. Oosterveld and van Oossanen (1975) performed detailed regression studies on the performance characteristics of the B-Screw series which relates thrust and torque to the propeller geometry and Reynold's number. It is the model of Oosterveld and van Oossanen (1975), (for the sake of brevity extensively referred to throughout this thesis as the OOVOO model), which is used as a tool for development and comparison of a modified propeller model. This propeller model was derived from open-water experiments conducted in flow arriving perpendicular to the propeller plane, and as such cannot account for flow arriving at oblique angles. Chapter 4 is devoted to the development of a propeller flow model which accounts for oblique flow.

Modelling the Environment

The environment that a ship experiences in this research is considered to be composed of wind, waves and surface (non-tidal) currents. As it is the intent of this research to focus on optimisation for in-service conditions, it is assumed that the ship will be travelling in deep water, and thus the effects of shallow water and banks are neglected.

Wind Model

Isherwood (1972) analysed results of wind resistance experiments carried out at different laboratories with models covering a wide range of merchant ships. He developed empirical formulae for determining the longitudinal and lateral (surge and sway) components of wind force, and the wind induced yawing moment on merchant ships, for a wind from any direction. Whilst this method has proven to be popular, ship forms have changed over the years and it is debatable if

Isherwood's formulae are still applicable.

Blendermann (1996) developed empirical formulae for determining the wind loading on various ship types, and whilst not as extensive as Isherwood's method, the ship's forms that where used in the analysis are modern, and cover the most popular types. Blendermann also developed a formula for wind induced roll, which can be accounted for in the manœuvring model of Inoue et al. (1981b). It is Blendermann's wind model that is used in this study.

Wave Model

Much work has been performed on the study of added resistance due to waves (Prpić-Oršić et al., 2008). These range from easy to apply approximate methods (Aertssen, 1969) to more complex theoretical methods (Salvesen, 1976).

In this study, the method proposed by Townsin et al. (1992) is used, as it is applicable to both tankers and container ships (the two case studies used as examples for this research), practical and easy to use. Disadvantages of this method are that it only considers the pure surge component of force on a hull due to waves encountering a ship from any angle (that is, the waves acting on the ship do not impose any sway or yawing motion). This method is regarded to be sufficient as a proof-of-concept for this research.

Current Model

In this research, the effects of surface currents on the ship are modelled by the principle of relative motion. For all velocities used in the formulation of forces and moments, relative velocities are used, for example $u = u_{\text{ship}} - u_{\text{current}}$. It is assumed that the velocity gradient of the current is zero.

Effects of seakeeping motions on propulsion characteristics

As mentioned earlier, due to the complexities of coupling a seakeeping analysis with a manœuvring one (Tello Ruiz et al., 2012), this research is based solely on manœuvring motion. It is however worthwhile detailing some of the aspects that seakeeping motions have on propulsion characteristics, and why, for added realism to the simulator and consequent analysis, seakeeping motions should ideally be taken in to consideration.

It has been stated that, although motions such as pitch or heave may have an

average value of near zero, the effect of these motions may have a noticeable effect on propulsion characteristics. This especially applies to the pitch motion, where the propeller is often situated far from the pitch centre, and therefore is subject to relatively large accelerations.

The flow into the propeller is clearly influenced by the wave pattern at the stern of a ship. For example, if there is a wave trough at the propeller plane, then the propeller will be operating in highly aerated water, or may even emerge. This causes a breakdown in thrust from cavitation, and propeller racing.

Another aspect to consider is the circular orbits of water particles from waves at the propeller plane. These have an effect on the inflow vectors to the propeller, and thus affect its characteristics.

When considering a ship which is pitching, it becomes apparent from the explanation of the previous paragraphs, that this particular motion could potentially cause the ship to perform sub-optimally, especially for ships who are sailing in the ballast condition.

Taking into account pitching motions during voyage analysis could potentially result in modified loading strategies, for example trimming by the stern during certain legs of a route.

A method to estimate the loss of thrust due to partial propeller submergence is given in Holtrop (1984).

1.3.4 Chapter 4: Propeller Flow Modelling in Steady and Unsteady Flow

The previous Subsection mentioned a mathematical model for propeller action which only considered flow arriving from directly in front of it (the "dead ahead" condition), also neglecting any sway or yaw induced on a ship's motions from the propeller. When the ship is in a seaway, she will have attained a drift angle, resulting in an oblique inflow angle to the propeller. This Chapter explains how the oblique drift angle and unsteady effects can be accounted for in modelling the propeller.

A Review of Modelling Propeller Action

This section provides a brief account of the more popular methods of modelling propeller action which were considered for this study. The list is in order of increasing complexity.

Momentum Theory

The axial momentum theory of Rankine (1865) is perhaps one of the earliest theories of propeller action. The propeller is reduced to a thin, infinitely bladed disc (or actuator disc) which accelerates the flow in the axial direction by somehow creating a pressure jump at the propeller plane. The same principle was applied by Froude (1889), in the angular direction, thus allowing the propeller to impart a rotational velocity in the wake.

A major disadvantage of this method is that it neglects the geometry of the propeller, blades and hub.

Blade Element Theory

Froude (1878) developed a propeller theory which considered the blade of a propeller to be divided up into a large number of elementary strips. These elementary strips are then regarded as a two-dimensional foil section which is subject to a resultant incident velocity. The lift and drag is then summed-up over the whole blade, and the resulting thrust and torque obtained.

A main disadvantage of this method is that is does not directly account for the induced velocity at the propeller plane.

Combined Blade Element Theory

The general momentum theory and the blade element theory can be combined to eliminate some of their inherent disadvantages. Burrill (1956)'s procedure is a combination of blade-element and momentum theory, with modifications to account for a finite number of blades in the momentum part, and empirical relations derived from wind tunnel tests for lift.

Lifting-Line

The propeller is reduced to radially aligned straight vortices (a lifting line) which vary in strength over the radius. Free vortices are shed in the flow and

viscous losses require empirical corrections. The lifting line is two-dimensional and therefore introduce considerable errors that need correcting.

Many lifting-line codes are adapted from the original formulation by Lerbs (1952) and are still popular today for preliminary design and analysis.

Lifting-Surface

With the advent of highly skewed propellers, the lifting line approach proved to be inadequate in capturing necessary three-dimensional flow phenomena (Carlton, 2007). The next level in advancement of propeller theories is the lifting-surface method, the most popular being the vortex-lattice method.

The propeller is reduced to a grid of horseshoe vortices, the pressure distribution on the blade is obtained from Bernoulli's law, which in turn yields forces and moments for the whole propeller. Corrections are needed for viscous effects, and the pressure distribution at the hub needs a correction.

Boundary Element or Panel Method

This is a formulation of the potential theory problem, with source or dipole panels.

The main disadvantages of this method are the complex programming involved corrections required for viscous effects, and the large number of panels necessary make it more computationally expensive compared to methods mentioned previously.

Computational Fluid Dynamics

This is a field method formulation of the three-dimensional viscous flow using various degrees of simplified Navier-Stokes equations, especially for turbulence modelling. It is very computationally expensive, and depends upon how well the particular turbulence model performs.

Propeller Model used in this Study

The method chosen for modelling the action of a propeller in this study is based on a heavily modified combined general momentum and blade element method. The reasons being that whilst perhaps not sufficient for detailed design work, the main physics of the flow can be adequately represented, resulting in realistic behaviour.

The propeller module is accessed at each time-step of the *SiS* simulator, therefore the mathematical propeller flow calculations are required to be fast. The modified combined general momentum and blade element method provides just such a practical and computationally fast procedure.

Details of the propeller model can be found in Chapter 4.

1.3.5 Chapter 5: Validation of Simulation Modules

The basis of the numerical models for simulating the manœuvring motion of a ship in a seaway have now been established, including the action of a propeller in oblique flow. This Chapter shows that the simulator behaves in a realistic manner by comparing the results of the *SiS* simulator with results from sea-trials and simulations carried out by various institutions.

1.3.6 Chapter 6: Simulation Methodology and Results

The *SiS* simulator has now been verified to work as expected. This Chapter describes the process of choosing a propeller that is optimised for conditions that the simulator predicts. Case studies are developed to show how modelling the propeller with different levels of fidelity affect the propeller's main particulars.

Results from these case studies are demonstrated using the *SiS* simulator, and show differences in efficiency, fuel consumption and CO_2 emissions from selecting a propeller that accounts for manœuvring motion compared to a propeller model that neglects it.

1.3.7 Chapter 7: Conclusions, Further Work and Recommendations

This Chapter summarises the main conclusions that are drawn from this research. It also proposes further work which could correct various assumptions.

1.4 Basis Ships

Different ship types behave differently to one another when they experience the same weather conditions. To determine the difference that ship type has on potential efficiency gains, two types were chosen for analysis in this study, a Very Large Crude Carrier (VLCC) (loaded), the *Esso Osaka*, and a 3600 Twenty Foot Equivalent Unit (TEU) container ship, the *KCS*.

The *Esso Osaka* has an unusually complete set of accurate sea-trials results, including corrections for weather (Crane, 1979). She has also had many captive and free-running model tests carried out by various laboratories, and as such has consequently been the subject of numerous numerical simulation studies (ITTC, 2002). The extensive amount of manœuvring data available for the *Esso Osaka* make it an excellent basis ship to verify manœuvring simulation development models. It is for these reasons, and the fact that oil tankers are now subject to efficiency regulations from the IMO that the *Esso Osaka* is chosen as a basis ship for this study.

The KRISO Container Ship (*KCS*) was conceived by the Korea Research Institute for Ships and Ocean Engineering (KRISO) as a modern (1997), efficient concept design of a container ship. No full-scale ship exists. The purpose of the design was to provide a benchmark for explication of flow physics and Computational Fluid Dynamics (CFD) validation. The *KCS* is one of the subject ships for SIMMAN (a workshop on verification and validation of ship manœuvring simulation methods) (SIMMAN, 2014), and as such has extensive manœuvring studies carried out on it. For this reason, the fact that it has a very different design to the *Esso Osaka*, and the fact that container ships are the subject of efficiency regulations from the IMO is the rationale behind why the *KCS* is chosen as a basis ship for this study.

	KCS (Container Ship)	*Esso Osaka* (*VLCC*)
$L_{pp}(m)$	230.0	325.0
$L_{wl}(m)$	232.5	335.0
$B_{wl}(m)$	32.2	53.0
$T(m)$	10.8	21.79
$\nabla(m^3)$	52030	311902
C_B	0.651	0.831
C_M	0.985	0.990
L_{CB} (%), fwd+	-1.48	3.169
No. of blades	5	5
$D(m)$	7.9	9.1
$P/D(0.7R)$	0.997	0.715
a_E	0.800	0.682

Table 1.1: Main particulars of the *Esso Osaka* and the *KCS*.

Table 1.1 shows the main dimensions of both the *Esso Osaka* and the *KCS*.

1.5 Practical Usage: The How-To Guide

This section is intended to provide the reader with a brief guide of how this research can be applied in practice.

- The ship's weight, major dimensions and service speed are determined from the ship owner's requirements.
- The ship's route is determined for which wind, wave and current statistics are obtained.
- The above parameters are input to the *SiS* simulator, and the simulation run.
- The *SiS* simulator can be used to either analyse an existing propeller's performance, or pick an optimised one from a standard series.
- The output of the simulator is extensive, parameters of most concern to powering applications include average, quasi-steady delivered power and open-water propeller efficiency.
- Scenarios can be played out to obtain the *overall* most efficient initial basis propeller for the ship and route in question. Simulation calculations should be combined with environment statistics for typical course trajectories.

1.6 Summary

This Chapter has provided an overview of the research carried out in this study. Figure 1.1 summaries the key components of the research. After describing the main approaches used to model the action of a propeller, it is concluded that, for the purposes of this research, a modified blade-element momentum method is the most suitable approach, due to its fast computation time, and sufficient accuracy.

This Chapter has defined the problem and motivation which has driven this research. It has described a novel approach to select an optimised propeller which accounts for the manœuvring motion of a ship. An How-To guide has been given which demonstrates the practical usage of the methodology.

The following Chapters depict in detail the different aspects of this research.

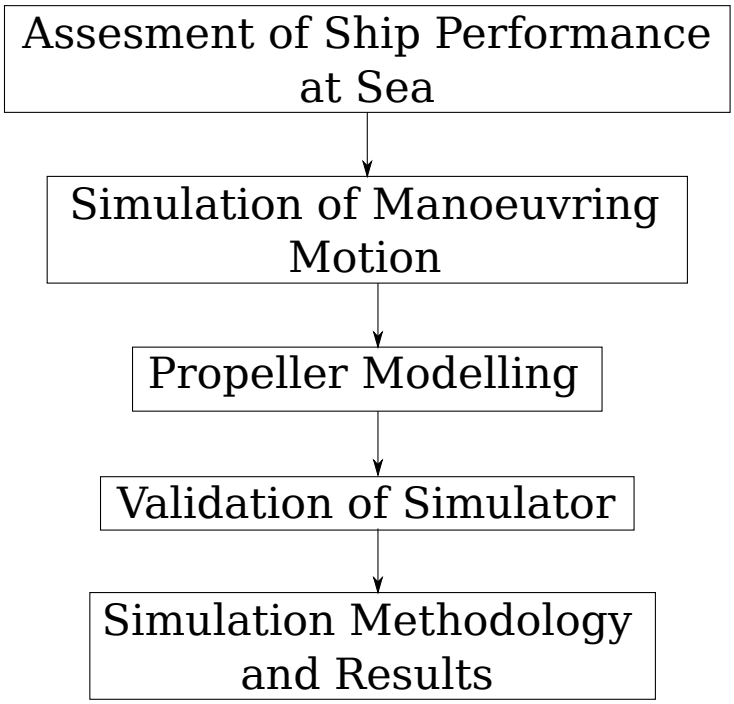

Figure 1.1: Key components of Research

Chapter 2. Ship Performance at Sea

This Chapter aims at describing the natural environment in which a ship operates, and how the ship's controls react if the ship is to reach her destination on time. It achieves this aim by describing the differences between the calm water environment, and the environment experienced by a ship in her normal, day-to-day operation. The forces considered to make up a seaway are assumed to arise from wind, waves and surface currents. These forces are described, along with how they can be estimated as a function of time from statistics. These external forces tend to move the ship off her desired track, and therefore the ship's controls must correct for these deviations. These deviations are also described in this Chapter.

Section 2.1 outlines the environmental conditions encountered in calm water (or sea trials) and why these conditions are important to consider. Section 2.2 describes the difference between calm water, and the environment encountered whilst the ship is in her expected conditions (or service conditions). This Section covers briefly why a ship would tend to change speed and course due to the effects of her environment, how the environment can be set up to be modelled for use in the developed *SiS* simulator, and how a ship would need to respond to counter the effects of the environment. Section 2.3 describes a method that can be used to predict a more accurate estimate of the sea-margin compared to commonly used traditional methods. This process involves the use of a simulator, which to the best of the author's knowledge is not used in practice and quite novel, but could provide the designer with more realistic loading conditions, and therefore design point. An example is given which demonstrates how the efficiency of a propeller deteriorates when operating away from its design point.

Section 2.4 discusses the importance of matching the correct engine to the selected propeller, to ensure optimum fuel efficiency and lowest CO_2 emissions.

2.1 Trial Conditions

As part of the contractual agreement with ship owner and builder, a ship is required to undergo *sea trials*. These trials are designed to ensure that the ship will meet the design specifications and International Maritime Organisation (IMO) criteria for such things as speed and manœuvrability (IMO, 1994). Sea trials are necessarily carried out in calm water, so as to minimise any effects from wind, waves and currents. Although most propeller designers design for service conditions, ensuring that their design will perform adequately under trial conditions, some designers do not, and optimise around trial conditions (and ensure that the propeller will operate adequately in service conditions). This is presumably due to pressure from the ship broker to ensure that the ship will meet her designed specifications - the penalties of not meeting the requirements can be very severe. As a rough estimate, Haakenstad (2012) indicates that: "A speed deviation of 0.3 knots between the trial speed (after correction) and that contractually stipulated, results in a fine of 100,000 United States Dollars (USD). Each additional 0.1 knots exceeding this discrepancy, increases the penalty by 100,000 USD. If the measured trial speed (after correction) is 0.8 knots or more below that contractually specified, the buyer has the right to cancel the contract."

The calculation of the Energy Efficiency Design Index (EEDI) is also verified from the results of the sea trials.

This research focuses on selecting an optimum propeller for a ship in service conditions, that is, a ship that is in the most probable conditions which she spends her voyage time.

2.2 In-Service Conditions

When a ship is in her normal day-to-day operation, she will be subject to the forces and moments imposed on her by the environment in which she is sailing.

When the wind blows over the surface of a body of water, friction at the interface between the air and water causes waves and also makes the surface of the water move (surface currents).

At the design stage, the effects of a seaway have traditionally been accounted for in the design by a constant of proportionality, known as the *sea-margin*. The sea-margin is usually calculated from rules of thumb (commonly around 1.2 to

1.5), or from previous experience. The value of the sea-margin is known to vary with the type of ship, speed and condition, but is mostly affected by the weather conditions that a ship will experience (Szelangiewicz and Żelazny, 2007) .

The ability of a ship to maintain speed and course whilst at sea reflects the success of the ship's design, that is, the ship is required to deliver cargo in a safe, timely and geographically precise manner whilst maintaining optimum efficiency. Different ship's operating profiles may have different assessment criteria, such as shortest time, lowest fuel consumption or lowest level of acceleration and thus discomfort. These other criteria must be taken into account also when selecting an optimum propeller.

2.2.1 Speed Loss in a Seaway

The loss of speed of a ship in a seaway consists of an involuntary loss and/or a voluntary speed loss. Speed loss can be regained up to the limit of the main engine power or the safe operating limits of the ship.

Involuntary Speed Loss

Speed loss will occur from:

- Added resistance caused by wind and waves.
- Added resistance from the motion response of the ship encountering these wind and waves.
- Loss of propulsive efficiency caused by an increase in propeller loading.
- Loss of propulsive efficiency caused by extreme events such as propeller racing or entrained air.

Voluntary Speed Loss

The ship's master may decide to voluntarily reduce the ship's speed or change course (which can be construed to be the same thing if time is of concern, please refer to section 2.2.5). This change in speed/course is brought about from the desire to maintain safety and efficiency. The main concerns include the risk of:

- Excessive vertical and horizontal accelerations.

- Excessive rolling.
- Green seas/deck wetness.
- Slamming.
- Propeller Racing.

It is assumed throughout the research that the weather does not get so bad that the operator needs to voluntarily reduce speed. This can be justified as the research is based around design for conditions which a ship is most probable to sail in.

2.2.2 Wind

The wind parameters which are input into the developed *SiS* simulator (please refer to Appendix A) consists of the mean true wind speed, and the mean true wind direction from North (positive clockwise). It is assumed in this research that the wind direction does not fluctuate about its mean value. This assumption is made from the fact that the author has been unable to find useful information regarding the numerical modelling of directionally varying wind. The majority of research effort on directionally varying wind seems to be based on observations and measurements in order to obtain clearer insight into how the wind effects the sea state (Donelan and Hamilton, 1985) and (Rieder and Smith, 1994).

The variation in mean wind speed (gusts) are accounted for by the following method:

The Davenport Wind Power Spectral Density Function

A power spectral density function (PSD) shows the strength of the variations of a signal as a function of frequency, that is, it shows at which frequencies the variations are strong and visa versa. It can be used to identify oscillatory signals in a time series and their amplitude. Figure 2.1 illustrates an example of the Davenport PSD.

Numerous wind gust spectra have been proposed over the years, perhaps the most popular include ones developed by Harris (1970), NPD (1992), API (2007) and Ochi and Shin (1988). Each model has its own strengths and weaknesses, for example, the Norwegian Petroleum Directive (NPD) spectrum has been developed

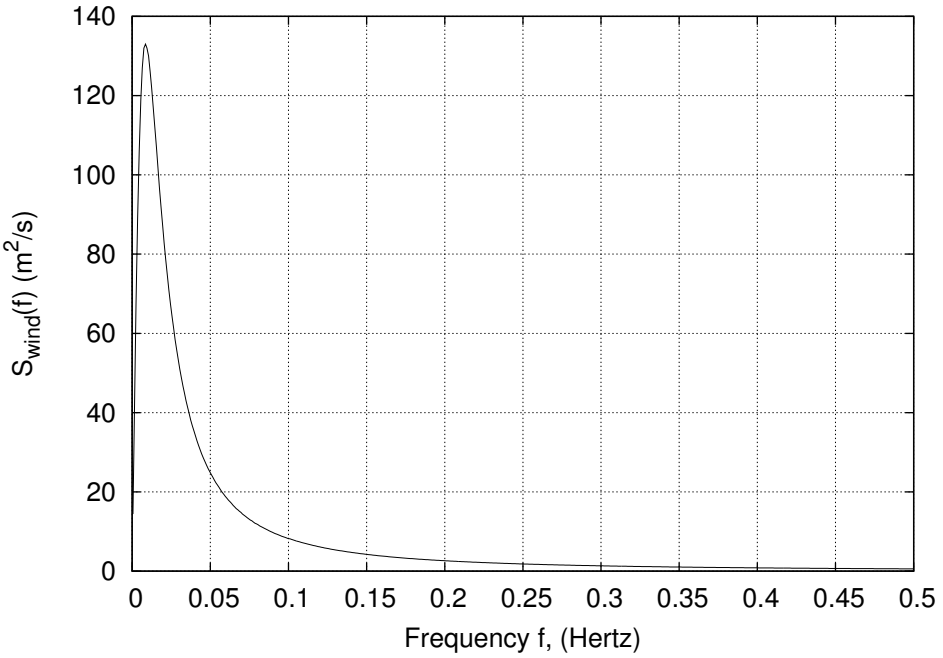

Figure 2.1: Davenport Power Spectral Density Function

from data around the Nordic countries. For initial design purposes, they all serve the same purpose, with not a great deal to choose between them. The main difference is that the offshore models contain more power at lower frequencies, the reason being that the other models are based over land, which has a different thermal structure.

An unsteady wind velocity model is incorporated into the *SiS* simulator (discussed in Section 3.8.1) using the Davenport (1978) spectrum for the variation in the longitudinal component of the wind due to gusting. This is a well established model and used in many time-domain analysis packages (e.g. MARIN (2013)), and is given in equation 2.1

$$S_W(f) = \frac{4\kappa L \bar{U}_W \chi}{(1+\chi^2)^{4/3}} \tag{2.1}$$

Where

$$\chi = \frac{fL}{\bar{U}_W} \tag{2.2}$$

S_W is the power spectral density (PSD) as a function of frequency, f (Hz). $\bar{U}_W$ is the mean wind speed at height z above the datum, usually 10 m. L is a scale length associated with fetch and is usually chosen to be 1200 m (Kaasen, 1999). κ is a surface drag coefficient and is usually chosen to be 0.005 for calm seas, and

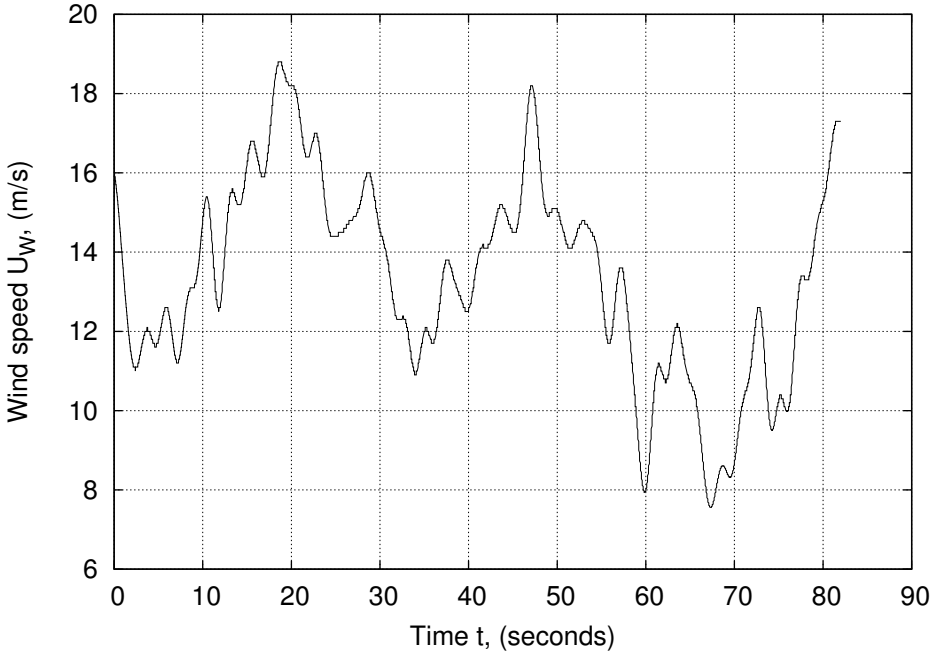

Figure 2.2: Time history of wind speed from Davenport PSD with $\bar{U}_W = 13.41 m/s$

0.0025 for rough seas.

Obtaining the Time-History from a Power Spectral Density function

The Spectral Representation Method developed by Shinozuka and Jan (1972) is used in this study to describe the time history of wind velocity from the power spectral density. The fluctuating velocity component, ΔU_W is a zero-mean random process simulated by superposition of harmonic waves.

From Shinozuka and Jan (1972):

$$\begin{aligned} U_W(t) &= \bar{U}_W + \Delta U_W(t) \\ &= \bar{U}_W + \sum_{j=1}^{N} \sqrt{2 S_W(f_j) \Delta f_j} \cos(2\pi f_j t + \phi_j) \end{aligned} \tag{2.3}$$

In order to apply equation 2.3, the frequency band of interest must be divided into N intervals such that:

$$\Delta f_j = f_{j+1} - f_j \tag{2.4}$$

ϕ_j is the random phase angle with a uniform probability distribution function between 0 and 2π.

Each time the `wind.f90` module is accessed, a new wind time-history is

generated. Due to the random nature of the wind, a single wind time-history data file is created which can be used instead of generating a new time series, and ensure that each run on the simulator uses the same environmental forces to provide comparable results (although the mean fluctuation of velocity is zero).

2.2.3 Waves

As a ship moves through a seaway, she will expend energy in deflecting waves from their original course. The waves will also excite the ship, causing her to move from her undisturbed position. These phenomena cause an increase in resistance, termed added resistance due to waves, or simply added resistance. There are several methods that can estimate the loss in speed, or added resistance (Prpić-Oršić et al., 2008), however, the method of Townsin et al. (1992) is used in this research due to its ease of use and practicality.

The method of Townsin et al. (1992) accounts for the speed loss in pure surge due to a ship encountering waves from any direction and is described in more detail in Section 3.8.2. It is considered to be suitable as a first step in modelling added resistance and will suffice as a proof-of-concept for this research.

2.2.4 Current

This study assumes that a ship is travelling in deep water, which is unaffected by tidal currents. Due to the action of the wind however a relative velocity can occur between the surface of the sea, and the sea bed. This surface current is accounted for in the research from the principle of relative motion, that is, the speed of the ship with respect to a point on Earth is equal to the velocity of the ship minus the velocity of the current.

It is assumed that the surface current has no velocity gradient along the length of the ship, and that the speed of the current is constant.

2.2.5 Leeway

Leeway can be defined as "The amount of drift motion to leeward of an object floating in the water caused by the component of the wind vector that is perpendicular to the object's forward motion" (Bowditch, 2002).

When a ship encounters a wind during her voyage, the force from the wind will

tend to push her off the desired course. Figure 2.3 shows a ship attempting to get from A to B. The wind has two effects upon the ship. Firstly it will impart a change in surge and sway velocities of the ship, and secondly, if the wind force does not happen to act through the centre of pressure in pure sway of the ship, a yawing moment will exist. Rudder application is required to compensate for these disturbances viz. The ship must be given a new course to steer so that she will end up at her final destination, or next waypoint. If the wind does not impart a yawing moment on the ship, then after the course has been corrected, the helm may be returned to zero (or the helm angle corresponding to zero rate of turn). If however, the wind is causing the ship to yaw, then some other rudder angle is constantly required, to check the yawing motion. When the effects of the environment are taken into account, the ship will now be sailing along at some drift angle, resulting in five additional effects:

1. The ship has now attained a sway velocity; the drag vector of which must be added to the forward resistance.

2. There is also a change in the forward resistance to account for, due to the new flow pattern around the ship, at this particular angle of incidence, resulting in a modified form coefficient.

3. If rudder action is required to check any yawing moments, then an induced drag from the rudder will also add to the ship's overall resistance.

4. The flow pattern into the propeller will be modified due to the ship's new attitude in the water.

5. The environment itself will be imparting extra forces and moments on the ship directly from the added resistance of wind and waves.

The power required to propel the ship at in-service conditions will be different to that of trial conditions. The reason for this is twofold:

- The distance through the water is different from the distance made good, thus the speed made good must change, that is, if the ship is to arrive at her destination on time.

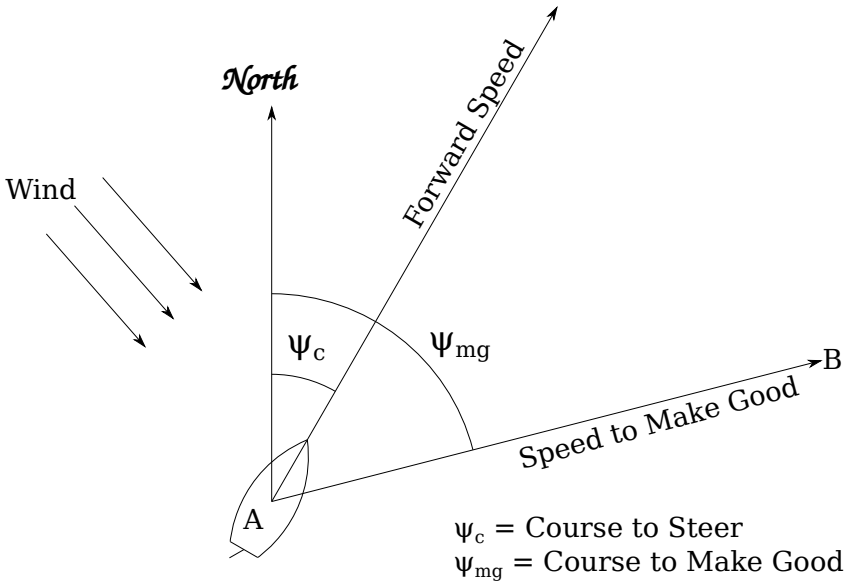

Figure 2.3: Leeway due to Wind

- The ship's powering requirements have changed due to the environmental loading itself, and also the ship's motion and propulsion response due to this environmental loading.

2.2.6 Passive Rudder

In the context of this research, the term passive rudder refers to the rudder being moved to a position which maintains the ship's desired course. If the helm angle is non-zero, then a lift induced drag force manifests itself to add to the total resistance of the ship.

2.3 A Method for Accurate Sea-Margin Prediction.

The speed at which a ship is able to travel in real weather conditions is one of the most important parameters which influences the ship's profitability.

Estimation of an accurate sea margin means being able to design for conditions that better represent day-to-day service conditions. One method of obtaining an accurate estimation of the sea-margin is predicting the long-term added resistance from wind and wave statistics for the area of service. This approach makes it possible to investigate with higher certainty than with a conventionally estimated sea-margin, the impact of power output of a particular main engine on a ship's

service parameters, and thereby service costs, and emissions footprint.

Wind and wave statistics are readily available for different areas from sources such as COGOW (2012) and GWS (2013).

A method to analyse propulsive efficiency over the whole voyage is to split the route up into different legs where the weather is significantly different. The propulsion system could then be selected that would have the greatest overall efficiency for the entire route (whilst still maintaining non-cavitating characteristics).

A study by Trodden and Woodward (2012) show how the open-water propeller efficiency changes with wind conditions for a 3600 TEU container ship in winter conditions in the North Sea. The study only considers changes in ship motions due to wind alone (no added wave resistance). As can be seen in fig. 2.4, the propeller efficiency varies with different relative wind directions. The centre of the polar plot, where the bars protrude outwards, represents a wind rose with the figures in magenta around the cardinal, intercardinal and secondary intercardinal points representing the probability that the wind is blowing *from* that direction. Wind rose plots and wind speed and direction data were obtained from Risien and Chelton (2006) and COGOW (2012), and were provided courtesy of Oregon State University's Cooperative Institute for Oceanographic Satellite Studies (CIOSS).

The scale of the polar plot (between 0.650 and 0.660) represents the open-water propeller efficiency, where the dotted green line represents the efficiency in calm water (a constant) and the red line represents the propeller's efficiency when the wind is blowing from the indicated direction. The outline of the ships hull indicates which direction the ship is heading, in this case North East. As can be seen, there is not a great deal of difference between the trial and service conditions figures, this is mainly due to the fact that only the effect of the wind has been modelled, however the methodology illustrates that designing for the most probable conditions has the potential to result in an overall greater efficient propeller.

In conjunction with the probability (in magenta), the red line indicates the most likely propeller efficiency resulting from a wind coming from the indicated direction. In this case it can be seen that the most probable wind does not result in any loss in efficiency, however, if the heading of the ship is rotated 180°, then the efficiency loss from the most probable wind will be relatively large, as this most probable wind has a high wind speed. These points demonstrate why, in the

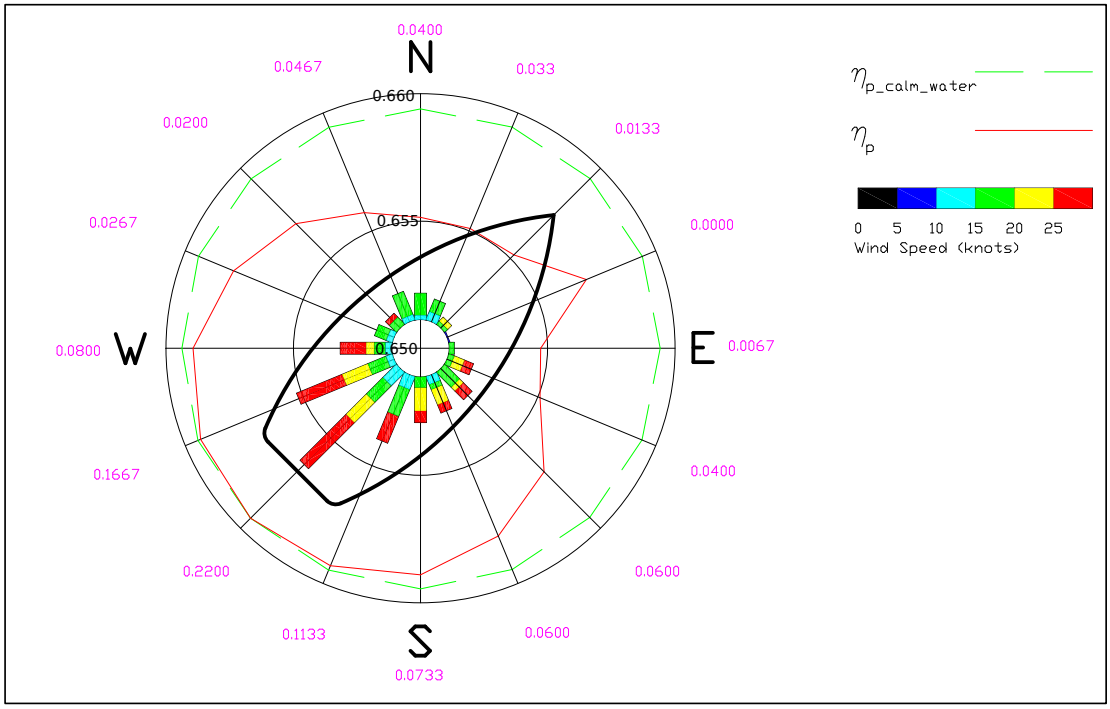

Figure 2.4: Propeller Efficiency Vs. Wind Probability

application of the methodology presented in this thesis, it is important to analyse the route as a whole, and select the propeller whose criteria produce the most efficient *overall* design.

The effect of wind on the open-water propeller efficiency depicted in the plot of fig. 2.4 is seen to be small. This is due to only accounting for the added wind resistance, and not the associated increase in added wave resistance due to action of this wind on the water. This plot also represents a propeller modelled using a *dead-ahead* flow model, and as such does not account for any change in propeller efficiency from operating in oblique flow. As noted in the paper of Trodden and Woodward (2012), there is an increase in shaft power of 9.2% on a route from Bergen to Newcastle for a South Westerly wind. This is quite a significant amount, which is attributed to the fact that the *KCS* is a relatively high power ship, travelling at 24 knots, and is subject to sharp increases in resistance (and therefore required power) from the environment at that speed. This illustrates, along with the discussions in Section 6.5, why relatively higher power ships benefit more from even small efficiency savings.

A study by Szelangiewicz and Żelazny (2007) investigated the influence of

realistic service margins, on the service parameters (speed, resistance) of a ship. This study calculated a service margin for different ship types over different shipping routes based on wind, wave and current statistics, and proposed a definition of Service Margin (or sea margin):

> "For a given ship sailing on a given shipping route, the service margin $k_{\dot{z}}$ should have such percentage value as the ship in assumed loading conditions and assumed state of its hull and propeller surface, would be able to maintain the service speed, V_{ZE}, assumed in the frame of long-term prediction, at the assumed exceeding probability P_{VE}."

Where P_{PVE} is the probability of a ship developing the service speed, and $k_{\dot{z}}$ is the notation used in the paper of Szelangiewicz and Żelazny (2007) to denote the service margin.

In order to make use of this definition, the designer needs to know the long-term service speed, and at the level of probability of maintaining the ship's speed that would make the ship operationally profitable.

The study by Szelangiewicz and Żelazny (2007) concluded that the influence of a ship's type and size on her speed or resistance is noticeable but not as great as that of the shipping route. Definite differences in the effectiveness (in terms of satisfying the owners requirements) of the same ship on a given shipping route can be observed, which is a result of a superior engine-propeller match.

2.4 Engine-Propeller Matching

It is important to match the engine power to the power required by the propeller, to avoid over/under loading the main engine, and producing excessive amounts of unwanted emissions. When the ship is in service, the engine is usually designed to operate between 85% and 90% of its Maximum Continuous Rated (MCR) Power. This is done to ensure the engine does not wear out too quickly, and also to provide extra power if it is required. In the following analysis, the engine margin has been selected to operate at 90% MCR in service conditions.

Figure 2.5 shows the KCS's propeller (c.f. Table 1.1) demand curve superimposed on a Wärtsilä 10 Cylinder RT-flex82C engine layout (Wärtsilä, 2011). The propeller demand curve represents the power required of the propeller to propel the ship at the desired speed. The propeller demand curve may be

obtained from the aforementioned simulator, or roughly estimated using the cubic 'Propeller Law' curve. If the resistance of the ship increases then the propeller demand curve will shift to the left and vice versa.

In fig. 2.5 PD represents the propeller's design point about trial-conditions. PD' is the propeller's design point at service conditions. SP is the service propulsion point, and MP is the engine's maximum continuous rated power. The grey area in fig. 2.5 shows the engine's overload range.

The light running propeller demand curve represents the power required to achieve the corresponding speed when the ship is in trial-conditions, that is the hull and propeller are smooth. The heavy running propeller demand curve represents the power required after the ship has been in the water for some time, when the hull and propeller are to some extend fouled. The difference between the heavy running and light running curves are usually between 4% and 7% and depends upon the ship's mission profile, dry docking interval and time between engine overhauls. This light running margin is usually selected from experience and in fig. 2.5 the light running margin is 5%.

As can be seen in fig. 2.5 the heavy running propeller whose design point is at PD will not provide enough thrust in service conditions to achieve the ship's service speed, therefore it is prudent to design the propeller to operate a few revolutions faster (the light running margin) than the service speed demands.

The sea margin of fig. 2.5 is stated as 15%, which is a typical rule-of-thumb figure. It is shown in this research that, with the use of a ship simulator at the design stage, a more realistic estimate of the sea margin can be obtained, and therefore the engine can be more closely matched to the propeller, resulting in lower fuel consumption and hence CO_2 emissions.

Figure 2.6 illustrates how the specific fuel consumption (and hence emissions) change when the engine-propeller is operated away from its optimal design point (Woodyard, 2004).

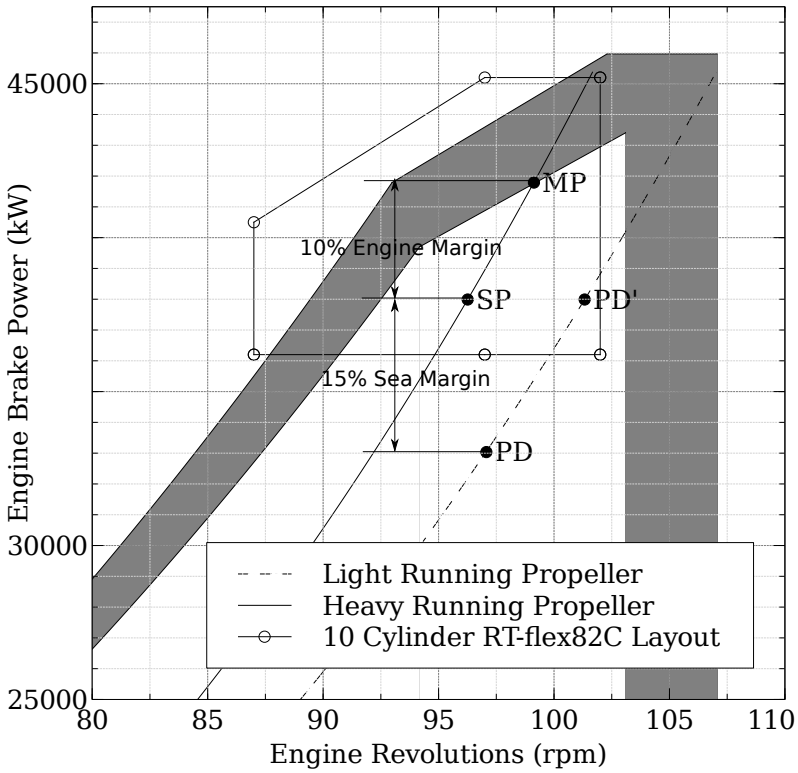

Figure 2.5: Wärtsilä 10 Cylinder RT-flex82C Main Engine & Propeller Demand Curve for KCS.

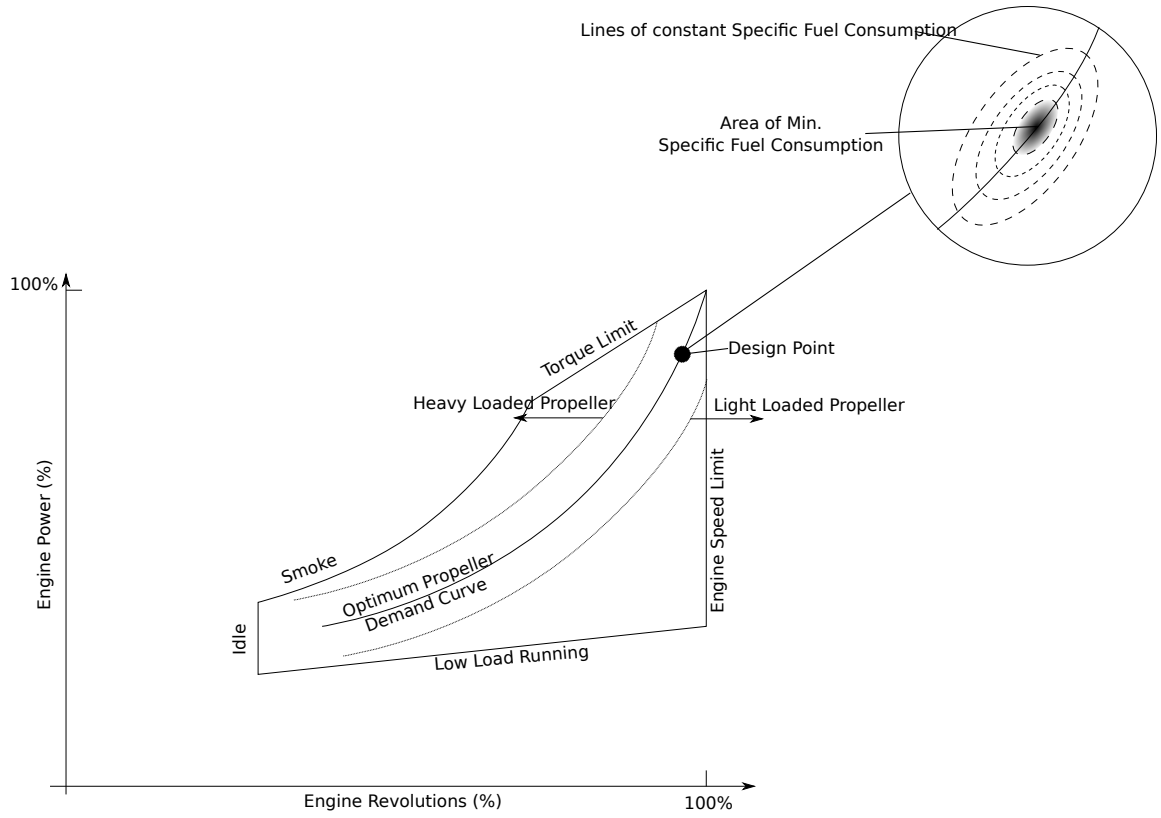

Figure 2.6: Impact on specific fuel consumption from operating engine away from optimum design point.

2.5 Summary

This Chapter has described the external forces that a ship will encounter in her day-to-day operation. It has been shown that the powering requirements of a ship in service conditions will be different to that in trial conditions, not just because of the fact that there are other forces and moments to consider directly, but also the forces and moments from the ship's response to the environment, and because the ship may have to travel at a different speed over the ground on a different heading in order to arrive at her final destination on time.

A methodology has been shown that relates how a realistic estimate of the sea margin can be obtained from a ship simulator, and thereby a more realistic design point. An example was given that shows how the efficiency of a propeller depreciates when operating away from its design point.

The importance of matching the engine to the propeller was demonstrated to ensure optimum overall propulsive efficiency.

Having explained the nature of the external forces a ship experiences whilst at sea, the next Chapter endeavors to describe how they can be modelled mathematically.

Chapter 3. Simulation of Manœuvring Motion

This Chapter aims at describing the mathematical modelling of a ship at sea in the manœuvring motions of surge, sway and yaw. The Chapter shows the development of a system of Ordinary Differential Equations (ODEs) from different components that affect the motion, these components comprise the ship's hull, rudder, propeller, wind and a limited added wave resistance model. ODEs are also developed to model engine and rudder machinery. A simple automatic pilot is described which allows the ship to stay on course and/or maintain speed when the ship is perturbed without any user (helmsman) intervention. The analysis needs to determine if the ship is dynamically stable, as a dynamically unstable ship would result in excessive helm correction and the role of the autopilot would play an essential role in the ship's overall efficiency. A method is described to determine whether or not a ship is dynamically stable. The process of solving simultaneously the ODEs numerically is described, followed by a brief summary.

Section 3.1 illustrates the coordinate systems that are used throughout this study. Section 3.2 defines the equations of motion that are solved by the developed *SiS* simulator, and shows the main components that are involved in the various mathematical models.

While Section 3.3 describes the rational behind the selected methodology for solving the manoeuvring equations of motion in the time-domain, Section 3.4 is devoted to describing the theory and mathematics behind the interaction between the hullform and the water. It also describes a method to determine if a ship is course stable. Section 3.5 details the effect of the rudder on a ship's manœuvring motion, and the interaction between the rudder, hull and propeller. It also specifies how the rudder's dynamics are modelled. Section 3.6 describes how a propeller's characteristics, that is, thrust and torque, are estimated. Section 3.7, outlines how the ship's main engine is modelled mathematically, and also how the dynamics of the combination of the engine and propeller are estimated. Section 3.8 explains

how the loading on a ship from her environment (wind, waves and surface currents) are estimated. Section 3.9 presents a method to correct the course and speed of a ship that is being pushed off her original course and speed due to her environment. Section 3.10 gives an account of the method used to solve the ordinary differential equations set out in this Chapter. Chapter 3.11 gives a summary of this Chapter.

General assumptions are that the ship is a rigid body, which is reasonable as deflections in the ship's hull are usually very small compared to the ship's manœuvring motion, and that the ship remains intact throughout the voyage. More specific assumptions are addressed throughout the various sections.

3.1 Coordinate System

In this study, a local, ship-fixed coordinate system, with its origin at the centre of gravity, is used to describe the manœuvring motions of a ship. It is convenient to describe the forces and moments on a ship with respect to midships, whilst motions are more conveniently described with respect to the centre of gravity. It is this approach that is taken throughout this study. This is illustrated in fig. 3.1.

A global, Earth-fixed coordinate system, is used to describe the navigational position and direction of a ship. The position and direction are obtained by integrating equations 3.1, 3.2 and 3.3.

$$\dot{x_o}(t) = \sqrt{u(t)^2 + v(t)^2} \times \cos\left[\psi(t) + \beta(t)\right] \qquad \text{Advance velocity w.r.t. Earth} \tag{3.1}$$

$$\dot{y_o}(t) = \sqrt{u(t)^2 + v(t)^2} \times \sin\left[\psi(t) + \beta(t)\right] \qquad \text{Transfer velocity w.r.t. Earth} \tag{3.2}$$

$$\dot{\psi_o}(t) = r(t) \qquad \text{Rate of change of heading} \tag{3.3}$$

3.2 Equations of Motion

This examination will focus on motions in the horizontal plane, namely surge, sway and yaw. The sea-keeping motions of heave, roll and pitch are neglected. In this proof-of-concept study, it is assumed that the predominant factor in an altered

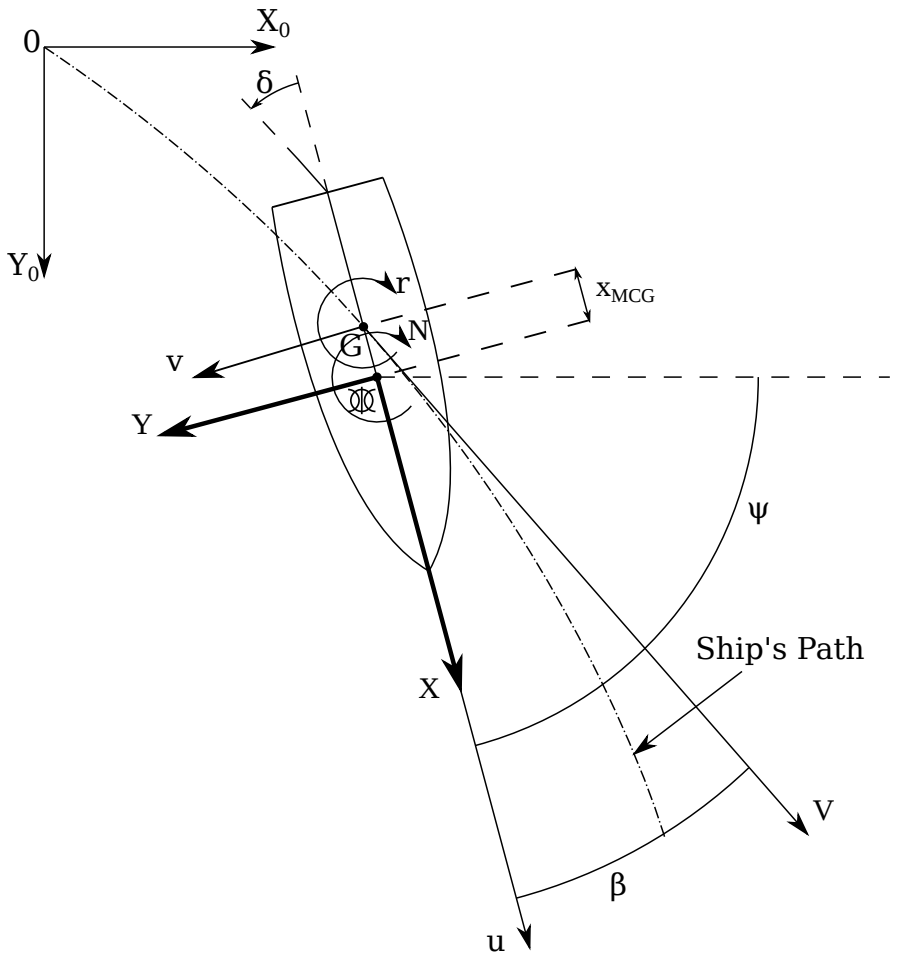

Figure 3.1: Coordinate System.

flow field will be drift angle, as when the ship has attained a quasi-steady state in a seaway, the averaged drift angle will be non-zero, whereas the other motions, with the exception of roll, can be assumed to have averaged values of near-zero (this does not necessarily mean however that these motions do not contribute to the overall efficiency of a propeller).

The equations of motion are defined in equations 3.4.

$$m\left(\dot{u} - rv\right) = X_H + X_R + X_P + X_W + X_A \qquad \text{SURGE} \qquad (3.4a)$$

$$m\left(\dot{v} + ru\right) = Y_H + Y_R + Y_P + Y_W + Y_A \qquad \text{SWAY} \qquad (3.4b)$$

$$I_{zz}\dot{r} = N_H + x_{MCG}Y_H + N_R + N_P + N_W + N_A \qquad \text{YAW} \qquad (3.4c)$$

The subscripts H, R, P, W and A in equations 3.4, denote the influences from the hull, rudder, propeller, waves and wind respectively. m is the mass of the ship, u is the velocity in pure surge, v is the velocity in pure sway and r is the yaw rate. x_{MCG} is the distance between the longitudinal centre of gravity and midships. I_{zz} is the mass moment of inertia of the ship about the z-axis.

3.3 Hydrodynamic Models for Time-Domain Simulation

The literature review of Section 1.3.3 highlights different methodologies that can be used to solve the equations of motion in surge sway and yaw and why the current method, which is broadly based on the one described by Inoue et al. (1981b) was chosen. There now follows a more detailed exposition of how these equations of motion are set-up.

3.4 Hull

The longitudinal force on the ship's hull, X_H, transverse force on the ship's hull, Y_H, and the yaw moment on the ship's hull, N_H can be written as equations 3.5, 3.6 and 3.7 respectively.

$$X_H = -m_x\dot{u} + \left(m_y + X_{vr}\right)v_o r + X_{H_o}\left(u\right) \qquad (3.5)$$

$$Y_H = -m_y\dot{v} - m_x ur + Y_{H_o}\left(v_o, r\right) \qquad (3.6)$$

$$N_H = -J_{zz}\dot{r} + N_{H_o}\left(v_o, r\right) \qquad (3.7)$$

Where m_x, and m_y are the surge and sway added mass respectively. J_{zz} is the

hull's added mass moment of inertia. v_o is the lateral sway velocity at midships: $v_o = v + x_{MCG}r$

The calm water, pure surge, resistance component, X_{H_o}, is estimated from the method proposed by Holtrop and Mennen (1982) and Holtrop (1984) and is summarised in appendix B.4. The fundamental force in pure sway, Y_{H_o} and yaw moment, N_{H_o} are obtained from the method given by Inoue et al. (1981a).

In the following notation, a $'$ symbol denotes a non-dimensionalised factor, and the standard SNAME nomenclature is used, whereby $Y_v \equiv \frac{\partial Y}{\partial v}$ etc.

$$X_{H_o} = R_f\,(1+k) + R_{app} + R_W + R_B + R_{tr} + R_a \tag{3.8a}$$

$$Y_{H_o} = \frac{1}{2}\rho L_{pp} T V_v^2 \left(Y'_v v'_o + Y'_r r' + Y'_{v|v|} v'_o |v'_o| + Y'_{v|r|} v'_o |r'| + Y'_{r|r|} r'|r'|\right) \tag{3.8b}$$

$$N_{H_o} = \frac{1}{2}\rho L_{pp} T V_v^2 \left(N'_v v'_o + N'_r r' + N'_{r|r|} r'|r'| + N'_{vrr} v'_o r'^2 + N'_{vvr} v'^2_o r'\right) \tag{3.8c}$$

The calm water resistance components of equation 3.8a are made up from viscous resistance ($R_f\,(1+k)$), where k is a form factor, the resistance of any appendages, R_{app}, the wave making resistance, R_W, the resistance of any bulbous bow, R_B, resistance from any imersion of a transom stern, R_{tr}, and a ship-model correlation allowance, R_a.

The non-dimensionalised components are $v'_o = v_o/V_v$ and $r' = rL_{pp}/V_v$, where V_v is the linear velocity of the origin in body axis (The resulting ship velocity).

The manœuvring coefficients in equations 3.8b and 3.8c are estimated from work by Inoue et al. (1981a), and can be found in appendix B.1.

The added mass and mass moment of inertia terms, m_x, m_y, I_{zz} and J_{zz} are obtained from Motora (1959 and 1960), formulae for which can be found in appendix B.3

The resistance component of a ship advancing at some drift angle is estimated from Inoue et al. (1981a)

$$X'_{vr} = -\left(1 - C_B\right) m'_y$$

3.4.1 Dynamic Stability

A ship is said to be dynamically stable (also sometimes referred to as directionally or course stable) if a deviation from a set course increases only while an external force or moment is acting to cause the deviation. If a ship's course deviates in the

absence of any external force or moment, then it is said to be dynamically unstable.

A ship that is not directionally stable will require constant rudder corrections to maintain her desired course. To prevent any excess rudder movement (and its associated resistance) from biasing results in any way, only course stable ships are analysed in this study. If the ship in question is found to be directionally unstable, then the simulation is aborted. Perhaps the easiest way to test if a ship is directionally stable is to analyse the linearised equations of motion, viz.

It can be shown that the linearised equations of motion can be written in the following form, as suggested by Nomoto (1966):

$$T_1' T_2' \ddot{r}' + (T_1' + T_2')\,\dot{r}' + r' = K'\delta + K' T_3' + \dot{\delta}'$$

Where T_1', T_2' and T_3' are the time constants of the yaw rate equation, and K' is the gain. The time and gain constants are related to the manœuvring coefficients by:

$$T_1' + T_2' = \frac{\left[\begin{array}{l}(Y_{\dot{v}}' - m')\,(N_r' - m' x_G') + (N_{\dot{r}}' - I_Z)\,Y_v' \\ \quad - (N_{\dot{v}}' - m' x_G')\,(Y_r' - m') - (Y_{\dot{r}}' - m' x_G')\,N_v'\end{array}\right]}{Y_v'\,(N_r' - m' x_G') - N_v'\,(Y_r' - m')} \tag{3.9}$$

$$T_1' T_2' = \frac{(Y_{\dot{v}}' - m')\,(N_{\dot{r}}' - I_Z) - (N_{dotv}' - m' x_G')\,(Y_{\dot{r}}' - m' x_G')}{Y_v'\,(N_r' - m' x_G') - N_v'\,(Y_r' - m')} \tag{3.10}$$

$$T_3' = \frac{(N_{\dot{v}}' - m' x_G')\,Y_\delta' - (Y_{\dot{v}}' - m')\,N_\delta'}{N_v' Y_\delta' Y_v' N_\delta'} \tag{3.11}$$

$$K' = \frac{N_v' Y_\delta' - Y_v' N_\delta'}{Y_v'\,(N_r' - m' x_G') - N_v'\,(Y_r' - m')} \tag{3.12}$$

For dynamic stability, the roots of the characteristic equation should have negative real parts. If the roots are given by σ_1 and σ_2 then it is also apparent that:

$$\sigma_1 = -\frac{1}{T_1'}$$
$$\sigma_2 = -\frac{1}{T_2'}$$

The stability boundary is reached when σ_1 or σ_2 becomes zero, or when T_1 or T_2 becomes infinite. By examining equation 3.10 when T_1 or T_2 is zero, it can be inferred that:

$$Y_v'\,(N_r' - m' x_G') - N_v\,(Y_r' - m') = 0$$

This is the stability criterion for ships, and should therefore be greater than zero.

$$Y'_v \left(N'_r - m'x'_G\right) - N_v \left(Y'_r - m'\right) > 0$$

or

$$\frac{N'_r - m'x'_G}{Y'_r - m'} > \frac{N'_v}{Y'_v} \tag{3.13}$$

Equation 3.13 physically meaning that if the centre of pressure in pure yaw is ahead of the centre of pressure in pure sway, then the ship is directionally stable.

As a linear model has been used to develop the stability criterion, it is important to use associated linear manœuvring coefficients. This is due to the fact that different expansion models have different values for their manœuvring coefficients. The linear manœuvring coefficients used to determine directional stability in this study are obtained from the work of Clarke et al. (1983).

3.5 Rudder

Once the rudder is deflected, a lift force is created by the rudder's pressure differential. c.f. Figure 3.2. This lift force deviates the ship from her original course, resulting in an angle of attack to the flow. This reduces the angle of attack of the rudder, but it still makes a small contribution that keeps the ship yawing. Meanwhile, the hull angle of attack causes a large drift force. The combination of drift and yawing are what is termed "turning".

3.5.1 Rudder Forces

The rudder angle is defined to be positive when the trailing edge is to the starboard side of the ship.

Referring to fig. 3.2, the rudder forces may be expressed in the following form:

$$X_R = -\left(1 - t_R\right) F_N \sin\delta_R \tag{3.14a}$$

$$Y_R = -\left(1 - a_H\right) F_N \cos\delta_R \tag{3.14b}$$

$$N_R = -\left(x_R + a_H x_H\right) F_N \cos\delta_R \tag{3.14c}$$

Where:

t_R is a rudder drag correction coefficient.

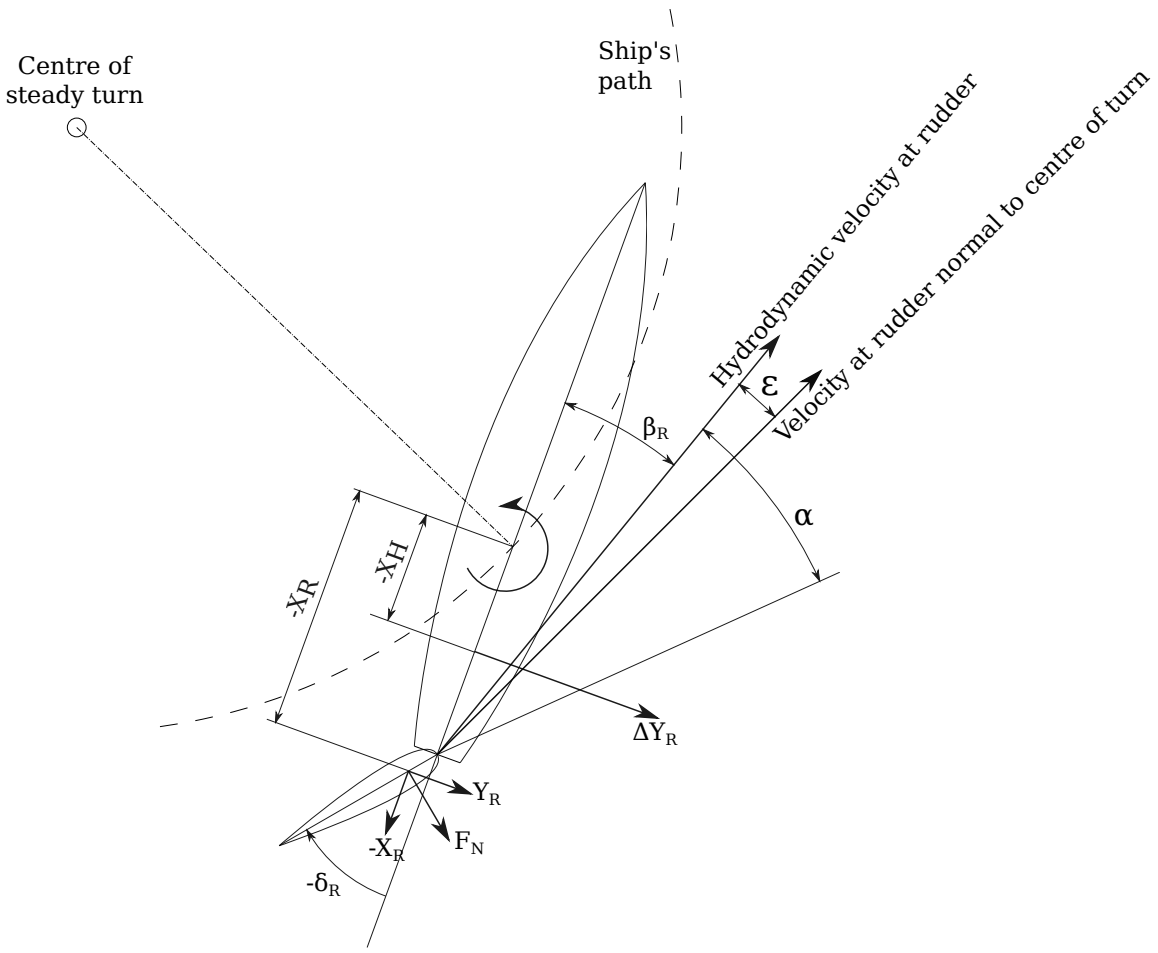

Figure 3.2: Velocity Vectors at the Rudder During a Steady Turn to Port

a_H is a coefficient to account for the interaction between the hull and rudder.
x_H is the distance between the point of application of the lift from the hull and amidships.
x_R is the distance between the centre of pressure of the rudder and amidships.
δ_R is the rudder's angle.

3.5.2 Hull - Rudder Interaction Coefficients

The longitudinal force of the rudder, $F_N \sin\delta_R$, yields an increase of resistance X_R. Usually $X_R < F_N \sin\delta_R$, hence the coefficient of t_R in equation 3.14a. The coefficient t_R can be determined from Meijing and Xiuheng (1990) as:

$$(1 - t_R) = 0.28 \times C_B + 0.55$$

The rudder induces an asymmetric flow which results not only in a lateral force, $F_N \cos\delta_R$ (at application point X_R), but also an extra lateral force $a_H F_N \cos\delta_R$ (at application point x_H) from the ship now being at an angle of attack to incoming flow. This leads to equation 3.14b.

The interaction coefficient, a_H and the application point x_H are estimated from Kijima et al. (1990a) as follows:

$$a_H = 0.627 C_B - 0.153$$

$$x_H = -0.5 L_{pp}$$

It is assumed that the ship is sailing in deep water, as the coefficients a_H and x_H increase and decrease respectively with decreasing water depth, although correction factors for shallow water can easily be applied to these coefficients (from the work of Yumuro (1985)). This assumption seems reasonable for the type of analysis that is undertaken in this study. The basis ships chosen for case studies in this research (c.f. Section 1.4) will spend the majority of their voyage time in deep water, and it is this condition for which the optimum propeller must be selected. A notable exception for this assumption is inland ships, for which shallow water cannot be disregarded. Inland ships must at present be excluded from this study.

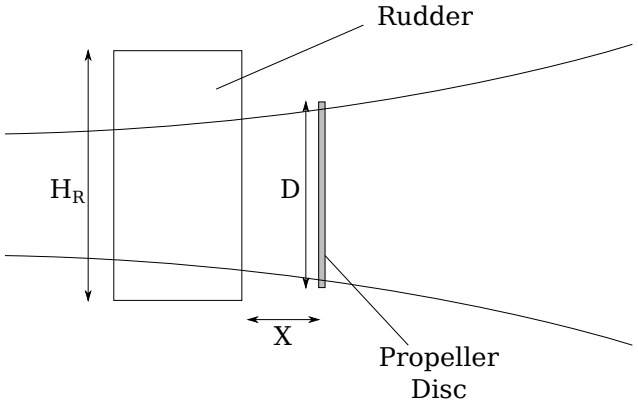

Figure 3.3: Schematic of longitudinal inflow velocity across a rudder.

3.5.3 Rudder Normal Force

The force normal to the rudder, F_N can be written as:

$$F_N = \frac{1}{2}\rho A_R f_a V_R^2 \sin\alpha_R$$

Where:

A_R is the area of the rudder.

V_R is the effective rudder inflow velocity.

α_R is the effective rudder inflow angle.

Fujii's prediction formula may be used to calculate the gradient of the lift coefficient of the rudder, f_a. viz.

$$f_a = \frac{6.13\Lambda}{2.25 + \Lambda}$$

Where Λ is the rudder's aspect ratio.

3.5.4 Effective Rudder Inflow Velocity

The rudder's normal force is considerably influenced by the nature of the propeller's slip stream, that is, it's wake contraction and velocity. Referring to fig. 3.3, the scheme described by Lee et al. (2003) is used to calculate the effective rudder inflow velocity, viz.

$$U_R = \varepsilon\,(1-w)\,u\sqrt{\eta\left[1+k\left(\sqrt{1+\frac{8K_T}{\pi J_P^2}}-1\right)\right]^2+1-\eta}$$

Where

$$\eta = D/H_R$$
$$\varepsilon = \frac{R_{R0}}{U_p} = \frac{1-w_R}{1-w}$$
$$k = k_x/\varepsilon$$
$$k_x = 0.5 + \frac{0.5}{\left[1+\left(\frac{0.15}{X/D}\right)\right]} \approx 0.6$$
$$J_R = u\frac{(1-w_R)}{nD}$$
$$w_R = w_{Ro}\exp -4.0\beta_P^2$$
$$\beta_P = \beta - x'_P r'$$

Where H_R is the height (span) of the rudder.

The $\sqrt{1+\frac{8K_T}{\pi J_P^2}}$ term represents the velocity of the wake far downstream (as can be shown from axial momentum theory), with the k factor correcting for the difference between the velocity far downstream and at the rudder (a function of distance of the rudder from the propeller (X/D).

3.5.5 Effective Rudder Inflow Angle

The effective rudder inflow angle, α_R, can be estimated using the following expressions:

$$\alpha_R = \delta_R - \gamma\beta_R$$

where

$$\gamma = -22.2\left(Cb\frac{B}{L_{pp}}\right)^2 + 0.02\left(Cb\frac{B}{L_{pp}}\right) + 0.68$$
$$\beta_R = \arcsin\left(\frac{v+x_R r}{V_v}\right)$$

γ represents the flow straightening factor due to the ship's hull, β_R is the drift angle at the rudder, and x_R is the distance of the x coordinate of the rudder from midships ($x_R \approx 0.5L_{PP}$).

The wake fraction at the rudder, w_R and flow straightening factor, γ significantly affect the results of the simulation (Kijima et al., 1990b) as they directly affect the inflow velocity into the rudder.

3.5.6 Rudder Dynamics

When an order for the rudder to be put over is given, the rudder does not instantaneously arrive at the given order, but takes a certain amount of time. The electromotive oil pressure steering gear model of Son (1989) is used:

$$\dot{\delta}_R = \begin{cases} \dfrac{(\delta_{R_c} - \delta_R)}{T_R} & \text{if } |\delta_{R_c} - \delta_R| \leq T_R |\dot{\delta}_{R_{\max}}| \\ \text{sign}\,(\delta_{R_c} - \delta_R)\,|\dot{\delta}_{\max}| & \text{if } |\delta_{R_c} - \delta_R| > T_R |\dot{\delta}_{R_{\max}}| \end{cases}$$

Where $\dot{\delta}_{R_{\max}}$ is the maximum slew rate, δ_{R_c} is the rudder command (or order) and T_R is the rudder time constant.

This equation is solved simultaneously with the other equations of motion to obtain the rudder angle at a particular time step.

3.6 Propeller

The propeller model described in this section is based upon the Wageningen B-Screw Series propellers and only considers the pure surge velocity component. A model that takes into account the ship's varying drift angle is described in Chapter 4.

The forces and moments imparted on the ship by the propeller can be written as equations 3.15, assuming that he side force and associated yawing moments generated by a single screw is negligible.

$$X_P = (1 - t)\,\rho n^2 D^4 K_T \tag{3.15a}$$

$$Y_P \approx 0 \tag{3.15b}$$

$$N_P \approx 0 \tag{3.15c}$$

Where t is the thrust deduction factor, due to the propeller modifying (reducing in the case of a ship making headway) the pressure distribution at the stern of a ship (thus increasing her resistance in forward motion or from another perspective, reducing the thrust).

Oosterveld and van Oossanen (1975) provide polynomials for calculating the open water characteristics of the Wageningen B-Screw Series propellers. For the sake of brevity, the propeller module that uses this method (as opposed to the methods described in Chapter 4) is often referred to, in this study, as the *OOVOO* model.

The thrust and torque coefficients, K_T and K_Q respectively are obtained from equations 3.16

$$K_T = \sum_{s,t,u,v} \left[C_{T_{s,t,u,v}} \cdot J_P^s \left(\frac{P}{D} \right)^t \left(\frac{A_E}{A_O} \right)^u Z^v \right] \tag{3.16a}$$

$$K_Q = \sum_{s,t,u,v} \left[C_{Q_{s,t,u,v}} \cdot J_P^s \left(\frac{P}{D} \right)^t \left(\frac{A_E}{A_O} \right)^u Z^v \right] \tag{3.16b}$$

The coefficients s, t, u, and v can be found in Appendix B.5. P is the propeller's pitch, D is the propeller's diameter, A_E is the expanded blade area and A_O is the area of a disc of diameter D. Z is the number of blades on the propeller. J_P is the effective advance ratio at the propeller, and is estimated by equation 3.17.

$$J_P = \frac{V_{a_p}}{nD} \tag{3.17}$$

Where n is the propeller revolutions, and V_{a_p} is the speed of advance at the propeller, as defined by equation 3.18

$$V_{a_p} = u\,(1 - w_p) \tag{3.18}$$

w_p is the wake fraction at the propeller, and is covered in the next subsection.

The thrust and torque are related to the thrust and torque coefficients by the identities of equations 3.19

$$T = \rho n^2 D^4 K_T \tag{3.19a}$$

$$Q = \rho n^2 D^5 K_Q \tag{3.19b}$$

3.6.1 Wake and Thrust Deduction Factor

The wake at the propeller plane for a ship at zero drift angle, w_{P0} and thrust deduction factor, t can be calculated from the analysis carried out by Holtrop (1984), equations for which can be found in Appendix B.4.

The following formulae from Hirano (1981) may be used to estimate the wake

fraction at the propeller plane:

$$w_P = w_{P0} \exp\left(-4.0\beta_P^2\right) \tag{3.20}$$

Where the drift angle at the propeller is given by:

$$\beta_P = \arcsin\left(\frac{v + x_P r}{V_v}\right) \tag{3.21}$$

Where x_P is the distance of the x-coordinate of the propeller from midships (a negative value $\approx -0.5L_{pp}$).

3.7 Main Engine Machinery Model

Expressions of the Main Engine Torque Q_E depend on engine types, and Q_E is modelled according to it's characteristics in each engine operating condition. In the following examination, the engine characteristics of a slow speed, directly coupled two-stroke diesel engine are described for the normal running mode. This engine type is the most popular for ship types like the basis ships of this study, due to the higher output power compared to their four-strokes counterparts.

The engine's torque characteristics are written in the form of equation 3.22, where $Q_{E_{\max}}$ is the maximum allowable torque of the main engine.

$$Q_E = \begin{cases} |Q_P| & \text{if } |Q_P| \leq Q_{E_{\max}} \\ Q_{E_{\max}} & \text{if } |Q_P| > Q_{E_{\max}} \end{cases} \tag{3.22}$$

3.7.1 Engine & Propeller Dynamics

The telegraph order sets the rate of propeller revolutions. This is achieved by altering the rate of fuel flow into the engine, thereby altering the torque the engine produces. The difference between the resisting torque of the water on the propeller, and the output torque from the engine, results in the acceleration of the drive train.

The rate of change of the propeller's speed can be written as equation 3.23.

$$\begin{aligned} \dot{n} 2\pi \left(I_{pp} + J_{pp}\right) &= Q_E - \rho n^2 D^5 K_Q \\ \dot{n} &= \frac{Q_E - Q_{prop}}{J_{shaft}} \end{aligned} \tag{3.23}$$

The added mass moment of inertia of the propeller, J_{pp} and mass moment of

inertia of the shaft system about it's axis, I_{pp} can be estimated from equation 3.24 (Ksnaj, 1996)

$$I_{pp} + J_{pp} = 20.0D^5 \tag{3.24}$$

It is noted, for equation 3.24 to be dimensionally correct, the constant 20.0 must have the units of $[Kg\ m^{-3}]$.

The torque from the engine (Q_E) is calculated from equation 3.25

$$Q_E = \chi_{gear} \cdot \eta_{shaft} \cdot \tau \cdot Q_{E_{max}} \tag{3.25}$$

Where χ_{gear} represents the gear ratio (which in the case of the slow speed directly coupled diesel engine is 1.0). Losses in the system are accounted for by the transmission efficiency (η_{shaft}). τ is the engine throttle setting.

In this analysis, it is assumed that a throttle setting of 100% corresponds to the engine producing maximum torque. The throttle setting is given between 0 to 100%, that is, the engine is not reversed in this analysis. The torque output from the engine does not respond instantaneously to the throttle setting, the response of the engine to the throttle setting is modeled with the use of the following expression:

$$\dot{\tau} = \begin{cases} \dfrac{(\tau_c - \tau)}{T_E} & \text{if } |\tau_c - \tau| \leq T_E \left|\dot{\tau}_{\max}\right| \\ \text{sign } (\tau_c - \tau) \left|\dot{\tau}_{\max}\right| & \text{if } |\tau_c - \tau| > T_E \left|\dot{\tau}_{\max}\right| \end{cases} \tag{3.26}$$

Where $\dot{\tau}$, is the throttle's rate of change with time, τ_c is the throttle command, τ is the instantaneous throttle setting, $\dot{\tau}_{\max}$ is the maximum rate of change of the throttle, and T_E is the engine's time constant.

Equations 3.26 and 3.23 are solved simultaneously along with the equations of motion ODEs.

3.8 Environment

Effects on the ship from the environment in which she sails was described in Chapter 2 and in a brief literature review in Chapter 1. There now follows a more detailed explanation as to how this environment is modelled mathematically.

3.8.1 Wind

The wind induced longitudinal and transverse forces and yawing moment imposed on a ship, in accordance with the current sign conventions and coordinate system, can be written as equations 3.27.

$$X_A = 0.5 C_{X_w} \rho V_{rw}^2 A_{F_w} \tag{3.27a}$$

$$Y_A = 0.5 C_{Y_w} \rho V_{rw}^2 A_{L_w} \tag{3.27b}$$

$$N_A = 0.5 C_{N_w} \rho V_{rw}^2 A_{L_w} L_{oa} + x_{MCG} Y_A \tag{3.27c}$$

Where V_{rw} is the velocity of the wind relative to the ship.

Blendermann (1996) gives semi-empirical formulae for estimating the wind force and wind-induced yawing moment coefficients on a ship for a wind from any direction. These are expressed as equations 3.28.

$$C_{X_w} = -CD_l \frac{A_{L_w}}{A_{F_w}} \left[\frac{\cos \gamma_{rw}}{1 - \frac{\delta}{2} \left(1 - \frac{CD_l}{CD_t} \right) \sin^2 (2\gamma_{rw})} \right] \tag{3.28a}$$

$$C_{Y_w} = CD_t \left[\frac{\sin \gamma_{rw}}{1 - \frac{\delta}{2} \left(1 - \frac{CD_l}{CD_t} \right) \sin^2 (2\gamma_{rw})} \right] \tag{3.28b}$$

$$C_{N_w} = \left[\frac{S_L}{L_{oa}} - 0.18 \left(\gamma_{rw} - \frac{\pi}{2} \right) \right] C_{Y_w} \tag{3.28c}$$

Where γ_{rw} is the relative wind direction, A_{L_w} is the lateral projected area, A_{F_w} is the transverse projected area and S_L is the horizontal distance to centroid of A_{L_w} from datum (midships). Values for δ, the cross-force parameter, CD_l the non-dimensional headwind drag coefficient and CD_t the non-dimensional beam-wind drag coefficient can be obtained from Table B.9.

Relative Wind Velocity and Direction

Referring to the diagram of fig 3.4, a ship is travelling on a course from A to B. The wind force is acting upon the ship, however the ship's course does not change, due to an application of the rudder, albeit, the ship's heading does change. The speed and direction of the wind, relative to the ship, can be calculated from

equations 3.29 and 3.30.

$$V_{RW} = \sqrt{\left[V_{TW}\cos\left(\gamma_{TW} - \psi\right) - V_v \cos\beta\right]^2 + \left[V_{TW}\sin\left(\gamma_{TW} - \psi\right) - V_v \sin\beta\right]^2} \tag{3.29}$$

$$\gamma_{RW} = \arctan\frac{V_{TW}\sin\left(\gamma_{TW} - \psi\right) - V_v \sin\beta}{V_{TW}\cos\left(\gamma_{TW} - \psi\right) - V_v \cos\beta} \tag{3.30}$$

Where V_{TW} = Velocity of true wind.

V_{RW} = Velocity of wind, relative to the ship's centre-line.

γ_{TW} = Direction of wind, relative to North, positive clockwise.

γ_{RW} = Direction of wind, relative to the ship's centre-line.

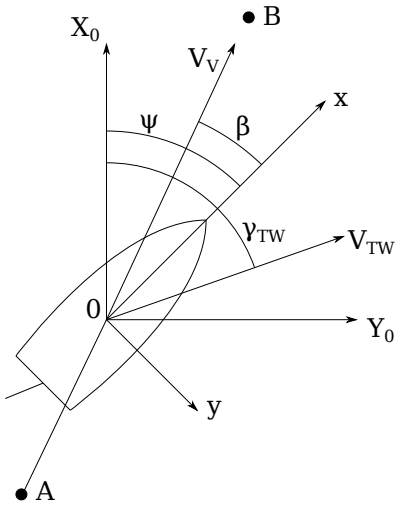

Figure 3.4: Relative Wind Velocity and Direction

3.8.2 Waves

As a starting point to account for added resistance due to waves, the method of Townsin et al. (1992) is used. This method estimates the added resistance in the pure surge direction caused by waves encountering a ship from any angle. The paper of Townsin et al. (1992) was written at a time when a 3600 TEU container ship such as the *KCS* used in this study was well within the size range for manufacture, the same applies to a ship such as the *Esso Osaka*, Rodrigue (2013). Caution should be exercised if this method is to be used for ships that are extreme in size, such as the Maersk Triple E Class, having a capacity of 18,340 TEU, as the validity of the method may not be applicable to such ships due to the semi-empirical nature of the method's formulation.

The percentage speed loss of a ship travelling in waves is given by:

$$\mu \frac{\Delta U}{U} 100\% = a\mathrm{BN} + \frac{\mathrm{BN}^b}{d\nabla^{2/3}} \tag{3.31}$$

Where a, b and d are obtained from Table 3.1, μ can be obtained from Table 3.2 and BN is the Beaufort Number which is obtained from the mean true wind speed as specified as input to the *SiS* simulator. A table to extract the Beaufort Number from wind speed is given in Table B.10.

	Tankers		Containerships
	Laden	Ballast	
a	0.5	0.7	0.7
b	6.5	6.5	6.5
d	2.7	2.7	22

Table 3.1: Coefficients for use in Townsin et al. (1992) method for added wave resistance.

	2μ
Head Sea (up to 30^o off bow)	2
Bow Sea (30^o - 60^o off bow)	$1.7 - 0.03\,(BN - 4)^2$
Beam Sea (60^o - 150^o off bow)	$0.9 - 0.06\,(BN - 6)^2$
Following Sea (150^o to 180^o off bow)	$0.4 - 0.03\,(BN - 8)^2$

Table 3.2: μ coefficient for use in Townsin et al. (1992) method for added wave resistance.

Now, assuming that the resistance force is directly proportional to the square of the velocity; $R \propto U^2$, then let

$$\frac{R}{R_1} = \frac{U_1^2}{U^2}$$

where

$$U = U_1 \left(1 - \frac{\Delta U}{U_1}\right)$$

then

$$X_W = R = \frac{R_1}{\left(1 - \frac{\Delta U}{U_1}\right)^2}$$

The subscript $_1$ denotes values at the previous time step, $t_{(i-1)}$, and the resistance due to waves in the pure surge direction, R is, in accordance with previous

notation, X_W. The values of U_1 and R_1 are obtained from the simulator.

3.8.3 Current

The approach taken in this study to model the effects of surface current on the manœuvring motion of a ship is to express the ship speed relative to the Earth fixed coordinate system as the sum of the ship speed relative to the water and the velocity of the current. This assumes that the steady state has been reached, and that no relative motions exist between a ship and the water due to the current. The velocity of a ship with respect to Earth can be written as:

$$u_G = u + V_c \cos(\gamma_c - \psi)$$
$$v_G = v + V_c \sin((\gamma_c - \psi)$$
$$r_G = r + r_c$$

Where γ_c is the direction of the current with respect to Earth, and V_c is the speed of the current.

3.9 Automatic Pilot

In order for the simulated ship to arrive at the intended destination at the intended time, an automatic pilot has been implemented to compensate for any speed and course deviations due to weather. The autopilot consists of Proportional, Integral, Derivative (PID) controllers, one PID controller for course keeping and another for speed keeping.

The output of the PID controller is expressed as equation 3.32

$$o(t) = K_P e(t) + K_I \int_0^t e(\tau) + K_D \frac{\mathrm{d}}{\mathrm{d}t} e(t) \tag{3.32}$$

Where K_P, K_I and K_D are the proportional, integral and derivative tuning parameters respectively. Also, e is the error, t is the discrete present time and τ is the variable of integration (values from time $t = 0$ to present time).

The error in the system is defined as the difference between the desired value, or set-point, (SP) and the output value of the process (PV).

$$e = SP - PV \tag{3.33}$$

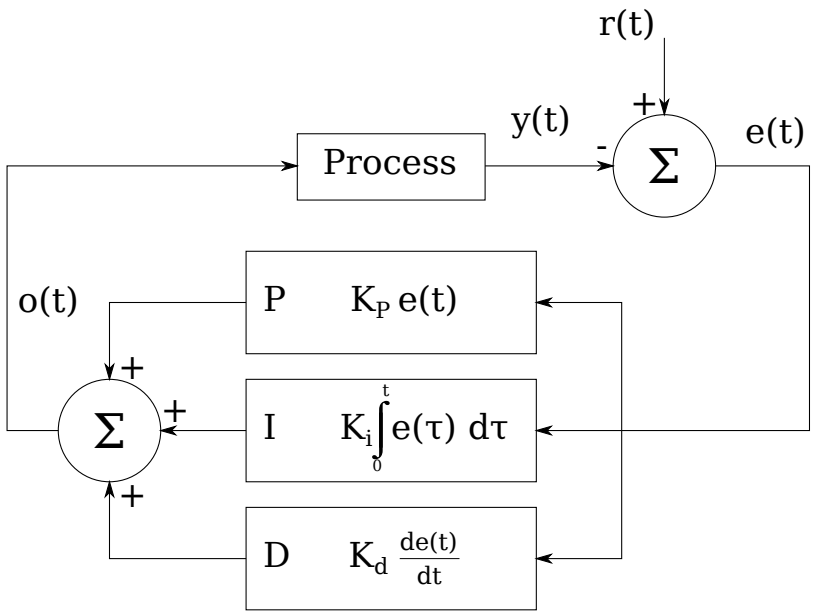

Figure 3.5: A block diagram of a PID controller in a feedback loop.

The error for the speed controller, e_s, is simply the difference between the designed service speed, V_s, and the ship's resultant velocity:

$$e_s = V_s - \sqrt{u\left(t\right)^2 + v\left(t\right)^2} \tag{3.34}$$

The error for the course controller, θ_e can be calculated with reference to fig.3.6.

$$\theta_c = \arctan\left(\frac{y_{wp} - y_{sp}}{x_{wp} - x_{sp}}\right) \tag{3.35}$$

$$\theta_e = \theta_c - (\psi - \beta) \tag{3.36}$$

Where θ_c is the ship's desired course, x_{sp} and y_{sp} are the Cartesian coordinates of the ship with respect to Earth, x_{wp} and y_{wp} are the coordinates of the next waypoint. In this analysis, the next waypoint is considered to be the ship's final destination, and is calculated as follows:

$$x_{wp} = V_s \times t_{\text{stop}} \sin\left(\psi_0\right) \tag{3.37}$$

$$y_{wp} = V_s \times t_{\text{stop}} \cos\left(\psi_0\right) \tag{3.38}$$

Where t_{stop} is the end time of the simulation, and ψ_0 is the ship's initial heading.

Providing the ship's resultant speed is kept the same as the starting speed (which for the purposes of this analysis is the ship's service speed), then the ship will arrive at her intended destination on time.

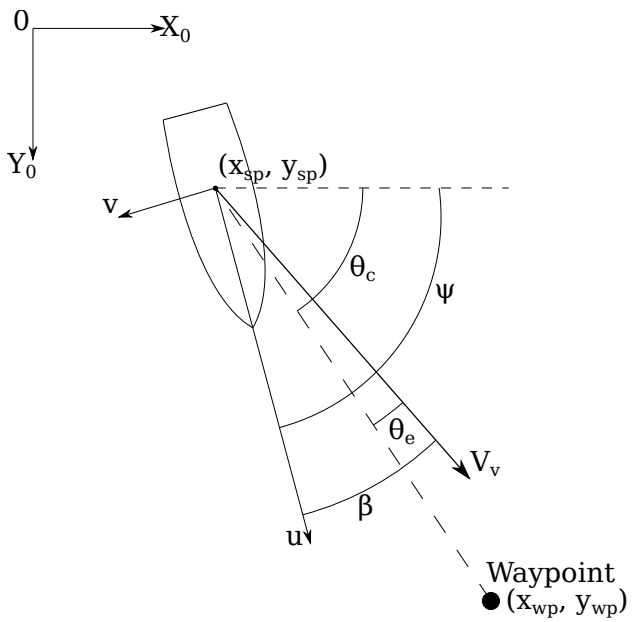

Figure 3.6: Calculation of Course Error.

3.9.1 Tuning the Automatic Pilot

The tuning parameters, K_P, K_I and K_D of the automatic pilot need to be chosen so that the system will reach its desired value (or set-point) within a reasonable time, without wild oscillations or becoming unstable (i.e. the output diverges). Several methods are available for determining the tuning parameters, one of the most popular being the Ziegler and Nichols (1942) method. This method requires knowledge of the oscillation period, which for an unsteady process is not an appropriate method.

A manual method of tuning the automatic pilot is used in this study, the process of which is outlined as follows:

- K_I and K_D are set to zero.
- K_P is increased until the output of the loop begins to oscillate (known as the *ultimate gain* K_U).
- K_P is then set to a half of the ultimate gain.
- K_I is then increased until any offset is corrected within a suitable time for the process. This statement effectively means that any offset does not grow so large that it cannot be corrected for within a reasonable time scale. "Reasonable" is rather a loose term, as for the purposes of this research,

where there are no tight manœuvres during a ship's voyage (with the exception of harbour manœuvres, which are not analysed), the accelerations and motions of a ship compared to the response of the control system are relatively slow, and therefore can usually be easily corrected within a time scale that would not result in a ship deviating drastically from her course. Care must be taken not to increase the value of K_I too much as this will cause instability.

- K_D is finally increased (if required) until the loop is acceptably quick at reaching the set point after a load disturbance. Again, "acceptably quick" is a loose term, meaning that any deviation is corrected within a time constraint so that after a disturbance, a ship can continue her voyage at the required specifications. Increasing the value of K_D results in a fast response, however, too much will result in excessive overshoot.

This tuning method is rather intuitive, and for the application of the ship's autopilot described in this research, the autopilot's tuning parameters are not sensitive to the results, and do not need to be finely optimised. It is thus difficult to quantify the tuning parameters, as for the purposes of this research they are not critical to results, and are rather subjective. The only time that the values of the tuning parameters become critical is when they result in an autopilot that does not do the job in hand and results in a ship that is unable to perform at her required specifications, or they produce such a sharp response that it results in an unstable system.

3.9.2 Automatic Pilot Review

Due to the assumption that the ship's resultant speed is kept constant, small errors creep into the calculations, due to the fact there are small fluctuations in the resultant ship speed. These small errors manifest themselves as an error in position near the end of the simulation's run, which are suddenly corrected by the autopilot when it realises that the waypoint is nearby. This sudden correction causes the ship to turn quickly, resulting in a transient response of the ship/propulsion system as seen, for example, in figs. C.1 and C.4. This transient stage towards the end of the simulation runs is discarded in the analysis of this research, however, it may be possible to avoid this sudden correction for, albeit, a small error in course,

from implementing a different methodology of automatic pilot.

One method to improve the automatic pilot's track keeping ability would be to incorporate a speed keeping algorithm in conjunction with a revised course-keeping algorithm. This revised course-keeping method would keep the ship on the desired track over each few time steps of the simulation, rather than the one waypoint at the end of the simulation, as presently implemented. This method would, however, probably require a faster response from the PID controllers, meaning that the tuning parameters would play a more critical role in the added resistance associated with the rudder's motion.

3.10 Numerical Integration of Ordinary Differential Equations

A forth-order Runge-Kutta method (Runge (1895) and Kutta (1901)) is used to solve the system of ODEs that together model the behaviour of the ship over time.

If the following N simultaneous differential equations represent the equations to be solved:

$$\frac{\mathrm{d}}{\mathrm{d}t} y_i\left(t, y_i\right) = f_i\left(t, y_i\right) \quad \text{for } i = 1, \ldots, N$$

Then the variables at the $(n+1)$th time step can be estimated from their values at the (n)th time step from the following algorithm (Abramowitz and Stegun, 1972):

$$y_i^{(n+1)} = y_i^{(n)} + \frac{1}{6}k_1 + \frac{1}{3}k_2 + \frac{1}{3}k_3 + \frac{1}{6}k_4 + O\left(h^5\right)$$

Where

$$\begin{aligned}
k_1 &= h f_i\left(t_n, y_i^{(n)}\right) \\
k_2 &= h f_i\left(t_n + \frac{1}{2}h, y_i^{(n)} + \frac{1}{2}k_1\right) \\
k_3 &= h f_i\left(t_n + \frac{1}{2}h, y_i^{(n)} + \frac{1}{2}k_2\right) \\
k_4 &= h f_i\left(t_n + h, y_i^{(n)} k_3\right)
\end{aligned}$$

and h is the size of the time increment, $i = 1, \ldots N$. The Bachmann-Landau symbol, O represents the local truncation error, and is set to zero in the present implementation.

3.10.1 Conversion of Second Order Ordinary Differential Equations Into System of First Order Ordinary Differential Equations

The equations of motion are expressed as a set of simultaneous second order Ordinary Differential Equations (ODE), however the Runge-Kutta method used in this analysis only solves first order ODEs. Fortunately one can easily convert a second order ODE into an equivalent set of simultaneous first order ODEs. viz.

If

$$\ddot{y}(x) = f[x, y(x), \dot{y}(x)] \tag{3.39}$$

with boundary conditions: $y(x_o) = y_o$ and $\dot{y}(x_o) = \dot{y}_o$, then let $Y_1(x) = y(x)$ and $Y_2(x) = \dot{y}(x)$. Equation 3.39 may be now be re-written as a system of two first order simultaneous equations:

$$\dot{Y}_1 = Y_2 \tag{3.40a}$$

$$\dot{Y}_2 = f(x, Y_1, Y_2) \tag{3.40b}$$

where $Y_1(x_o) = y_o$ and $Y_2(x_o) = \dot{y}_o$

Q.E.D.

3.11 Summary

This Chapter has laid out the mathematical structure for setting up and solving the components that form a ship simulator in the manœuvring motions of surge, sway and yaw. These components comprise the forces and moment from the ship's hull, propeller and rudder, and external forces and moment from the wind and the pure surge component of added wave resistance. An autopilot has been addressed, so that the simulation may be run without user interaction for correction of course and speed. This simulation methodology has been realised in a set of FORTRAN (2008 standard) subprogrammes, for which the descriptions and function list can be found in Appendix A.3.

Validation of the simulator is addressed in Chapter 5.

Chapter 4. Propeller Flow Modelling in Steady and Unsteady Flow

This Chapter details a theoretical basis for the unsteady dynamics of a marine propeller when accounting for the changing inflow vectors imparted to it by the manœuvring motion of a ship. For the purposes of this study, unsteady flow means that at a discrete polar coordinate in the propeller plane, the velocity vector there will be varying with time. The study excludes the variations due to hull wake.

A description of various theories to model the propeller flow was outlined in Chapter 1. In the early work on the theory of propeller action there were two main streams of thought; one based on the general conservation of momentum, chiefly attributed to Rankine (1865), and the other based upon elemental strips of the propeller's blade, attributed to Froude (1878). The combination of these two theories is known as the Blade-Element Momentum Theory ($BEMT$).

The mathematical propeller flow model that is used in this research is that of the combined Blade-Element Momentum Theory, the reason being is that it is considered to be the most amenable to integrating into a simulator (due to its relatively quick computation time, and the fact that the propeller module is called at each time-step throughout the simulation).

The $BEMT$ in its basic form is not considered to be accurate enough to capture some of the physical flow phenomena encountered by the propeller (certainly in the case of oblique flow). This Chapter explains the workings of the $BEMT$ and the modifications necessary to account for various flow phenomena, including unsteady flow effects.

Section 4.1 briefly describes the basis propeller series which is used to calculate steady propeller forces and to calibrate the unsteady propeller flow model. Section 4.2 describes the theory and mathematics behind the general conservation of momentum theory and how it is adapted to account for a finite number of blades, and an oblique inflow angle. Section 4.3 details the theory and mathematics

behind the blade element theory, and how it is modified to account for oblique inflow angle. Section 4.4 presents a method which combines the general conservation of momentum theory and the blade-element theory, thereby overcoming certain drawbacks that are inherent in each theory alone. Section 4.5 describes how the sectional lift and drag coefficients are obtained. These coefficients are necessary for the blade-element part and include effects of unsteady flow. This section also describes a method used to determine the flow regime (fully attached, transitional or separated). Whilst Section 4.6 describes how to predict the stall angle for the blade sections, Section 4.7 briefly outlines how the variation in inflow due to the ship's wake is used to further optimise a propeller, and why it has been neglected in this analysis. Section 4.8 demonstrates how the mathematics of the previous Sections are assembled into a Fortran subprogramme. Section 4.9 shows how the developed modified $BEMT$ propeller flow model is calibrated against the B-Screw Series via the polynomials developed by Oosterveld and van Oossanen (1975). This calibration is done to ensure that when comparisons are made between flow models, the base-line figure is identical between the flow models. Section 4.10 summarises the development and findings of the Chapter on Propeller Flow Modelling.

4.1 The Wageningen B-Screw Series

The Wageningen B-Screw Series has been chosen as a basis propeller to calibrate and compare the mathematical propeller flow model developed in this Chapter. The B-Screw Series has been extensively studied in the past, the performance can readily be calculated from the polynomials provided by Oosterveld and van Oossanen (1975), which have been based on accurate regression analyses from experimental data. An example of a B-Screw Series blade which has been output from `gplot.f90` is depicted in fig. 4.1.

4.2 The General Conservation of Momentum Theory

Rankine (1865) proposed a simple theory of propeller action based on the axial momentum of water passing through a propeller disc. The assumptions Rankine made in his theory were:

- The fluid in which the propeller operates is *ideal* (does not experience energy

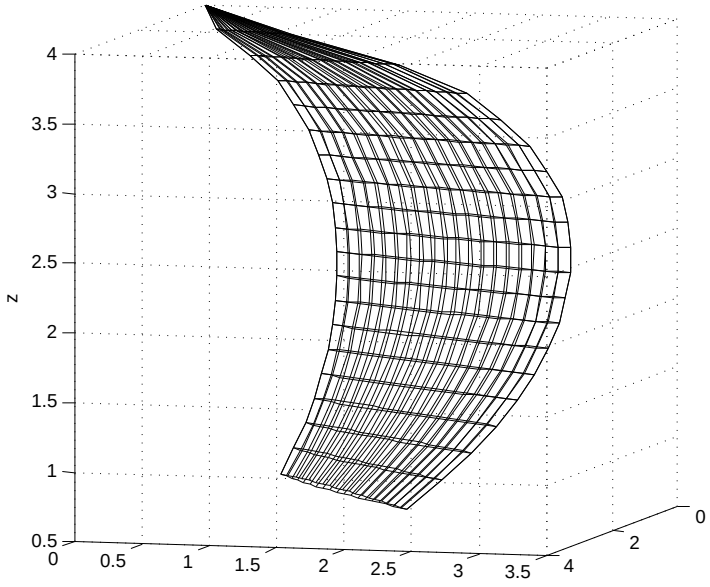

Figure 4.1: Example output from `b_screw_geom.f90` for propeller with $a_E = 0.8$, $P/D = 1.0$

losses due to friction).

- The propeller has an infinite number of blades (known as an actuator disc).
- The propeller does not impart any rotation into the slipstream.
- The thrust is assumed to be distributed uniformly over the disc.

The concept of the actuator disc (which is akin to a propeller with an infinite number of blades and infinitesimal thickness) is a common way to represent a propeller in early propeller theories. The actuator disc is considered to absorb all of the energy imparted in to it from the engine or appropriate source, and dissipate this power by causing an instantaneous increase in pressure across the two faces of the disc.

The power absorbed by the propeller, P_D is equal to the increase in kinetic energy of the slipstream per unit time, and the thrust the propeller generates, T, is equal to the increase in axial momentum of the slipstream: c.f. fig. 4.2

$$P_D = \frac{1}{2}\dot{m}\left(V_w^2 - V_a^2\right) \tag{4.1}$$

$$T = \dot{m}\left(V_w - V_a\right) \tag{4.2}$$

Where $\dot{m}$ is the mass flux , V_a is the velocity far upstream of the disc, and V_w is the velocity far downstream of the disc.

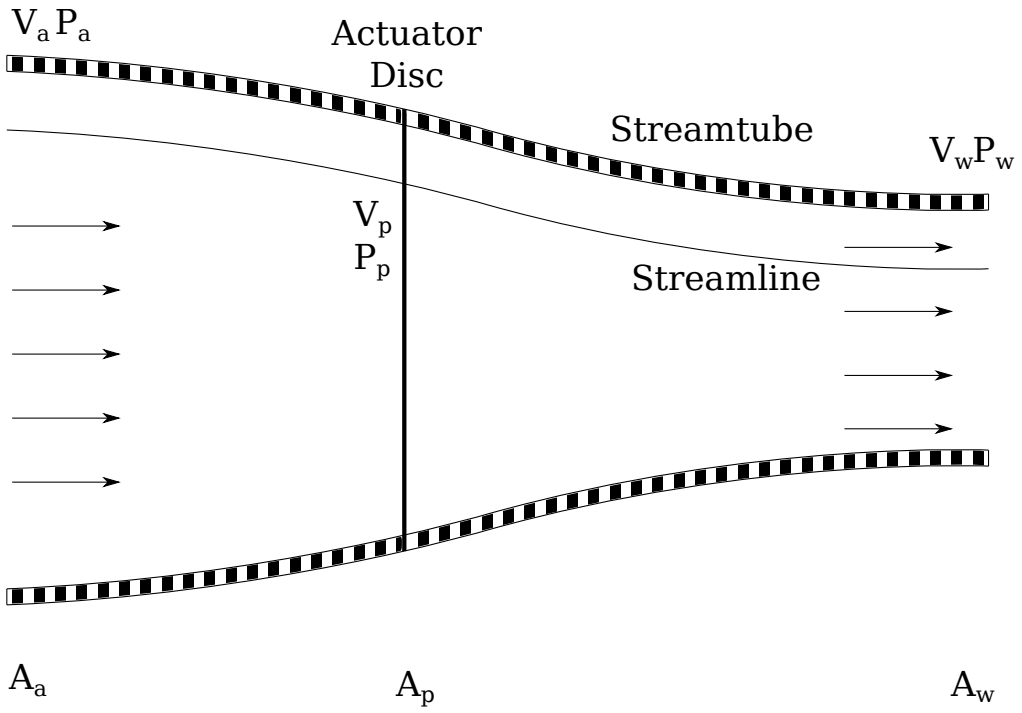

Figure 4.2: Axial Momentum Model of an Actuator Disc

Considering that power is equal to the work done by the thrust force of the propeller $P_D = TV_p$, where V_p is the velocity at the propeller disc, it can be shown from equations 4.1 and 4.2 that the velocity through the actuator disc is equal to the average of the velocities in the streamtube far upstream, and far down stream of the disc.

$$V_p = \frac{1}{2}(V_w + V_a) \tag{4.3}$$

Combining equations 4.3 and 4.2 and substituting $\dot{m} = \rho A_p V_p$ yields:

$$\begin{aligned} T &= 2\rho A_p V_p (V_p - V_a) \\ &= 2\rho A_p V_i (V_i + V_a) \end{aligned} \tag{4.4}$$

The increment of velocity added to the freestream velocity is called the induced velocity, V_i, such that $V_i = V_p - V_a$.

4.2.1 Accounting for Changes in Angular Momentum

The classical momentum model in its original form, as developed by Rankine (1865) assumed that the actuator disc would only accelerate fluid in the axial

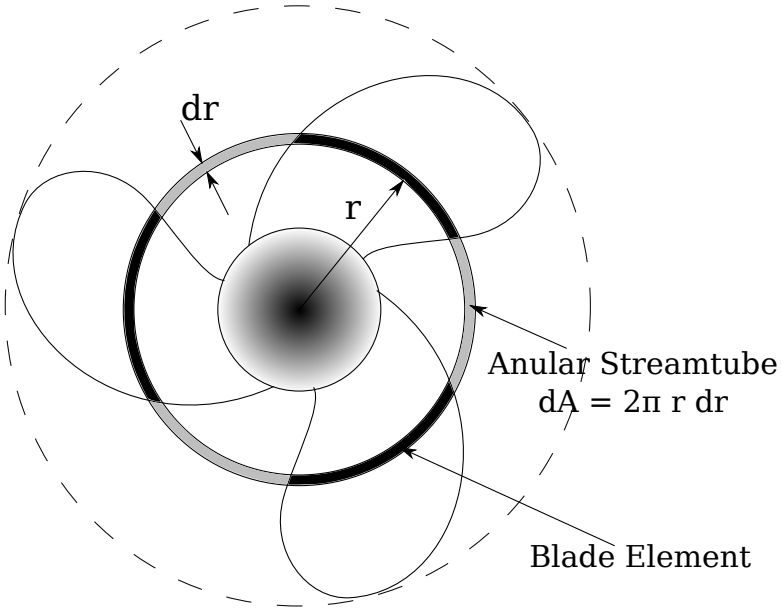

Figure 4.3: Concept of the Annular Streamtube

direction i.e. the slipstream's rotation was neglected. This assumption was addressed by Froude (1889) who applied an 'angular momentum' theory to the propeller action, analogous to Rankine's 'axial momentum' theory. This allows the propeller to impart a rotational velocity to the slipstream, and an overall more realistic model. This addition to the axial momentum theory is sometimes referred to as the *general* momentum theory.

The model assumes that the axial and angular velocities are uniformly distributed over the disc. Following the fashion of the classical axial momentum theory, the angular velocity of the flow is assumed to be zero far upstream of the disc and equal to ω at the disc.

The angular velocity at the disc, ω, can be written for a radius, r, in terms of the tangential induced velocity as $\omega = V_{\theta i}(r)/r$, where $V_{\theta i}$ is the tangential component of induced velocity.

Figure 4.3 represents the control volume of an annular streamtube. The torque on each element of the disc's annulus at radius r is equal to the angular change in momentum per unit time of the entire annular streamtube.

$$\begin{aligned} dQ &= \dot{m}\,(2\omega)\,r^2 \\ &= \dot{m}\left(2\frac{V_{\theta i}}{r}\right)r^2 \end{aligned}$$

Where the mass flux, $\dot{m}$, through the disc annulus at radius r is defined as:

$$\dot{m} = 2\pi dr\rho\left(V_a + V_{ai}\right)$$

Thus the elementary torque on each element in the disc annulus is:

$$\frac{dQ}{dr} = 4\pi\rho r^2 V_{\theta i}\left(V_a + V_{ai}\right) \tag{4.5}$$

Where V_{ai} and $V_{\theta i}$ are the axial and tangential components of the induced velocity, respectively, at the disc at radius r. The total propeller torque is the integration of each elemental differential torque in each annulus over the radius of the disc.

4.2.2 Glauert's Thrust Hypothesis

In 1897 H.S. Maxim observed that an airscrew when moved perpendicular to its axis of rotation experiences an increased thrust for a given power output. Glauert (1928) investigated the thrust behaviour of an helicopter rotor for all possible flight conditions (hover, vertical and horizontal flight). He developed an hypothesis relating the thrust of the rotor blade to the inflow velocity vector.

Glauert drew an analogy between an helicopter rotor in high-speed horizontal flight (with the rotor's axis perpendicular to direction of flight), and an elliptically loaded wing. He then used vortex theory to apply a lifting line to the elliptically loaded wing with the result that the induced velocity (or downwash as it is sometimes referred to) is related to the lift by:

$$L = \rho V_a \pi \left(\frac{b}{2}\right)^2 2V_i \tag{4.6}$$

Where b is the wing span, V_a is the advance velocity.

Glauert applied equation 4.6 to the lift of an helicopter rotor in high speed horizontal flight, with the hypothesis that the induced velocity at the rotor is related by:

$$T = \rho V \pi R^2 2V_i = 2\rho A V_i V \tag{4.7}$$

Where the velocity V is the resulting inflow velocity vector arriving at the disc (i.e. $V = V_a + V_i$). Glauert went on to assert that for the general case of a rotor at an arbitrary angle δ to the free-stream velocity, as shown in fig. 4.4, the total

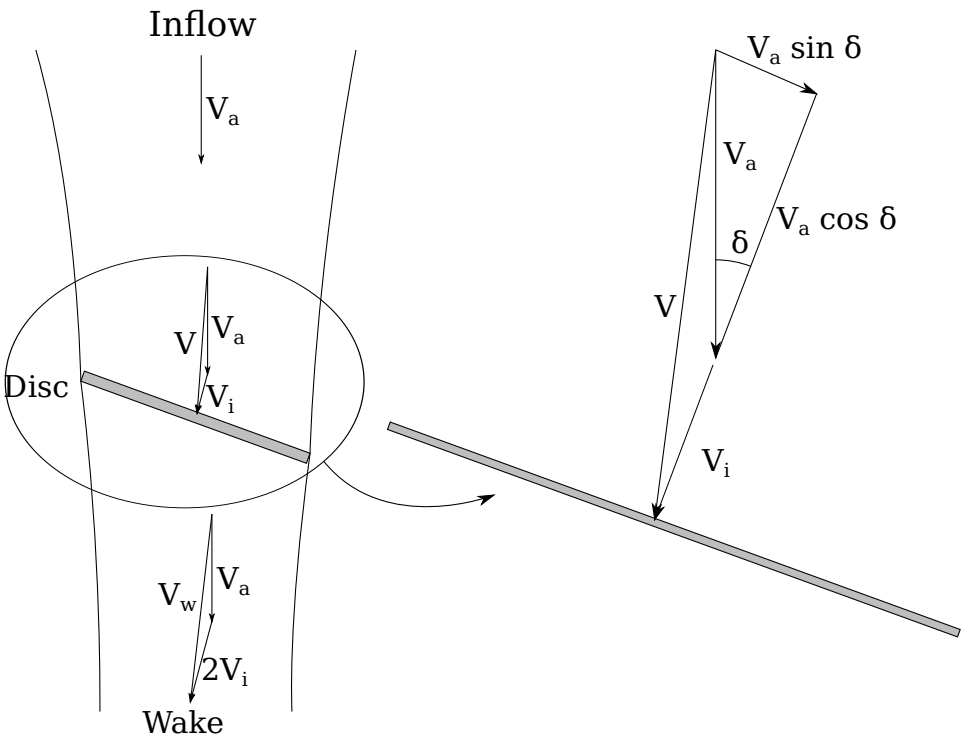

Figure 4.4: Glauert's concept of an helicopter rotor in oblique flow.

vector sum of the velocity at the disc would be:

$$V = \sqrt{(V_a \cos\delta + V_i)^2 + (V_a \sin\delta)^2} \tag{4.8}$$

$$= \sqrt{V_a^2 + 2V_i V_a \cos\delta + V_i^2} \tag{4.9}$$

Although Glauert based his hypothesis on an helicopter in high speed forward flight, Stepniewski and Keys (1984) prove that, with the help of numerical methods, Glauert's results are valid for all cases, and are applicable for the current application of providing for the extra lift that Maxim observed for a propeller disc in oblique flow.

4.2.3 Momentum Theory Accounting for Finite Blade Number

Consideration of vortex theory requires the trailing vortices in the wake lie on a regular helical surface. The velocity system of the wake can be obtained if this regular vortex sheet is assumed to be a rigid membrane which moves aft with constant velocity. The fluid velocity at the interior part of the slipstream (the term slipstream is also referred to as the wake) mainly has axial and rotational components, which move with the vortex sheets. Near the exterior of the

slipstream, the fluid tends to flow around the edges of the vortex sheets, from the higher pressure to the lower pressure regions, imparting a radial velocity component to the slipstream. This process is referred to as "leakage" or "tip-loss".

The general momentum theory does not account for any velocity distribution as a function of radius, and therefore on its own does not model leakage. Prandtl, in his Appendix of Betz (1919) first developed an approximate method for estimating the effect of leakage of flow around the edges of the vortex sheets. This method can be thought of as a momentum reduction factor, and is applied directly to the general momentum equations.

Goldstein (1929) used vortex theory to analyse the flow induced by a system of helical surfaces of infinite length. He developed a method which accounts for the difference between the average inflow factors of an actuator disc and propeller with a finite number of blades. This averaging factor, K, is known as the Goldstein factor. The application of this averaging factor is used in a manner identical to Prandtl's momentum reduction factor. The approximation that the trailing vortices form regular helices is equivalent to neglecting the contraction of the slipstream (and thus is only valid for small values of the thrust coefficient, i.e. lightly and moderately loaded propellers).

A practical estimation for the Goldstein K factor is given by (Molland et al., 2011):

$$K = \begin{cases} \frac{2}{\pi} \arccos\left[\frac{\cosh(xF)}{\cosh(F)}\right] & \text{if } F \leq 85 \\ 1 & \text{if otherwise} \end{cases} \tag{4.10}$$

where $F = \frac{Z}{2x \tan\phi} - \frac{1}{2}$, Z is the number of blades, ϕ is the local section hydrodynamic pitch angle and x is the radius of the propeller at the annulus in question.

4.3 Blade-Element Theory

A drawback with the pure general momentum theory approach is that the propeller's geometry does not play any role in the calculations of the propeller's action. The blade-element theory, originally developed by Froude (1878) considers the force experienced by the blades of the propeller in their motion through the fluid. (And as such, this method does take into account the blade's geometry.) A

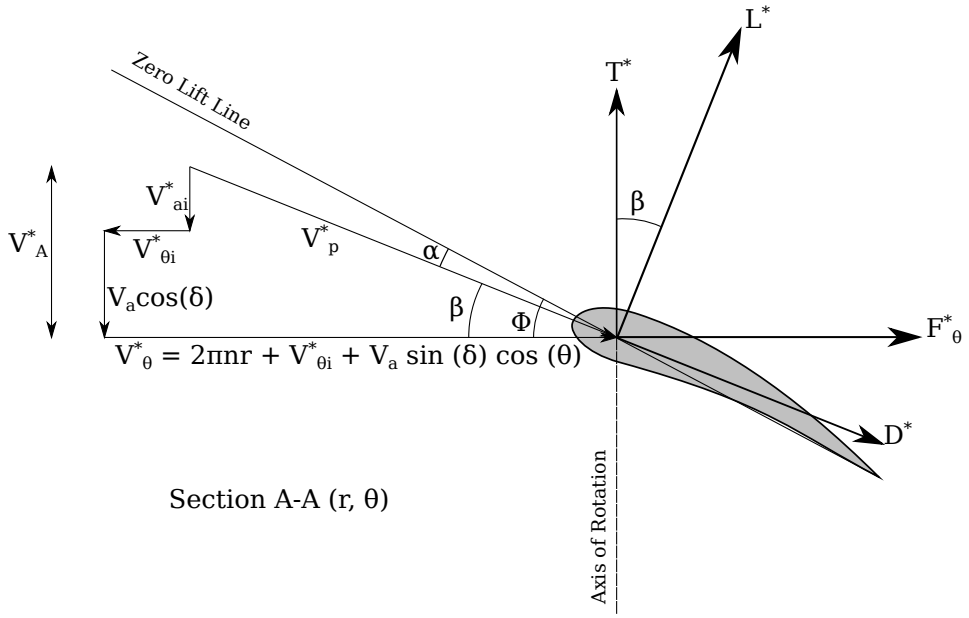

Figure 4.5: Oblique Flow into a Propeller

drawback with the blade-element theory approach is the uncertainty of the generation of the blade-element's lift and drag characteristics. This aspect is addressed in Section 4.5.

4.3.1 Blade-Element Theory Accounting for Wake-Skew Effects

The original blade-element method assumes that the induced axial and tangential velocities are constant around each annulus. When the propeller is at an inclined angle to the freestream, the resulting wake will also be inclined at some angle, defined here as the skew angle, χ, as depicted in fig. 4.7 . The original blade-element method ignores this aspect. A wake skew angle produces an asymmetry of induced velocities with respect to blade azimuthal angle, θ, around the annular ring. Coleman et al. (1945) applied the Biot-Savart law to a vortex wake represented by an elliptic cylindrical shell, with a continuous distribution of vortex "rings" representing the mean helical surfaces of the vortex wake, whose planes are parallel to the disc (fig. 4.7). The resulting expression for the induced velocity was a complex expression, yet found to be a very nearly linear distribution over the diameter of the disc. The linearised expression for the distribution of

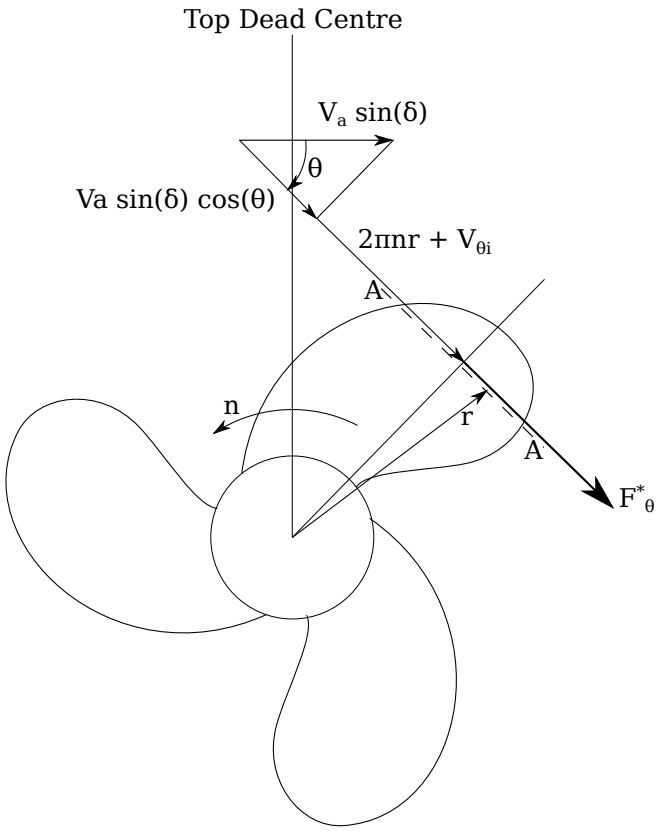

Figure 4.6: Oblique Flow Velocity Vectors at a Propeller Blade Element

induced velocity, V_i, over a helicopter rotor in forward flight is given by:

$$V_i = V_{i0}\left[1 + \frac{r}{R}\tan\left(\frac{\chi}{2}\right)\cos\psi\right] \tag{4.11}$$

Where V_{i0} is the mean induced velocity (i.e. at the center of the disc), r is the radial coordinate on the disc, ψ is the azimuthal angle measured from the downstream direction, and χ is the wake skew angle (in the downstream direction).

Coleman et al. (1945) went on to combine the Glauert thrust hypothesis (discussed in section 4.2.2) with their own results, to obtain an expression relating the mean induced velocity and the wake skew angle and advance velocity, viz.

$$\frac{V_{i0}}{V_a} = \frac{\cos\left(\chi + \alpha_D\right)}{2\tan\frac{\chi}{2}} \tag{4.12}$$

Where α_D is the angle of incidence the disc makes to the incoming flow, in terms of a ship's perspective, the drift angle at the propeller.

The mathematics and assumptions that Coleman et. al. base their results on are geometric and kinematic considerations of the helical vortex wake relative to the disc, and is shown to be applicable to the marine propeller in oblique flow by

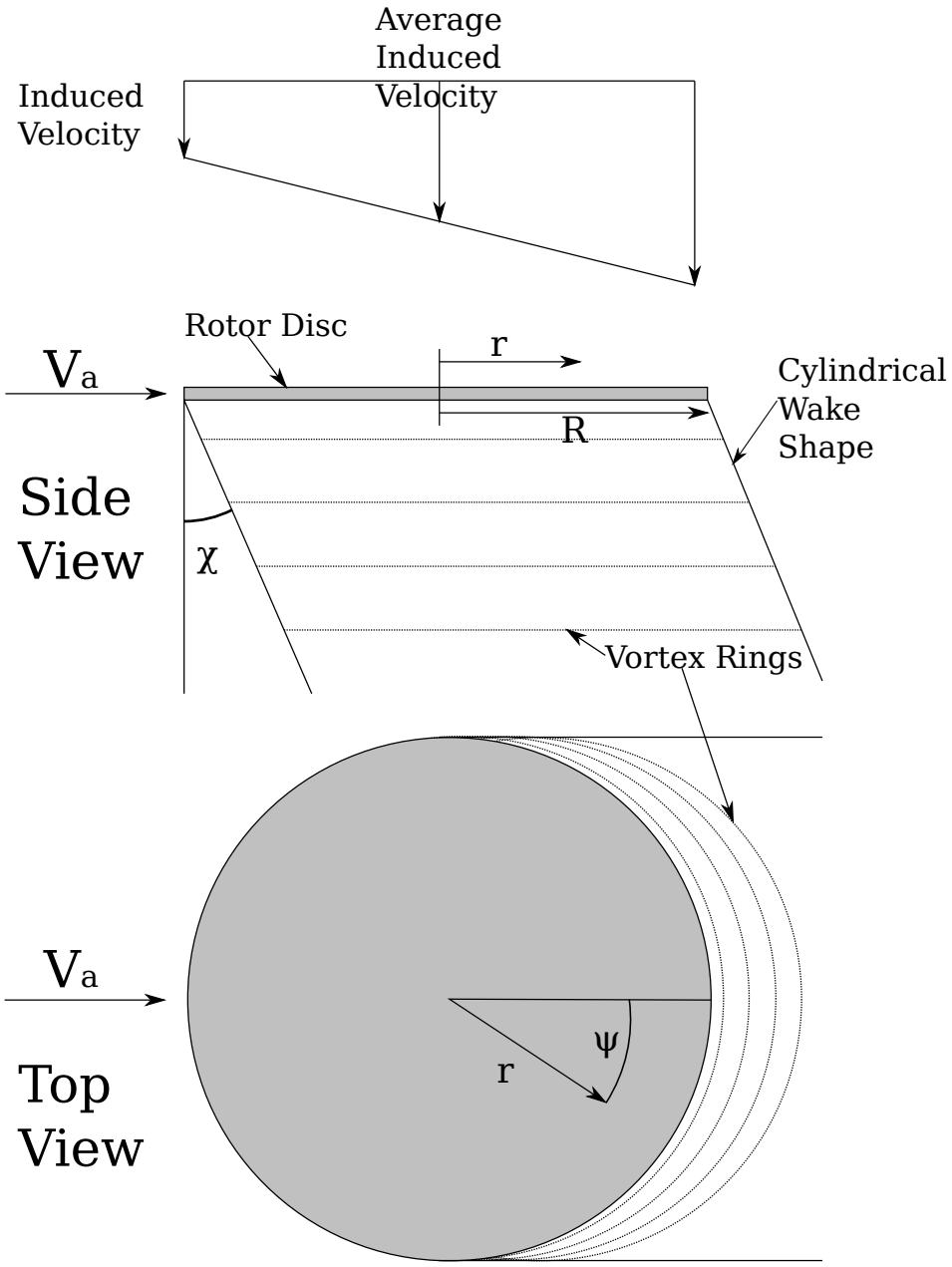

Figure 4.7: Wake Skew Angle

Stettler (2004). Stettler used fluorescent paint to visualise the helical wake of an azimuthing propeller in transient conditions. The radial distribution of axial induced velocity can be calculated from:

$$V_{Ai}\left(r,\theta\right) = V_{Ai0}\left[1 + \frac{r}{R}\tan\left(\frac{\chi}{2}\right)\sin\theta\right] \tag{4.13}$$

Where R is the radius of the propeller, and R_H is the radius of the propeller's hub. Referring to fig. 4.8, if the wake skew angle, χ is considered as a constant across the radius and for all azimuthal positions (equivalent to taking the average of the spatial variations of inflow and induced velocities, to attain a single spatially-averaged wake skew angle), it is possible to calculate the wake skew angle from:

$$\chi = \arctan\left(\frac{V_a\sin\delta + \bar{V}_{Ti}}{V_a\cos\delta + \bar{V}_{Ai}}\right) \tag{4.14}$$

Where $\bar{V}_{Ti}$ is the disc-averaged in-plane (or cross-flow) transverse induced velocity component, and $\bar{V}_{Ai}$ is the disc-averaged axial induced velocity component.

The spatially-averaged disc-averaged induced velocities can be calculated from:

$$\bar{V}_{Ti} = \frac{1}{\pi R^2 - R_H^2}\int_{R_H}^{R}\int_{0}^{2\pi} V_{\theta i}\left(r,\theta\right)\cos\theta\,\mathrm{d}\theta r\,\mathrm{d}r \tag{4.15}$$

$$\bar{V}_{Ai} = \frac{1}{\pi R^2 - R_H^2}\int_{R_H}^{R}\int_{0}^{2\pi} V_{Ai}\left(r,\theta\right)\,\mathrm{d}\theta r\,\mathrm{d}r \tag{4.16}$$

4.4 Combined Blade-Element Momentum Theory

A combination of the blade-element theory and the general momentum theory provides the basis to model the action of a propeller in this study, and can overcome some of the weaknesses that are inherent in each of the separate theories. At each blade section (element) along the radius, a force balance is applied from the two-dimensional lift and drag forces, with the thrust and torque. The result is then summed up over the circumference drawn out at that particular radius. Simultaneously, an axial and angular momentum balance is applied to the annular ring of the streamtube through which that particular blade section passes. By equating the thrust and torque determined from the blade element method

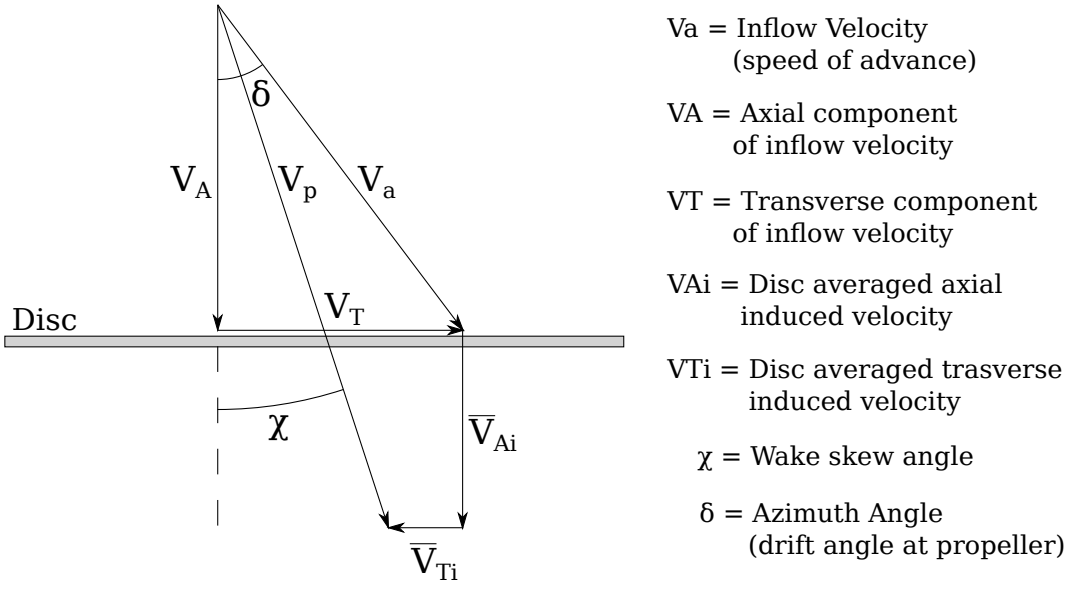

Figure 4.8: Velocity Vectors to Calculate Wake Skew Angle.

(multiplied by the number of blades on the propeller) to the thrust and torque required to balance the axial and angular momentum within the annular streamtube, a resulting pair of non-linear simultaneous differential equations are obtained for each differential annular ring along the propeller's radius. The induced velocities can be obtained from solving these equations, and the resulting thrust and torque of the propeller can then be calculated by integrating the elemental values over the propeller's radius.

As mentioned by citetStettler-2004, the application of the combined blade-element momentum theory assumes that the annular blade elements do not interact with one another, that is, the flow can be considered locally to be two-dimensional at that particular blade section. This has the effect of neglecting any radial induced velocities. As the induced velocities vary with the blade's position around the annular ring, neglecting radial induced velocities seems to invalidate the method's use for a propeller in oblique flow. If annular-averaged induced velocities are used however, the thrust and torque are calculated from spatial averaging around each annulus, so the average induced velocity values can be used, and the combined blade-element momentum theory can be applied.

The total local axial and tangential components of velocity at each blade

element, referring to figs. 4.5 and 4.6 can be written as:

$$V_a^* = (r,\theta) = V_a \cos\delta + V_{Ai}\,(r,\theta) \tag{4.17}$$

$$V_\theta^* = 2\pi nr + V_{\theta i}\,(r,\theta) + V_a \sin\delta\cos\theta \tag{4.18}$$

The angle of attack, α at each blade element location can be written

$$\alpha\,(r,\theta) = \phi\,(r,\theta) - \beta\,(r) \tag{4.19}$$

Where β is the hydrodynamic pitch angle (c.f. fig. 4.5), and ϕ is the inflow angle calculated by:

$$\phi\,(r,\theta) = \arctan\left(\frac{V_A^*\,(r,\theta)}{V_\theta^*\,(r,\theta)}\right) \tag{4.20}$$

The elementary thrust force and in-plane tangential force can be written in terms of the elementary lift and drag forces

$$L^*\,(r,\theta) = L^*\cos\phi - D^*\sin\phi \tag{4.21}$$

$$D^*\,(r,\theta) = L^*\sin\phi + D^*\cos\phi \tag{4.22}$$

Where the elementary lift and drag forces can be written

$$L^*\,(r,\theta) = \frac{1}{2}\rho V_p^{*2} c C_L \tag{4.23}$$

$$D^*\,(r,\theta) = \frac{1}{2}\rho V_p^{*2} c C_D \tag{4.24}$$

Where c is the chord length, C_L and C_D are the sectional lift and drag coefficients, respectively. V_p^* is the total velocity vector across the blade element.

Equation 4.25, based upon linear lifting theory for a thin foil with a camber (Hoerner and Borst, 1985) can be used as a first approximation to section lift coefficient.

$$C_L = k_1\left[2\pi\alpha + 4\pi\left(\frac{\delta_F}{C_M}\right)_{\max}\right] \tag{4.25}$$

Where α is the effective angle of attack on the blade and $\left(\frac{\delta_F}{C_M}\right)_{\max}$ is the maximum camber ratio of the blade section: δ_F is the maximum camber of the section, and C_M is the chord length. k_1 is an empirical coefficient used to calibrate the model with the polynomials developed by Oosterveld and van Oossanen (1975).

Equation 4.26 is an approximation for the drag coefficient of a thin blade

section, and is a combination of parasitic and lift-induced drag (Hoerner, 1965).

$$C_D = k_2 \left(0.008\right) + 0.06 C_L^2 \tag{4.26}$$

Where k_2 is an empirical coefficient used to calibrate the model with the polynomials developed by Oosterveld and van Oossanen (1975). Section 4.9 describes how the coefficients k_1 and k_2 are obtained.

Equations 4.25 and 4.26 are useful for achieving a fast, quasi-static solution to the $BEMT$.

The differential thrust, torque, normal force and steering moment (about axis perpendicular to shaft) for each annular ring at the propeller disc (radius) are calculated by integrating the blade elemental thrust force and tangential force over the annulus given in equations 4.27, 4.28, 4.29 and 4.30, respectively.

$$\tilde{T}\left(r\right) = Z \frac{1}{2\pi} \int_0^{2\pi} T^*\left(r, \theta\right) \mathrm{d}\theta \tag{4.27}$$

$$\tilde{Q}\left(r\right) = Z \frac{1}{2\pi} \int_0^{2\pi} F_\theta^*\left(r, \theta\right) r \mathrm{d}\theta \tag{4.28}$$

$$\tilde{N}\left(r\right) = Z \frac{1}{2\pi} \int_0^{2\pi} F_\theta^*\left(r, \theta\right) \cos\theta \mathrm{d}\theta \tag{4.29}$$

$$\tilde{M}\left(r\right) = Z \frac{1}{2\pi} \int_0^{2\pi} -T^*\left(r, \theta\right) r \sin\theta \mathrm{d}\theta \tag{4.30}$$

As discussed previously, the differential thrust and torque of each annular ring at the propeller disc, as calculated from blade-element theory, must be equal to the differential thrust and torque of the corresponding annular streamtube as calculated from general momentum theory. Using the equations 4.7 and 4.8 proposed from Glauert's Thrust Hypothesis, the thrust for each annular streamtube can be written as:

$$\tilde{T} = 4\rho\pi r \bar{V}_{Ai}\left(r\right) \sqrt{\bar{V_A}^2\left(r\right) + 2\bar{V}_{Ai}\left(r\right)\bar{V}_A\left(r\right) + \bar{V}_{Ai}^2\left(r\right)} \tag{4.31}$$

The torque for each annular streamtube can be written from equation 4.5 in the form:

$$\tilde{Q} = 4\rho\pi r^2 \bar{V}_{\theta i}\left(r\right) \sqrt{\bar{V_A}^2\left(r\right) + 2\bar{V}_{Ai}\left(r\right)\bar{V}_A\left(r\right) + \bar{V}_{Ai}^2\left(r\right)} \tag{4.32}$$

Where $\bar{V}_{Ai}(r)$ and $\bar{V}_{\theta i}(r)$ are annulus-averaged values of the induced axial and tangential velocities respectively at the disc.

$$\bar{V}_{Ai}(r) = \frac{1}{2\pi}\int_0^{2\pi} V_{Ai}(r,\theta)\,\mathrm{d}\theta \tag{4.33}$$

$$\bar{V}_{\theta i}(r) = \frac{1}{2\pi}\int_0^{2\pi} V_{\theta i}(r,\theta)\,\mathrm{d}\theta \tag{4.34}$$

By equating the thrust and torque from equations 4.27 and 4.28 with equations 4.31 and 4.32, the annulus-averaged axial and tangential induced velocities can be calculated. Once the calculations for the induced velocities have converged to a solution (c.f. Section 4.8 for a calculation scheme), the total propeller's thrust, torque, normal force and steering moment can be calculated by integration of the annulus values over the propeller disc, viz.

$$T = \int_{R_H}^{R} \bar{T}(r)\,\mathrm{d}r \tag{4.35}$$

$$Q = \int_{R_H}^{R} \bar{Q}(r)\,\mathrm{d}r \tag{4.36}$$

$$N = \int_{R_H}^{R} \bar{N}(r)\,\mathrm{d}r \tag{4.37}$$

$$M = \int_{R_H}^{R} \bar{M}(r)\,\mathrm{d}r \tag{4.38}$$

4.5 Lift and Drag

The requirement for calculating the coefficient of lift, C_L, and drag, C_D, with sufficient accuracy is of paramount importance to the results obtained from the Blade Element Method.

Figure. 4.9 shows an example output from the developed model, showing the inflow angle distribution on blade sections from root to tip, when the ship has zero drift angle. Manœuvering conditions change the ship's wake at the propeller plane. For comparison, fig 4.10 shows the inflow angle distribution on blade sections from root to tip, when the ship has a steady drift angle of 8.89°. Large spatial variations can be seen in fig. 4.10 which, as can be seen from figs. 4.11, 4.12, and summarised

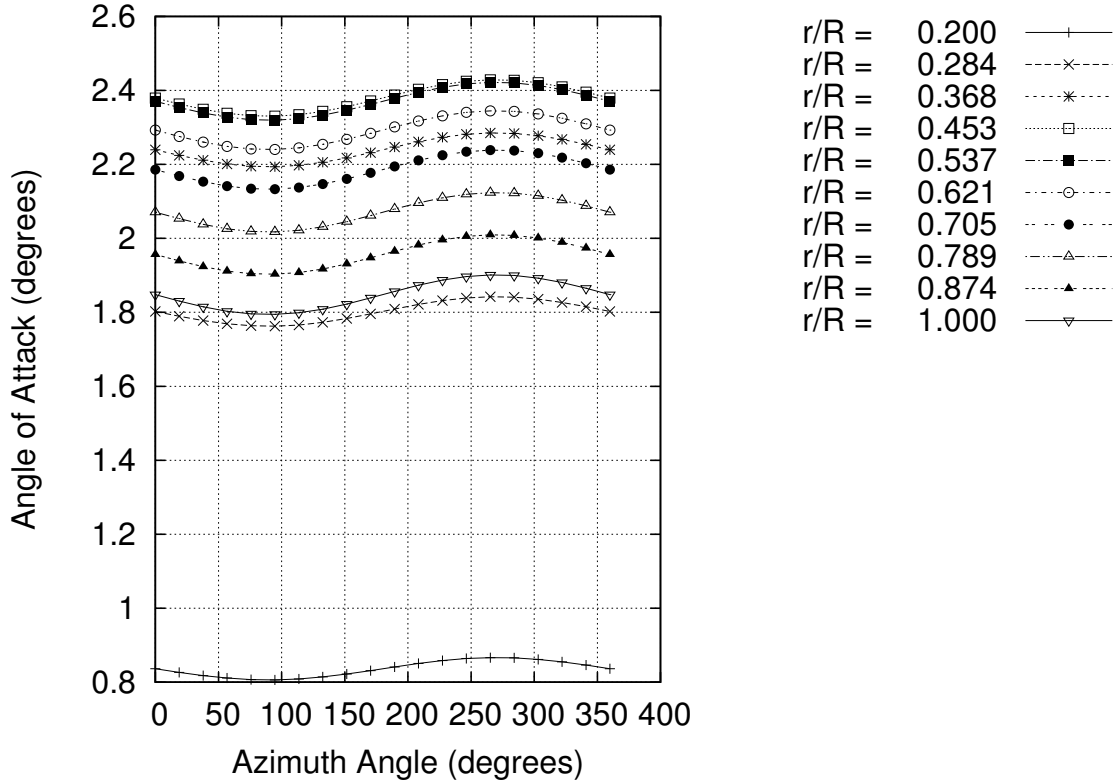

Figure 4.9: Angle of attack vs azimuth (position "around the clock") angle at a drift angle of 0.00°

in fig. 4.13 increase with increasing drift angle. Quantitatively this indicates that with a rapid variation in inflow angle across the blade section, the unsteady effects on the propeller's forces will not be small. Incidentally, it is interesting to note that the small variation in angle of attack with azimuth angle when the ship has zero drift angle, as depicted in fig. 4.9, is due to the variation in inflow caused by the tangential component of induced velocity.

The following section explains the construction of an unsteady sectional lift and drag model for input to the blade-element module. In order to ensure that the calculations are computationally fast, semi-empirical methods are used to model the dynamics of the model.

4.5.1 Effects of Unsteady Inflow Velocity on Lift and Drag

Figure 4.15 has been plotted from the methodology described in this Chapter and is typical of a propeller's lift and drag characteristics. The values of the sectional lift and drag are dependant on η, which is a function of Reynolds number, section profile and thickness and camber distributions. The value of η can be used to

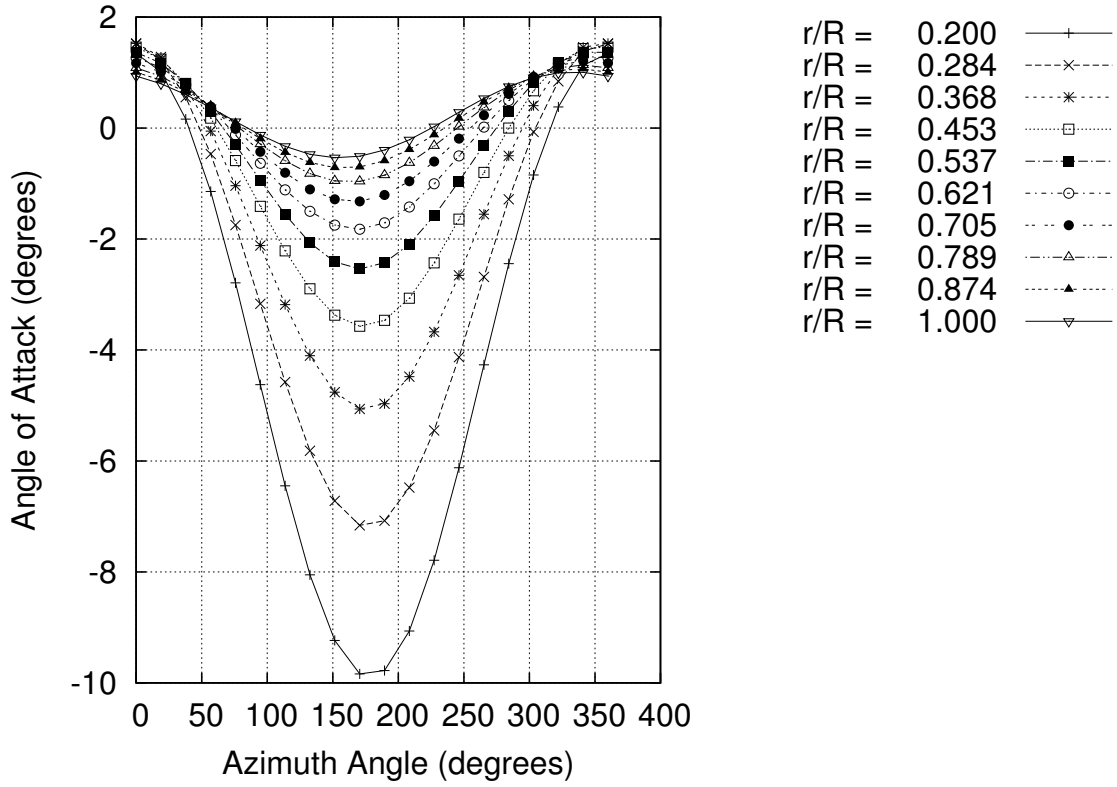

Figure 4.10: Angle of attack vs azimuth angle at a drift angle of 8.89°

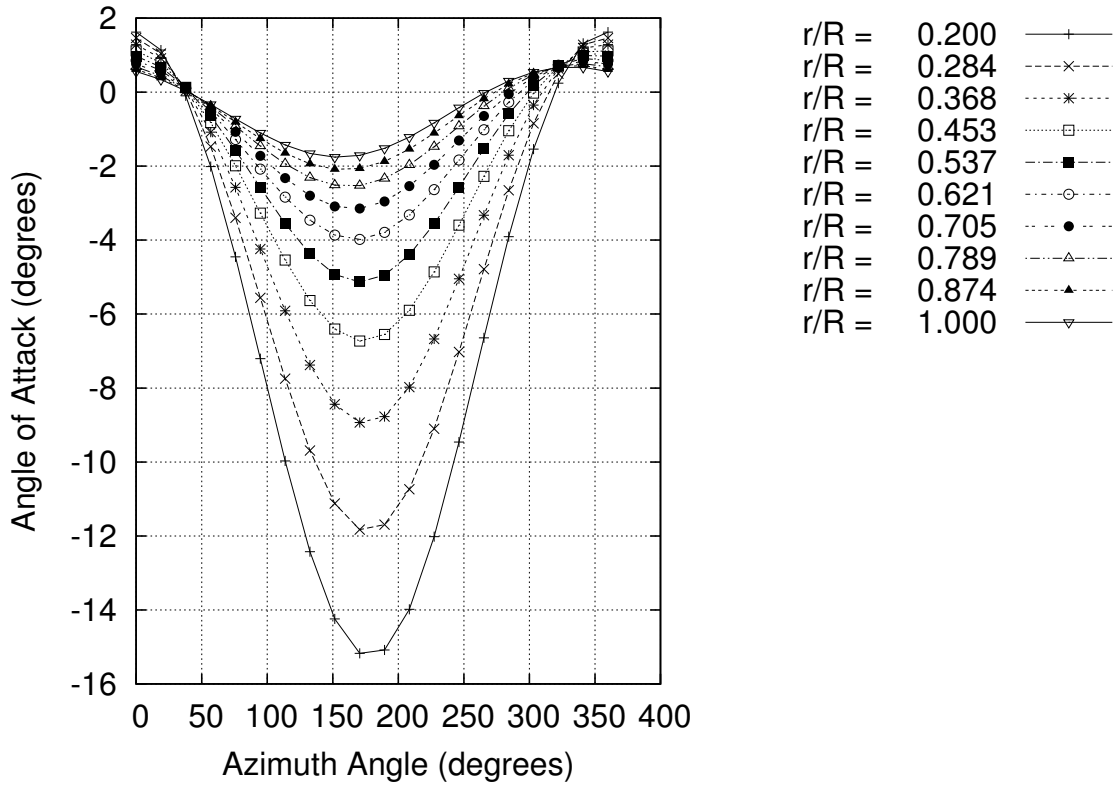

Figure 4.11: Angle of attack vs azimuth angle at a drift angle of 13.33°

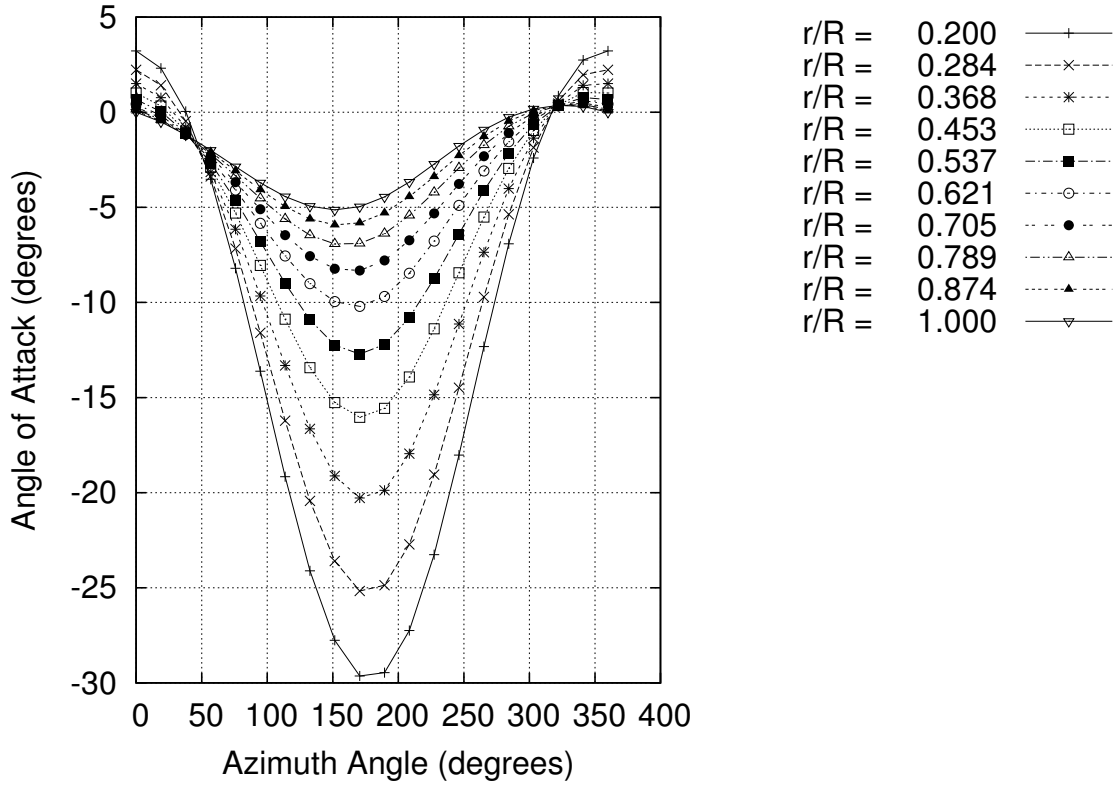

Figure 4.12: Angle of attack vs azimuth angle at a drift angle of 26.67°

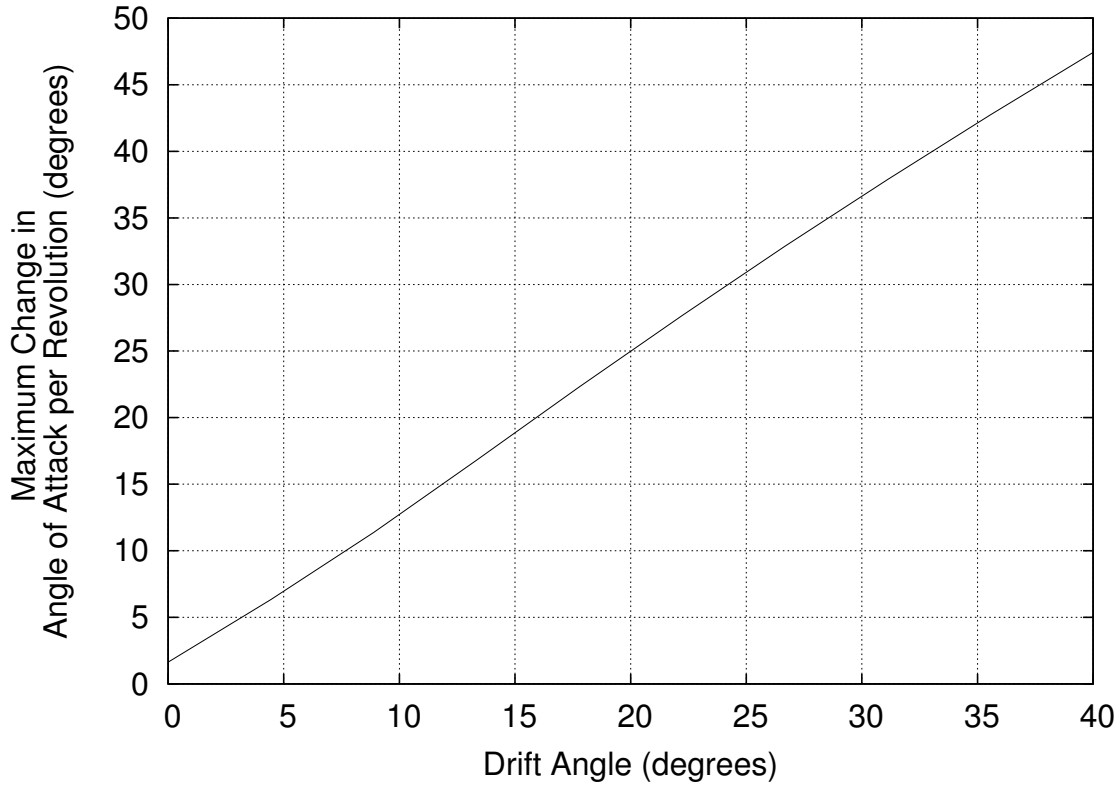

Figure 4.13: Maximum change in Angle of Attack vs. drift angle

account for, to some extent, three dimensional, viscous flow phenomena, as discussed in the following Sections. Referring to fig. 4.15, at low angles of attack, that is between the hydrofoil angles at points 1 and 4, the flow is fully attached. The lift is seen to increase linearly with the hydrofoil's angle. Further increase in foil angle results in a sharp drop in lift. The foil at this point 4 is said to be in static stall, the angle of which is denoted as α_{ss}. Between points 4 and 5 the boundary layer at the foil's surface begins to experience flow separation. This transitional region between fully attached and fully separated flow is complex and unstable. For the foil angle between points 5 and 6, the flow on the upper surface is fully separated. The lift is seen to increase almost linearly with hydrofoil angle, but with a smaller value for the lift slope compared to the fully attached case.

Shen and Fuhs (1997) developed a semi-empirical method for predicting the dynamic flow effects on a propeller blade section's lift and drag coefficients. The approach taken by Shen and Fuhs (1997) was to derive expressions for various sections of curves depicted in graphs such as 4.14 and 4.15. They compared their results to the experimental ramp-up, ramp-down tests of Francis and Keesee (1985) and Ham and Garelick (1968).

To characterise this unsteady motion, a non-dimensional pitch rate, R is defined:

$$R = \dot{\alpha}\frac{c}{2V_p^*} \tag{4.39}$$

Where $\dot{\alpha}$ is the instantaneous foil angle's time derivative. The pitch rate defines the degree of unsteadiness of a problem.

Figure 4.17 shows the change in lift coefficient for different angles of attack over a range of pitch rate (as output from `lift_drag.f90`). From this plot it can be seen that:

- The stall angle increases with increasing reduced frequency.
- The lift coefficient increases with increasing reduced frequency.
- The slope of the lift curve is independent of reduced frequency.

These results correspond to experimental work done by Ericsson and Reding (1972).

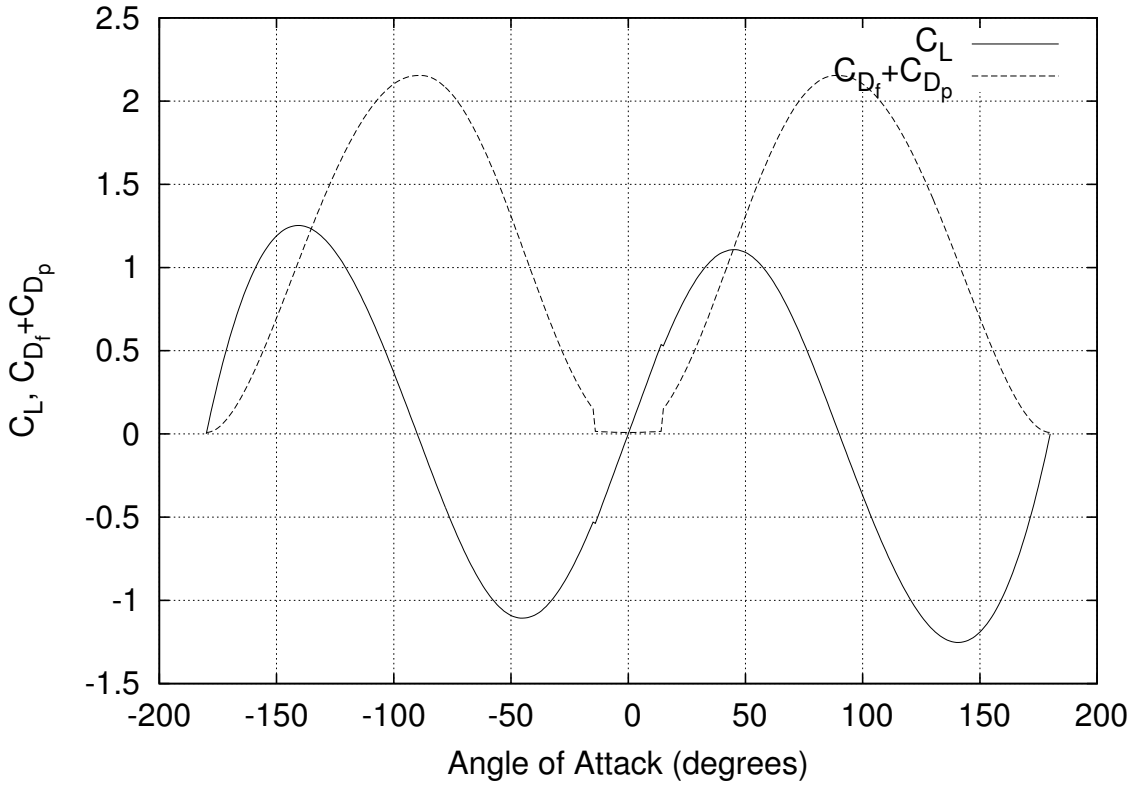

Figure 4.14: Lift and drag coefficients vs. angle of attack for symmetrical foil, when $\eta = 0.35$

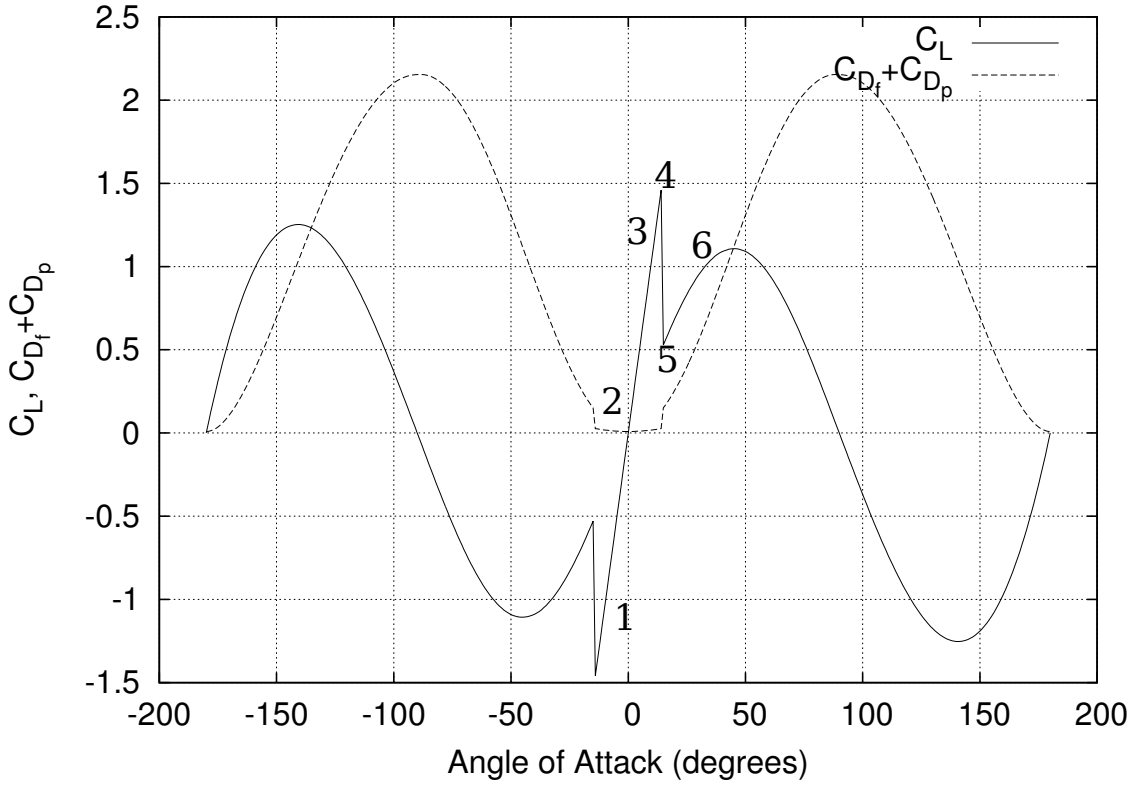

Figure 4.15: Lift and drag coefficients vs. angle of attack for symmetrical foil, when $\eta = 0.95$

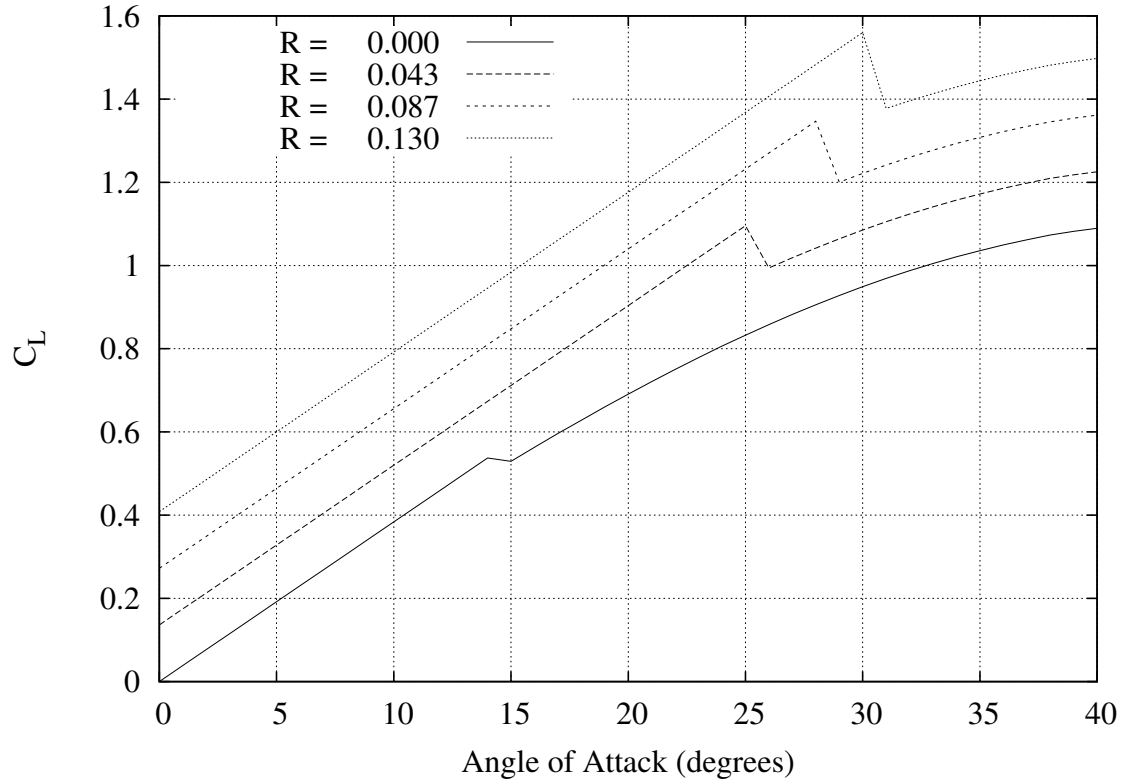

Figure 4.16: Lift coefficient vs. angle of attack over various non-dimensionalised pitch rate, when $\eta = 0.35$

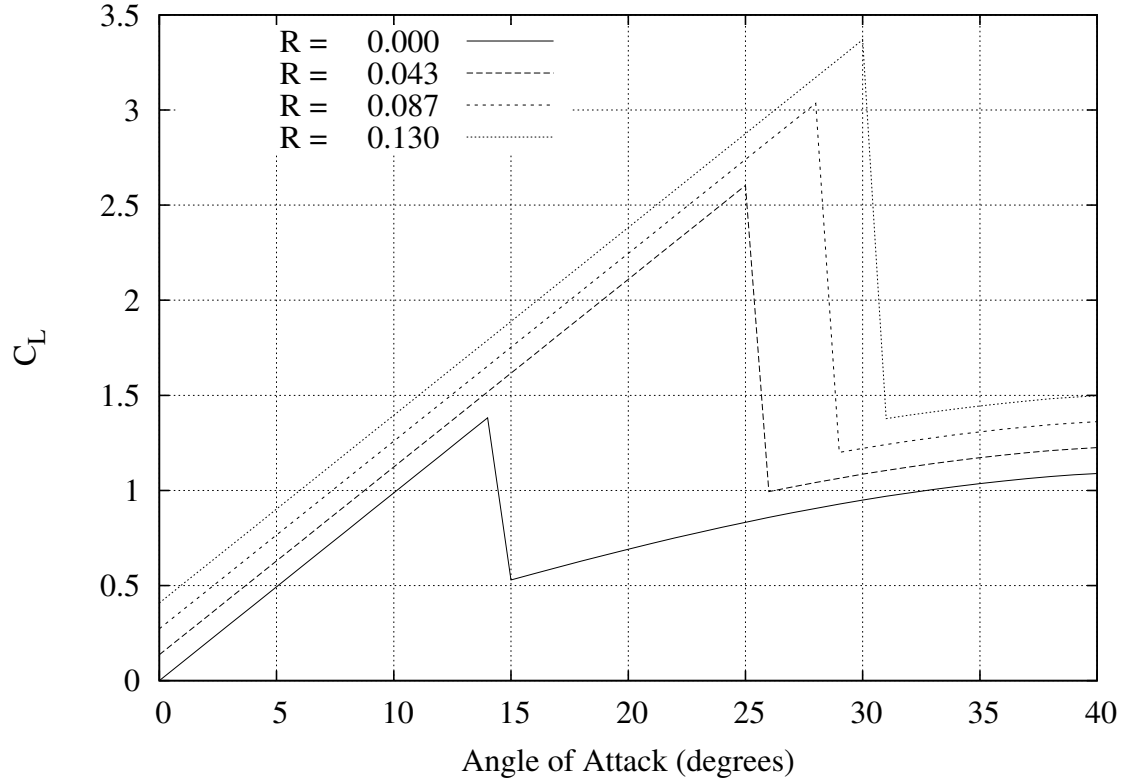

Figure 4.17: Lift coefficient vs. angle of attack over various non-dimensionalised pitch rate, when $\eta = 0.95$

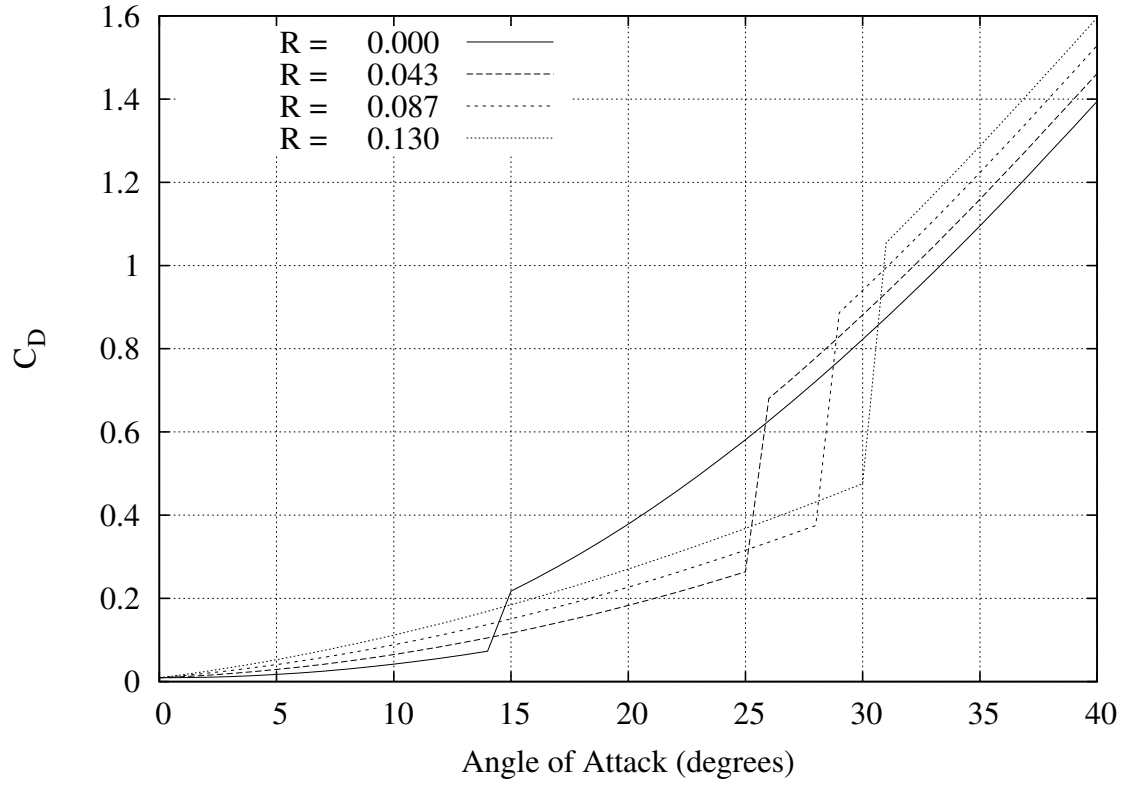

Figure 4.18: Drag coefficient vs. angle of attack over various non-dimensionalised pitch rate, when $\eta = 0.35$

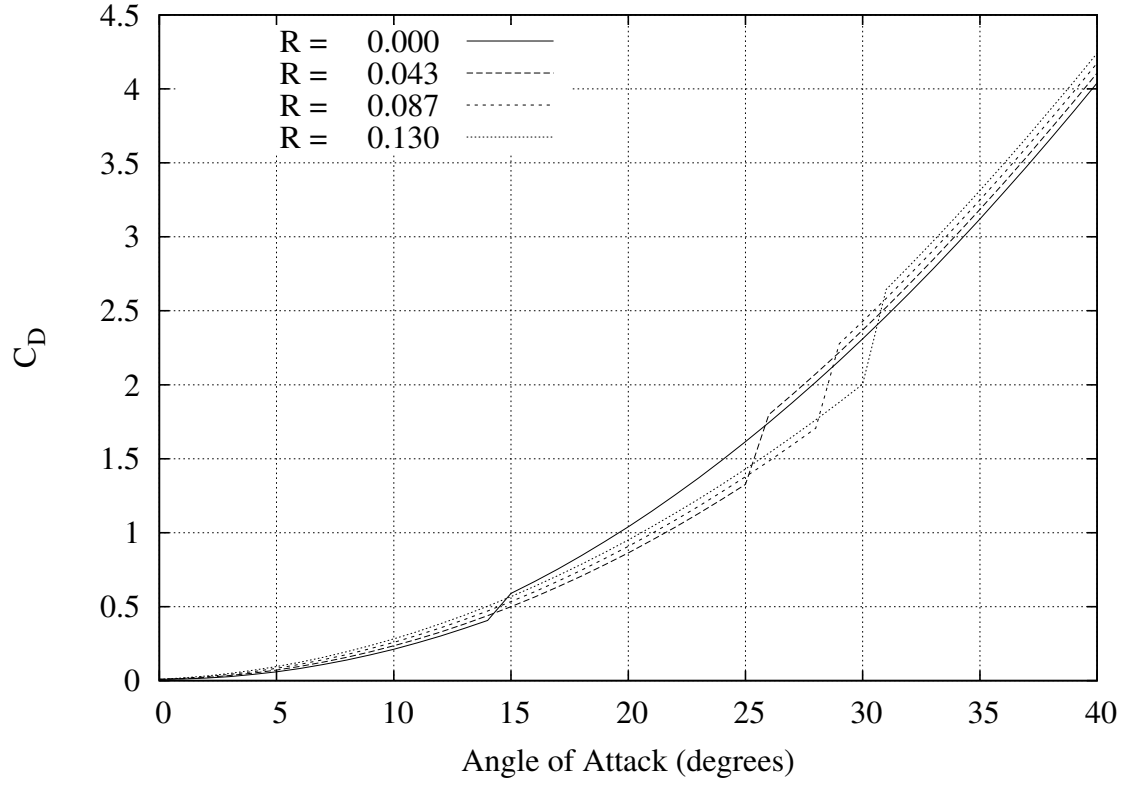

Figure 4.19: Drag coefficient vs. angle of attack over various non-dimensionalised pitch rate, when $\eta = 0.95$

The unsteady effects on the lift and drag coefficients can be seen to be substantial, whether the flow is fully attached or fully separated. A plot of lift coefficient vs angle of attack over different pitch rates is given in fig. 4.16 for relatively lower values of η (η is mainly dependent on aspect ratio). For flow in the fully attached regime, the typical example of fig. 4.17, the unsteady (dynamic) lift coefficient at a non-dimensional pitch rate of 0.043 is about 20% higher than the static lift coefficient. Again, the lift coefficient for a foil in unsteady flow is seen to be significantly higher than the static lift coefficient. Figures 4.18 and 4.19 show the differences in drag coefficients for steady and unsteady flow.

The variation in the non-dimensionalised pitch rate can be seen for different ship's drift angles in figs. 4.20, 4.21, 4.22 and 4.23. Figure 4.24 shows a plot of the maximum values of pitch rate encountered, vs drift angle.

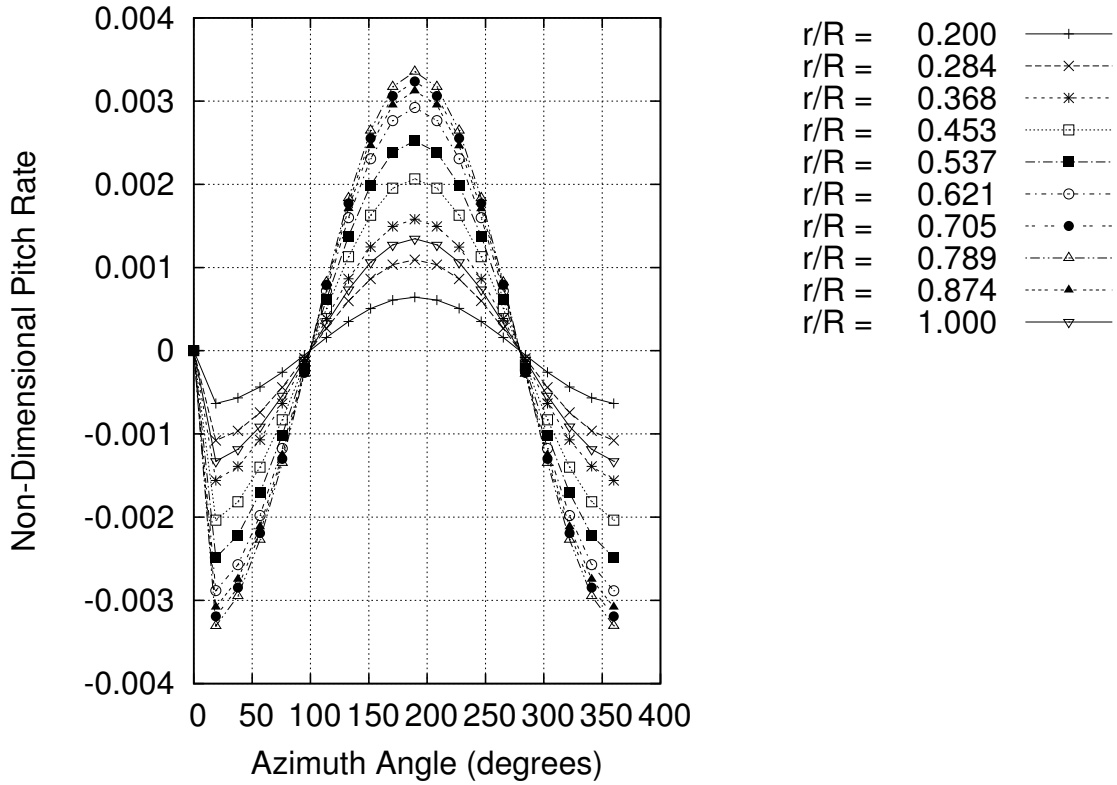

Figure 4.20: Non-dimensionalised Pitch Rate vs azimuth angle at a drift angle of 0.00°

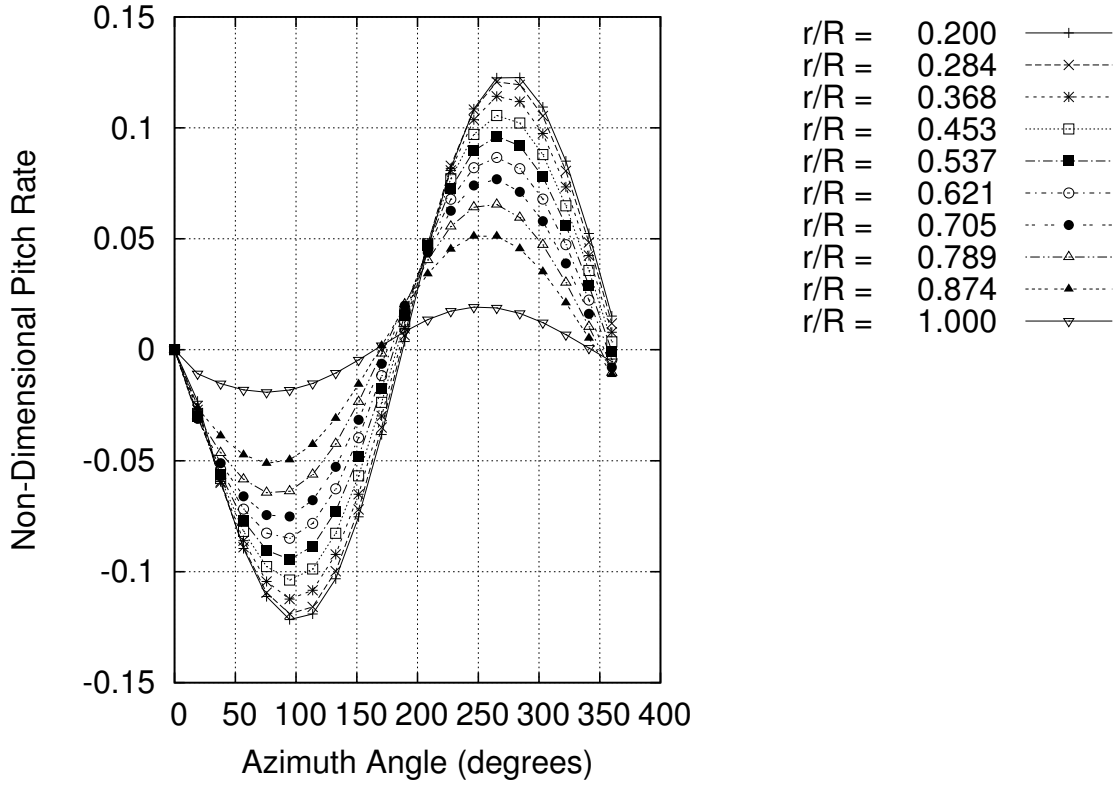

Figure 4.21: Non-dimensionalised Pitch Rate vs azimuth angle at a drift angle of 8.89°

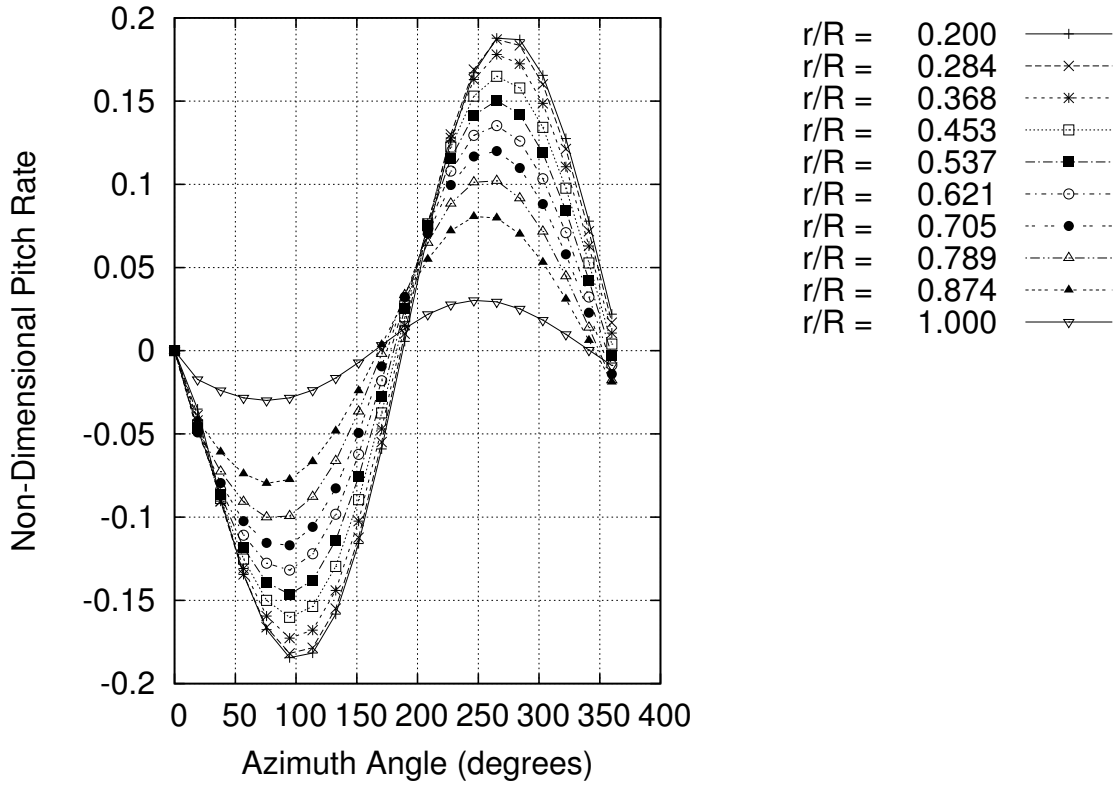

Figure 4.22: Non-dimensionalised Pitch Rate vs azimuth angle at a drift angle of 13.33°

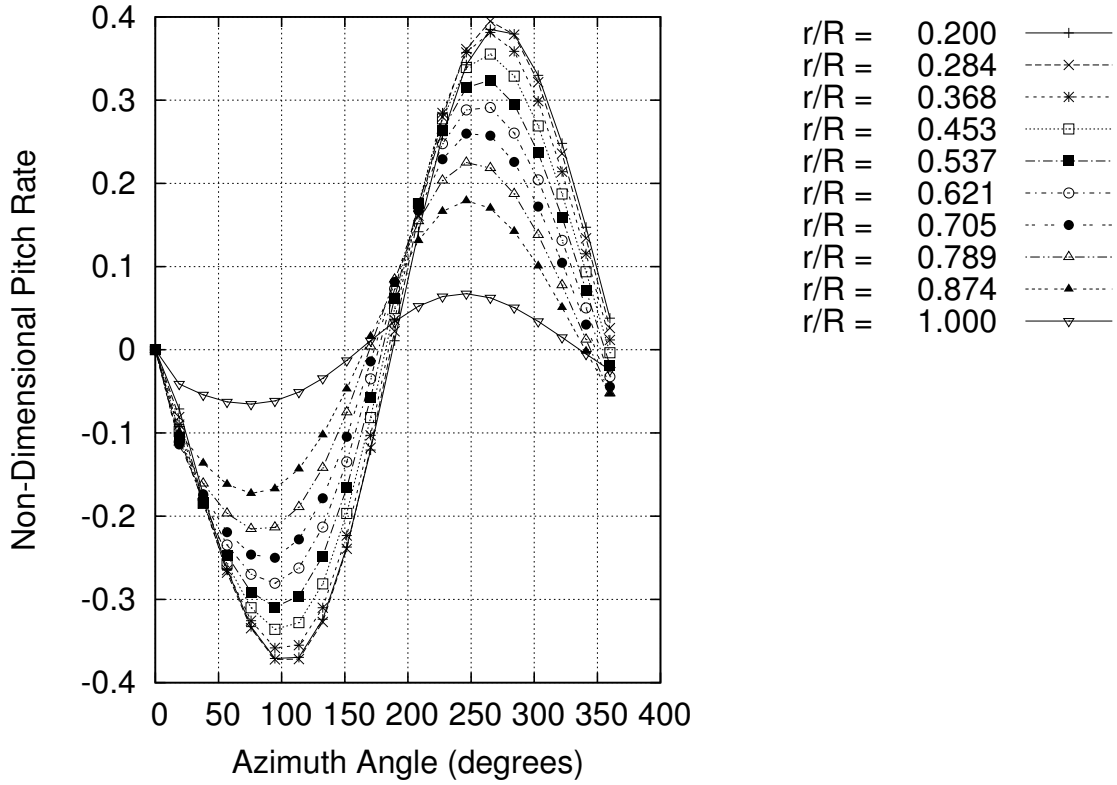

Figure 4.23: Non-dimensionalised Pitch Rate vs azimuth angle at a drift angle of 26.67°

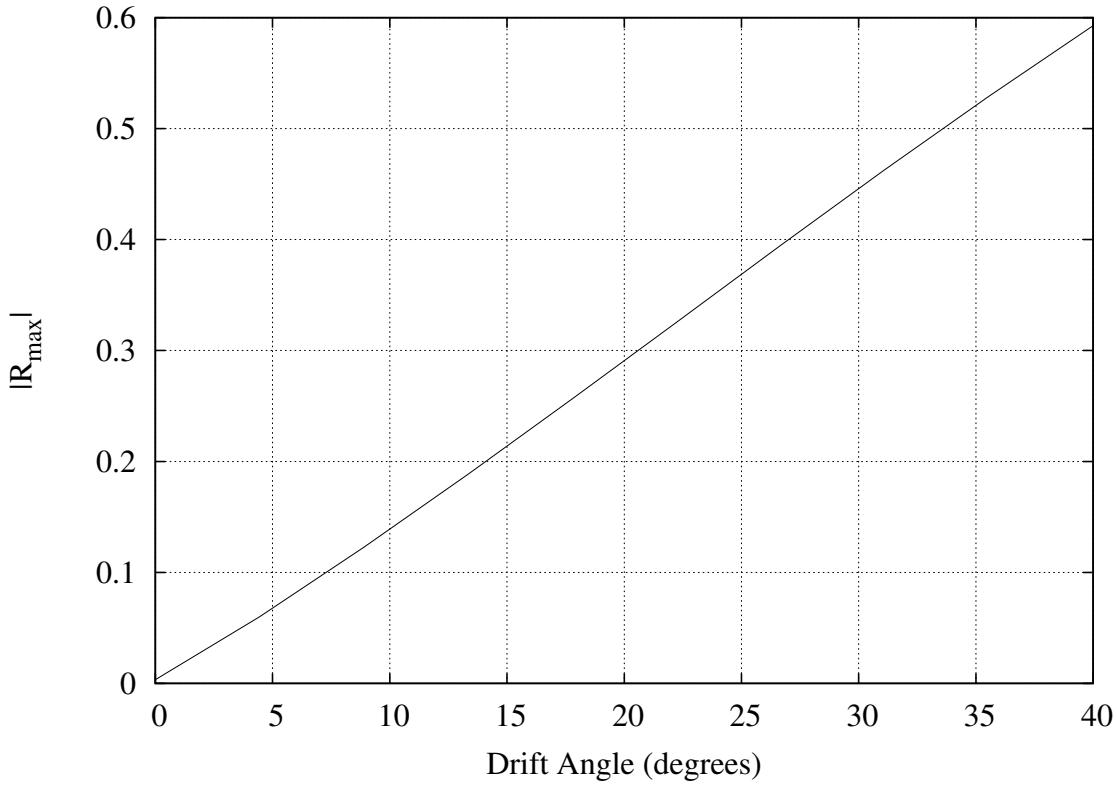

Figure 4.24: Absolute maximum value of non-dimensional pitch rate vs. drift angle

4.5.2 Static Lift

Fully Attached Flow

The static lift is related to the foil angle by:

$$C_L = \left(\frac{\partial C_L}{\partial \alpha}\right)\alpha \qquad \text{for } \alpha < \alpha_{ss} \tag{4.40}$$

Where α_{ss} is the angle at which static stall occurs, α represents the *effective* angle of attack. In the case of a cambered foil, $\alpha = \alpha_G + \alpha_{C_L=0}$, where α_G is the geometric angle of attack, and $\alpha_{CL=0}$ is the angle of zero lift. For a symmetric foil, the zero lift angle is zero. The zero lift angle can be obtained from experiment (a good source of experimental data is Abbott and Von Doenhoff (1959)), or Reynolds Averaged Navier Stokes (RANS) code. The method used in this analysis to estimate $\alpha_{C_L=0}$ is detailed later in this Section.

For a two-dimensional foil, the static lift slope can be written as:

$$\frac{\partial C_L}{\partial \alpha} = 2\pi\eta \qquad \text{for } \alpha < \alpha_{ss} \tag{4.41}$$

The value of η depends upon Reynolds number, section profile and thickness and camber distributions. It can be determined from experiments, or RANS computations. In the case of this study, η is calibrated to match existing data from the Wageningen B-Screw Series (c.f. section 4.9). The value of η can be used to account for, to some extent, three dimensional and viscous flow phenomena, as discussed in the following Sections.

Fully Separated Flow

From the model that Shen and Fuhs (1997) developed for fully separated flow, the lift coefficient can be approximated by:

$$C_L = \frac{2\pi \sin\alpha}{4 + \pi \sin\alpha}\left[1 + \sigma + \frac{\sigma^2}{8\left(\pi + 4\right)}\right]\cos\alpha \tag{4.42}$$

Where σ is the non-dimensional pressure coefficient inside the separated flow (cavity). This is also sometimes referred to as the cavitation number, and is given by:

$$\sigma = \frac{P_0 - P_v}{0.5\rho\left(V_p^*\right)^2} \tag{4.43}$$

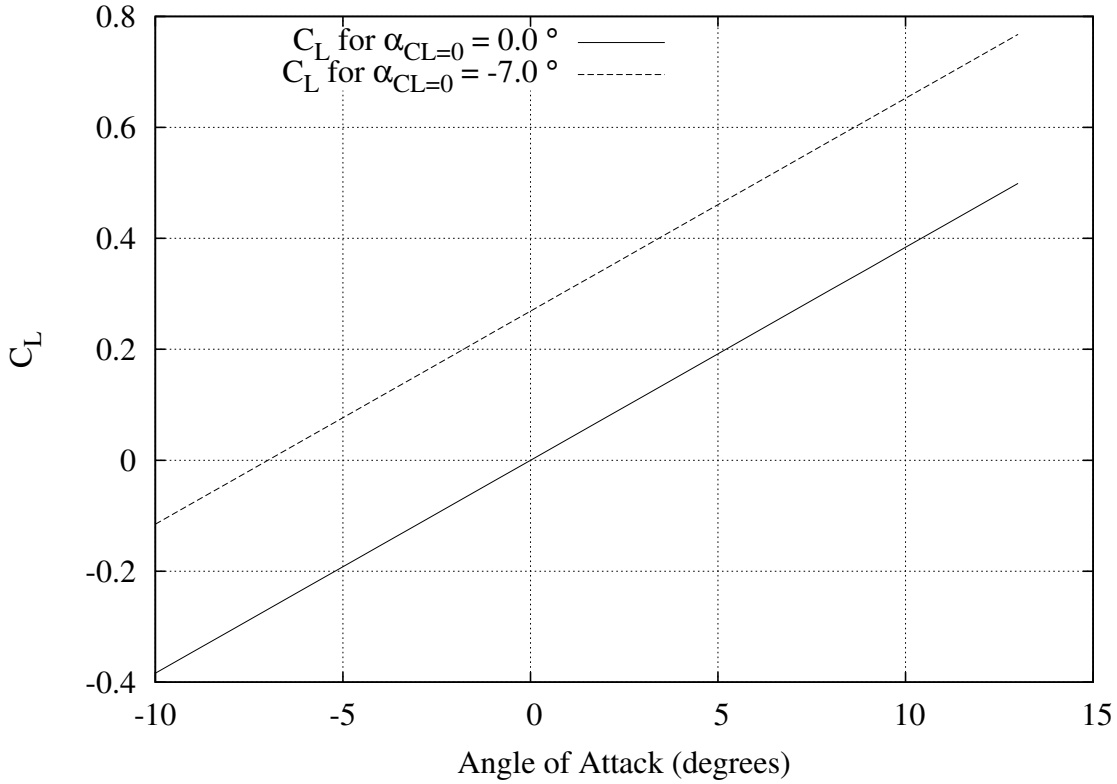

Figure 4.25: Effect of camber on lift coefficient.

Where P_0 is the reference pressure, taken to be the static pressure at the shaft centreline, and P_v is the vapour pressure of the fluid.

4.5.3 Static Drag

The static sectional drag coefficient, C_D can be expressed as the sum of the static friction coefficient, C_{DF}, static pressure drag, C_{DP} and lift induced drag, C_{DI}.

$$C_D = C_{DF} + C_{DP} + C_{DI} \tag{4.44}$$

At low angles of attack, the frictional drag dominates. At high angles of attack the pressure drag dominates.

Friction Drag

If the foil is asymmetrical, i.e. it has a camber, then the foil's lift slope becomes displaced, as shown in fig. 4.25. As can be seen in the example, positive lift is still produced, even at a negative angle of attack. Camber therefore offsets the angle at which stall will occur (Abbott and Von Doenhoff, 1959).

Most marine propellers have varying camber/chord ratios distributed over their

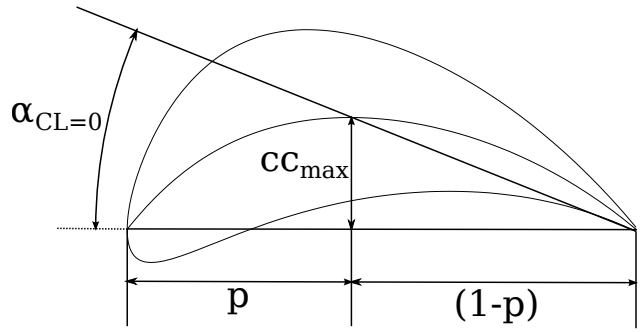

Figure 4.26: Method to estimate zero lift angle.

radii. To account for the camber, the angle at which the blade section produces zero lift must be calculated. Referring to fig. 4.26, the zero-lift angle, $\alpha_{C_L=0}$, can be estimated as follows (Jones, 1988):

$$\alpha_{C_L=0} = -\arctan\left(\frac{cc_{\max}}{1-p}\right) \tag{4.45}$$

Where $cc_{\max}$ is the camber from nose-tail line, and p the camber-line high point.

$$C_L = \frac{\partial C_L}{\partial \alpha}\left(\alpha - \alpha_{C_L=0}\right) \tag{4.46}$$

The thickness of the blade section has an effect on the frictional resistance (as local velocities on the surface may be higher than the freestream, thus increasing shearing stress), and is accounted for from the following relationship of Hoerner (1965):

$$C_{DF} = 2 \times C_f\left(1 + 2\frac{t}{c}\right) \tag{4.47}$$

Where t is the thickness of the section, and c is the chord.

The coefficient of friction is obtained from the formula of Hughes (1954) viz.

$$C_f = 0.067 \log\left(R_n - 2\right)^{-2} \tag{4.48}$$

Where R_n is the Reynolds Number.

Induced Drag

For a two-dimensional section, that is, when the width of the blade section tends towards zero, the aspect ratio tends to infinity, which would indicate that the

induced drag tends towards zero. It has been found that the induced drag on the blade is certainly not negligible, and needs to be accounted for in some way.

$$C_{DI} = \frac{C_L^2}{\pi e \Lambda} = \kappa \times C_L^2 \tag{4.49}$$

Where e is the Oswald planform efficiency factor. This is a correction factor that represents the difference in drag with lift of a three-dimensional wing compared to a two-dimensional one. Λ is the aspect ratio.

The value of κ is used to calibrate the model with the basis Wageningen B-Screw Series. c.f. Section 4.9

Pressure Drag in Fully Attached Flow

The pressure drag in terms of a suction recovery factor, ξ can be expressed from Leishman and Beddoes (1989):

$$C_{DP} = \frac{1}{2} C_L \left(1 - \xi\right) \sin 2\alpha \tag{4.50}$$

ξ represents the failure of the hydrofoil to achieve the leading edge suction it would achieve in potential flow. Good agreement between the above theory and measurements is achieved when $\xi = 0.96, 0.97, 0.974$ for Reynolds numbers of $R_n = 3.0, 6.0, 9.0 \times 10^6$ respectively.

Pressure Drag in Fully Separated Flow

In the model developed by Shen and Fuhs (1997), the foil's pressure drag in separated flow is predicted well from:

$$C_{DP} = \frac{2\pi \sin \alpha}{4 + \pi \sin \alpha} \left[1 + \sigma + \frac{\sigma^2}{8\left(\pi + 4\right)}\right] \sin \alpha \tag{4.51}$$

4.5.4 Dynamic Lift

$$C_{LC} = \frac{\partial C_L}{\partial \alpha} \alpha_E \left(s\right) \tag{4.52}$$

Where

$$\alpha_E \left(s\right) = \alpha \left(0\right) \phi \left(s\right) + \int \frac{\mathrm{d}\alpha}{\mathrm{d}u} \phi \left(s - u\right) \mathrm{d}u \tag{4.53}$$

Where $\phi\left(s\right)$ is the Wagner function, and s denotes a non-dimensional time parameter, given by: $s = 2V_p^* t/c$.

Leishman and Beddoes (1989) presents the following numerical approximation for Duhamel's integral for the effective angle of attack.

$$\alpha_E(s) = \alpha(0)\,\phi(s) + \sum_{n=1}^{m} \Delta\alpha_n - X_n - Y_n \tag{4.54}$$

Where

$$X_0 = 0 \quad \text{and} \quad X_n = X_{n-1}\exp(-b_1\Delta s) + A_1\Delta\alpha_n \tag{4.55a}$$

$$Y_0 = 0 \quad \text{and} \quad Y_n = Y_{n-1}\exp(-b_2\Delta s) + A_2\Delta\alpha_n \tag{4.55b}$$

Where Δs is the distance travelled by the foil in semi-chords over a sample interval Δt and $\Delta\alpha_n$ is the corresponding change in angle of attack over that time interval. Beddoes (1976) provides the constantsA_1, A_2, b_1 and b_2 to be 0.165, 0.335. 0.0455 and 0.3 respectively. The Wagner function, $\phi(s)$ can be approximated with sufficient accuracy from Bisplinghoff et al. (1996)

$$\phi(s) = \frac{s+2}{s+4} \tag{4.56}$$

Where

$$s = \frac{2V_p^* t}{c} = \frac{2V_p^* \psi\omega}{c} \qquad \text{for } 0 \le \psi \le 2\pi \tag{4.57}$$

McLaughlin (1992) compiled an extensive data set of lift slopes for several airfoil sectional profiles. A functional relationship between static and dynamic lift slope can be expressed as:

$$\left(\frac{\partial C_L}{\partial\alpha}\right)_{\text{dynamic}} = 0.94\left(\frac{\partial C_L}{\partial\alpha}\right)_{\text{static}} \tag{4.58}$$

Fully Attached Flow

From the work of Shen and Fuhs (1999), the dynamic lift for fully attached flow is expressed as:

$$C_L = (C_L)_{\text{static}} - \left(\frac{\partial C_L}{\partial\alpha}\right)_{\text{dynamic}} \alpha_w(s) + \text{sign}(\alpha')\,\pi R \qquad \text{for } \alpha \le \alpha_{ss} \tag{4.59}$$

Where

$$\text{sign}(\dot{\alpha}) = \begin{cases} 1 & \text{if } \dot{\alpha} \text{ is positive} \\ -1 & \text{if } \dot{\alpha} \text{ is negative} \end{cases} \tag{4.60}$$

Where $\alpha_w = \alpha - \alpha_E$ and accounts for the time history effects of the change in α

Transitional Flow

From the work of Shen and Fuhs (1999), the dynamic lift in transitional flow is given by:

$$C_L = (C_L)_{ss} + \left(\frac{\partial C_L}{\partial \alpha}\right)_{\text{static}} (\alpha - \alpha_{ss}) - \left(\frac{\partial C_L}{\partial \alpha}\right)_{\text{dynamic}} \alpha_w(s) + \text{sign}(\alpha')\,\pi R \quad \text{for } \alpha_{ss} < \alpha \leq \alpha_{DM} \tag{4.61}$$

Fully Separated Flow

From the work of Shen and Fuhs (1999), the dynamic lift in fully separated flow is expressed as:

$$C_L = \frac{2\pi \sin\alpha}{4 + \pi \sin\alpha}\left[1 + \sigma + \frac{\sigma^2}{8(\pi + 4)}\right]\cos\alpha + \text{sign}(\alpha')\,\pi R \quad \text{for } \alpha > \alpha_{DM} \tag{4.62}$$

4.5.5 Dynamic Drag

Kottapalli and Pierce (1979) studied the effects of an oscillating airfoil in a fluctuating free stream. This data was further analysed by Leishman (1989) who show that fluctuations in unsteady viscous drag are small and negligible when compared with the pressure drag. It is assumed that friction drag is not frequency dependent.

$$(C_{DF})_{\text{dynamic}} = (C_{FD})_{\text{static}} \tag{4.63}$$

This assumption implies that the unsteady effect on the drag force comes from the pressure drag. The dynamic effect on pressure drag is calculated as follows.

Fully Attached Flow

$$C_D = C_{DF} + C_{DP} \tag{4.64}$$

$$= \left[C_{DF} + \frac{1}{2} C_L (1 - \xi)\sin(2\alpha)\right]_{\text{static}} + \text{sign}(\alpha')\,\pi R \cos\alpha \sin\alpha \qquad \text{for } \alpha \leq \alpha_{ss} \tag{4.65}$$

Transitional Flow

$$C_D = \left\{ C_{DF} + \frac{1}{2}\left[(C_L)_{ss} + \left(\frac{\partial C_L}{\partial \alpha} \right)_{\text{static}} (\alpha - \alpha_{ss}) \right] (1-\xi) \sin(2\alpha) \right\}_{\text{static}} + \text{sign}(\alpha')\, \pi R \cos\alpha \sin\alpha \qquad \text{for } \alpha_{ss} < \alpha \leq \alpha_{DM} \tag{4.66}$$

Fully Separated Flow

$$C_D = \frac{2\pi \sin\alpha}{4 + \pi \sin\alpha} \left[1 + \sigma + \frac{\sigma^2}{8(\pi+4)} \right] \sin\alpha + \text{sign}(\alpha')\, \pi R \cos\alpha \sin\alpha \qquad \text{for } \alpha > \alpha_{DM} \tag{4.67}$$

4.5.6 Effects of Aspect Ratio

Although the Blade Element Theory incorporates two-dimensional sections, the aspect ratio of the blade has an effect on the lift and drag characteristics that need to be accounted for. From Lifting line theory, the 3D-lift coefficient for an elliptically loaded foil is depicted in fig. 4.27 and can be estimated from:

$$C_L = C_{L_\alpha} \left(\frac{\Lambda}{2 + \Lambda} \right) \alpha \tag{4.68}$$

Where C_{L_α} is the two-dimensional lift coefficient slope, and the aspect ratio, Λ, is defined as:

$$\Lambda = \frac{b^2}{S} \tag{4.69}$$

Where b is the span of the foil, and S is the area of the foil planform. The aspect ratio is taken into account in this study using equation 4.70 where η is obtained from calibrations made with the steady model of Oosterveld and van Oossanen (1975) (referred to in this research as the *OOVOO* model), c.f. Section 4.9

$$\frac{\partial C_L}{\partial C_D} = 2\pi\eta \quad \alpha < \alpha_{ss} \tag{4.70}$$

4.6 Prediction of Stall Angles

The present model assumes that the static stall angle remains constant for all foil types. Most foils have a static stall angle of around 15° (Abbott and Von Doenhoff, 1959), and is the value used in the current analysis.

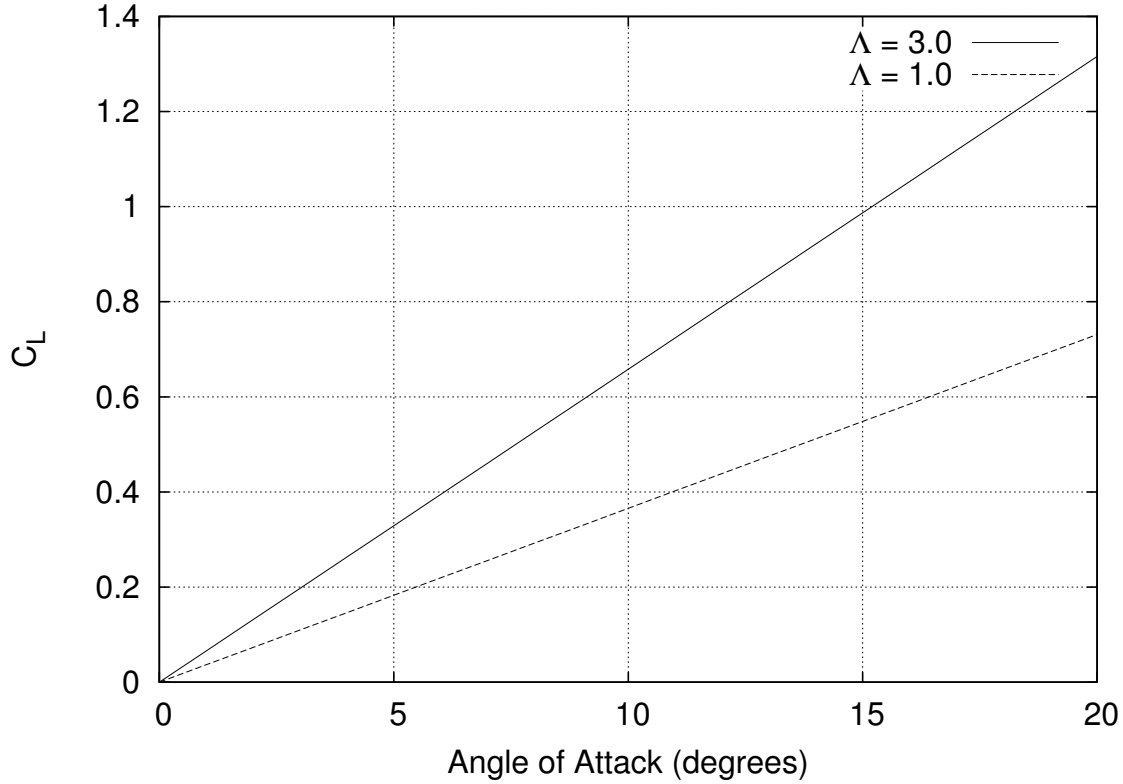

Figure 4.27: Effect of aspect ratio on lift coefficient.

Shen and Fuhs (1999) developed an empirical formula relating the dynamic moment stall angle, α_{DM} with reduced frequency from the work done on oscillating foil tests of McCroskey (1981), and the ramp-up tests of Francis and Keesee (1985) and Green and Galbraith (1994). viz.

$$\alpha_{DM} = \begin{cases} \alpha_{ss} + 340R & \text{if } R \leq 0.03 \\ \alpha_{ss} + 10.2 + 53.5\,(R - 0.03) & \text{if } R > 0.03 \end{cases} \tag{4.71}$$

The dynamic moment stall angle is the critical angle, above which the flow is considered to be fully separated.

4.7 The Variation in Inflow Velocity Due to the Ship's Wake

The shape of a ship's hull will greatly affect the wake field at the propeller plane, the wake field will therefore vary for different ships. Experiments are commonly performed to obtain the propeller-behind-hull wake field (the wake survey) so that the propeller's blade sections can be optimised for the velocity vectors at a particular radius. This process is known as wake adaptation. It is, however, extremely difficult to obtain experimental wake surveys for a ship at different drift

angles. This is due to the fact that conventional blade-section optimisation assumes that the ship has zero drift angle.

In this study, the wake field's *variation* in inflow velocity due to the ship's hull is neglected. To elaborate somewhat, the "shadow" that the underwater part of the ship's hull casts over the propeller is neglected. The effect that this shadow has is to modify the velocity vectors at a particular propeller radius. This variation in velocity at the propeller plane is the aspect which is currently neglected in this research. The disc-averaged wake that is modified due to the ship's drift angle is, of course taken into account (equation 3.20).

The reason for neglecting the modified wake velocity vectors from the ship's hull is due to the author being unable to obtain wake field data for ships sailing at angles of drift. Whilst neglecting the effect of the ship's wake will affect the accuracy of the results, it is not expected to change the outcome. Neglecting the modifications of a ship's wake due to her stern lines also has the effect of normalising the variation in wake-field of different hullforms, removing any bias that an extremely efficient hullform has over an inefficient one.

4.8 Calculation Scheme

Figure 4.28 shows the basic algorithm which is used to solve the $BEMT$. As with all of the other subprogrammes developed as part of this research, algorithms are coded in Fortran (2008 standard).

When including the non-linear effects of stall, combined with the non-linear nature of the system of differential equations of thrust and torque, obtaining a converging solution is a significant challenge. The HYBRD1 algorithm from the MINPACK (Moré et al., 1980) library was chosen to solve the system of non-linear equations, however, in certain circumstances, this can become unstable. The HYBRD1 algorithm is implemented at the point in the algorithm where the thrust and torque are balanced from the blade-element theory and momentum theory. The HYBRD1 algorithm is a minimisation routine which, in this case, chooses values for the induced velocities which minimise the difference between values of thrust and torque obtained from the blade-element theory to those of the momentum theory. Perhaps a more robust method to solve the thrust-torque balance equations is to use the recently published method of Ning (2013).

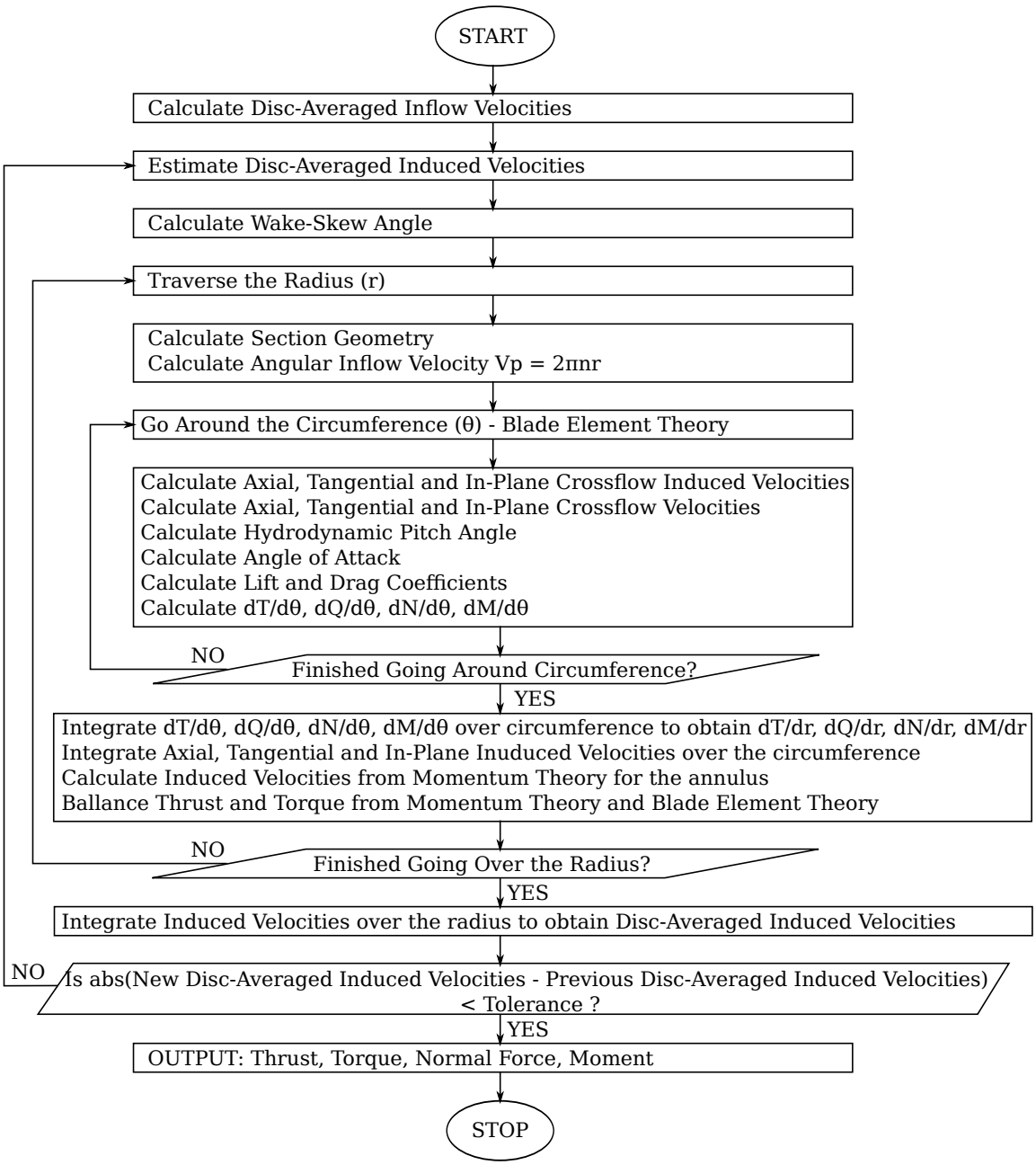

Figure 4.28: Blade-Element Momentum Theory Algorithm

Unfortunately, this paper was released too late for the author to utilise in the present work.

The Fortran module `mbemt.f90` is responsible for calculating the thrust and torque on the propeller using the modified $BEMT$. It uses several other modules, including `b_screw_geom.f90` which calculates the geometry of the propeller based on the Wageningen B-Screw series. This geometry is calculated from work by Oosterveld and van Oossanen (1975), and appropriate formulae for geometry calculations can be found in Appendix B.5.1. `lift_drag.f90` is also used as an external module to obtain sectional lift and drag coefficients. The module `gplot.f90` is used to plot various graphs, as in the ones included in this Chapter.

4.9 Calibration of Lift and Drag Coefficients.

The accurate calculation of the blade sectional lift and drag coefficients is imperative to the accuracy of the propeller model as a whole. Whilst the calculations for lift and drag coefficients presented in the previous sections are shown to behave as expected, and their values to be approximately correct, this is not considered to be good enough when comparing different propeller models. To illustrate this point; as will be shown in Chapter 6, a propeller design selected with the $OOVOO$ model is compared to one selected with the unsteady $MBEMT$ model. These two models obviously need to produce the same results (within tolerance) when analysing the same propeller under the same conditions. To achieve this matching, the $MBEMT$ models are calibrated to the results obtained from the $OOVOO$ model (The $OOVOO$ model is known to mimic the B-Screw series precisely)

Calibration for both the quasi-static and the unsteady propeller models described in this Chapter are carried out against the Wageningen B-Screw Series at zero drift angle (i.e. the propeller shaft is aligned with the incoming flow). The propeller blade geometry is obtained from the formula presented by Oosterveld and van Oossanen (1975), details of which can be found in B.5.1.

The geometry of the propeller affects the values of the calibration coefficients, the coefficients have therefore been calculated for the diameters of propeller found on the *Esso Osaka* and *KCS*, over a range of a_E and P/D. Calculation of the calibration coefficients over such a range is necessary as, from the results of the

simulation, an optimum basis propeller is selected from this range. c.f. Section 6.1.

4.9.1 Calibration of Quasi-Static $MBEMT$ Propeller Model

The lift and drag coefficients used in the quasi-static propeller model are shown in equations 4.25 and 4.26. Values for $k1$ and $k2$ were systematically adjusted so as to closely align with the results obtained from the $OOVOO$ model. The outcome of the calibration is shown in Table 4.1. It is noted that the drag calibration factor, $k2$ can be considered equal to 1.5 over the entire range of a_E and P/D.

	Esso Osaka		*KCS*	
a_E	$k1$	$k2$	$k1$	$k2$
$P/D = 0.6$				
0.3	0.35	1.5	0.3	1.5
0.6	0.51	1.5	0.6	1.5
0.9	0.80	1.5	0.9	1.5
1.2	1.10	1.5	1.2	1.5
1.5	1.10	1.5	1.5	1.5
$P/D = 0.8$				
0.3	0.35	1.5	0.35	1.5
0.6	0.50	1.5	0.45	1.5
0.9	0.65	1.5	0.50	1.5
1.2	0.65	1.5	0.55	1.5
1.5	0.70	1.5	0.55	1.5
$P/D = 1.0$				
0.3	0.30	1.5	0.30	1.5
0.6	0.50	1.5	0.45	1.5
0.9	0.60	1.5	0.50	1.5
1.2	0.65	1.5	0.50	1.5
1.5	0.65	1.5	0.45	1.5
$P/D = 1.2$				
0.3	0.30	1.5	0.30	1.5
0.6	0.50	1.5	0.45	1.5
0.9	0.60	1.5	0.50	1.5
1.2	0.65	1.5	0.50	1.5
1.5	0.65	1.5	0.50	1.5
$P/D = 1.4$				
0.3	0.40	1.5	0.40	1.5
0.6	0.50	1.5	0.45	1.5
0.9	0.60	1.5	0.50	1.5
1.2	0.60	1.5	0.50	1.5
1.5	0.50	1.5	0.40	1.5

Table 4.1: Parameters used in the calibration of the lift and drag coefficients for the quasi-static $MBEMT$ propeller model.

Calibration results for the quasi-static $MBEMT$ model can be seen for the

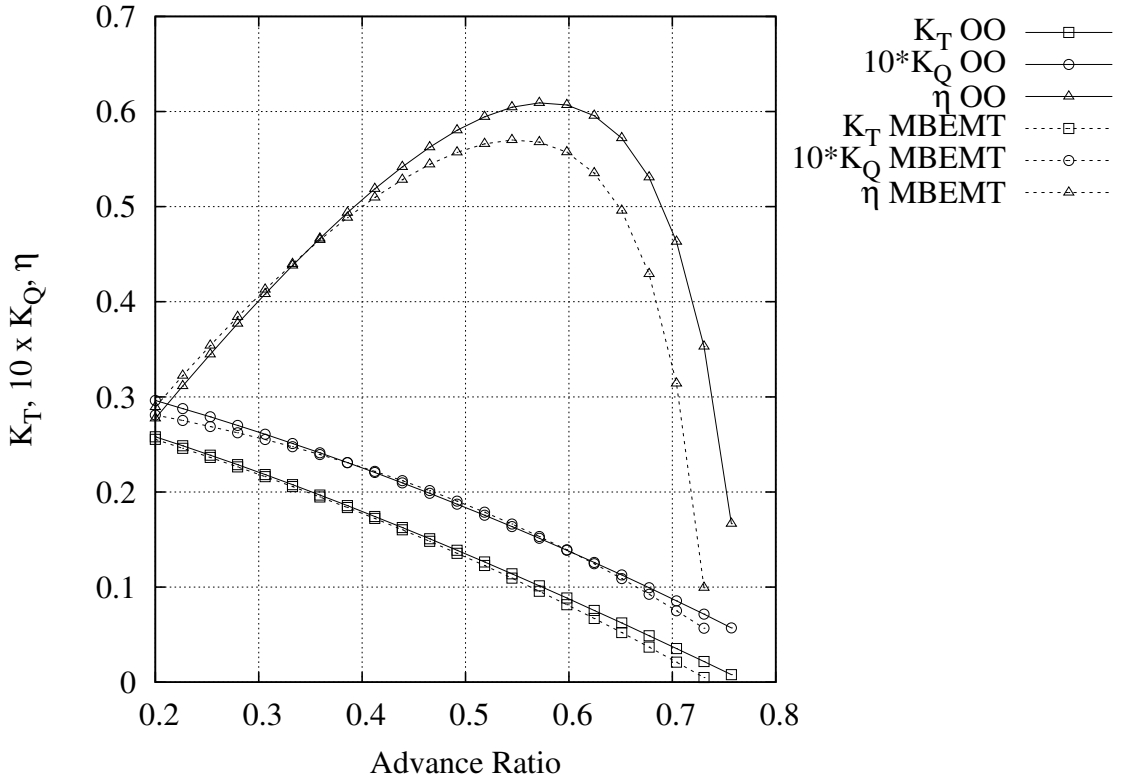

Figure 4.29: Comparison plot of *OOVOO* and calibrated quasi-static *MBEMT* propeller models for *Esso Osaka* stock propeller

stock propellers of the *Esso Osaka* and *KCS* in figures 4.29 and 4.30.

4.9.2 Calibration of Unsteady MBEMT Propeller Model

Figure 4.31 shows the comparison between propeller characteristics as calculated from Oosterveld and van Oossanen (1975) and the unsteady *MBEMT* model as described in this Chapter. As can be seen, the gradients of the K_T, K_Q lines are very similar. This is a result of obtaining an accurate value for the static lift slope, η beforehand. The magnitude of the K_T, K_Q curves obtained from the unsteady *MBEMT* model are lower than expected. This is attributed to three-dimensional flow phenomena that are not captured in the model due its two-dimensional nature.

To correct this, calibration constants are applied to the basic static lift and induced drag expressions, viz.

$$C_L = 2\pi\eta\alpha_{eff} + f_L \tag{4.72}$$

$$C_{DI} = \kappa C_L^2 + f_D \tag{4.73}$$

Where η, f_L, κ and f_D are estimated such that the resulting K_T, K_Q curves match

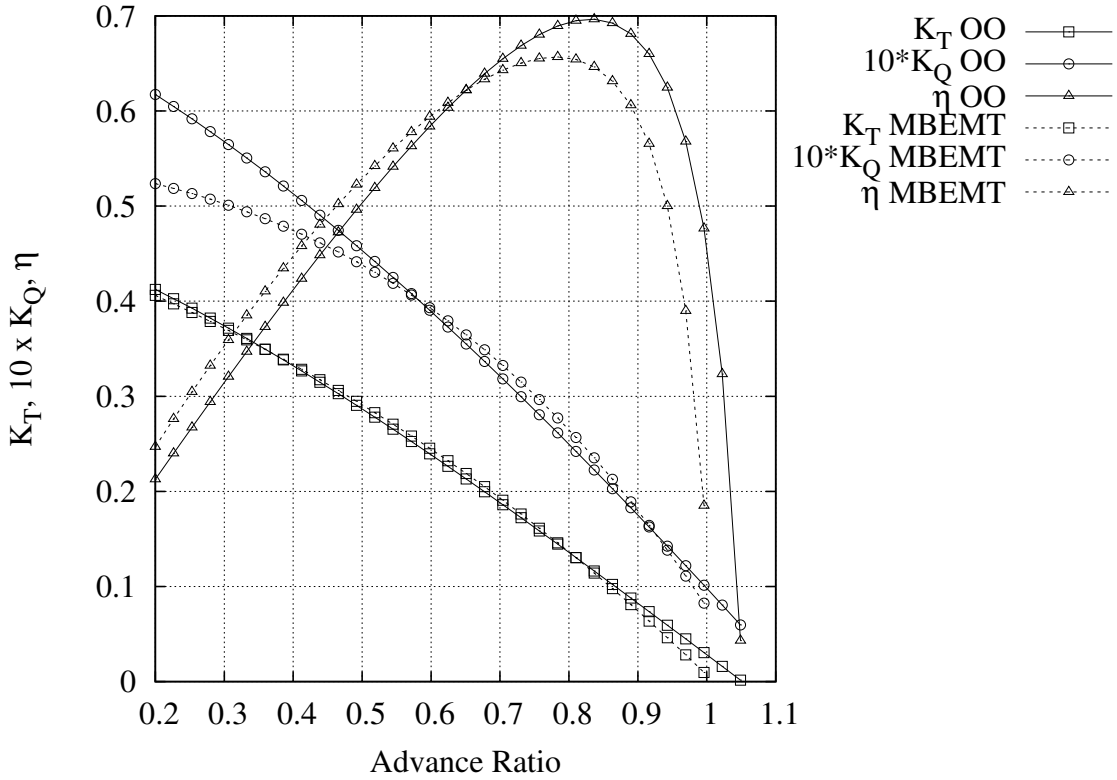

Figure 4.30: Comparison plot of *OOVOO* and calibrated quasi-static *MBEMT* propeller models for *KCS* stock propeller

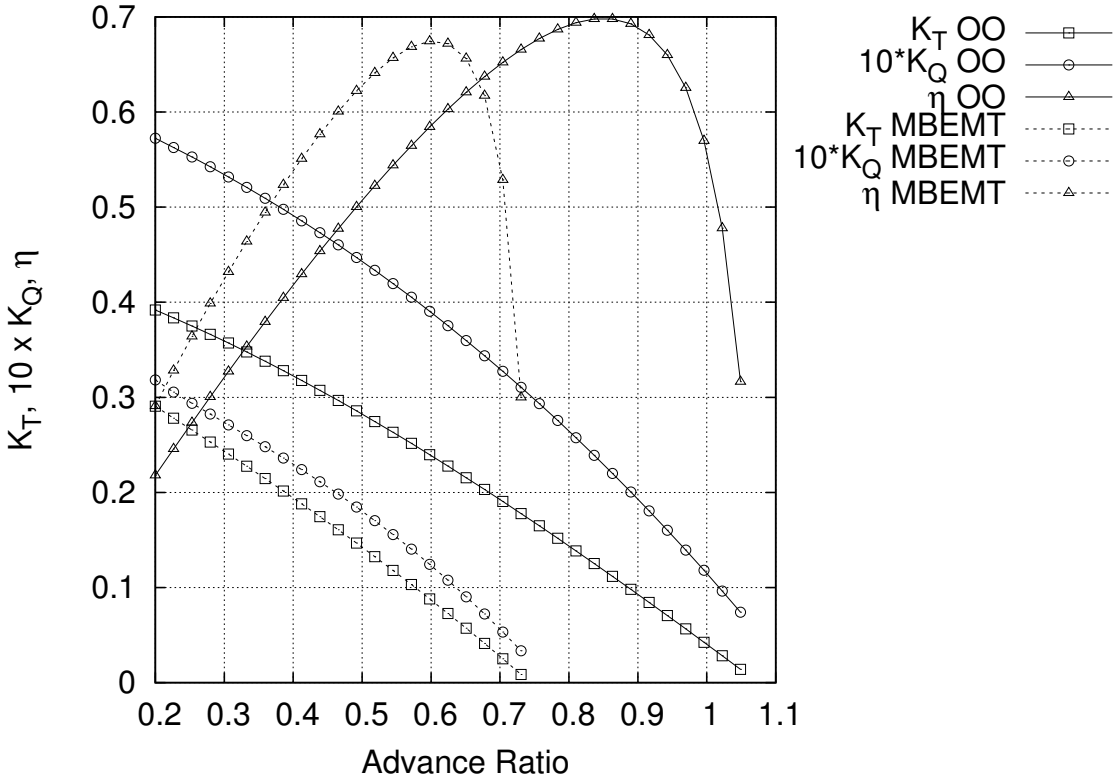

Figure 4.31: Comparison plot of *OOVOO* and uncalibrated unsteady *MBEMT* propeller models when $\frac{P}{D} = 1.0$ and $a_E = 0.6$

with the $OOVOO$ results.

Calibration was done based on a trial and error principle by adjusting values of η, f_L, κ and f_D systematically until the difference between the $OOVOO$ K_T, K_Q values were within an acceptable tolerance. Results from the calibration are presented in table 4.2.

	Esso Osaka				*KCS*			
a_E	η	f_L	κ	f_D	η	f_L	κ	f_D
$P/D = 0.6$								
0.3	0.970	0.800	0.001	0.0250	0.970	0.730	0.001	0.025
0.6	0.600	0.430	0.050	0.0070	0.590	0.380	0.050	0.007
0.9	0.410	0.270	0.050	0.0050	0.410	0.240	0.050	0.005
1.2	0.285	0.175	0.050	0.0060	0.285	0.155	0.050	0.006
1.5	0.220	0.120	0.100	0.0070	0.200	0.100	0.050	0.007
$P/D = 0.8$								
0.3	0.890	0.750	0.020	0.0290	0.890	0.680	0.02	0.0290
0.6	0.575	0.420	0.100	0.0030	0.575	0.370	0.10	0.0030
0.9	0.450	0.300	0.100	0.0045	0.450	0.260	0.10	0.0045
1.2	0.350	0.220	0.100	0.0060	0.400	0.240	0.10	0.0060
1.5	0.250	0.160	0.100	0.0070	0.250	0.140	0.10	0.0070
$P/D = 1.0$								
0.3	0.850	0.730	0.040	0.0200	0.850	0.680	0.04	0.0200
0.6	0.570	0.420	0.100	0.0060	0.570	0.380	0.10	0.0060
0.9	0.500	0.320	0.100	0.0040	0.500	0.280	0.10	0.0040
1.2	0.410	0.240	0.100	0.0044	0.410	0.210	0.10	0.0044
1.5	0.300	0.200	0.100	0.0075	0.300	0.160	0.10	0.0075
$P/D = 1.2$								
0.3	0.780	0.720	0.100	0.0030	0.780	0.700	0.10	0.003
0.6	0.550	0.420	0.100	0.0050	0.550	0.390	0.10	0.005
0.9	0.500	0.340	0.100	0.0050	0.500	0.290	0.10	0.005
1.2	0.400	0.250	0.100	0.0050	0.400	0.210	0.10	0.005
1.5	0.350	0.200	0.100	0.0100	0.380	0.180	0.10	0.010
$P/D = 1.4$								
0.3	0.800	0.750	0.050	0.0200	0.800	0.680	0.05	0.020
0.6	0.620	0.450	0.100	0.0050	0.620	0.360	0.10	0.005
0.9	0.530	0.350	0.100	0.0050	0.530	0.270	0.10	0.005
1.2	0.450	0.260	0.100	0.0050	0.450	0.210	0.10	0.010
1.5	0.450	0.220	0.100	0.0300	0.450	0.210	0.10	0.010

Table 4.2: Parameters used in the calibration of the lift and drag coefficients for the unsteady $MBEMT$ propeller model.

Calibration results for the unsteady $MBEMT$ model can be seen for the stock propellers (table 1.1) of the *Esso Osaka* and *KCS* in figures 4.32 and 4.33. Calibration constants for intermediate values of P/D and a_E are obtained via cubic spline interpolation. These figures illustrate that the unsteady $MBEMT$

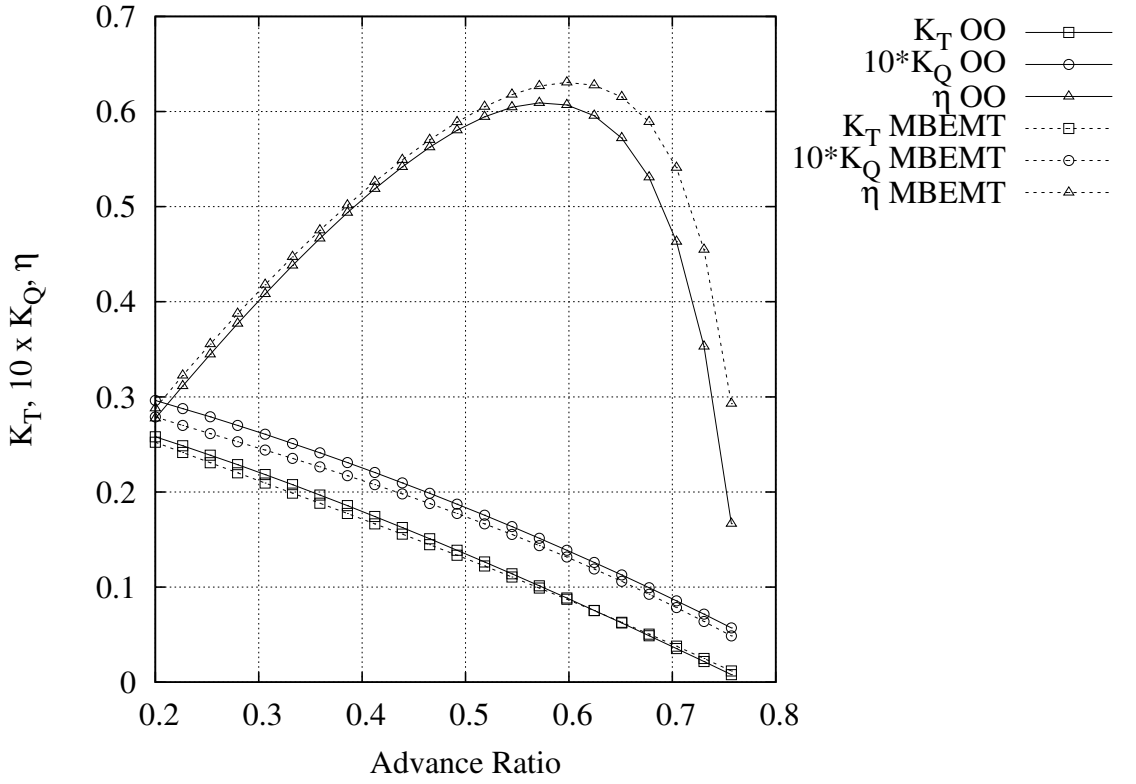

Figure 4.32: Comparison plot of $OOVOO$ and calibrated unsteady $MBEMT$ propeller models for *Esso Osaka* stock propeller

model mimics the behaviour of the B-Screw more closely than the quasi-static $MBEMT$ model over a larger range of advance coefficient. There is a larger difference however between the K_T, K_Q curves at certain ratios, compared with the quasi-static model. This is due to fast changing calibration parameters, and hence the unsteady calibration could be improved with a greater number of data points.

Benini (2004) compared a $BEMT$ model to that of a RANS model for a B3-50 propeller. He found that the $BEMT$ model was only accurate when the three-dimensional effects are of a secondary order. The quantities which most influenced the performance prediction of the $BEMT$ as a function of J are the incidence angle, α, the inflow velocity, V_p^* and the radial elementary thrust and torque distributions, $\frac{\mathrm{d}T}{\mathrm{d}r}$ and $\frac{\mathrm{d}Q}{\mathrm{d}r}$,respectively. The major discrepancy found between the two models was the incidence angle.

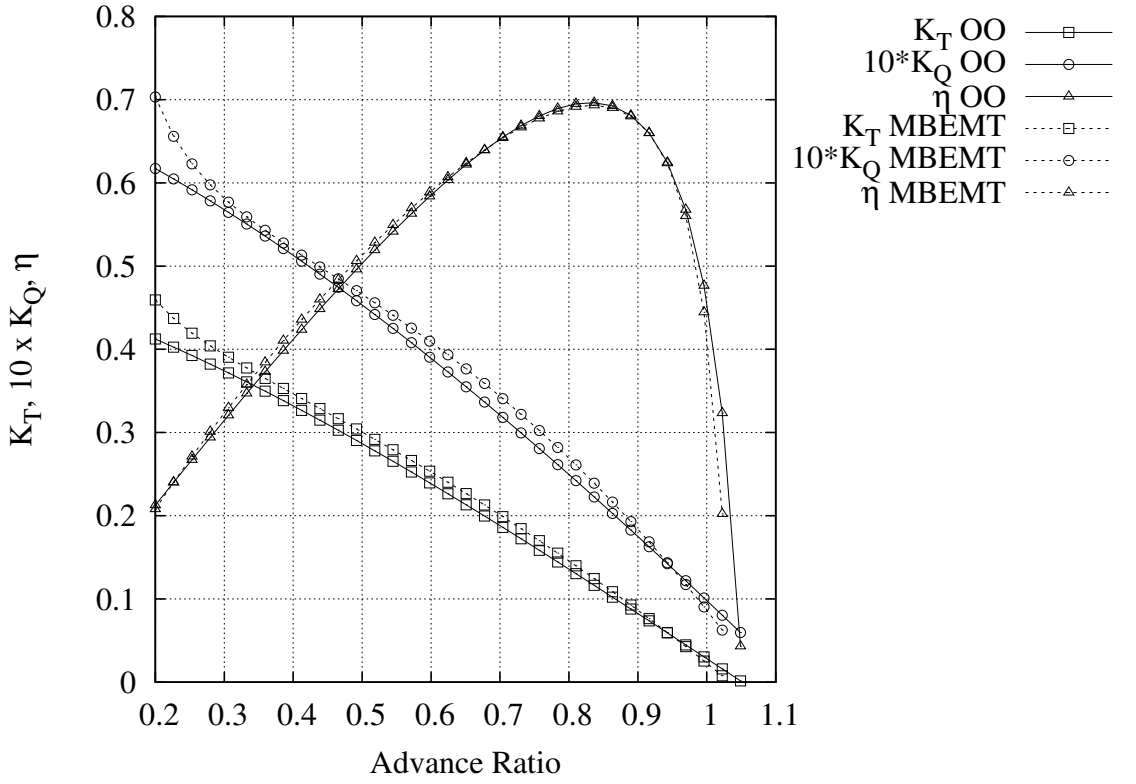

Figure 4.33: Comparison plot of $OOVOO$ and calibrated unsteady $MBEMT$ propeller models for *KCS* stock propeller

4.9.3 Comparison between Quasi-Static and Unsteady Propeller Models at Non-Zero Drift Angles

In order to display a level of confidence in the results of the unsteady $MBEMT$, comparisons can be shown with the quasi-static $MBEMT$ model, whose mathematics is based chiefly on physical geometry, with a minimum of semi-empirical formulæ. Figures 4.34, 4.35 and 4.36 show the difference between the quasi-static, and the unsteady $MBEMT$ propeller models.

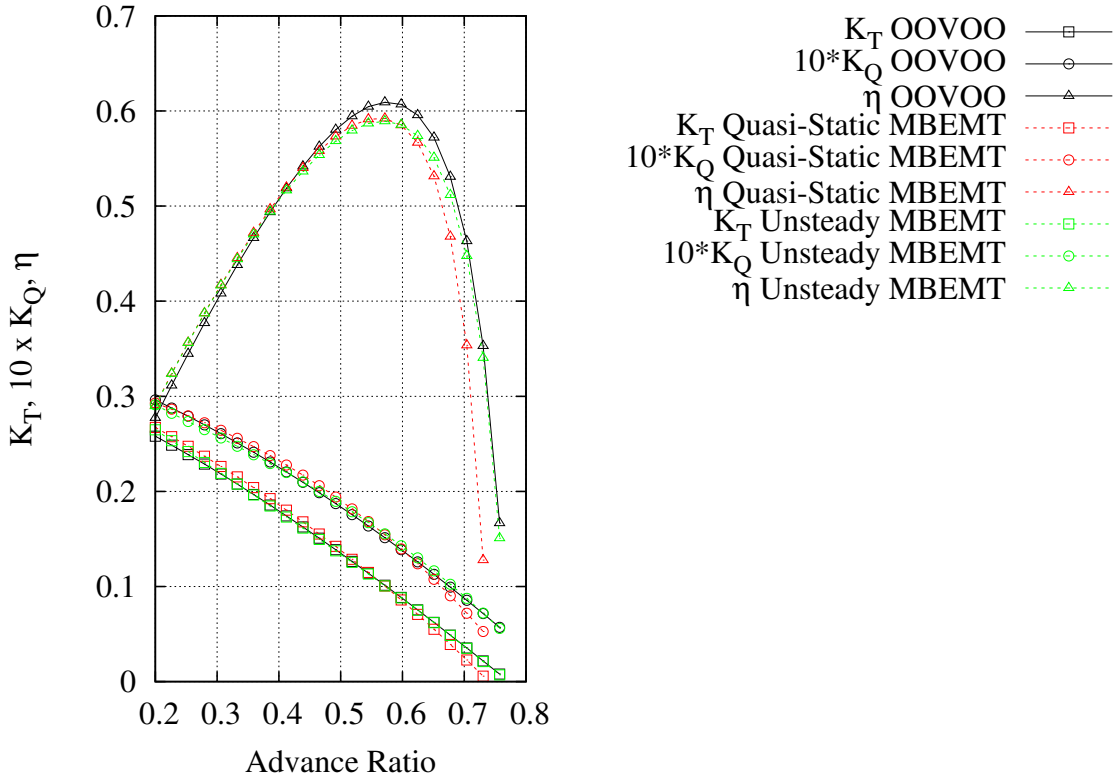

Figure 4.34: Comparison plot of calibrated quasi-static and unsteady *MBEMT* propeller models when drift angle = 0.0°

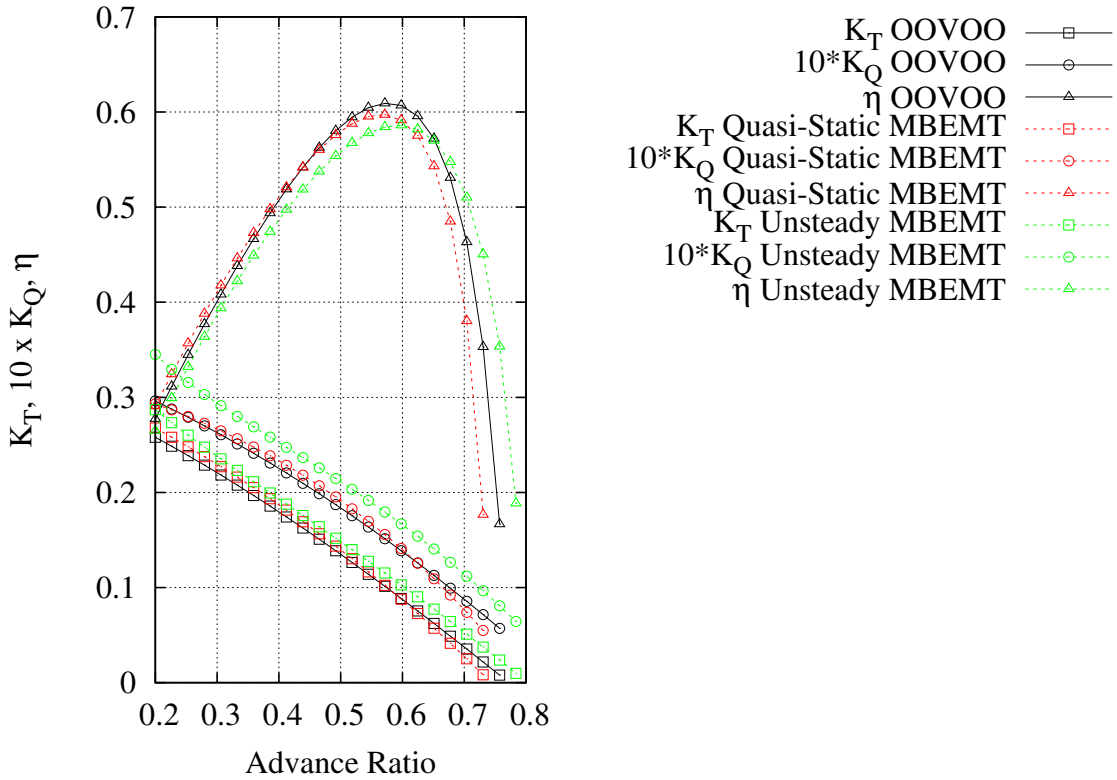

Figure 4.35: Comparison plot of calibrated quasi-static and unsteady *MBEMT* propeller models when drift angle = 5.0°

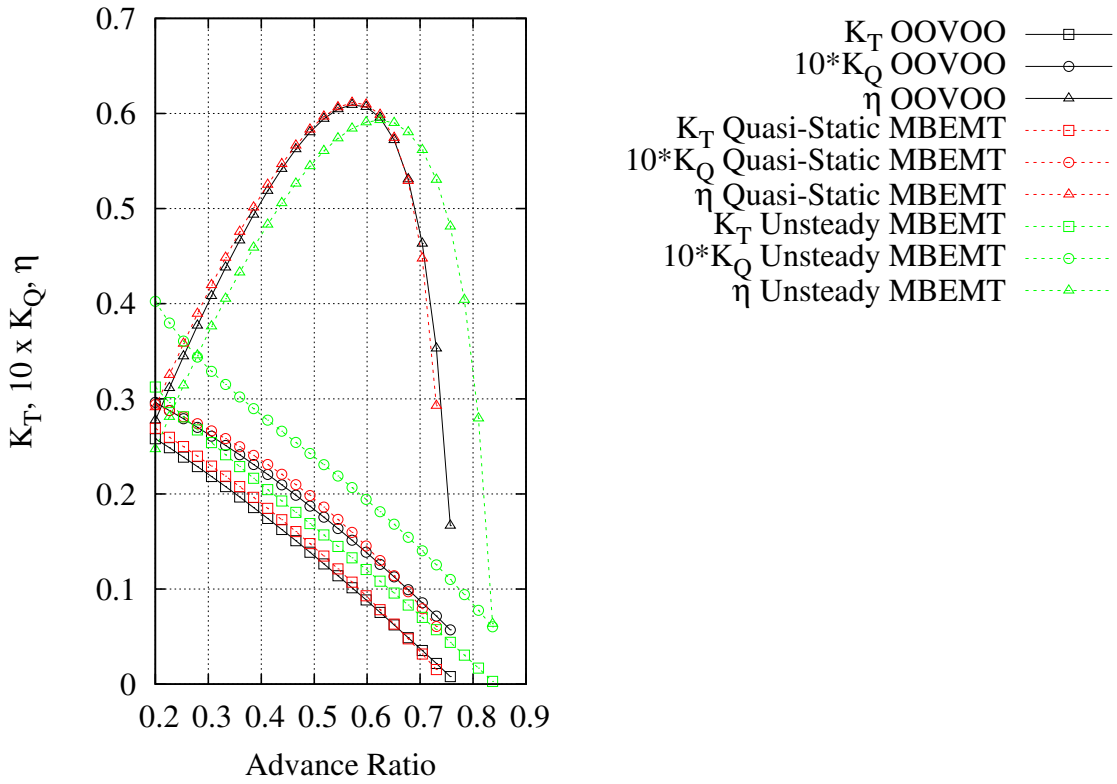

Figure 4.36: Comparison plot of calibrated quasi-static and unsteady *MBEMT* propeller models when drift angle = 10.0°

4.10 Summary

This Chapter presented a method to model the action of a propeller that is propelling a ship when sailing at some arbitrary drift angle. Modifications to the general blade-element momentum theory are explained to account for drift angle, and a strategy for modelling the dynamic lift and drag of a propeller section are described.

Due to neglecting the variation in wake due to the ship's hull (from lack of data in that particular area), the results will be somewhat different to reality, however, the overall trend and outcome is not expected to change.

Various algorithms have been developed and implemented as Fortran modules which, in turn, can be used in the ship manœuvring simulator.

The effects of unsteady flow on lift and drag coefficients, represented in terms of a non-dimensional pitch rate, have been shown, and output plots from the developed code confirm that unsteady effects are not negligible.

In order to make use of the $MBEMT$ propeller flow model in further analysis, it has been calibrated, for a ship at zero drift angle, with that of the thrust and torque obtained by Oosterveld and van Oossanen (1975). This ensures that differences between the two models are from oblique inflow angle (with associated unsteady effects) alone.

The early observations of H. S. Maxim are confirmed, and depicted in figs. 4.34, 4.35 and 4.36. These show graphically how the thrust on a propeller increases when the propeller is moved perpendicular to its axis of rotation (or in this case not perpendicular, but at some oblique angle)

The propeller model presented in this Chapter is shown to perform as expected compared to the Oosterveld and van Oossanen (1975) polynomials and, once calibrated, is shown to accurately mimic the B-Screw Series.

Chapter 5. Validation of Simulation Modules

The aim of this Chapter is to provide the reader with a level of confidence that the mathematical models of the previous Chapters behave in a realistic manner. To achieve this, comparisons between manœuvring simulations are made for the *Esso Osaka* using models presented thus far, and experimental and theoretical results from other institutions.

As validation of the *SiS* simulator, a series of standard manœuvring tests are run, and compared with the results from the Korea Research Institute of Ship and Ocean (KRISO), the Hydronautics Ship Model Basin (HSMB) and Seoul National University (SNU). These results are presented in the ITTC Specialist Committee on Esso Osaka (ITTC, 2002), and were selected by the ITTC committee from many data sets, as having the most reliable data, with the least scatter between them.

Results show a scatter in data from all models, however, the trend from the results are all similar. The ITTC Specialist Committee on Esso Osaka (ITTC, 2002) concluded that the reason for scatter in the results from various institution's manoeuvring simulations could not be determined.

Section 5.1 describes a standard turning circle manœuvre, how and why it is performed, and compares results obtained by the *SiS* simulator (a ship manœuvring simulator developed as part of this research) with results from other institutions and sea-trials. The results of Section 5.1 also show how the degree of fidelity of the propeller model affects the turning characteristics.

Section 5.2 presents the results of a standard 10-10 zig-zag manœuvre obtained from the *SiS* simulator and compares them with other research institutions and sea-trials.

Section 5.3 shows results from turning circle and zig-zag manœuvres as performed by the *KCS* with the *SiS* simulator. The author has been unable to find independently verified manœuvring results on the *KCS*, and so the results presented in this Section are informational purposes.

The different propeller models used in the *SiS* simulator for these experiments comprise a set of polynomials developed by Oosterveld and van Oossanen (1975) (referred to in this work as the $OOVOO$ model, for the sake of brevity), a quasi-static $BEMT$, and an unsteady $BEMT$ propeller flow model. Please refer to Chapter 4 for details on the $BEMT$ models. These different models are used in this analysis to highlight the effects of different levels of fidelity that a propeller model has on the characteristics of a manœuvring ship.

To ensure the accuracy of the propulsion model, the modified $BEMT$ propeller flow models are calibrated against a propeller's characteristics as obtained from the $OOVOO$ model. The $OOVOO$ model is considered to mimic the behaviour of the B-Screw series propellers accurately. Please refer to Section 4.9 for details on how the calibration was performed.

Figure 5.1 shows the resulting comparison between the propeller characteristics as calculated from the $OOVOO$ model, and the unsteady $MBEMT$ model. It is noted that the Abscissa is limited to a range of advance ratio above 0.2. This is due to the `MINPACK` library having difficulties in converging to a solution at low advance ratios. In practice, these low values of advance ratio are never reached in the practical application of this research, as a low speed of advance means a relatively high propeller speed for a relatively low ship speed. If bollard pull is to be analysed using this simulator, then the way the `MINPACK` library is used would need revision. As can be seen from fig. 5.2, the range of advance ratio at the propeller, J encountered during the turning circle is between about 0.157 and 0.405. The thrust and torque characteristics from fig. 5.1 match very closely over this range.

5.1 Turning Circle Manœuvre

The turning circle manœuvre provides a measure of turning ability. To perform the manœuvre, the ship reaches a steady approach speed, with zero yaw rate, and then throws the rudder hard over (that is, to its maximum extent for the given speed, but not more than 35°). This procedure is repeated for both starboard and port turns. The essential information retrieved from this test consists of the tactical diameter (the transfer distance at 180° change of heading), the advance, transfer, speed loss in the turn, and peak and final yaw rates. To meet IMO

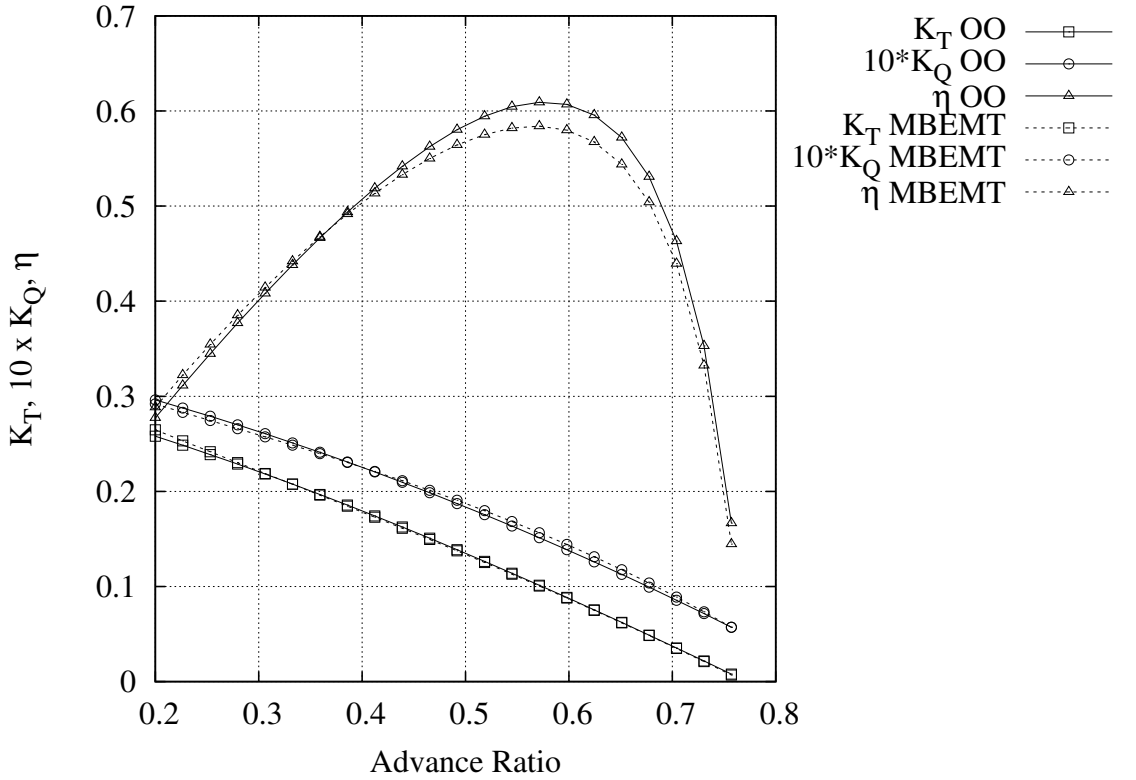

Figure 5.1: *OOVOO* and unsteady *MBEMT* comparison for propeller used in the turning circle manœuvre.

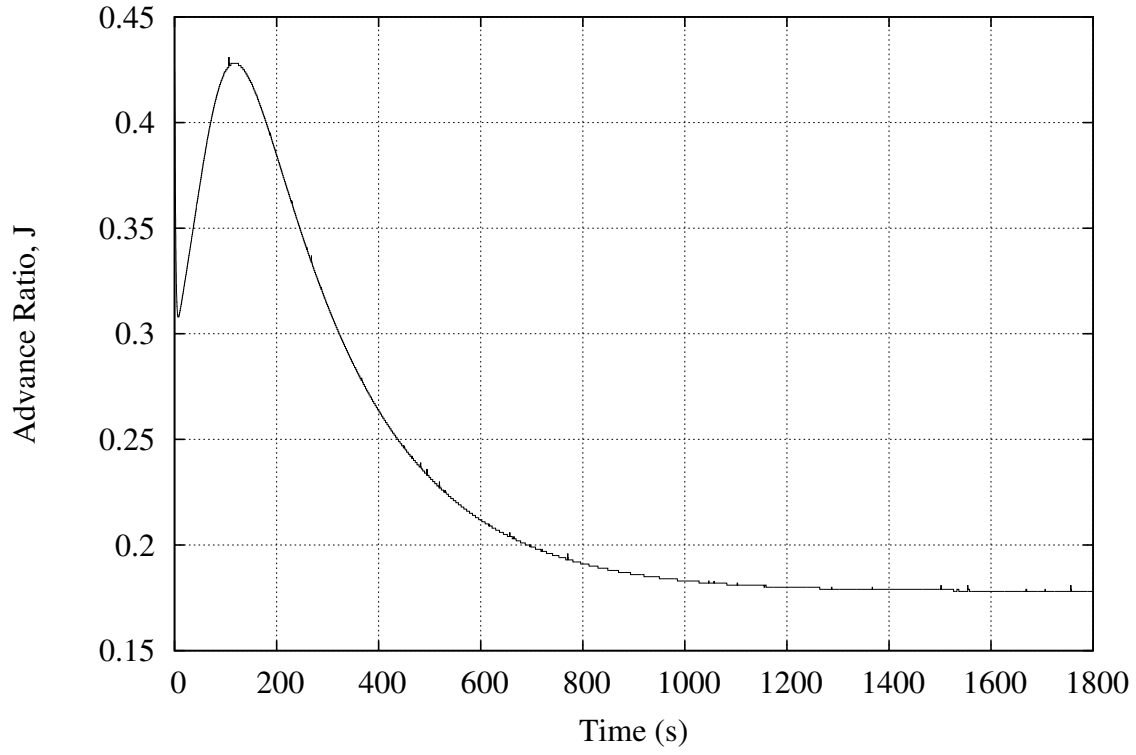

Figure 5.2: Variation of advance ratio at the propeller during turning circle manœuvre

criteria, the tactical diameter should not exceed five ship lengths, and the advance at 90° heading change should not exceed four and a half ship lengths.

The turning circle performed in this section is of the Esso Osaka, with a steady approach speed of 10.0 knots, with a 35° starboard rudder. The simulation is run on the *SiS* simulator, and the results are superimposed on data obtained from ITTC (2002).

Figures 5.3, 5.4, 5.5 and 5.6 show, for comparison, the results obtained from the $OOVOO$, quasi-static $MBEMT$ and unsteady $MBEMT$ propeller models. These figures show the results for a starboard turning circle from sea trials, numerical manœuvring models developed by KRISO, HSMB and SNU, as well as the numerical manœuvring models developed in this research. To recapitulate, the $OOVOO$ propeller model is based on the polynomials carried out by the regression analysis of Oosterveld and van Oossanen (1975), and considers the thrust and torque characteristics of a propeller with flow arriving perpendicular to the propeller plane. The $OOVOO$ model also neglects any induced sway or yaw imparted to a ship from the action of the propeller. The quasi-static $MBEMT$ propeller flow model accounts for flow arriving at an oblique angle to the propeller plane, whilst the unsteady $MBEMT$ model also accounts for unsteady effects that the oblique flow imposes. Both $MBEMT$ propeller flow models can account for the induced sway and yaw imparted to a ship from the propeller's action.

In order to distinguish the effects of including sway and yaw induced from the propeller, figs. 5.7, 5.8, 5.9 and 5.10 show comparisons for the turning circle when the induced sway and yaw by the propeller from the $MBEMT$ models has been set to zero.

The plots of transfer and advance (figs. 5.3 and 5.7) are difficult to compare results with. A bar chart has been composed of figs. 5.3 and 5.7, which plot two specific points around the turning circle, enabling easy comparison between the different methods and institutions. The resulting bar chart is found in fig. 5.11. Ordinarily, tactical diameter (i.e. the transfer at 180 degree heading change) and advance (i.e. advance at 90 degree heading change) would be plotted. In this case transfer at 180 degree course change (designated Turning Diameter* on the graph), and advance at 90 degree course change (designated Advance* on the graph) are plotted, the reason being it is more readily obtained from turning circle plots (which do not have details of heading angles).

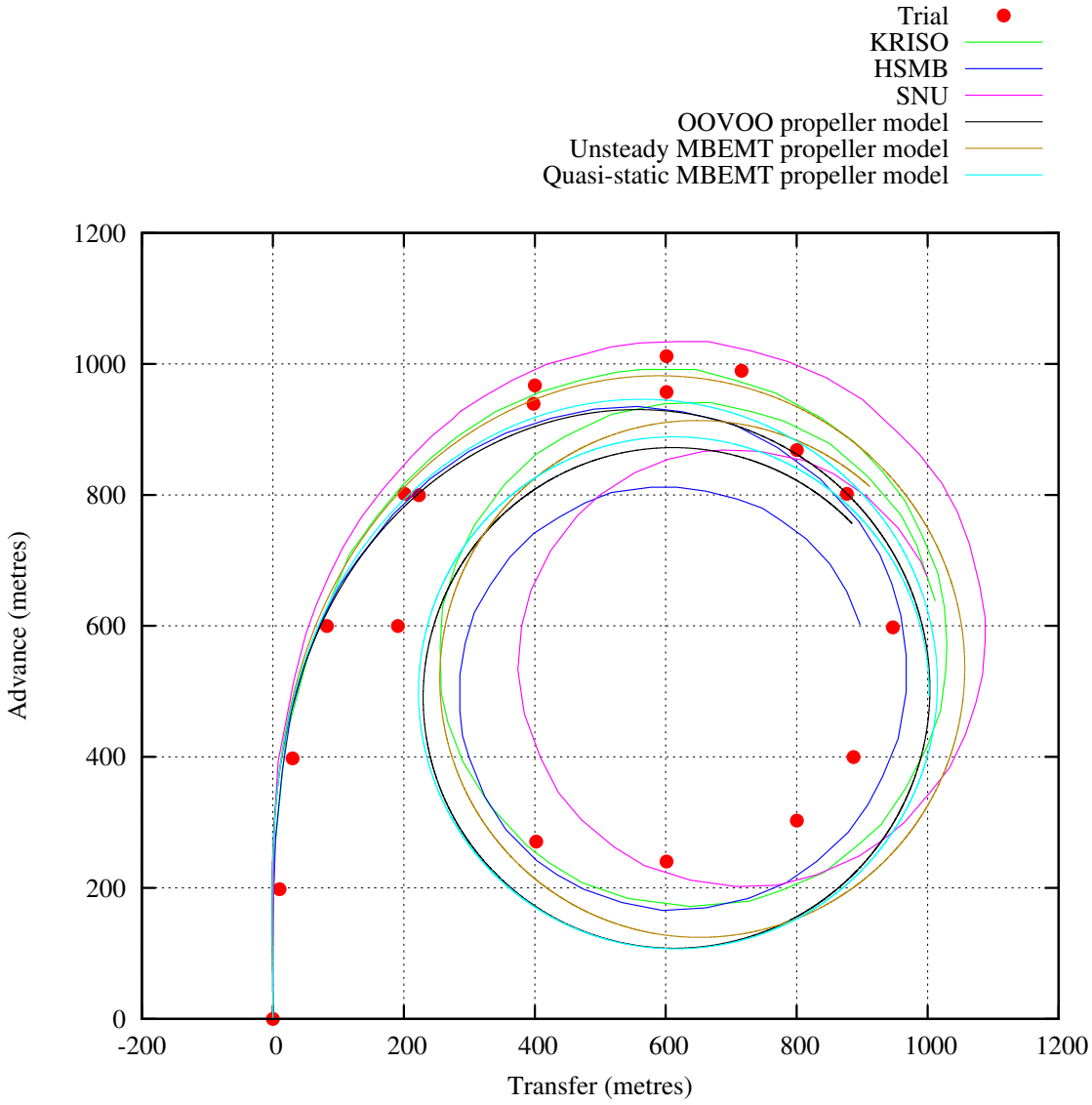

Figure 5.3: Track of 35^o starboard turning circle (V = 10.0 knots)

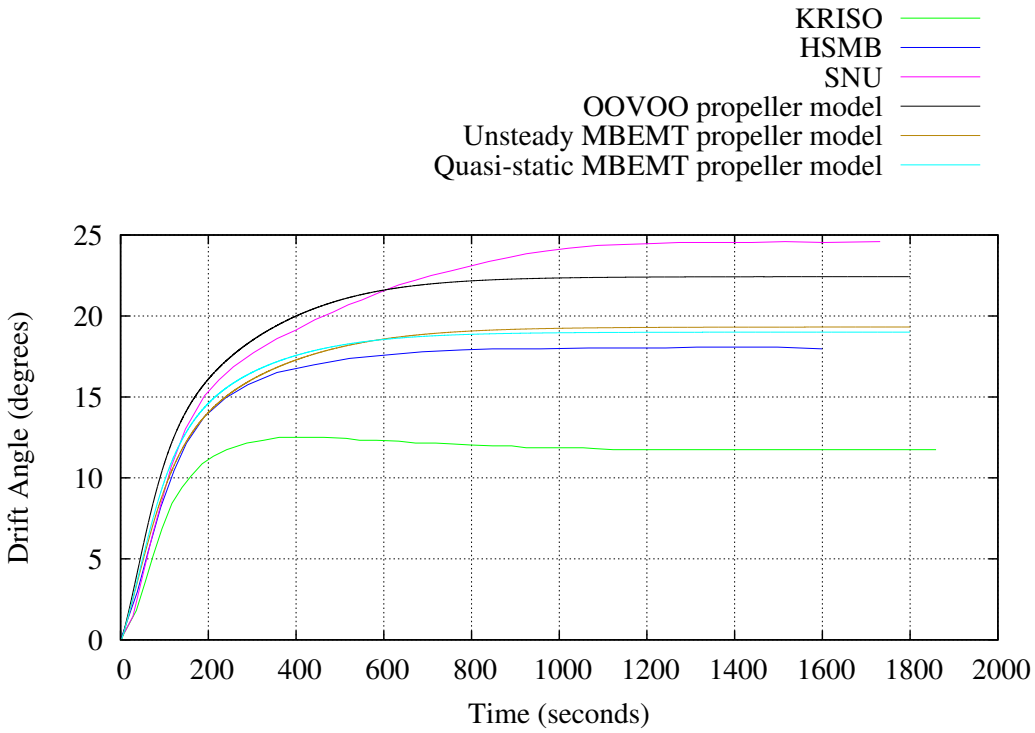

Figure 5.4: Drift Angle Time History of 35^o starboard turning circle (V = 10.0 knots)

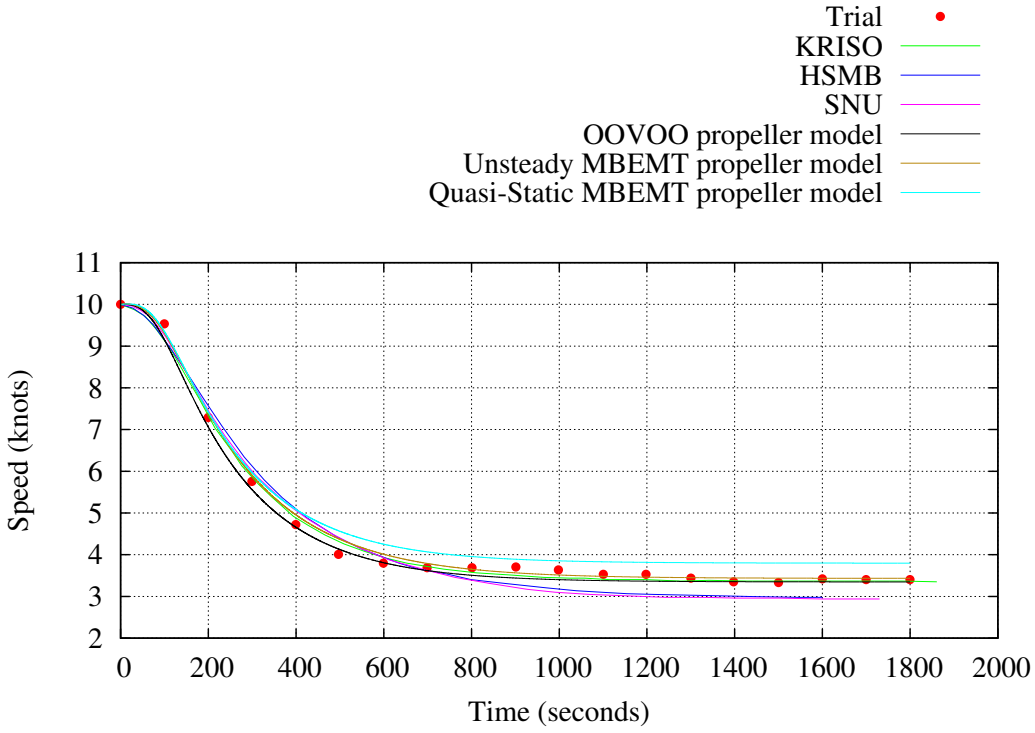

Figure 5.5: Speed Time History of 35^o starboard turning circle (V = 10.0 knots)

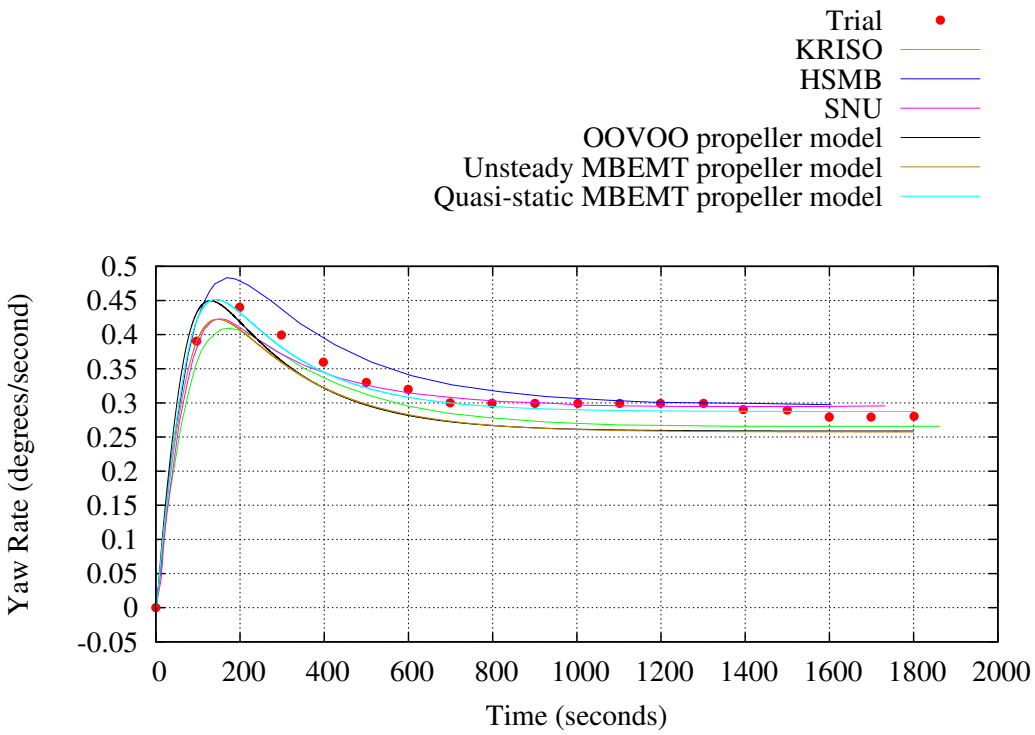

Figure 5.6: Yaw Angle Time History of 35^o starboard turning circle (V = 10.0 knots)

The values for advance are expected to more faithfully represent the trials results compared to the tactical diameter. This stems from the fact that the tactical diameter is necessarily measured at a point further forward in time than the advance. Any errors that arise in the simulator are cumulative over each time step, and thus increase with time.

As can be seen from the turning circle plots, the effects of unsteady propeller action, *and* effects of induced sway and yaw from the propeller both have a noticeable outcome on the simulation's results. When the effects of induced sway and yaw from the propeller are included in the model, it is observed that the advance and tactical diameter is reduced, that is, the side force produced by the propeller aids the ship in attaining a tighter starboard turn. This is indicative of a left handed propeller (anticlockwise rotation as viewed from the stern), which tends to push the stern to port. The plot of fig. 5.11 also illustrates that the effect of unsteady flow tends to increase the advance and tactical diameter.

For the sake of completeness, a 35° turning circle to port has been plotted in figs. 5.12, 5.13, 5.14 and 5.15 using the developed *SiS* simulator with the *OOVOO* propeller model, and compared with the results of the same institutions as the starboard turning circle. As can be seen there is a certain asymmetry compared to

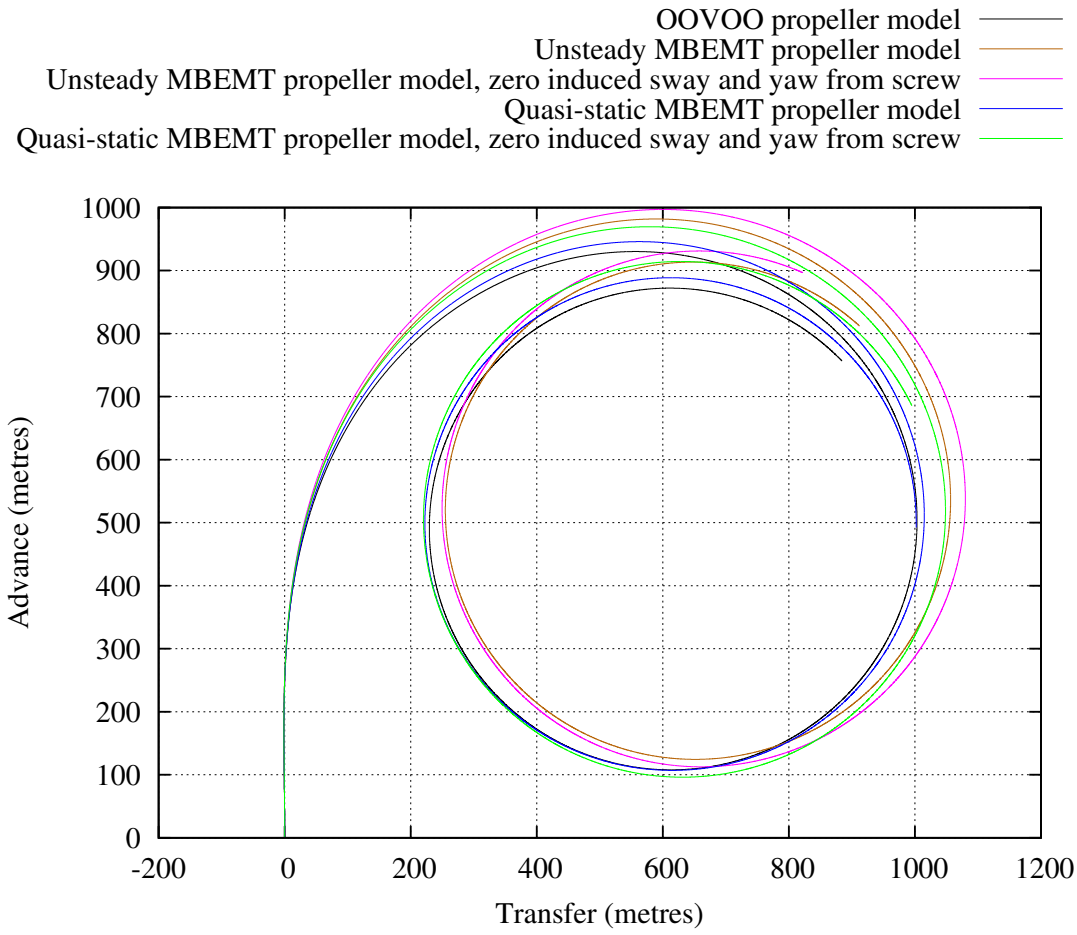

Figure 5.7: Track of 35^o starboard turning circle (V = 10.0 knots) without influence of sway and yaw from propeller.

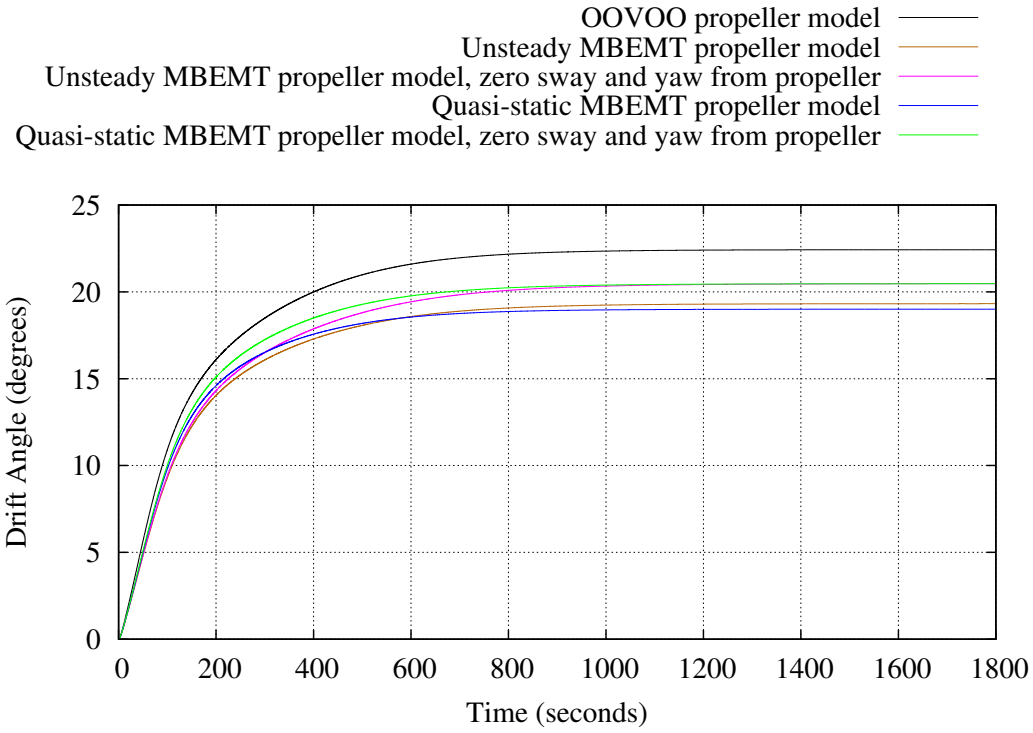

Figure 5.8: Drift Angle Time History of 35^o starboard turning circle (V = 10.0 knots) without influence of sway and yaw from propeller.

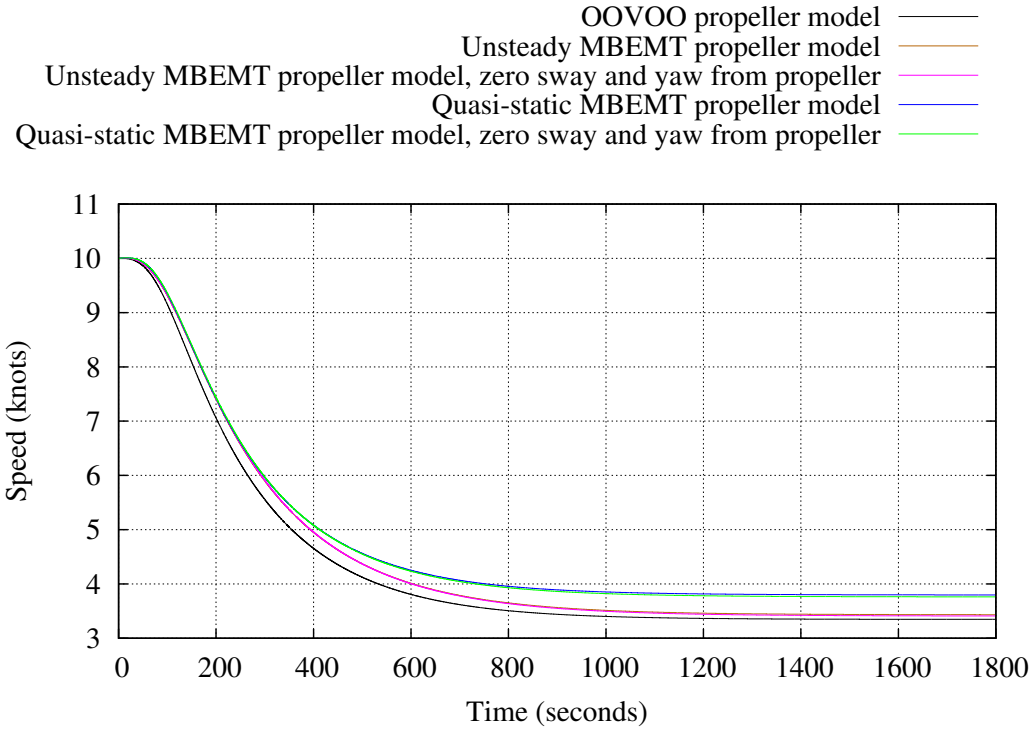

Figure 5.9: Speed Time History of 35^o starboard turning circle (V = 10.0 knots) without influence of sway and yaw from propeller.

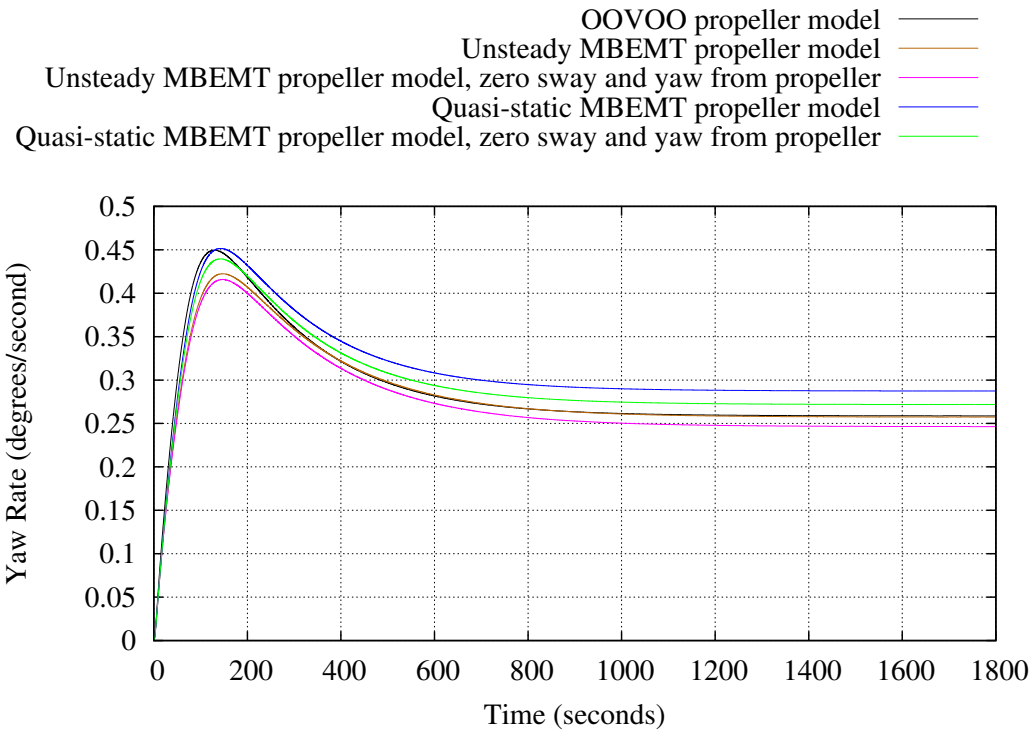

Figure 5.10: Yaw Angle Time History of 35^o starboard turning circle (V = 10.0 knots) without influence of sway and yaw from propeller.

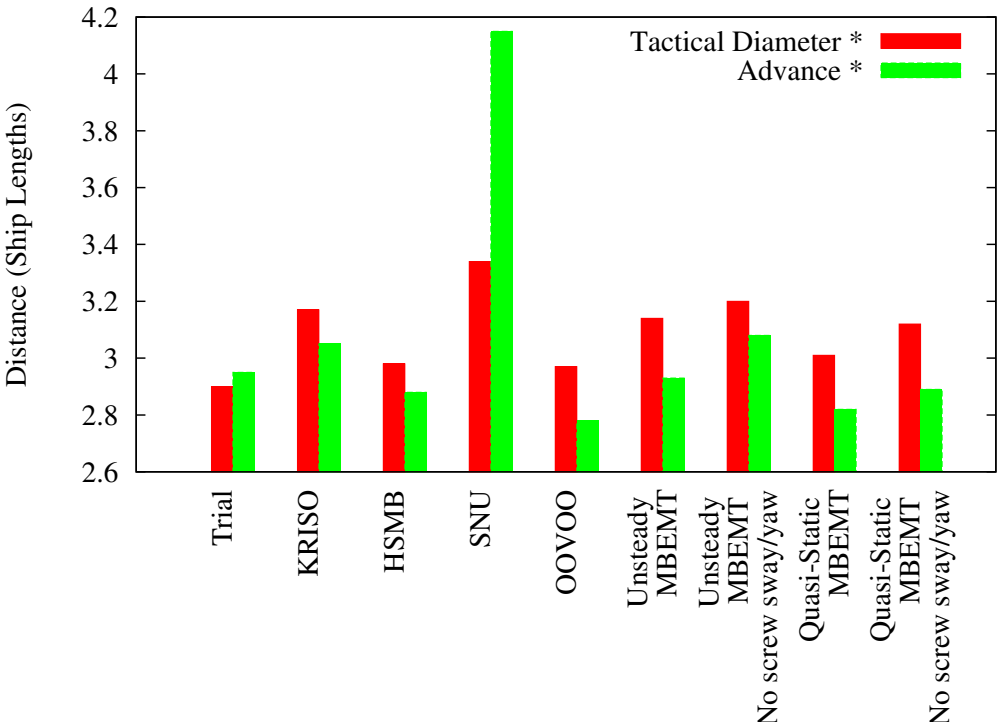

Figure 5.11: Comparison of Tactical Diameter* and Advance* of different institutions and propeller models, (refer to main text for definition of Tactical Diameter* and Advance*).

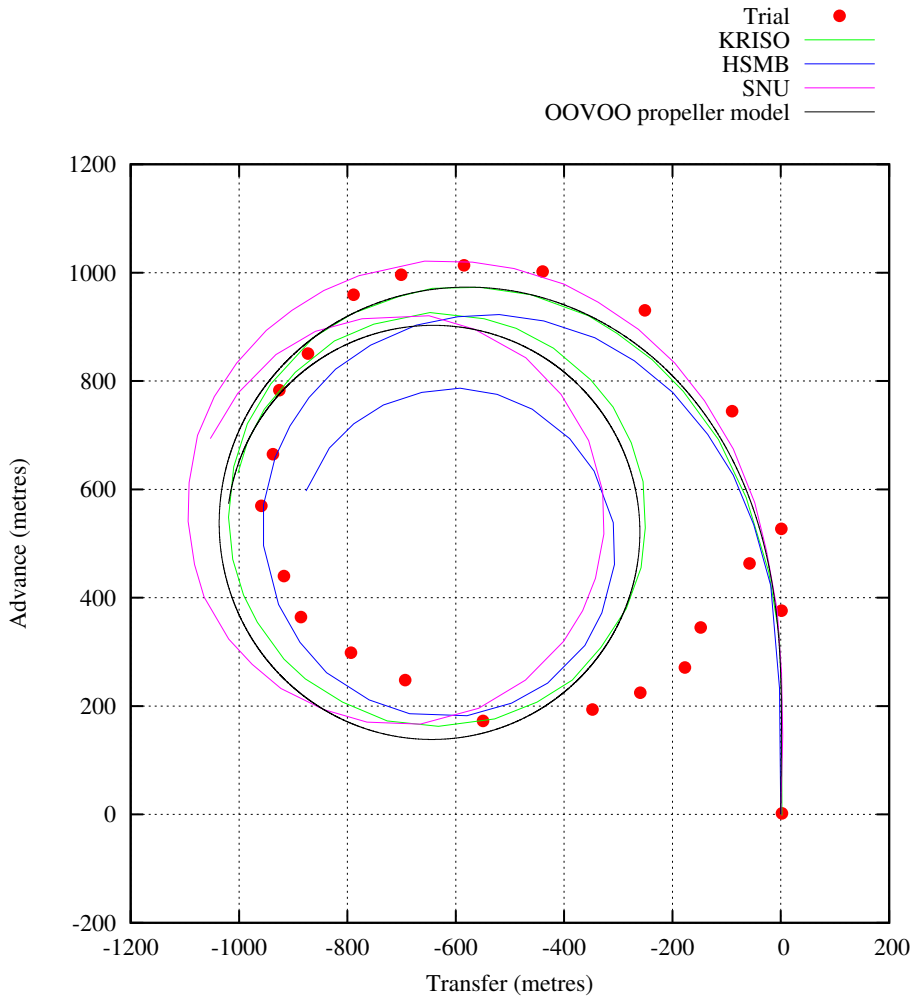

Figure 5.12: Track of 35^o port turning circle (V = 7.7 knots).

the starboard turn (aside from the fact that the approach speed is different). This asymmetry principally arises from "propeller walk" which is like a paddle wheel effect. A propeller, as well as propelling a ship ahead or astern, will also tend to rotate it. A right-handed propeller will tend to push the stern to starboard, whereas a left-handed propeller will tend to push the stern to port.

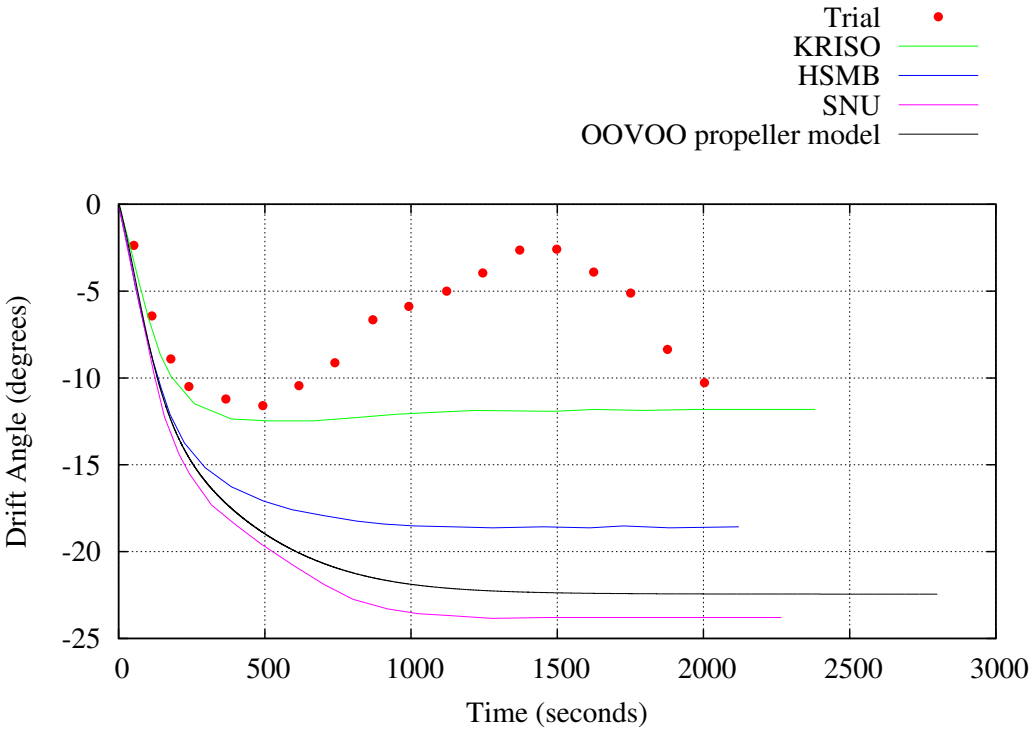

Figure 5.13: Drift Angle Time History of 35^o port turning circle (V = 7.7 knots).

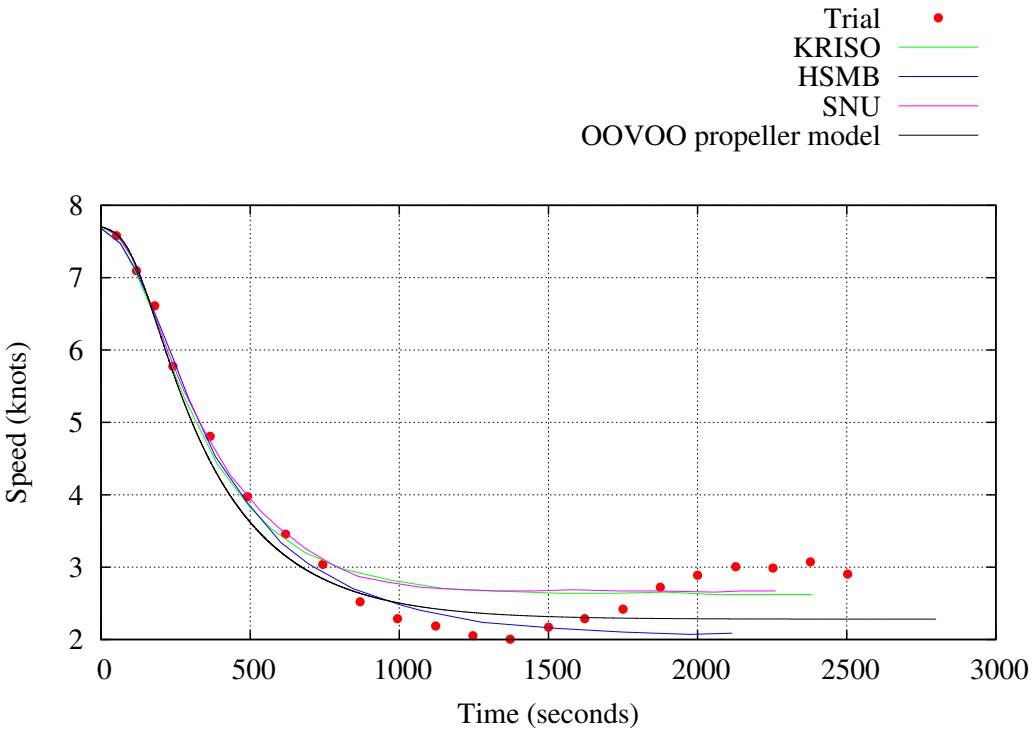

Figure 5.14: Speed Time History of 35^o port turning circle (V = 7.7 knots).

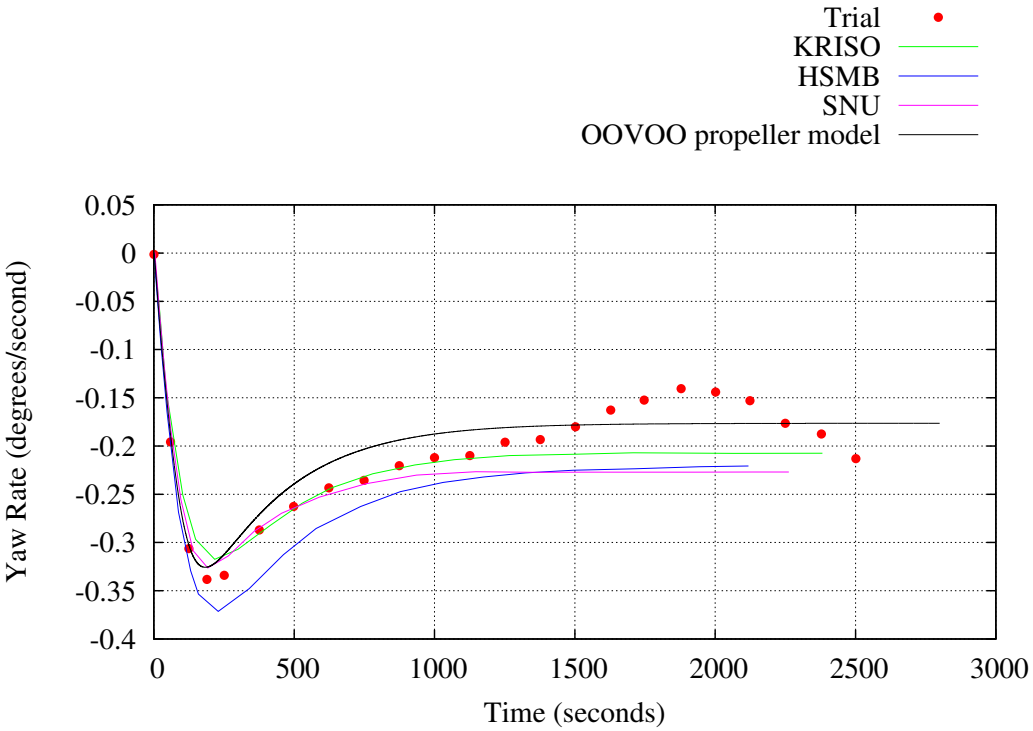

Figure 5.15: Yaw Rate Time History of 35^o port turning circle (V = 7.7 knots).

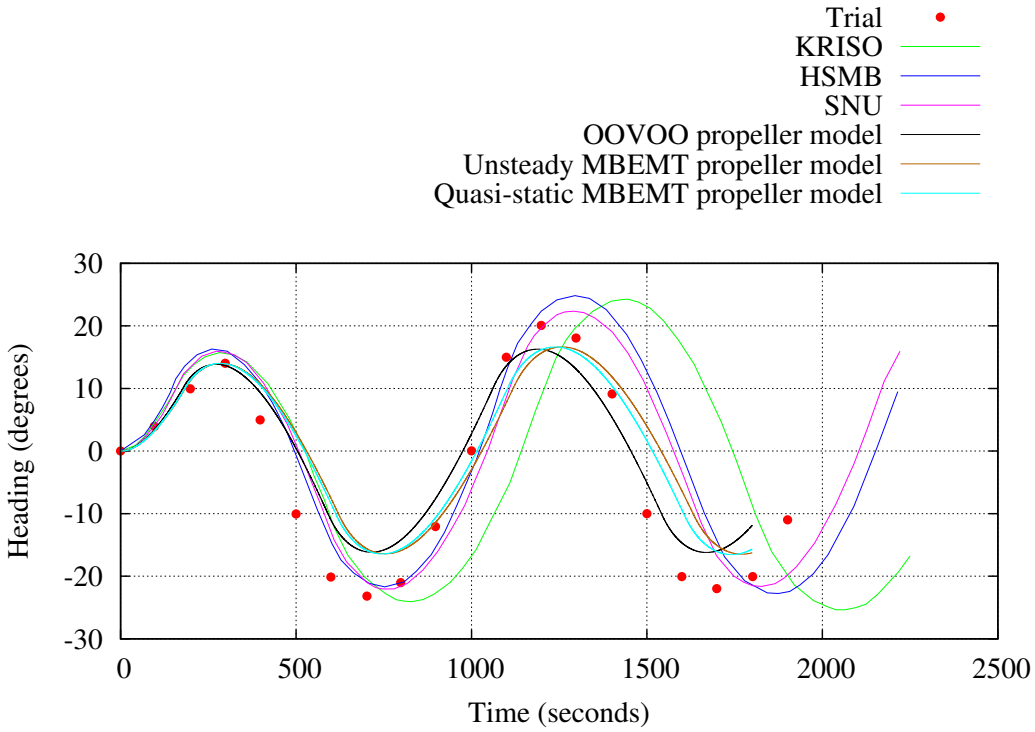

Figure 5.16: Heading Angle Time History of 10-10 ZigZag (V = 7.5 knots)

5.2 Zig-Zag Manœuvre

A zig-zag manœuvre provides a measure of the directional stability, but by its nature is also a measure of the initial turning ability. The initial turning ability is defined by the change-of-heading response to a moderate helm, in terms of distance covered before realising a certain heading deviation. The zig-zag manœuvre is initiated from a steady approach speed with zero yaw rate, the rudder is then put over a specified angle, δ (first run). When the heading has changed to δ degrees off the original heading, the rudder is put over to $-\delta$ degrees (second run). After the rudder has been put over, the ship will continue turning, with a decreasing yaw rate, the ship will respond to the rudder, and eventually turn to port/starboard. When the ship's heading has reached $-\delta$ from the original course, the ruder is again put over to δ degrees (third run). The first overshoot angle is the additional heading deviation experienced in the zig-zag test following the second run. The second overshoot angle is the additional heading deviation experienced in the zig-zag test following the third run. Figures 5.16, 5.17 and 5.18 show the results of the developed *SiS* simulator when the *Esso Osaka* is run during a 10-10 zig-zag manœuvre.

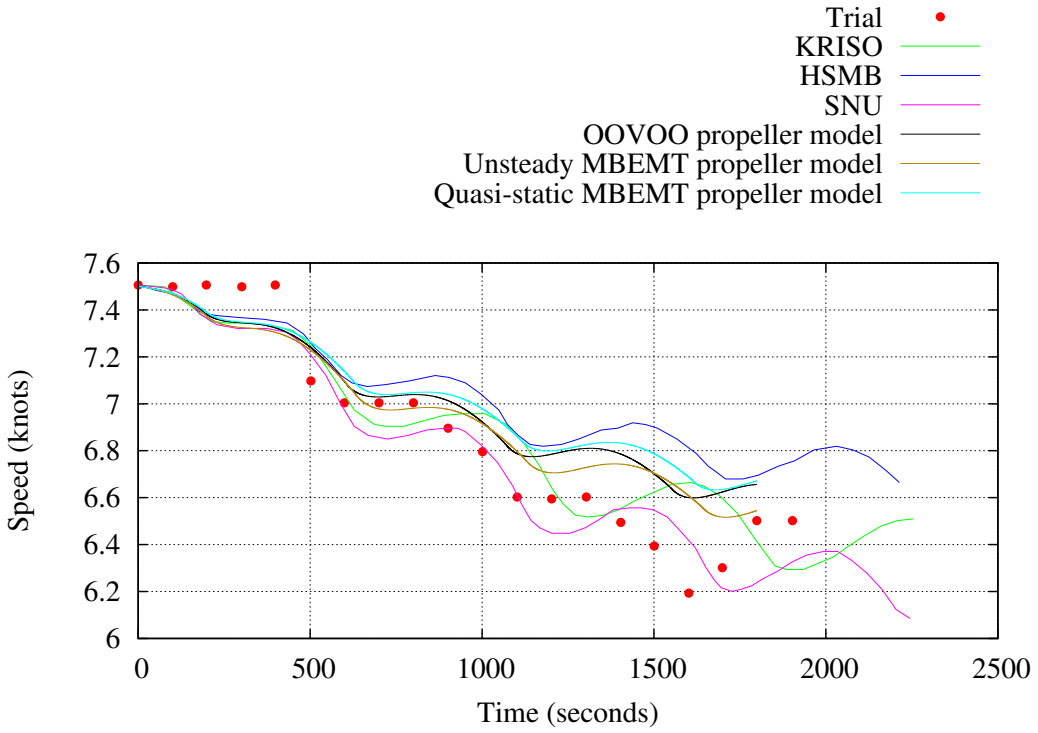

Figure 5.17: Speed Time History of 10-10 ZigZag (V = 7.5 knots)

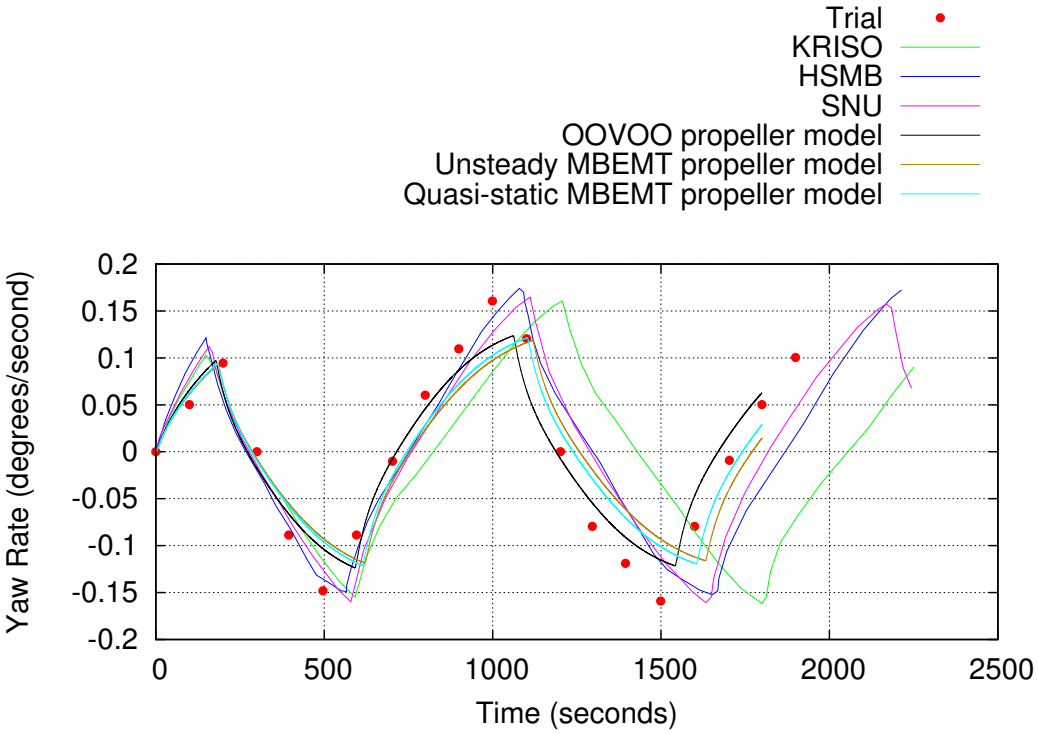

Figure 5.18: Yaw Rate Time History of 10-10 ZigZag (V = 7.5 knots)

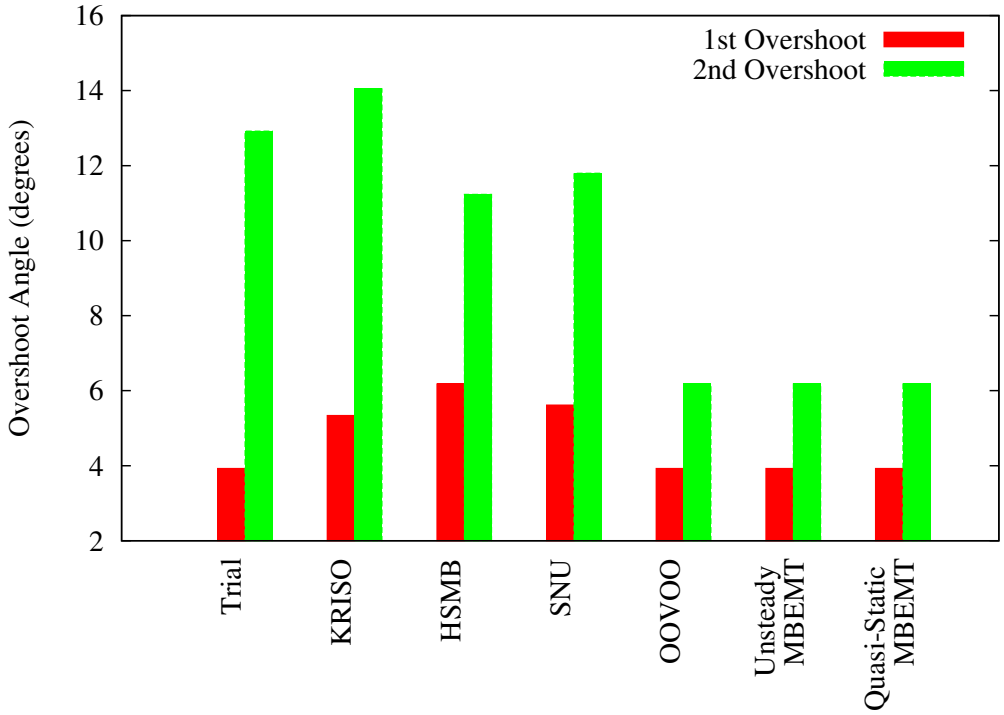

Figure 5.19: Comparison of 1st and 2nd Overshoot Angles from different institutions and propeller models.

As with the case of the transfer and advance plots of the turning circle manœuvre, it is difficult to compare results with the plot of fig. 5.16. The bar chart of fig. 5.19 present the 1st and 2nd overshoot angles from the results of the zig-zag heading angles, making it easier to compare results. As can be seen from fig. 5.19, the different propeller models have no effect on the 1st and 2nd overshoot angles. By examining fig. 5.20 it is seen that the drift angle oscillates between $\approx 4.5°$ and $\approx -4.5°$. It is the author's conjecture, that the period is too small to show any discernible difference when compared to the other institution's results. As further work, it may be interesting to plot a 20-20 zig-zag manœuvre, which would have a larger period, to determine if this conjecture is true.

5.3 Standard Manœuvres for the *KCS*

This Section shows results from some standard manœuvres carried out by the *SiS* Simulator on the *KCS*. The author has been unable to find any independently verified manœuvring results on the *KCS*, and so the results of this Section are more for information than anything else.

It can be seen from observations of the previous Sections, that the results of the

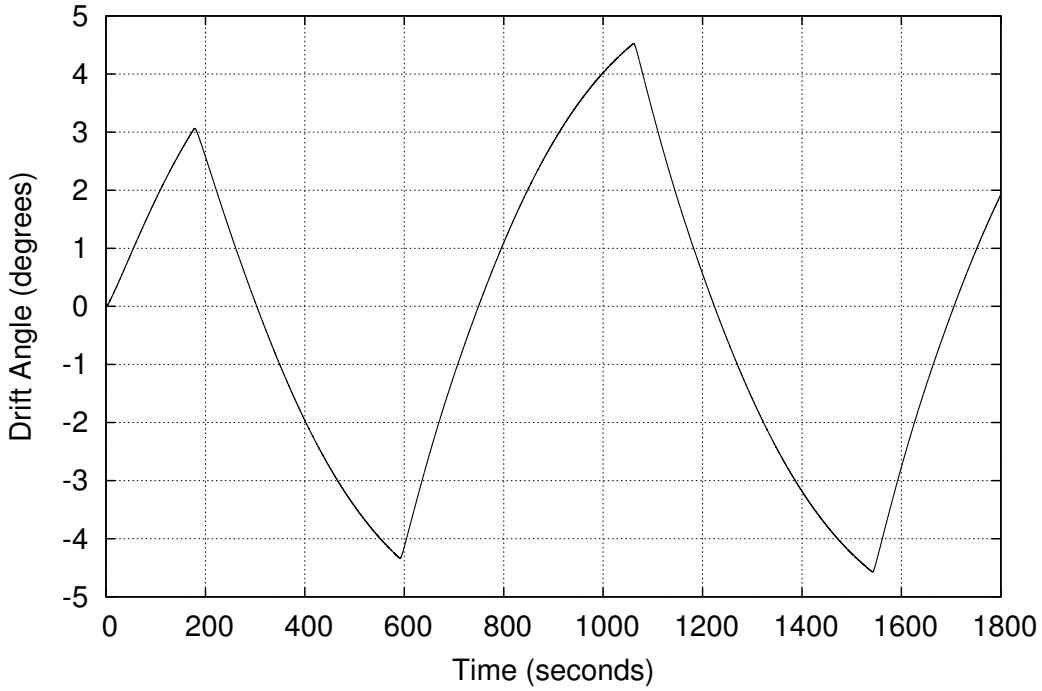

Figure 5.20: Local drift angle at propeller of *Esso Osaka* during 10-10 Zig-Zag Manœuvre

manœuvres for the *KCS* follow similar trends to that of the *Esso Osaka*.

5.3.1 Turning Circle Manœuvre

Figures 5.21, 5.22, 5.23 and 5.24 show results for a 35° starboard turning circle as performed by the *KCS* on the *SiS* Simulator. The approach speed was 15 knots.

For the sake of completeness, figs. 5.25, 5.26, 5.27 and 5.28 show plots from a 35° port turning circle, with an approach speed of 15 knots. These plots have been calculated using the $OOVOO$ propeller model of the *SiS* simulator.

5.3.2 10-10 Zig-Zag Manœuvre

Figures 5.29, 5.30, 5.31 and 5.32 show results for a 35° starboard turning circle as performed by the *KCS* on the *SiS* Simulator. The approach speed was 15 knots.

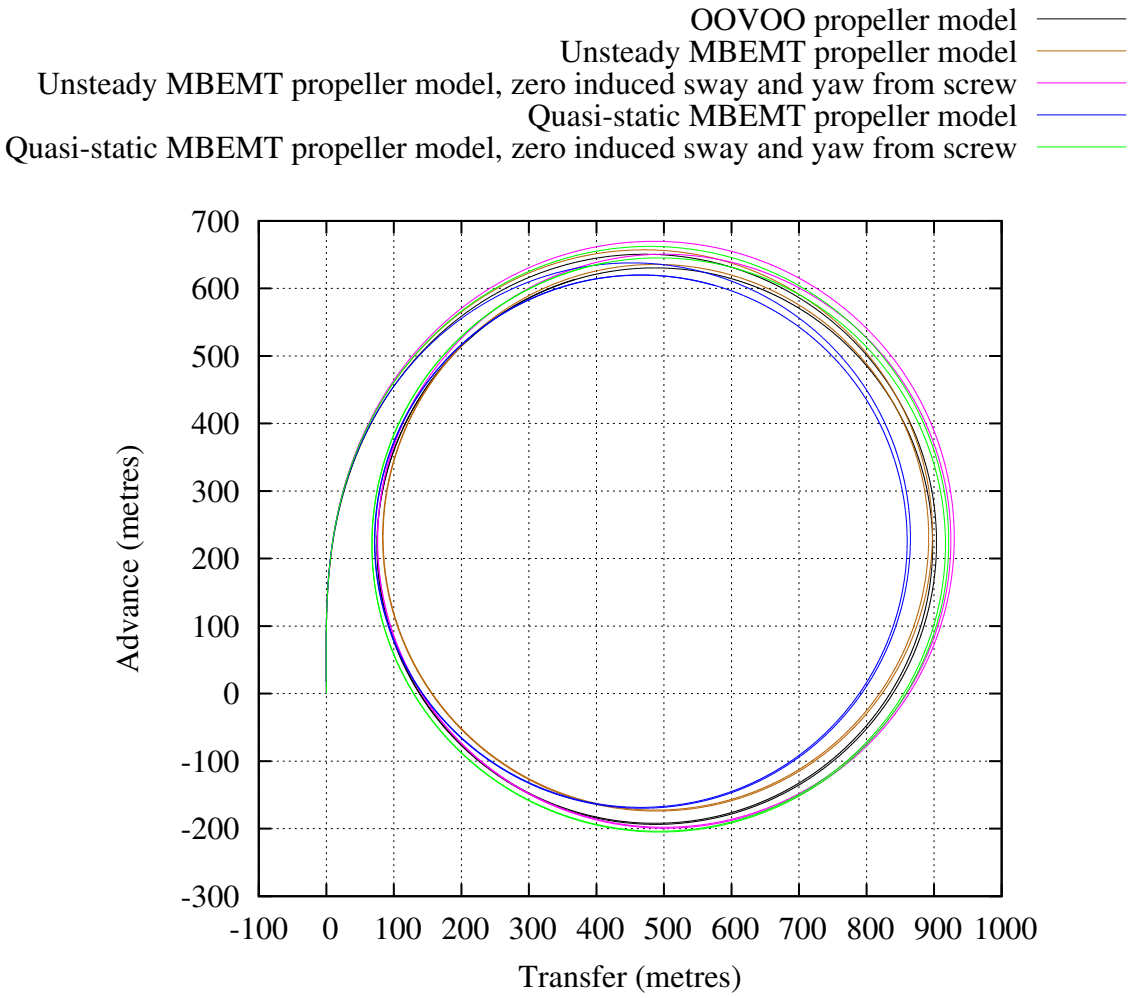

Figure 5.21: Track of 35^o starboard turning circle (V = 15.0 knots)

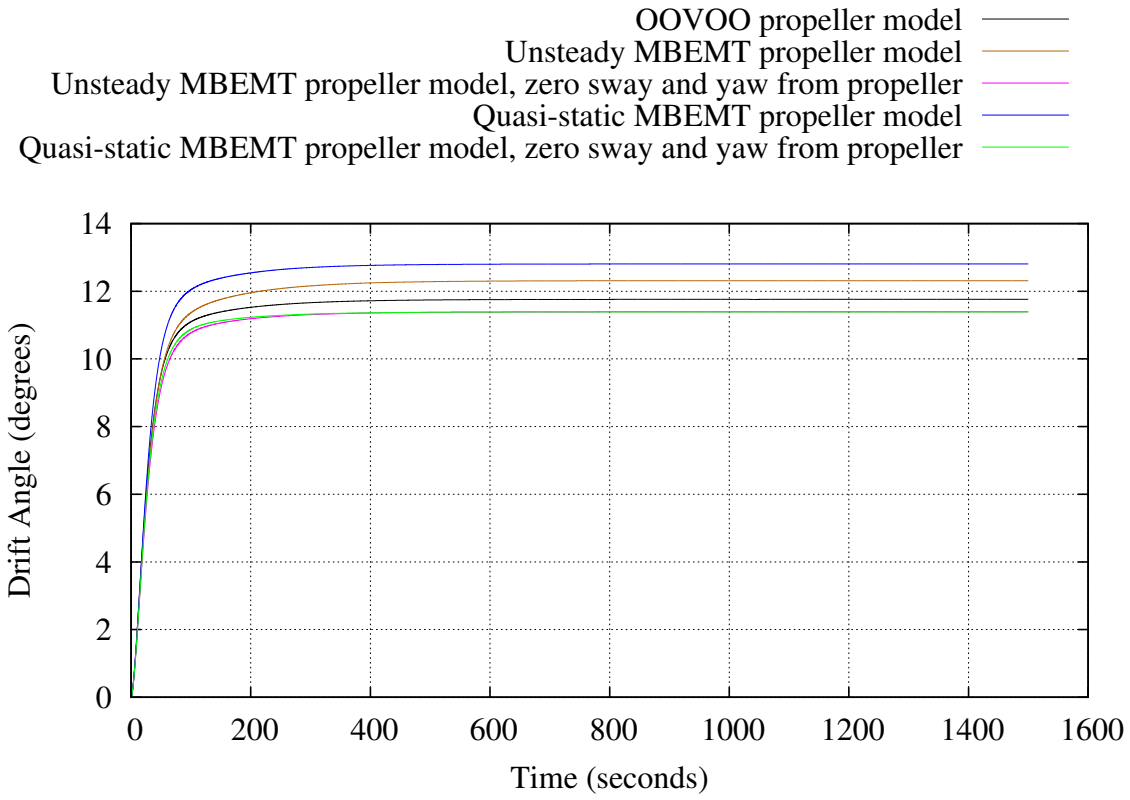

Figure 5.22: Drift Angle Time History of 35^o starboard turning circle (V = 15.0 knots)

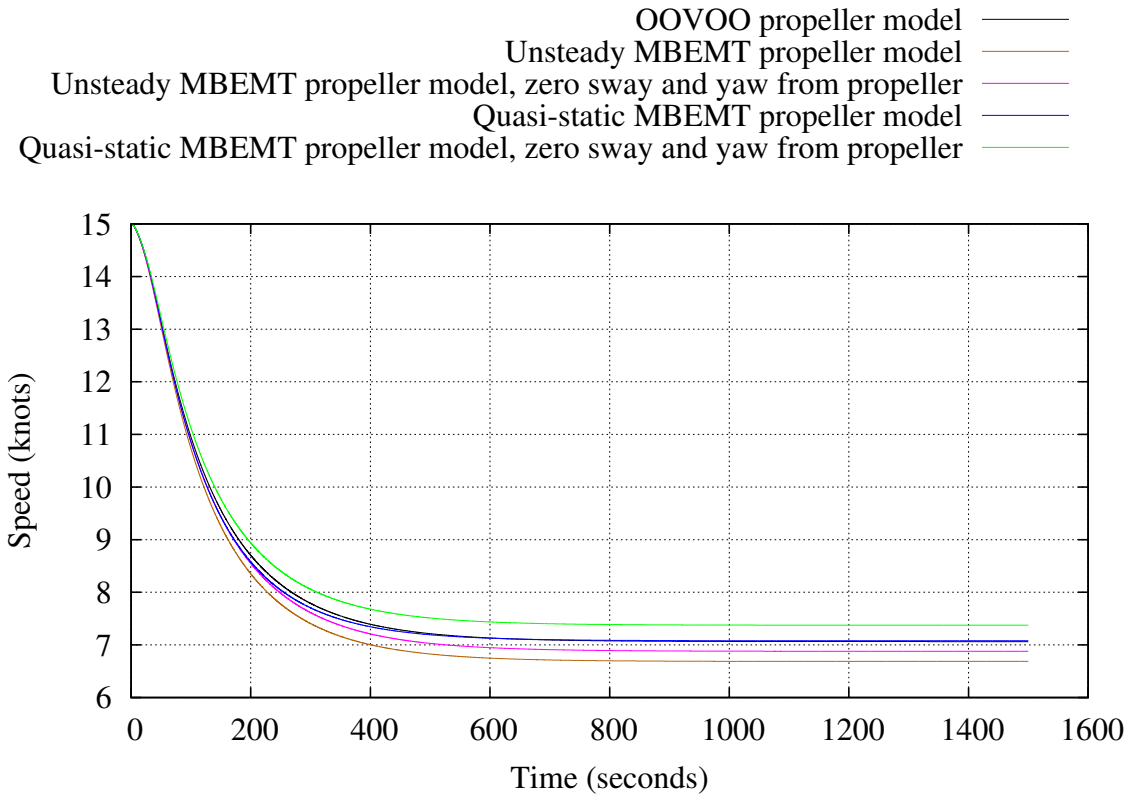

Figure 5.23: Speed Time History of 35^o starboard turning circle (V = 15.0 knots)

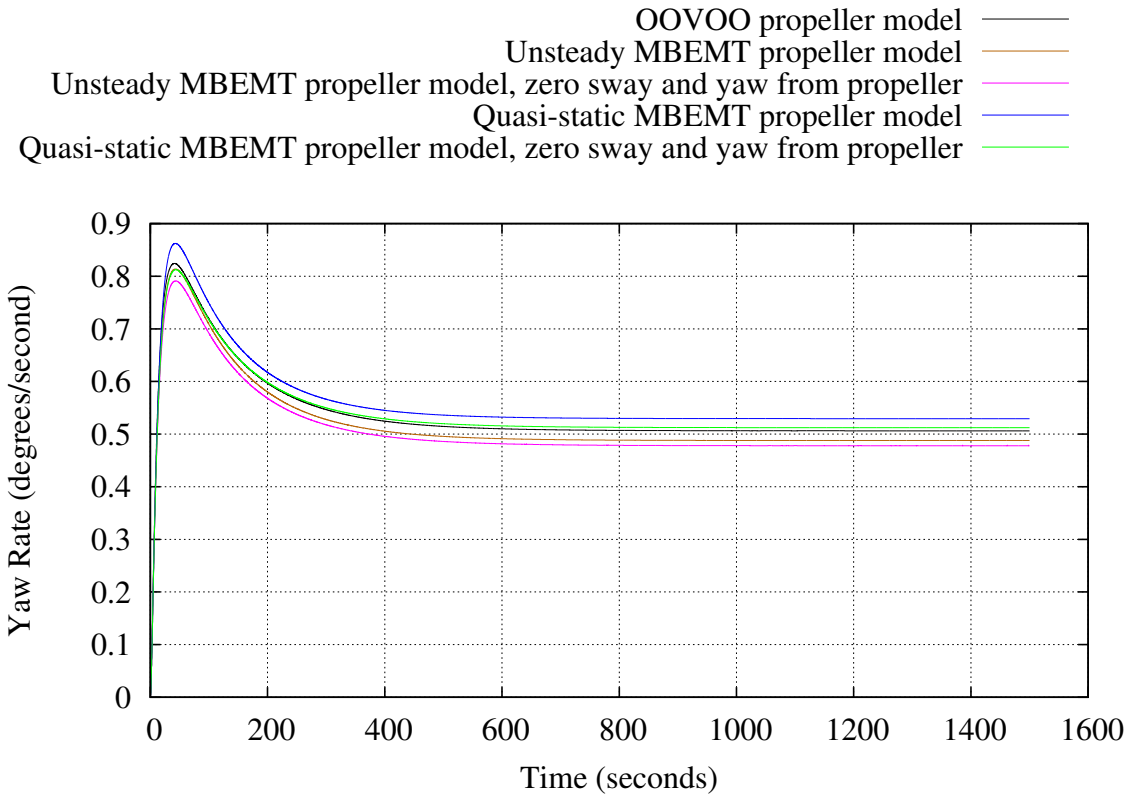

Figure 5.24: Yaw Angle Time History of 35^o starboard turning circle (V = 15.0 knots)

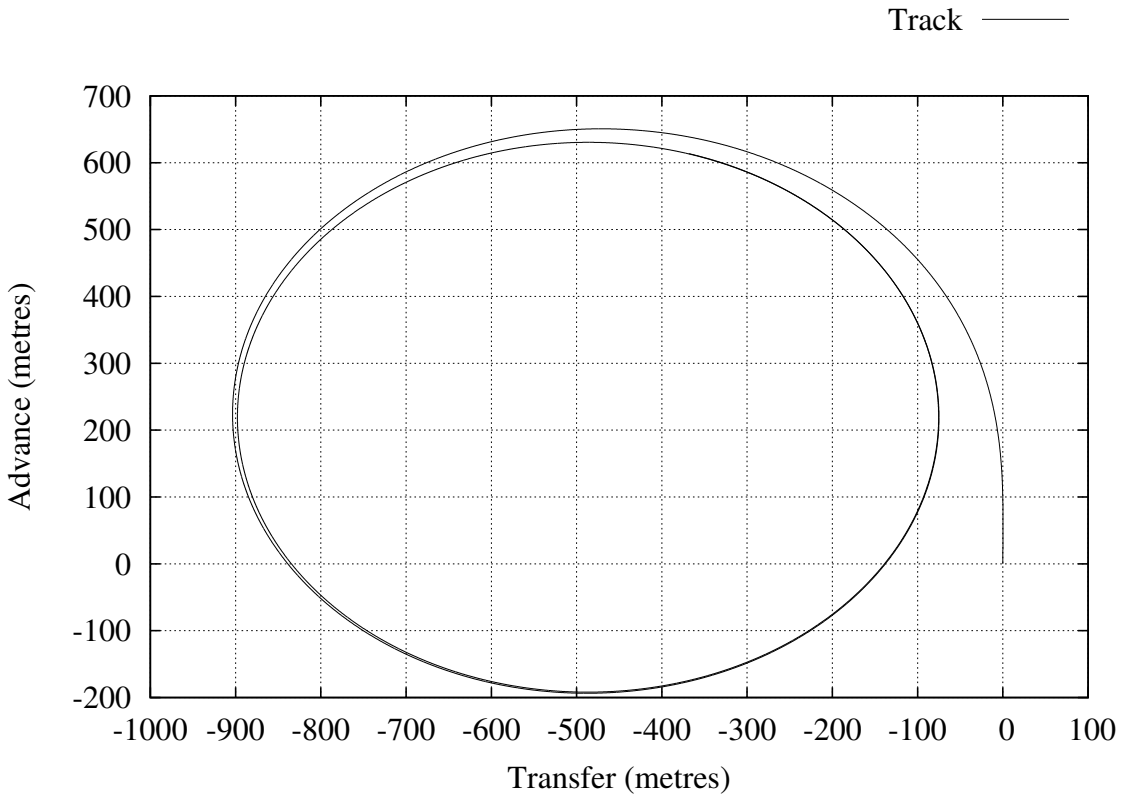

Figure 5.25: Track of 35^o port turning circle (V = 15.0 knots)

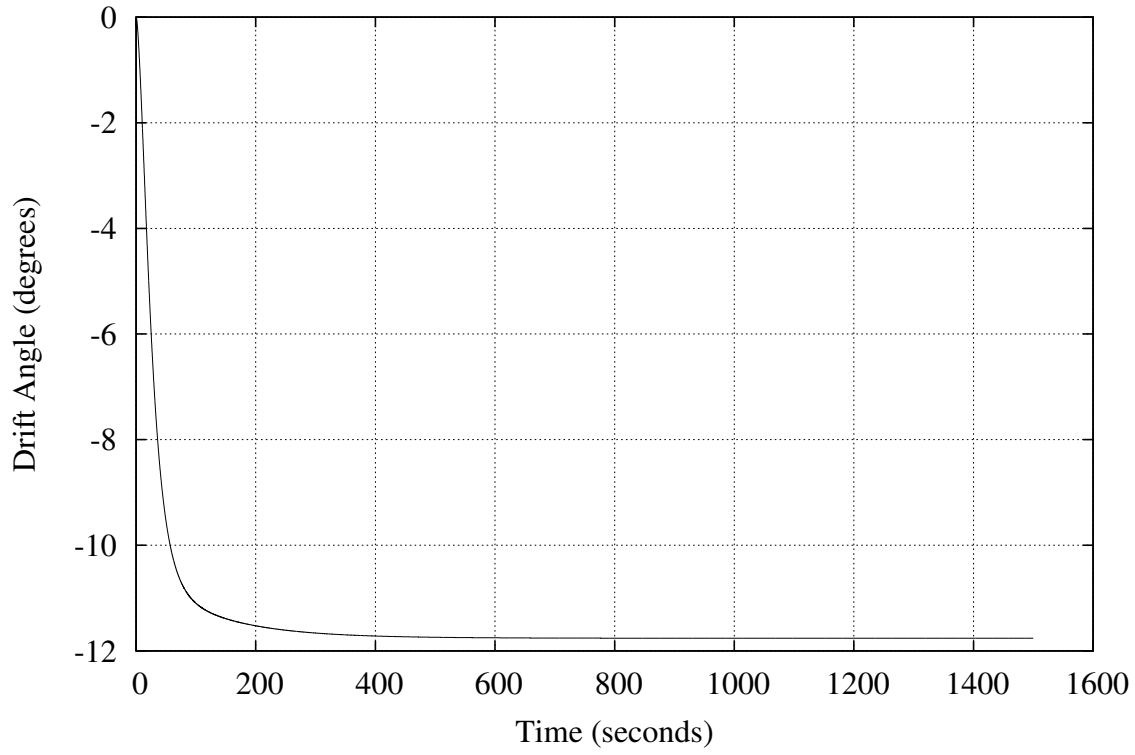

Figure 5.26: Drift Angle Time History of 35^o port turning circle (V = 15.0 knots)

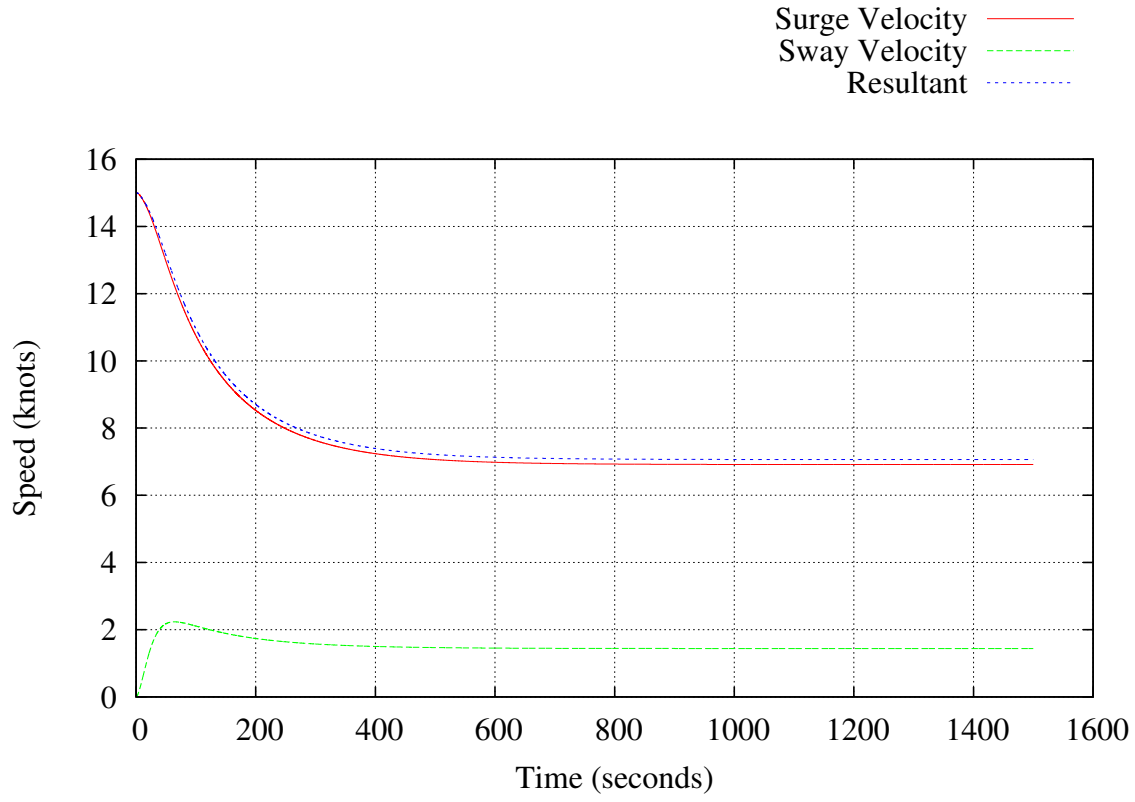

Figure 5.27: Speed Time History of 35^o port turning circle (V = 15.0 knots)

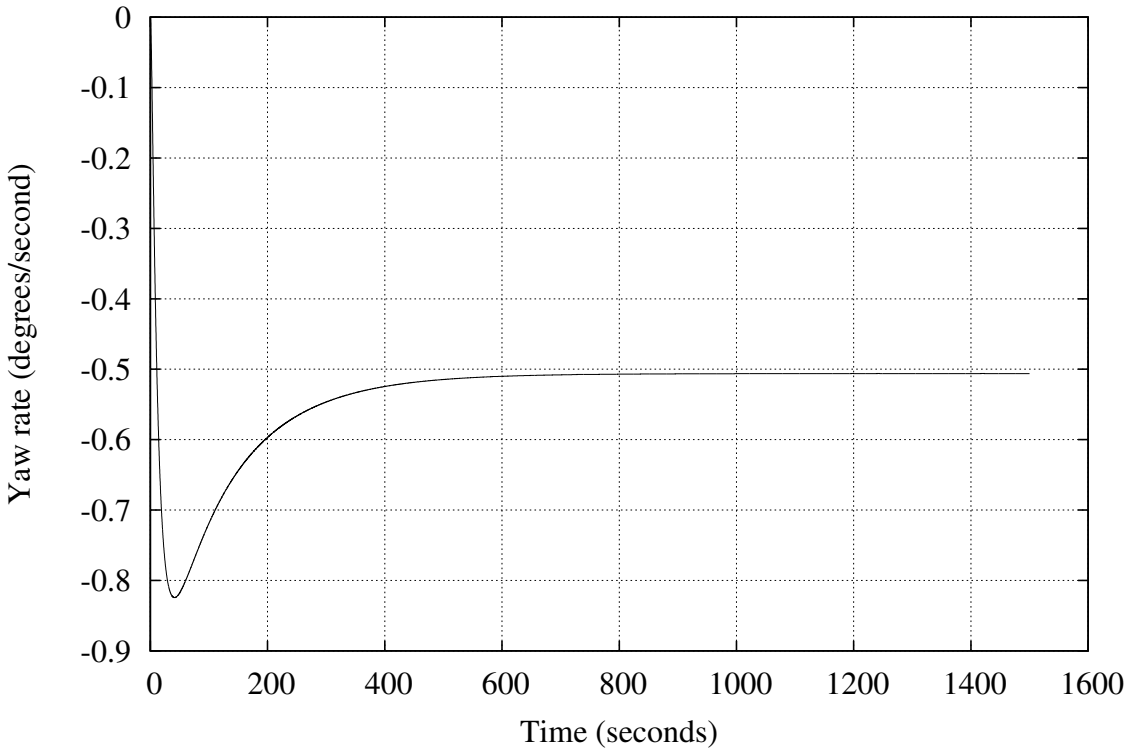

Figure 5.28: Yaw Angle Time History of 35^o port turning circle (V = 15.0 knots)

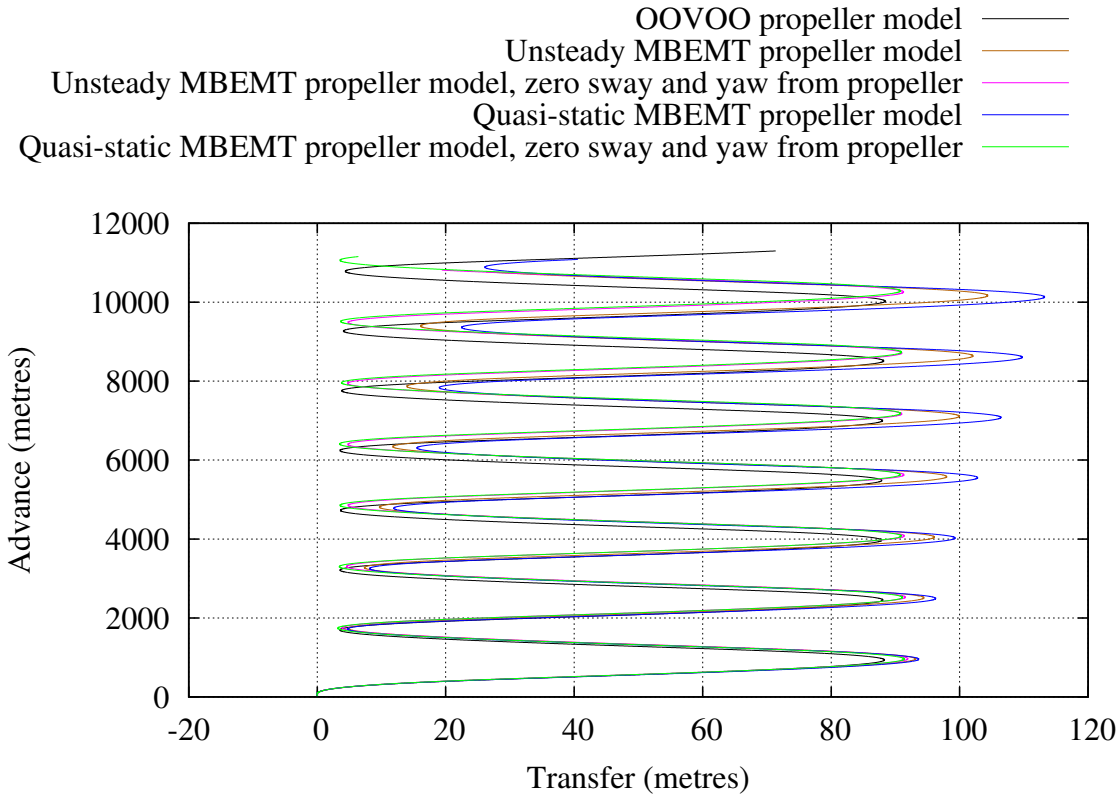

Figure 5.29: Track of 10-10 Zig-Zag manœuvre (V = 15.0 knots)

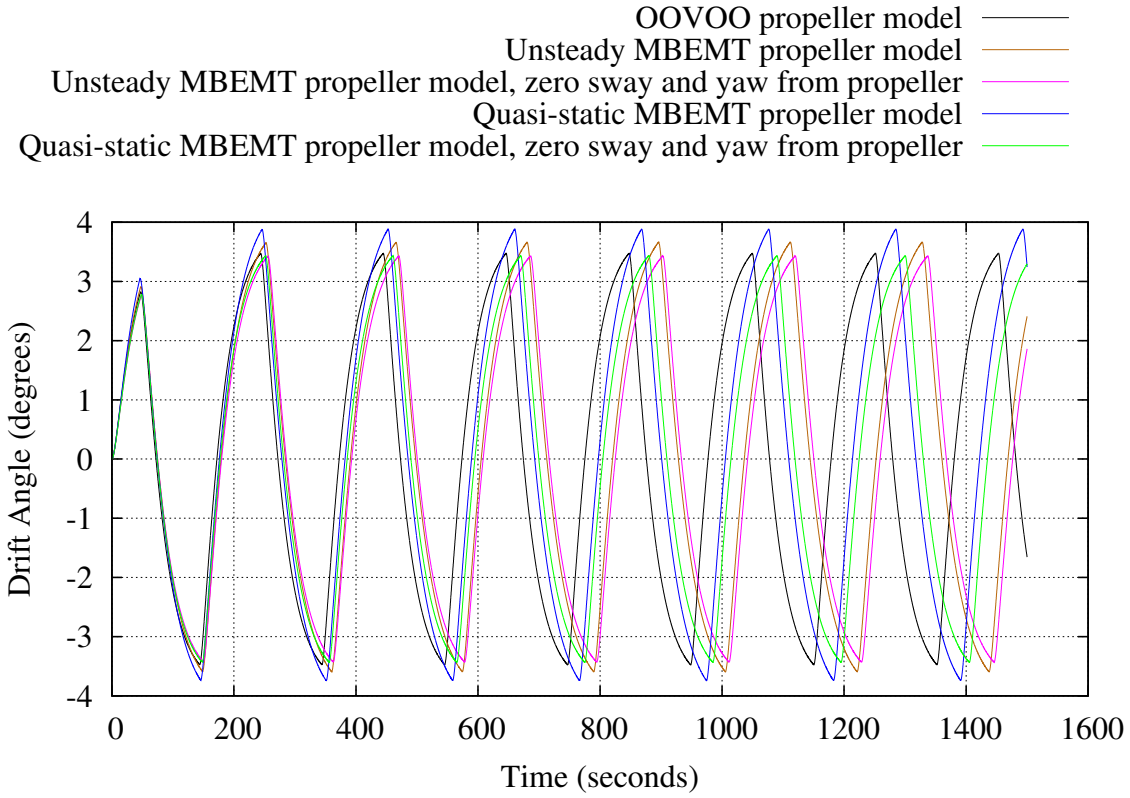

Figure 5.30: Drift Angle Time History of 10-10 Zig-Zag manœuvre (V = 15.0 knots)

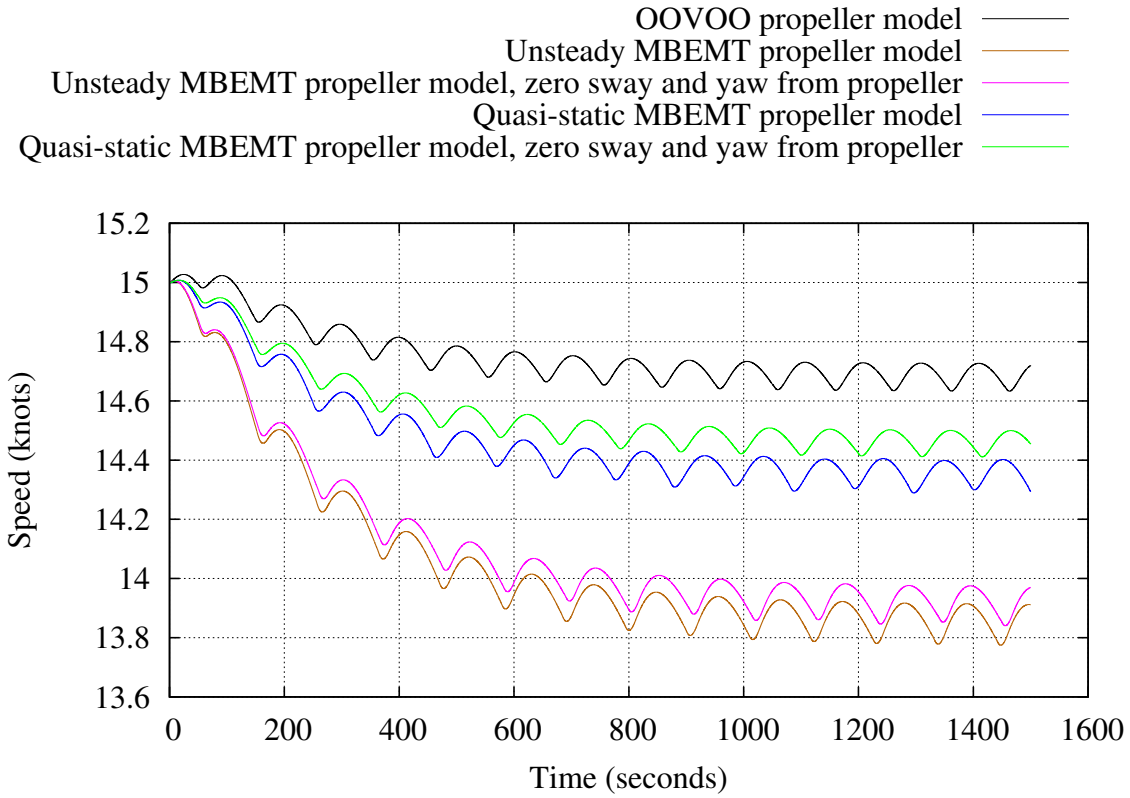

Figure 5.31: Speed Time History of 10-10 Zig-Zag manœuvre (V = 15.0 knots)

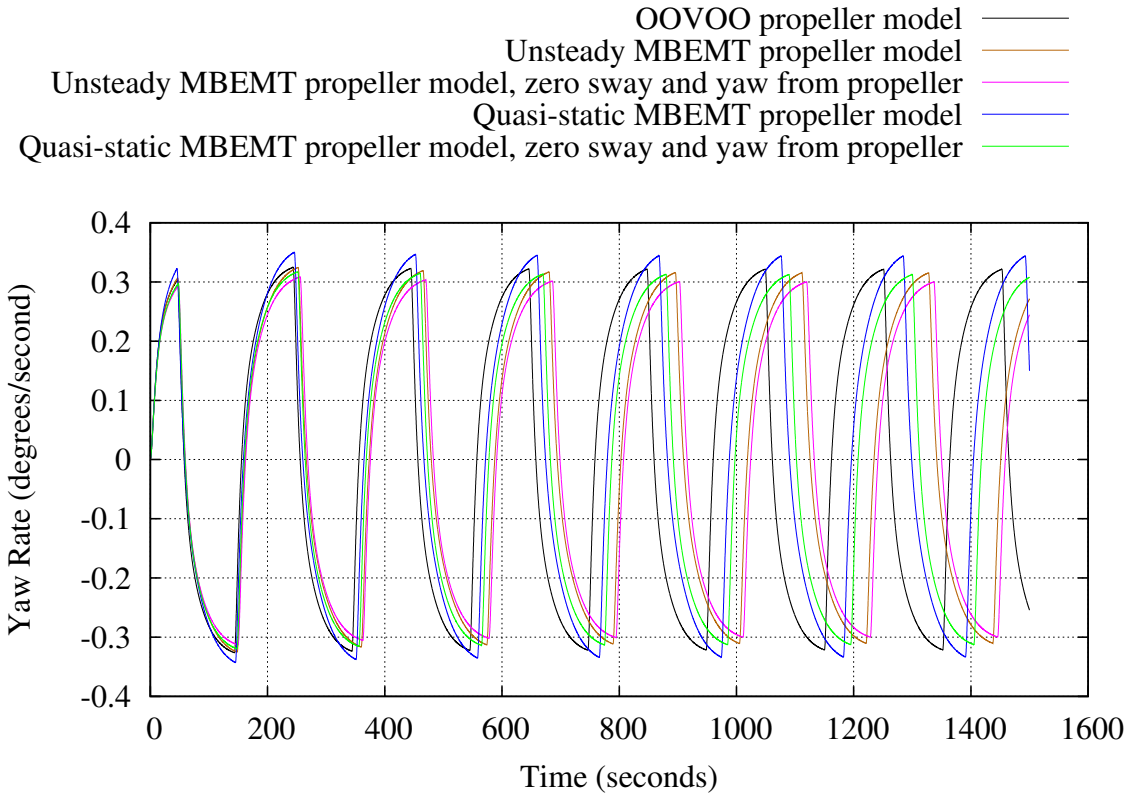

Figure 5.32: Yaw Angle Time History of 10-10 Zig-Zag manœuvre (V = 15.0 knots)

5.4 Summary

The results of the specially developed *SiS* ship manœuvring simulator have been presented when the *Esso Osaka* is run with a 35° starboard turning-circle, and 10-10 zig-zag manœuvres. The results from the *SiS* simulator are compared to ones obtained from various other research institutions and sea-trials and found to be consistent.

The turning-circle and zig-zag manœuvres were carried out using a propeller model which neglects incoming oblique flow angle (the $OOVOO$ model), a propeller flow model which accounts for oblique flow, but not its dynamic effects (the quasi-steady $MBEMT$ model) and a propeller flow model which accounts for oblique flow and its dynamic effects (the unsteady $MBEMT$ model). To ensure that each propeller model has the same "baseline" figure, that is, the same characteristics when operated in flow that is purely perpendicular to the propeller plane, the two $MBEMT$ models are calibrated to that of the $OOVOO$ model.

By observation of turning circle plots, it can be seen that the impact on ship manœuvring of including the induced sway force and yawing moment from a propeller are not inconsiderable. The difference in a ship's manœuvring behaviour from including unsteady flow in the propeller model is also seen to affect results.

The *SiS* simulator is shown to behave as expected and can now be used to run analysis on the basis ships when they are sailing in realistic scenarios, which is the subject of the next Chapter.

Chapter 6. Simulation Methodology and Results

Conventionally when a basis propeller is selected for a particular ship, the manœuvring motion of the ship is neglected (and hence the dynamic effects of the seaway). In this research, the effect of a ship's manœuvring motion on a propeller's performance is taken into account.

The aim of this Chapter is to show how a propeller can be selected from using a flow model that accounts for the manœuvring motion of a ship, that has an higher overall efficiency compared to a model that just accounts for "dead ahead" flow (i.e. flow arriving perpendicular to the propeller plane).

To achieve this aim, the following objectives are met.

- A description of what is meant in this research by the term *propeller optimisation*.
- A method of selecting an optimum propeller is presented.
- Case studies are developed which show how the *SiS* simulator can be used as an optimum propeller selection tool.
- Results are shown from the output of the *SiS* simulator of these case studies. The simulator records the time-history of the motions of a ship (and velocity vectors at the propeller) when the ship is sailing in realistic weather conditions in the motions of surge, sway and yaw.
- Analysis of fuel consumption and CO_2 emission savings for an unsteady propeller flow model over a "dead ahead" model are presented.

Section 6.1 defines the term "optimum propeller" as used in the context of this research, and details the process of selecting an optimised propeller. Section 6.2 describes how the developed *SiS* manœuvring simulator is used in conjunction with the propeller models set forth in Chapters 3 and 4 to select an optimum propeller for a ship sailing in her expected environment. Section 6.2 also presents

the development of case studies which illustrates how comparisons are made between the propeller flow models. Section 6.3 presents the results of the case studies, in terms of propeller geometry, efficiency and power requirements. Section 6.4 portrays the calculations of fuel saving, and thereby CO_2 emissions from the different case studies.

It is emphasised that this is not a design process per se (id est designing blade sections for ideal angle of attack, ensuring separation-free flow conditions with the lowest flow drag losses), but a selection process for a basis propeller, the design of which can then be further optimised for a particular ship's hull.

As mentioned in Chapter 1, two ship types are specifically examined in this study, a loaded VLCC, the *Esso Osaka* and a container carrier, the *KCS*. Both these ships have been determined, by the process described in Section 3.4.1, to be directionally stable. This is an important aspect to consider in order to avoid excessive rudder movements, and associated drag. Example input files for the *SiS* simulator, for these two ships can be found in Section A.2.

The route that is being examined assumes that the wind is blowing from a constant direction with respect to North, and a constant mean speed. In a practical application, actual wind conditions can be obtained from statistics as described in Chapter 2.

6.1 The Optimisation Strategy

Throughout this section, the word *selection* is used interchangeably with *optimisation* as the process selects the "best" propeller (in terms of efficiency) from a propeller series. This selected propeller can then be further optimised using techniques such as wake adaptation for the particular hull in question. This further optimisation process is not addressed in this study due to extensive experiments required on a propeller behind a hull, ideally at various drift angles. The author has been unable to obtain wake field data for ships at drift angles and believes that if they indeed exist, they are not in the public domain.

The process of selecting an optimised basis propeller is as follows:

A first approximation of a propeller design must be obtained, so it can be run through the simulator and analysed to see how it performs in service conditions. This initial propeller is obtained from optimising around calm water resistance

calculations obtained from Holtrop and Mennen (1982) and Holtrop (1984). The propeller's main parameters (Z, a_E, P/D) are then run through the simulation. The environmental conditions that a ship experiences are not calm weather and so the propeller's efficiency will not be equal to the initial design when running in weather. From the output of the simulator (that is, required thrust, speed of advance and drift angle at the propeller), a new optimised propeller is chosen. This propeller's parameters are passed to the simulator module and the simulation run again. Because the propeller is different, the output from the simulation will be different, and thus an iterative procedure takes place of optimising the propeller, then running it in the simulator, until the efficiency from the previous run is within tolerance of the present run.

6.1.1 The Process of Optimised Propeller Selection

To analyse a propeller's performance, certain main parameters are required to be known. If the diameter of the ship's propeller is not supplied to the input file of the *SiS* simulator, then the propeller diameter for bulk carriers and tankers is assumed to be 65% of the draught, and for container ships 74% of the draught Molland et al. (2011). These are maximum diameter limits that can safely be installed (restrictions on diameter are imposed to avoid unduly high pressure pulses and vibration on the ship's hull). The maximum diameter is capped at 10.0 m, as at the time of writing, it is challenging to manufacture a propeller over 10 m diameter.

Generally, the larger the diameter of propeller that can be employed, the higher the efficiency attained, so, in this analysis, propeller diameter for each basis ship is kept constant at it's maximum limit. The reason behind the association of large diameter and high efficiency can be explained by considering equation 6.1.

$$\begin{aligned} \eta_o &= \frac{\text{Propulsive Power Out}}{\text{Shaft Power In}} \\ &= \frac{T \times V_a}{Q \times 2\pi n} \end{aligned} \tag{6.1}$$

To maximise the open water propeller efficiency, η_o, the propeller revolutions, n need to be low, whilst maintaining the required thrust. Now, from examining equation 6.2, to maintain the required thrust and speed of advance, V_a, whilst

keeping the revolutions low, implies a large diameter.

$$T = \rho V_a^2 D^2 f\left(\frac{nD}{V_a}\right) \tag{6.2}$$

To determine the optimum propeller, it is necessary to obtain the optimum propeller rotation rate for a given propeller diameter, knowing the required thrust (obtained from the simulator). The speed of advance at the propeller is also obtained from the simulator. As only the required thrust, propeller diameter and speed of advance are known, the unknown values of thrust coefficient, K_T and rotation rate n of equation 6.3a cannot yet be calculated. However, the value for $\frac{K_T}{J^2}$ can be calculated, following equations 6.3:

$$K_T = \frac{T}{\rho n^2 D^4} \tag{6.3a}$$

$$J = \frac{Va}{nD} \tag{6.3b}$$

$$\frac{K_T}{J^2} = \frac{T}{\rho V_a^2 D^2} \tag{6.3c}$$

Referring to fig. 6.1 a scheme to calculate the optimum propeller is described as follows.

The expanded blade area ratio a_E is incremented from 0.3 to 1.5 (the range of the standard B-Screw series propellers). For each value of a_E, K_T, K_Q, $\frac{K_T}{J^2}$ and open water propeller efficiency, η_o are calculated over a range of J and P/D and recorded in an array. Each propeller in the array is then checked for excessive cavitation. In the case of the $OOVOO$ propeller model, this can be easily achieved by comparing the present value of a_E to the minimum value for a_E to avoid cavitation as obtained from Keller (1966), however, the validity of this formula starts to break down when a ship reaches a speed of about 24 knots (the service speed of the KCS), so the charts developed by Burrill (1963) are used. When the simulation is run using the unsteady propeller model, the point at which excessive cavitation occurs is estimated from the method described in Section 4.5. This method is chosen over Burrill (1963) as it takes into account dynamic effects. If the propeller is found to cavitate excessively, then it is discarded by setting the value of $\frac{K_T}{J^2}$ to zero (so that it is not equal to the *required* $\frac{K_T}{J^2}$).

The cavitation criteria for merchant ship propellers from the work by Burrill is set to approximately 4% back cavitation. To ensure that cavitation criteria remain consistent between methods, a subroutine within `mbemt.f90` determines if 4% of

the blade's back is covered in cavitation, when used with the unsteady $MBEMT$ method.

Once a table of propeller characteristics has been generated over a range of J and P/D, for the particular value of a_E an array is populated containing possible propeller parameters that match the *required* value of $\frac{K_T}{J^2}$.

When the a_E has reached its final increment, the propeller with the highest efficiency is selected from the array of possibles.

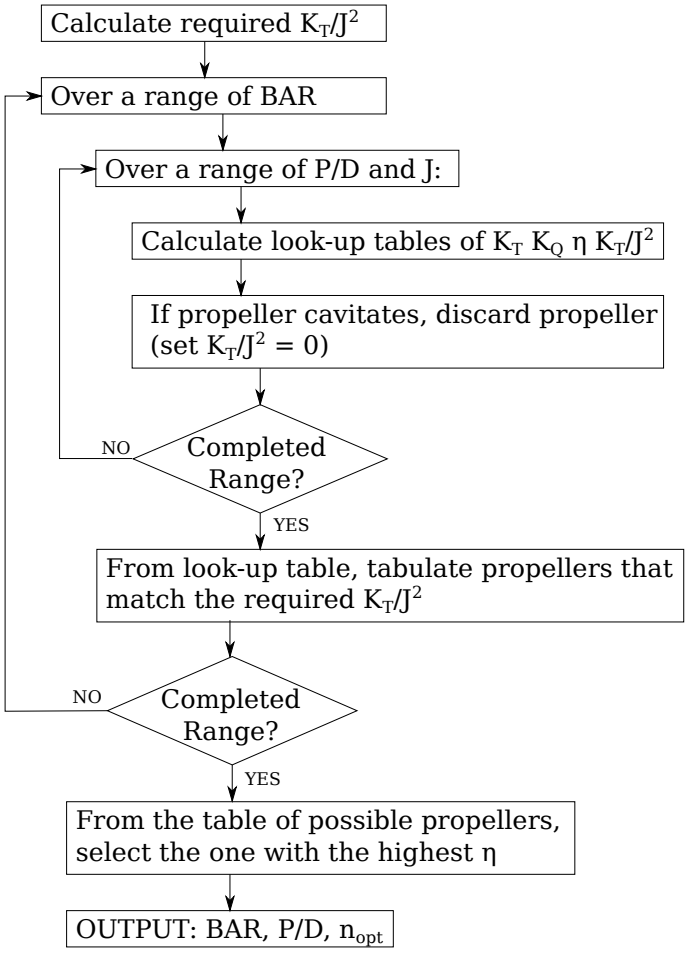

Figure 6.1: Propeller Optimization Algorithm

6.2 Methodology of Simulations with Different Propeller Models

This section details a method of investigating how accounting for the manœuvring motion and unsteady flow into the propeller can result in a different basis propeller selection, compared to one selected on the "dead ahead" concept. "Dead ahead" in this context meaning that the angle of incoming flow due to the ship's drift angle

is neglected, and therefore, any dynamic effects due to the blade's acceleration at this inclined flow is also neglected.

To recapitulate, the $OOVOO$ model calculated thrust and torque from the propeller using the polynomials developed by Oosterveld and van Oossanen (1975). This model does not take into account any oblique inflow angle to the propeller that may result from a ship's drift angle, and thus does not model any dynamic effects from the blade's acceleration with respect to incoming flow. The $OOVOO$ model also neglects any sway or yaw imposed on the ship from the propeller's action. This model works on the "dead ahead" principle.

The unsteady $MBEMT$ model accounts for oblique inflow angle, the dynamic effects of the blade's acceleration with respect to the incoming flow, and sway and yaw induced on a ship from the propeller's action.

A set of three case studies has been developed for each of the two basis ship types (making a total of six cases). For ease of reference, the cases are summarised in Table 6.1

Case Number	Description
1	*Esso Osaka*, propeller is optimised based on $OOVOO$ model.
2	*Esso Osaka*, propeller is optimised based on unsteady $MBEMT$ model.
3	*Esso Osaka*, propeller selected from Case 1 is run using the unsteady $MBEMT$ model and analysed.
4	Same as case 1, but run on the *KCS*.
5	Same as case 2, but run on the *KCS*.
6	Same as case 3, but run on the *KCS*.

Table 6.1: Case studies for propeller selection analysis.

The three case studies are explained in more detail, viz.

1. The first case represents the selection of a propeller optimised for the environmental conditions in which the ship is expected to experience, as output from the *SiS* simulator. The simulation considers the manœuvring motion of the ship, but neglects any sway or yaw induced by the propeller. The propeller model only accounts for the flow arriving at the propeller from directly in front of it (i.e. perpendicular to the propeller plane), and therefore also neglects any dynamic effects due to the propeller accelerating into/away from the incoming oblique flow.

2. The second case better represents what is happening in reality. An optimised propeller is selected for the environmental conditions in which a ship is expected to experience (the same as in the first case). This case however considers the manœuvring motion of the ship, sway and yaw induced by the propeller, and the dynamic effects from a propeller working in oblique flow.

3. The third case is a simulation run on a ship in the environmental conditions in which she is expected to sail (the same as Case 1 & 2). This case differs from the other two in that it does not select an optimised propeller, but rather analyses an existing one. The propeller that this case analyses is the one that Case 1 selected to be the most efficient, however, like Case 2, this case considers the manœuvring motion of the ship, sway and yaw induced by the propeller, and the dynamic effects from a propeller working in inclined flow. This case highlights the difference in propeller performance from selecting a propeller based upon "dead ahead" conditions, compared to when accounting for effects of oblique flow.

So, in short, Case 1's propeller is optimised on the dead ahead flow model, Case 2's propeller is optimised accounting for oblique flow, and Case 3 represents how the propeller from Case 1 would fair in oblique flow. (A ship's propeller is conventionally designed from the perspective that flow is dead ahead).

The environmental conditions for each case study are identical. A mean wind speed of 20 knots (a fresh breeze) is coming from the West.

Both ships are expected to maintain their service speed, and maintain a course due North. The service speed of the *Esso Osaka* is 10 knots, and the service speed of the *KCS* is 24 knots.

6.3 Results

Full time-history plots of simulation output can be found for all the case studies in Appendix C.

It should be noted that during the simulation, at time $t = 0$, the forces and moments from the environment are instantaneously applied to the particular ship in question. This will result in an initial transient that will settle down, once the automatic pilot and speed control have re-established the set point. Due to imperfections in the simple automatic controllers that have been implemented in

the study, towards the end of the run, the ship will respond quickly to try to correct for a relatively small error. This sudden correction results in another transient stage at the end of the run.

The results that occur between the end of the initial transient and the beginning of the final transient are denoted the quasi-steady results. To avoid the initial and final transients from biasing the results, it is these quasi-steady results that are further analysed and recorded in this Chapter.

It is noted that, depending on route and environmental conditions, a ship will usually never reach a steady state, due to the unsteady nature of the environment, hence the term 'quasi-steady results'. The quasi-steady results are the ones taken between the initial and final transients of the simulation run, so very roughly the middle third of the voyage. The stop time of the simulation was chosen so that there would be adequate time to collect results during this middle third of the voyage.

Tables 6.2 and 6.3 show the results from the Cases listed in Table 6.1. They summarise how the propeller's main parameters change, depending on which propeller model is used (Cases 1 and 2), and shows the difference when the optimised propeller from Case 1 is run using a method which accounts for oblique flow (Case 3). The main engine's brake power required to propel the ship at her service speed is also included in the table.

	Esso Osaka		
	Case 1 Optimisation base on dead-ahead *OOVOO* model	**Case 2** Optimisation base on unsteady MBEMT model	**Case 3** Analysis of propeller from Case 1 run with unsteady MBEMT model
Z	5	5	5
$D(m)$	9.1	9.1	9.1
$P(m)$	7.69	6.95	7.69
a_E	0.643	0.692	0.643
$\overline{\eta_{p_o}}$	0.513	0.520	0.511
Required $\overline{P_B}(kW)$	7696.89	7645.53	7782.29
$\overline{J}$	0.477	0.419	0.488
$\overline{n}$(rpm)	50.629	54.047	50.509

Table 6.2: Results from running the *SiS* simulator on the *Esso Osaka* for different case studies.

As can be seen from Tables 6.2 and 6.3, cases 2 and 5 have the highest efficiency

	KCS		
	Case 4 Optimisation base on dead-ahead *OOVOO* model	**Case 5** Optimisation base on unsteady MBEMT model	**Case 6** Analysis of propeller from Case 4 run with unsteady MBEMT model
Z	5	5	5
$D(m)$	7.9	7.9	7.9
$P(m)$	8.09	9.25	8.09
a_E	0.863	0.471	0.863
$\overline{\eta_{p_o}}$	0.640	0.656	0.641
Required $\overline{P_B}(kW)$	40120.27	38040.023	39302.24
$\overline{J}$	0.964	0.813	0.744
$\overline{n}$(rpm)	106.20	90.662	98.99

Table 6.3: Results from running the *SiS* simulator on the *KCS* for different case studies.

(and therefore the lowest required power), meaning that a propeller which has been selected using a propeller model which accounts for oblique flow fairs better than a one optimised for dead-ahead flow, but operated in oblique flow (cases 3 and 6).

The *Esso Osaka* has a higher propeller thrust loading compared to the *KCS*, which is why she has a lower open-water propeller efficiency. Compared to the dead-ahead case, the thrust loading will increase further in in-service conditions, due to a full form ship moving through the water at an oblique angle. This requires the propeller to develop relatively more revolutions compared to the case of the *KCS*.

Inspecting Table 6.3 for the *KCS*, it is seen that the propeller revolutions are reduced, due to the extra thrust arising as a consequence of oblique flow into the propeller. (This oblique inflow angle is far greater for the *KCS* compared to the *Esso Osaka*. The *KCS*'s drift angle is approximately 1.5°, whereas the *Esso Osaka*'s is approximately 0.5°.) The main engine therefore does not need to produce as much thrust, reducing the propeller loading, which in turn reduces the risk of cavitation, which in turn reduces the required expanded blade area ratio, a_E, reducing the frictional resistance of the blades. All these effects result in an increase of the efficiency of the newly proposed propeller, compared to the more conventional method.

The open water propeller efficiency gain from selecting a propeller from a model which accounts for oblique flow for the *Esso Osaka* (i.e. the percentage difference

between case 2 and 3) is $\frac{0.520-0.511}{0.511} = 1.761\%$

The open water propeller efficiency gain from selecting a propeller from a model which accounts for oblique flow for the *KCS* (i.e. the percentage difference between case 5 and 6) is $\frac{0.656-0.641}{0.641} = 2.340\%$

6.4 Fuel and CO_2 Emissions Savings

The specific fuel consumption of an engine will vary depending on whereabouts in the engine load diagram the operating point is (c.f. fig. 2.6). This operating point will vary dynamically as the engine load varies throughout the course of the ship's voyage. To obtain an accurate forecast of fuel consumption and emissions output, it is necessary to incorporate a sophisticated engine simulator into the manœuvring simulator, the scope of which is beyond this study.

To simplify the fuel and CO_2 emissions calculations, it is assumed that the mean quasi-steady main engine's brake power results in the mean quasi-steady values for fuel consumption and CO_2 emissions.

To calculate the CO_2 emissions from a fuel, the Carbon content of the fuel must be multiplied by the ratio of molecular weight of CO_2 to the molecular weight of C, that is 44:12.

The Carbon content of Heavy Fuel Oil (HFO) (ISO 8217 Grades RME through RMK) is 84.93%, therefore, 1 gramme of HFO produces $0.8493 \times \frac{44}{12} = 3.1141$ grammes of CO_2 when fully combusted.

If it is assumed that the specific fuel consumption (SFC) vs. brake engine power output trend is similar to all slow-speed engine manufacturers (referring to figs. 6.2 and 6.3), that is, constant over the range of brake power from the different case studies, then the comparative differences in fuel consumption between case studies are independent of the value of SFC, and therefore engine manufacturer.

6.4.1 Esso Osaka

A Wärtsilä RTA82T is chosen as an example of an engine that has the necessary requirements to satisfy the propulsion of the *Esso Osaka*. Referring to fig. 6.2, obtained from Wärtsilä (2013b), the specific fuel consumption is regarded to be a constant of $166g/kWhr$ over the range of brake power output from case studies 1, 2 and 3. This fuel consumption can be equated to grammes of CO_2 produced per

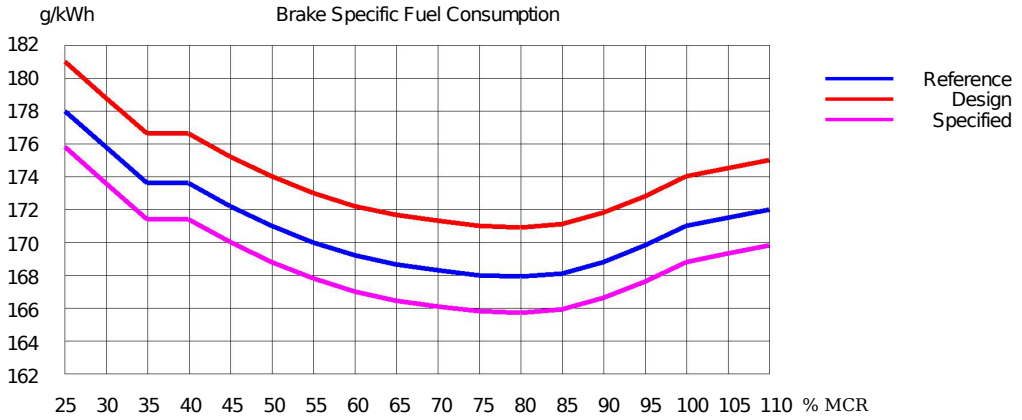

Figure 6.2: Brake specific fuel consumption for 6 cylinder RTA82T, suitable for the *Esso Osaka* (obtained from Wärtsilä (2013b)).

	Case Study		
	1	2	3
Required $P_B(kW)$	7696.89	7645.53	7782.29
Fuel Consumption (t/hr)	1.278	1.269	1.292
CO_2 Produced (t/hr)	3.979	3.952	4.023

Table 6.4: Fuel Consumption and CO_2 Emissions for the *Esso Osaka*

$kWhr$.

$$CO_2 \text{ produced}/kWhr = 166 \times 3.1141$$
$$= 516.94 g/kWhr$$

Table 6.4 summarises the fuel consumption and CO_2 emissions from the cases described in Section 6.2.

The saving in fuel for the *Esso Osaka* from selecting an optimum propeller for in-service conditions using an unsteady $MBEMT$ model compared to the "dead ahead" $OOVOO$ model (and run in service conditions) (i.e. the percentage difference between cases 2 and 3) is $\frac{1.292-1.269}{1.292} = 1.780\%$. The corresponding CO_2 emissions savings $\frac{4.023-3.952}{4.023} = 1.765\%$

6.4.2 KCS

An RTA82C from Wärtsilä is chosen as an example of an engine that has the necessary requirements to satisfy the propulsion of the *KCS*. Figure 6.3 shows the

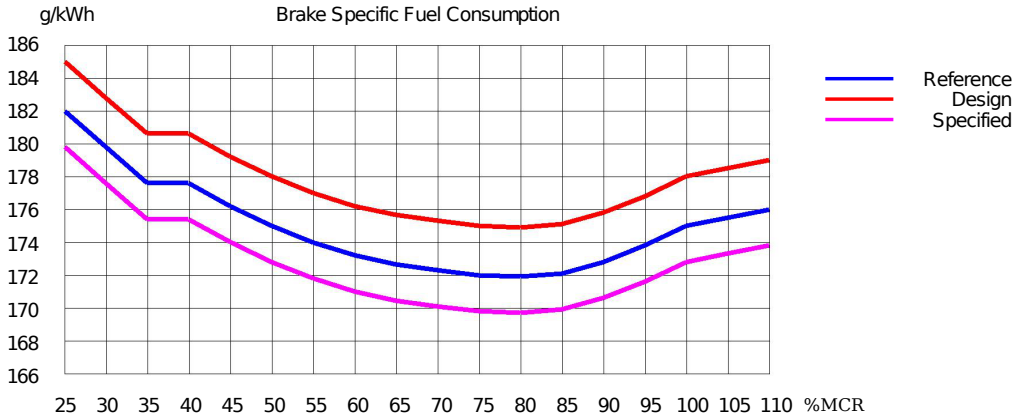

Figure 6.3: Brake specific fuel consumption for 10 cylinder RTA82C, suitable for the *KCS* (obtained from Wärtsilä (2013b)).

	Case Study		
	4	5	6
Required $P_B(kW)$	40120.27	38040.02	39302.24
Fuel Consumption (t/hr)	6.820	6.467	6.681
CO_2 Produced (t/hr)	21.240	20.138	20.807

Table 6.5: Fuel Consumption and CO_2 Emissions for the *KCS*

specific fuel consumption, as calculated from Wärtsilä's General Technical Data (Wärtsilä, 2013b). Referring to fig. 6.3, over the range of brake power output from Case Studies 4, 5 and 6, the specific fuel consumption is regarded to be a constant of $170g/kWhr$. This fuel consumption can be equated to grammes of CO_2 produced per $kWhr$ in an identical manner to that for the *Esso Osaka*.

$$\begin{aligned} CO_2 \text{ produced}/kWhr &= 170 \times 3.1141 \\ &= 529.40g/kWhr \end{aligned}$$

Table 6.5 summarises the fuel consumption and CO_2 emissions from the cases described in Section 6.2. The saving in fuel for the *KCS* from selecting an optimum propeller for in-service conditions using an unsteady $MBEMT$ model compared to the "dead ahead" $OOVOO$ model (and run in service conditions) (i.e. the percentage difference between cases 5 and 6) is $\frac{6.681-6.467}{6.681} = 3.203\%$. The corresponding CO_2 emissions savings $\frac{20.807-20.138}{20.807} = 3.215\%$

6.5 Discussion of Results

Figures 6.4, 6.5 and 6.6 summarises the comparison of the two different propeller selection strategies described in the previous section. Briefly, the two different propeller strategies are:

1. Based on the assumption that flow is moving from bow to stern, parallel to the ship's centreline (this is the conventional perspective of initial propeller selection).

2. Based on a model which accounts for oblique flow into the propeller plane, representing the drift angle which a ship will attain whilst travelling in her expected environmental conditions.

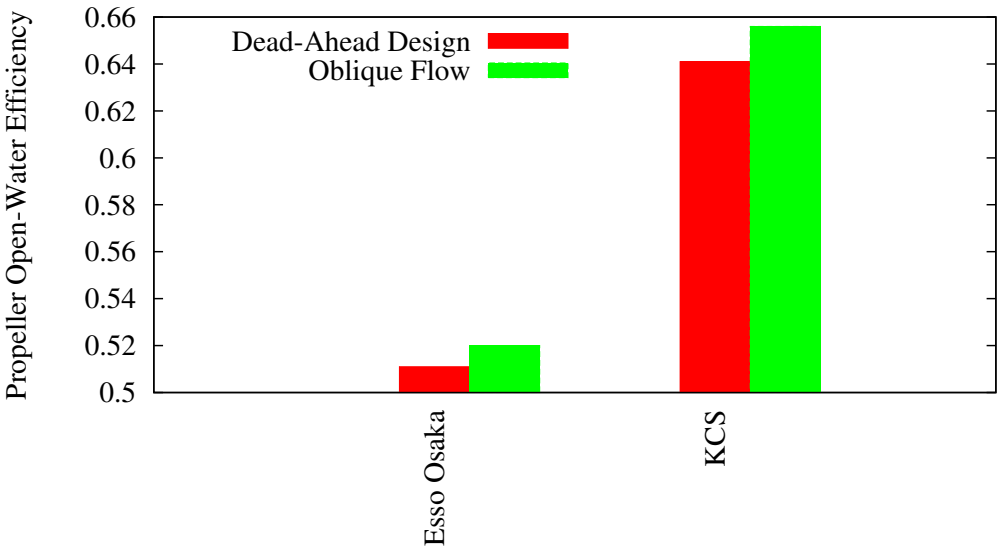

Figure 6.4: Comparison of optimised open-water propeller efficiency from accounting for, and neglecting a ship's drift angle in propeller selection.

As can be seen from fig. 6.4, for both the *Esso Osaka* and the *KCS*, the open-water propeller efficiency is higher for the propeller which has been selected from the model which considers oblique flow. The *KCS* has a relatively higher efficiency gain over the *Esso Osaka*.

A significant difference between the two ships is their motion response to the environment in which they are operating. The environmental factors were identical for the two ships, yet, due to the larger above-water area of the *KCS*, it attains a higher drift angle when underway, compared to the *Esso Osaka*. The larger drift

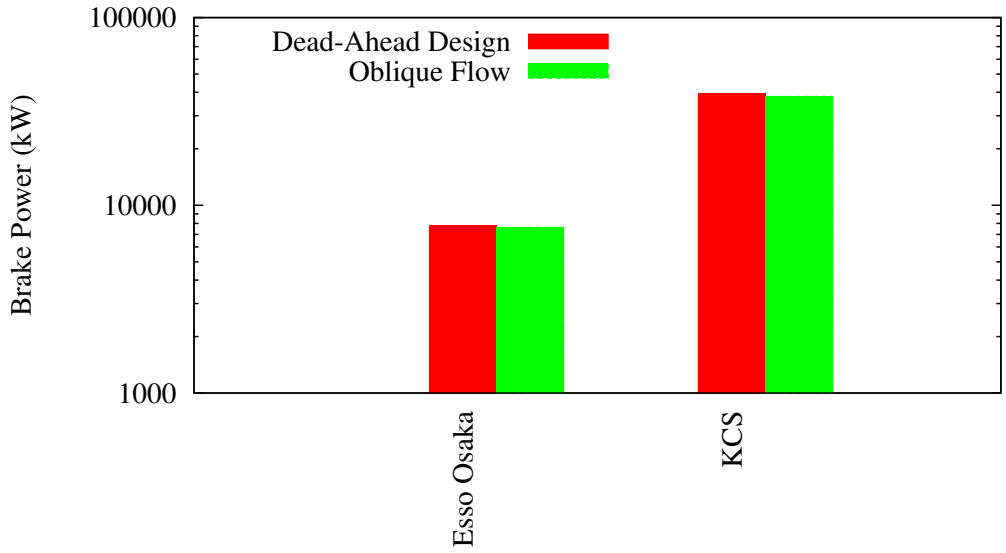

Figure 6.5: Comparison of required brake power from accounting for, and neglecting a ship's drift angle in propeller selection.

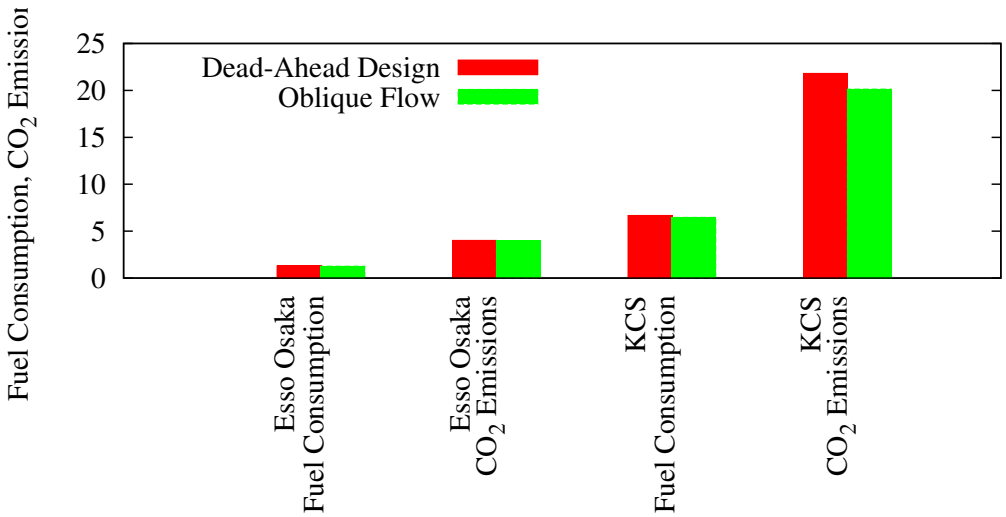

Figure 6.6: Comparison of fuel consumption and CO_2 emissions from accounting for, and neglecting a ship's drift angle in propeller selection.

angle relates to a larger angle of inclined flow at the propeller plane. Figure 6.4 suggests that ships which are more susceptible to larger drift angles could benefit more from the proposed propeller selection methodology, compared to ships which tend to attain low drift angles. (Time-history of drift angles and other results can be found in Appendix C).

From fig. 6.5, it can be seen that the propeller which has been selected from the model which accounts for oblique flow results in a ship which requires less brake power, compared to one whose propeller has been selected on the dead-ahead

principle (as expected from the conclusions drawn from fig. 6.4). Again, the *KCS* has a relatively higher improvement over the *Esso Osaka*.

From fig. 6.6, it is seen that, continuing the trend, the *KCS* fairs to a greater degree than the improvement of the *Esso Osaka*. In this plot, the reader is able to observe that there is a proportionately greater reduction in CO_2 emissions over fuel consumption. This is a significant result, as it means that an increase in propeller efficiency results in a proportionally larger reduction in CO_2 emissions. How large the proportion is depends on the required power (and therefore fuel consumption). The greater the required power, the higher the savings in CO_2 emissions.

Ships which will benefit the most from the proposed method of propeller selection, therefore, are ones which are susceptible to higher drift angles, and/or ones which require higher engine power.

It can be said that it is physically extremely challenging to measure differences in propeller efficiency of less than $\approx 2\%$, due to the uncertainties in calibration of measuring devices, bearing in mind shaft torsional stiffness is very rarely, if ever measured (Woodward, 2014). Although not physically measurable at the propeller shaft, a difference in propeller efficiency may manifest itself as a significant, measurable change in fuel consumption and CO_2 emission reduction. Of course, proving that this reduction in CO_2 emissions is actually attributable to an increase in propeller efficiency is perhaps even more challenging than measuring it at the shaft, as there are now many more processes to measure, each with their own degrees of uncertainty.

6.5.1 The Performance of the Newly Proposed Propellers in Calm Water, Trial Conditions

It is of interest to illustrate the performance of the propellers selected from the newly proposed methodology in the calm water, trials condition scenario. These results are presented in Sections C.7 and C.8 of Appendix C for the *Esso Osaka* and *KCS* respectively.

These calm water simulation runs were carried out using the Unsteady $MBEMT$ propeller model of the *SiS* Simulator. It can be seen that a very slight course correction from the autopilot is necessary. This is due to the fact that the sway force and yaw moment induced on the hull by the propeller is taken into

account.

The average, steady-state open-water propeller efficiency for the *Esso Osaka* is 0.531 when run in calm water, compared to that of 0.520 when run in service conditions.

The average, steady-state open-water propeller efficiency for the *KCS* is 0.672 when run in calm water, compared to that of 0.656 when run in service conditions.

These results are as expected, as the lower resistance experienced in the calm water environment results in lower propeller disc loading. Referring to equation 6.4, the lower loading requires less torque, resulting in a higher efficiency.

$$\eta_o = \frac{\text{Power Out}}{\text{Power In}} = \frac{TV_a}{2\pi Qn} \tag{6.4}$$

It may also be of interest to show how a propeller designed for calm-water trial conditions fairs in service conditions, however, at present, the *SiS* simulator when used with the Unsteady $MBEMT$ does not account for the thrust *lost* due to cavitation. It only gives the user an indication of cavitation inception (in order to reject any unsuitable propellers at the design stage).

6.5.2 Estimation of Sea-Margin using the SiS Simulator

This section shows a practical demonstration of how a simulator, like the *SiS* simulator, can give an estimate as to the sea-margin of a ship, which takes into account the most probable weather conditions. A more accurate sea margin enables more correct design points not only for the propeller (which is demonstrated in this research), but also allows for closer engine/propeller matching, resulting in further fuel consumption reduction.

Referring to Section C.2, Appendix C, the average quasi-steady state in-service resistance for the *Esso Osaka* is $915.190kN$. The calm-water resistance is $801.324kN$. This equates to a sea-margin of 12.44%.

Referring to Section C.5, Appendix C, the average quasi-steady state in-service resistance for the *KCS* is $2091.773kN$. The calm-water resistance is $1842.203kN$. This equates to a sea-margin of 11.93%.

Not knowing the real-life sea-margin (that is, not one based on rule-of-thumb or similar, but the actual difference in resistance between calm water and a typical voyage) it is not possible to state if the sea margins calculated above are

particularly accurate, however, the values are typical.

6.5.3 A Note on Computing Time

The time it takes to run a simulation depends upon a number of factors, perhaps the most influential being:

- the stop time of the simulation.
- the time step used in the calculations.
- the CPU speed and number of threads.

From profiling the *SiS* programme, it is seen that the vast majority of the CPU's time is spent in the `MINPACK` subroutines. It is difficult to quantify the ability of the `MINPACK` library to solve for the induced velocities in the $MBEMT$ routines. Some inflow vectors take longer to solve than others.

In the following analysis, the stop time of the simulation is 2800 seconds, with a time step of 0.1 seconds. The CPU was an Haswell-MB (Mobile) Intel® Core™i5-4200U CPU @ 1.60GHz × 4.

The Wall Time (that is, the time it takes as measured by a clock on the wall), for a turning circle to be performed using the $OOVOO$ propeller model was 2.55 seconds. For a turning circle performed using the Unsteady $MBEMT$ model, the wall time was 8264.13 seconds.

A typical Wall Time for a simulation run in service conditions for the *Esso Osaka* is 8471 seconds, whereas for the *KCS*, the Wall Time is 11453 seconds. This difference illustrates the extra degree of difficulty the `MINPACK` library has in converging to a solution under certain circumstances. It must be noted that this is for one run, or each iteration of the design loop.

From the above timings, it can be seen that the *SiS* Simulator when used with the $OOVOO$ propeller model, is well suited for adaptation in a real-time simulator, however, if the Unsteady $MBEMT$ model is to be considered for inclusion in a real-time simulator, mechanisms to speed up the computation time need consideration.

One method to speed up processing time would be to make use of the Graphics Processing Unit (GPU) of a personal computer, for example CUDA Parallel Computing (Nvidia, 2014). This process was not implemented in the current work,

as the present version is sufficiently fast for the author's purpose. The downside of this method, is that it is heavily hardware dependent requiring different libraries for different hardware.

6.6 Summary

This Chapter shows how a propeller can be selected using a flow model that accounts for oblique flow (as established by the manœuvring motion of a ship), which has an higher overall efficiency compared to a model that just accounts for "dead ahead" flow.

A definition of an *optimised propeller* in the context of this research has been specified, followed by a methodology of how a propeller is optimised for in-service conditions using the specially developed *SiS* simulator.

Case studies have been developed that show how the performance of a propeller varies in the same conditions depending on how completely the propeller model represents actual flow phenomena. Two ship types are analysed, the *Esso Osaka*, a VLCC, and a container ship, the *KCS*.

Results from running the case studies on the simulator are presented and fuel and CO_2 emissions savings are calculated.

It is shown that efficiency gains (and therefore fuel and CO_2 emission savings) can be made by selecting an optimised propeller using an unsteady $MBEMT$ model compared to a propeller that has been selected using a model which neglects the effects of a ship's manœuvring motion. Gains in efficiency and reductions in fuel consumption and CO_2 emissions from the proposed propeller selection methodology are presented in table 6.6.

	Esso Osaka	*KCS*
Open-water propeller efficiency gain (%)	1.761	2.340
Fuel consumption reduction (%)	1.780	3.203
CO_2 emissions reduction (%)	1.765	3.215

Table 6.6: % gain in Efficiency and % reduction in fuel consumption and CO_2 emissions from the newly proposed propeller selection methodology.

The results are encouraging, and suggest that the more susceptible a ship is to drift, the higher the potential efficiency gains from the newly proposed propeller selection method. It is also noted that if a ship has a relatively high required

power, even a small increase in propeller efficiency can manifest itself into a large CO_2 emission reduction.

Chapter 7. Conclusions, Further Work and Recommendations

The purpose of this Chapter is to present major achievements and conclusions that this study has identified, and further work that could be done to potentially improve upon the developed methods. It briefly revisits each Chapter of the Thesis, highlighting the aims and objectives and how they were met, novelty and achievements.

The aim of Chapter 1 was to give the reader an overview of the entire research study. It achieved this aim by defining the motivation driving this research, as well as the aims and objectives, and then went on to summarise the methodology used, which included a literature review of existing methods to predict manœuvring motions and propeller forces. It also provided a practical guide as to how the newly proposed propeller selection methodology can be used.

Main outcomes and achievements from Chapter 1 are listed as follows:

Primary objective: The overall aim of this research was to reduce the amount of Carbon Dioxide (CO_2) produced from operating ships. The approach taken by the Author to address this aim was to increase the efficiency (and thereby reduce fuel consumption and emissions) by selecting a propeller whose design-point better represents the conditions in which it is expected to operate.

Methodology outline: Conventionally, a propeller is selected on the assumption that a ship is sailing with zero drift angle. When a ship is in her natural environment it is likely that when she is full-away on passage, she will have attained some drift angle due to environmental forces and moments imposed on her.

The overall methodology of analysing, and accounting for the ship's motion response to her environment, in propeller selection has been sub-divided into

the following items.

- In order to obtain an estimate of the loading conditions on a ship's propeller whilst in her day-to-day operations at sea, a ship manœuvring simulator, coded in Fortran, (the Ship-in-Service, *SiS* simulator) has been developed by the Author. The effects of wind, waves and surface current are accounted for by the simulator, and automatic controllers are used to maintain the ship's speed and desired course.

  The *SiS* simulator estimates a ship's motion in the horizontal plane of surge, sway and yaw. This plane is considered to be the most influential to the outcome of propeller efficiency, as, when a ship is in a seaway, the average drift angle is likely to be non-zero, whereas the other motions (with the exception of roll) are likely to average near zero.

- A numerical model is required to calculate the propulsion characteristics of a propeller, while considering the manœuvring motion of a ship in a seaway. This Chapter concluded that, for the purposes of this study, a heavily modified Blade-Element-Momentum theory model would be most appropriate, due to its fast computation time (the routine needs to be called at every time-step of the simulation).

- A unique and novel methodology has been developed which selects an optimum propeller from a standard B-Screw series for a ship which is travelling along her intended route, encountering the most probable weather conditions.

- Case studies have been developed which show how the efficiency of a propeller fairs from the newly proposed method of propeller selection, compared to conventional methods.

The approach of using a simulator to obtain loading conditions for use as design points is believed to be novel. It is the first time, to the best of the Author's knowledge, that the procedures outlined in this Thesis have been assembled in such a way as to produce a robust method of selecting an optimised propeller which accounts for the manœuvring motion of a ship sailing in an environment in which she is expected to encounter.

The aim of Chapter 2 was to describe the environment which a ship will

encounter, how this environment affects the ship, and how a ship's controls need to respond in order for her to arrive at her intended destination on time. It achieved this aim by presenting differences between trial-conditions (calm water) and in-service conditions, outlining wind, wave and surface current forces and moments and how these can be obtained from statistics. The Chapter went on to explain how these external forces tend to alter a ship's desired speed and course, and hence the loading.

Main outcomes and achievements from Chapter 2 are listed as follows:

- Although it is imperative that a ship passes her sea-trials (due to IMO regulations and owner's requirements), the ship will very rarely operate in calm water, trial conditions, devoid of any weather. This Chapter has demonstrated from an example, that once a ship's propulsion system is operated away from her design point, the efficiency of the system will diminish. It is therefore more economical and environmentally friendly to design the propeller about a point which it is most likely to operate at. This fact raises the issue that a design optimised around expected service conditions will perform sub-optimally when run during sea-trials.

- This Chapter illustrated that it is possible to get an estimate of the sea-margin from the use of a simulator. This is believed to be a novel concept, making it possible to predict powering requirements with a greater degree of fidelity over conventional, rule-of-thumb methods for sea-margin estimates.

- It was also shown that to avoid excessive fuel consumption and exhaust gas emissions, it is important to match the loading requirements of the propeller to the power output of the main engine.

The aim of Chapter 3 was to describe how the motions of a ship, and the environment in which she is operating, can be estimated from numerical models. This aim was achieved by describing a modular approach of representing forces and moments of hull, propeller, rudder and their interactions. It also presents models for forces and moments imposed on a ship from wind, waves and surface currents. System dynamics are also accounted for, so the rudder does not instantly attain its command, or the main engine's fuel rack does not provide an

instantaneous change of power. An automatic pilot is also described, which keeps the speed and course of a ship at her set point. All these models are in the form of ordinary differential equations, which are solved in the time domain using a forth order Runge-Kutta method.

Main outcomes and achievements from Chapter 3 are listed as follows:

- A modular approach allows different elements to be modified, without affecting other parts of the model (unlike a whole-ship approach). This makes it possible to develop new models (in this case a propeller model) and use the simulator as an analysis tool to estimate performance of those entities for a ship in manœuvring motion over her route.

- The propeller model depicted in this Chapter is based on the polynomials of Oosterveld and van Oossanen (1975), and as such ignore effects of a ship's motion (apart from dead-ahead surge). A new propeller model is therefore required which accounts for a ship's manœuvring motion.

- To assist in modelling propeller flow, various outputs from the simulator can be used, for example velocity vectors at the propeller plane.

- A simple PID controller has been implemented to counteract the effects of speed and course deviation due to the environment. The autopilot is an important component in overall propulsive efficiency, as excessive rudder movement results in greater drag. When comparing results from the newly proposed method of propeller selection, and the conventional method, the case studies (discussed in Chapter 6) have been put together in such a way as to keep weather conditions constant, and thereby autopilot movements constant, thus removing the autopilot as a component in the comparison of overall propulsive efficiency.

- The model which is used to estimate added resistance due to waves only considers loading in the pure surge direction. This has the effect of neglecting any leeway from the action of waves. In reality, the waves would indeed impart sway and yaw velocities to a ship, and so, to some extent, the present method under-predicts drift angle. The results indicate that, potentially, higher efficiency gains can be made over the published ones, due to this under-prediction of drift angles.

The aim of Chapter 4 was to produce a numerical model which would estimate the action of a propeller when accounting for flow arriving at the propeller plane from some oblique angle, as would happen on a ship sailing with a drift angle. It achieved this aim by explaining how the combined Blade-Element-Momentum Theory ($BEMT$) can be modified to account for oblique inflow angles, and then went on to develop the model further and account for unsteady flow effects from a propeller's blade accelerating towards and away from the incoming flow.

Main outcomes and achievements from Chapter 4 are listed as follows:

- It is observed that the general effects from inclined flow into the propeller plane result in an increase in thrust from the propeller, for a given power. This is due, in part, to an increased resultant velocity across the blade, but also from unsteady flow effects. The general blade-element-momentum theory has been adapted to account for this oblique flow.

- As a consequence of using the Modified Blade-Element Momentum Theory ($MBEMT$), the resulting force which acts perpendicular to the propeller shaft is estimated. This allows the effects of sway and yaw induced on a ship from propeller action to be accounted for, which was neglected in the previous model.

- As the propeller is working in oblique flow, the blades will be accelerating towards and away from the flow. It has been shown that these unsteady effects modify the sectional lift and drag, and can result in substantial differences between the dead-ahead flow scenario. A typical example for the dynamic lift coefficient being 20% higher than the static lift coefficient.

- The shape of a ship's hull will modify the flow into a propeller, also, when a ship is at some drift angle, the hull will cast a "shadow" over the propeller, resulting in modified velocity vectors at the propeller plane. These aspects are neglected in the present study, due to lack of available data of hullforms tested at different speeds and different drift angles. By neglecting these aspects, the results published from this work are expected to be somewhat different to actual results from a whole ship experimental model, however, the trend in results and overall outcome is not expected to change.

  Neglecting the modifications of a ship's wake due to her stern lines also has

the effect of normalising the variation in wake-field of different hullforms, removing any bias that an extremely efficient hullform has over an inefficient one.

Of course, certain flow modifications from the hull are accounted for in the model, such as wake (as a function of main ship geometry) and the modification of this wake due to drift angle.

- To balance the equations of thrust and torque, that is solve for the induced velocities in the $MBEMT$ model, a robust solver is required, as the component equations, especially the lift and drag terms, are non-linear, and can lead to instabilities. The minimisation algorithms from the MINPACK library (Moré et al., 1980), are successfully employed in this study to balance the thrust and torque equations.

- To ensure that changes in efficiency from different flow models yield the same results for the same propeller, the $MBEMT$ model is calibrated against the model from Oosterveld and van Oossanen (1975) (the $OOVOO$ model) at zero drift angle. This is achieved by adjusting parameters pertaining to lift and drag coefficients until the difference between the two models are within tolerance. At non-zero drift angle, then there will be a difference between the models, as the $OOVOO$ model neglects non-zero drift angle.

The developed unsteady $MBEMT$ propeller flow model was incorporated into the *SiS* simulator, producing a tool which can be used to analyse the performance of a propeller which accounts for the manœuvring motion of a ship. It is the first time, to the best of the Author's knowledge, that results have been published over a range of operating conditions, and for the full range of a propeller series using this method, certainly when considering unsteady flow effects. This is possibly due to the challenges involved in balancing the thrust/torque equations.

The aim of Chapter 5 was to provide the reader with a level of confidence that the mathematical models previously presented behave in an expected manner. It achieved this aim by showing results from the developed *SiS* simulator for a 35° starboard turning circle, and a 10-10 zig-zag manœuvre performed by the *Esso Osaka*. It compared these results with results from other institutions.

Main outcomes and achievements from Chapter 5 are listed as follows:

- It is demonstrated that, for zero drift angle, the characteristics for each propeller model are in close agreement, meaning that any difference between the models during manoeuvres is attributable to the degree of fidelity of the model, and the flow phenomena that they represent.

- The developed model is observed to behave in an expected manner, and deviation from trials results is in-line with other institutions.

- The effect of sway and yaw induced by the propeller is seen to be modelled correctly, as are the effects of unsteady flow.

- There is no discernible effect on the 1^{st} and 2^{nd} overshoot angles of the zig-zag manœuvre when using any of the developed propeller models. This implies that the directional stability of the *Esso Osaka* is not dependant on unsteady propeller flow, or induced sway or yaw arising from the propeller's action.

The aim of Chapter 6 was to show how a propeller can be selected from using a flow model that accounts for the manœuvring motion of a ship, which has an higher overall efficiency compared to a model that just accounts for flow arriving perpendicular to the propeller plane (the conventional propeller selection perspective). It achieved this aim by developing a new methodology of propeller selection, which includes a manœuvring simulator to predict propeller loading for the environment in which a ship is expected to encounter. Case studies are constructed which allow propeller efficiency comparisons between the newly proposed method, and the conventional approach.

Main outcomes and achievements from Chapter 6 are listed as follows:

- A scheme to calculate the optimum propeller geometry (given some known parameters as obtained from the simulator) is given. This is an iterative procedure, whereby a propeller selection process is successively run through the simulation until the optimised efficiency has converged.

- The developed case studies are designed to show the potential gain in efficiency from using the newly proposed selection process, over the conventional one.

- Two ship types were examined, a VLCC, the *Esso Osaka*, and a container ship, the *KCS*. The *Esso Osaka*'s open water propeller efficiency increased by 1.76%, from using the newly proposed propeller selection method, and the *KCS*'s open water propeller efficiency increased by 2.34%. This equates to a saving in CO_2 emissions for the *Esso Osaka* of 1.77% and 3.22% for the *KCS*.

- The results suggest that the more susceptible a ship is to drift, the higher the potential efficiency gains from the newly proposed propeller selection method.

- From further analysis of results, it is shown that if a ship has a relatively high required power, seemingly small increases in propeller efficiency can manifest itself as a large CO_2 emission reduction, and noticeable reductions in fuel consumption.

The results of this work show great potential for the reduction of CO_2 emissions from a propeller selection method which accounts for the manœuvring motion of a ship (that is, design which accounts for a ship's motion response in an environment in which she is expected to operate).

The ship simulator can be used as a valuable tool at the initial design stage, not only for analysing the ship's motions, but as a method of obtaining more realistic loading estimates (and therefore design-points) for a ship in her natural environment, rather than the usual synthetic calm-water plus sea-margin.

It must be noted that this research is considered to be in the proof-of-concept stage, actual values given in the results are expected to differ from physical experiments due to various simplifying assumptions, highlighted in the next Section. The Author is, however, confident that the inferences drawn and general outcome and conclusions are not expected to differ from physical experiments.

7.1 Suggested Further Work and Recommendations

It is shown that the nearer the design-point is to physical reality, and the greater the level of representing that physical reality, then the more efficient the design will be. If the operating profile of a ship is variable, then the different design points can be analysed, and a design with the highest *overall* efficiency obtained. To add more fidelity to the model presented in this Thesis, a number of recommendations for further work are made, viz.

This study has focused on the manœuvring motion of a ship in a seaway. In a true seaway, a ship will be subjected to six degrees of freedom, which should ideally be accounted for. The sea-keeping motions are, however, expected to have less impact on results in moderate sea conditions as their quasi-steady average is likely to be near zero (with, perhaps, the exception of roll, which is not expected to alter the flow-field significantly).

The modified combined blade-element momentum theory propeller model developed in this research provides a relatively low level of precision. Whilst suitable as a proof of concept, and initial analysis, it is unsuitable for blade section design. To further optimise a propeller (eg wake adaptation) using the technique described in this study, a flow model with a greater degree of precision, such as a panel method, should be used (at the expense of greatly increased computation time).

The analysis neglected the change in wake-field due to the ship's hull at oblique angles. The modified wake from the ship's hull is expected to alter the results somewhat, however, the general outcome is not expect to change. It is suggested that model experiments are designed and completed in a cavitation tunnel for a propeller-behind-hull configuration, in combined sea-keeping and manœuvring motion, to compare with the numerical model and highlight any discrepancies which require refinement.

The model that is used to predict added resistance due to waves only considers the added force in purely a longitudinal direction. In reality the waves will impart other forces and moments on the ship, including sway and yaw. It is expected that if a more realistic wave model is substituted for the present one, a ship will attain a somewhat greater drift (or leeway) angle than presently predicted, and therefore the energy savings are expected to be potentially higher than the ones presented.

A designer should concentrate on optimising for the in-service scenario, rather than the calm-water trials condition, if the design is to produce a minimum amount of Carbon Dioxide in service. The Energy Efficiency Design Index (EEDI) is a mechanism developed by the IMO to ensure that ships meet a required standard for CO_2 emissions. The EEDI is finalised from the results of sea-trials, now, if a ship is optimised around service conditions, it follows that it will perform sub-optimally at trial, perhaps leading to failure of EEDI requirements at trial, but in normal day-to-day operation surpass them. It is suggested that the

mechanism in which the EEDI is attained and verified is reviewed.

References

Abbott, I. H. A. and Von Doenhoff, A. E. *Theory of Wing Sections: Including a Summary of Airfoil Data*. Courier Dover Publications, 1959.

Abkowitz, M. A. Lectures on ship hydrodynamics - steering and maneuverability. Technical Report HY-5, Hydro and Aerodynamic's Laboratory. Lyngby, Denmark., 1964.

Abramowitz, M. and Stegun, I. A. *Handbook of Mathematical Functions with Formulas, Graphs, and Mathematical Tables*. Dover, ninth dover printing, tenth gpo printing edition, 1972.

Aertssen, G. Service performance and trials at sea. In *12th ITTC Performance Committee.*, 1969.

API. Recommended practice for planning, designing and constructing fixed offshore platforms - working stress design. Technical Report RP 2A-WSD, American Petroleum Institute, 2007.

Beddoes, T. A synthesis of unsteady aerodynamic effects including stall hysteresis. *Vertica*, 1:113 – 123, 1976.

Benini, E. Significance of blade element theory in performance prediction of marine propellers. *Ocean Engineering*, 31:957–974, 2004.

Betz, A. Schraubenpropellers mit geringstem energieverlust. *Nachrichten von der Gesellschaft der Wissenschaften zu Göttingen, Mathematisch-Physikalische Klasse*, 1919:193–217, 1919. In German, Appendix written by Prandtl, L.

Bisplinghoff, R., Ashley, H., and Halfman, R. *Aeroelasticity*. Dover Books on Aeronautical Engineering Series. Dover Publications Inc., 1996. ISBN 9780486691893.

Blendermann, W. Wind loading of ships - collected data from wind tunnel tests in uniform flow. Technical Report 574, Institut für Schulungsmaßnahmen, University of Hamburg, 1996.

Bowditch, N. *The American Practical Navigator*. Defense Mapping Agency Hydrographic/Topographic Center. Bethesda, MD., 2002.

Burrill, L. C. Propeller cavitation: Further tests on 16in. propeller models in the kings college cavitation tunnel. *Transactions of The North East Coast Institution of Engineers and Shipbuilders*, 1963.

Burrill, L. The optimum diameter of marine propellers: A new design approach. *Transactions of the North East Coast Institution of Engineers and Shipbuilders*, 72, 1956.

Carlton, J. *Marine Propellers and Propulsion.* Butterworth Heinemann, 2nd edition, 2007.

Clarke, D., Gedling, P., and Hine, G. The application of manoeuvring criteria in hull design using linear theory. *Transactions of Royal Institution of Naval Arhchitects.*, 125:45 – 68, 1983.

COGOW. Climatology of global ocean winds. `http://cioss.coas.oregonstate.edu/cogow`, 2012. last accessed: 19th November 2013.

Coleman, R., Feingold, A., and Stempin, C. Evaluation of the induced velocity field of an idealized helicopter rotor. Technical Report ARR No. L5E10, National Advisory Committee for Aeronautics, 1945.

Crane, C. L. Maneuvering trials of the 278,000 dwt esso osaka in shallow and deep water. *Transactions of the SNAME*, 87, 1979.

Davenport, A. G. Wind structure and wind climate. In *International Research Seminar on Safety of Structures under Dynamic Loading.*, pages 209–237, Trondheim, 1978. Norwegian Institute of Technology.

DNV and PSE. Dnv and pse report on ship carbon capture & storage. Press Release, 2013.

Donelan, M. and Hamilton, W. H., J. andHui. Directional spectra of wind-generated waves. *Philosophical Transactions of the Royal Society*, 315(1534 509-562), 1985.

Eloot, K., Vantorre, M., and Delefortrie, G. Prediction of ship manoeuvrability of an 8000 teu containership in deep and shallow water: mathematical modelling and captive model testing. In *Proceedings MARSIM 2006.* Maritime Institute Willem Barentsz, 2006.

Ericsson, L. E. and Reding, J. Dynamic stall of helicopter blades. *American Helicopter Society*, 17:1–19, 1972.

Francis, M. S. and Keesee, J. E. Airfoil dynamic stall performance with large amplitude motions. *AIAA Journal*, 23, 1985.

Froude, R. On the part played in the operation of propulsion differences in fluid pressure. *Transactions of the Institue of Naval Architects.*, 30, 1889.

Froude, W. On the elementary relation between pitch, slip and propulsive efficiency. *Transactions of the Institue of Naval Architects.*, 19, 1878.

Glauert, H. On the horizontal flight of a helicopter. Technical Report 1157, British Aeronautical Research Council: Reports & Memoranda, 1928.

Goldstein, S. On the vortex theory of screw propellers. In *Proceedings of the Royal Society, London Series A.*, volume 123, pages 440–465, 1929.

Green, R. and Galbraith, R. A. A demonstration of the effect of the testing environment on unsteady aerodynamics experiments. *Aeronautical Journal*, 98, 1994.

GWS. Bmt fluid mehcanics: Global wave statistics online. `http://www.globalwavestatisticsonline.com/`, 2013. last accessed: 19th November 2013.

Haakenstad, K. Analysis and correction of sea trials. Master's thesis, Department of Marine Technology, Norwegian University of Science and Technology, 2012.

Hadler, J. B. Coefficients for international towing tank conference 1957 model correlation line. Technical Report 1185, David Taylor Model Basin., 1957.

Ham, N. and Garelick, M. Dynamic stall considerations in helicopter rotors. *American Helicopter Society*, 13(2):49 – 55, 1968.

Harris, R. I. The nature of the wind. In *Proceedings of the Seminar on the Modern Design of Wind Sensitive Structures*, pages 29–55. Institution of Civil Engineers, London, 1970.

Hirano, M. A practical calculation method of ship maneuvring motion at initial design stage. *Naval Architecture and Ocean Engineering.*, 19, 1981.

Hochkirch, K. and Bertram, V. Engineering options for more fuel efficient ships. In *Proceedings of First International Symposium on Fishing Vessel Energy Efficiency.*, 2010.

Hoerner, S. *Fluid Dynamic Drag: Practical Information on Aerodynamic Drag and Hydrodynamic Resistance.* Hoerner Fluid Dynamics, 2 edition, 1965.

Hoerner, S. and Borst, H. *Fluid-Dynamic Lift: Practical Information on Aerodynamic and Hydrodynamic Lift.* L.A. Hoerner, 1985.

Holtrop, J. A statistical re-analysis of resistance and propulsion data. *International Shipbuilding Progress.*, pages 272 – 276, 1984.

Holtrop, J. and Mennen, G. An approximate power prediction method. *International Shipbuilding Progress.*, 29:166 – 170, 1982.

Hughes, G. Friction and form resistance in turbulent flow and a proposed formulation for use in model and ship correlation. *Transactions of the Royal Institution of Naval Architects.*, 96, 1954.

IMO. Imo resolution a.751: Interim standards for ship manoeuvrability. Technical Report CFR Section: 33 CFR 157.444(a), International Maritime Organisation, 1994.

IMO. Second imo ghg study 2009. Technical report, International Maritime Organisation, 2009.

Inoue, S., Hirano, M., and Kijima, K. Hydrodynamic derivatives on ship manoeuvring. *International Shipbuilding Progress.*, 28, 1981a.

Inoue, S., Hirano, M., Kijima, K., and Takashina, J. A practical calculation method of ship manoeuvring motion. *International Shipbuilding Progress.*, 28, 1981b.

Isherwood, R. Wind resistance of merchant ships. *Transactions of Royal Institution of Naval Arhchitects.*, 114:327 – 338, 1972.

ITTC. The specialist committee on esso osaka - final report and recommendations to the 23rd ittc. In *23rd ITTC*. International Towing Tank Conference, 2002.

ITTC. The seakeeping committee - final report and recommendations to the 25th ittc. In *Proceedings of 25th International Towing Tank Conference*, volume 1, 2008.

ITTC. The specialist committee on computational fluid dynamics. In *Proceedings of the 26th International Towing Tank Committee, Volume II.*, 2011.

Jones, R. T. *Modern Subsonic Aerodynamics*. Martin Hollmann Aircraft Designs, Inc., 1988.

Kaasen, E., Karl. Time domain model representations of standard wind gust spectra. In *Ninth International Offshore and Polar Engineering Conference*. MARINTEK, 1999.

Keller, J. a. Enige aspecten bij het ontwerpen van scheepsschroeven. *Schip en Werf*, 24, 1966. In Dutch.

Kijima, K., Katsuno, T., Nakiri, Y., and Furakawa, Y. On the manoeuvring performance of a ship with the parameter of loading condition. *Society of Naval Architects of Japan*, 168, 1990a.

Kijima, K., Nakiri, Y., Tanaka, S., and Furukawa, Y. On a numerical simulation for predicting of ship manoeuvring performance. In *19th International Towing Tank Conference*, pages 559–568. Kyushu University, 1990b.

Kose, K., Yumuro, A., and Yoshimura, Y. Concrete of mathematical model for ship manoeuvrability. *3rd Symposium on Ship Manoeuvrability, Society of Naval Architects of Japan*, 1981. In Japanese.

Kottapalli, S. B. and Pierce, G. A. Drag on an oscillating airfoil in a fluctuating free stream. *Fluids Engineering*, 101, 1979.

Ksnaj. *Handbook of Ship Design*. Kansai Society of Naval Architects, Japan, 1996. In Japanese.

Kutta, W. Beitrag zur naherungsweisen integration von differentialgleichungen. *Z. Math. und Phys.*, 46:435–453, 1901. In German.

Lammeren, W., van Mennen, J., and Oosterveld, M. The wageningen b-screw series. *Transactions of SNAME*, 77, 1969.

Lee, T., Ahn, K., Lee, H., and Yum, D. On an empirical prediction of hydrodynamic coefficients for modern ship hulls. In *MARSIM 03*. Hyundai Heavy Industries Co., Ltd, Korea, 2003.

Leishman, J. G. Two-dimensional model for airfoil unsteady drag below stall. *Journal of Aircraft.*, 25(7), 1989.

Leishman, J. G. and Beddoes, T. S. A semi-empirical model for dynamic stall. *American Helicopter Society*, 34(3):3–17, 1989.

Lerbs, H. Moderatley loaded propellers wiht a finite number of blades and an arbitrary distribution of circulation. *Transactions of SNAME*, 60, 1952.

MARIN. Time domain analysis of multi body dynamics for offshore operations. `https://wiki.marin.nl/index.php/ANYwiki/`, 2013. Last accessed: 18th November 2013.

McCroskey, W. J. The phenomenon of dynamic stall. Technical Report TM 81264, NASA, 1981.

McLaughlin, T. E. *Aerodynamic Foundations for Use of Unsteady Aerodynamic Effects in Flight Control*. PhD thesis, University of Colorado, Department of Aerospace Engineering Sciences., 1992.

Meijing, L. and Xiuheng, W. Simulation calculation and comprehensive assessment on ship maneuverabilities in wind, wave, current and shallow water. In *MARSIM & ICSM 90*, pages 403 – 411, 1990.

MEPC. Resolution mepc.159(55). Technical report, International Maritime Organisation, 2006.

Molland, A. F., Turnock, S. R., and Hudson, D. A. *Ship Resistance and Propulsion, Practical Estimation of Ship Propulsive Power.*, page 346. Cambridge University Press, 2011. ISBN: 978-0-521-76052-2.

Moré, J. J., Garbow, B. S., and Hillstrom, K. E. User guide for minpack-1. Technical Report ANL-80-74, Argonne National Laboratory, 1980.

Motora, S. On the measurement of added mass and added moment of inertia for ship motions. *Transactions of Society of Naval Architects of Japan*, 105 and 106, 1959 and 1960.

Ning, S. A. A simple solution method for the blade element momentum equations with guaranteed convergence. *Wind Energy*, 2013.

Nomoto, K. Researches on the manoeuvrability of ships in japan. *Transactions of the Society of Naval Architects of Japan, 60th Aniversary Series Publication.*, 11, 1966.

Norrbin, N. Theory and observations on the use of a mathematical model for ship manoeuvring in deep and conned water. Technical Report 63, Swedish State Shipbuilding Experimental Tank., Gothenburg, 1971.

NPD. Guidelines concerning loads and load effects to regulations concerning load bearing structures in the petroleum activities. Technical report, The Norwegian Petroleum Directorate, 1992.

Nvidia. `http://www.nvidia.co.uk/object/cuda-parallel-computing-uk.html/`, 2014. Last accessed: 16th August 2014.

Ochi, M. and Shin, Y. Wind turbulent spectra for design consideration of offshore structures. In *20th Annual Offshore Technology Conference*. University of Florida and American Bureau of Shipping, 1988.

Ogawa, A. and Kasai, H. On the mathematical model of manoeuvring motion of ship. *International Shipbuilding Progress*, 25, 1978.

Oltmann, P. and Sharma, S. Simulation of combined engine and rudder maneuvers using an improved model of hull-propeller-rudder interactions. Technical Report 444, Technische Universität Hamburg-Harburg, Hamburg, 1984. Prepared for the Fifteenth ONR Symposium on Naval Hydrodynamics.

Oosterveld, M. and van Oossanen, P. Further computer-analysed data of the wageningen b-screw series. *International Shipbuilding Progress.*, 22, 1975.

OpenMP. The openmp application programming interface. `http://www.openmp.org/`, 2013. last accessed: 28th August 2013.

Peric, M. and Bertram, V. Trends in industry applications of computational fluid dynamics for maritime flows. *Ship Production and Design*, 27(4), 2011.

Prpić-Oršić, J., Nabergoj, R., and Trincas, G. The methods of added resistance estimation for ships in a seaway. In *18th Symposium on Theory and Practice of Shipbuilding*. University of Rijeka and University of Trieste, 2008.

Rankine, W. J. On the mechanical principles of the action of propellers. *Transactions of the Institue of Naval Architects.*, 6, 1865.

Rieder, K. and Smith, J. Observed directional characteristics of the wind, wind stress, and surface waves on the open ocean. *Geophysical Research*, 99, 1994.

Risien, C. M. and Chelton, D. A satellite-derived climatology of global ocean winds. *Remote Sensing of Environment*, 105(3):221–236, 2006.

Rodrigue, J.-P. *The Geography of Transport Systems*. Routledge, 2013.

Runge, C. Ueber die numerische auflösung von differentialgleichungen. *Math. Ann.*, 46:167–178, 1895. In German.

Salvesen, N. Added resistance of ships in waves. Technical report, David Taylor Naval Ship R&D Center, 1976.

Shen, Y. and Fuhs, D. Blade section lift coefficients for propellers at extreme off-design conditions. Technical Report CRDKNSWC/HD-1205-02, Hydrodynamic Directorate Research and Development Report, Naval Surface Warfare Centre, Carderock Division, 1997.

Shen, Y. and Fuhs, D. Dynamic effects on propellers blade section lift, drag, and pitching moment coefficients. Technical Report CRDKNSWC/HD-1205-0, Hydrodynamic Directorate Research and Development Report, Naval Surface Warfare Centre, Carderock Division, 1999.

Shinozuka, M. and Jan, C. M. Digital simulation of random process and its applications. *Journal of Sound and Vibration.*, 25:111âĂŞ128, 1972.

SIMMAN. `http://www.simman2013.dk/`, 2014. Last accessed: 19th April 2014.

Son, K. On the mathematical model for estimating the manoeuvring performance of ships. *Society of Korea Voyage.*, 13(2), 1989.

Stepniewski, W. and Keys, C. *Rotary Wing Aerodynamics*. Dover Publications, 1984.

Stettler, J. *Steady and Unsteady Dynamics of an Azimuthing Podded Propulsor Related to Vehicle Maneuvering.* PhD thesis, Massachusetts Institute of Technology., 2004.

Szelangiewicz, T. and Żelazny, K. Calculation of the mean long-term service speed of transport ship, part iii, influence of shipping route and parameters on its service speed. *Polish Maritime Research*, 2, 2007.

Tello Ruiz, M., M., C., Vantorre, M., Delefortrie, G., Peeters, D., and Mostaert, F. Ship manoeuvring in waves. a literature review. Technical Report WL2012R00_096_18rev2_0, Flanders Hydraulics Research, 2012.

Townsin, R. L., Kwon, Y. J., Baree, M. S., and Kim, D. Y. Estimating the influence of weather on ship performance. *Transactions of RINA*, 135:191–209, 1992.

Trodden, D. and Woodward, M. Optimal propeller design when accounting for thea manœuvring response due to environmental loading. In *MARSIM 2012*. Newcastle University, UK, 2012.

Troost, L. Open-water test series with modern propeller forms. Technical Report 33, Netherlands Ship Model Basin (NSMB), Wageningen, 1938a.

Troost, L. Open-water test series with modern propeller forms. *Transactions of the North East Coast Institute of Engineers and Shipbuilders (NECIES)*, 56, 1938b.

Troost, L. Open-water test series with modern propeller forms. *Transactions of the North East Coast Institute of Engineers and Shipbuilders (NECIES)*, 67, 1938c.

Wärtsilä. *RT-Flex82 Marine Installation Manual*, 2011.

Wärtsilä. Mbr systems. `http://www.wartsila.com/en/water-management/waste-water-management/MBR-systems`, 2013a. last accessed: 16th December 2013.

Wärtsilä. General technical data for wärtsilä marine low-speed engines. `http://www.wartsila.com/en/marine-solutions/products/netGTD`, 2013b. last accessed: 18th December 2013.

Woodward, M. In private communication, 2014. Member of the ITTC Specialist Committee on Uncertainty Analysis.

Woodyard, D., editor. *Pounder's Marine Diesel Engines and Gas Turbines*, page 144. Elsevier, 8th edition, 2004.

Yumuro, A. Some experiments on shallow water effects on manoeuvring hydrodynamic forces acting on a ship model. *IHI Engineering Review*, 25(4), 1985.

Ziegler, J. and Nichols, N. Optimum settings for automatic controllers. *American Society of Mechanical Engineers.*, 64:759–768, 1942.

Appendix A. SiS User Manual

This Appendix describes the basic operation of the *SiS* simulator, along with example input files for the basis ships used in the analysis of this research.

A.1 Introduction

The *SiS* ship manœuvring simulator has been specially developed for use in this research. It is written in Fortran 2008 standard, using the OpenMP specification for parallel programming, and is known to compile on UNIX clones with either the Intel Fortran Compiler (`ifort`) or the GNU Fortran Compiler (`gfortran`).

The programme is designed to be run without user intervention, so it can conveniently be run in batch mode.

Figure A.1 shows the directory tree of the *SiS* simulator. The input/output file names and directories are hard-coded, meaning that the programme will expect to find them where they are illustrated in the figure.

When the *SiS* is invoked, the first thing it will do is read and parse the input file `input.dat` (for examples please see Section A.2). This input file serves to supply the programme with ship specific data, and also to configure the type of analysis that it will perform.

Having read the input file the general flow of the programme is depicted in fig. A.2.

A.2 Example Input Files

In the following examples of input files for the *SiS* simulator, comments have been made at the end of each line to indicate the significance of each line. The "Ship Type" entry needs further explanation as there is too little space to depict them in the input file. Ship type designations are found in Table A.1.

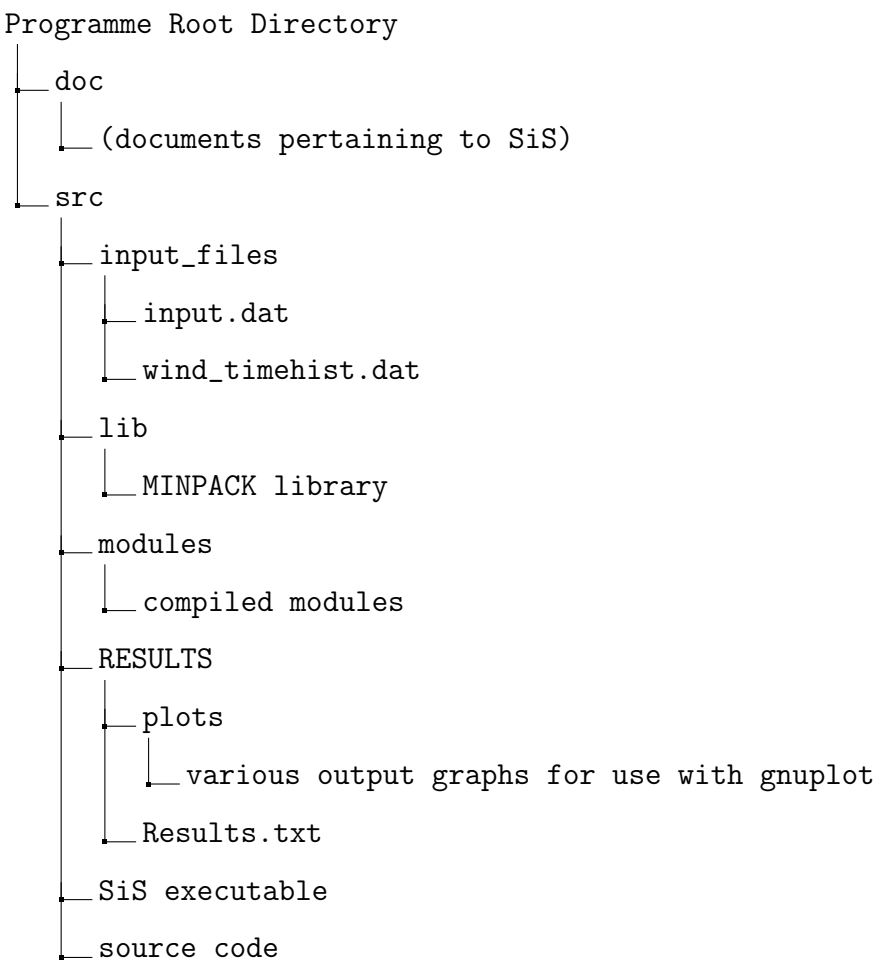

Figure A.1: Directory structure of *SiS* simulator.

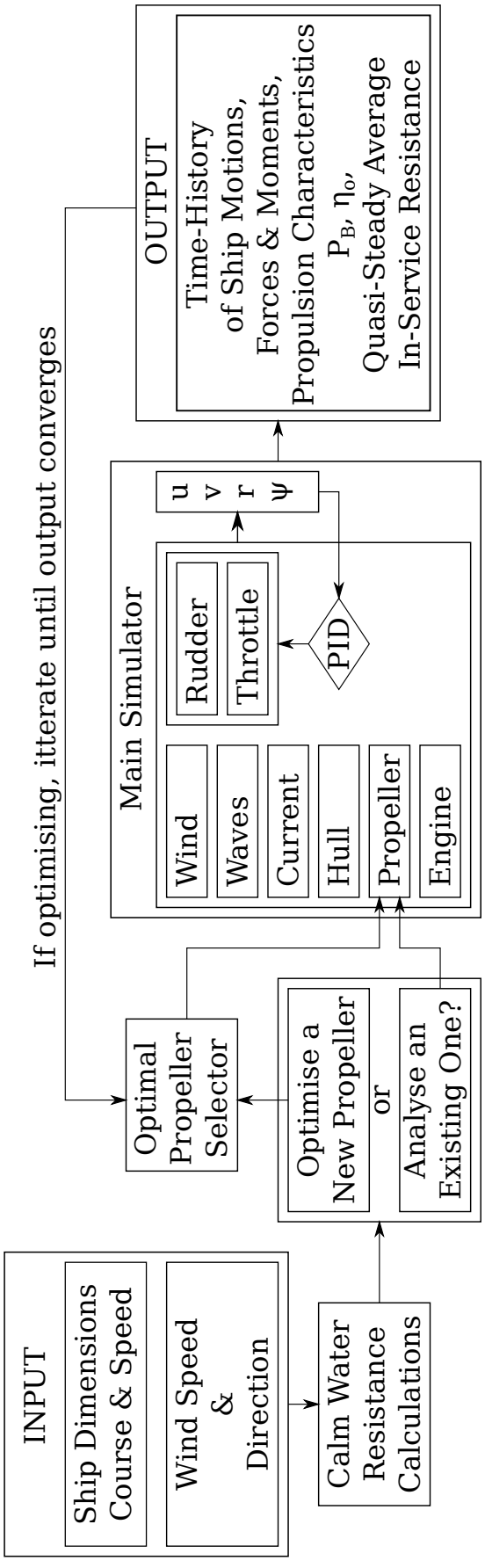

Figure A.2: *SiS* Programme Flow

Number Designation	Ship Type
1	Car carrier
2	Cargo vessel, loaded
3	Cargo vessel, container on deck
4	Container ship, loaded
5	Destroyer
6	Diving support vessel
7	Drilling vessel
8	Ferry
9	Fishing vessel
10	Liquefied natural gas tanker
11	Offshore supply vessel
12	Passenger liner
13	Research vessel
14	Speed boat
15	Tanker, loaded
16	Tanker, in ballast
17	Tender

Table A.1: Ship type designation as used in the input file for the *SiS* simulator

A.2.1 Example Input File for the Esso Osaka

```
"Esso Osaka VLCC - Loaded Test Case"
311901.5  ! Volume of Displacement (m^3)
325.0     ! Length between Perpendiculars (m)
335.0     ! Length along the Waterline (m)
53.0      ! Beam (m)
21.79     ! Draught at Forward Perpendicular (m)
21.79     ! Draught at After Perpendicular (m)
3.169     ! Longitudinal Centre of Buoyancy (relative to midships +ve forward [%])
0.99      ! Midship Coefficient
0.85      ! Waterplane Coefficient
10.0      ! Service Speed (knots)
2         ! Rudder Type
13.85     ! Rudder Span (m)
9.0       ! Rudder Chord (m)
249.3     ! Wetted Surface Area of Rudder (m^2)
0.0       ! Wetted Surface Area of Bilge Keels (m^2)
0.0       ! Wetted Surface Area of Skeg (m^2)
0.0       ! Wetted Surface Area of Strut Bossings (m^2)
0.0       ! Wetted Surface Area of Hull Bossings (m^2)
0.0       ! Wetted Surface Area of Shafts (m^2)
0.0       ! Wetted Surface Area of Shaft Brackets (m^2)
0.0       ! Wetted Surface Area of Stabiliser Fins (m^2)
0.0       ! Wetted Surface Area of Radar Dome (m^2)
16.53     ! Transverse Area of Bulbous Bow (m^2)
3.59      ! Height of Centre of Bulb from Keel (m)
3.0       ! Bow Thruster Tunnel Diameter (m)
0.005     ! Bow Thruster Opening Coefficient
2         ! After-Body Form Type
9.86      ! Immersed Area of Transom (m^2)
y         ! Optimise a propeller for in-service conditions, or analyse existing one (y/n)?
1         ! Number of Propellers
9.1       ! Propeller Diameter (m)
5         ! Number of Blades on Propeller
6.507     ! Pitch of Propeller (m)
0.682     ! Propeller's Expanded Blade Area Ratio
0.273     ! Clearance between Propeller and Keel (m)
15        ! Ship Type
2         ! Engine Type
1.0       ! Main Engine Gearbox Ratio
1.0       ! Shaft efficiency
```

```
343.0     ! Length Overall (m)
3550.0    ! Lateral Projected Area (m^2)
909.0     ! Transverse Projected Area (m^2)
191.0     ! Distance from Bow of Centroid of Lateral Projected Area (m)
20.0      ! True Wind Speed (knots)
90.0      ! Wind Direction - Cardinal Points (degrees)
0.0       ! Current Speed (knots)
0.0       ! Current Direction - Cardinal Points (degrees)
0.0       ! Ship's Course (Direction of travel) - Cardinal Points (degrees)
t         ! Do we generate a new time-history of wind velocity, or use an existing file
          ! (True or False)
s         ! Which propulsion model should we use; 's' for quasi-static BEMT,
          ! 'd' for dynamic BEMT or 'o' for Oosterveld & van Oossanen (LOWER CASE ONLY!)
a         ! Analysis type; c = turning circle, z = zig-zag, a = autotrack & autospeed,
          ! n = no control
0.485     ! Autopilot proportional coefficient for course control
0.4       ! Autopilot integral coefficient for course control
0.02      ! Autopilot derivative coefficient for course control
0.6       ! Autopilot proportional coefficient for speed control
0.015     ! Autopilot integral coefficient for speed control
0.0       ! Autopilot derivative coefficient for speed control
```

A.2.2 Example Input File for the KCS

```
"KCS - KRISO Container Ship"
50885.0   ! Volume of Displacement (m^3)
232.0     ! Length between Perpendiculars (m)
237.58    ! Length along the Waterline (m)
32.2      ! Beam (m)
11.343    ! Draught at Forward Perpendicular (m)
11.343    ! Draught at After Perpendicular (m)
-2.03     ! Longitudinal Centre of Buoyancy (relative to midships +ve forward [%])
0.985     ! Midship Coefficient
0.802     ! Waterplane Coefficient
24.0      ! Service Speed (knots)
2         ! Rudder Type
9.9       ! Rudder Span (m)
5.5       ! Rudder Chord (m)
115.0     ! Wetted Surface Area of Rudder (m^2)
0.0       ! Wetted Surface Area of Bilge Keels (m^2)
0.0       ! Wetted Surface Area of Skeg (m^2)
0.0       ! Wetted Surface Area of Strut Bossings (m^2)
0.0       ! Wetted Surface Area of Hull Bossings (m^2)
0.0       ! Wetted Surface Area of Shafts (m^2)
0.0       ! Wetted Surface Area of Shaft Brackets (m^2)
0.0       ! Wetted Surface Area of Stabiliser Fins (m^2)
0.0       ! Wetted Surface Area of Radar Dome (m^2)
9.55      ! Transverse Area of Bulbous Bow (m^2)
9.25      ! Height of Centre of Bulb from Keel (m)
0.0       ! Bow Thruster Tunnel Diameter (m)
0.0       ! Bow Thruster Opening Coefficient
3         ! After-Body Form Type
0.0       ! Immersed Area of Transom (m^2)
n         ! Optimise a propeller for in-service conditions, or analyse existing one (y/n)?
1         ! Number of Propellers
7.9       ! Propeller Diameter (m)
5         ! Number of Blades on Propeller
7.8763    ! Pitch of Propeller (m)
0.8       ! Propeller's Expanded Blade Area Ratio
0.336     ! Clearance between Propeller and Keel (m)
4         ! Ship Type
2         ! Engine Type
1.0       ! Main Engine Gearbox Ratio
1.0       ! Shaft efficiency
253.8     ! Length Overall (m)
5472.08   ! Lateral Projected Area (m^2)
914.65    ! Transverse Projected Area (m^2)
113.81    ! Distance from Bow of Centroid of Lateral Projected Area (m)
0.0       ! True Wind Speed (knots)
90.0      ! Wind Direction - Cardinal Points (degrees)
0.0       ! Current Speed (knots)
0.0       ! Current Direction - Cardinal Points (degrees)
0.0       ! Ship's Course (Direction of travel) - Cardinal Points (degrees)
t         ! Do we generate a new time-history of wind velocity, or use an existing file
```

```
          ! (True or False)
d         ! Which propulsion model should we use; 's' for quasi-static BEMT,
          ! 'd' for dynamic BEMT or 'o' for Oosterveld & van Oossanen (LOWER CASE ONLY!)
n         ! Analysis type; c = turning circle, z = zig-zag, a = autotrack & autospeed,
          ! n = no control
0.485     ! Autopilot proportional coefficient for course control
0.4       ! Autopilot integral coefficient for course control
0.02      ! Autopilot derivative coefficient for course control
0.6       ! Autopilot proportional coefficient for speed control
0.015     ! Autopilot integral coefficient for speed control
0.0       ! Autopilot derivative coefficient for speed control
```

A.3 *SiS* Subprogram Descriptions

Table A.2

Module Name	Main Subprograms
`added_wave_resistance.f90`	`subroutine townsin_kwon(...)` - Calculates the added resistance in pure surge due to waves. `function BN(...)` - Calculates the Beaufort Number from the true wind speed.
`blendermann94.f90`	`function blendermann(...)` - Calculates the wind force and moment coefficients.
`b_screw.f90`	`function Okt(...)` - Calculates thrust coefficient from Oosterveld and van Oossanen (1975) polynomials. `function Okq(...)` - Calculates torque coefficient from Oosterveld and van Oossanen (1975) polynomials.
`b_screw_geom.f90`	`subroutine b_geom(...)` - Calculates blade offsets, chord length, maximum thickness, zero lift angle. `subroutine b_chord(...)` - Calculates the chord length at a given radius. `subroutine propeller_offsets(...)` - Writes out the propeller offsets to a file.
`course_stability.f90`	`subroutine clarke(...)` - Calculates linearised manœuvring coefficients. `subroutine dstability(...)` - Assesses the dynamic stability of the ship.

Continued on next page

Table A.2 – continued from previous page

Module Name	Main Subprograms
	`subroutine tprime(...)` - Checks if the ship meets IMO Turning Criteria.
`gms.f90`	Defines various physical constants and some general mathematical and science routines, including: `function linintpol(...)` - Linear interpolation. `function cubic_spline(...)` - Cubic spline interpolation.
`gplot.f90`	Numerous subroutines to plot graphs via *gnuplot*.
`holtrop_mennen.f90`	`hm_coeff(...)` - Calculates coefficients used in Holtrop and Mennen (1982) ship resistance calculations. `cw_res(...)` - Calculates the calm water (pure surge) resistance of a ship. `wPo(...)` - Estimates the (Taylor) Wake Fraction from Holtrop and Mennen (1982) `tdfo(...)` - Estimates the Thrust Deduction Fraction from Holtrop and Mennen (1982) `etaR(...)` - Estimates the Relative Rotative Efficiency from Holtrop and Mennen (1982)
`hydrostatics.f90`	`bhydro(...)` - Calculates various hydrostatics, including mass, centre of gravity, mass moments of inertia, block coefficient.
`input_data.f90`	`subroutine gobble(...)` - Read in ship and environment data from input file.
`isherwood72.f90`	`isherwood(...)` - Alternative method of calculating the wind force and moment coefficients.
`lift_drag.f90`	`subroutine C_Lift(...)` - Calculates the lift coefficient of a two-dimensional hydrofoil in unsteady conditions, for both fully attached and separated flow.

Continued on next page

Table A.2 – continued from previous page

Module Name	Main Subprograms
`mbemt.f90`	`subroutine C_Drag(...)` - Calculates the drag coefficient of a two-dimensional hydrofoil in unsteady conditions, for both fully attached and separated flow. `subroutine bem_theory(...)` - Calculates the thrust and torque on the propeller using quasi-static or unsteady models. `subroutine f_Vi_cl(...)` - Implements the modified combined blade-element momentum theory.
`opt_b_screw.f90`	Various routines to select a propeller with the highest efficiency for the environmental conditions that the ship encounters. c.f. 6.1
`power.f90`	`subroutine power_calc(...)` - Calculates the required propeller torque and revolution rate to propel the ship at the given speed. (used for initial estimate when propeller data is not given)
`report.f90`	Various routines to write output data to a file on disc.
`simulator.f90`	Main simulation subprograms. Major routines include: `subroutine hull(...)` - Calculates instantaneous hull forces and moment at each time-step of the simulation. `subroutine rudder(...)` - Calculates instantaneous rudder forces and moment at each time-step of the simulation. `subroutine propeller(...)` - Uses either `b_screw.f90` or `mbemt` (depending on the analysis) to calculate the instantaneous propeller forces and moment at each time-step of the simulation.

Continued on next page

Table A.2 – continued from previous page

Module Name	Main Subprograms
	`subroutine wind(...)` - Uses `blendermann94.f90` to calculate the instantaneous wind forces and moment at each time-step of the simulation. `subroutine seaway(...)` - uses `added_wave_resistance.f90` to calculate the instantaneous added wave resistance. `subroutine sim(...)` - The main calling routine, sets up initial conditions and uses `rk4sys(...)` to run the simulation. `subroutine eqn_m(...)` - Calls `hull(...)`, `rudder(...)`, `propeller(...)` `wind(...)` and `seaway(...)` to set up the system of equations of motion. Also simultaneous ODEs are setup for rudder slew rate and throttle fuel rack rate. `subroutine Q_Engine(...)` - Calculates the torque from the engine. `subroutine rk4sys(...)` - Solves the system of ODEs that are generated from `eqn_m(...)`. Also calls (required) control commands. `subroutine turncircle(...)` - Gives the order for the rudder to be put over for a turning circle manœuvre. `subroutine zigzag(...)` - Gives rudder orders for the ship to perform a zigzag manœuvre. `subroutine autopilot(...)` - Gives rudder and throttle orders to keep the ship on course at the required speed.

Continued on next page

Table A.2 – continued from previous page

Module Name	Main Subprograms
	`subroutine post_process(...)` - Analyses the data from the simulation, writes results to disc and calls various plotting routines.

Table A.2: FORTRAN modules and main subprograms used in propeller modelling calculations.

Appendix B. Miscellaneous Calculations

This Appendix describes various calculations that are necessary to repeat the analysis of this research. They are listed here, as opposed to the main Chapters where they are referenced, as they are considered to divert the reader away from the main flow of the topic.

B.1 Non-Linear Manœuvring Coefficients

Non-Linear Manœuvring coefficients are estimated from Inoue et al. (1981b)

$$Y'_v = -\left(\frac{\pi T}{L_{pp}} + 1.4\frac{C_B B}{L_{pp}}\right)\left[1 + \frac{2}{3}\left(\frac{\tau}{T}\right)\right]$$

$$Y'_r = \frac{1}{2}\frac{\pi T}{L_{pp}}\left(1 + 0.8\frac{\tau}{T}\right)$$

$$N'_v = -\frac{2T}{L_{pp}} + 0.54\frac{\tau}{L_{pp}}\left(0.5\pi + 0.7\frac{C_B B}{T}\right)$$

$$N'_r = -\left(1.08\frac{T}{L_{pp}} - \frac{4T^2}{L_{pp}^2}\right)\left(1 + 0.3\frac{\tau}{T}\right)$$

$$Y'_{v|v|} = -6.49\,(1 - C_B)\,\frac{T}{B} + 0.0795$$

$$Y'_{v|r|} = 1.82\,(1 - C_B)\,\frac{T}{B} - 0.447$$

$$Y'_{r|r|} = -0.4664\,(1 - C_B)\,\frac{T}{B}$$

$$N'_{vvr} = -\left[3.25\frac{C_B B}{L_{pp}} - 0.35 + 10^{-7}\left(\frac{L_{pp}}{C_B B}\right)^6\right]$$

$$N'_{vrr} = 0.444\frac{C_B T}{B} - 0.064$$

$$N'_{r|r|} = -\left[1.7\left(\frac{C_B B}{L_{pp}} - 0.157\right)^{1.5} + 0.01\right]$$

B.1.1 Non Dimensionalising Factors

Forces : $\frac{1}{2}\rho V_v^2 T L_{pp}$

$$\text{Moments} : \frac{1}{2}\rho V_v^2 T L_{PP}^2$$

B.2 Linear Manœuvring Coefficients

Linear Manœuvring coefficients are estimated from Clarke et al. (1983)

$$Y'_v = -\pi \left(\frac{T}{L}\right)^2 \left[1 + 0.4 C_B \frac{T}{L}\right]$$

$$Y'_r = -\pi \left(\frac{T}{L}\right)^2 \left[-\frac{1}{2} + 2.2\frac{B}{L} - 0.080\frac{B}{T}\right]$$

$$N'_v = -\pi \left(\frac{T}{L}\right)^2 \left[\frac{1}{2} + 2.4\frac{T}{L}\right]$$

$$N'_r = -\pi \left(\frac{T}{L}\right)^2 \left[\frac{1}{4} + 0.039\frac{B}{T} - 0.56\frac{B}{L}\right]$$

$$Y'_{\dot{v}} = -\pi \left(\frac{T}{L}\right)^2 \left[1 + 0.16 C_B \frac{B}{T} - 5.1\left(\frac{B}{L}\right)^2\right]$$

$$Y'_{\dot{r}} = -\pi \left(\frac{T}{L}\right)^2 \left[0 + 0.67\frac{B}{L} - 0.0033\left(\frac{B}{T}\right)^2\right]$$

$$N'_{\dot{v}} = -\pi \left(\frac{T}{L}\right)^2 \left[0 + 1.1\frac{B}{L} - 0.041\frac{B}{T}\right]$$

$$N'_{\dot{r}} = -\pi \left(\frac{T}{L}\right)^2 \left[\frac{1}{12} + 0.017 C_B \frac{B}{T} - 0.33\frac{B}{L}\right]$$

B.2.1 Non Dimensionalising Factors

$$\text{Forces} : \frac{1}{2}\rho V_v^2 L_{PP}^2$$

$$\text{Moments} : \frac{1}{2}\rho V_v^2 L_{PP}^3$$

B.3 Added Mass and Added Mass Moment of Inertia Terms

Added Mass Equations derived from the charts of Motora (1959 and 1960):

$$\begin{aligned} m_x = \frac{m}{100}\Bigg[& 2.246 + 17.242\left(\frac{T}{B}\right) + 5.873 C_B - 1.472\left(\frac{L_{pp}}{B}\right) \\ & - 7.406\left(\frac{T}{B}\right)^2 + 4.687 C_B^2 + 0.175\left(\frac{L_{pp}}{B}\right)^2 \\ & + 22.979\left(\frac{T}{B}\right) C_B - 1.701 C_B\left(\frac{L_{pp}}{B}\right) - 2.198\left(\frac{L_{pp}}{B}\right)\left(\frac{T}{B}\right)\Bigg] \end{aligned}$$

$$m_y = \frac{m}{100}\left[13.97 + 359.23\left(\frac{T}{B}\right) + 29.03C_B - 5.52\left(\frac{L_{pp}}{B}\right) - 198.58\left(\frac{T}{B}\right)^2 - 1.39C_B^2 + 0.49\left(\frac{L_{pp}}{B}\right)^2 - 152.89\left(\frac{T}{B}\right)C_B - 5.69C_B\left(\frac{L_{pp}}{B}\right) + 11.40\left(\frac{L_{pp}}{B}\right)\left(\frac{T}{B}\right)\right]$$

$$J_{zz} = m\left\{\frac{L_{pp}}{100}\left[19.29 + 65.81\left(\frac{T}{B}\right) - 52.56C_B + 1.53\left(\frac{L_{pp}}{B}\right) - 34.41\left(\frac{T}{B}\right)^2 + 38.97C_B^2 - 0.07\left(\frac{L_{pp}}{B}\right)^2 - 30.53\left(\frac{T}{B}\right)C_B - 0.10C_B\left(\frac{L_{pp}}{B}\right) + 0.07\left(\frac{L_{pp}}{B}\right)\left(\frac{T}{B}\right)\right]\right\}^2$$

$$I_{zz} = m\left(0.25L_{pp}\right)^2$$

B.4 Calm Water Ship Calculations

The total resistance, R_{total} of a ship advancing in pure surge is estimated from the method proposed by Holtrop and Mennen (1982) and Holtrop (1984) viz.

B.4.1 Calm Water Ship Resistance Calculations

$$R_{\text{total}} = R_F\left(1+k\right) + R_{app} + R_B + R_W + R_{tr} + R_a$$

Where:

R_f is the frictional resistance according to the ITTC-1957 friction formula for a flat plate.

$(1+k)$ is the form factor describing the viscous reisistance of the hull form.

R_{app} is the resistance of any appendages.

R_W is the resistance due to wave-makeing and wave-breaking.

R_B is the additional reistance of a bulbous bow near the water surface.

R_{tr} is the additional pressure reistance of an immersed transom stern.

R_a is the model-ship correlation resistance.

Frictional Resistance, R_F

The Frictional Resistance, R_F can be estimated as follows:

$$R_F = \frac{1}{2}\rho u^2 S\left(1+k_1\right)C_F$$

Appendage Resistance, R_{app}

$$R_{\text{app}} = \frac{1}{2}\rho u^2 S_{\text{app}} \left(1 + k_2\right)_{\text{eq}} C_F$$

Wave Making/Breaking Resistance, R_W

$$R_W = \begin{cases} C_1 C_2 C_5 \nabla \rho g \exp\left[m_1 F_n^{-0.9} + m_4 \cos\left(\lambda F_n^{-2}\right)\right] & \text{if } (F_n \leq 0.4) \\ R_W|_{F_n=0.4} + (10F_n - 4)\,\dfrac{R_W|_{F_n=0.55} - R_W|_{F_n=0.4}}{1.5} & \text{if } (0.4 < F_n < 0.55) \\ C_{17} C_2 C_5 \nabla \rho g \exp\left[m_3 F_n^{-0.9} + m_4 \cos\left(\lambda F_n^{-2}\right)\right] & \text{if } (F_n \geq 0.55) \end{cases}$$

Pressure Resistance due to Bulbous Bow, R_B

$$R_B = 0.11 \rho g \frac{\exp\left(-3P_B^{-2}\right) F_{ni}^3 A_{BT}^{1.5}}{1 + F_{ni}^2}$$

Pressure Resistance due to Transom Immersion, R_{tr}

$$R_{tr} = \frac{1}{2}\rho u^2 A_T C_6$$

Model – Ship Correlation Allowance R_A

$$R_A = \frac{1}{2}\rho u^2 S C_A$$

B.4.2 Calm Water Propeller Wake Fraction, w_P *Calculation*

Single Screw Ship

$$\begin{aligned} w_P =& C_9 C_{20} C_v \frac{L}{T_A}\left(0.050776 + 0.93405 C_{11} \frac{C_v}{1 - C_P 1}\right) \\ &+ 0.27915 C_{20} \sqrt{\frac{B}{L\left(1 - C_{P1}\right)}} + C_{19} C_{20} \end{aligned}$$

Twin Screw Ship

$$w_P = 0.3095 C_B + 10 C_v C_B - \frac{0.23 D}{\sqrt{BT}}$$

B.4.3 Calm Water Thrust Deduction Factor, t Calculation

Single Screw Ship

$$t = \frac{0.25014\left(\frac{B}{L}\right)^{0.28956}\left(\frac{\sqrt{BT}}{D}\right)^{0.2624}}{\left(1 - C_P + 0.0225\text{LCB}\right)^{0.01762}} + 0.0015C_{\text{stern}}$$

Twin Screw Ship

$$t = 0.325C_B - 0.1885\frac{D}{\sqrt{BT}}$$

B.4.4 Parameters and Coefficients Used in Calm Water Calculations

C_F can be calculated via the ITTC 1957 line from Hadler (1957)

$$C_F = \frac{0.075}{\left(\log R_n - 2\right)^2}$$

$$\begin{aligned}(1 + k_1) =& 0.93 + 0.487118C_{14}\left(\frac{B}{L}\right)^{1.06806}\left(\frac{T}{L}\right)^{0.46106} \\ &\times \left(\frac{L}{L_R}\right)^{0.121563}\left(\frac{L^3}{\nabla}\right)^{0.36486}(1 - C_P)^{-0.604247}\end{aligned}$$

The equivalent appendage form factor $(1 + k_2)$ may be determined from

$$(1 + k_2)_{\text{eq}} = \frac{\Sigma\left(1 + k_2\right)S_{\text{app}}}{\Sigma S_{\text{app}}}$$

and $(1 + k_2)$ values can be found in table B.2

Where,

$$C_6 = \begin{cases} 0.2\left(1 - 0.2F_{nT}\right) & \text{if } (F_{nT} < 5) \\ 0 & \text{if } (F_{nT} \geq 5) \end{cases}$$

and F_{nT} is the Froude Number based on transom immersion:

$$F_{nT} = \frac{u}{\sqrt{\frac{2gA_T}{(B + BC_W)}}}$$

Where

$$C_A = 0.006\left(L + 100\right)^{-0.16} - 0.00205 + 0.003\sqrt{\frac{L}{7.5}}C_B^4 C_2\left(0.04 - C_4\right)$$

Afterbody Form	C_{stern}
Pram with Gondola	-25
V shaped sections	-10
Normal shaped sections	0
U shaped sections	10

Table B.1: Stern Shape Factors

Appendage	$(1 + k_2)$
Rudder behind skeg	1.5 – 2.0
Rudder behind stern	1.3 – 1.5
Twin-screw balance rudders	2.8
Shaft brackets	3.0
Skeg	1.5 – 2.0
Strut bossings	3.0
hull bossings	2.0
Shafts	2.0 – 4.0
Stabiliser fins	2.8
Radar dome	2.7
Bilge keels	1.4

Table B.2: Approximate $(1 + k_2)$ values

Where

$$L_R = L\left(1 - C_P + 0.06C_P\frac{\text{LCB}}{4C_P - 1}\right)$$

Where P_B is a measure of the emergence of the bow:

$$P_B = 0.56\frac{\sqrt{A_{BT}}}{(T_F - 1.5h_B)}$$

and F_{ni} is the Froude Number based on bow immersion:

$$F_{ni} = \frac{u}{\sqrt{g\left(T_F - h_B - 0.25\sqrt{A_{BT}}\right) + 0.15u^2}}$$

The stern shape factor C_{14} is:

$$C_{14} = 1 + 0.011C_{\text{stern}}$$

Where the C_{stern} can be found in table B.1

Where,

$$C_1 = 2223105C_7^{3.78613}\left(\frac{T}{B}\right)^{1.07961}(90 - i_E)^{-1.37565}$$

$$C_2 = \exp\left(-1.89\sqrt{C_3}\right)$$

$$C_3 = \frac{0.56A_{BT}^{1.5}}{BT\left(0.31\sqrt{A_{BT}} + T_F - h_B\right)}$$

$$C_5 = 1 - \frac{0.8A_T}{BTC_M}$$

$$C_7 = \begin{cases} 0.229577\left(\dfrac{B}{L}\right)^{1/3} & \text{if } (B/L \leq 0.11) \\ \dfrac{B}{L} & \text{if } (0.11 < B/L < 0.25) \\ 0.5 - 0.0625\dfrac{L}{B} & \text{if } (B/L \geq 0.25) \end{cases}$$

$$C_{15} = \begin{cases} -1.69385 & \text{if } \left(L^3/\nabla \leq 512\right) \\ -0.69385 + \dfrac{\left(\frac{L}{\nabla^{1/3}} - 8\right)}{2.36} & \text{if } \left(512 < L^3/\nabla < 1726.91\right) \\ 0 & \text{if } \left(L^3/\nabla \geq 1726.91\right) \end{cases}$$

$$C_{16} = \begin{cases} 8.07981C_P - 13.8673C_P^2 + 6.984388C_P^3 & \text{if } (C_P < 0.8) \\ 1.73014 - 0.7067C_P & \text{if } (C_P > 0.8) \end{cases}$$

$$C_{17} = 6919.3C_M^{-}1.3346\left(\frac{\nabla}{L^3}\right)^{2.00977}\left(\frac{L}{B}\right)^{1.40692}$$

$$m_1 = 0.0140407\frac{L}{T} - 1.75254\frac{\nabla^{1/3}}{L} - 4.79323\frac{B}{L} - C_{16}$$

$$m_3 = -7.2035\left(\frac{B}{L}\right)^{0.326869}\left(\frac{T}{B}\right)^{0.605375}$$

$$m_4 = 0.4C_{15}\exp\left(-0.034F_n^{-3.29}\right)$$

$$\lambda = \begin{cases} 1.446C_P - 0.03\dfrac{L}{B} & \text{if } (L/B \leq 12) \\ 1.446C_P - 0.36 & \text{if } (L/B > 12) \end{cases}$$

$$i_E = 1 + 89\,\exp\left\{\left[-\left(\frac{L}{B}\right)^{0.80856}(1 - C_W)^{0.30484}(1 - C_P - 0.0225\text{LCB})^{0.6367}\left(\frac{L_R}{B}\right)^{0.34574}\left(100\frac{\nabla}{L^3}\right)^{0.16302}\right]\right\}$$

Where i_E is the half angle of entrance off the bow, h_B is the vertical position of the centre of A_{BT} above the keel ($h_B \leq 0.6T_F$), and A_T is the immersed part of the

transverse area of the transom stern at rest.

$$C_4 = \begin{cases} \dfrac{T_F}{L} & \text{if } (T_F/L \leq 0.04) \\ 0.04 & \text{if } (T_F/L > 0.04) \end{cases}$$

Hull Wetted Surface Area, S

The projected wetted surface area, S can be estimated as

$$\begin{aligned} S =& L\left(2T + B\right)\sqrt{C_M} \\ & \times \left(0.453 + 0.4425C_B - 0.2862C_M - 0.003467\frac{B}{T} + 0.3696C_W\right) \\ & + 2.38\frac{A_{BT}}{C_B} \end{aligned}$$

Where

$$C_8 = \begin{cases} \dfrac{BS}{LDT_A} & \text{if } (B/T_A \leq 5) \\ S\dfrac{\left(\frac{7B}{T_A} - 25\right)}{LD\left(\frac{B}{T_A} - 3\right)} & \text{if } (B/T_A > 5) \end{cases}$$

$$C_9 = \begin{cases} C_8 & \text{if } (C_8 \leq 28) \\ 32 - \dfrac{16}{C_8 - 24} & \text{if } (C_8 > 28) \end{cases}$$

$$C_{11} = \begin{cases} \dfrac{T_A}{D} & \text{if } (T_A/D \leq 2) \\ 0.0833333\left(\dfrac{T_A}{D}\right)^3 + 1.33333 & \text{if } (T_A/D > 2) \end{cases}$$

$$C_{19} = \begin{cases} \dfrac{0.12997}{0.95 - C_B} - \dfrac{0.11056}{0.95 - C_P} & \text{if } (C_P \leq 0.7) \\ \dfrac{0.18567}{1.3571 - C_M} - 0.72476 + 0.38648C_P & \text{if } (C_P > 0.7) \end{cases}$$

$$C_{20} = 1 + 0.015C_{\text{stern}}$$

$$C_{P1} = 1.45C_P - 0.315 - 0.0225\text{LCB}$$

$$C_v = \left(1 + K_1\right)C_F + C_A$$

Where C_v is the viscous resistance coefficient.

B.5 Formulae used for the Wageningen B-Screw Series Calculations

Equations presented in this section are from the work carried out by Oosterveld and van Oossanen (1975). The thrust coefficient, K_T and torque coefficient K_Q are calculated from equations B.1

$$K_T = \sum_{s,t,u,v} \left[C_{T_{s,t,u,v}} \cdot J_P^s \left(\frac{P}{D}\right)^t \left(\frac{A_E}{A_O}\right)^u Z^v \right] \tag{B.1a}$$

$$K_Q = \sum_{s,t,u,v} \left[C_{Q_{s,t,u,v}} \cdot J_P^s \left(\frac{P}{D}\right)^t \left(\frac{A_E}{A_O}\right)^u Z^v \right] \tag{B.1b}$$

The thrust and torque coefficients of equations B.1 are applicable for a Reynold's Number of 2×10^6. Corrections for Reynold's Numbers between 2×10^6 and 2×10^9 can be obtained from equations B.2.

For $R_n \neq 2 \times 10^6$

$$K_T\left(R_n\right) = K_T + \Delta K_T \tag{B.2a}$$

$$K_Q\left(R_n\right) = K_Q + \Delta K_Q \tag{B.2b}$$

Where

$$\begin{aligned}
\Delta K_T =& 0.000353485 \\
&- 0.00333758 \left(\frac{A_E}{A_O}\right) J^2 \\
&- 0.00478125 \left(\frac{A_E}{A_O}\right) \frac{P}{D} J \\
&+ 0.000257792 \left(\log R_n - 0.301\right)^2 \frac{A_E}{A_O} J^2 \\
&+ 0.0000643192 \left(\log R_n - 0.301\right) \frac{P}{D}^6 J^2 \\
&- 0.0000110636 \left(\log R_n - 0.301\right)^2 \frac{P}{D}^6 J^2 \\
&- 0.0000276305 \left(\log R_n - 0.301\right)^2 Z \frac{A_E}{A_O} J^2 \\
&+ 0.0000954 \left(\log R_n - 0.301\right) Z \frac{A_E}{A_O} \frac{P}{D} J \\
&+ 0.0000032049 \left(\log R_n - 0.301\right) Z^2 \frac{A_E}{A_O} \frac{P}{D}^3 J
\end{aligned}$$

$$
\begin{aligned}
\Delta K_Q = &- 0.000591412 \\
&+ 0.00696898\frac{P}{D} \\
&- 0.0000666654Z\frac{P}{D}^6 \\
&+ 0.0160818\frac{A_E}{A_O}^2 \\
&- 0.000938091\left(\log R_n - 0.301\right)\frac{P}{D} \\
&- 0.00059593\left(\log R_n - 0.301\right)\frac{P}{D}^2 \\
&+ 0.0000782099\left(\log R_n - 0.301\right)^2\frac{P}{D}^2 \\
&+ 0.0000052199\left(\log R_n - 0.301\right)Z\frac{A_E}{A_O}J^2 \\
&- 0.00000088528\left(\log R_n - 0.301\right)^2 Z\frac{A_E}{A_O}\frac{P}{D}J \\
&+ 0.0000230171\left(\log R_n - 0.301\right)Z\frac{P}{D}^6 \\
&- 0.00000184341\left(\log R_n - 0.301\right)^2 Z\frac{P}{D}^6 \\
&- 0.00400252\left(\log R_n - 0.301\right)\frac{A_E}{A_O}^2 \\
&+ 0.000220915\left(\log R_n - 0.301\right)^2\frac{A_E}{A_O}^2
\end{aligned}
$$

B.5.1 Geometry of the Wageningen B-Screw Series Propellers

Formulae for the calculation of the geometry of the B-Screw series propeller are presented in the work of Oosterveld and van Oossanen (1975) and summarised here, with reference to fig. B.1.

$$
\left.
\begin{aligned}
Y_{\text{face}} &= V_1\left(t_{\max} - t_{\text{t.e.}}\right) \\
Y_{\text{back}} &= \left(V_1 + V_2\right)\left(t_{\max} - t_{\text{t.e.}}\right) + t_{\text{t.e.}}
\end{aligned}
\right\} \quad \text{For} P \leq 0 \tag{B.4}
$$

$$
\left.
\begin{aligned}
Y_{\text{face}} &= V_1\left(t_{\max} - t_{\text{l.e.}}\right) \\
Y_{\text{back}} &= \left(V_1 + V_2\right)\left(t_{\max} - t_{\text{l.e.}}\right) + t_{\text{l.e.}}
\end{aligned}
\right\} \quad \text{For} P \geq 0 \tag{B.5}
$$

Y_{face} and Y_{back} are the vertical ordinate of a point on a blade section on the face and on the back with respect to the pitch line. $t_{\max}$ is the maximum thickness of blade section. $t_{\text{t.e}}$ and $t_{\text{l.e}}$ is the extrapolated blade section thickness at the trailing

n	$C_{T_{s,t,u,v}}$	$S(J)$	$t(P/D)$	$u(A_e/A_o)$	$v(Z)$
1	0.008804960	0	0	0	0
2	-0.204554000	1	0	0	0
3	0.166351000	0	1	0	0
4	0.158114000	0	2	0	0
5	-0.147581000	2	0	1	0
6	-0.481497000	1	1	1	0
7	0.415437000	0	2	1	0
8	0.014404300	0	0	0	1
9	-0.053005400	2	0	0	1
10	0.014348100	0	1	0	1
11	0.060682600	1	1	0	1
12	-0.012589400	0	0	1	1
13	0.010968900	1	0	1	1
14	-0.133698000	0	3	0	0
15	0.006384070	0	6	0	0
16	-0.001327180	2	6	0	0
17	0.168496000	3	0	1	0
18	-0.050721400	0	0	2	0
19	0.085455900	2	0	2	0
20	-0.050447500	3	0	2	0
21	0.010465000	1	6	2	0
22	-0.006482720	2	6	2	0
23	-0.008417280	0	3	0	1
24	0.016842400	1	3	0	1
25	-0.001022960	3	3	0	1
26	-0.031779100	0	3	1	1
27	0.018604000	1	0	2	1
28	-0.004107980	0	2	2	1
29	-0.000606848	0	0	0	2
30	-0.004981900	1	0	0	2
31	0.002598300	2	0	0	2
32	-0.000560528	3	0	0	2
33	-0.001636520	1	2	0	2
34	-0.000328787	1	6	0	2
35	0.000116502	2	6	0	2
36	0.000690904	0	0	1	2
37	0.004217490	0	3	1	2
38	0.000056523	3	6	1	2
39	-0.001465640	0	3	2	2

Table B.3: Coefficients for K_T polynomials

n	$C_{Q_{s,t,u,v}}$	$S(J)$	$t(P/D)$	$u(A_e/A_o)$	$v(Z)$
1	0.003793680	0	0	0	0
2	0.008865230	2	0	0	0
3	-0.032241000	1	1	0	0
4	0.003447780	0	2	0	0
5	-0.040881100	0	1	1	0
6	-0.108009000	1	1	1	0
7	-0.088538100	2	1	1	0
8	0.188561000	0	2	1	0
9	-0.003708710	1	0	0	1
10	0.005136960	0	1	0	1
11	0.020944900	1	1	0	1
12	0.004743190	2	1	0	1
13	-0.007234080	2	0	1	1
14	0.004383880	1	1	1	1
15	-0.026940300	0	2	1	1
16	0.055808200	3	0	1	0
17	0.016188600	0	3	1	0
18	0.003180860	1	3	1	0
19	0.015896000	0	0	2	0
20	0.047172900	1	0	2	0
21	0.019628300	3	0	2	0
22	-0.050278200	0	1	2	0
23	-0.030055000	3	1	2	0
24	0.041712200	2	2	2	0
25	-0.039772200	0	3	2	0
26	-0.003500240	0	6	2	0
27	-0.010685400	3	0	0	1
28	0.001109030	3	3	0	1
29	-0.000313912	0	6	0	1
30	0.003598500	3	0	1	1
31	-0.001421210	0	6	1	1
32	-0.003836370	1	0	2	1
33	0.012680300	0	2	2	1
34	-0.003182780	2	3	2	1
35	0.003342680	0	6	2	1
36	-0.001834910	1	1	0	2
37	0.000112451	3	2	0	2
38	-0.000029723	3	6	0	2
39	0.000269551	1	0	1	2
40	0.000832650	2	0	1	2
41	0.001553340	0	2	1	2
42	0.000302683	0	6	1	2
43	-0.000184300	0	0	2	2
44	-0.000425399	0	3	2	2
45	0.000086924	3	3	2	2
46	-0.000465900	0	6	2	2
47	0.000055419	1	6	2	2

Table B.4: Coefficients for K_Q polynomials

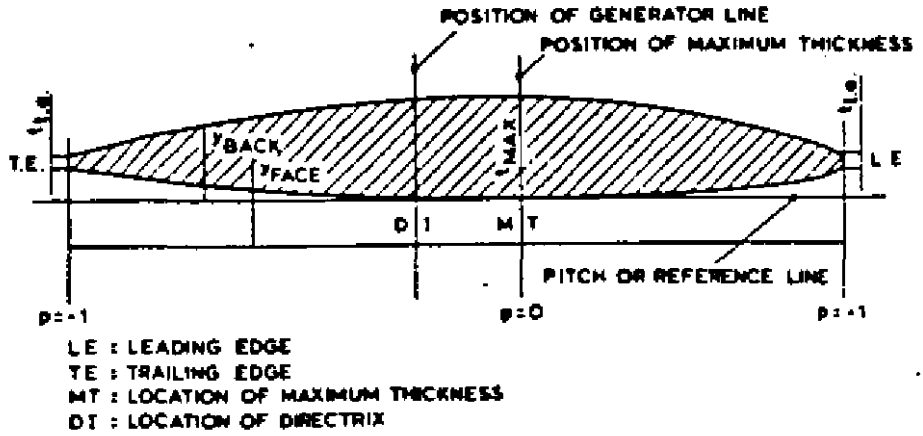

Figure B.1: Geometry of B-Screw Propeller (Oosterveld and van Oossanen, 1975)

r/R	$\frac{c}{D}\frac{Z}{A_E/A_O}$	$\frac{a}{c}$	$\frac{b}{c}$	A_r	B_r
0.2	1.662	0.617	0.350	0.0526	0.0040
0.3	1.882	0.613	0.350	0.0464	0.0035
0.4	2.050	0.601	0.351	0.0402	0.0030
0.5	2.152	0.586	0.355	0.0340	0.0025
0.6	2.187	0.561	0.389	0.0278	0.0020
0.7	2.144	0.524	0.443	0.0216	0.0015
0.8	1.970	0.463	0.479	0.0154	0.0010
0.9	1.582	0.351	0.500	0.0092	0.0005
1.0	0.000	0.000	0.000	0.0030	0.0000

Table B.5: B-Screw Dimensions for Four, Five, Six and Seven-Bladed Propellers

and leading edges respectively. V_1 and V_2 are the tabulated functions dependent on r/R and P. P is the non-dimensional coordinate along pitch line from position of maximum thickness to leading edge (where $P = 1$), and from position of maximum thickness to trailing edge (where $P =$ -1).

Where

$$\frac{t}{D} = A_r - B_r Z \tag{B.6}$$

a is the distance between leading edge and generator line at r, b is the distance between leading edge and location of maximum thickness, c is the chord length of the blade's section at radius r and t is the maximum blade section thickness at radius r.

r/R	$\frac{c}{D}\frac{Z}{A_E/A_O}$	$\frac{a}{c}$	$\frac{b}{c}$	A_r	B_r
0.2	1.633	0.616	0.350	0.0526	0.0040
0.3	1.832	0.611	0.350	0.0464	0.0035
0.4	2.000	0.599	0.350	0.0402	0.0030
0.5	2.120	0.583	0.355	0.0340	0.0025
0.6	2.186	0.558	0.389	0.0278	0.0020
0.7	2.168	0.526	0.442	0.0216	0.0015
0.8	2.127	0.481	0.478	0.0154	0.0010
0.9	1.657	0.400	0.500	0.0092	0.0005
1.0	0.000	0.000	0.000	0.0030	0.0000

Table B.6: B-Screw Dimensions for Three-Bladed Propellers

B.6 Coefficients for use in Blendermann's Wind Force Model

The coefficients for use in the wind force model of Blendermann (1996) are presented in Table B.9 Where $CD_{l_{AF_{\text{bow}}}}$ is the longitudinal drag coefficient if the relative wind direction is coming from the bow. $CD_{l_{AF_{\text{stern}}}}$ is the longitudinal drag coefficient if the relative wind direction is coming from the stern. δ is the cross-force parameter, and κ is a rolling moment factor.

B.7 The Beaufort Scale

The Beaufort scale can be used to define the sea's conditions that correspond to wind speed and wave height. It is used in this study in conjunction with the Townsin et al. (1992) method of estimating added resistance due to waves. The scale is given in table B.10

P / r/R	-1.0	-0.95	-0.9	-0.8	-0.7	-0.6	-0.5	-0.4	-0.2	0.0
0.15	0.3000	0.2824	0.2650	0.2300	0.1950	0.1610	0.1280	0.0955	0.0365	0.0
0.20	0.2826	0.2630	0.2400	0.1967	0.1570	0.1207	0.0880	0.0592	0.0172	0.0
0.25	0.2598	0.2372	0.2115	0.1651	0.1246	0.0899	0.0579	0.0350	0.0084	0.0
0.30	0.2306	0.2040	0.1790	0.1333	0.0943	0.0623	0.0376	0.0202	0.0033	0.0
0.40	0.1467	0.1200	0.0972	0.0630	0.0395	0.0214	0.0116	0.0044	0.0000	0.0
0.50	0.0522	0.0420	0.0330	0.0190	0.0100	0.0040	0.0012	0.0000	0.0000	0.0
0.60	0.0000	0.0000	0.0000	0.0000	0.0000	0.0000	0.0000	0.0000	0.0000	0.0
0.70	0.0000	0.0000	0.0000	0.0000	0.0000	0.0000	0.0000	0.0000	0.0000	0.0
0.80	0.0000	0.0000	0.0000	0.0000	0.0000	0.0000	0.0000	0.0000	0.0000	0.0
0.90	0.0000	0.0000	0.0000	0.0000	0.0000	0.0000	0.0000	0.0000	0.0000	0.0
1.00	0.0000	0.0000	0.0000	0.0000	0.0000	0.0000	0.0000	0.0000	0.0000	0.0
P / r/R	+0.2	+0.4	+0.5	+0.6	+0.7	+0.8	+0.85	+0.9	+0.95	+1.0
0.15	0.0096	0.0384	0.0615	0.0920	0.1320	0.1870	0.2230	0.2642	0.3150	0.3860
0.20	0.0049	0.0304	0.0520	0.0804	0.1180	0.1685	0.2000	0.2353	0.2821	0.3560
0.25	0.0031	0.0224	0.0417	0.0669	0.1008	0.1465	0.1747	0.2068	0.2513	0.3256
0.30	0.0027	0.0148	0.0300	0.0503	0.0790	0.1191	0.1445	0.1760	0.2186	0.2923
0.40	0.0000	0.0033	0.0090	0.0189	0.0357	0.0637	0.0833	0.1088	0.1467	0.2181
0.50	0.0000	0.0000	0.0008	0.0034	0.0085	0.0211	0.0328	0.0500	0.0778	0.1278
0.60	0.0000	0.0000	0.0000	0.0000	0.0000	0.0006	0.0022	0.0067	0.0169	0.0382
0.70	0.0000	0.0000	0.0000	0.0000	0.0000	0.0000	0.0000	0.0000	0.0000	0.0000
0.80	0.0000	0.0000	0.0000	0.0000	0.0000	0.0000	0.0000	0.0000	0.0000	0.0000
0.90	0.0000	0.0000	0.0000	0.0000	0.0000	0.0000	0.0000	0.0000	0.0000	0.0000
1.00	0.0000	0.0000	0.0000	0.0000	0.0000	0.0000	0.0000	0.0000	0.0000	0.0000

Table B.7: Values for V_1 as used in equations B.4 and B.5

P / r/R	-1.0	-0.95	-0.9	-0.8	-0.7	-0.6	-0.5	-0.4	-0.2	0.0
0.15	0.0	0.0540	0.1325	0.2870	0.4280	0.5585	0.6770	0.7805	0.9360	1.0
0.20	0.0	0.0640	0.1455	0.3060	0.4535	0.5842	0.6995	0.7984	0.9446	1.0
0.25	0.0	0.0725	0.1567	0.3228	0.4740	0.6050	0.7184	0.8139	0.9519	1.0
0.30	0.0	0.0800	0.1670	0.3360	0.4885	0.6195	0.7335	0.8265	0.9583	1.0
0.40	0.0	0.0905	0.1810	0.3500	0.5040	0.6353	0.7525	0.8415	0.9645	1.0
0.50	0.0	0.0950	0.1865	0.3569	0.5140	0.6439	0.7580	0.8456	0.9639	1.0
0.60	0.0	0.0965	0.1885	0.3585	0.5110	0.6415	0.7530	0.8426	0.9613	1.0
0.70	0.0	0.0975	0.1900	0.3600	0.5100	0.6400	0.7500	0.8400	0.9600	1.0
0.80	0.0	0.0975	0.1900	0.3600	0.5100	0.6400	0.7500	0.8400	0.9600	1.0
0.85	0.0	0.0975	0.1900	0.3600	0.5100	0.6400	0.7500	0.8400	0.9600	1.0
0.90	0.0	0.0975	0.1900	0.3600	0.5100	0.6400	0.7500	0.8400	0.9600	1.0
1.00	0.0	0.0975	0.1900	0.3600	0.5100	0.6400	0.7500	0.8400	0.9600	1.0
P / r/R	+0.2	+0.4	+0.5	+0.6	+0.7	+0.8	+0.85	+0.9	+0.95	+1.0
0.15	0.9760	0.8825	0.8055	0.7105	0.5995	0.4520	0.3665	0.2600	0.1300	0.0
0.20	0.9750	0.8875	0.8170	0.7277	0.6190	0.4777	0.3905	0.2840	0.1560	0.0
0.25	0.9751	0.8899	0.8259	0.7415	0.6359	0.4982	0.4108	0.3042	0.1758	0.0
0.30	0.9750	0.8020	0.8315	0.7520	0.6505	0.5130	0.4265	0.3197	0.1890	0.0
0.40	0.9725	0.8933	0.8345	0.7593	0.6590	0.5220	0.4335	0.3235	0.1935	0.0
0.50	0.9710	0.8880	0.8275	0.7478	0.6430	0.5039	0.4135	0.3056	0.1750	0.0
0.60	0.9690	0.8790	0.8090	0.7200	0.6060	0.4620	0.3775	0.2720	0.1485	0.0
0.70	0.9675	0.8660	0.7850	0.6840	0.5615	0.4140	0.3300	0.2337	0.1240	0.0
0.80	0.9635	0.8520	0.7635	0.6545	0.5265	0.3765	0.2925	0.2028	0.1050	0.0
0.85	0.9615	0.8450	0.7550	0.6455	0.5160	0.3660	0.2830	0.1950	0.1000	0.0
0.90	0.9600	0.8400	0.7500	0.6400	0.5100	0.3600	0.2775	0.1900	0.0975	0.0
1.00	0.9600	0.8400	0.7500	0.6400	0.5100	0.3600	0.2775	0.1900	0.0975	0.0

Table B.8: Values for V_2 as used in equations B.4 and B.5

Vessel Type	CD_t	$CD_{l_{AF_{\text{bow}}}}$	$CD_{l_{AF_{\text{stern}}}}$	δ	κ
Car Carrier	0.95	0.55	0.60	0.80	1.2
Cargo Vessel, Loaded	0.85	0.65	0.55	0.40	1.7
Cargo Vessel, Container on Deck	0.85	0.55	0.50	0.40	1.4
Container Ship, Loaded	0.90	0.55	0.55	0.40	1.4
Destroyer	0.85	0.60	0.65	0.65	1.1
Diving Support Vessel	0.90	0.60	0.80	0.55	1.7
Drilling Vessel	1.00	0.85	0.93	0.10	1.7
Ferry	0.90	0.45	0.50	0.80	1.1
Fishing Vessel	0.95	0.70	0.70	0.40	1.1
Liquefied Natural Gas Carrier	0.70	0.60	0.65	0.50	1.1
Offshore Supply Vessel	0.90	0.55	0.80	0.55	1.2
Passenger Liner	0.90	0.40	0.40	0.80	1.2
Research Vessel	0.85	0.55	0.65	0.60	1.4
Speed Boat	0.90	0.55	0.60	0.60	1.1
Tanker, Loaded	0.70	0.90	0.55	0.40	3.1
Tanker, in Ballast	0.70	0.75	0.55	0.40	2.2
Tender	0.85	0.55	0.55	0.65	1.1

Table B.9: Blendermann's Coefficients

Beaufort Number	Description	Wind Speed (knots)	Wave Height (m)	Sea Conditions
0	Calm	<1	0.0	Flat.
1	Light Air	1 - 3	0.0 - 0.2	Ripples without crests.
2	Light Breeze	4 - 6	0.2 - 0.5	Small wavelets. Crests of glassy appearance, not breaking.
3	Gentle Breeze	7 - 10	0.5 - 1.0	Large wavelets. Crests begin to break; scattered whitecaps.
4	Moderate Breeze	11 - 16	1.0 - 2.0	Small waves with breaking crests. Fairly frequent whitecaps.
5	Fresh Breeze	17 - 21	2.0 - 3.0	Moderate waves of some length. Many whitecaps. Small amounts of spray.
6	Strong Breeze	22 - 27	3.0 - 4.0	Long waves begin to form. White foam crests are very frequent. Some airborne spray is present.
7	Near Gale	28 - 33	4.0 - 5.5	Sea heaps up. Some foam from breaking waves is blown into streaks along wind direction. Moderate amounts of airborne spray.
8	Gale	34 - 40	5.5 - 7.5	Moderately high waves with breaking crests forming spindrift. Well-marked streaks of foam are blown along wind direction. Considerable airborne spray.
9	Severe Gale	41 - 47	7.0 - 10.0	High waves whose crests sometimes roll over. Dense foam is blown along wind direction. Large amounts of airborne spray may begin to reduce visibility.
10	Storm	48 - 55	9.0 - 12.5	Very high waves with overhanging crests. Large patches of foam from wave crests give the sea a white appearance. Considerable tumbling of waves with heavy impact. Large amounts of airborne spray reduce visibility.
11	Violent Storm	56 - 63	11.5 - 16.0	Exceptionally high waves. Very large patches of foam, driven before the wind, cover much of the sea surface. Very large amounts of airborne spray severely reduce visibility.
12	Hurricane	≥ 64	≥ 14.0	Huge waves. Sea is completely white with foam and spray. Air is filled with driving spray, greatly reducing visibility

Table B.10: The Beaufort Scale

Appendix C. Simulation Results

This Appendix presents the output of the *SiS* simulator for each of the case studies described in Chapter 6 of this research.

C.1 Case 1. Esso Osaka, 20 Knot Wind (Fresh Breeze), oovoo Propulsion Model, Automatic Control, Propeller Optimisation

```
    |=============================================|
    | Ship-in-Service Performance Estimator       |
    |=============================================|
    | (c) 2013 David Trodden                      |
    | School of Marine Science and Technology     |
    | Newcastle University, UK                    |
    |=============================================|

"Esso Osaka VLCC - Loaded Test Case"
====================================


Simuation Parameters
--------------------
  Simulation is speed and track automatic pilot.
  Using the Oosterveld and van Oossanen propulsion model.
  Mean true wind speed =                                  20.00 knots
  Mean true wind direction =                              90.00 degrees


Ship Main Particulars
---------------------
  Service Speed =                                         10.00 knots
  Lpp =                                                  325.00 m
  Lwl =                                                  335.00 m
  B =                                                     53.00 m
  T =                                                     21.79 m
  Volume of Displacement =                            311901.50 m^3
  Mass of Ship =                                      319699.06 tonnes
  LCB relative to midships +Fwd (%) =                     3.169
  Midship Coefficient, Cm =                               0.990
  Waterplane Coefficient, Cwp =                           0.850
  Block Coefficient, Cb =                                 0.831
  Prismatic Coefficient, Cp =                             0.839


Resistance Calculations from Holtrop & Mennen (Calm Water)
----------------------------------------------------------
  Friction Resistance =                                 704.530 kN
  Appendage Resistance =                                  8.309 kN
  Wave Making Resistance =                                0.266 kN
  Added Pressure Resistance of Bulbous Bow =              0.000 kN
  Added Pressure Resistance of Immersed Transom Stern =   7.152 kN
  Model-Ship Correlation Line =                          81.067 kN
  Total Calm Water Resistance =                         801.324 kN


Iteration:  1
==============


  Optimised Propeller Selection
```

```
  ------------------------------
    Number of Propellers =                    1
    Number of Blades =                        5
    Diameter =                             9.10 m
    Pitch =                                7.84 m
    Expanded Blade Area Ratio =           0.643
    Optimum Open Water Efficiency =       0.533
    Optimum Revolutions =                 47.84 rpm


In-Service Propulsion Characteristics
-------------------------------------
  Average 'quasi-steady state' resultant resistance =          911.999 kN
  Average 'quasi-steady state' resultant ship speed =            9.939 knots
  Average 'quasi-steady state' propeller efficiency =            0.512
  Average 'quasi-steady state' propeller revolutions =          49.948 rpm
  Average 'quasi-steady state' advance ratio =                   0.453
  Average 'quasi-steady state' Delivered Power =              7613.606 kW
  Average 'quasi-steady state' Engine Brake Power =           7682.621 kW
  Average 'quasi-steady state' drift angle at propeller =       -0.368 degrees


Iteration:  2
==============


  Optimised Propeller Selection
  ------------------------------
    Number of Propellers =                    1
    Number of Blades =                        5
    Diameter =                             9.10 m
    Pitch =                                7.69 m
    Expanded Blade Area Ratio =           0.643
    Optimum Open Water Efficiency =       0.513
    Optimum Revolutions =                 50.59 rpm


In-Service Propulsion Characteristics
-------------------------------------
  Average 'quasi-steady state' resultant resistance =          913.140 kN
  Average 'quasi-steady state' resultant ship speed =            9.945 knots
  Average 'quasi-steady state' propeller efficiency =            0.512
  Average 'quasi-steady state' propeller revolutions =          50.629 rpm
  Average 'quasi-steady state' advance ratio =                   0.447
  Average 'quasi-steady state' Delivered Power =              7627.761 kW
  Average 'quasi-steady state' Engine Brake Power =           7696.889 kW
  Average 'quasi-steady state' drift angle at propeller =       -0.365 degrees
```

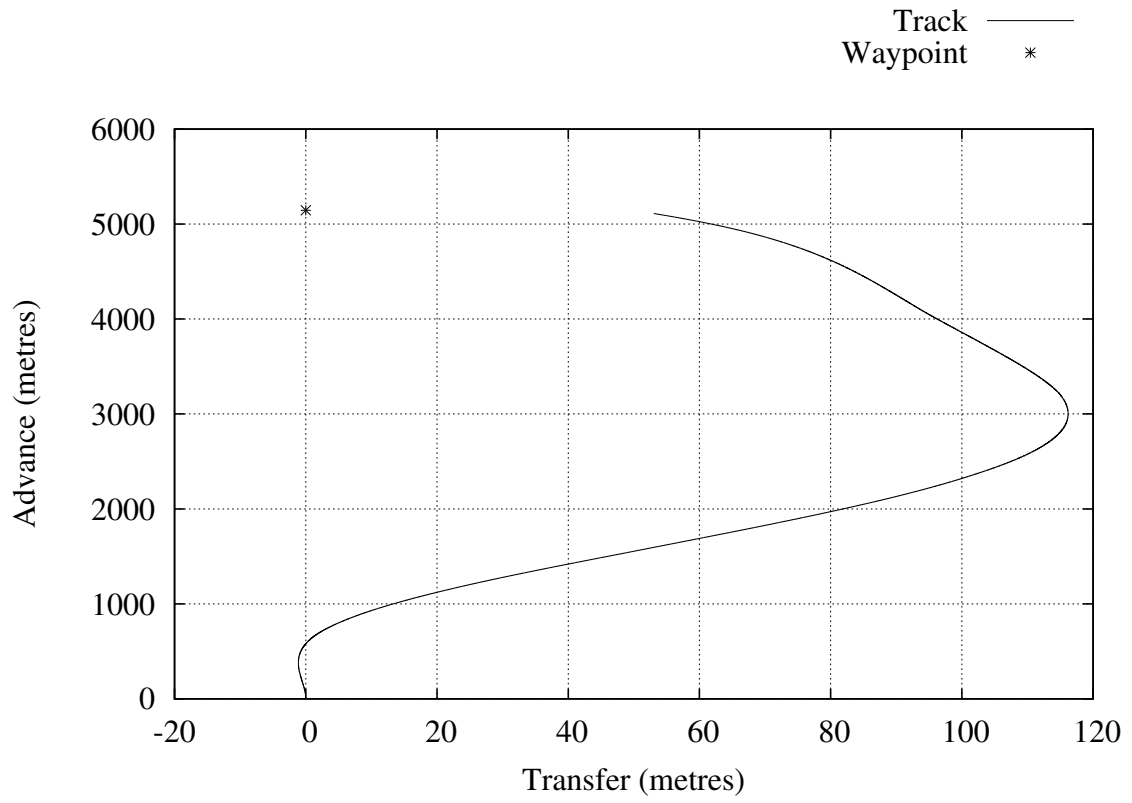

Figure C.1: Case 1: Ship Track

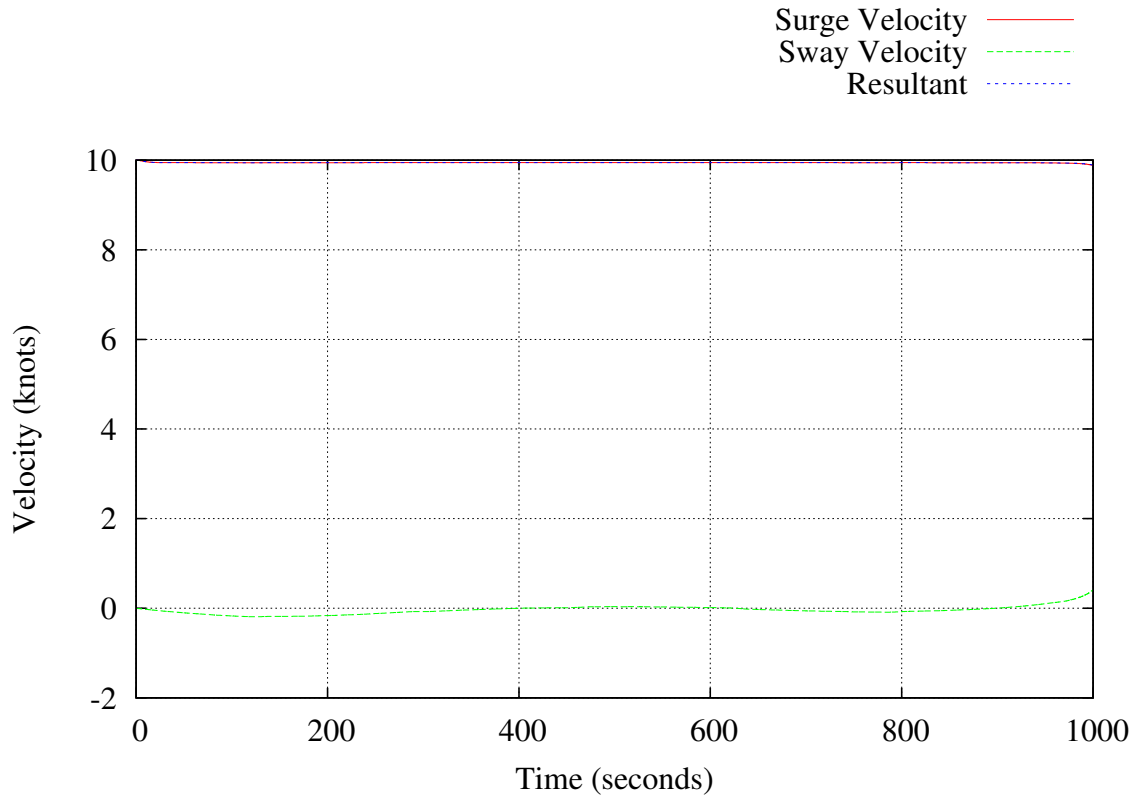

Figure C.2: Case 1: Speed vs. Time

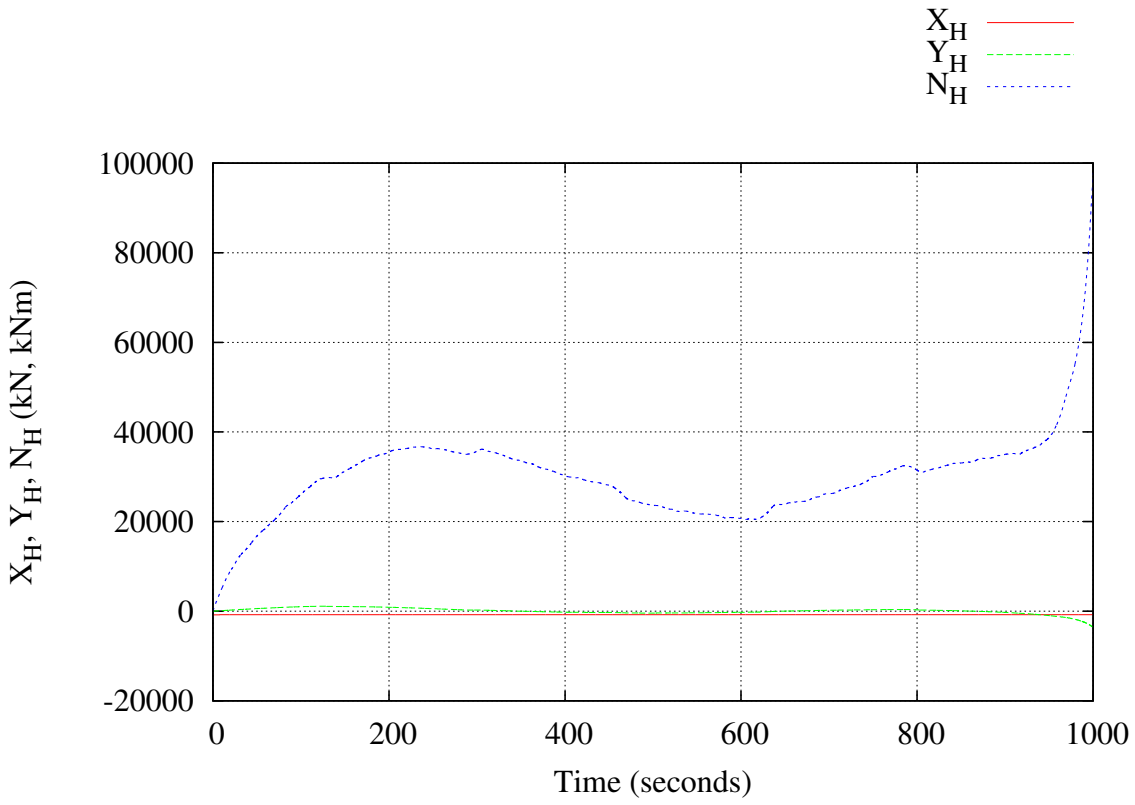

Figure C.3: Case 1: Hull Forces vs. Time

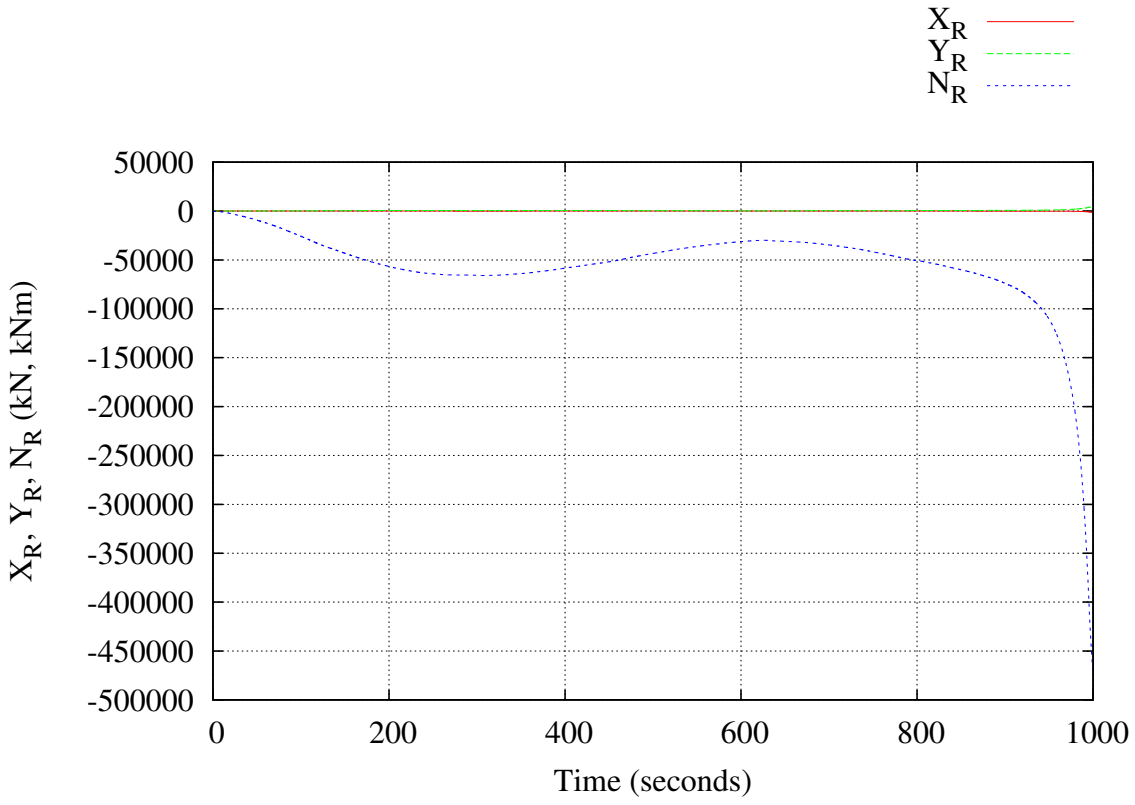

Figure C.4: Case 1: Rudder Force vs. Time

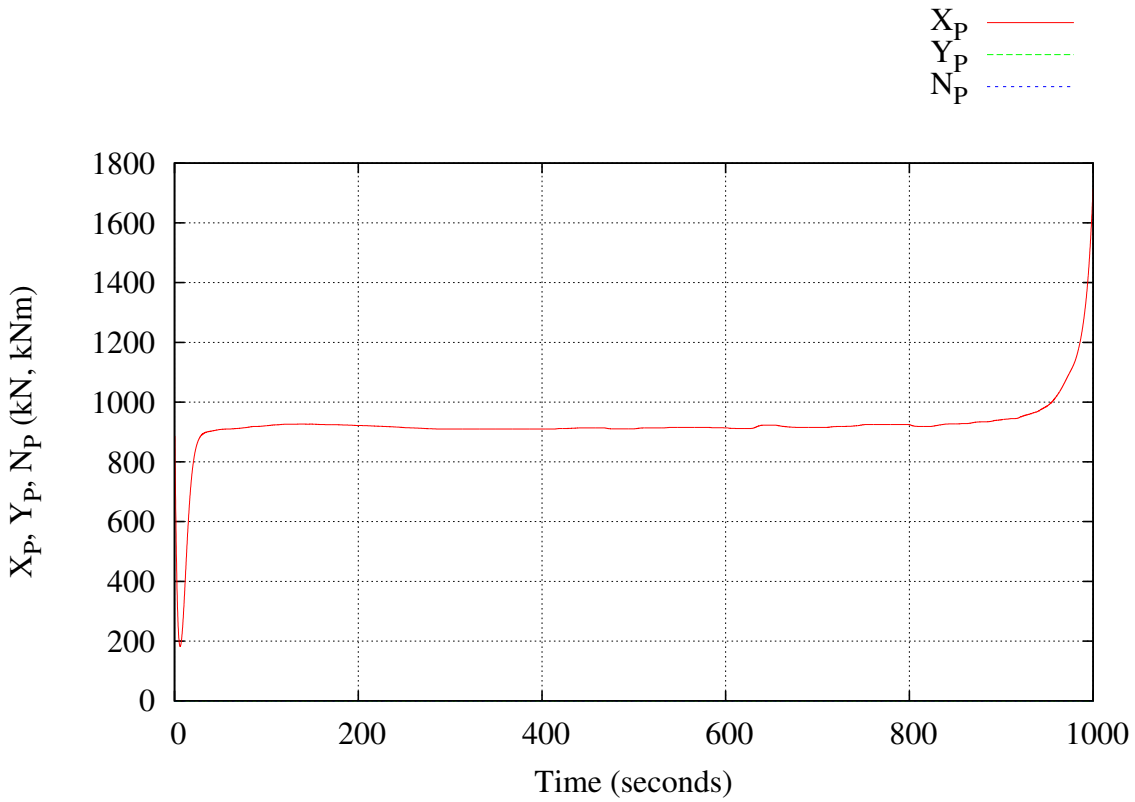

Figure C.5: Case 1: Propeller Force vs. Time

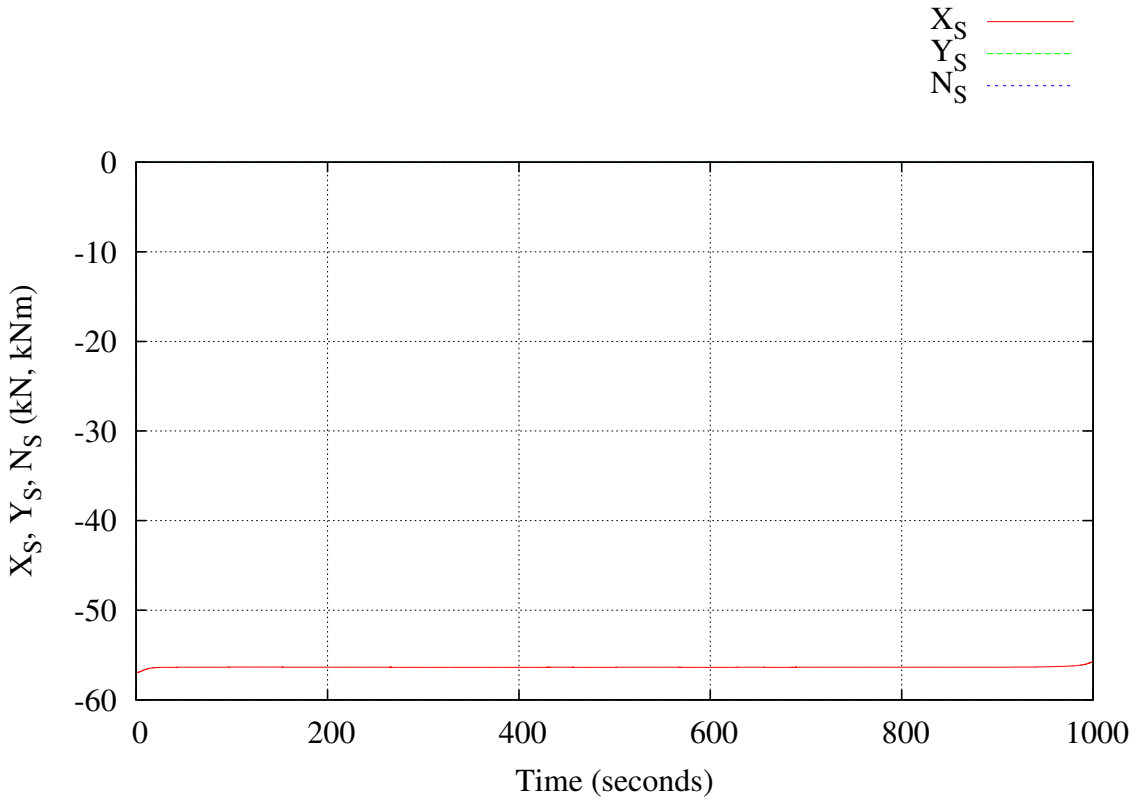

Figure C.6: Case 1: Seaway Force vs. Time

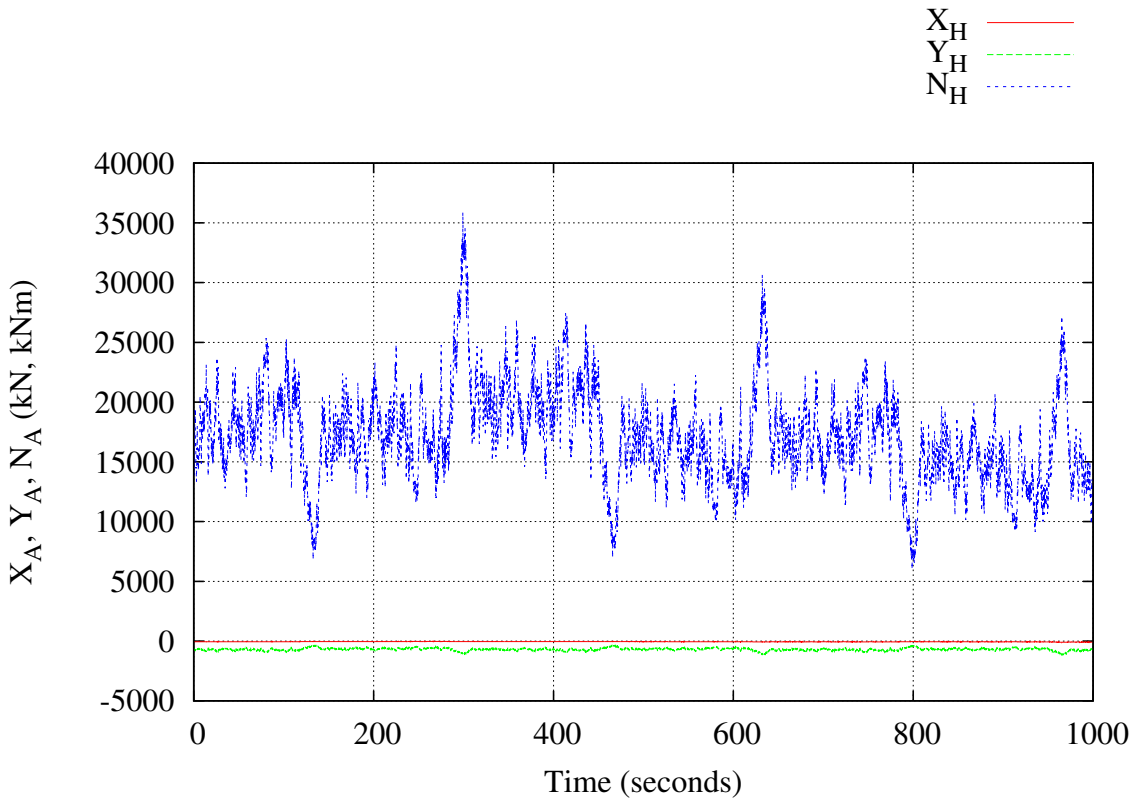

Figure C.7: Case 1: Wind Force vs. Time

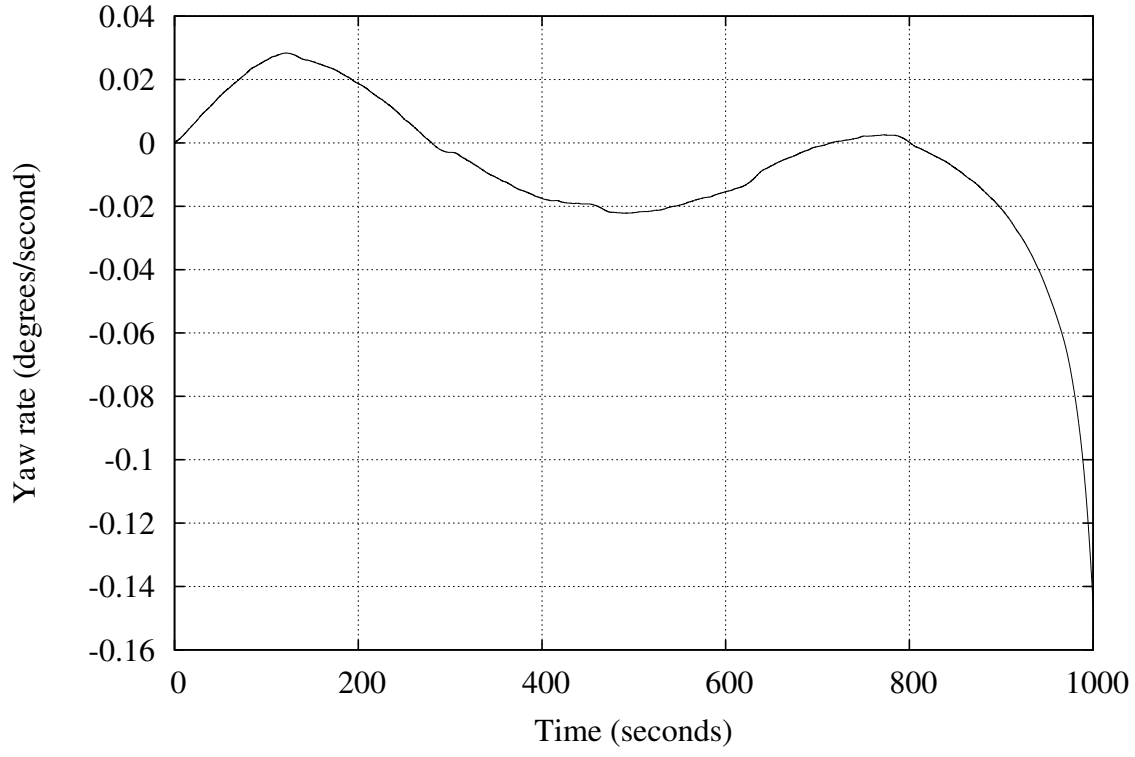

Figure C.8: Case 1: Yaw Rate vs. Time

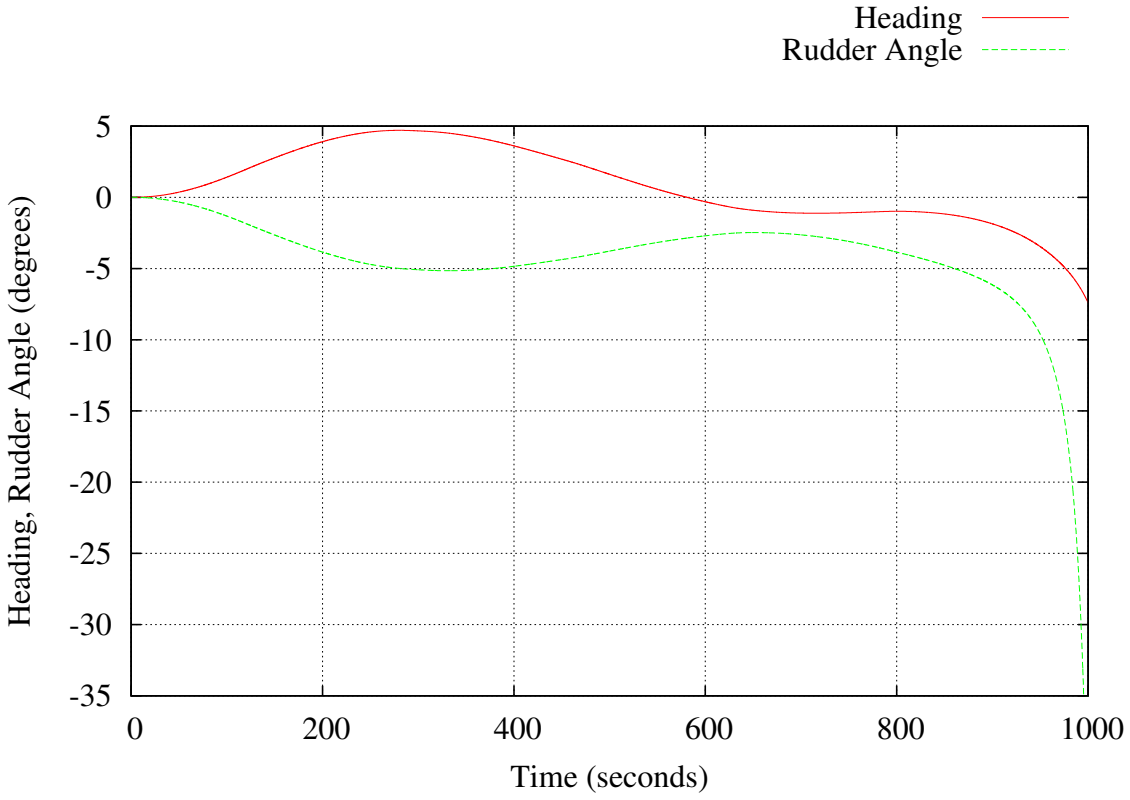

Figure C.9: Case 1: Rudder Command and Heading vs. Time

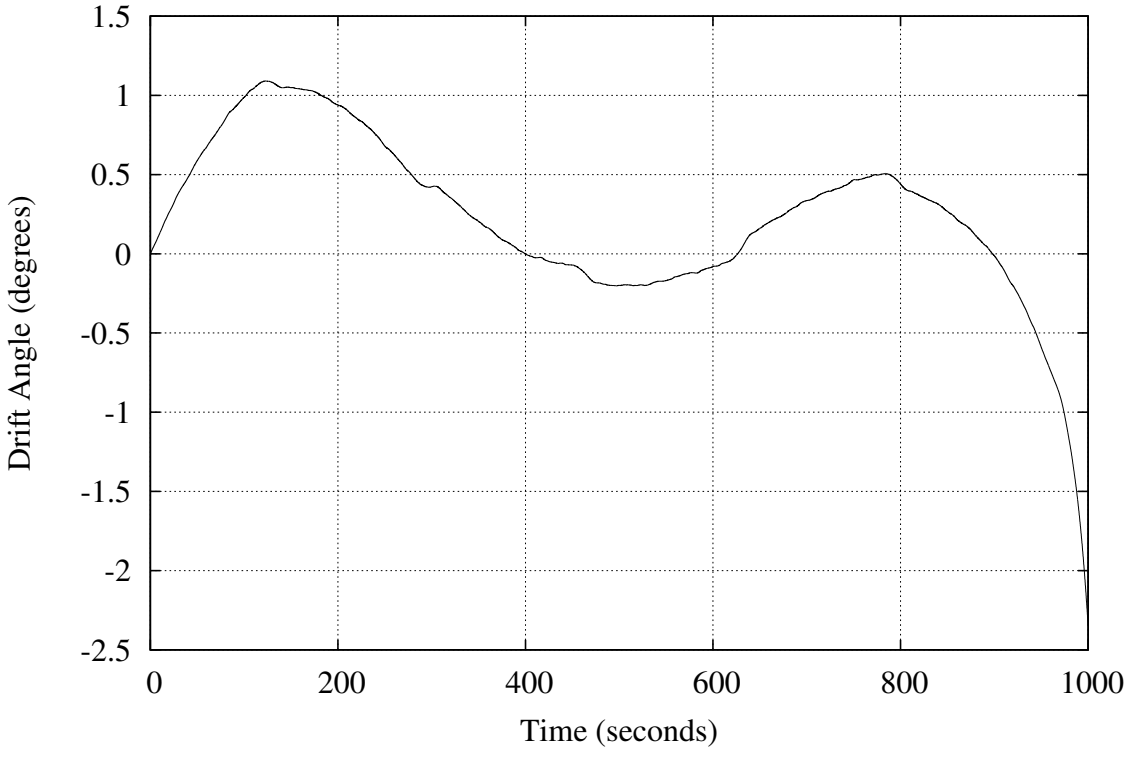

Figure C.10: Case 1: Drift Angle vs. Time

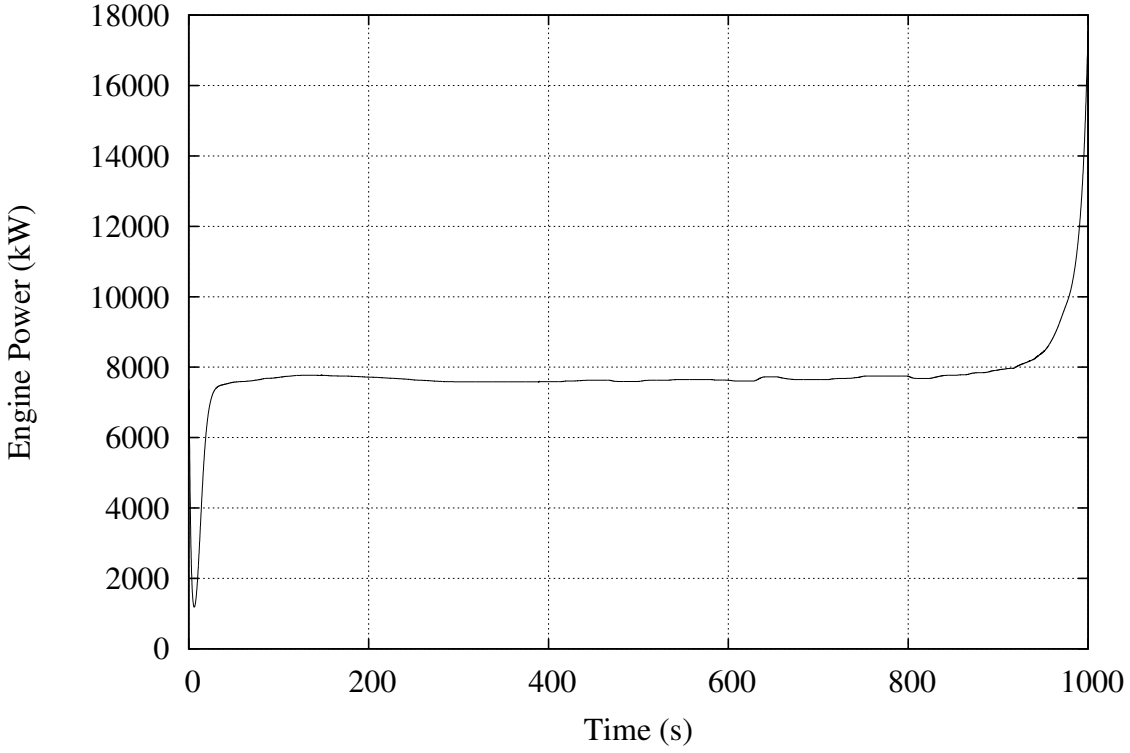

Figure C.11: Case 1: Engine Power vs. Time

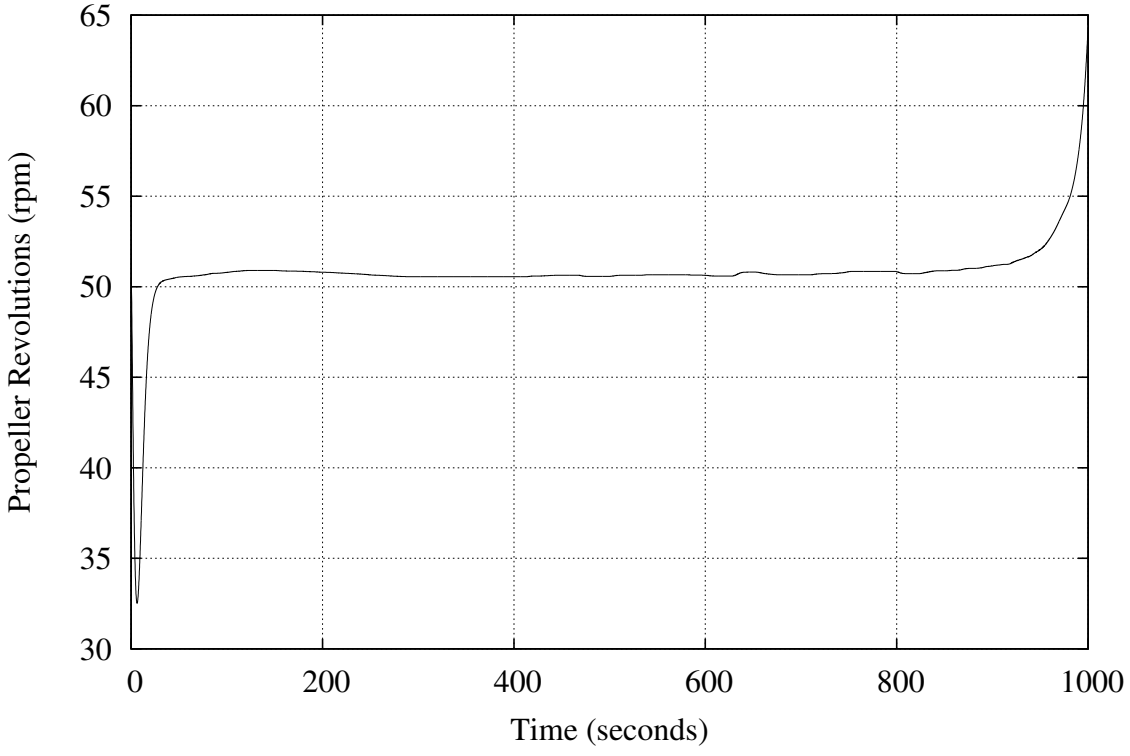

Figure C.12: Case 1: Propeller Revolutions vs. Time

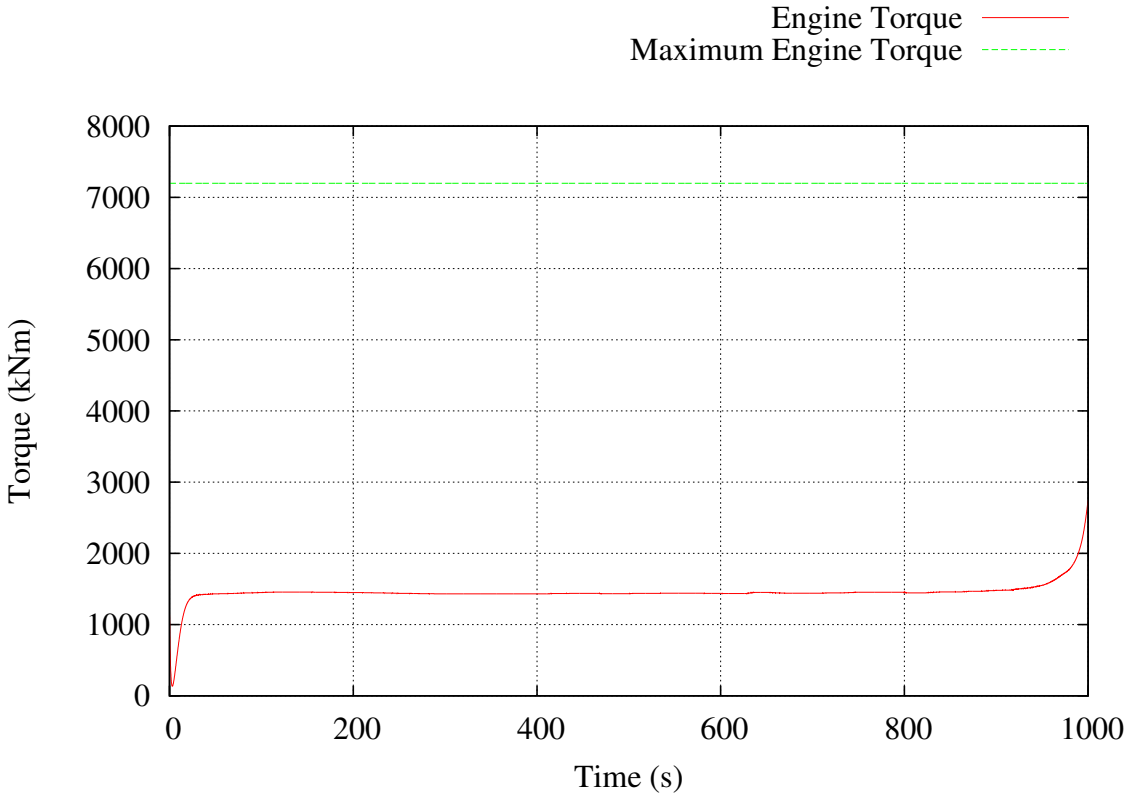

Figure C.13: Case 1: Engine Torque vs. Time

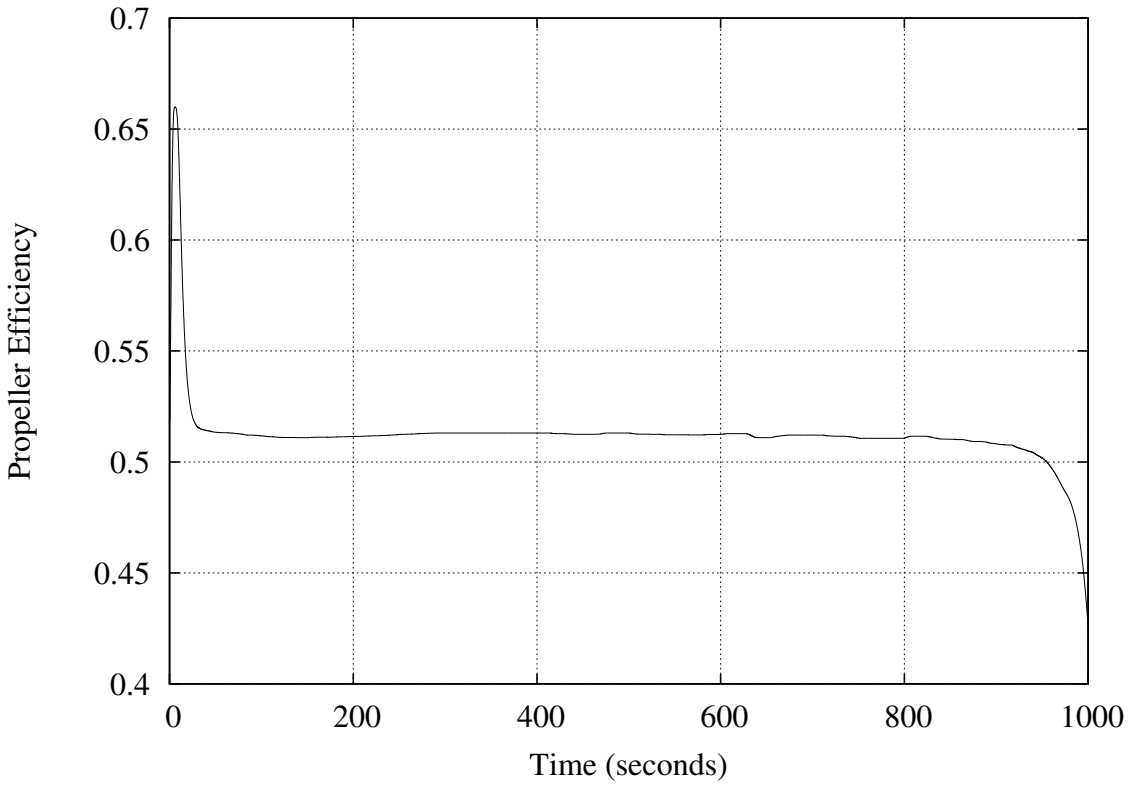

Figure C.14: Case 1: Open Water Propeller Efficiency vs. Time

C.2 Case 2. Esso Osaka, 20 Knot Wind (Fresh Breeze), Unsteady MBEMT Propulsion Model, Automatic Control, Propeller Optimisation

```
    |=============================================|
    | Ship-in-Service Performance Estimator       |
    |=============================================|
    | (c) 2013 David Trodden                      |
    | School of Marine Science and Technology     |
    | Newcastle University, UK                    |
    |=============================================|


"Esso Osaka VLCC - Loaded Test Case"
====================================


Simuation Parameters
--------------------
  Simulation is speed and track automatic pilot.
  Using an unsteady BEMT propulsion model.
  Mean true wind speed =                                  20.00 knots
  Mean true wind direction =                              90.00 degrees


Ship Main Particulars
---------------------
  Service Speed =                                         10.00 knots
  Lpp =                                                  325.00 m
  Lwl =                                                  335.00 m
  B =                                                     53.00 m
  T =                                                     21.79 m
  Volume of Displacement =                            311901.50 m^3
  Mass of Ship =                                      319699.06 tonnes
  LCB relative to midships +Fwd (%) =                     3.169
  Midship Coefficient, Cm =                               0.990
  Waterplane Coefficient, Cwp =                           0.850
  Block Coefficient, Cb =                                 0.831
  Prismatic Coefficient, Cp =                             0.839


Resistance Calculations from Holtrop & Mennen (Calm Water)
----------------------------------------------------------
  Friction Resistance =                                 704.530 kN
  Appendage Resistance =                                  8.309 kN
  Wave Making Resistance =                                0.266 kN
  Added Pressure Resistance of Bulbous Bow =              0.000 kN
  Added Pressure Resistance of Immersed Transom Stern =   7.152 kN
  Model-Ship Correlation Line =                          81.067 kN
  Total Calm Water Resistance =                         801.324 kN


Iteration:  1
==============


  Optimised Propeller Selection
  -----------------------------
    Number of Propellers =                    1
    Number of Blades =                        5
    Diameter =                             9.10 m
    Pitch =                                6.95 m
    Expanded Blade Area Ratio =            0.692
    Optimum Open Water Efficiency =        0.542
    Optimum Revolutions =                 51.77 rpm


In-Service Propulsion Characteristics
-------------------------------------
  Average 'quasi-steady state' resultant resistance =              915.190 kN
  Average 'quasi-steady state' resultant ship speed =                9.938 knots
  Average 'quasi-steady state' propeller efficiency =                0.519
  Average 'quasi-steady state' propeller revolutions =              54.069 rpm
  Average 'quasi-steady state' advance ratio =                       0.418
  Average 'quasi-steady state' Delivered Power =                  7594.118 kW
  Average 'quasi-steady state' Engine Brake Power =               7684.934 kW
```

```
  Average 'quasi-steady state' drift angle at propeller =          -0.813 degrees

Iteration:  2
==============


  Optimised Propeller Selection
  -----------------------------
    Number of Propellers =                    1
    Number of Blades =                        5
    Diameter =                             9.10 m
    Pitch =                                6.95 m
    Expanded Blade Area Ratio =           0.692
    Optimum Open Water Efficiency =       0.519
    Optimum Revolutions =                53.96 rpm


In-Service Propulsion Characteristics
-------------------------------------
  Average 'quasi-steady state' resultant resistance =            914.647 kN
  Average 'quasi-steady state' resultant ship speed =              9.945 knots
  Average 'quasi-steady state' propeller efficiency =              0.520
  Average 'quasi-steady state' propeller revolutions =            54.047 rpm
  Average 'quasi-steady state' advance ratio =                     0.419
  Average 'quasi-steady state' Delivered Power =                7555.176 kW
  Average 'quasi-steady state' Engine Brake Power =             7645.531 kW
  Average 'quasi-steady state' drift angle at propeller =         -0.527 degrees
```

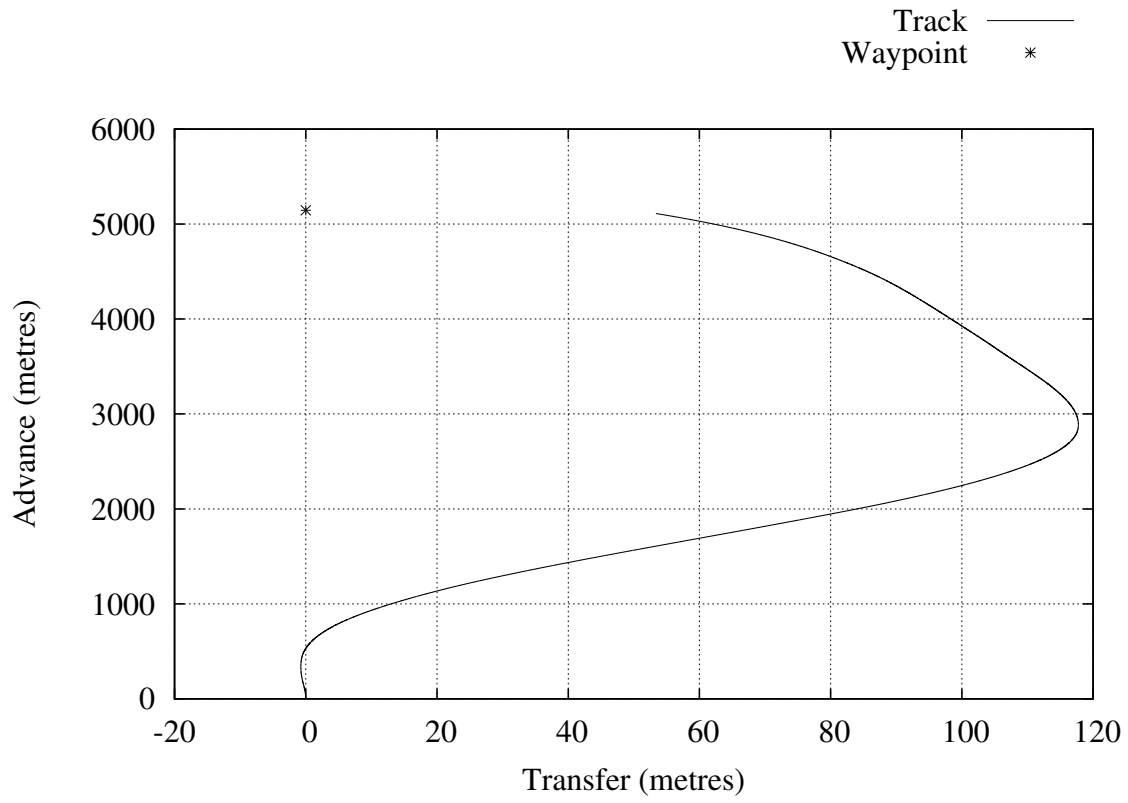

Figure C.15: Case 2: Ship Track

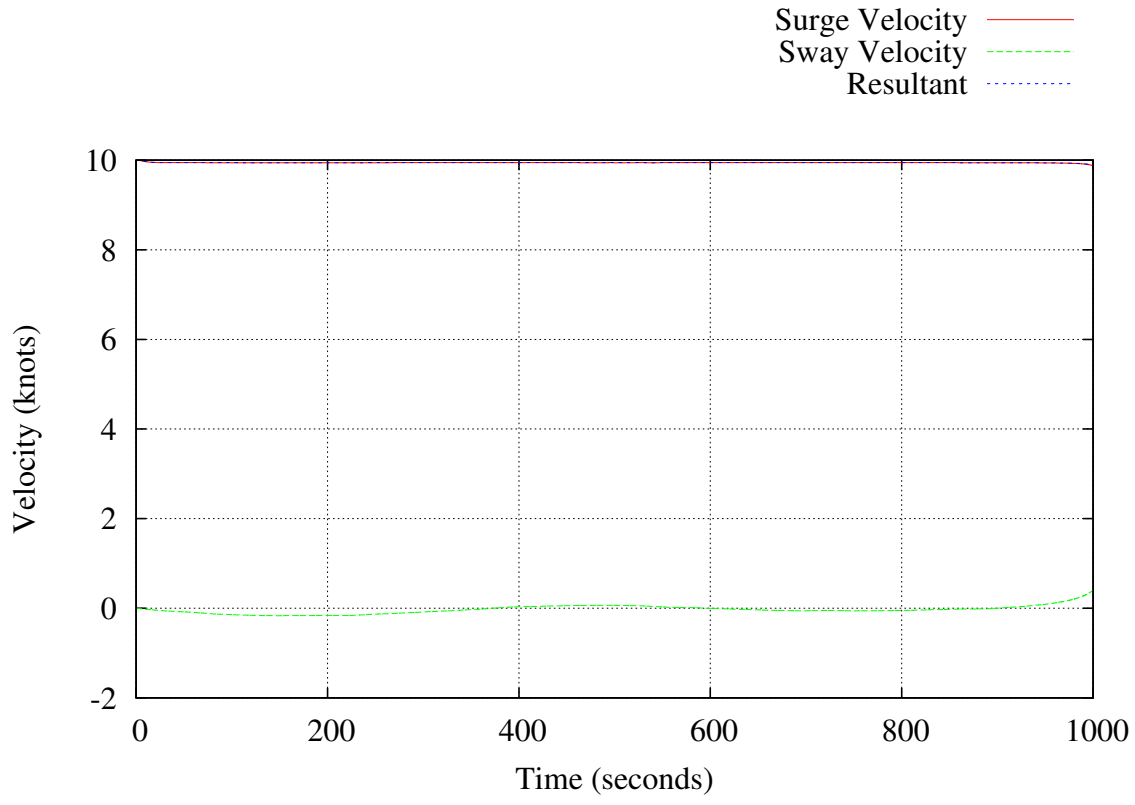

Figure C.16: Case 2: Speed vs. Time

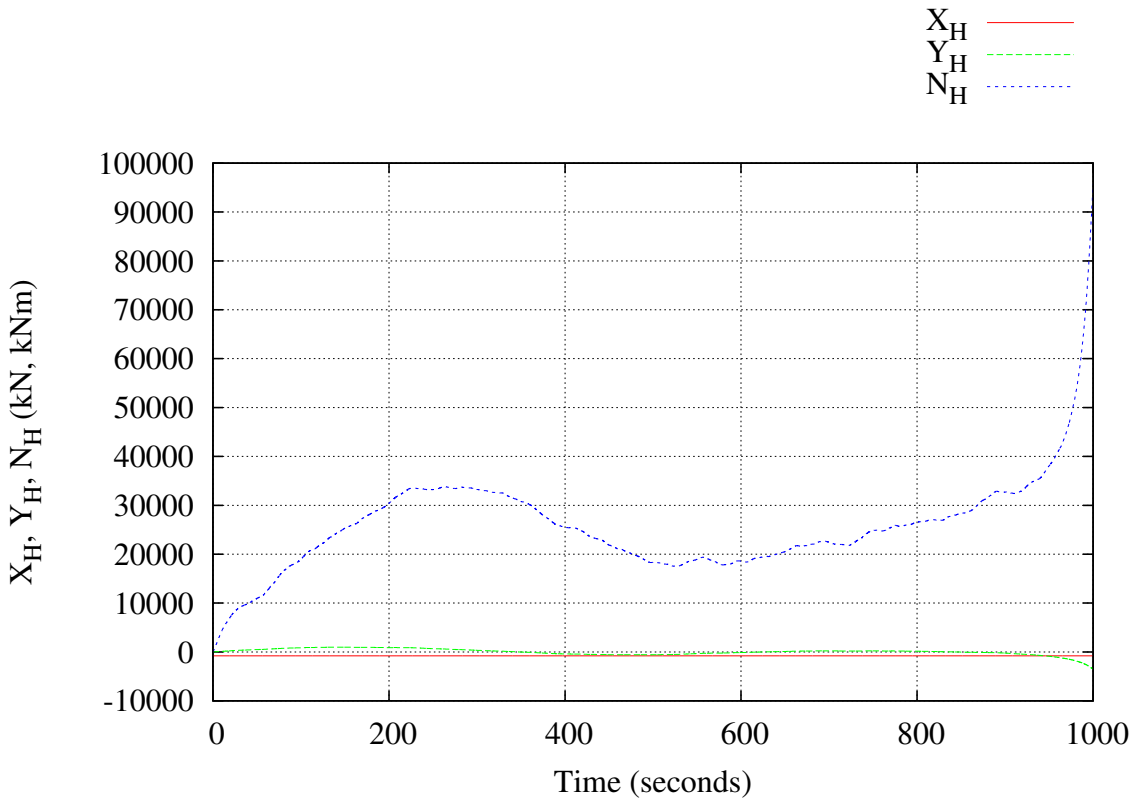

Figure C.17: Case 2: Hull Forces vs. Time

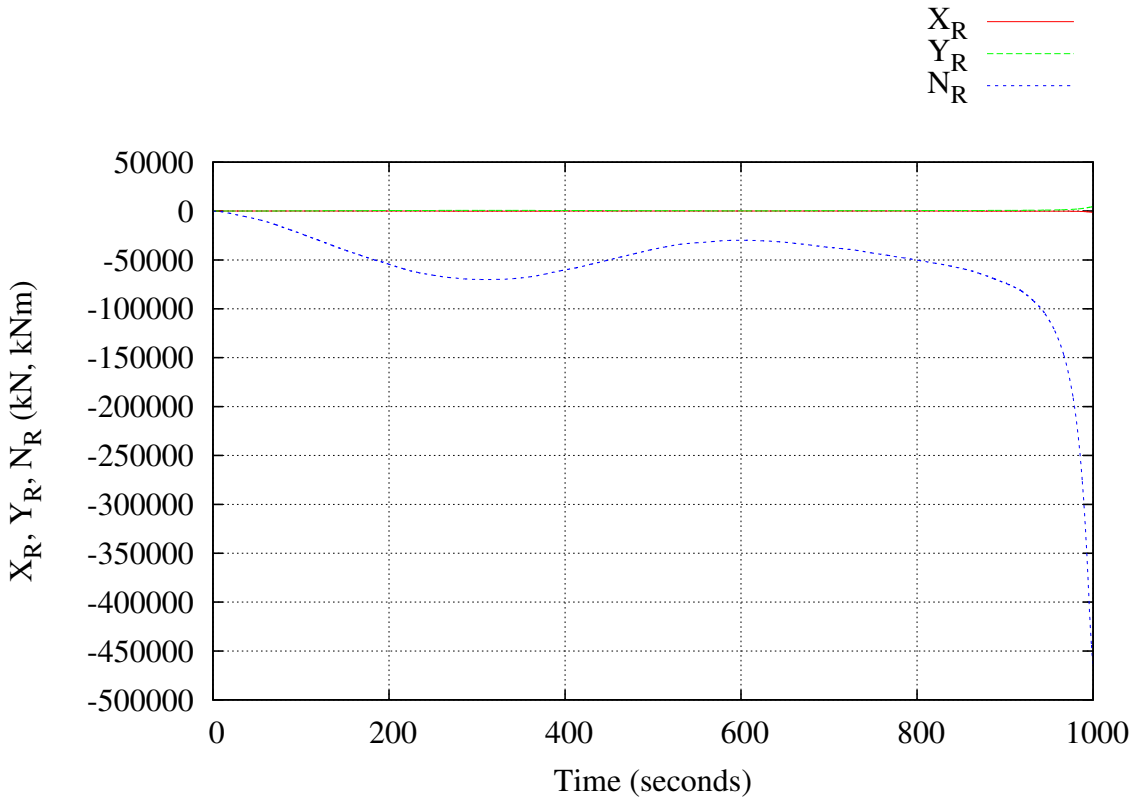

Figure C.18: Case 2: Rudder Force vs. Time

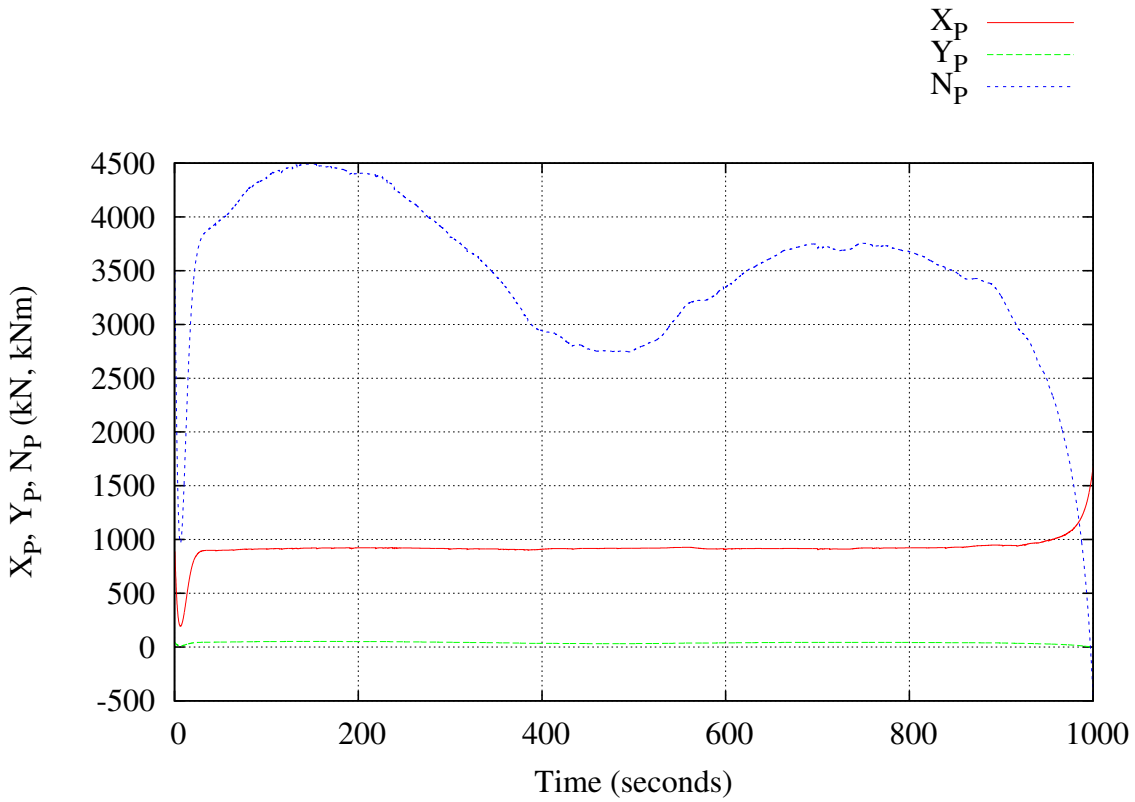

Figure C.19: Case 2: Propeller Force vs. Time

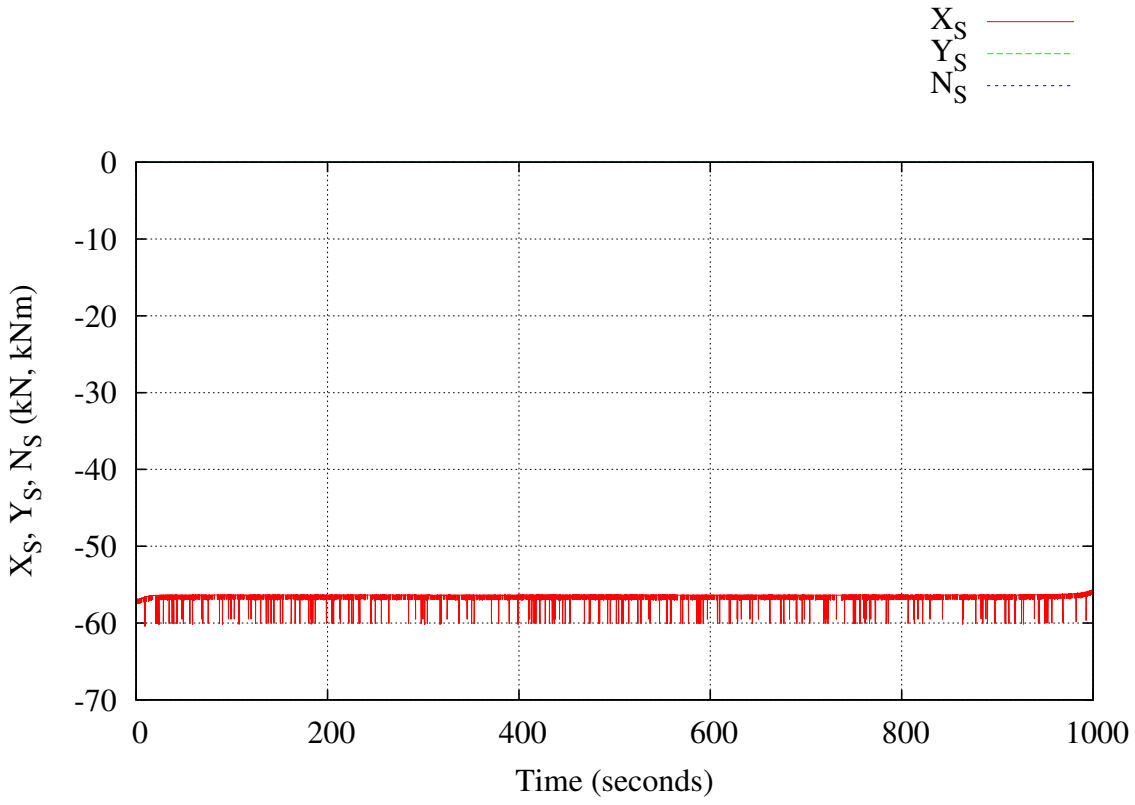

Figure C.20: Case 2: Seaway Force vs. Time

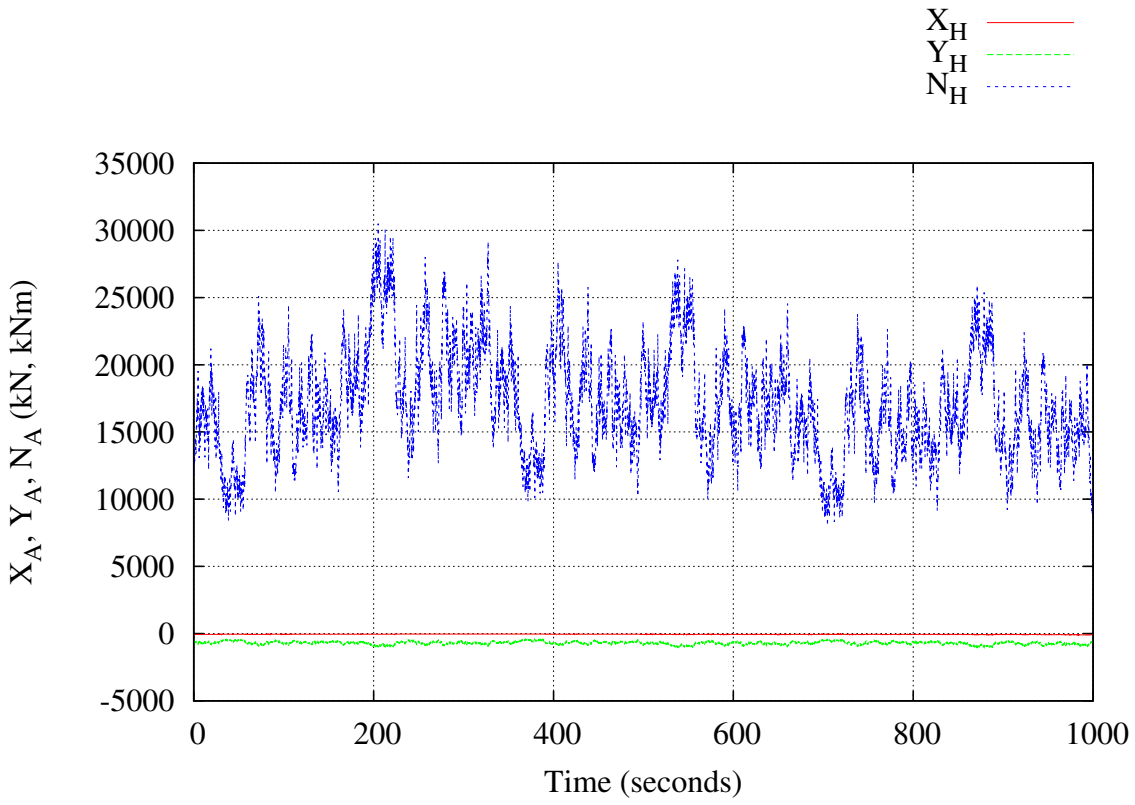

Figure C.21: Case 2: Wind Force vs. Time

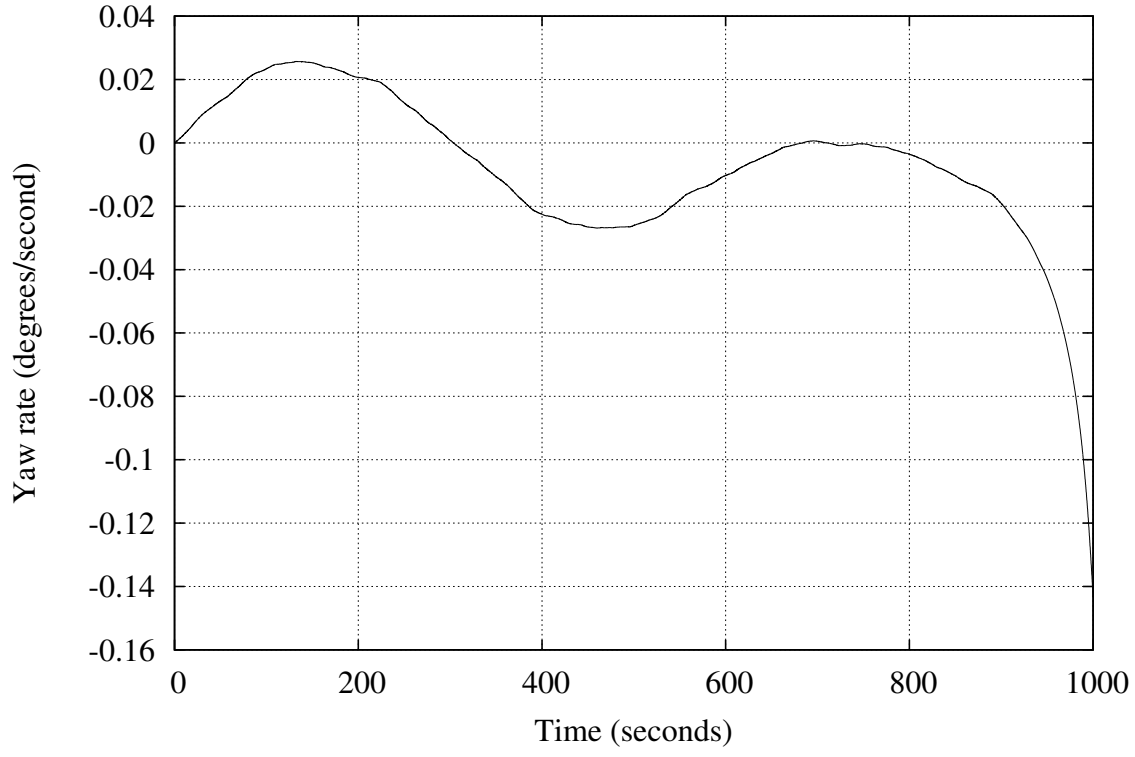

Figure C.22: Case 2: Yaw Rate vs. Time

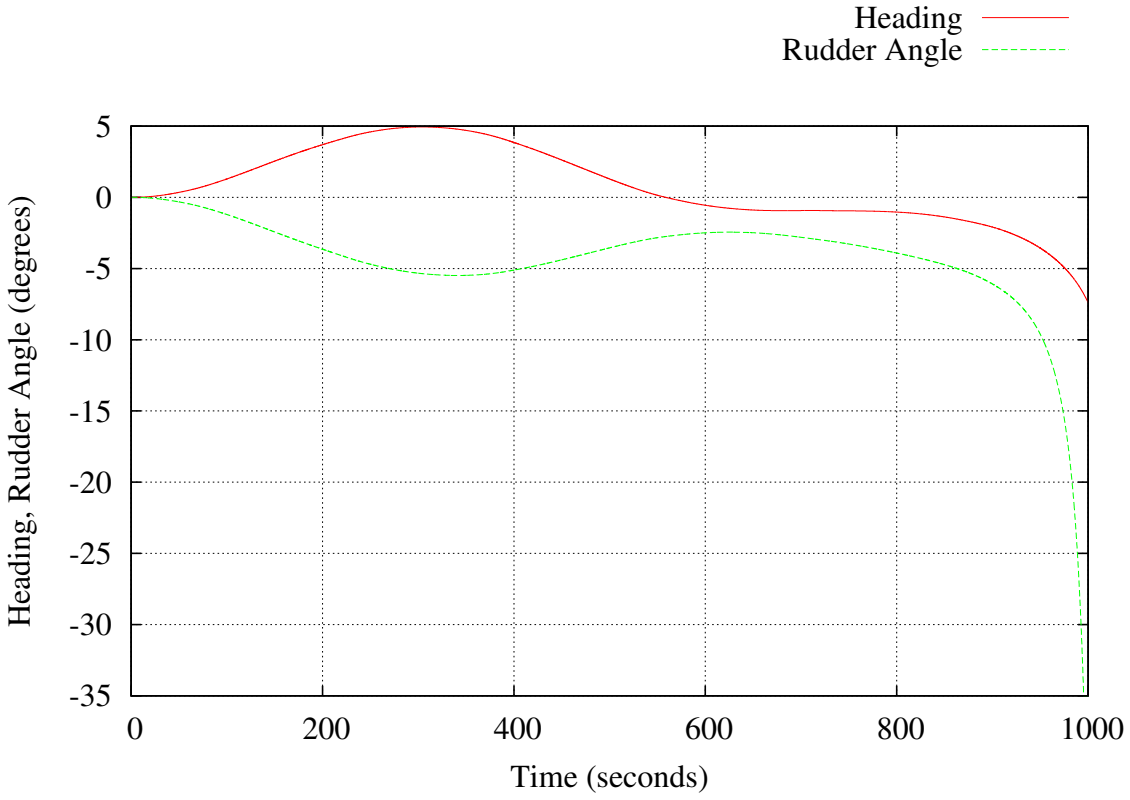

Figure C.23: Case 2: Rudder Command and Heading vs. Time

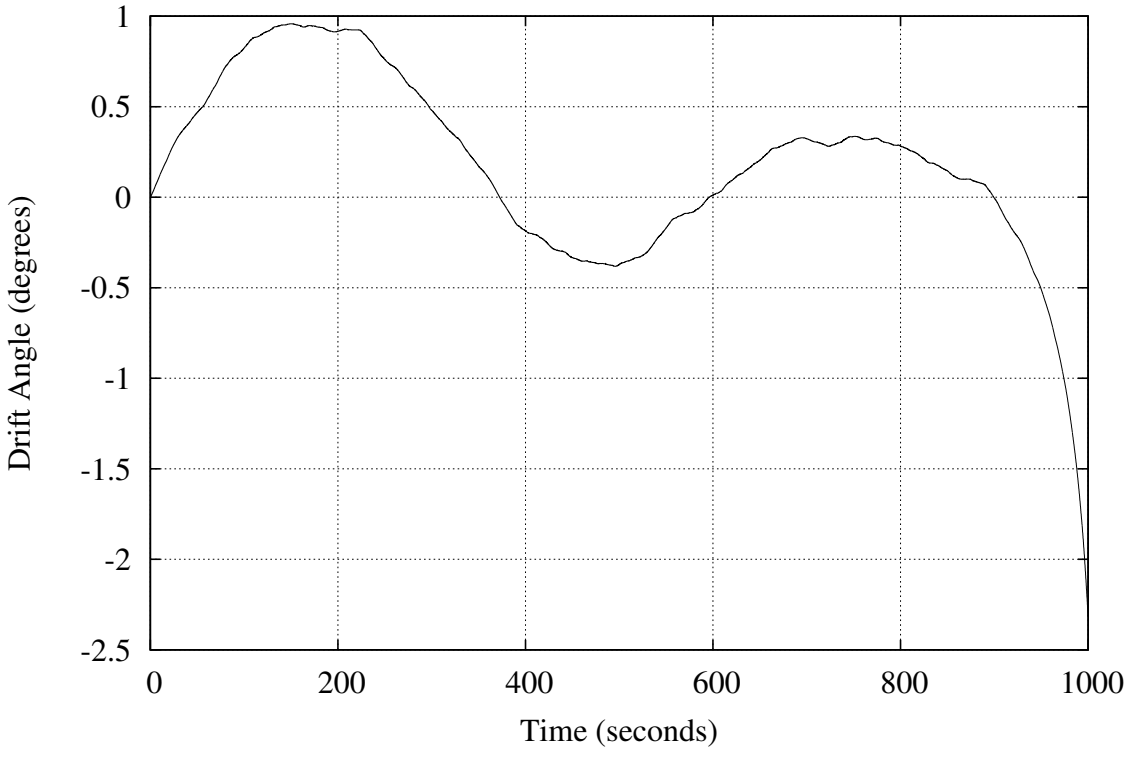

Figure C.24: Case 2: Drift Angle vs. Time

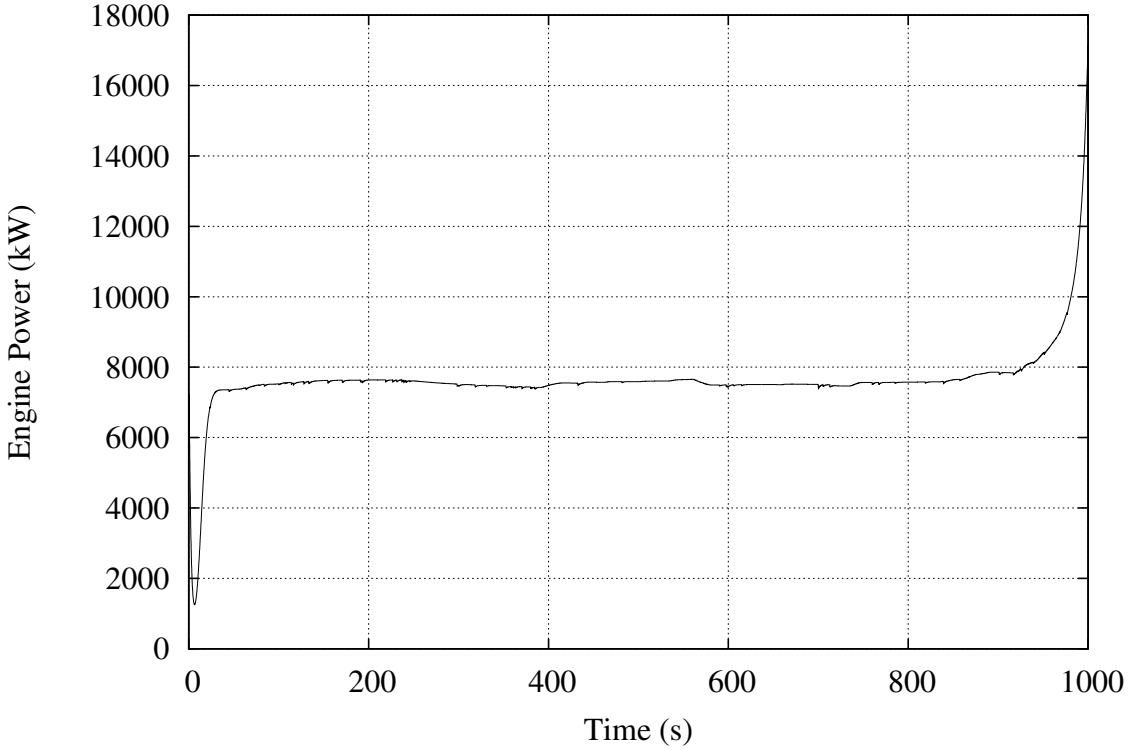

Figure C.25: Case 2: Engine Power vs. Time

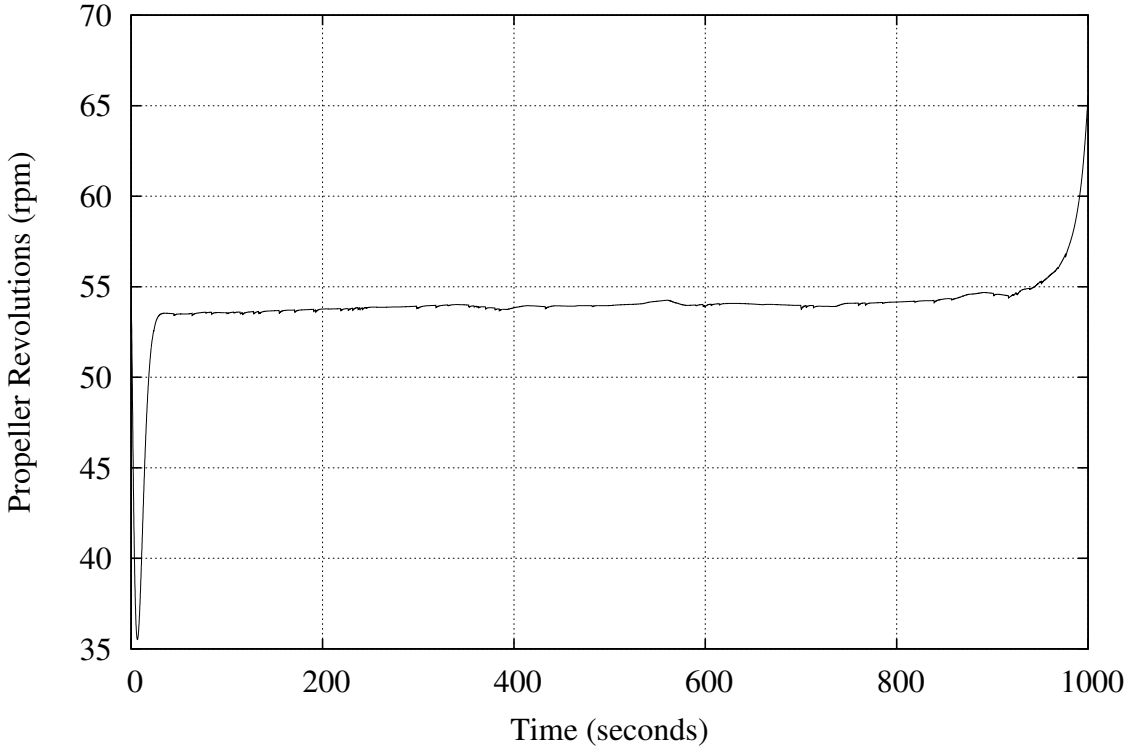

Figure C.26: Case 2: Propeller Revolutions vs. Time

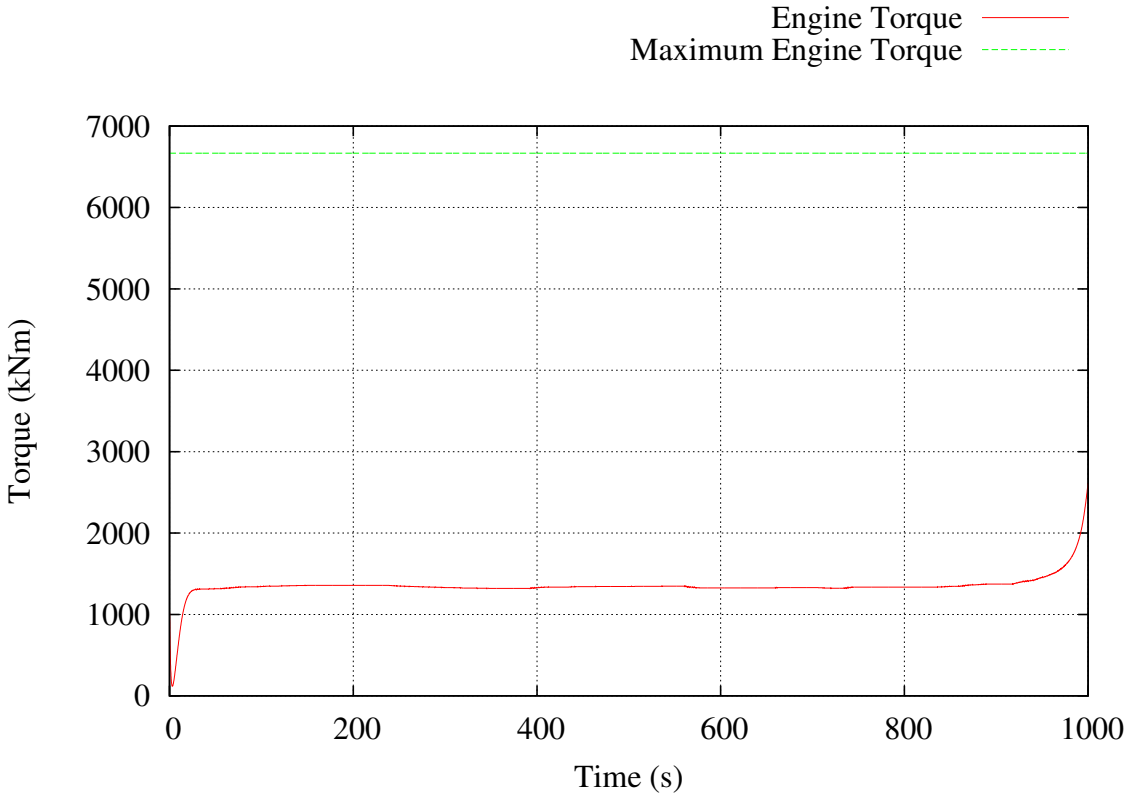

Figure C.27: Case 2: Engine Torque vs. Time

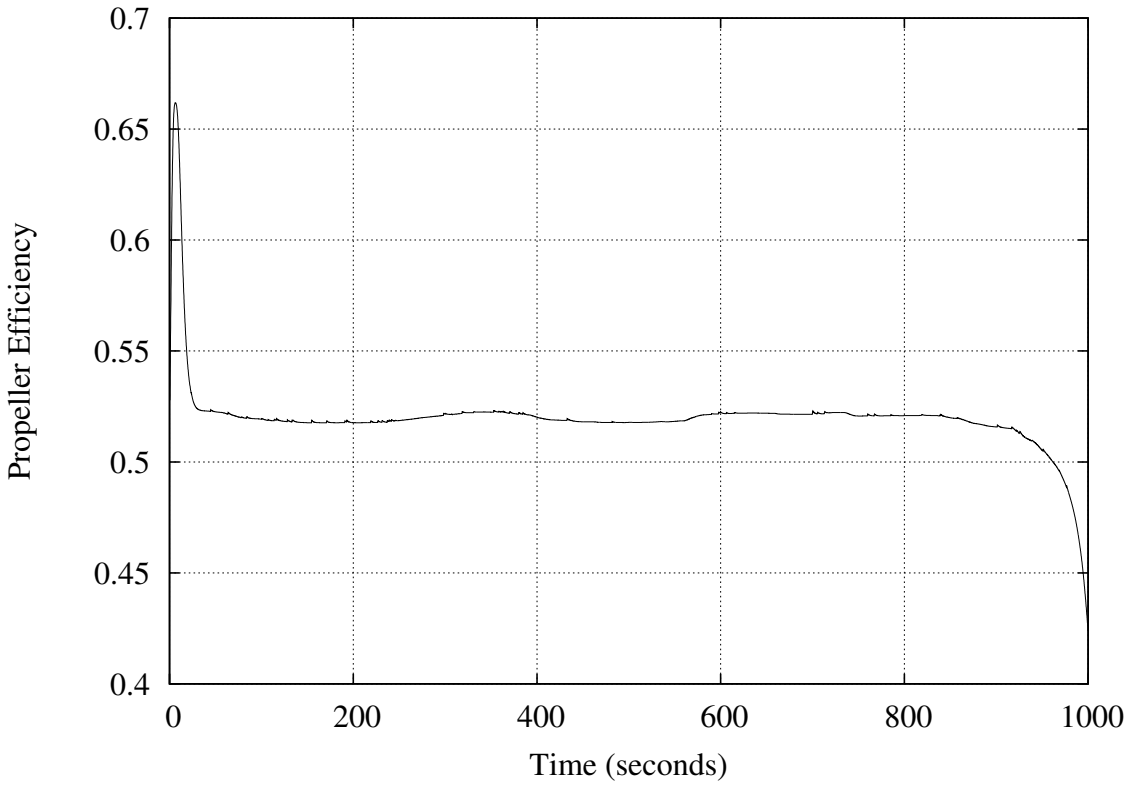

Figure C.28: Case 2: Open Water Propeller Efficiency vs. Time

C.3 Case 3. *Esso Osaka*, 20 Knot Wind (Fresh Breeze), Unsteady $MBEMT$ Propulsion Model, Automatic Control, with Propeller Selected from $OOBOO$ Model

```
    |=============================================|
    | Ship-in-Service Performance Estimator       |
    |=============================================|
    | (c) 2013 David Trodden                      |
    | School of Marine Science and Technology     |
    | Newcastle University, UK                    |
    |=============================================|


"Esso Osaka VLCC - Loaded Test Case"
====================================


Simuation Parameters
--------------------
  Simulation is speed and track automatic pilot.
  Using an unsteady BEMT propulsion model.
  Mean true wind speed =                                  20.00 knots
  Mean true wind direction =                              90.00 degrees


Ship Main Particulars
---------------------
  Service Speed =                                         10.00 knots
  Lpp =                                                  325.00 m
  Lwl =                                                  335.00 m
  B =                                                     53.00 m
  T =                                                     21.79 m
  Volume of Displacement =                            311901.50 m^3
  Mass of Ship =                                      319699.06 tonnes
  LCB relative to midships +Fwd (%) =                      3.169
  Midship Coefficient, Cm =                                0.990
  Waterplane Coefficient, Cwp =                            0.850
  Block Coefficient, Cb =                                  0.831
  Prismatic Coefficient, Cp =                              0.839


Propeller geometry has been provided
------------------------------------
  Number of Propellers =                                      1
  Number of Blades on each Propeller =                        5
  Propeller Diameter =                                     9.10 m
  Propeller Pitch =                                        7.69 m
  Expanded Blade Area Ratio =                              0.64


Resistance Calculations from Holtrop & Mennen (Calm Water)
----------------------------------------------------------
  Friction Resistance =                                 704.530 kN
  Appendage Resistance =                                  8.309 kN
  Wave Making Resistance =                                0.266 kN
  Added Pressure Resistance of Bulbous Bow =              0.000 kN
  Added Pressure Resistance of Immersed Transom Stern =   7.152 kN
  Model-Ship Correlation Line =                          81.067 kN
  Total Calm Water Resistance =                         801.324 kN


Calm Water Propulsion Characteristics
-------------------------------------
  Required Engine Power for Service Speed =            5137.812 kW
  Propeller Revolutions =                                48.250 rpm
  Open Water Propeller Efficiency =                       0.534


In-Service Propulsion Characteristics
-------------------------------------
  Average 'quasi-steady state' resultant resistance =             915.716 kN
  Average 'quasi-steady state' resultant ship speed =               9.938 knots
  Average 'quasi-steady state' propeller efficiency =               0.511
  Average 'quasi-steady state' propeller revolutions =             50.509 rpm
  Average 'quasi-steady state' advance ratio =                      0.448
  Average 'quasi-steady state' Delivered Power =                 7712.330 kW
  Average 'quasi-steady state' Engine Brake Power =              7782.294 kW
```

```
Average 'quasi-steady state' drift angle at propeller =          -0.768 degrees
```

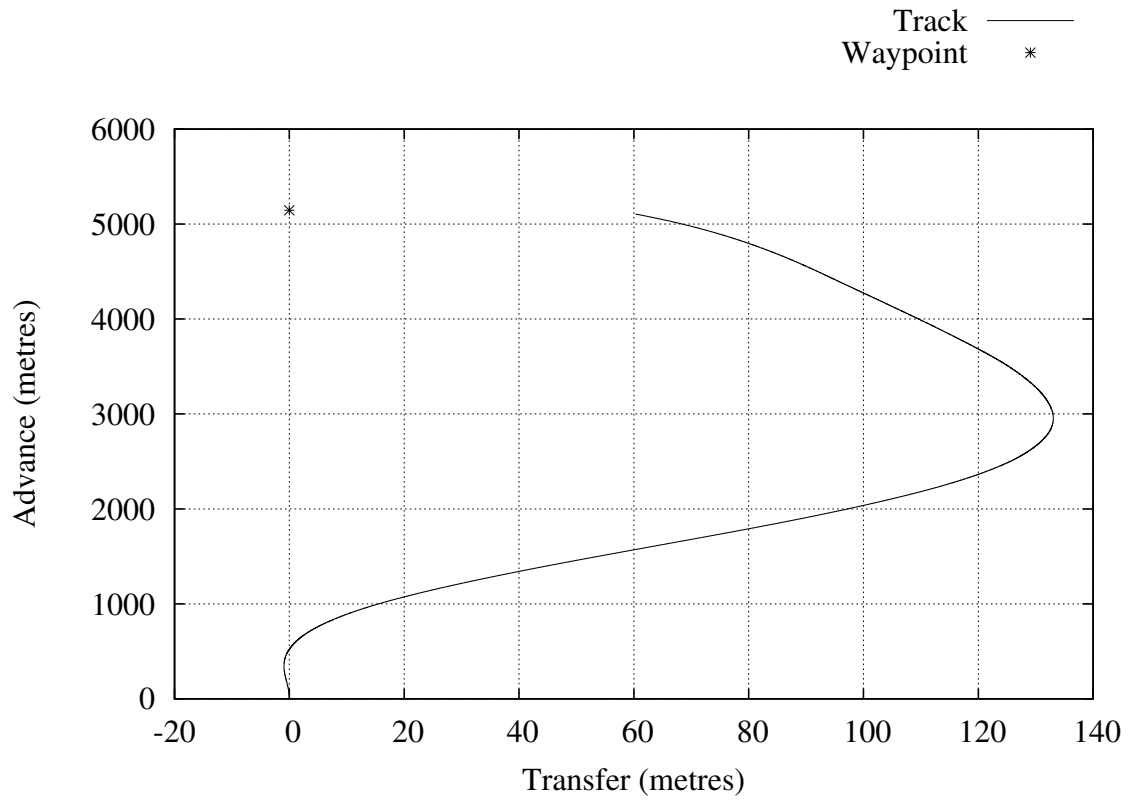

Figure C.29: Case 3: Ship Track

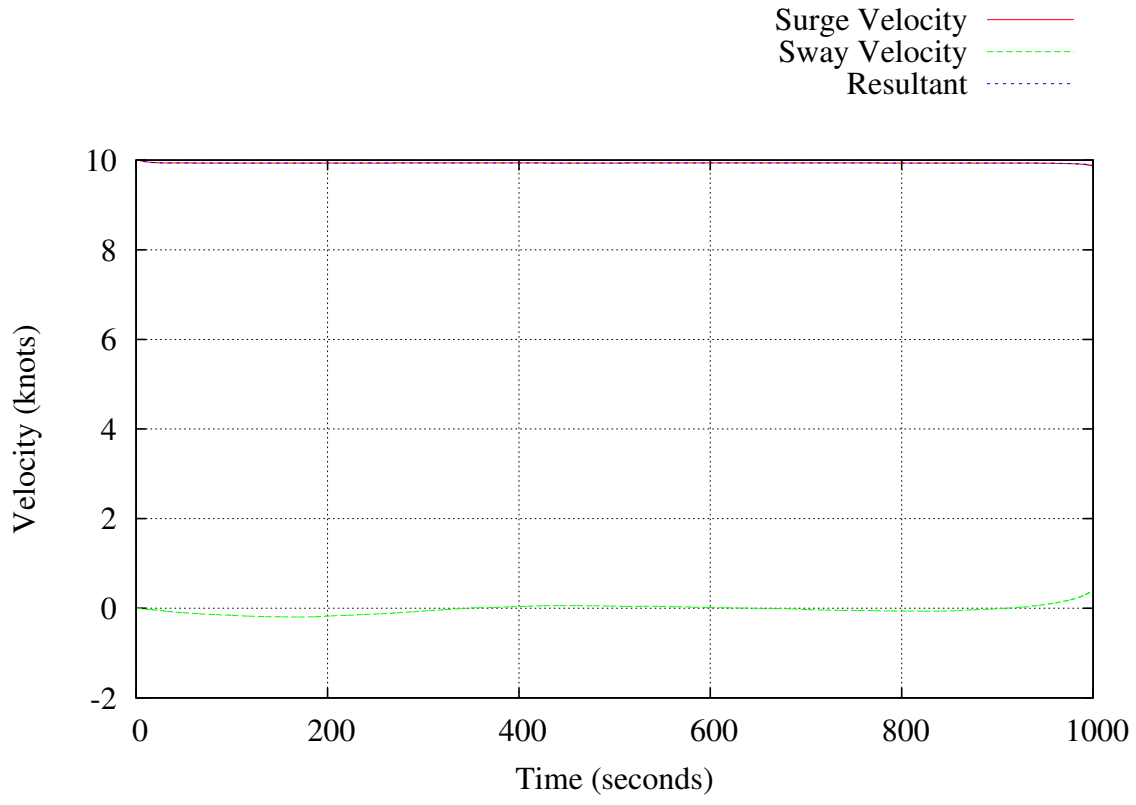

Figure C.30: Case 3: Speed vs. Time

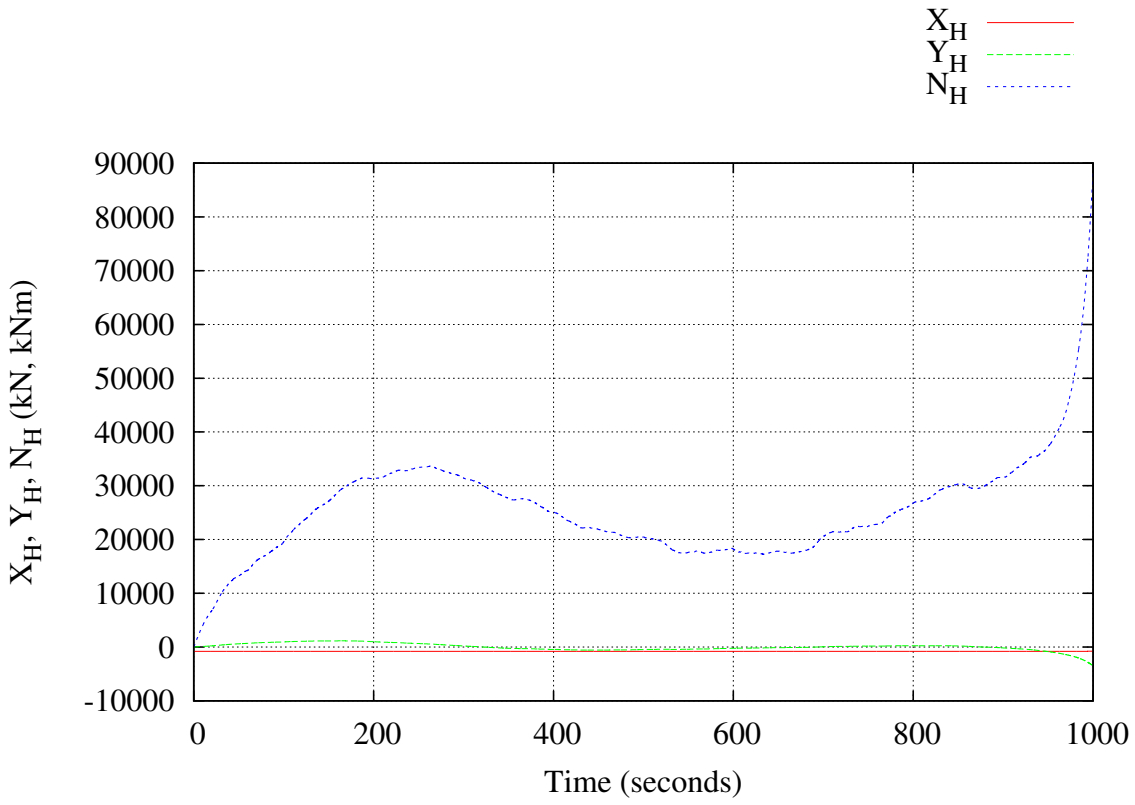

Figure C.31: Case 3: Hull Forces vs. Time

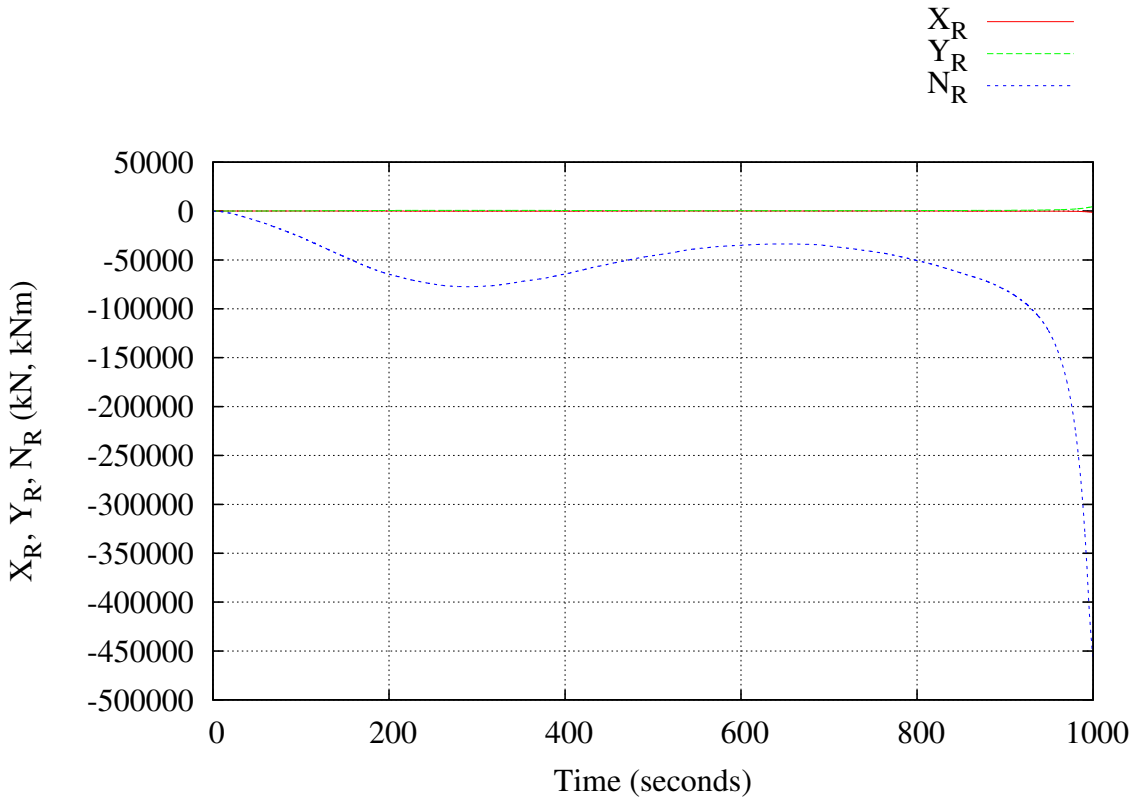

Figure C.32: Case 3: Rudder Force vs. Time

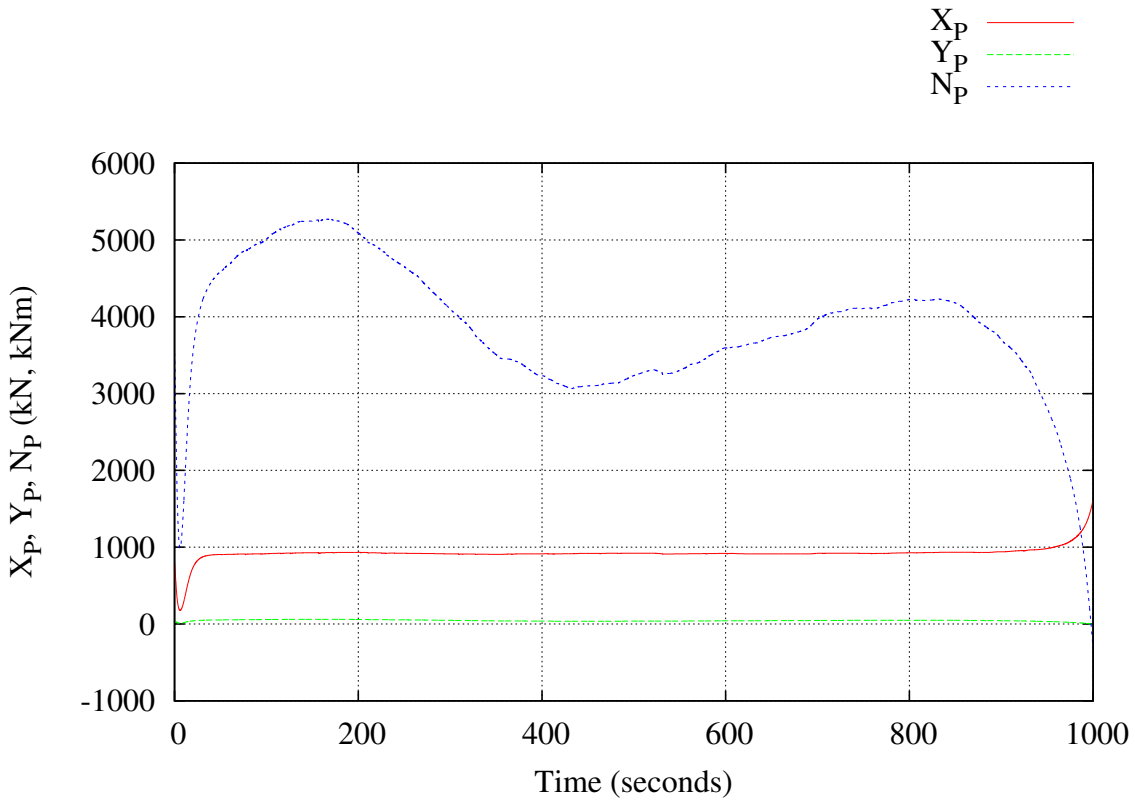

Figure C.33: Case 3: Propeller Force vs. Time

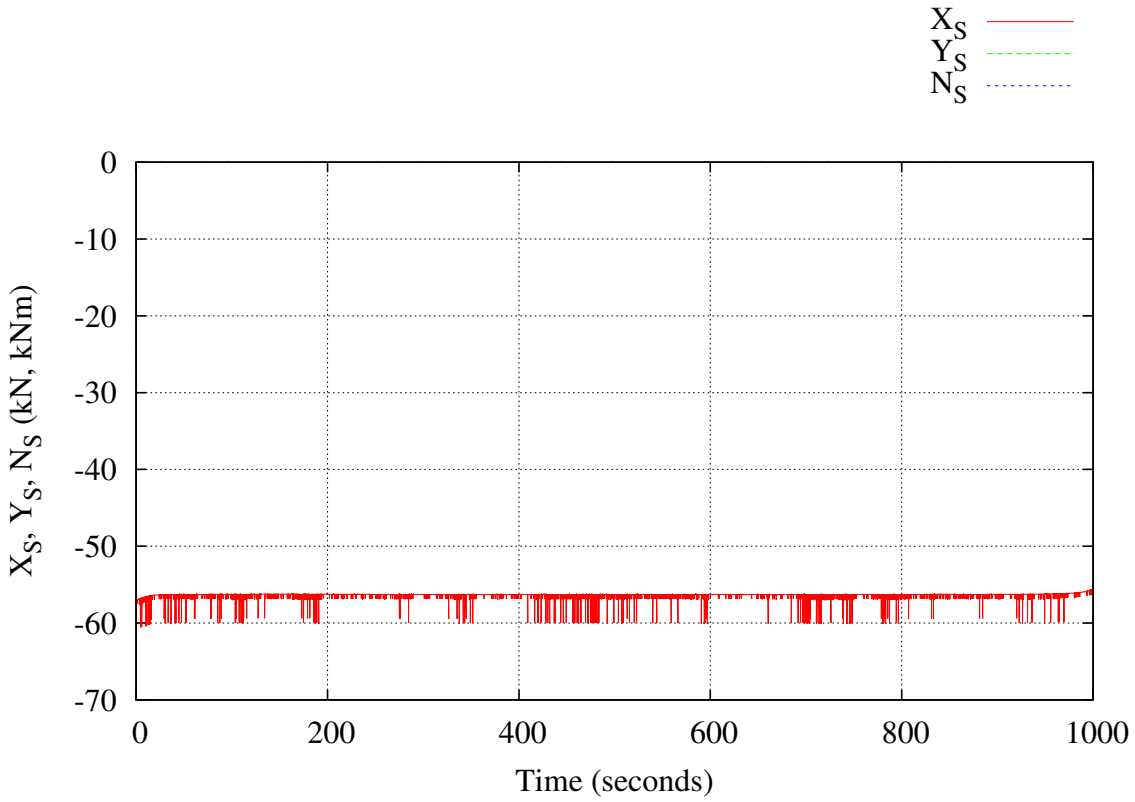

Figure C.34: Case 3: Seaway Force vs. Time

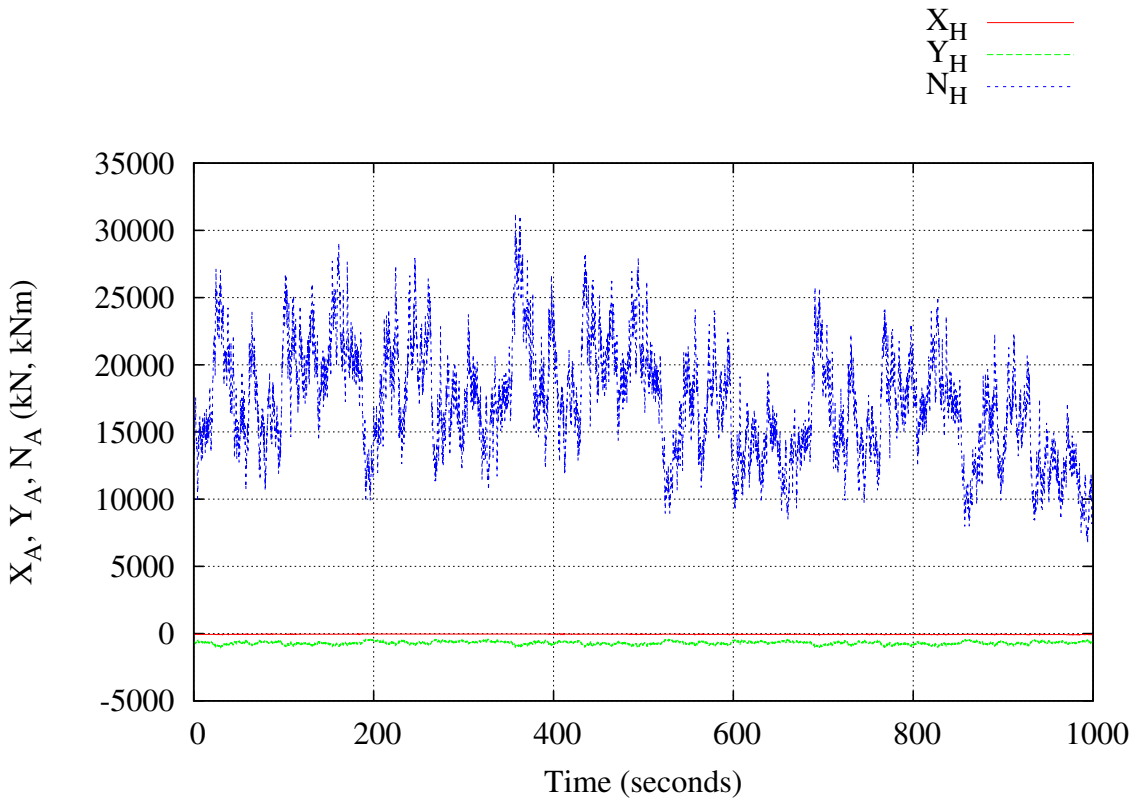

Figure C.35: Case 3: Wind Force vs. Time

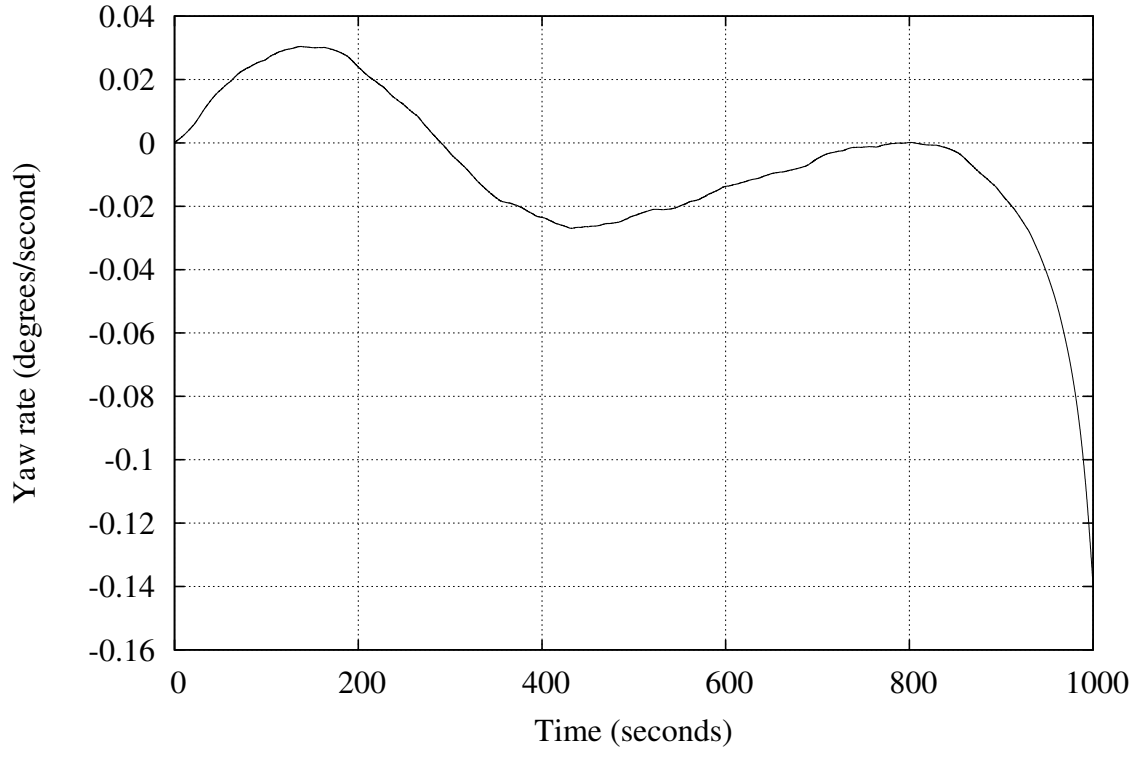

Figure C.36: Case 3: Yaw Rate vs. Time

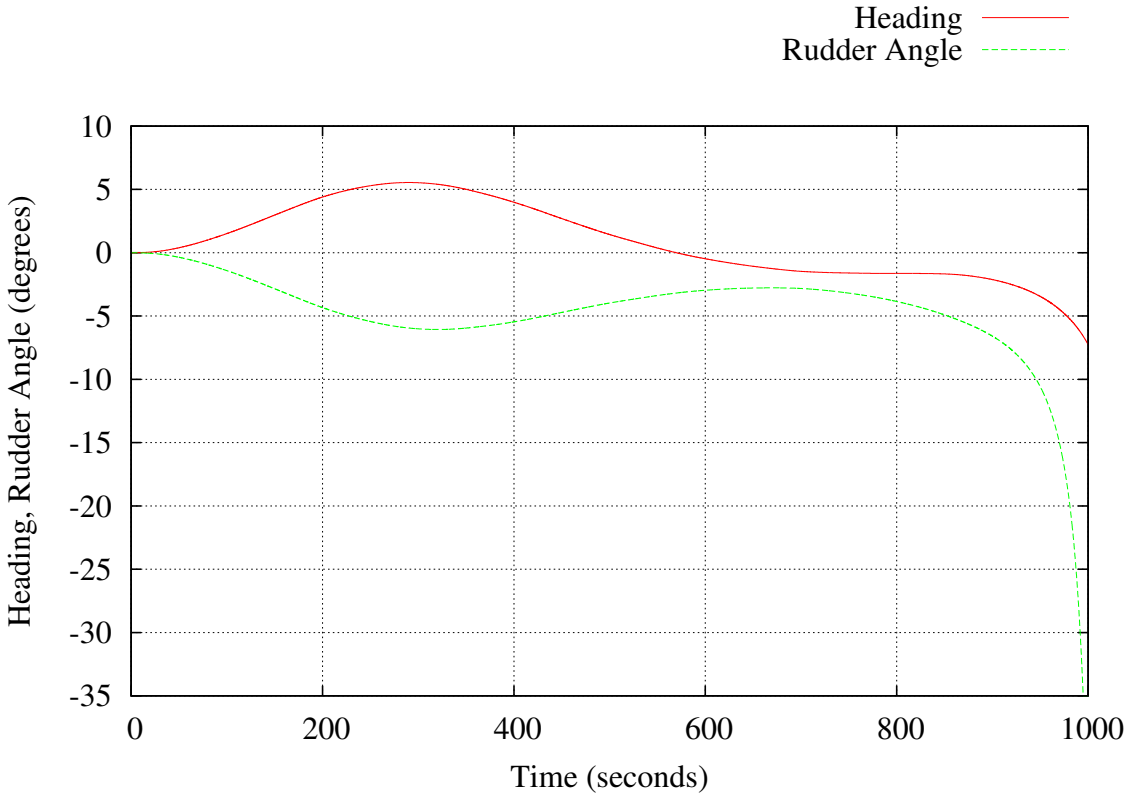

Figure C.37: Case 3: Rudder Command and Heading vs. Time

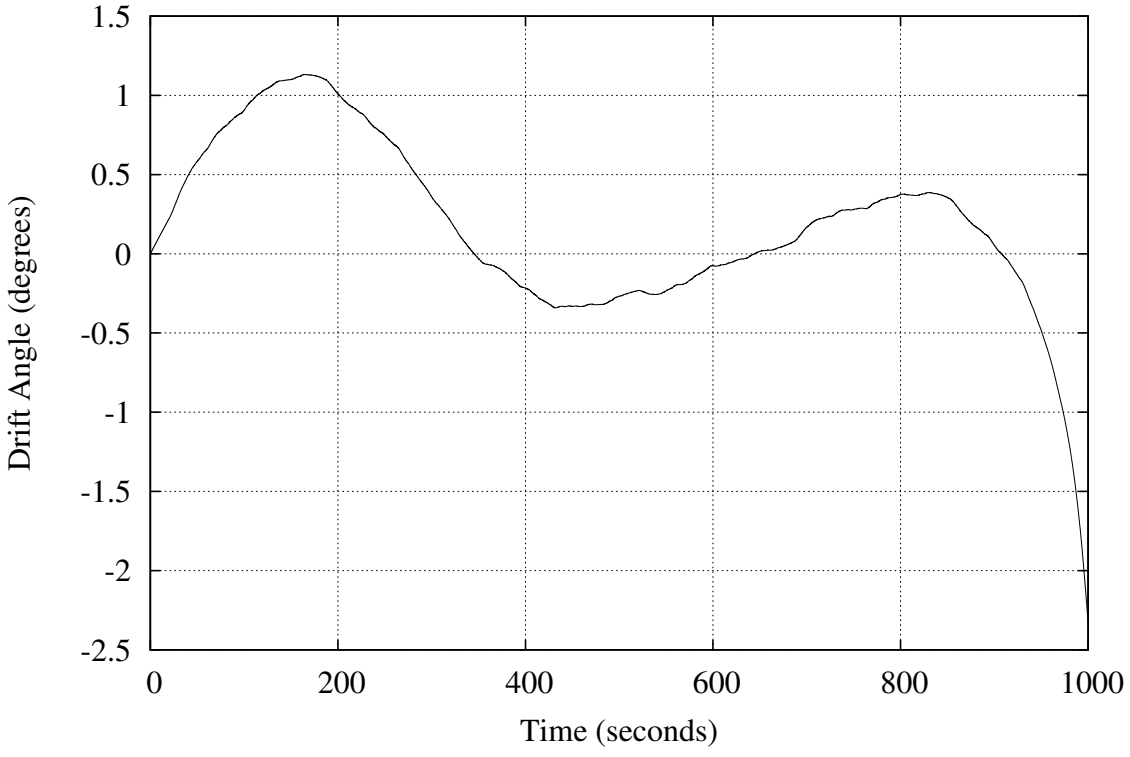

Figure C.38: Case 3: Drift Angle vs. Time

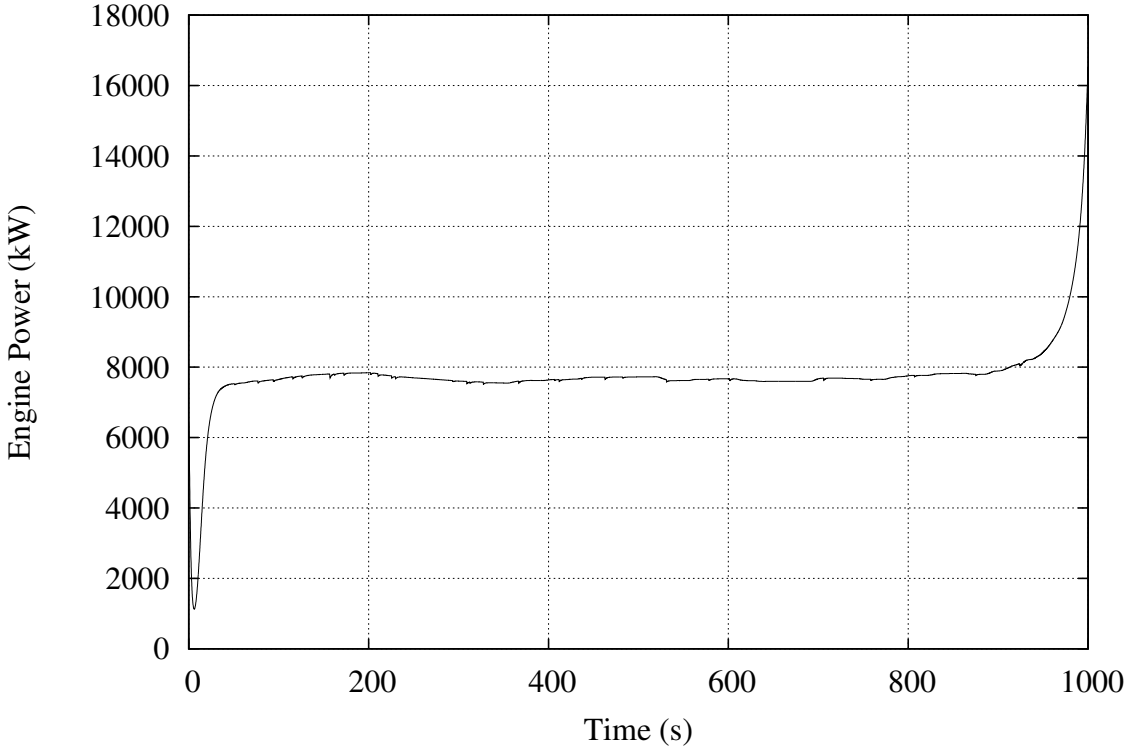

Figure C.39: Case 3: Engine Power vs. Time

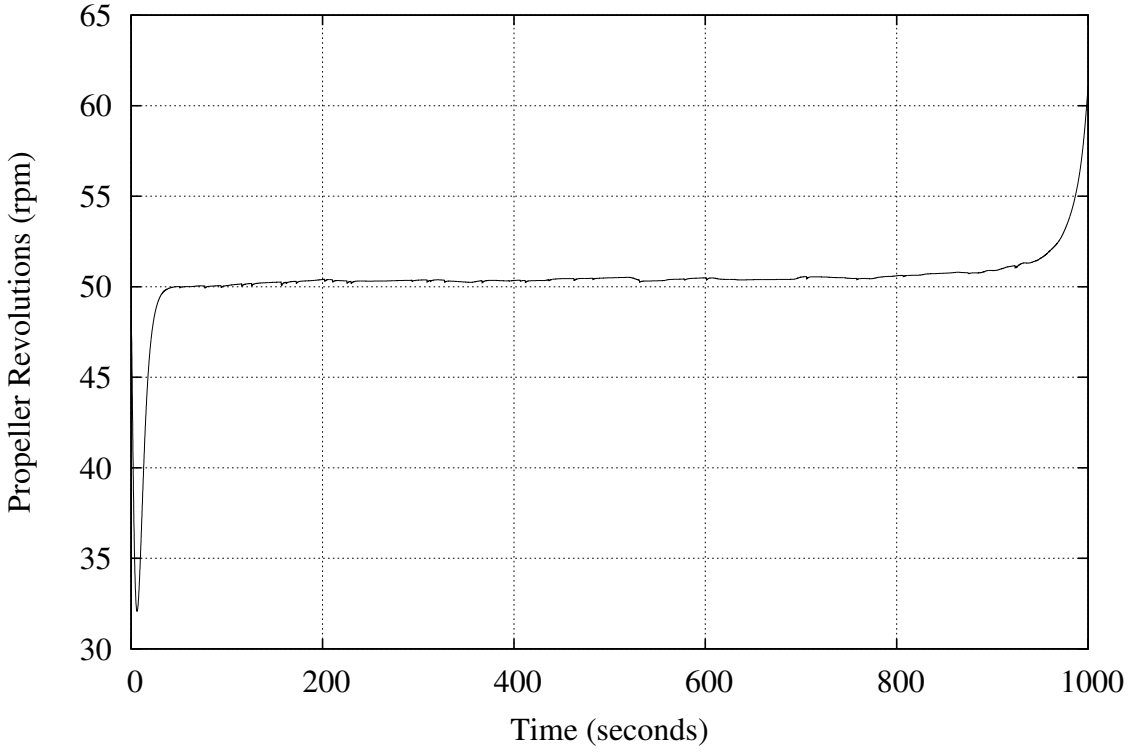

Figure C.40: Case 3: Propeller Revolutions vs. Time

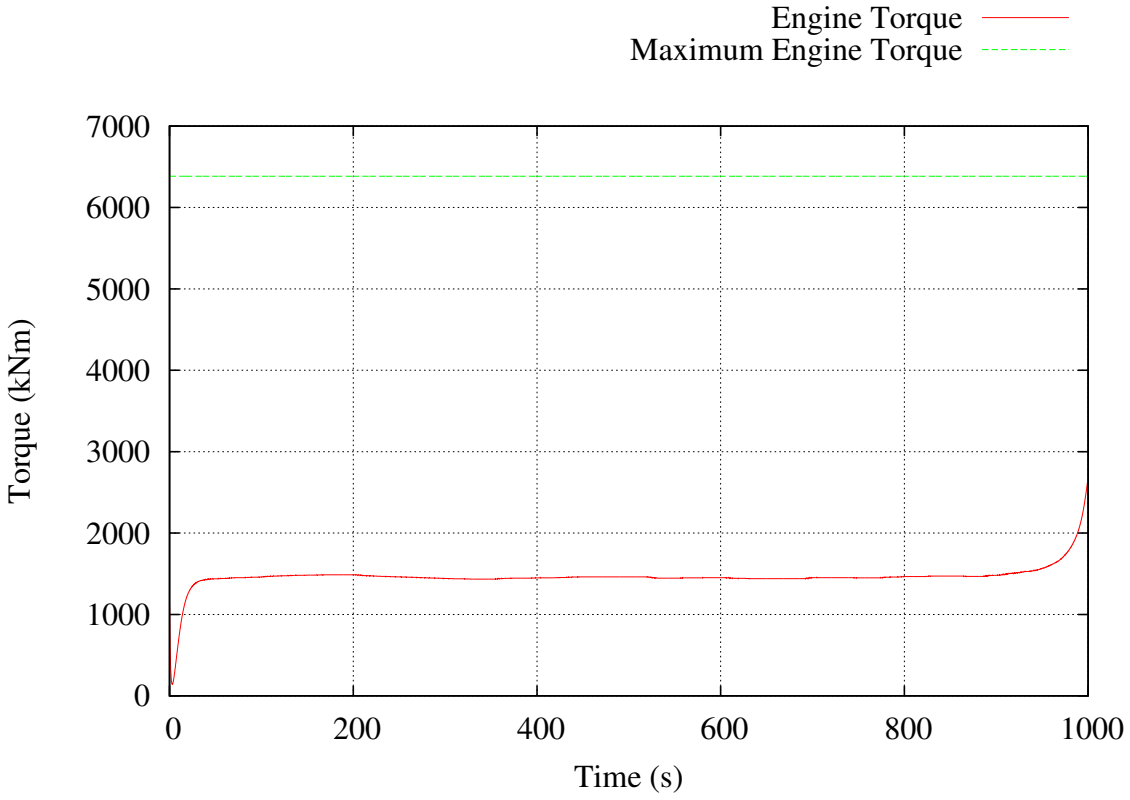

Figure C.41: Case 3: Engine Torque vs. Time

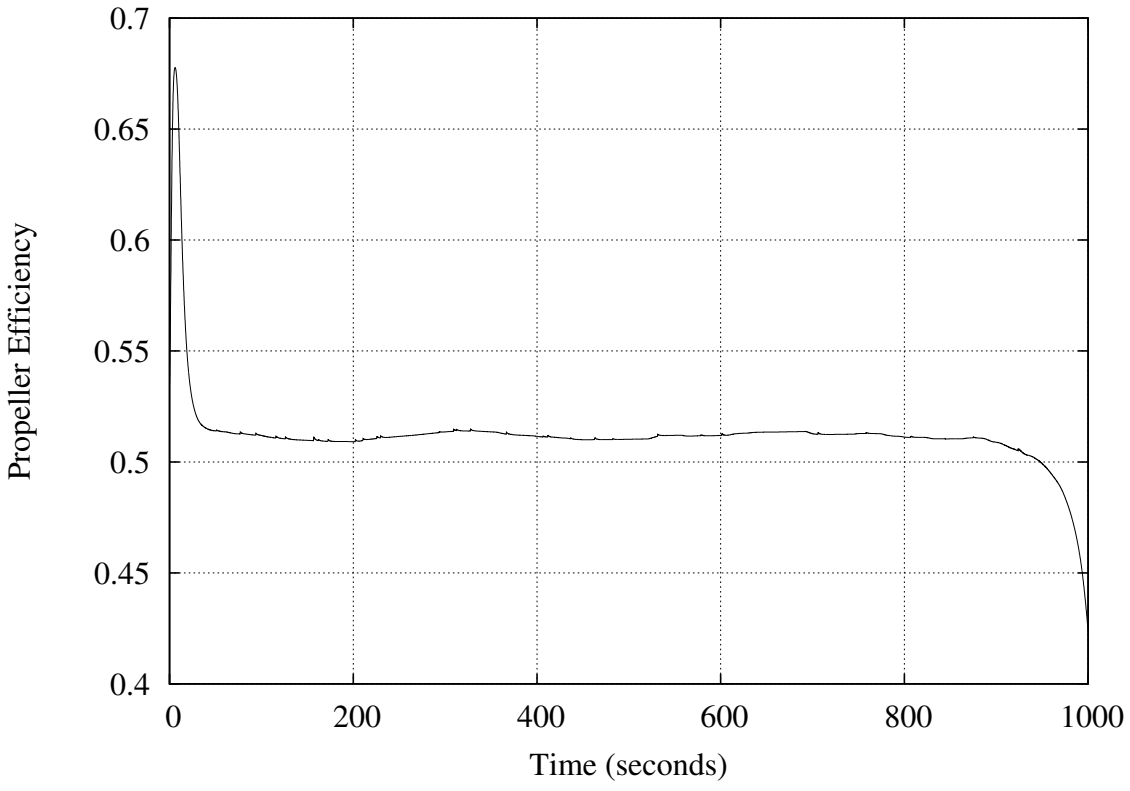

Figure C.42: Case 3: Open Water Propeller Efficiency vs. Time

C.4 Case 4. KCS, 20 Knot Wind (Fresh Breeze), Unsteady MBEMT Propulsion Model, Automatic Control, Propeller Optimisation

```
    |=============================================|
    | Ship-in-Service Performance Estimator       |
    |=============================================|
    | (c) 2013 David Trodden                      |
    | School of Marine Science and Technology     |
    | Newcastle University, UK                    |
    |=============================================|


"KCS - KRISO Container Ship"
============================


Simuation Parameters
--------------------
  Simulation is speed and track automatic pilot.
  Using the Oosterveld and van Oossanen propulsion model.
  Mean true wind speed =                                    20.00 knots
  Mean true wind direction =                                90.00 degrees


Ship Main Particulars
---------------------
  Service Speed =                                           24.00 knots
  Lpp =                                                    232.00 m
  Lwl =                                                    237.58 m
  B =                                                       32.20 m
  T =                                                       11.34 m
  Volume of Displacement =                               50885.00 m^3
  Mass of Ship =                                         52157.13 tonnes
  LCB relative to midships +Fwd (%) =                       -2.030
  Midship Coefficient, Cm =                                  0.985
  Waterplane Coefficient, Cwp =                              0.802
  Block Coefficient, Cb =                                    0.601
  Prismatic Coefficient, Cp =                                0.610


Resistance Calculations from Holtrop & Mennen (Calm Water)
----------------------------------------------------------
  Friction Resistance =                                  1174.728 kN
  Appendage Resistance =                                   17.524 kN
  Wave Making Resistance =                                419.418 kN
  Added Pressure Resistance of Bulbous Bow =                0.089 kN
  Added Pressure Resistance of Immersed Transom Stern =     0.000 kN
  Model-Ship Correlation Line =                           230.444 kN
  Total Calm Water Resistance =                          1842.203 kN


Iteration:  1
==============


  Optimised Propeller Selection
  -----------------------------
    Number of Propellers =                      1
    Number of Blades =                          5
    Diameter =                               7.90 m
    Pitch =                                  8.48 m
    Expanded Blade Area Ratio =             0.790
    Optimum Open Water Efficiency =         0.658
    Optimum Revolutions =                   99.10 rpm


In-Service Propulsion Characteristics
-------------------------------------
  Average 'quasi-steady state' resultant resistance =            2102.316 kN
  Average 'quasi-steady state' resultant ship speed =              23.939 knots
  Average 'quasi-steady state' propeller efficiency =               0.642
  Average 'quasi-steady state' propeller revolutions =            102.477 rpm
  Average 'quasi-steady state' advance ratio =                      0.719
  Average 'quasi-steady state' Delivered Power =                38714.078 kW
  Average 'quasi-steady state' Engine Brake Power =             39734.996 kW
  Average 'quasi-steady state' drift angle at propeller =           1.283 degrees
```

```
Iteration:  2
==============


  Optimised Propeller Selection
  -----------------------------
    Number of Propellers =                    1
    Number of Blades =                        5
    Diameter =                             7.90 m
    Pitch =                                8.09 m
    Expanded Blade Area Ratio =           0.863
    Optimum Open Water Efficiency =       0.640
    Optimum Revolutions =                106.36 rpm


In-Service Propulsion Characteristics
-------------------------------------
  Average 'quasi-steady state' resultant resistance =          2104.251 kN
  Average 'quasi-steady state' resultant ship speed =            23.946 knots
  Average 'quasi-steady state' propeller efficiency =             0.640
  Average 'quasi-steady state' propeller revolutions =          106.203 rpm
  Average 'quasi-steady state' advance ratio =                    0.694
  Average 'quasi-steady state' Delivered Power =              38918.773 kW
  Average 'quasi-steady state' Engine Brake Power =           40120.266 kW
  Average 'quasi-steady state' drift angle at propeller =         1.283 degrees
```

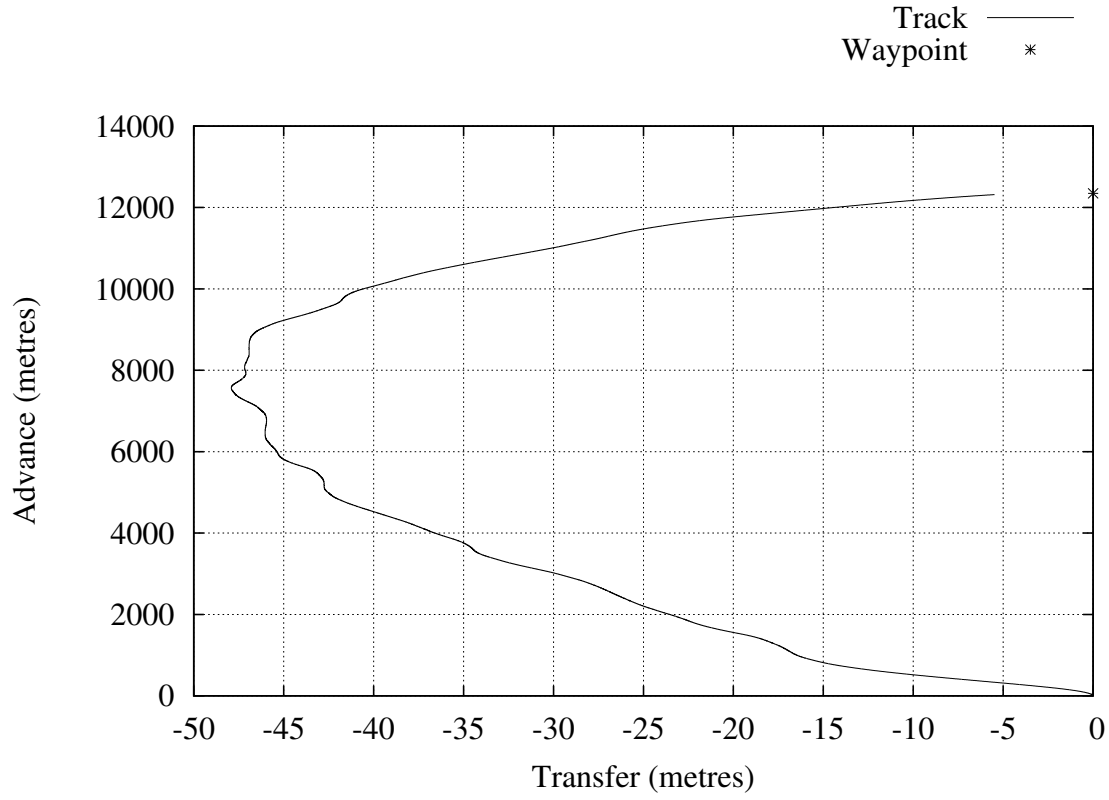

Figure C.43: Case 4: Ship Track

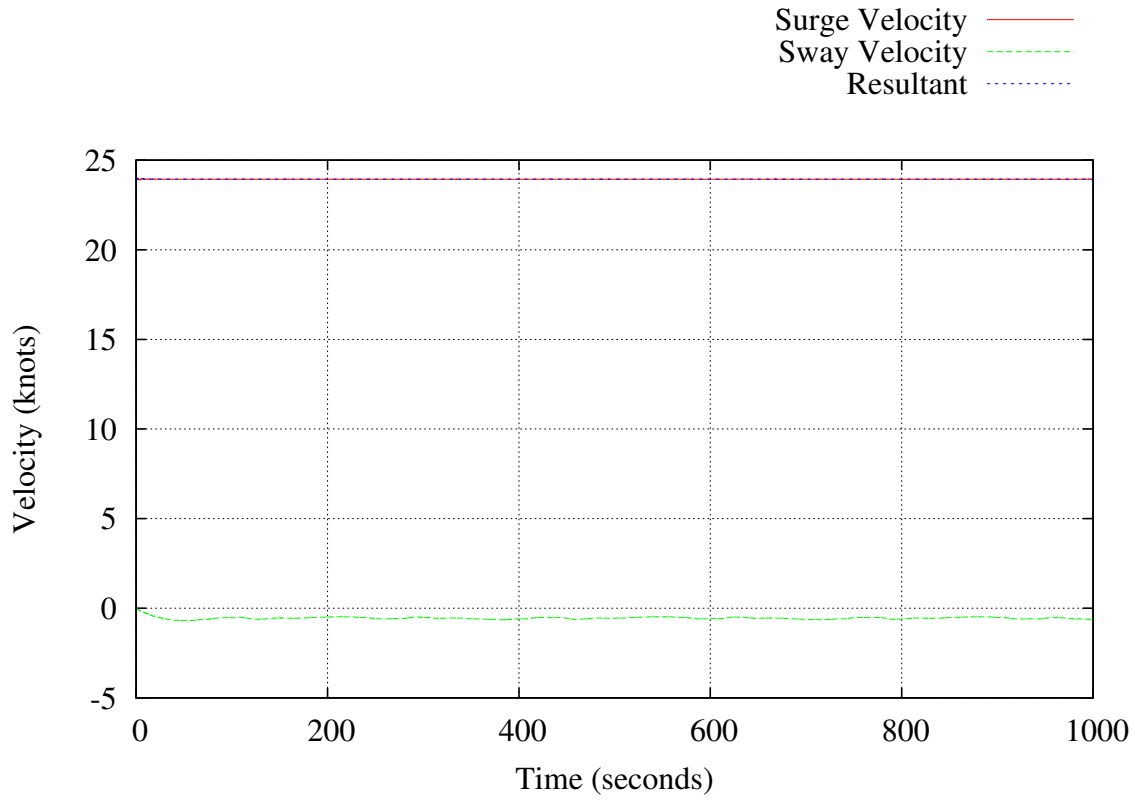

Figure C.44: Case 4: Speed vs. Time

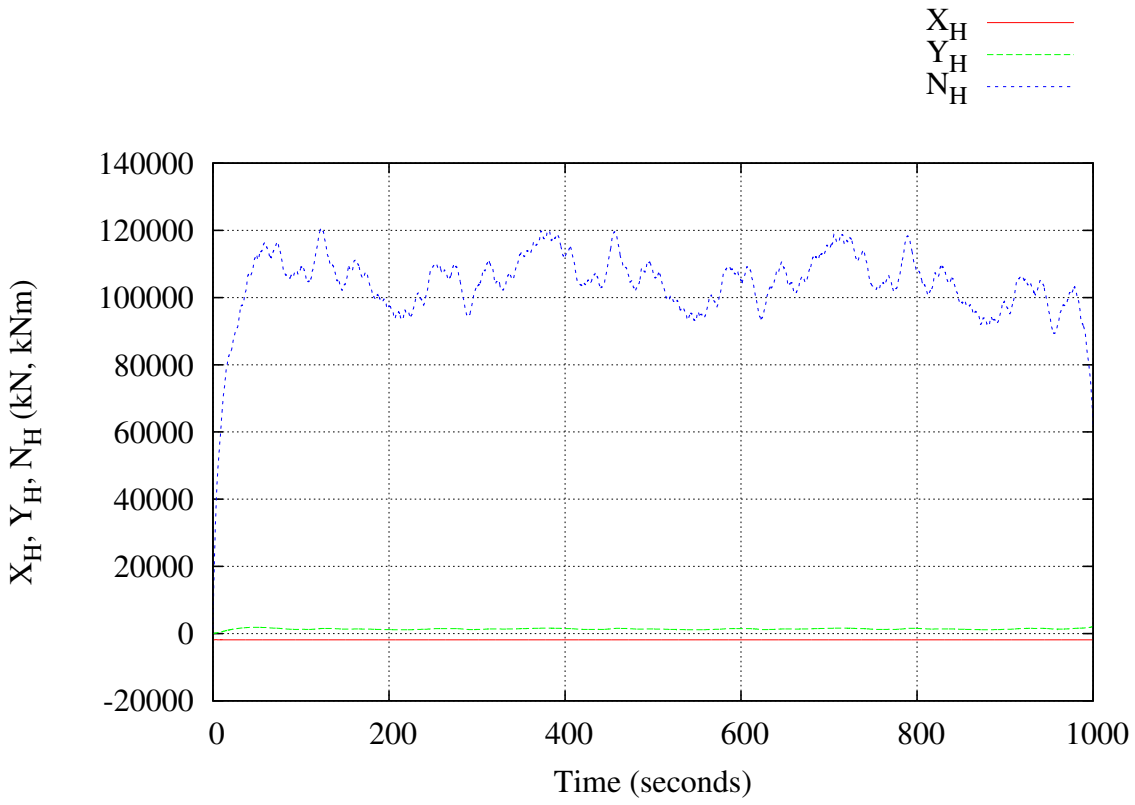

Figure C.45: Case 4: Hull Forces vs. Time

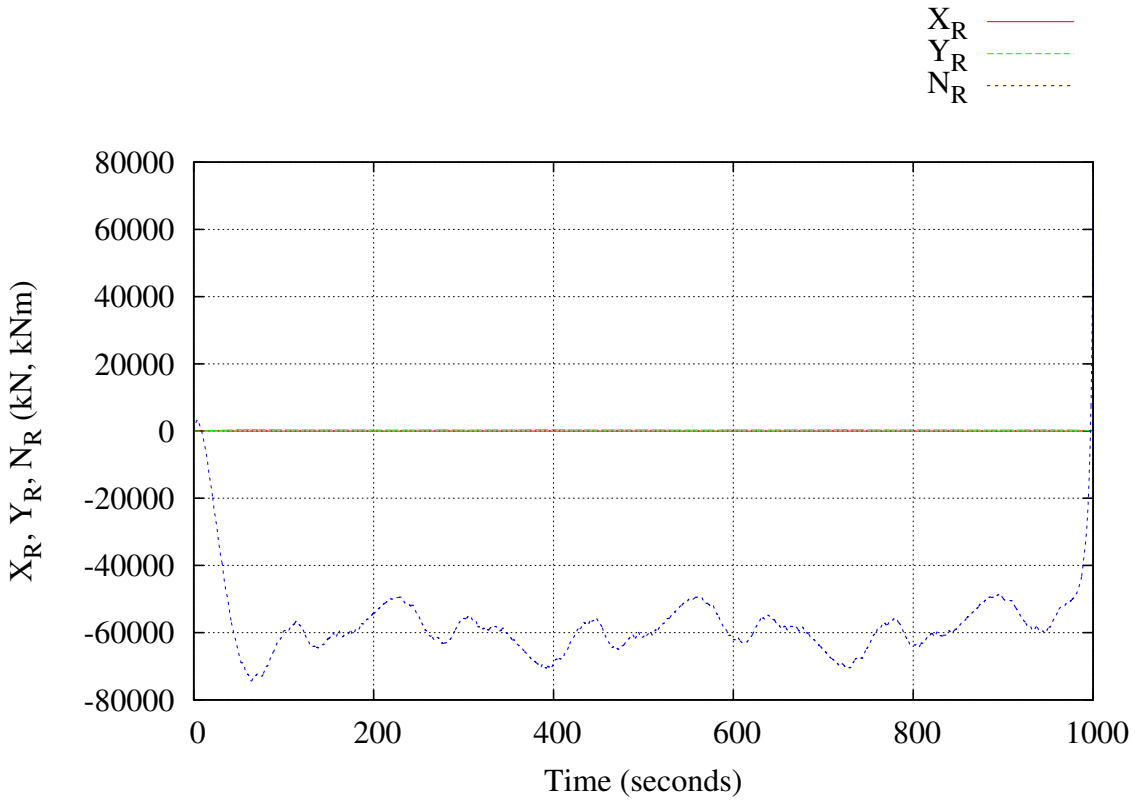

Figure C.46: Case 4: Rudder Force vs. Time

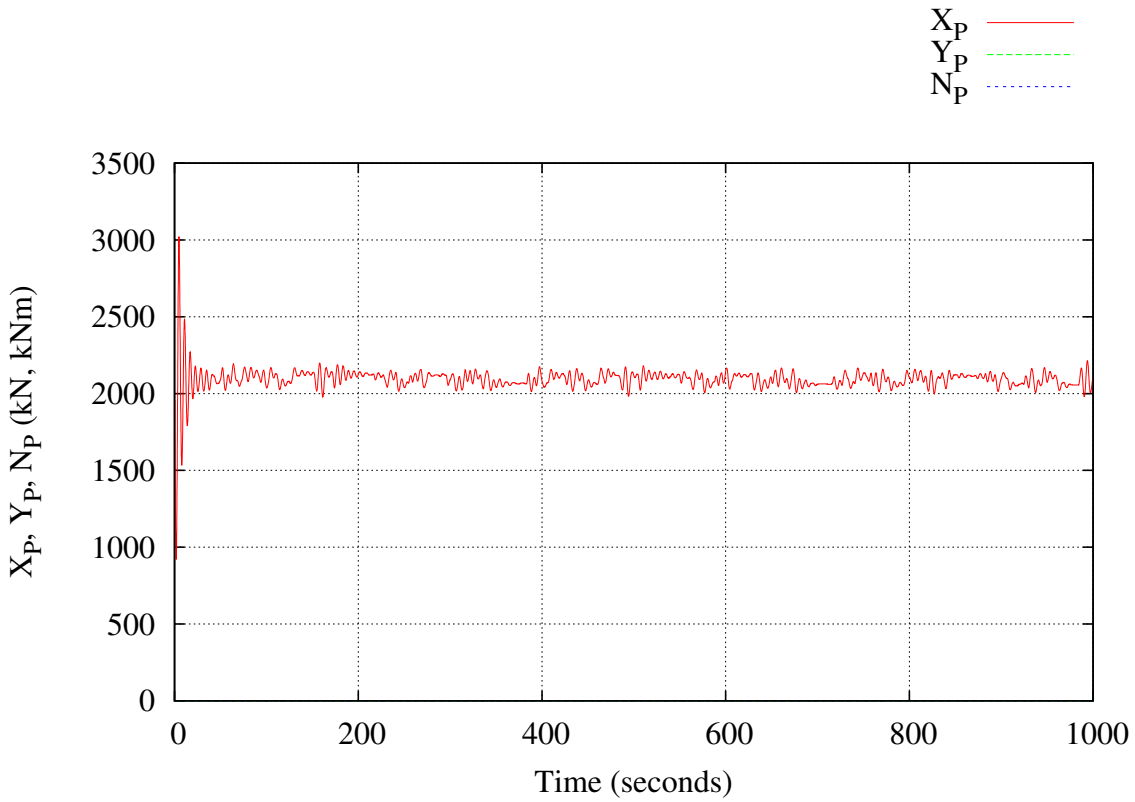

Figure C.47: Case 4: Propeller Force vs. Time

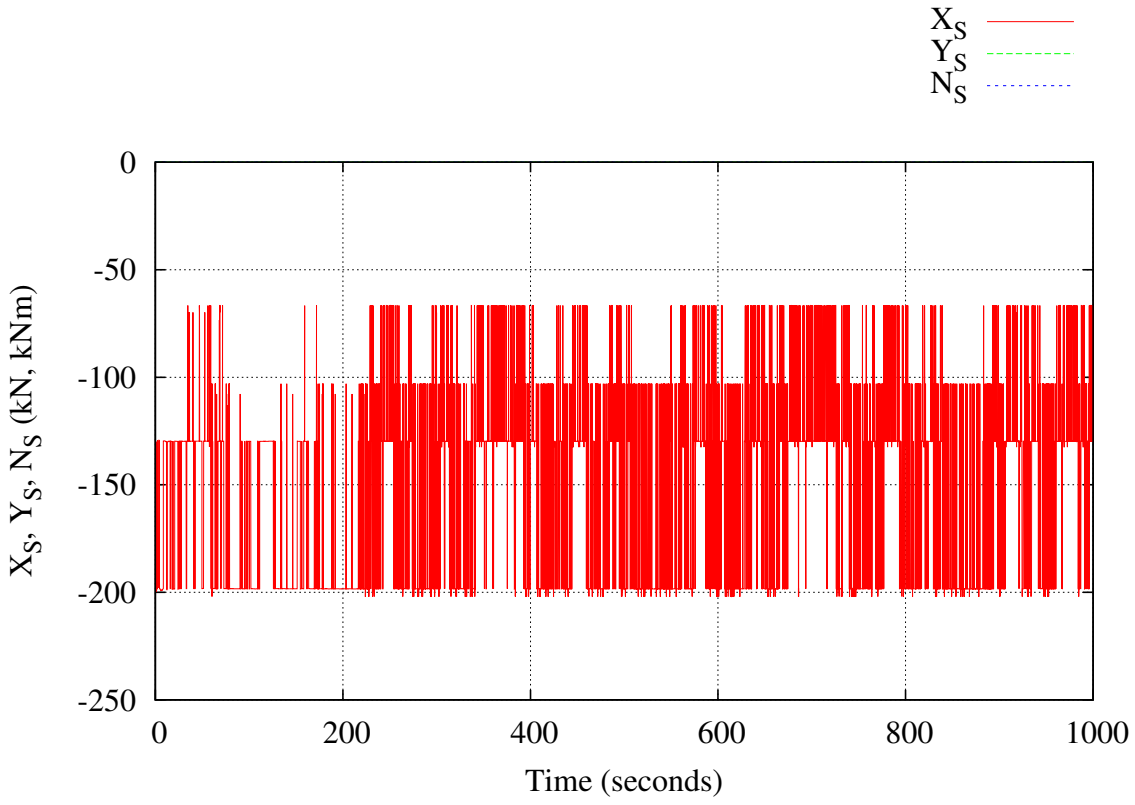

Figure C.48: Case 4: Seaway Force vs. Time

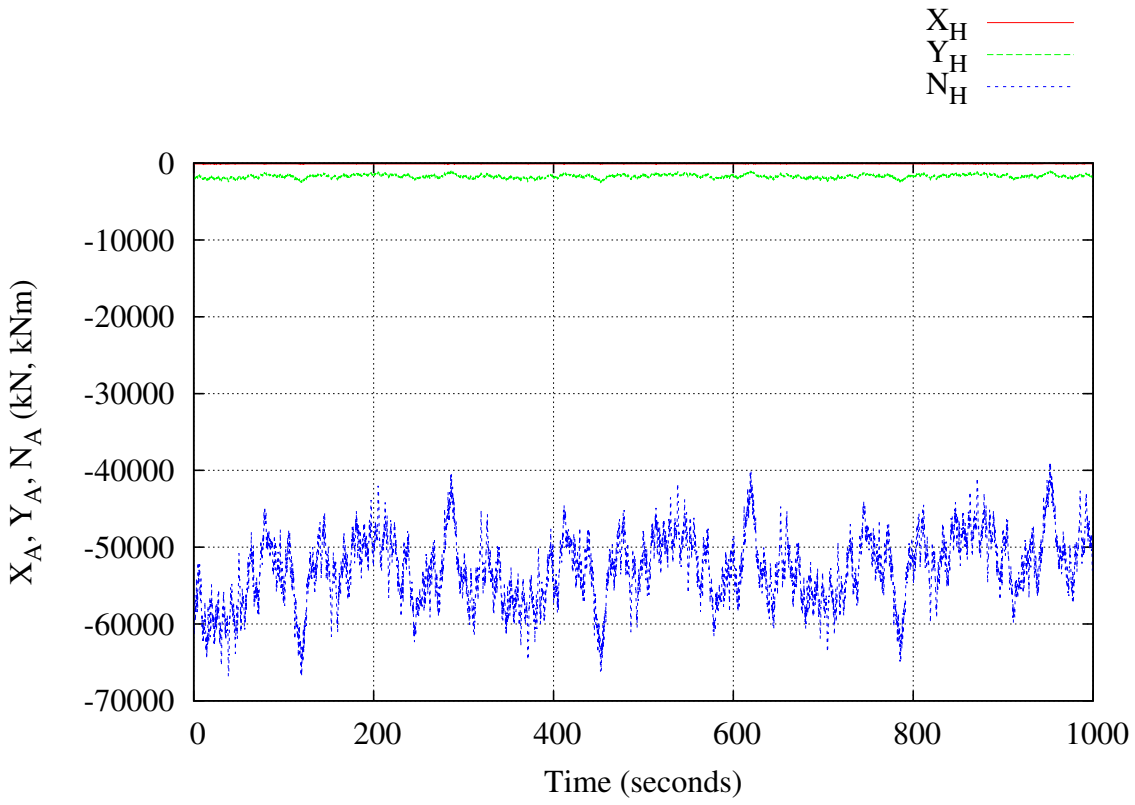

Figure C.49: Case 4: Wind Force vs. Time

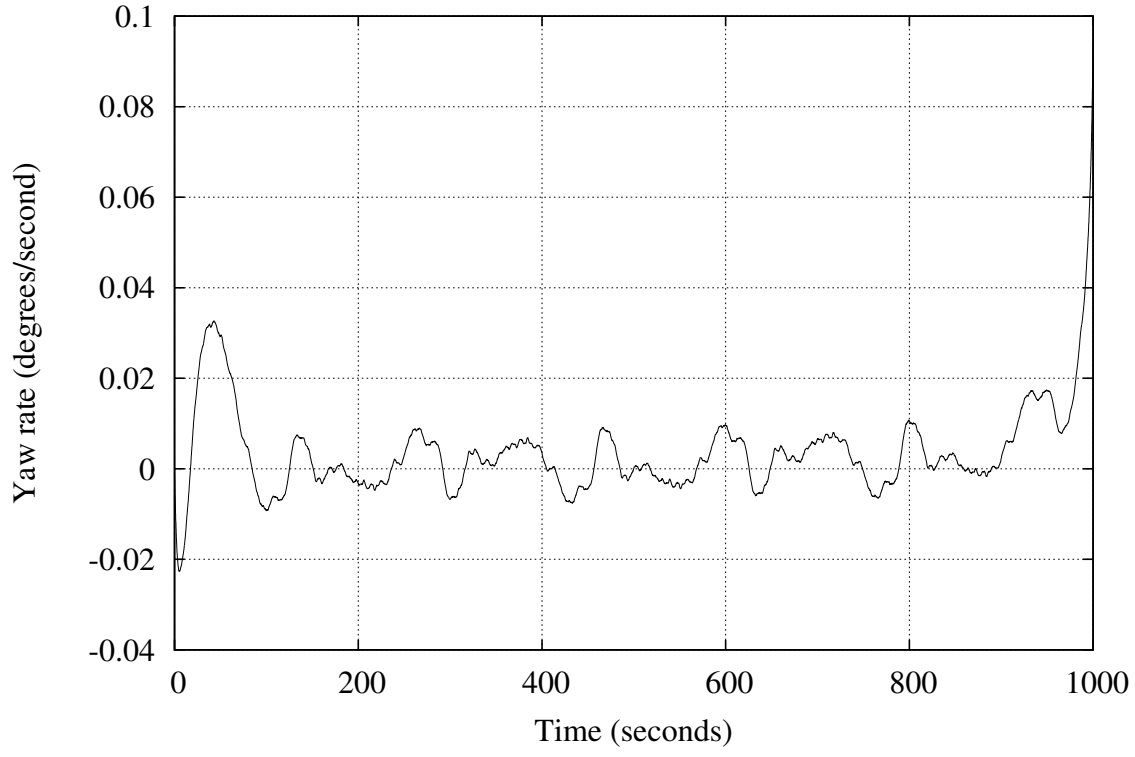

Figure C.50: Case 4: Yaw Rate vs. Time

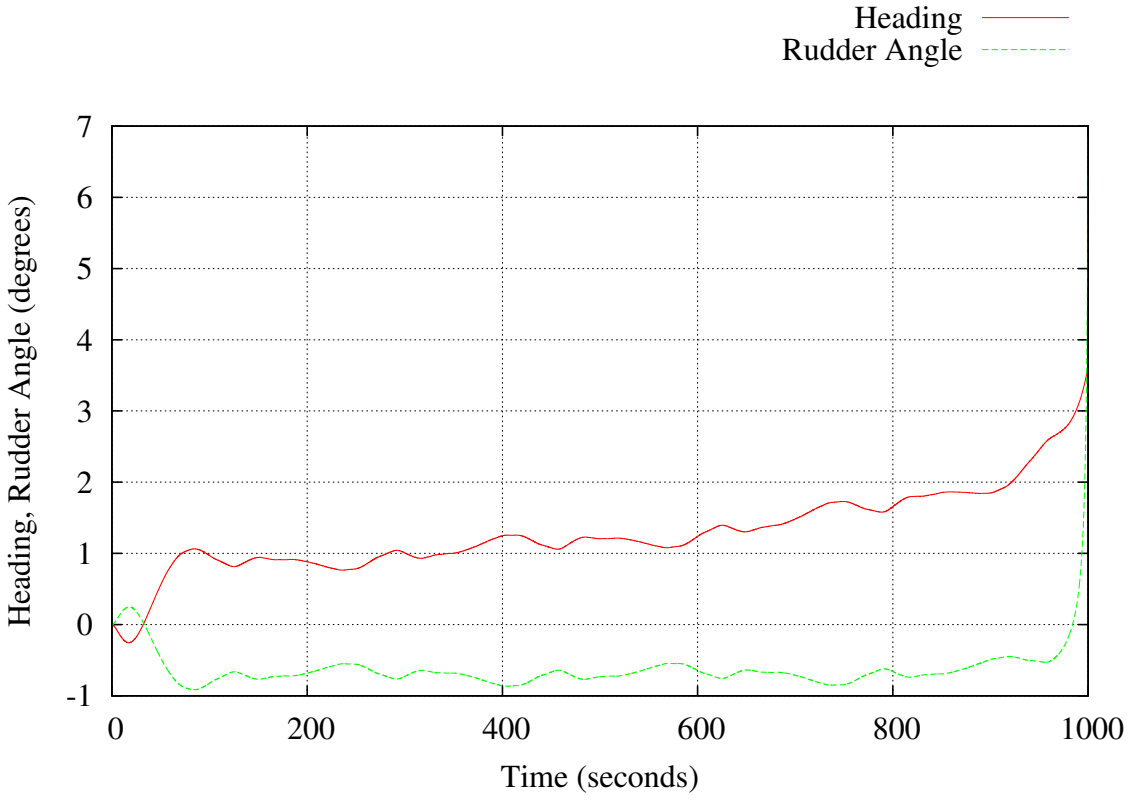

Figure C.51: Case 4: Rudder Command and Heading vs. Time

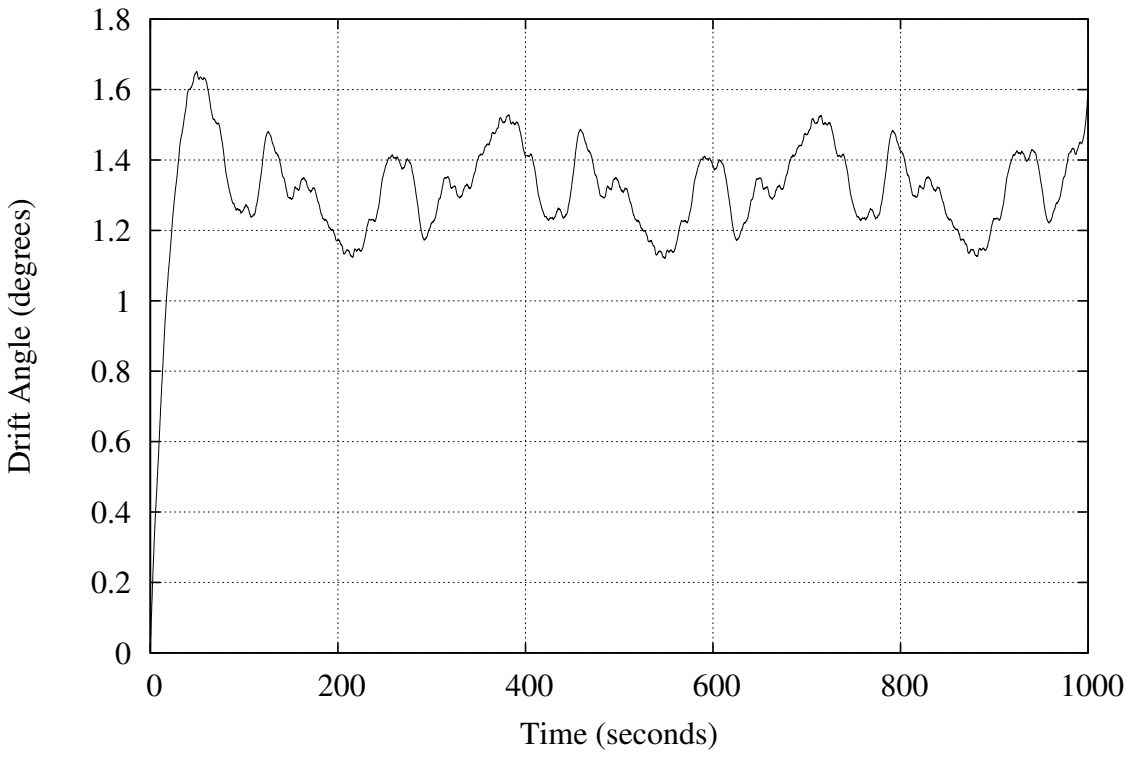

Figure C.52: Case 4: Drift Angle vs. Time

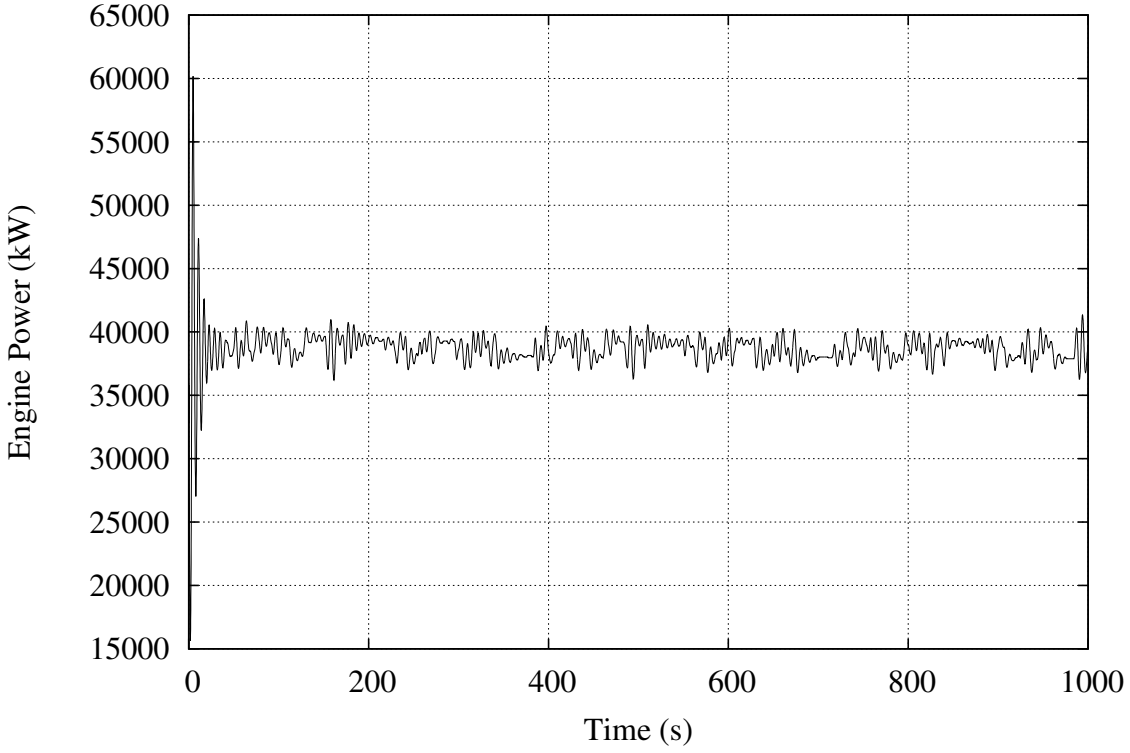

Figure C.53: Case 4: Engine Power vs. Time

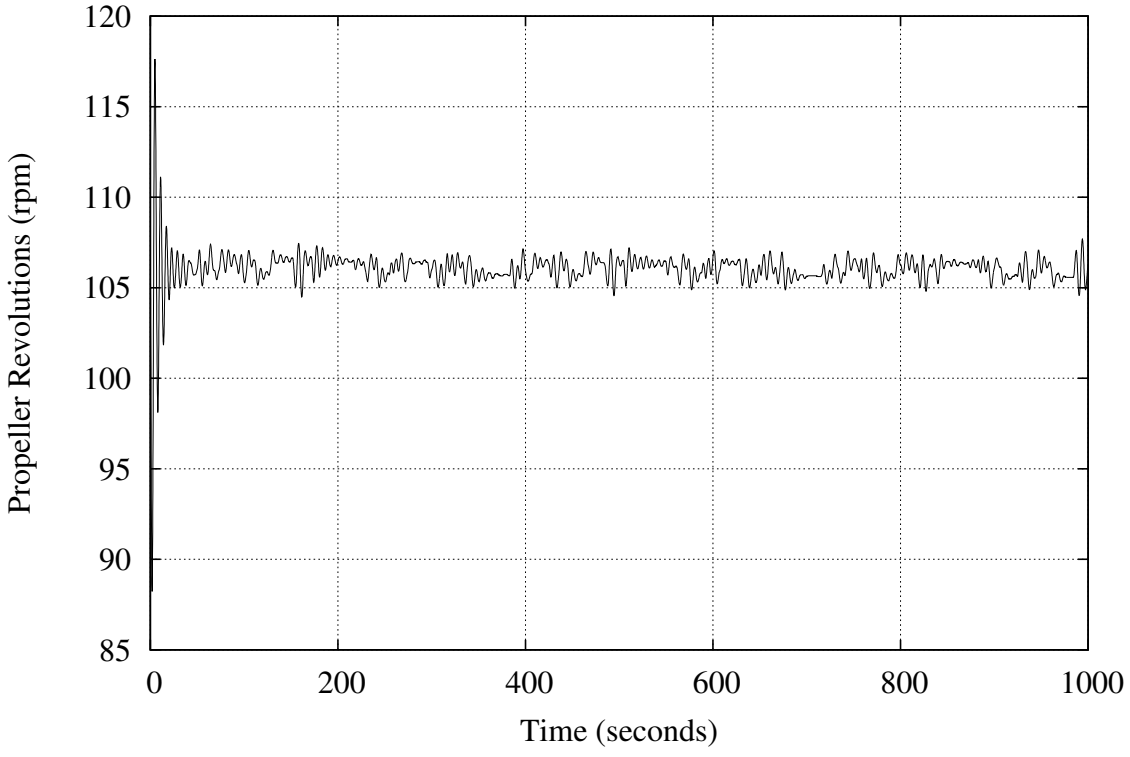

Figure C.54: Case 4: Propeller Revolutions vs. Time

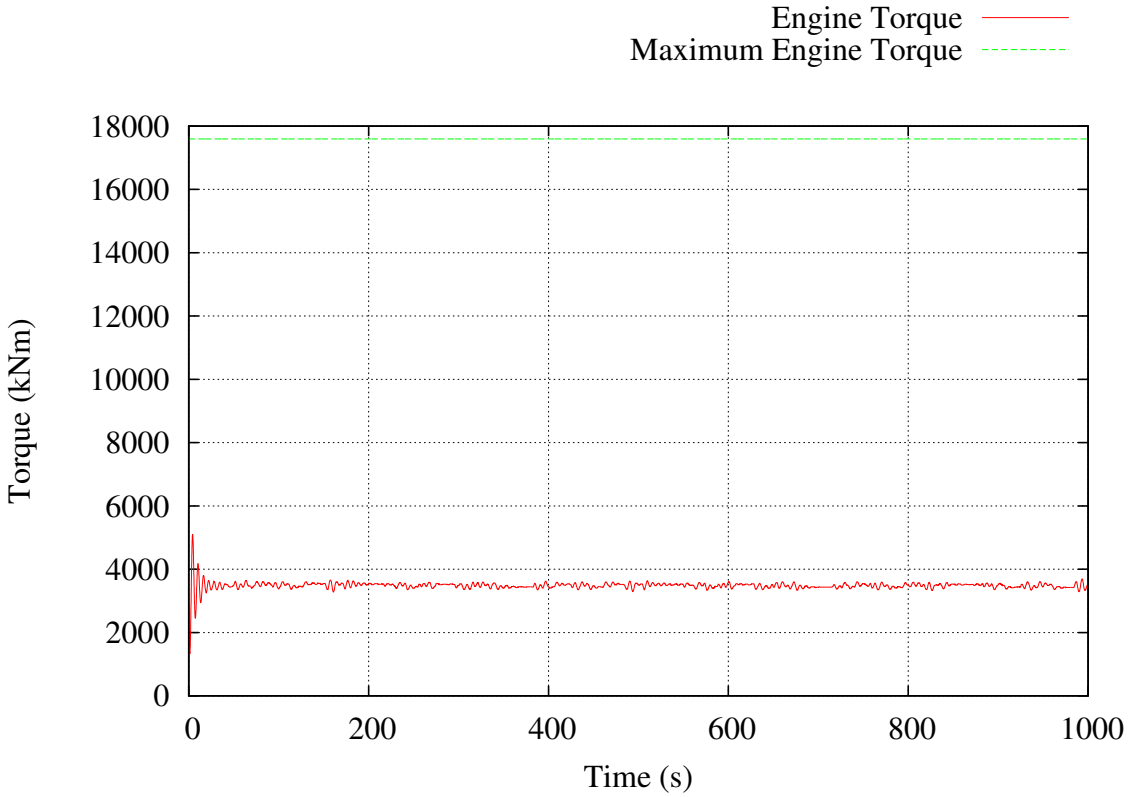

Figure C.55: Case 4: Engine Torque vs. Time

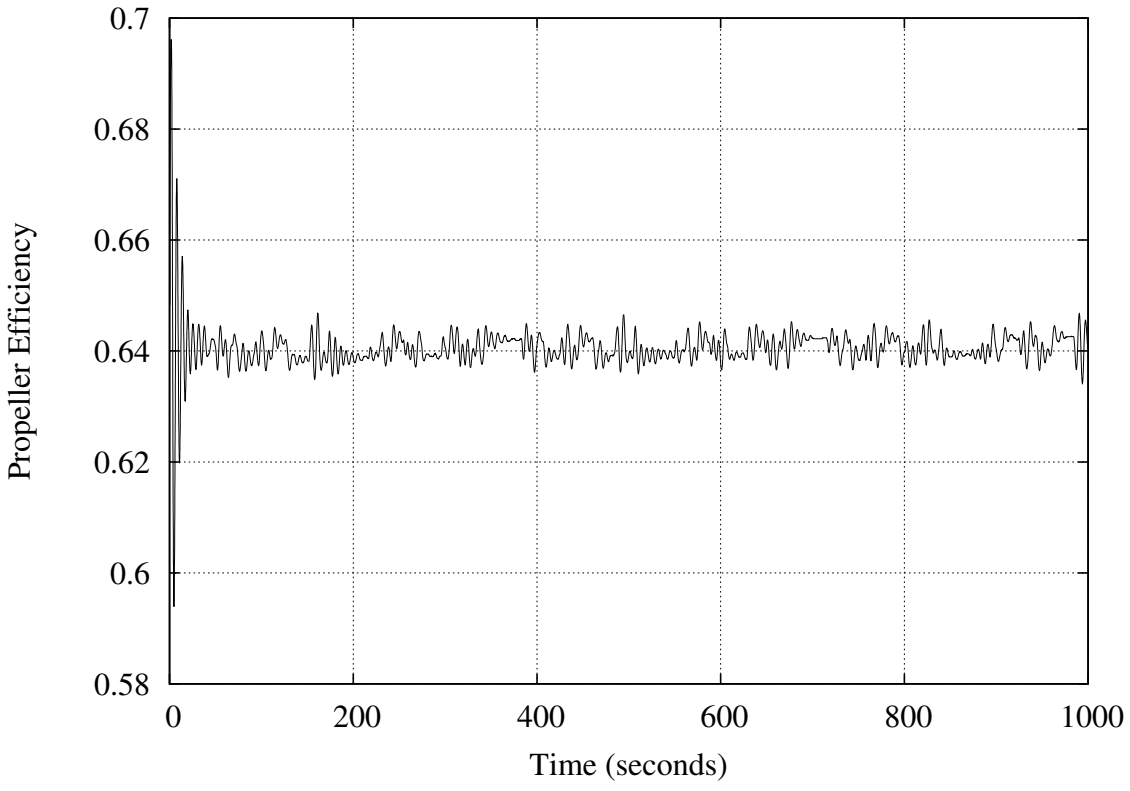

Figure C.56: Case 4: Open Water Propeller Efficiency vs. Time

C.5 Case 5. KCS, 20 Knot Wind (Fresh Breeze), Unsteady MBEMT Propulsion Model, Automatic Control, Propeller Optimisation

```
    |=============================================|
    | Ship-in-Service Performance Estimator       |
    |=============================================|
    | (c) 2013 David Trodden                      |
    | School of Marine Science and Technology     |
    | Newcastle University, UK                    |
    |=============================================|


"KCS - KRISO Container Ship"
============================


Simuation Parameters
--------------------
  Simulation is speed and track automatic pilot.
  Using an unsteady BEMT propulsion model.
  Mean true wind speed =                                    20.00 knots
  Mean true wind direction =                                90.00 degrees


Ship Main Particulars
---------------------
  Service Speed =                                           24.00 knots
  Lpp =                                                    232.00 m
  Lwl =                                                    237.58 m
  B =                                                       32.20 m
  T =                                                       11.34 m
  Volume of Displacement =                               50885.00 m^3
  Mass of Ship =                                         52157.13 tonnes
  LCB relative to midships +Fwd (%) =                       -2.030
  Midship Coefficient, Cm =                                  0.985
  Waterplane Coefficient, Cwp =                              0.802
  Block Coefficient, Cb =                                    0.601
  Prismatic Coefficient, Cp =                                0.610


Resistance Calculations from Holtrop & Mennen (Calm Water)
----------------------------------------------------------
  Friction Resistance =                                  1174.728 kN
  Appendage Resistance =                                   17.524 kN
  Wave Making Resistance =                                419.418 kN
  Added Pressure Resistance of Bulbous Bow =                0.089 kN
  Added Pressure Resistance of Immersed Transom Stern =     0.000 kN
  Model-Ship Correlation Line =                           230.444 kN
  Total Calm Water Resistance =                          1842.203 kN


Iteration:  1
==============


  Optimised Propeller Selection
  -----------------------------
    Number of Propellers =                      1
    Number of Blades =                          5
    Diameter =                               7.90 m
    Pitch =                                  6.29 m
    Expanded Blade Area Ratio =             0.667
    Optimum Open Water Efficiency =         0.721
    Optimum Revolutions =                 114.60 rpm


In-Service Propulsion Characteristics
-------------------------------------
  Average 'quasi-steady state' resultant resistance =            2088.626 kN
  Average 'quasi-steady state' resultant ship speed =              23.934 knots
  Average 'quasi-steady state' propeller efficiency =               0.640
  Average 'quasi-steady state' propeller revolutions =            120.812 rpm
  Average 'quasi-steady state' advance ratio =                      0.610
  Average 'quasi-steady state' Delivered Power =                38634.930 kW
  Average 'quasi-steady state' Engine Brake Power =             39367.301 kW
  Average 'quasi-steady state' drift angle at propeller =           1.285 degrees
```

```
Iteration:  2
==============


  Optimised Propeller Selection
  -----------------------------
    Number of Propellers =                    1
    Number of Blades =                        5
    Diameter =                             7.90 m
    Pitch =                                9.25 m
    Expanded Blade Area Ratio =           0.471
    Optimum Open Water Efficiency =       0.656
    Optimum Revolutions =                 90.57 rpm


In-Service Propulsion Characteristics
-------------------------------------
  Average 'quasi-steady state' resultant resistance =          2091.773 kN
  Average 'quasi-steady state' resultant ship speed =            23.945 knots
  Average 'quasi-steady state' propeller efficiency =             0.656
  Average 'quasi-steady state' propeller revolutions =           90.662 rpm
  Average 'quasi-steady state' advance ratio =                    0.813
  Average 'quasi-steady state' Delivered Power =              37763.824 kW
  Average 'quasi-steady state' Engine Brake Power =           38040.023 kW
  Average 'quasi-steady state' drift angle at propeller =         1.245 degrees
```

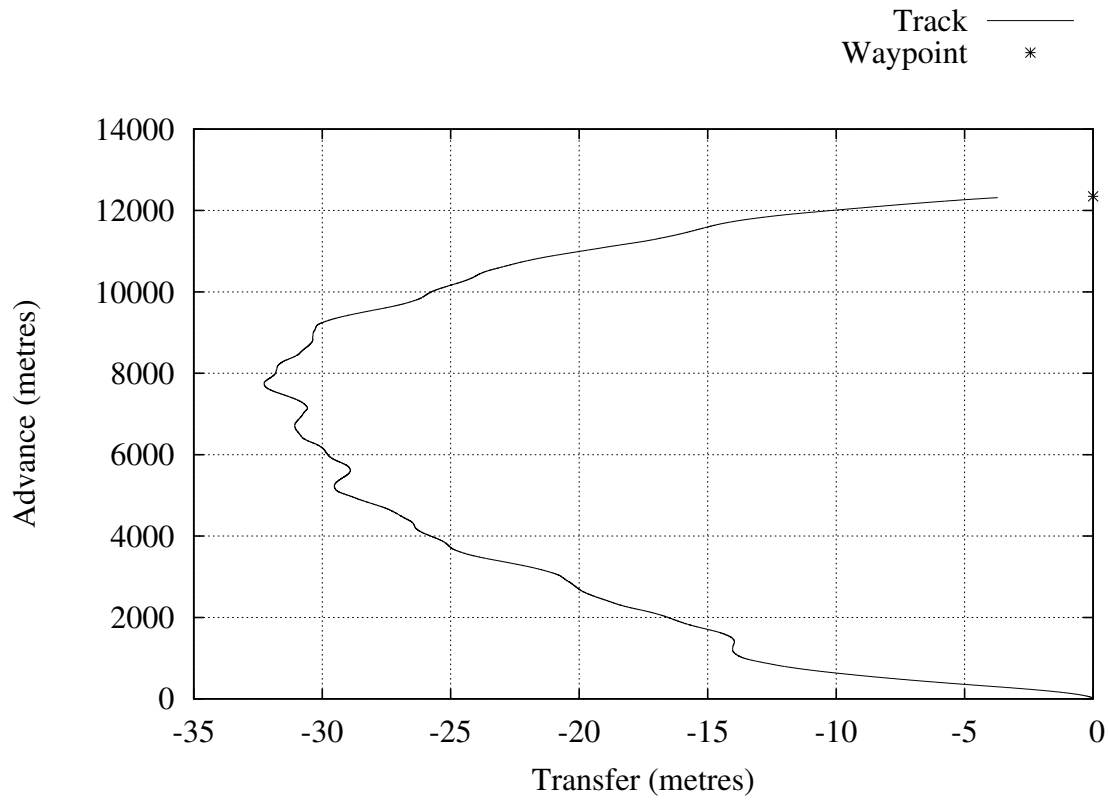

Figure C.57: Case 5: Ship Track

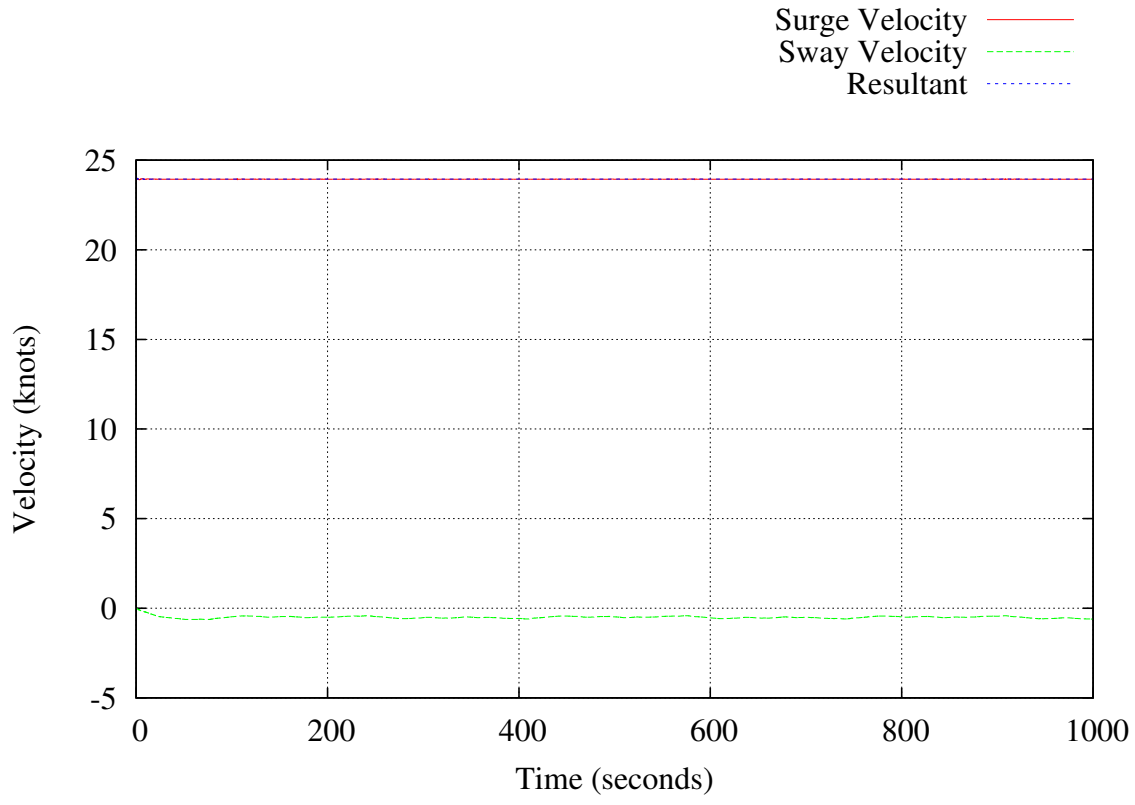

Figure C.58: Case 5: Speed vs. Time

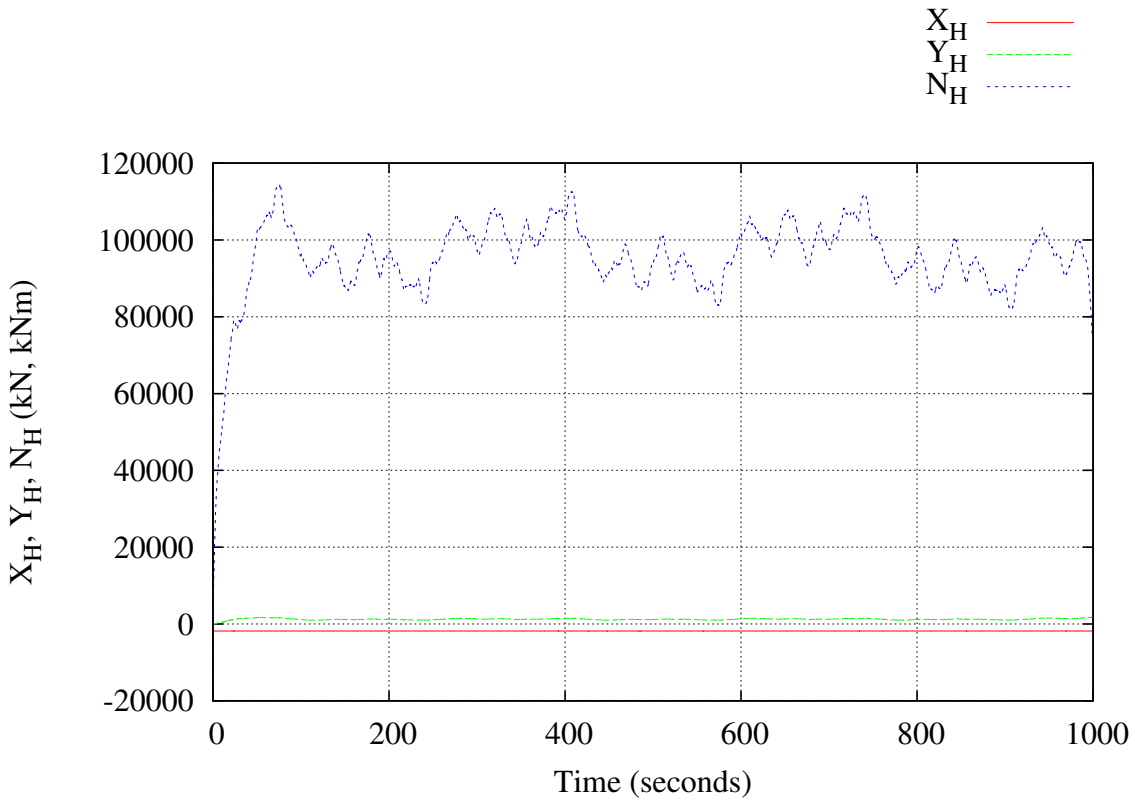

Figure C.59: Case 5: Hull Forces vs. Time

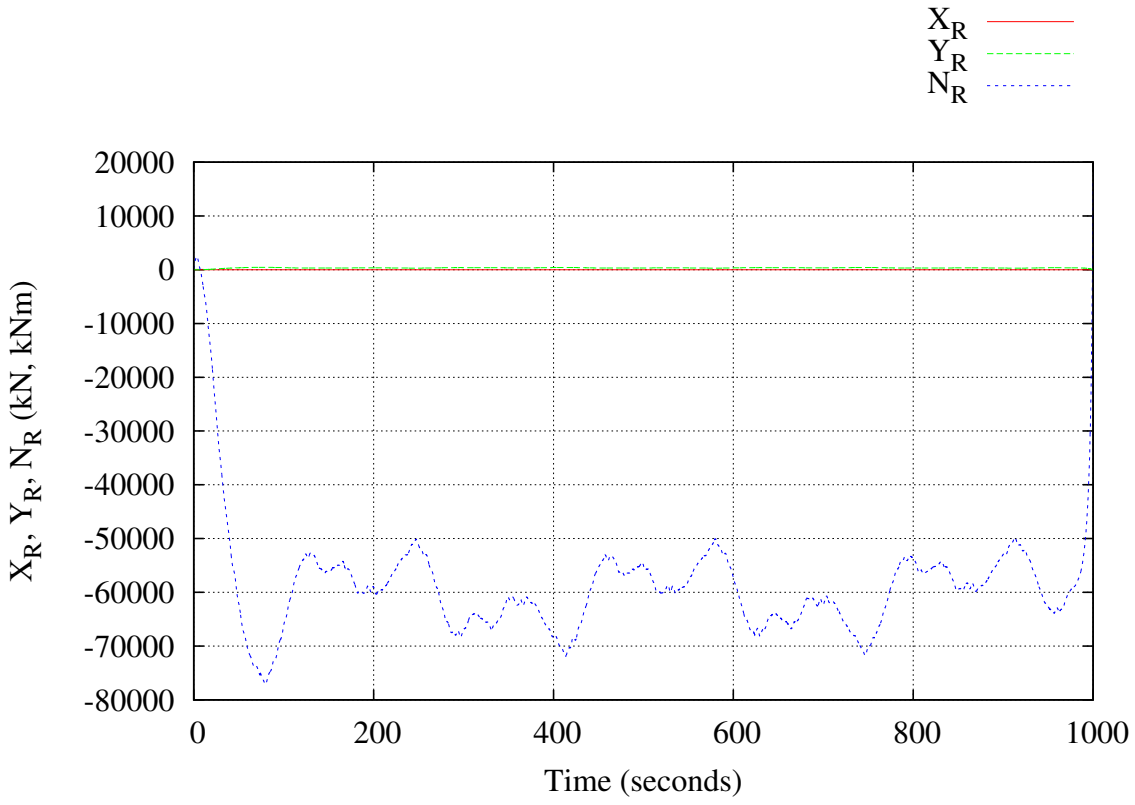

Figure C.60: Case 5: Rudder Force vs. Time

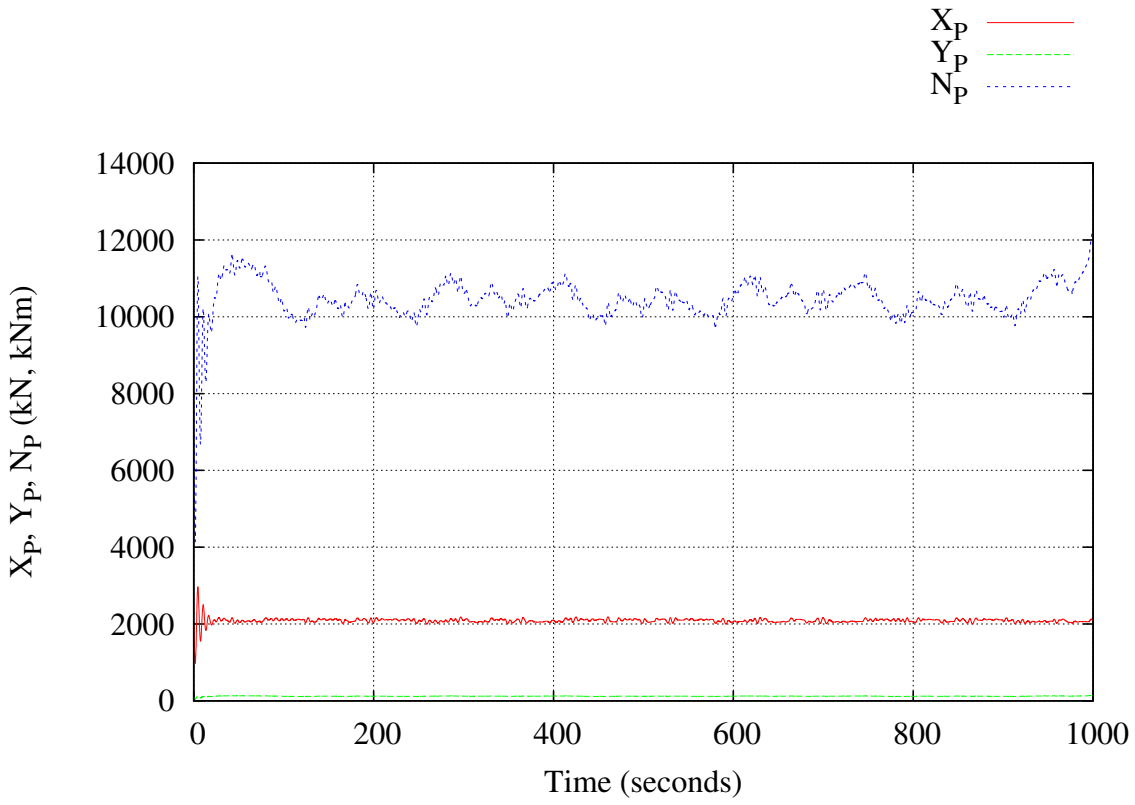

Figure C.61: Case 5: Propeller Force vs. Time

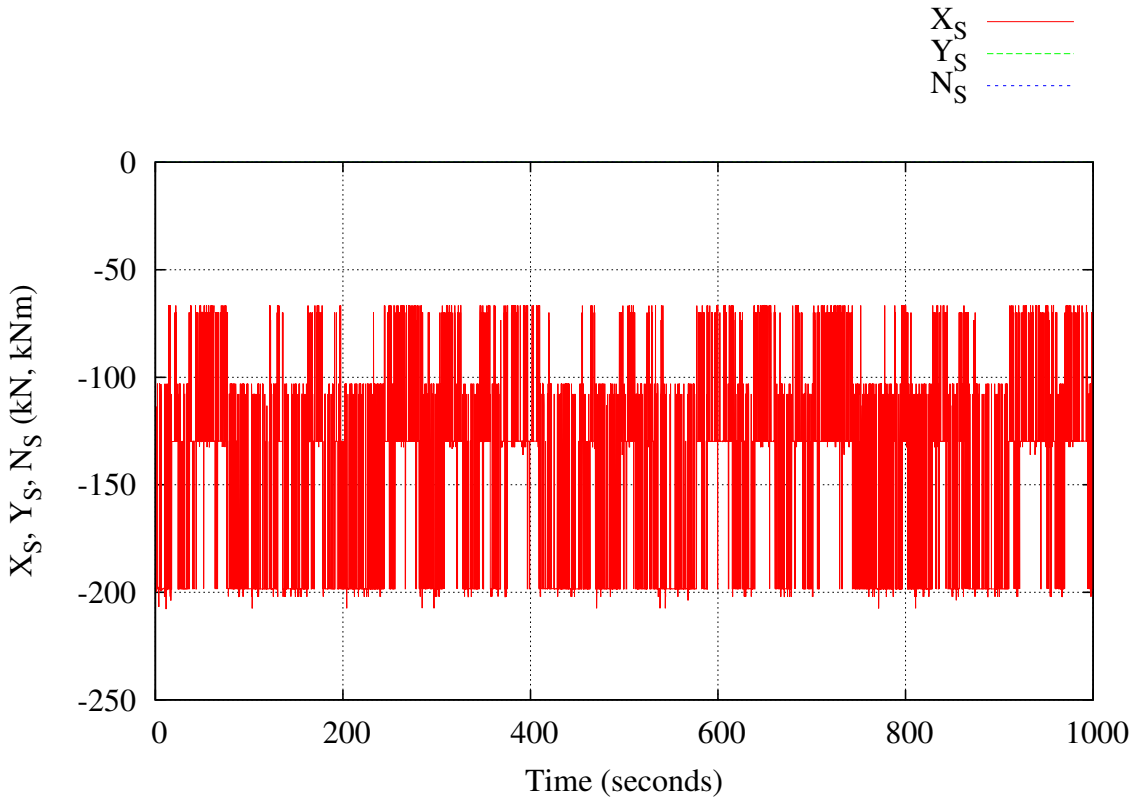

Figure C.62: Case 5: Seaway Force vs. Time

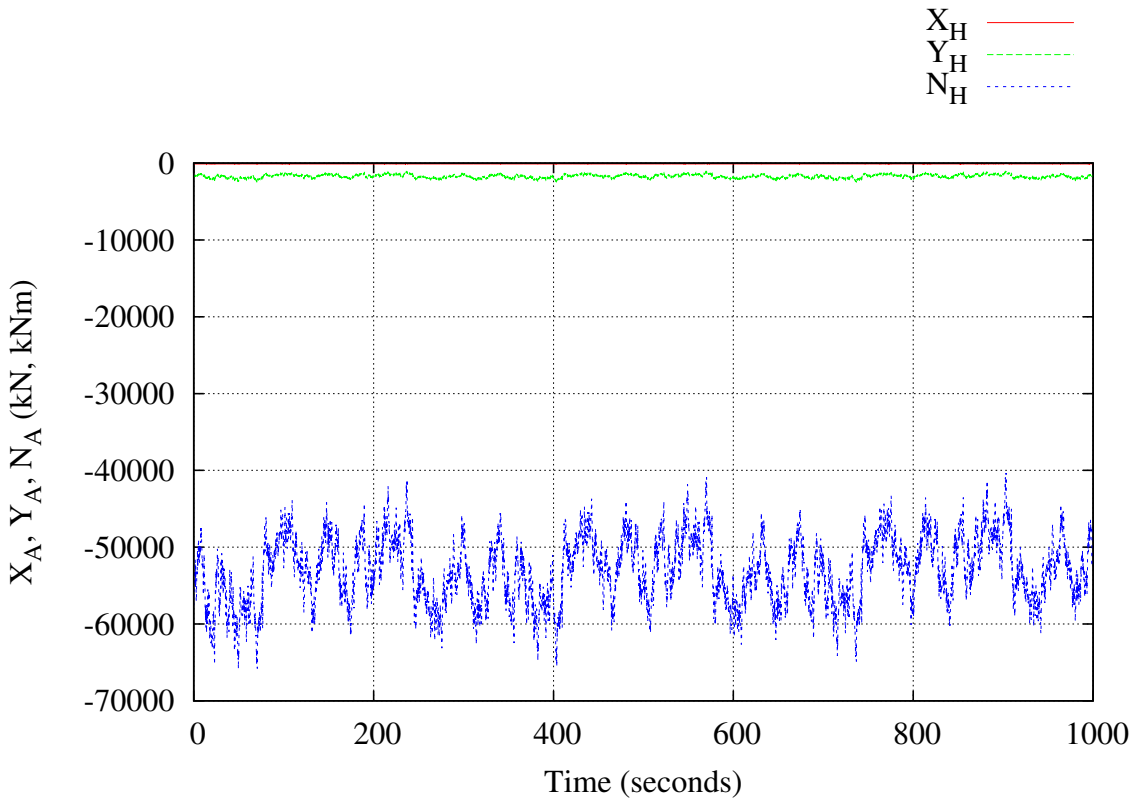

Figure C.63: Case 5: Wind Force vs. Time

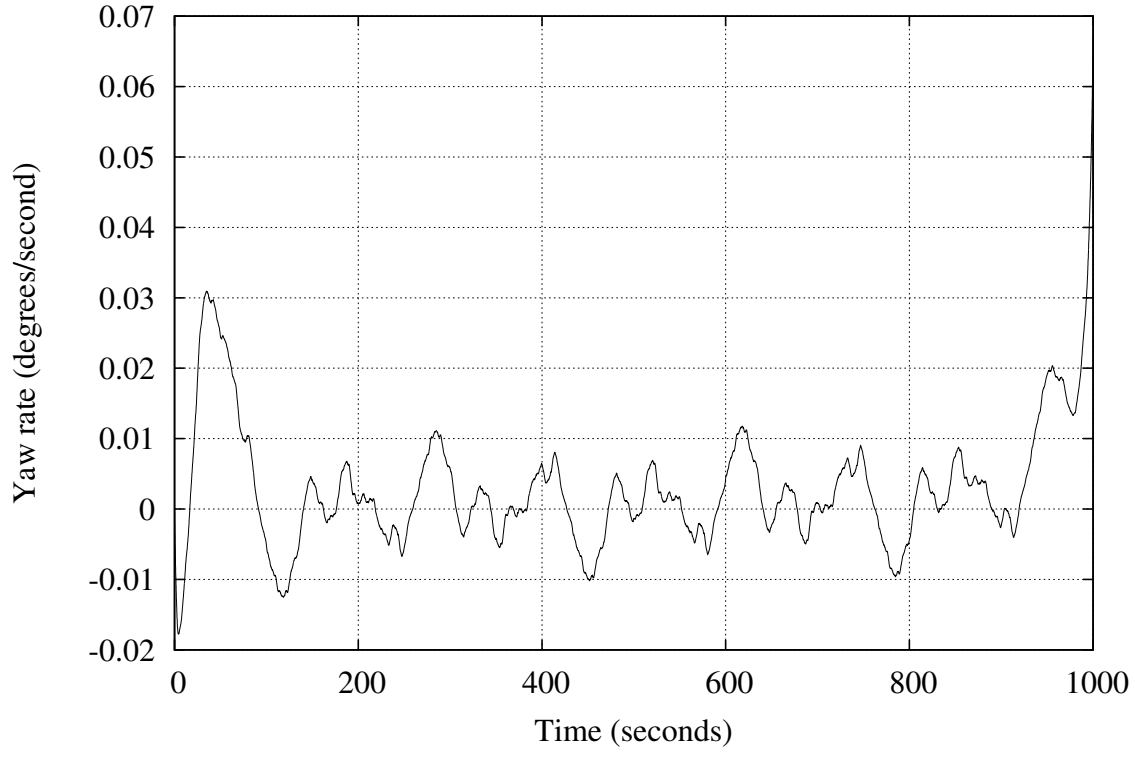

Figure C.64: Case 5: Yaw Rate vs. Time

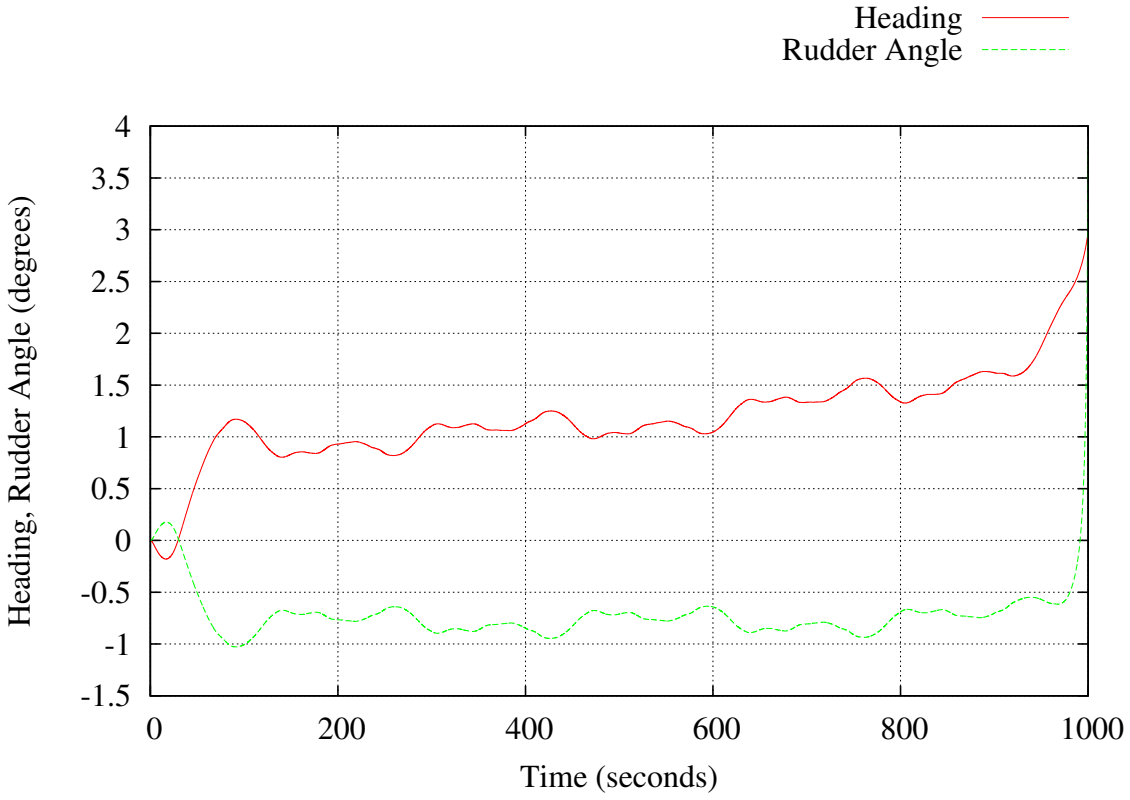

Figure C.65: Case 5: Rudder Command and Heading vs. Time

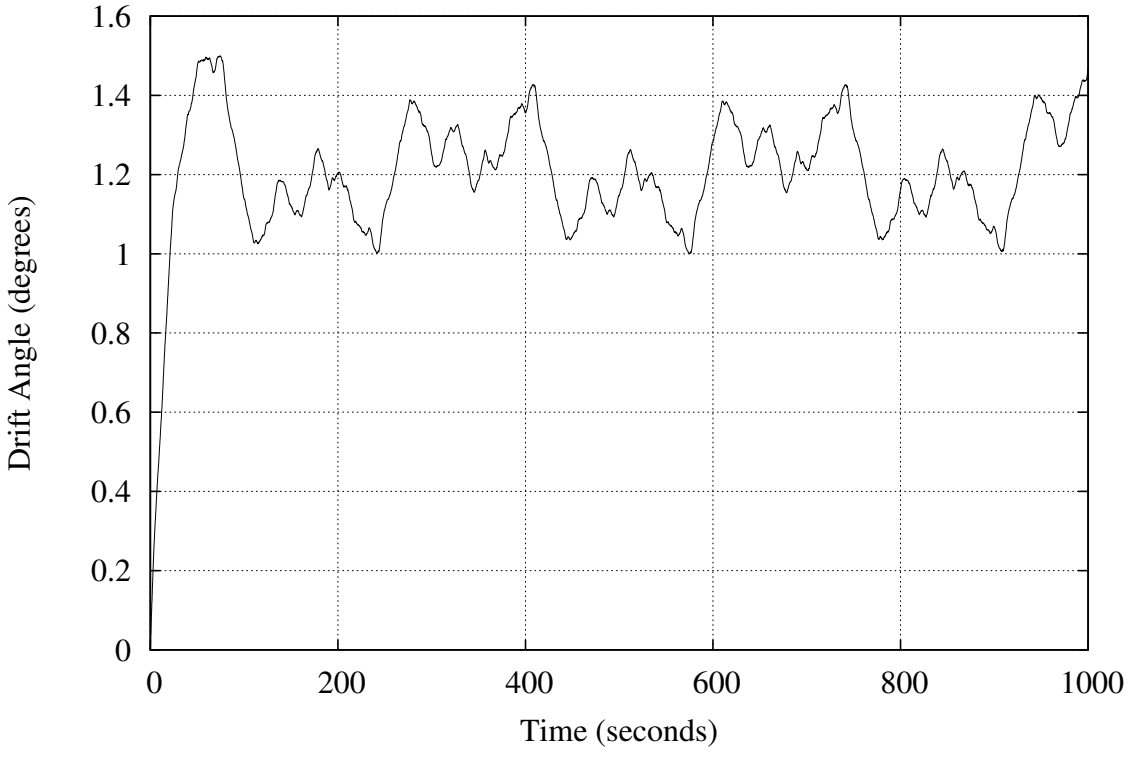

Figure C.66: Case 5: Drift Angle vs. Time

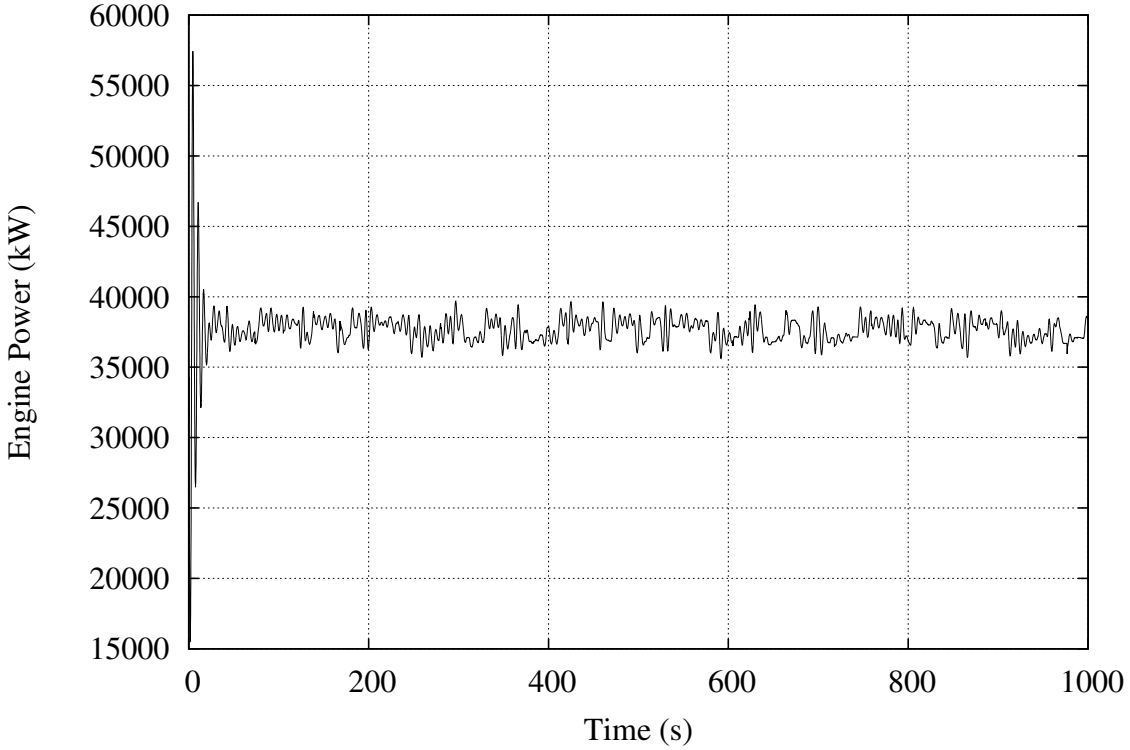

Figure C.67: Case 5: Engine Power vs. Time

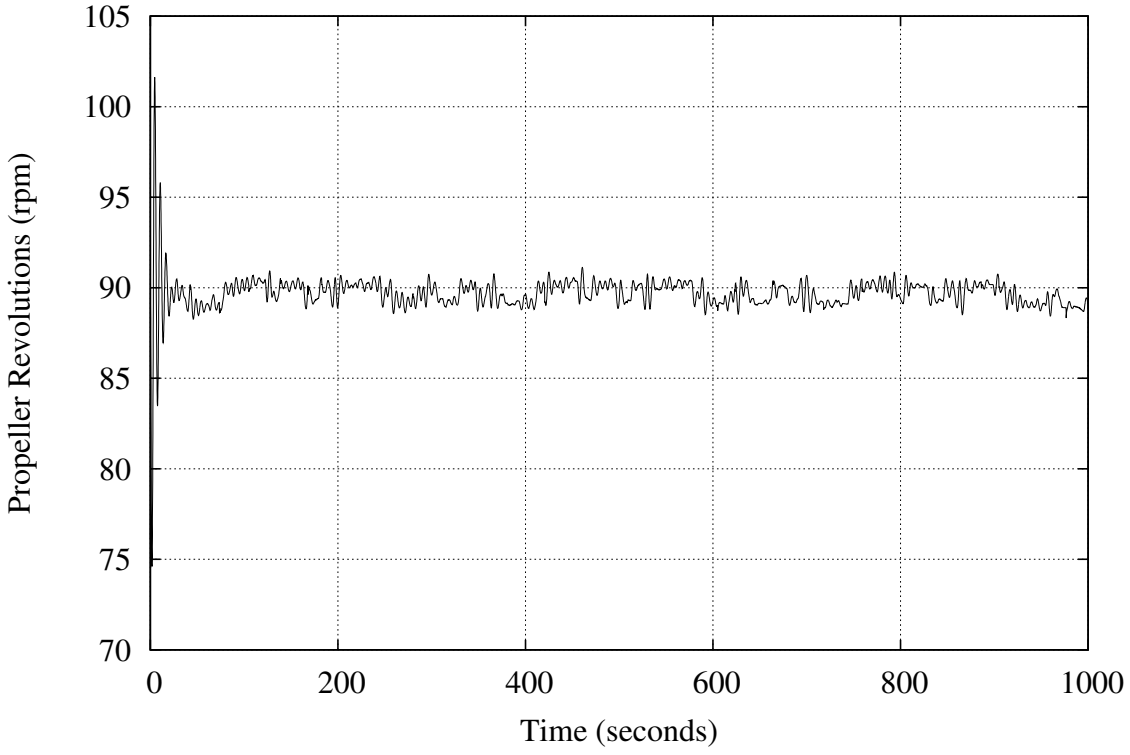

Figure C.68: Case 5: Propeller Revolutions vs. Time

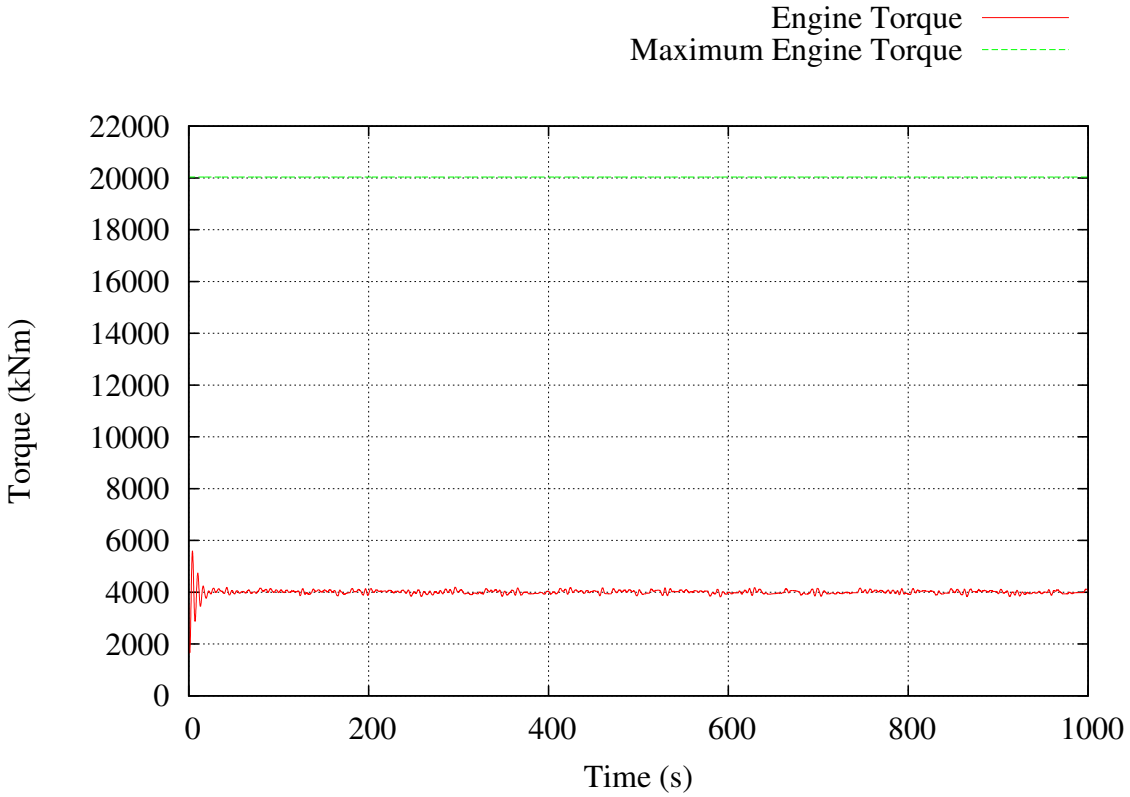

Figure C.69: Case 5: Engine Torque vs. Time

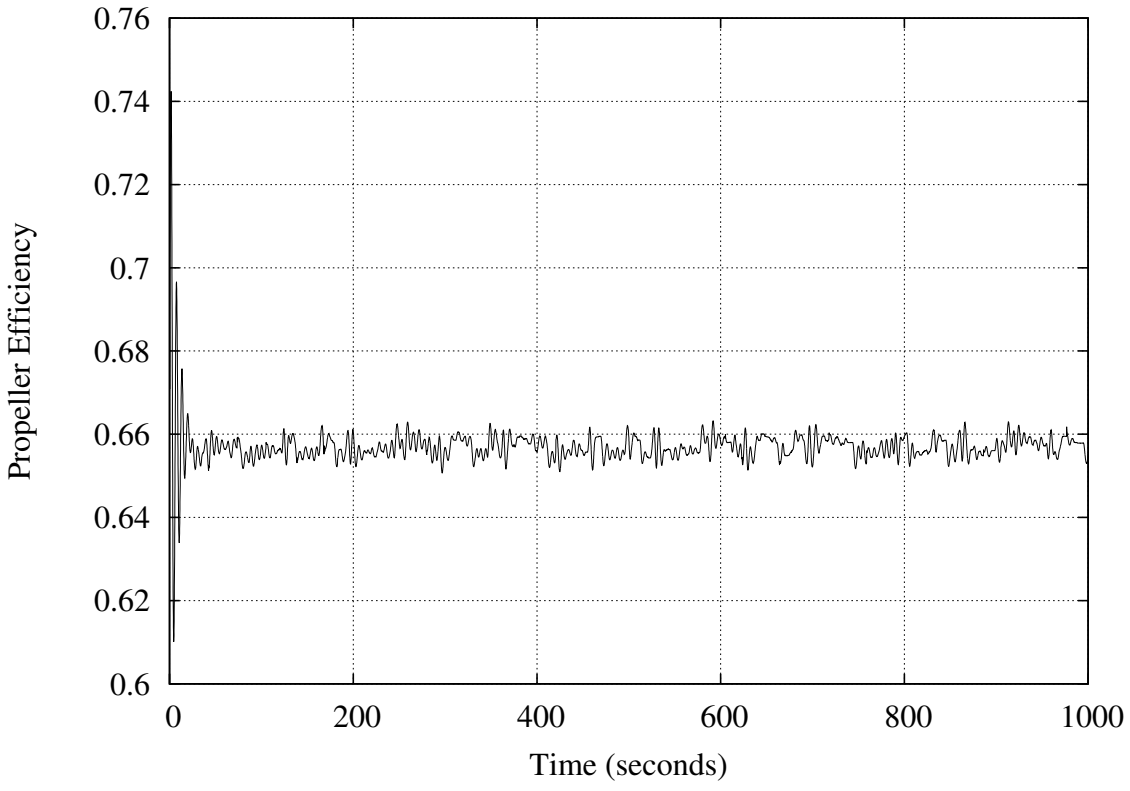

Figure C.70: Case 5: Open Water Propeller Efficiency vs. Time

C.6 Case 6. *KCS*, 20 Knot Wind (Fresh Breeze), Unsteady *MBEMT* Propulsion Model, Automatic Control, with Propeller Selected from *OOBOO* Model

```
    |=============================================|
    | Ship-in-Service Performance Estimator       |
    |=============================================|
    | (c) 2013 David Trodden                      |
    | School of Marine Science and Technology     |
    | Newcastle University, UK                    |
    |=============================================|

"KCS - KRISO Container Ship"
============================


Simuation Parameters
--------------------
  Simulation is speed and track automatic pilot.
  Using an unsteady BEMT propulsion model.
  Mean true wind speed =                                  20.00 knots
  Mean true wind direction =                              90.00 degrees


Ship Main Particulars
---------------------
  Service Speed =                                         24.00 knots
  Lpp =                                                  232.00 m
  Lwl =                                                  237.58 m
  B =                                                     32.20 m
  T =                                                     11.34 m
  Volume of Displacement =                             50885.00 m^3
  Mass of Ship =                                       52157.12 tonnes
  LCB relative to midships +Fwd (%) =                     -2.030
  Midship Coefficient, Cm =                                0.985
  Waterplane Coefficient, Cwp =                            0.802
  Block Coefficient, Cb =                                  0.601
  Prismatic Coefficient, Cp =                              0.610


Propeller geometry has been provided
------------------------------------
  Number of Propellers =                                      1
  Number of Blades on each Propeller =                        5
  Propeller Diameter =                                     7.90 m
  Propeller Pitch =                                        8.09 m
  Expanded Blade Area Ratio =                              0.86


Resistance Calculations from Holtrop & Mennen (Calm Water)
----------------------------------------------------------
  Friction Resistance =                                1174.728 kN
  Appendage Resistance =                                 17.524 kN
  Wave Making Resistance =                              419.417 kN
  Added Pressure Resistance of Bulbous Bow =              0.089 kN
  Added Pressure Resistance of Immersed Transom Stern =   0.000 kN
  Model-Ship Correlation Line =                         230.444 kN
  Total Calm Water Resistance =                        1842.203 kN


Calm Water Propulsion Characteristics
-------------------------------------
  Required Engine Power for Service Speed =           27743.639 kW
  Propeller Revolutions =                                96.351 rpm
  Open Water Propeller Efficiency =                       0.674


In-Service Propulsion Characteristics
-------------------------------------
  Average ship resistance =                            2088.377 kN
  Average resultant ship speed =                         23.935 knots
  Average propeller efficiency =                          0.641
  Average propeller revolutions =                        95.923 rpm
  Average Delivered Power =                           38516.203 kW
  Average Engine Brake Power =                        39302.242 kW
```

```
Average 'steady state' resultant resistance =          2083.865 kN
Average 'steady state' resultant ship speed =            23.935 knots
Average 'steady state' propeller efficiency =             0.641
Average 'steady state' propeller revolutions =           95.839 rpm
Average 'steady state' advance ratio =                    0.769
Average 'steady state' Delivered Power =              38441.281 kW
Average 'steady state' Engine Brake Power =           39225.793 kW
Average 'steady state' drift angle at propeller =         1.259 degrees
```

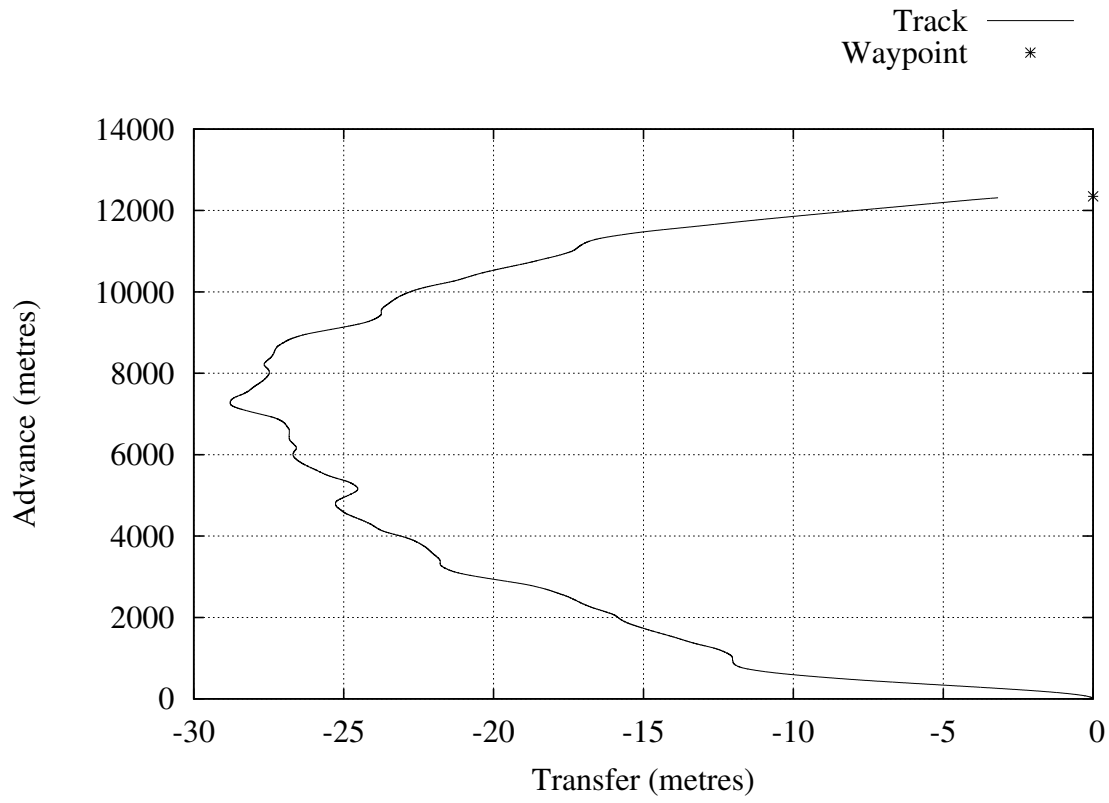

Figure C.71: Case 6: Ship Track

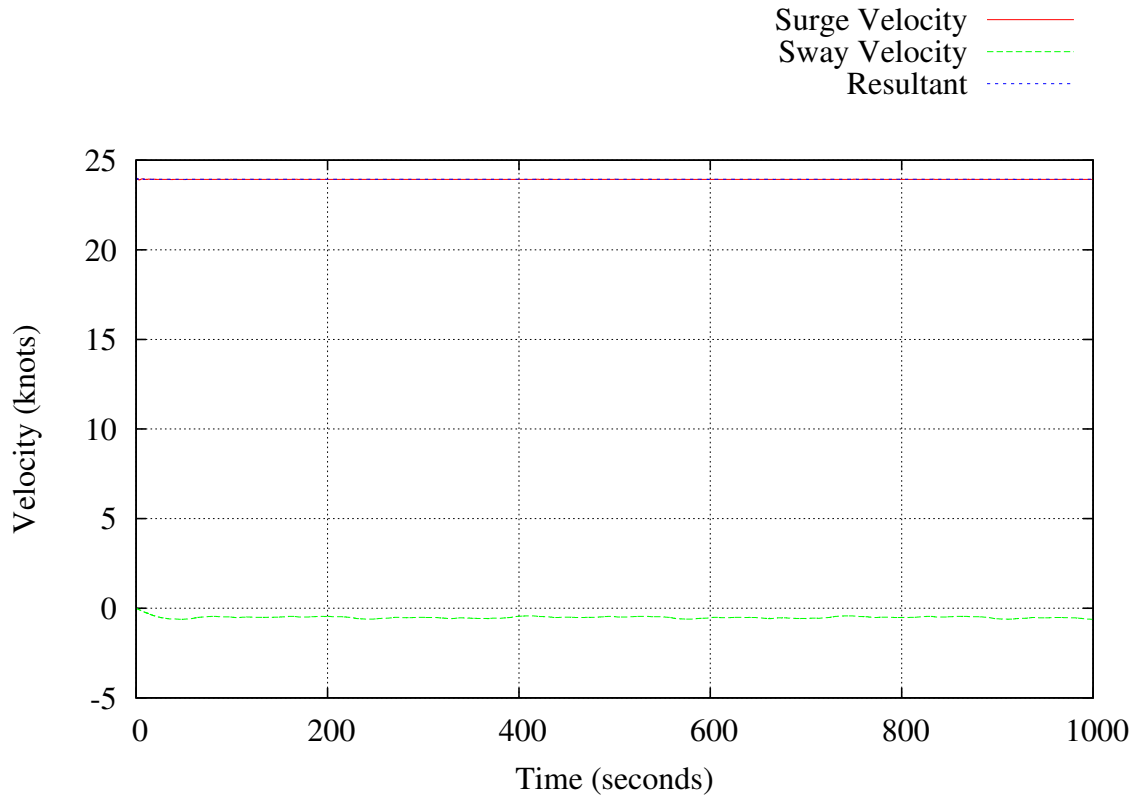

Figure C.72: Case 6: Speed vs. Time

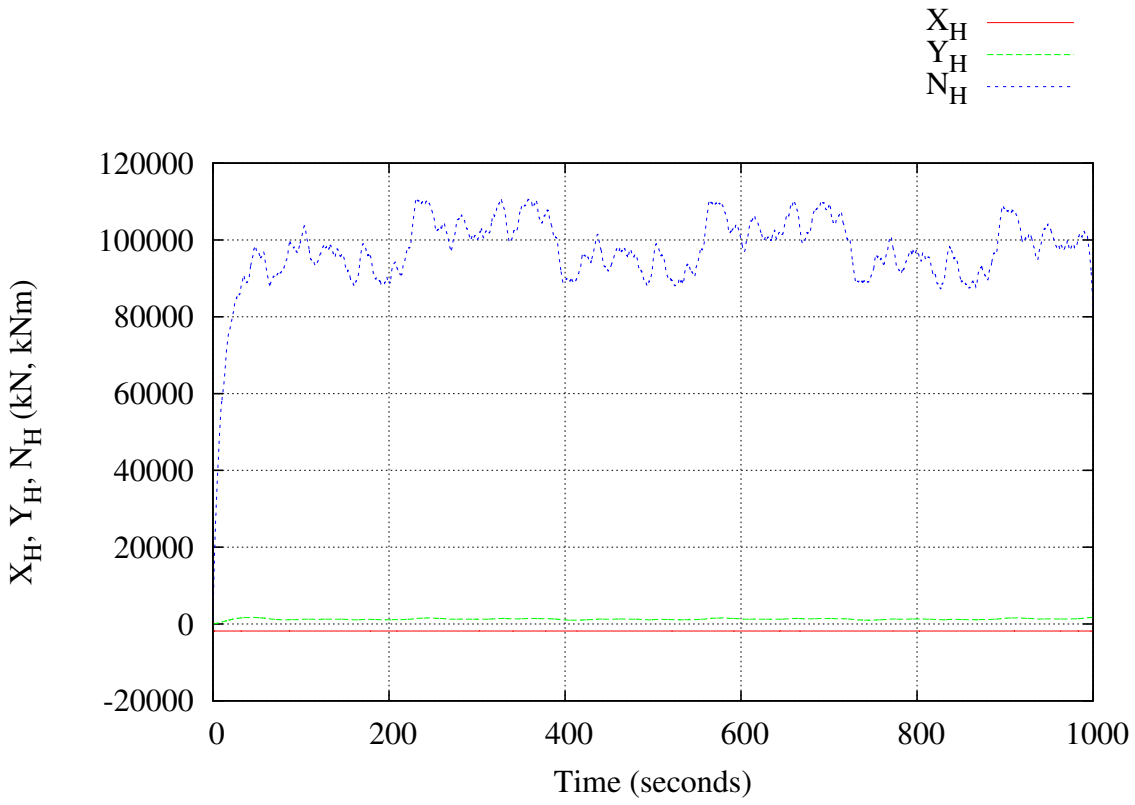

Figure C.73: Case 6: Hull Forces vs. Time

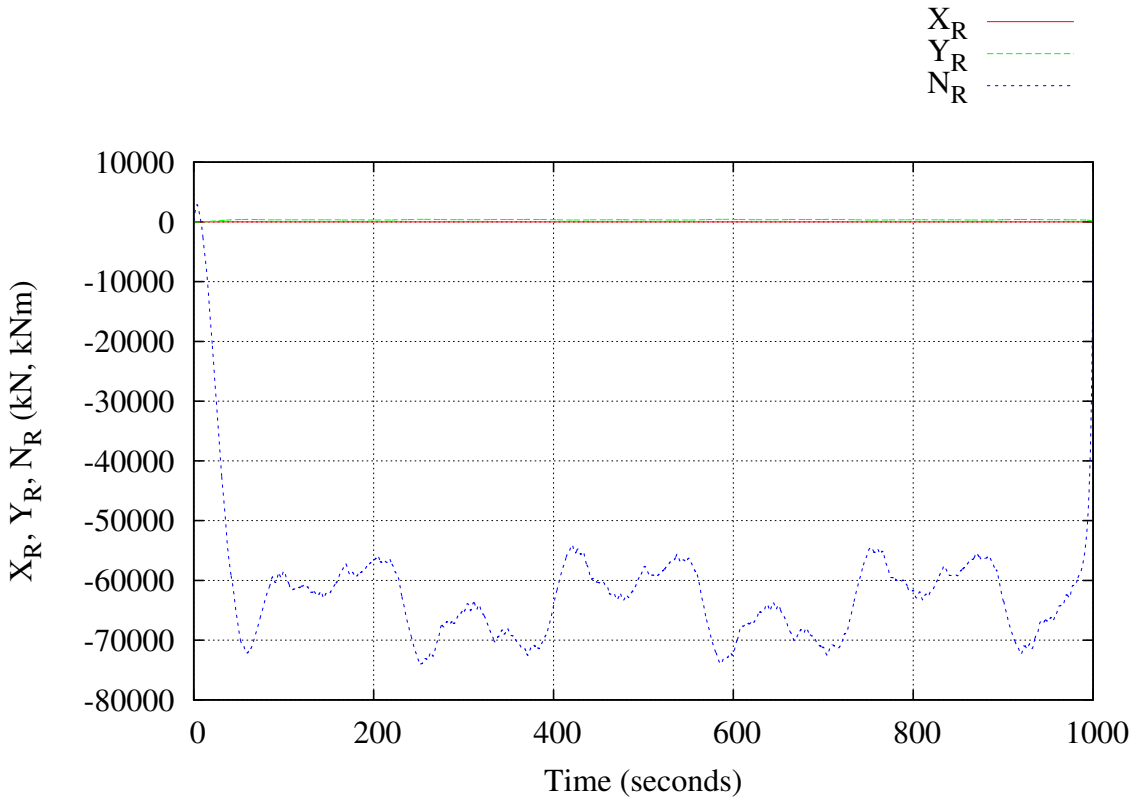

Figure C.74: Case 6: Rudder Force vs. Time

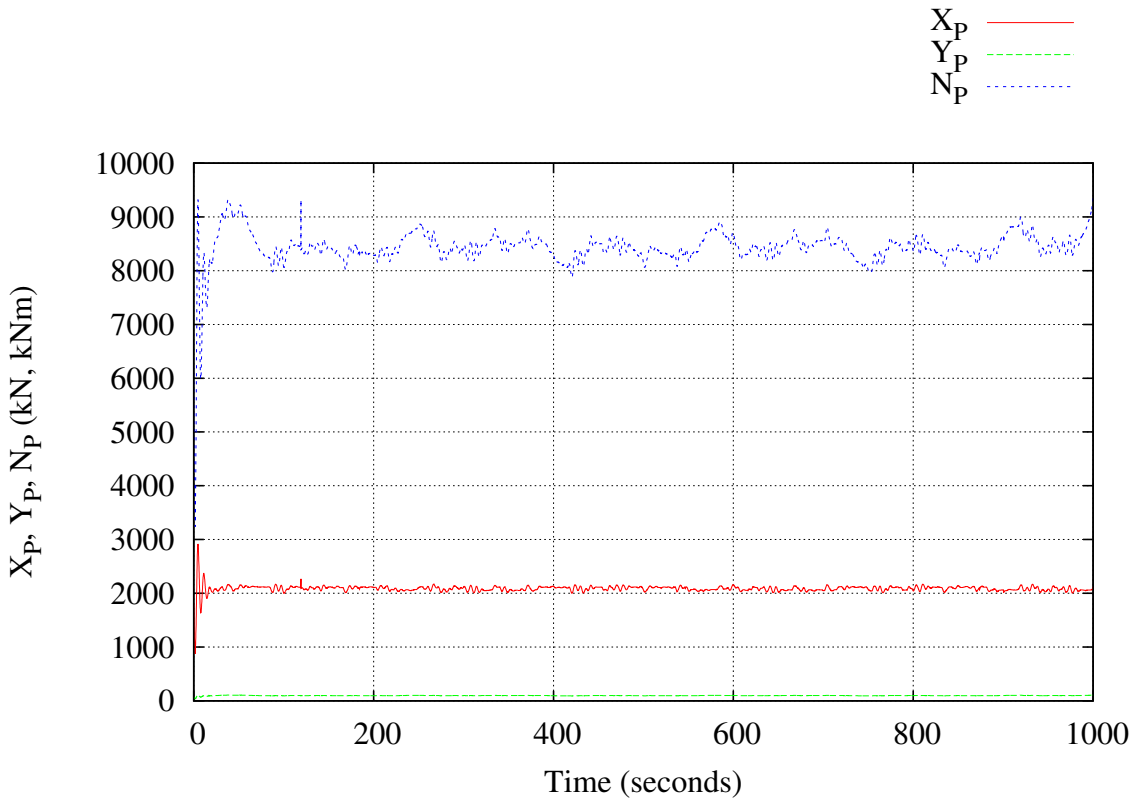

Figure C.75: Case 6: Propeller Force vs. Time

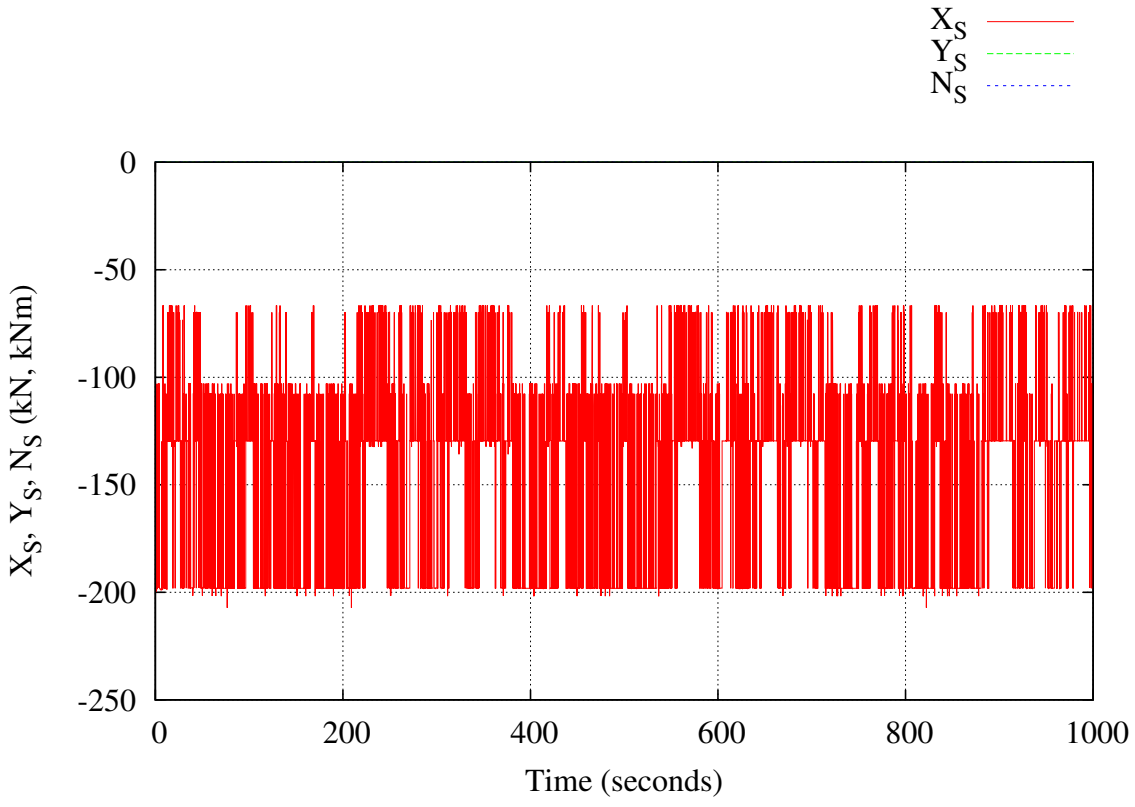

Figure C.76: Case 6: Seaway Force vs. Time

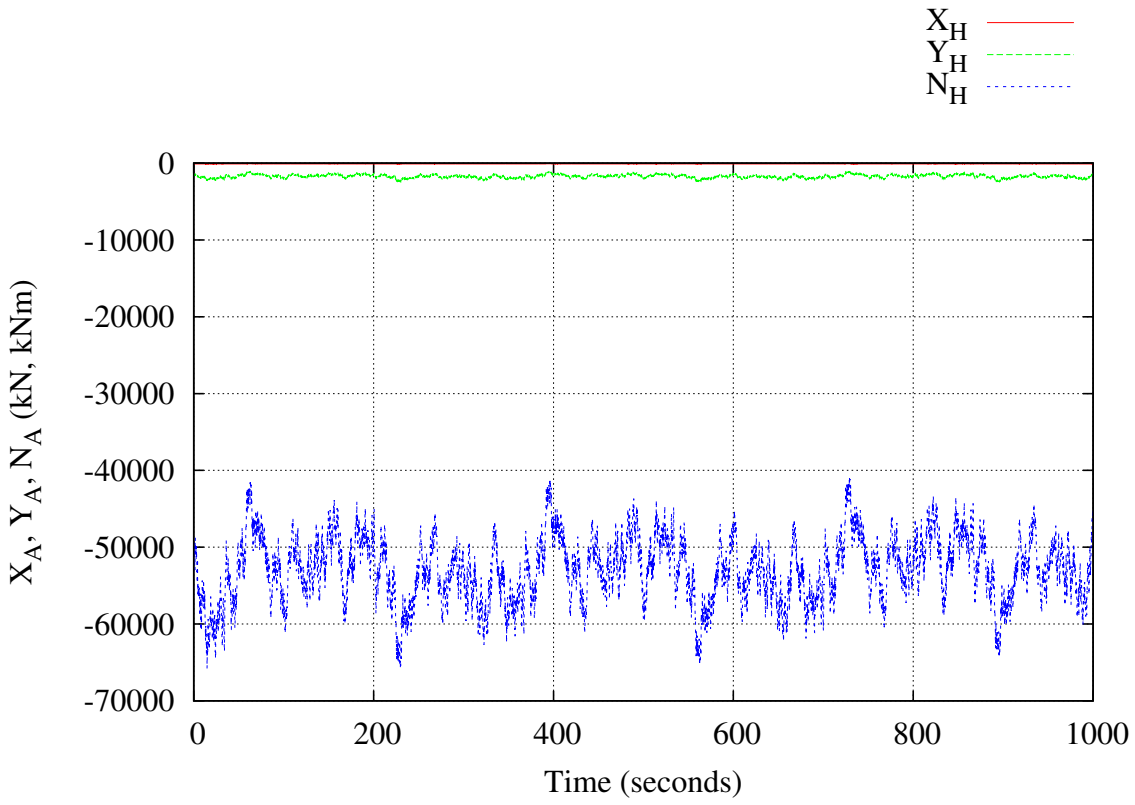

Figure C.77: Case 6: Wind Force vs. Time

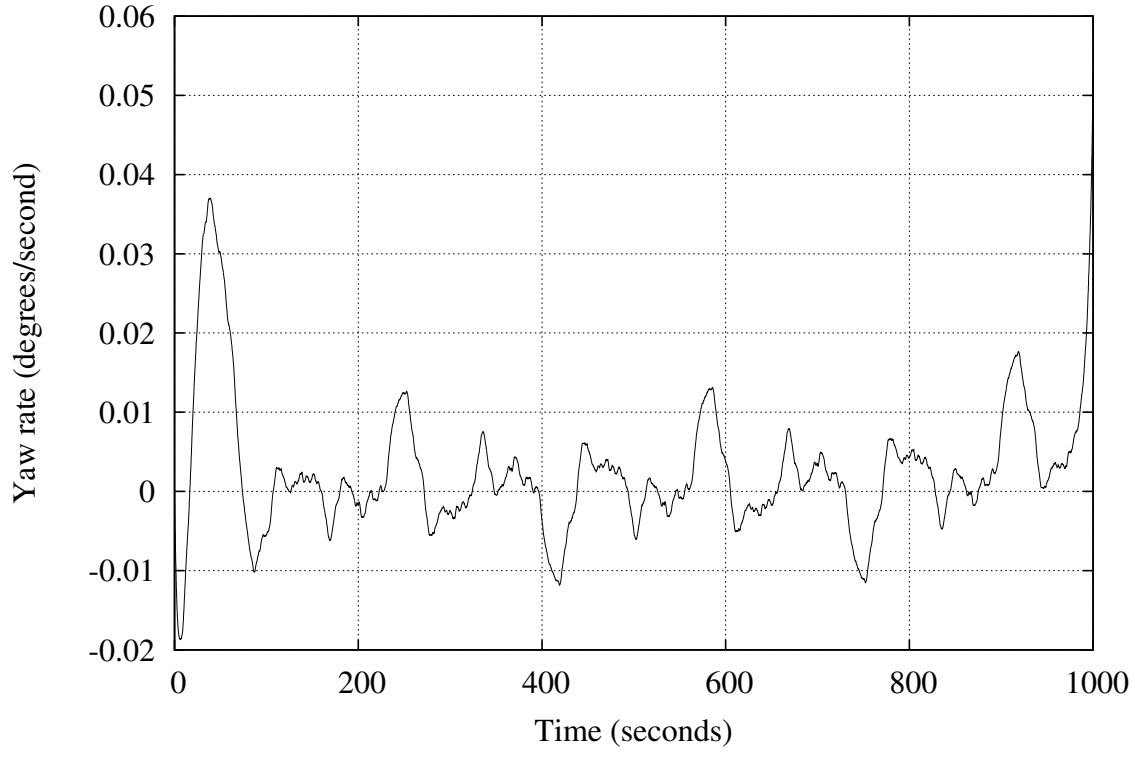

Figure C.78: Case 6: Yaw Rate vs. Time

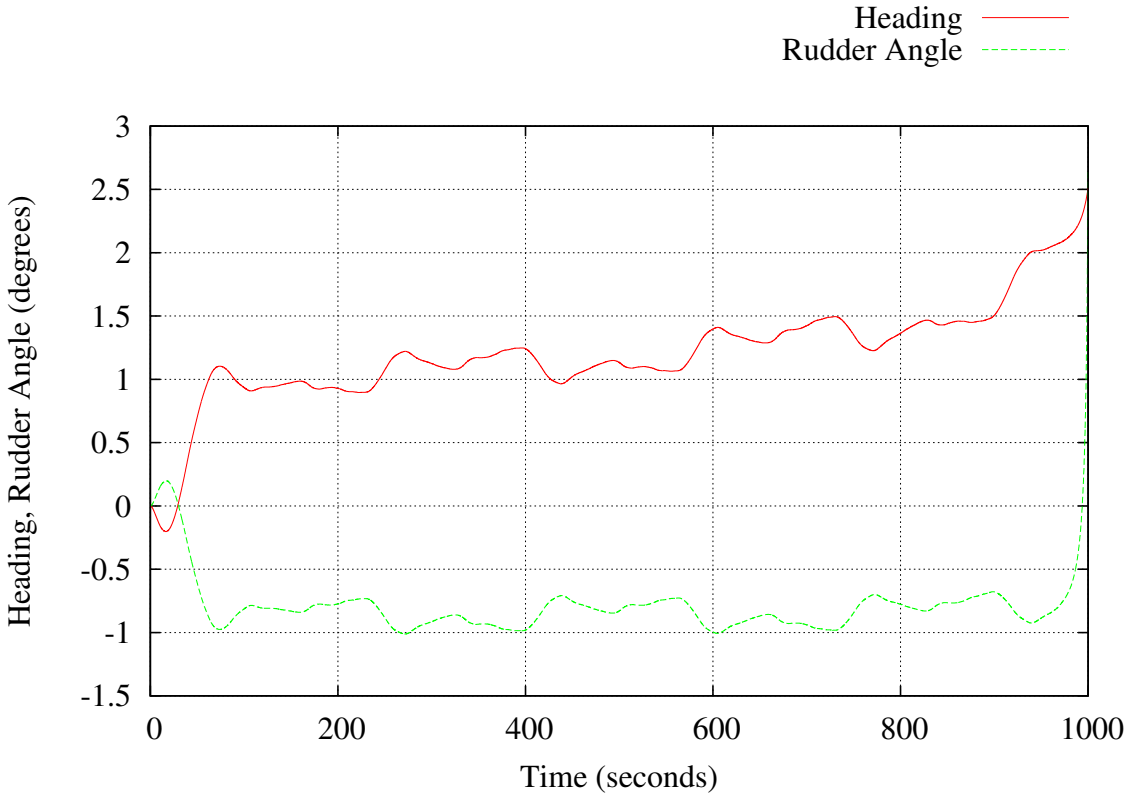

Figure C.79: Case 6: Rudder Command and Heading vs. Time

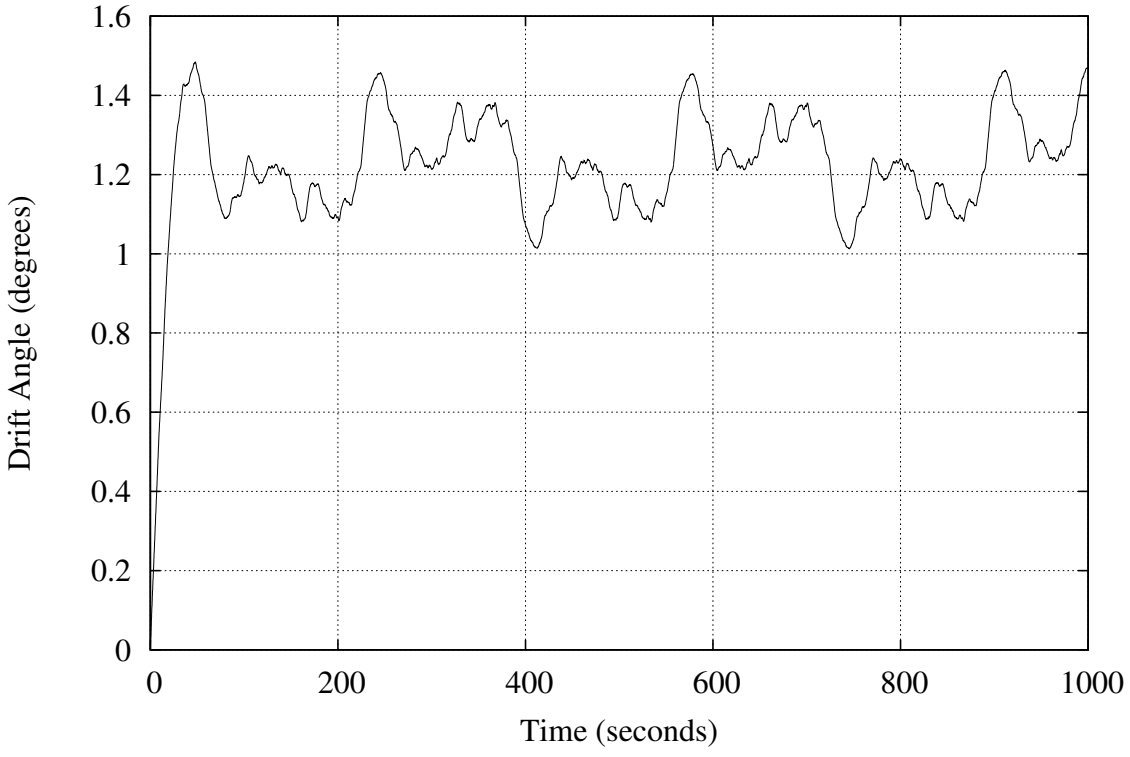

Figure C.80: Case 6: Drift Angle vs. Time

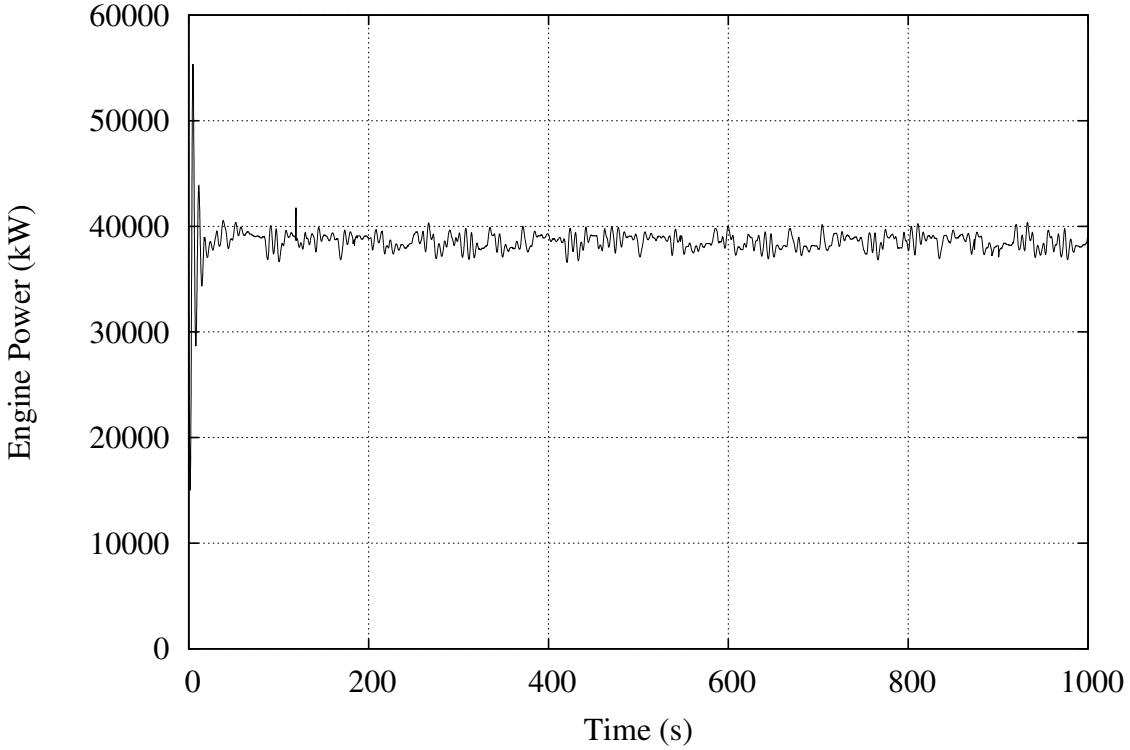

Figure C.81: Case 6: Engine Power vs. Time

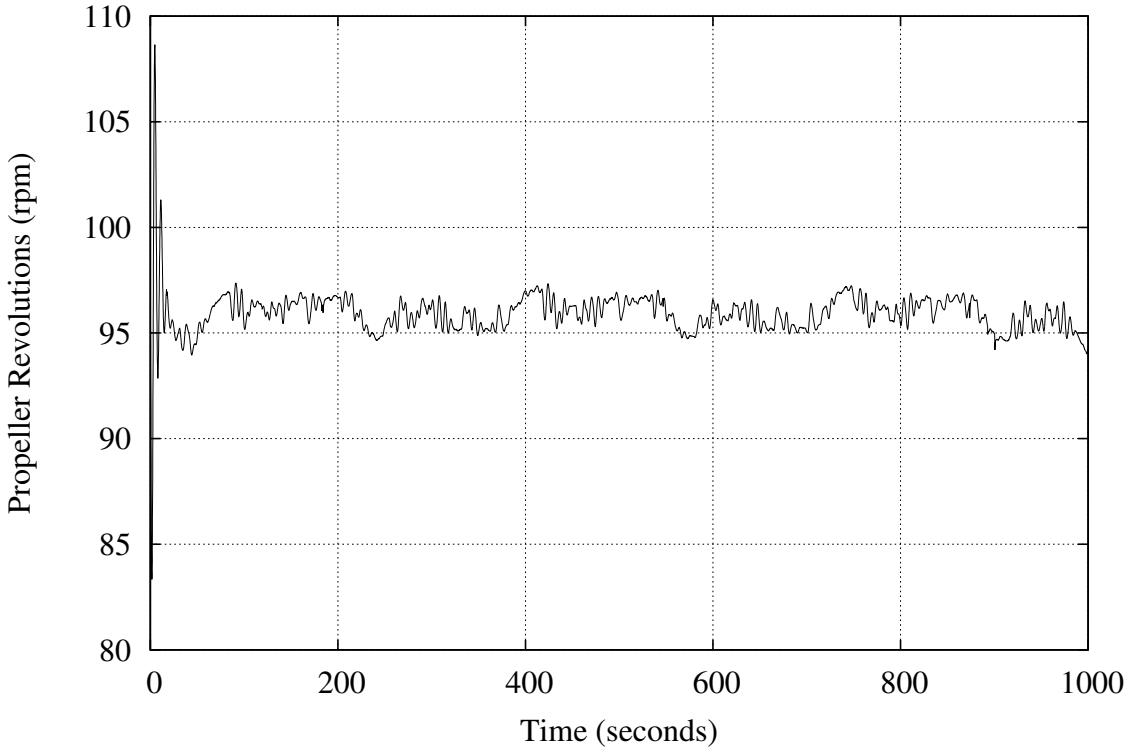

Figure C.82: Case 6: Propeller Revolutions vs. Time

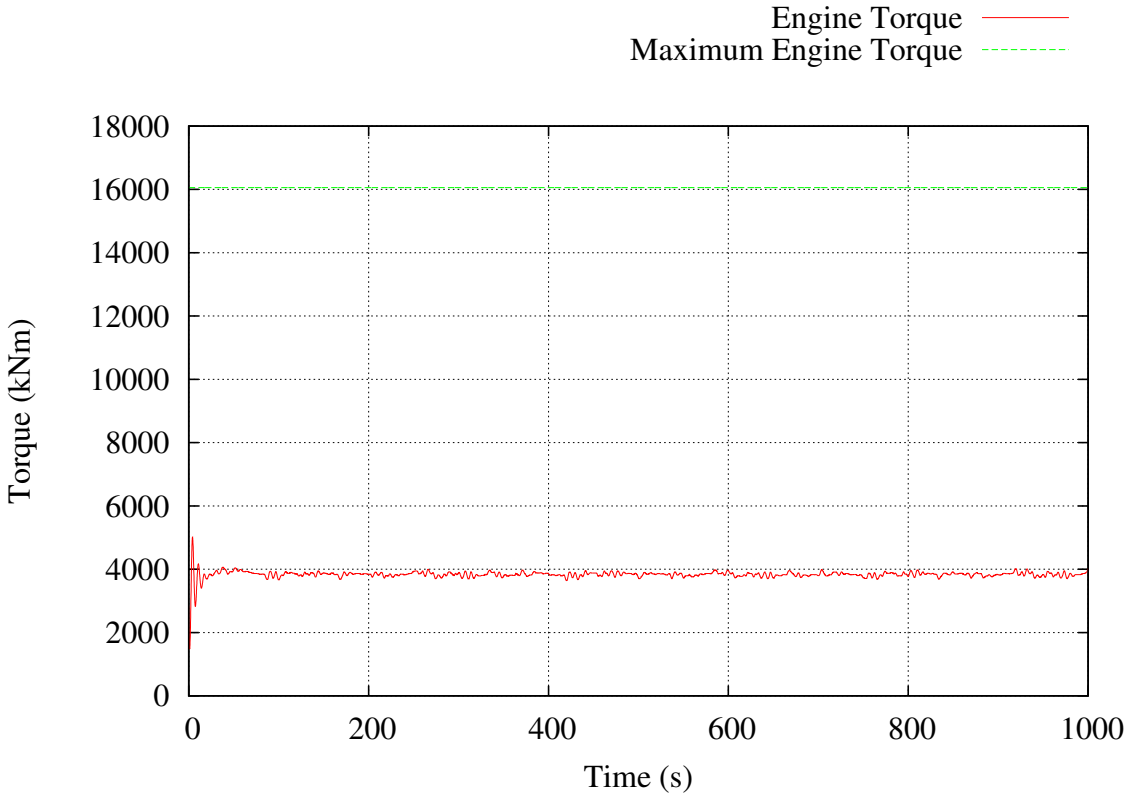

Figure C.83: Case 6: Engine Torque vs. Time

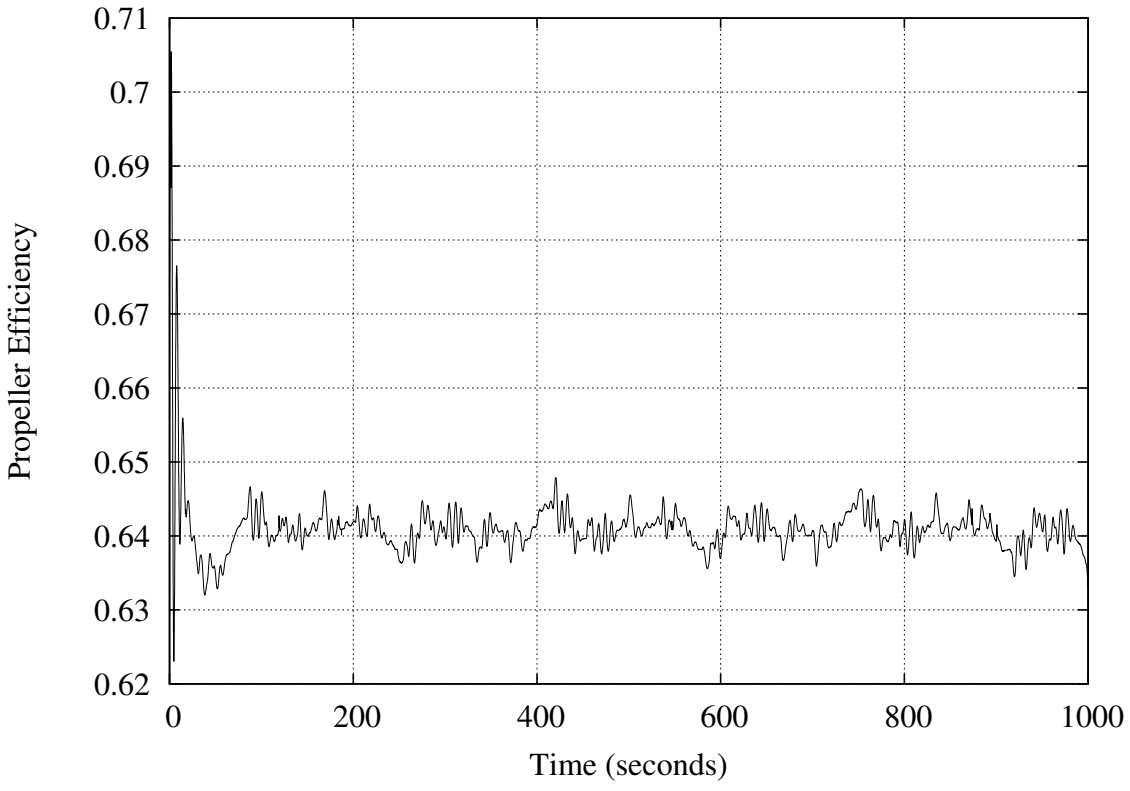

Figure C.84: Case 6: Open Water Propeller Efficiency vs. Time

C.7 The *Esso Osaka* with the Newly Proposed Propeller, Run in Calm Water, with the Unsteady $MBEMT$ Propulsion Model.

```
    |=============================================|
    | Ship-in-Service Performance Estimator       |
    |=============================================|
    | (c) 2013 David Trodden                      |
    | School of Marine Science and Technology     |
    | Newcastle University, UK                    |
    |=============================================|


"Esso Osaka VLCC - Loaded Test Case"
====================================


Simuation Parameters
--------------------
  Simulation is speed and track automatic pilot.
  Using an unsteady BEMT propulsion model.
  Mean true wind speed =                                    0.00 knots
  Mean true wind direction =                               90.00 degrees


Ship Main Particulars
---------------------
  Service Speed =                                          10.00 knots
  Lpp =                                                   325.00 m
  Lwl =                                                   335.00 m
  B =                                                      53.00 m
  T =                                                      21.79 m
  Volume of Displacement =                             311901.50 m^3
  Mass of Ship =                                       319699.06 tonnes
  LCB relative to midships +Fwd (%) =                       3.169
  Midship Coefficient, Cm =                                 0.990
  Waterplane Coefficient, Cwp =                             0.850
  Block Coefficient, Cb =                                   0.831
  Prismatic Coefficient, Cp =                               0.839


Propeller geometry has been provided
------------------------------------
  Number of Propellers =                                       1
  Number of Blades on each Propeller =                         5
  Propeller Diameter =                                      9.10 m
  Propeller Pitch =                                         7.69 m
  Expanded Blade Area Ratio =                               0.64


Resistance Calculations from Holtrop & Mennen (Calm Water)
----------------------------------------------------------
  Friction Resistance =                                   704.530 kN
  Appendage Resistance =                                    8.309 kN
  Wave Making Resistance =                                  0.266 kN
  Added Pressure Resistance of Bulbous Bow =                0.000 kN
  Added Pressure Resistance of Immersed Transom Stern =     7.152 kN
  Model-Ship Correlation Line =                            81.067 kN
  Total Calm Water Resistance =                           801.324 kN


Calm Water Propulsion Characteristics
-------------------------------------
  Required Engine Power for Service Speed =              5137.812 kW
  Propeller Revolutions =                                  48.250 rpm
  Open Water Propeller Efficiency =                         0.534


In-Service Propulsion Characteristics
-------------------------------------
  Average ship resistance =                                806.654 kN
  Average resultant ship speed =                             9.945 knots
  Average propeller efficiency =                             0.532
  Average propeller revolutions =                           48.204 rpm
  Average Delivered Power =                               6459.308 kW
  Average Engine Brake Power =                            6517.766 kW


  Average 'steady state' resultant resistance =            806.637 kN
```

```
Average 'steady state' resultant ship speed =              9.945 knots
Average 'steady state' propeller efficiency =              0.531
Average 'steady state' propeller revolutions =            48.281 rpm
Average 'steady state' advance ratio =                     0.469
Average 'steady state' Delivered Power =                6485.335 kW
Average 'steady state' Engine Brake Power =             6544.182 kW
Average 'steady state' drift angle at propeller =         -0.011 degrees
```

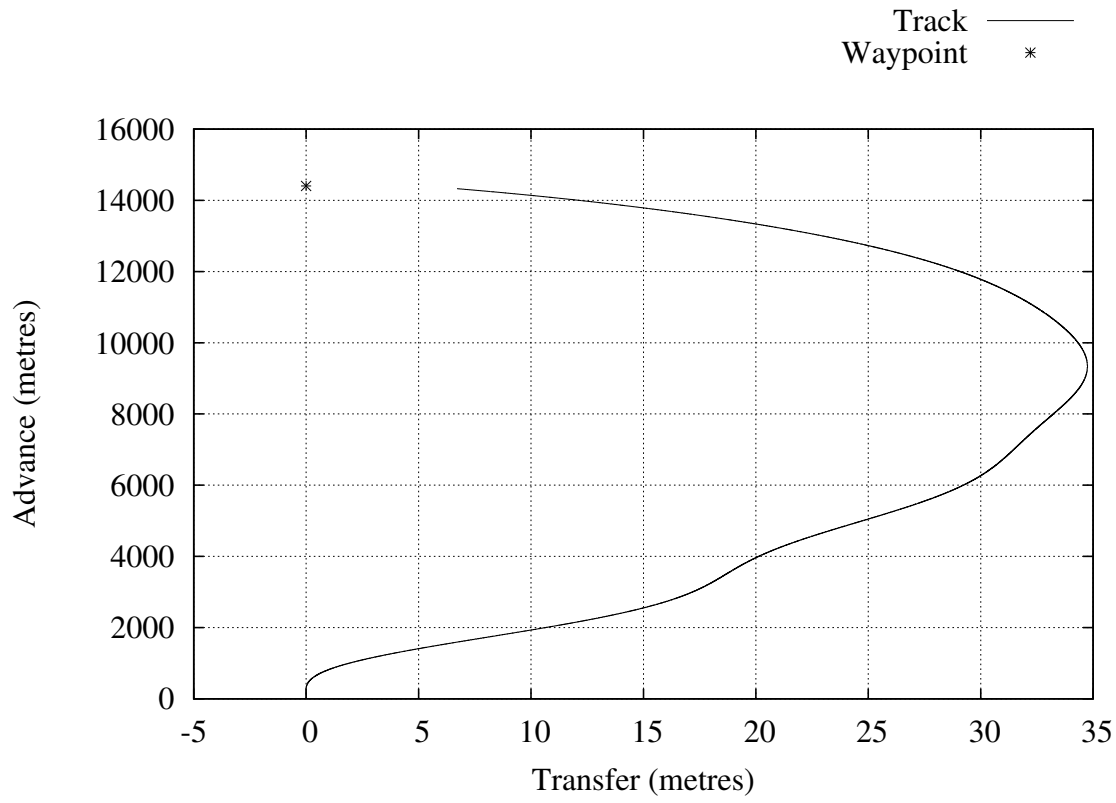

Figure C.85: *Esso Osaka* in Calm Water: Ship Track

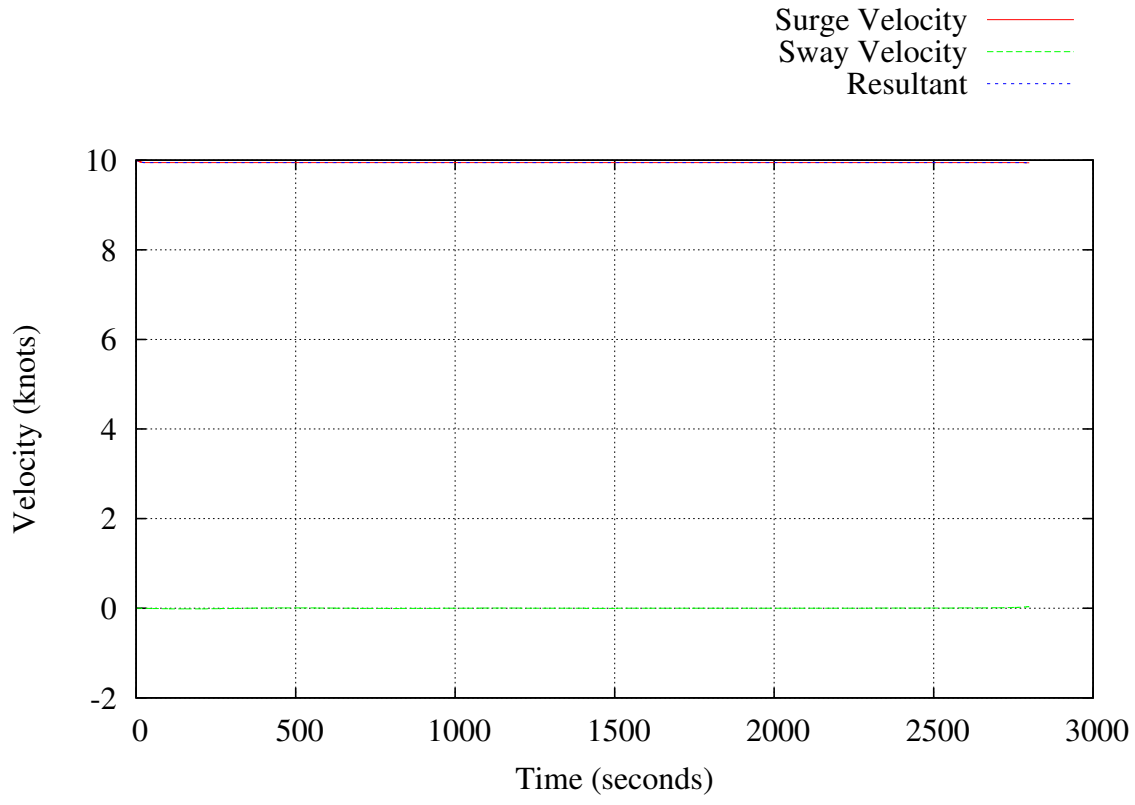

Figure C.86: *Esso Osaka* in Calm Water: Speed vs. Time

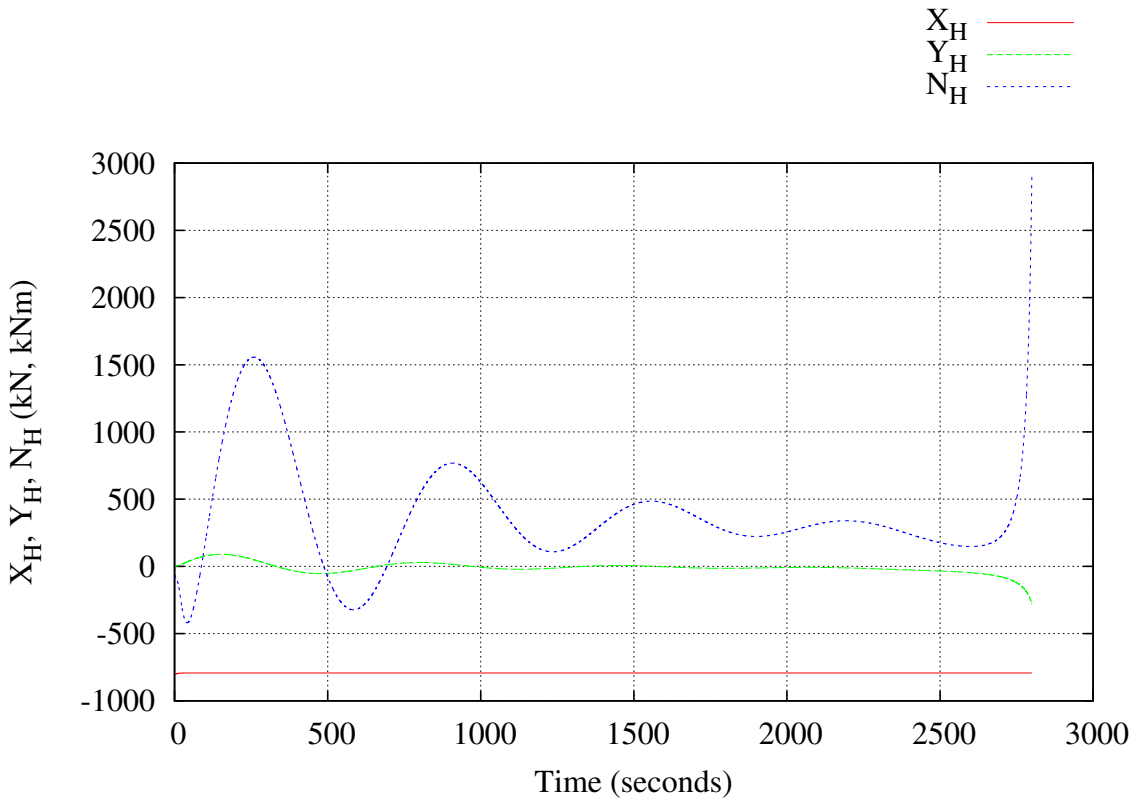

Figure C.87: *Esso Osaka* in Calm Water: Hull Forces vs. Time

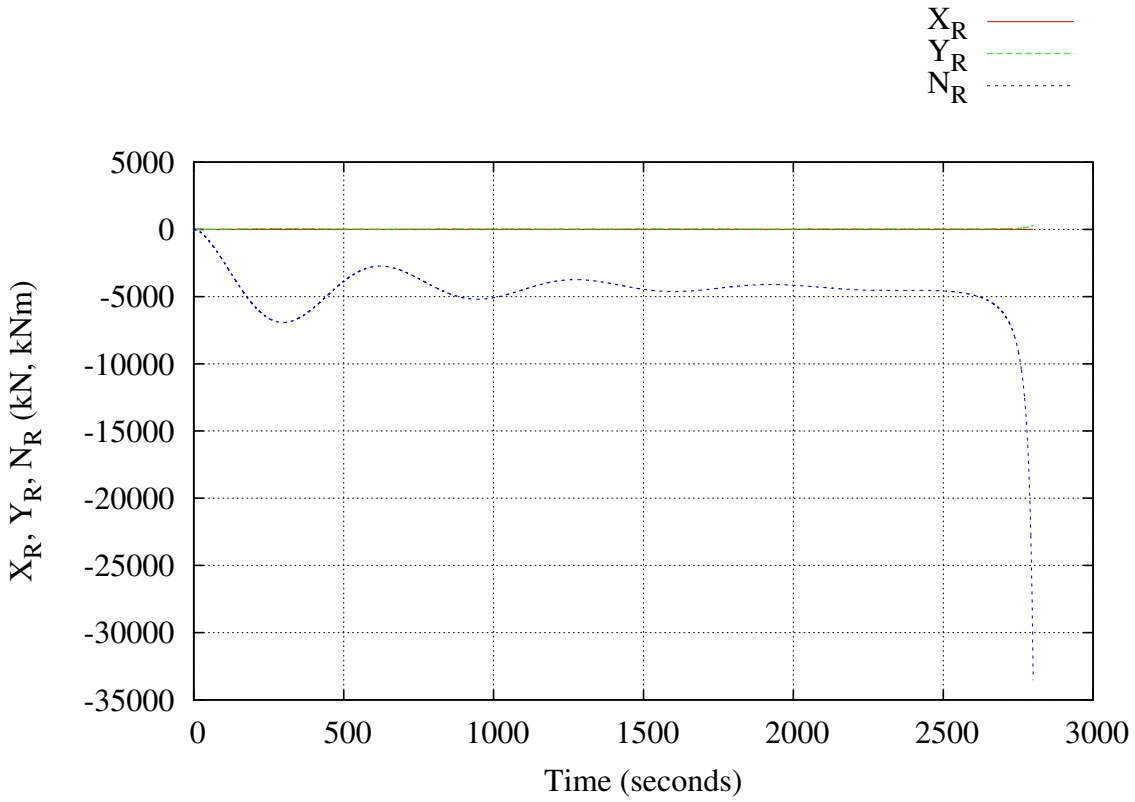

Figure C.88: *Esso Osaka* in Calm Water: Rudder Force vs. Time

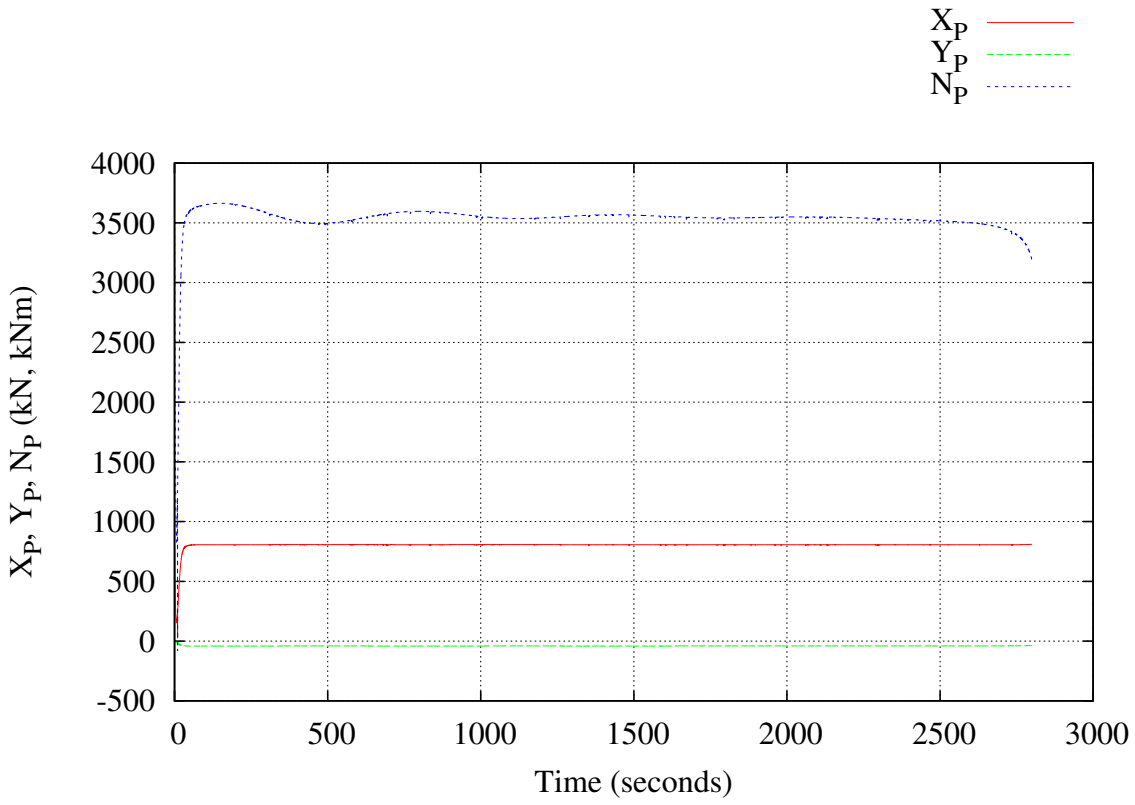

Figure C.89: *Esso Osaka* in Calm Water: Propeller Force vs. Time

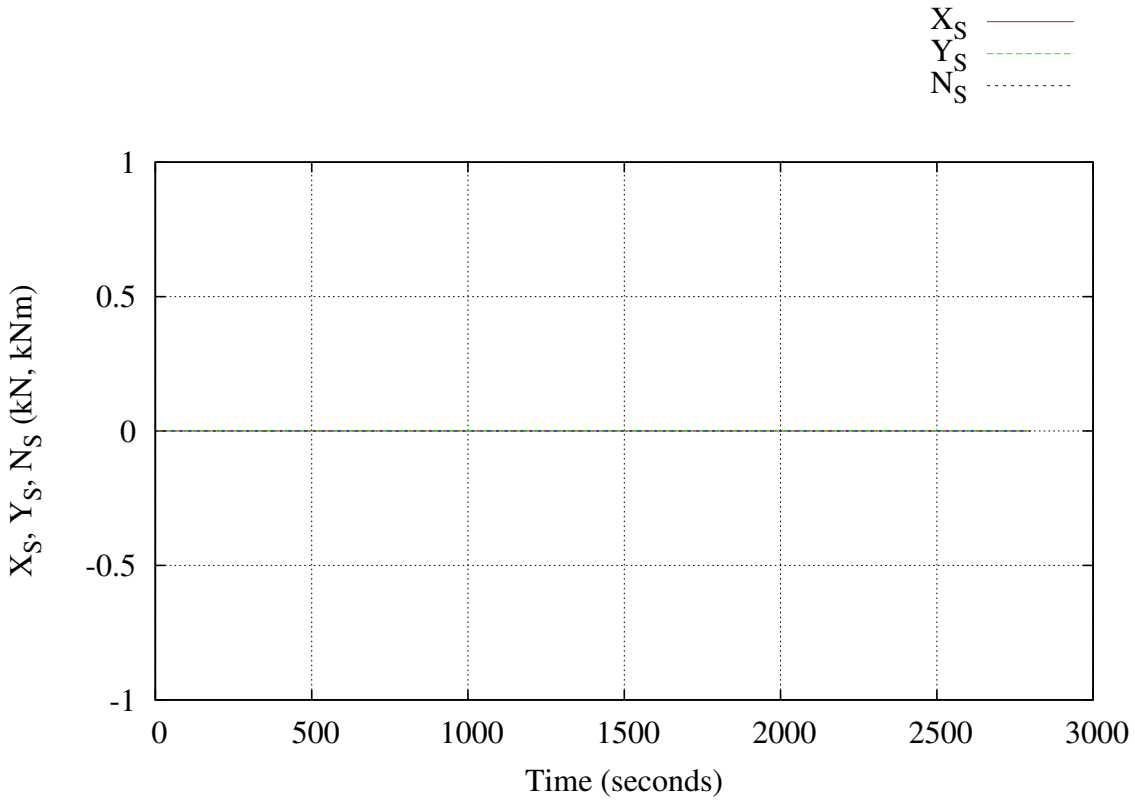

Figure C.90: *Esso Osaka* in Calm Water: Seaway Force vs. Time

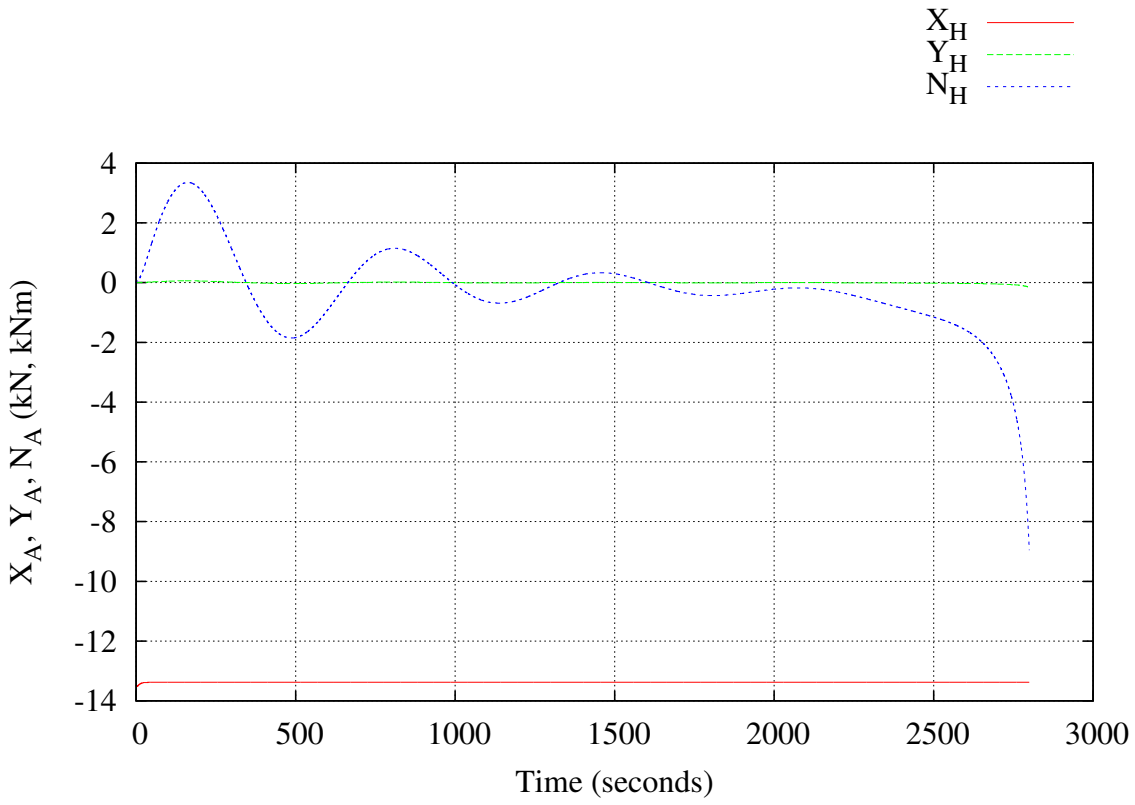

Figure C.91: *Esso Osaka* in Calm Water: Wind Force vs. Time

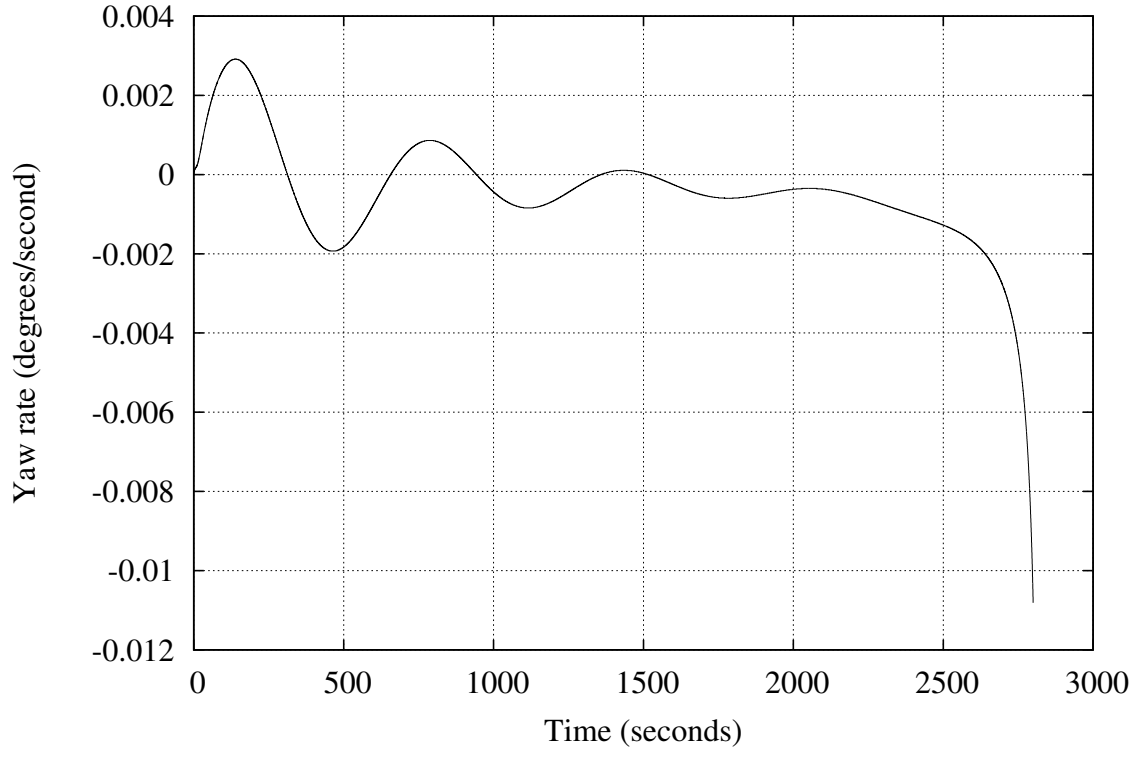

Figure C.92: *Esso Osaka* in Calm Water: Yaw Rate vs. Time

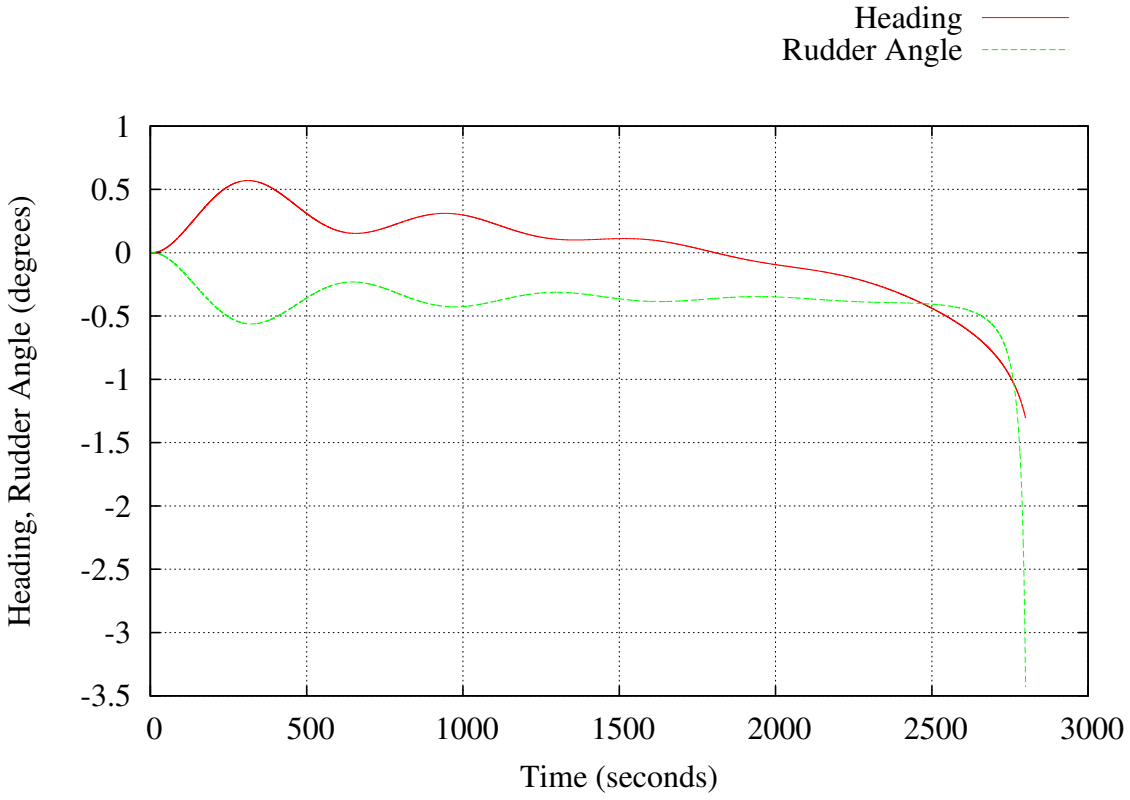

Figure C.93: *Esso Osaka* in Calm Water: Rudder Command and Heading vs. Time

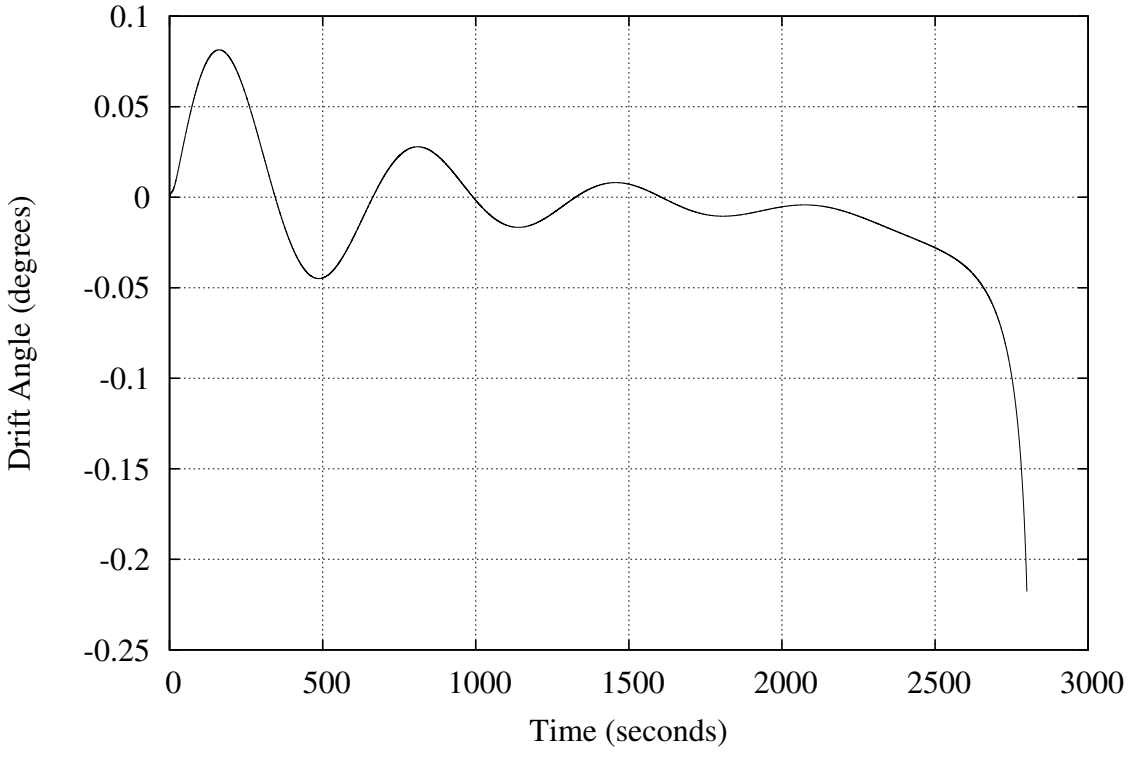

Figure C.94: *Esso Osaka* in Calm Water: Drift Angle vs. Time

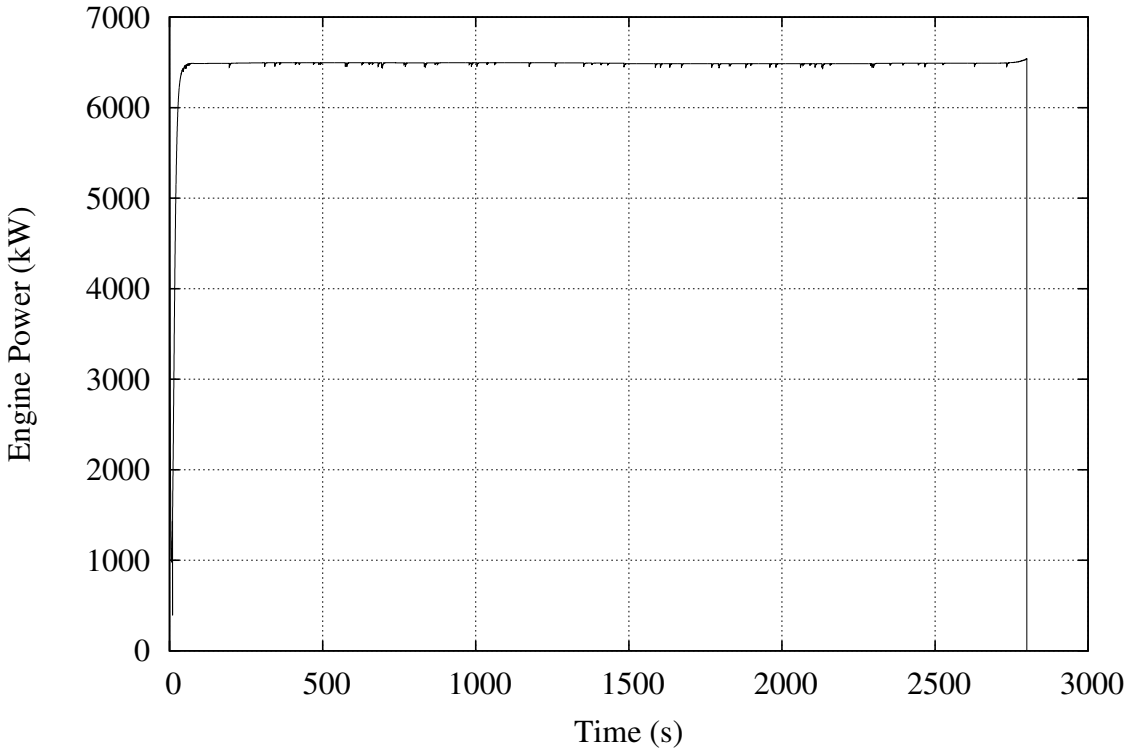

Figure C.95: *Esso Osaka* in Calm Water: Engine Power vs. Time

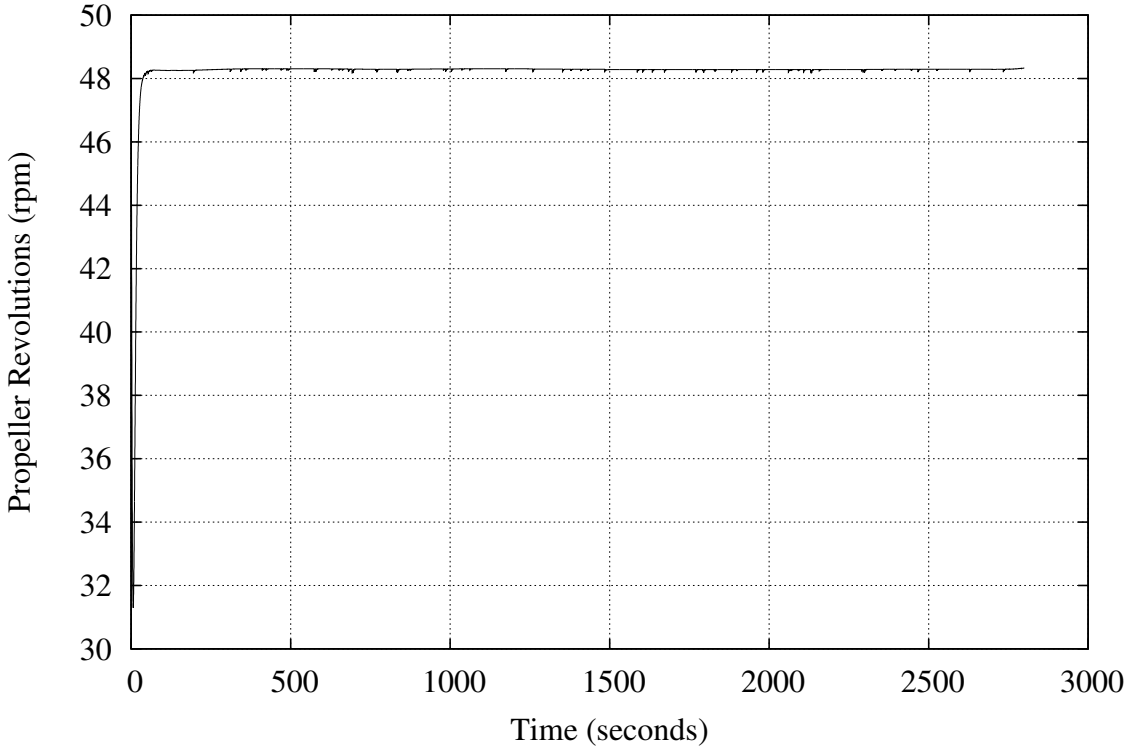

Figure C.96: *Esso Osaka* in Calm Water: Propeller Revolutions vs. Time

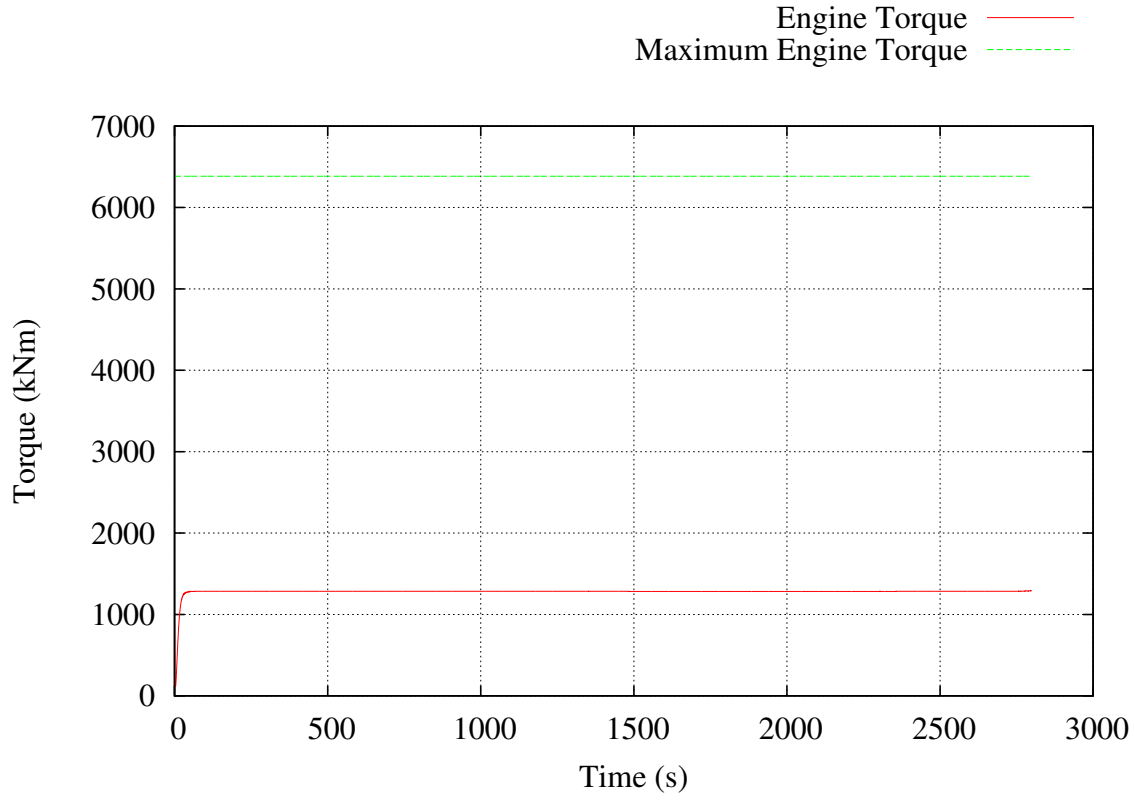

Figure C.97: *Esso Osaka* in Calm Water: Engine Torque vs. Time

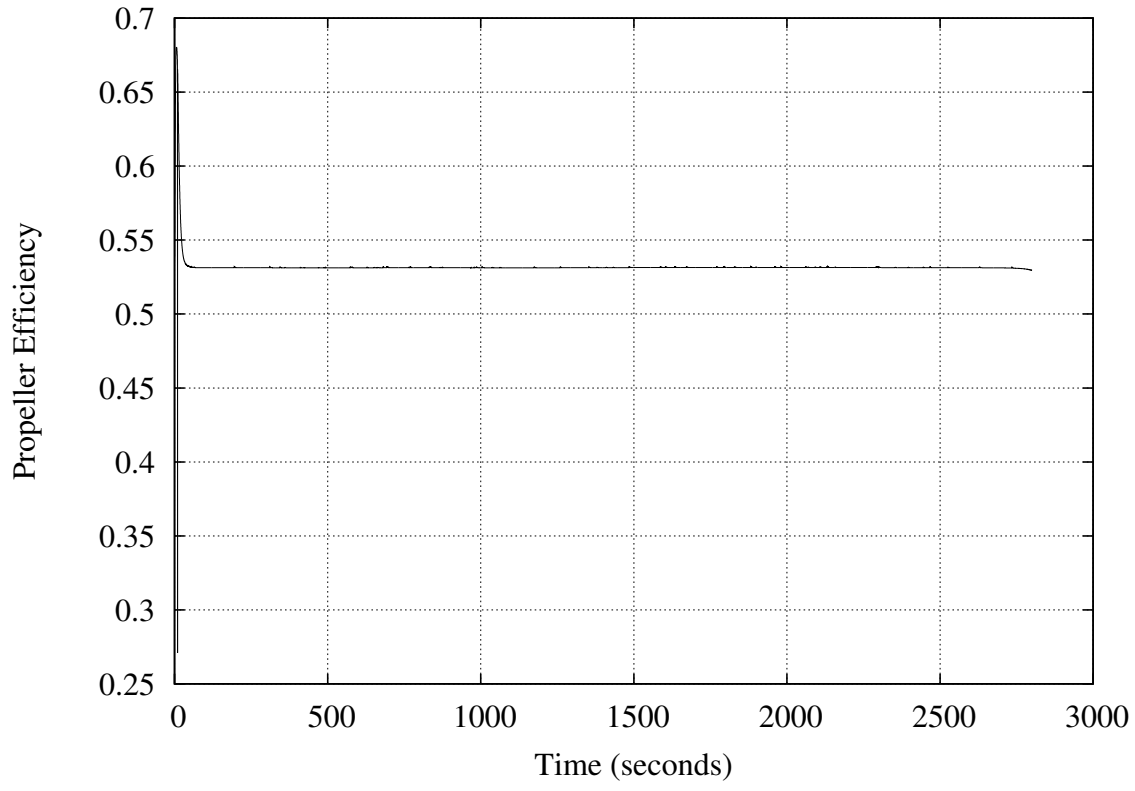

Figure C.98: *Esso Osaka* in Calm Water: Open Water Propeller Efficiency vs. Time

C.8 The *KCS* with the Newly Proposed Propeller, Run in Calm Water, with the Unsteady *MBEMT* Propulsion Model.

```
    |=============================================|
    | Ship-in-Service Performance Estimator       |
    |=============================================|
    | (c) 2013 David Trodden                      |
    | School of Marine Science and Technology     |
    | Newcastle University, UK                    |
    |=============================================|


"KCS - KRISO Container Ship"
============================


Simuation Parameters
--------------------
  Simulation is speed and track automatic pilot.
  Using an unsteady BEMT propulsion model.
  Mean true wind speed =                                    0.00 knots
  Mean true wind direction =                               90.00 degrees


Ship Main Particulars
---------------------
  Service Speed =                                          24.00 knots
  Lpp =                                                   232.00 m
  Lwl =                                                   237.58 m
  B =                                                      32.20 m
  T =                                                      11.34 m
  Volume of Displacement =                              50885.00 m^3
  Mass of Ship =                                        52157.12 tonnes
  LCB relative to midships +Fwd (%) =                      -2.030
  Midship Coefficient, Cm =                                 0.985
  Waterplane Coefficient, Cwp =                             0.802
  Block Coefficient, Cb =                                   0.601
  Prismatic Coefficient, Cp =                               0.610


Propeller geometry has been provided
------------------------------------
  Number of Propellers =                                       1
  Number of Blades on each Propeller =                         5
  Propeller Diameter =                                      7.90 m
  Propeller Pitch =                                         8.09 m
  Expanded Blade Area Ratio =                               0.86


Resistance Calculations from Holtrop & Mennen (Calm Water)
----------------------------------------------------------
  Friction Resistance =                                 1174.728 kN
  Appendage Resistance =                                  17.524 kN
  Wave Making Resistance =                               419.418 kN
  Added Pressure Resistance of Bulbous Bow =               0.089 kN
  Added Pressure Resistance of Immersed Transom Stern =    0.000 kN
  Model-Ship Correlation Line =                          230.444 kN
  Total Calm Water Resistance =                         1842.203 kN


Calm Water Propulsion Characteristics
-------------------------------------
  Required Engine Power for Service Speed =            27743.648 kW
  Propeller Revolutions =                                 96.351 rpm
  Open Water Propeller Efficiency =                        0.674


In-Service Propulsion Characteristics
-------------------------------------
  Average ship resistance =                              1878.208 kN
  Average resultant ship speed =                           23.944 knots
  Average propeller efficiency =                            0.672
  Average propeller revolutions =                          96.664 rpm
  Average Delivered Power =                             33069.004 kW
  Average Engine Brake Power =                          34089.961 kW


  Average 'steady state' resultant resistance =          1878.210 kN
```

```
Average 'steady state' resultant ship speed =              23.945 knots
Average 'steady state' propeller efficiency =               0.672
Average 'steady state' propeller revolutions =             96.677 rpm
Average 'steady state' advance ratio =                      0.762
Average 'steady state' Delivered Power =                33077.516 kW
Average 'steady state' Engine Brake Power =             34098.398 kW
Average 'steady state' drift angle at propeller =           0.021 degrees
```

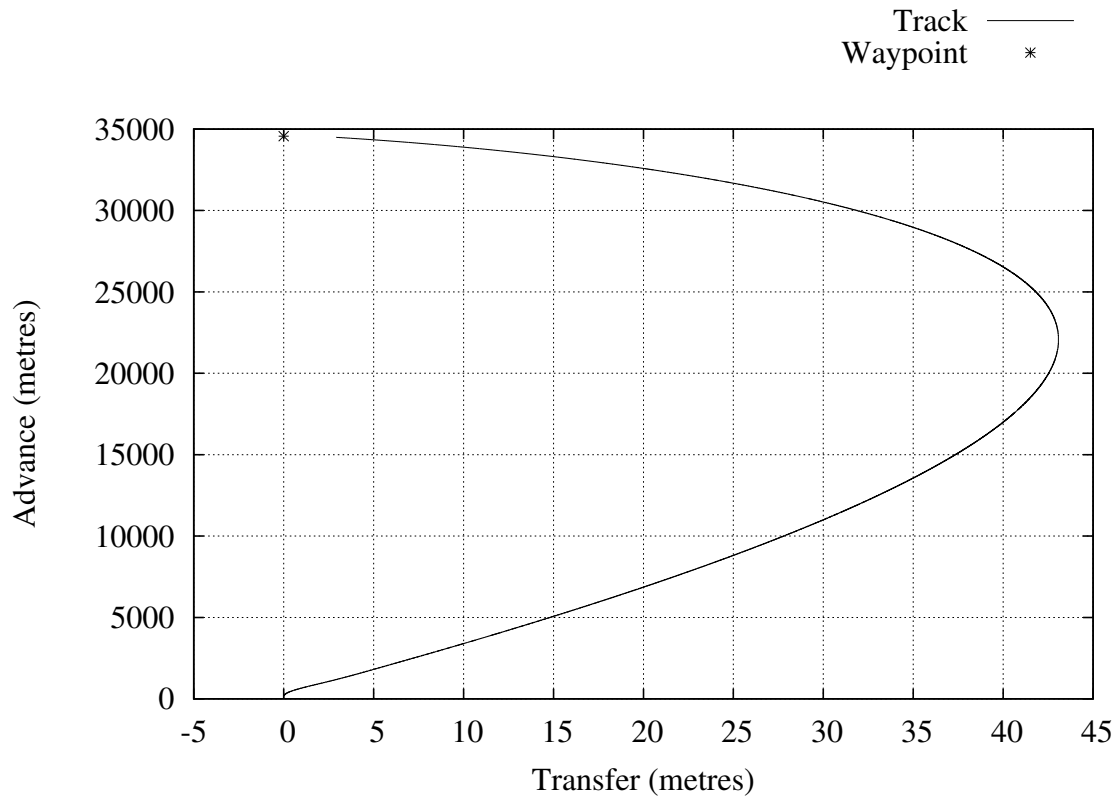

Figure C.99: *KCS* in Calm Water: Ship Track

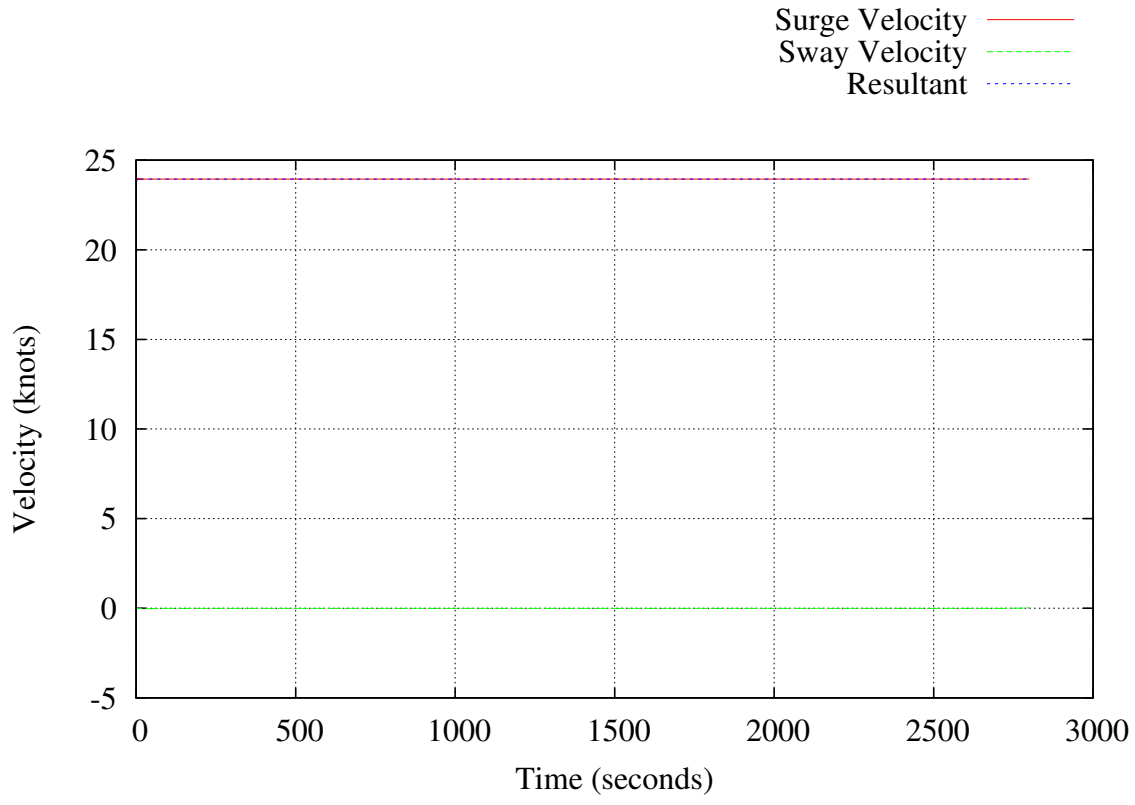

Figure C.100: *KCS* in Calm Water: Speed vs. Time

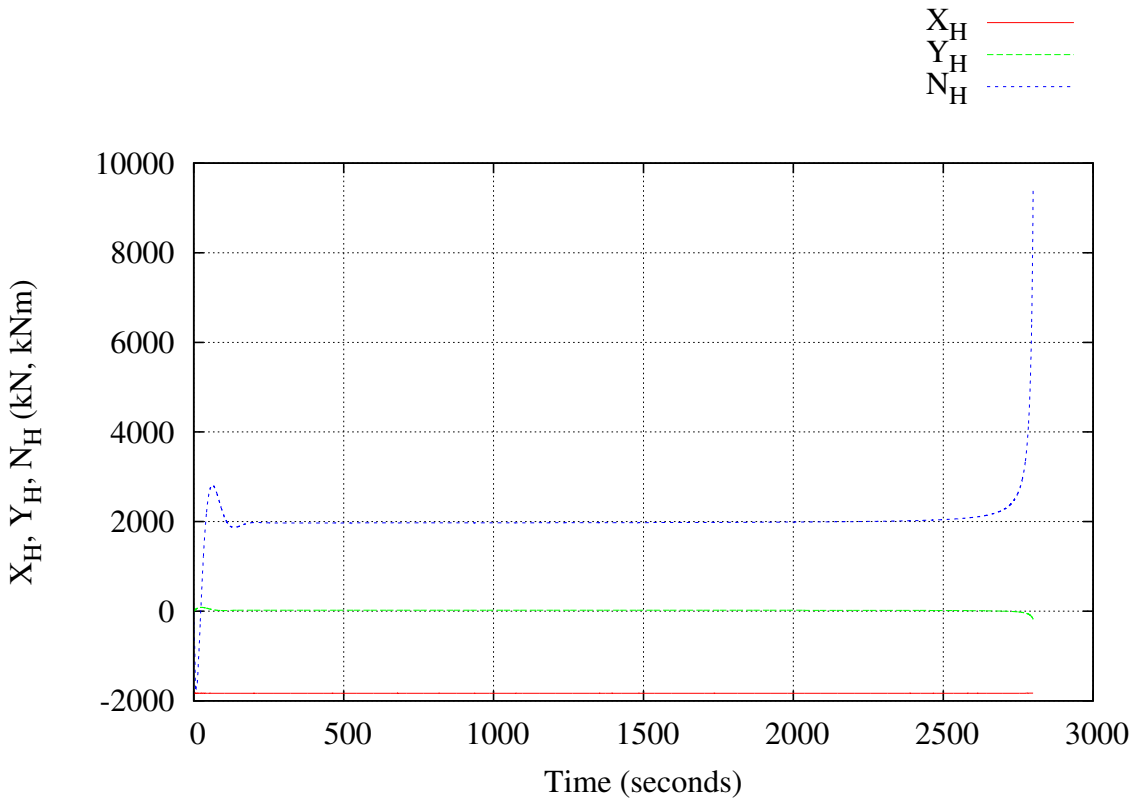

Figure C.101: *KCS* in Calm Water: Hull Forces vs. Time

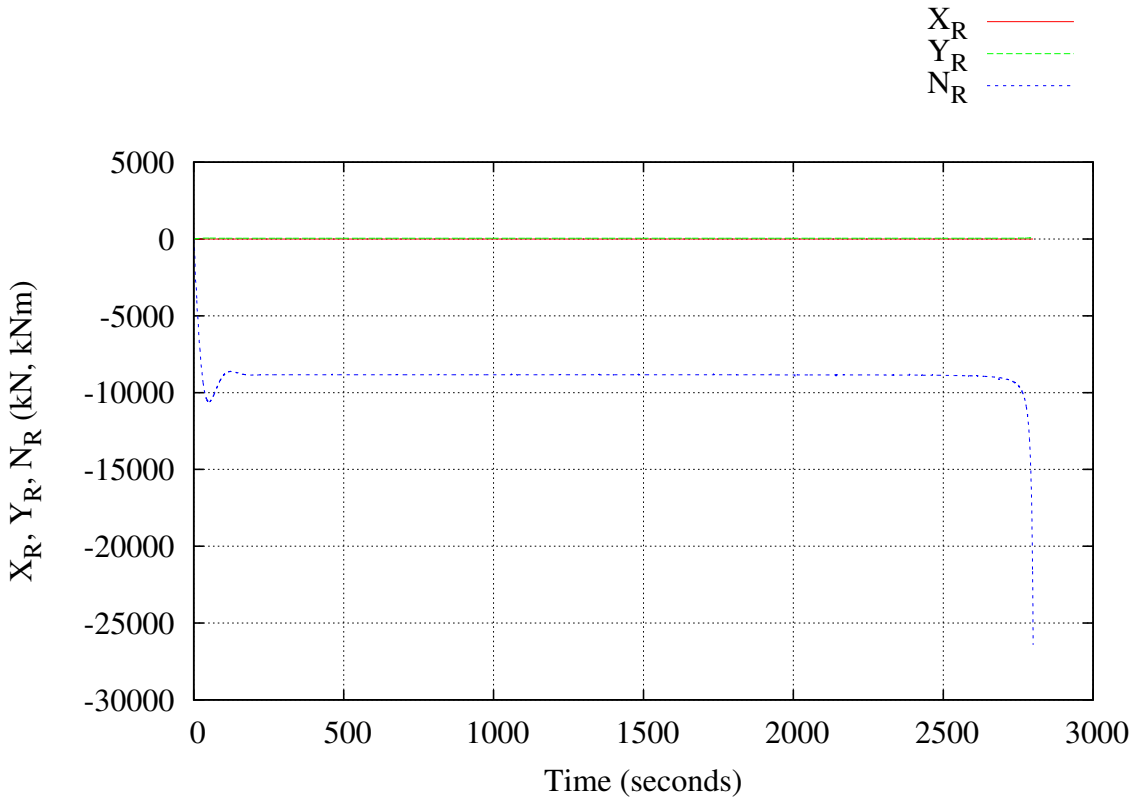

Figure C.102: *KCS* in Calm Water: Rudder Force vs. Time

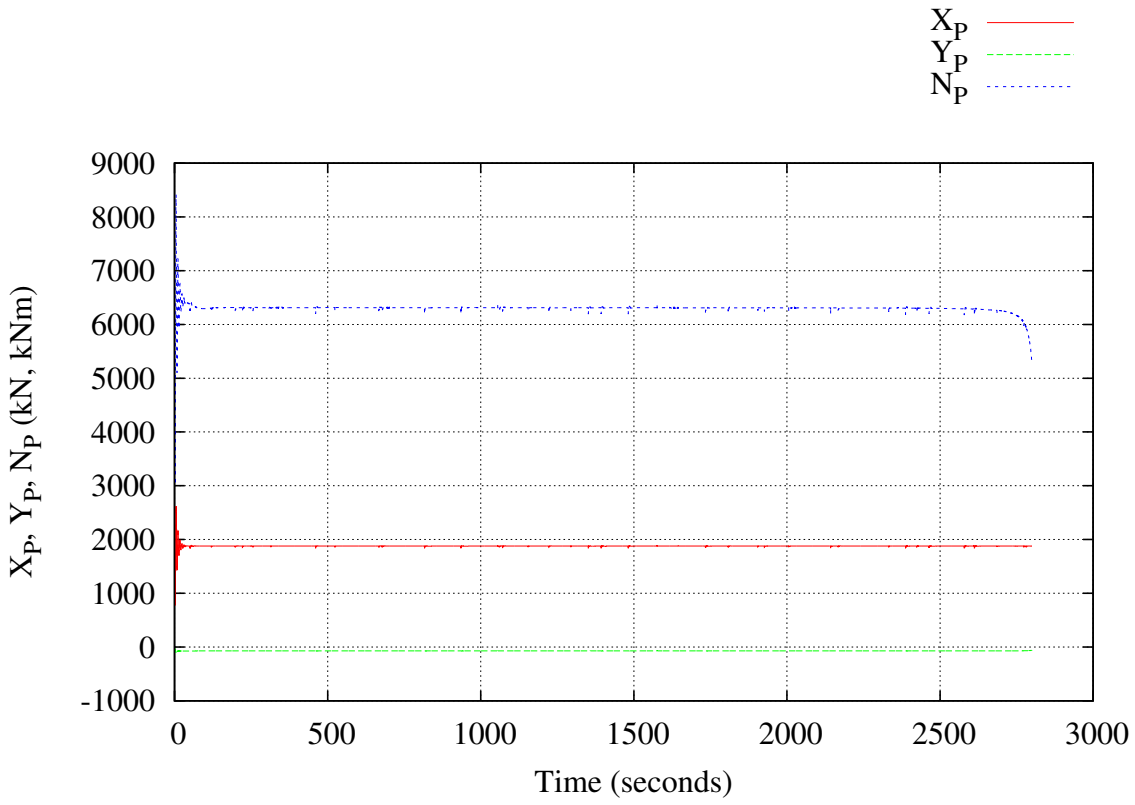

Figure C.103: *KCS* in Calm Water: Propeller Force vs. Time

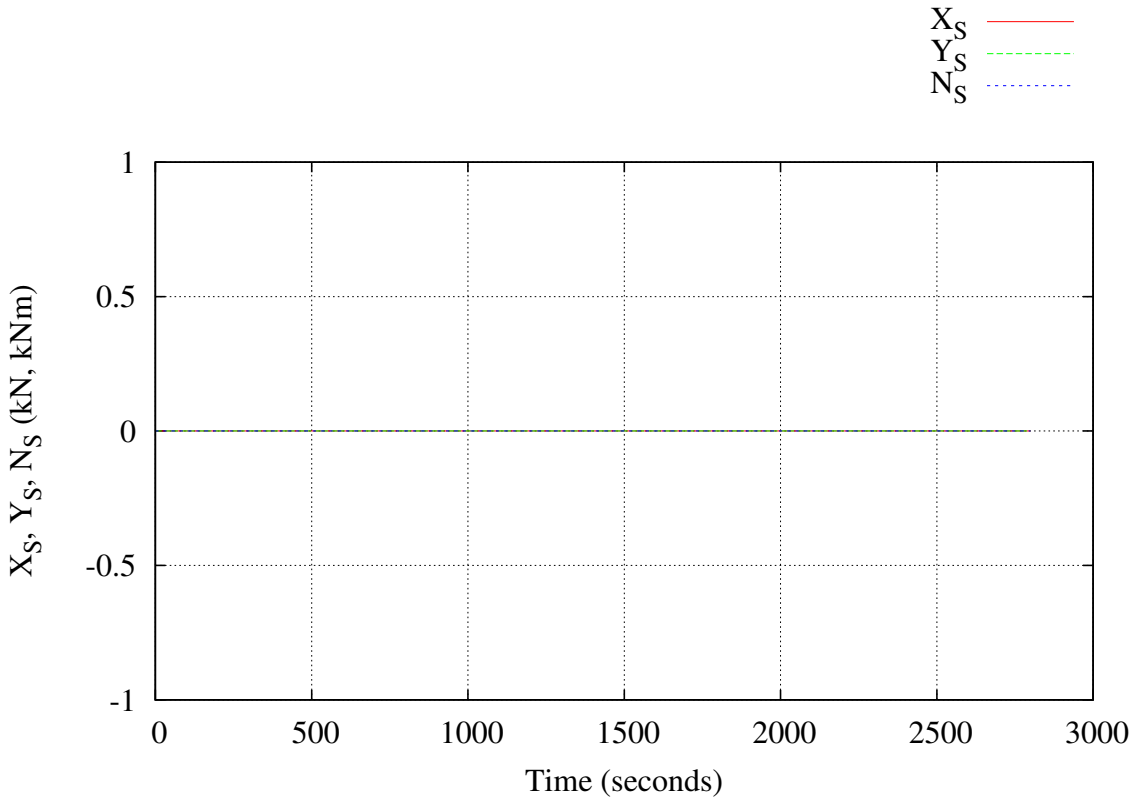

Figure C.104: *KCS* in Calm Water: Seaway Force vs. Time

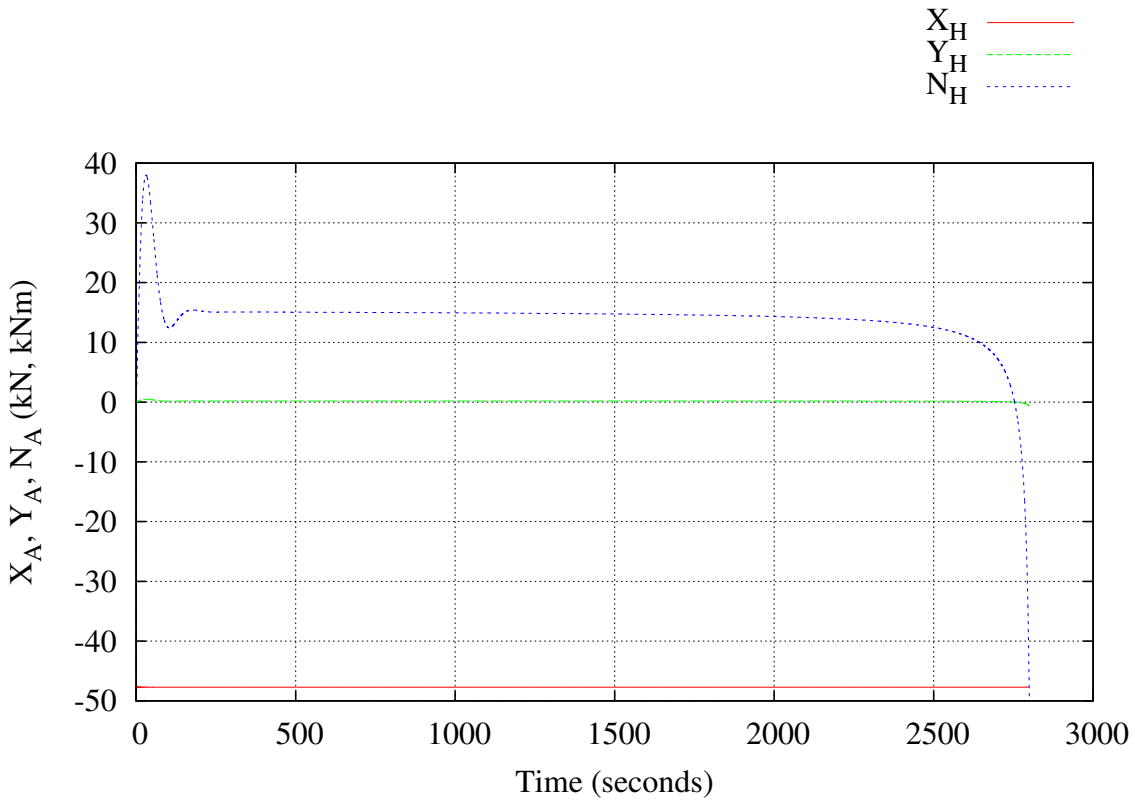

Figure C.105: *KCS* in Calm Water: Wind Force vs. Time

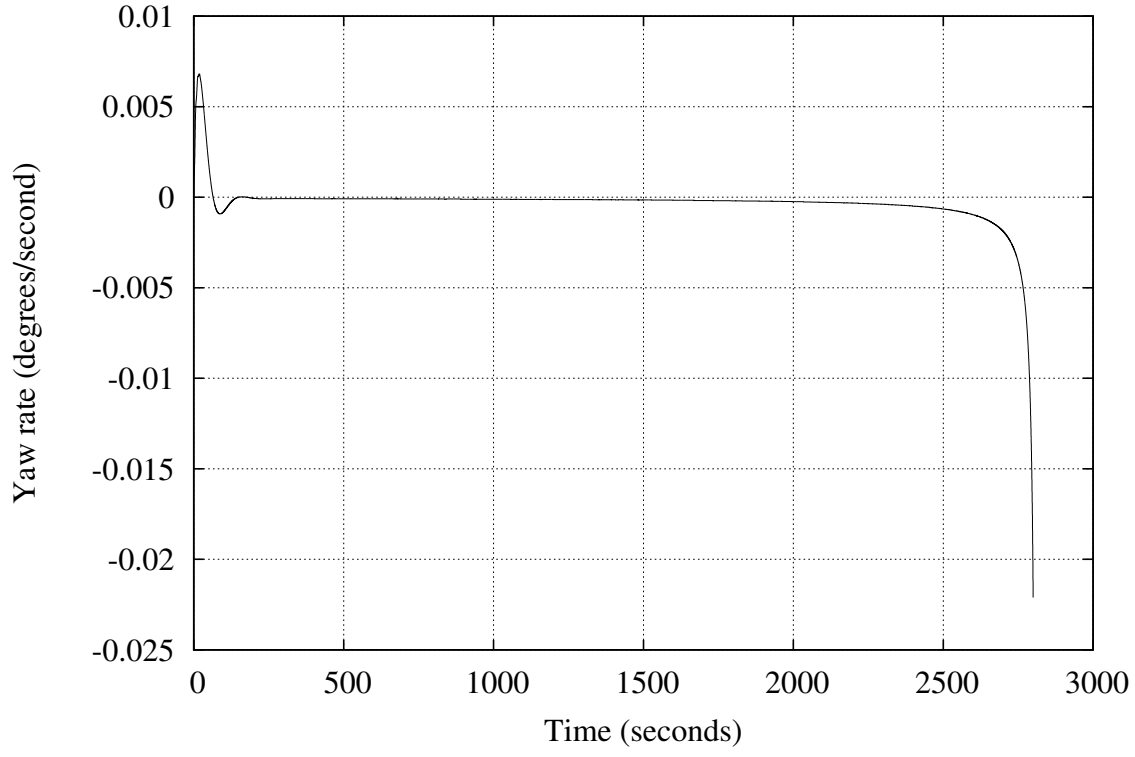

Figure C.106: *KCS* in Calm Water: Yaw Rate vs. Time

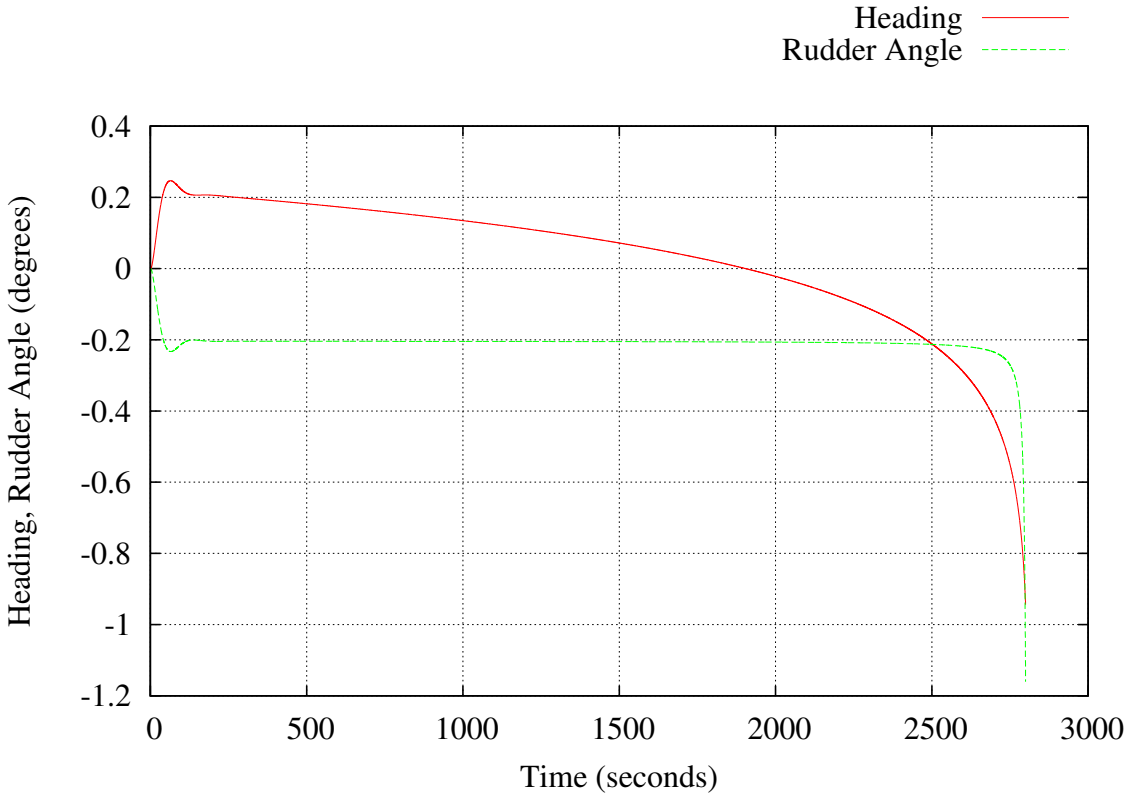

Figure C.107: *KCS* in Calm Water: Rudder Command and Heading vs. Time

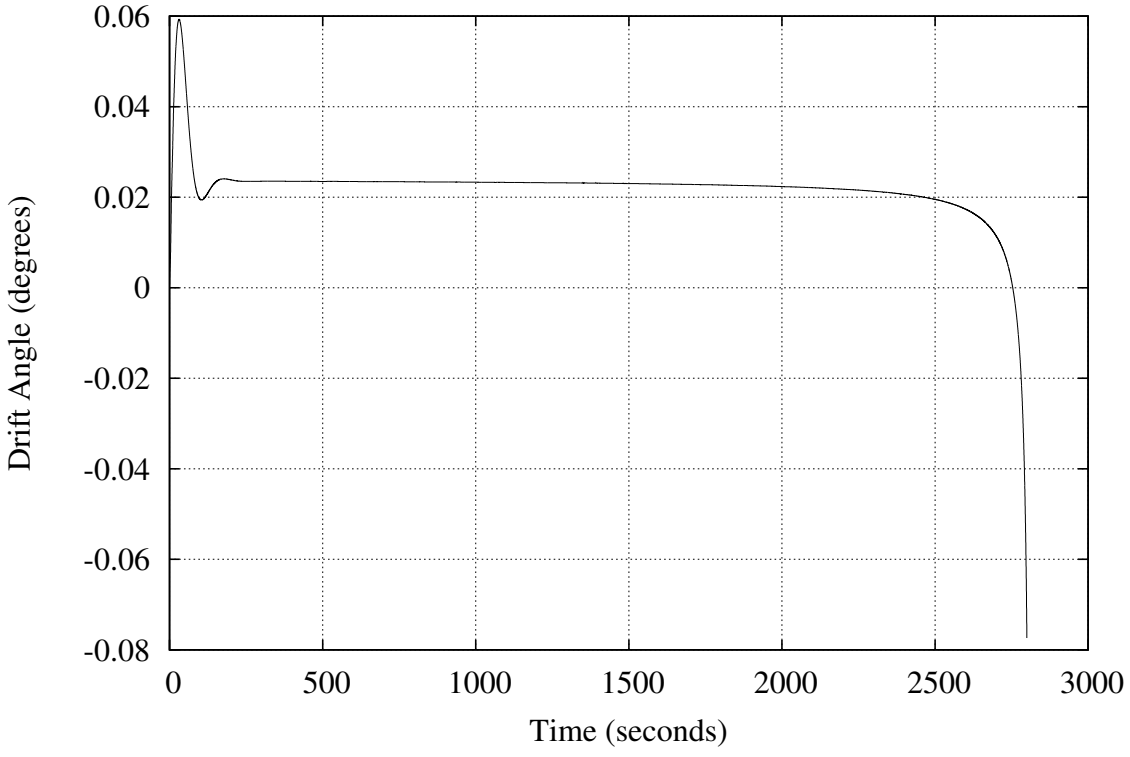

Figure C.108: *KCS* in Calm Water: Drift Angle vs. Time

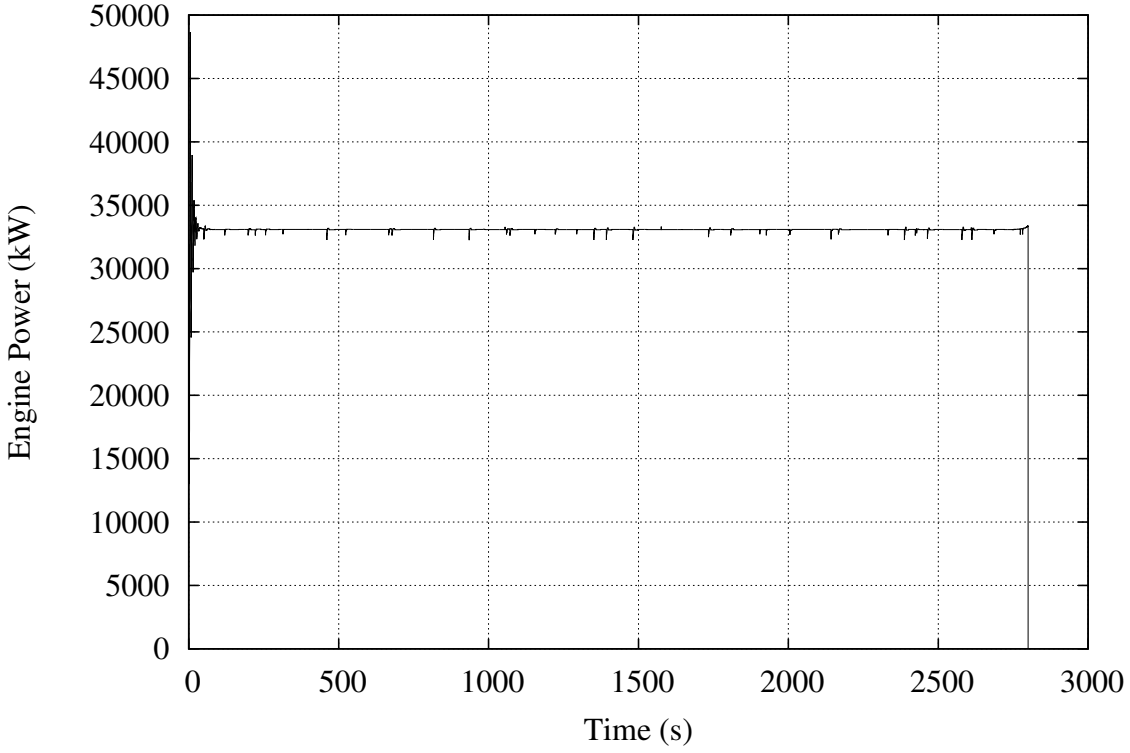

Figure C.109: *KCS* in Calm Water: Engine Power vs. Time

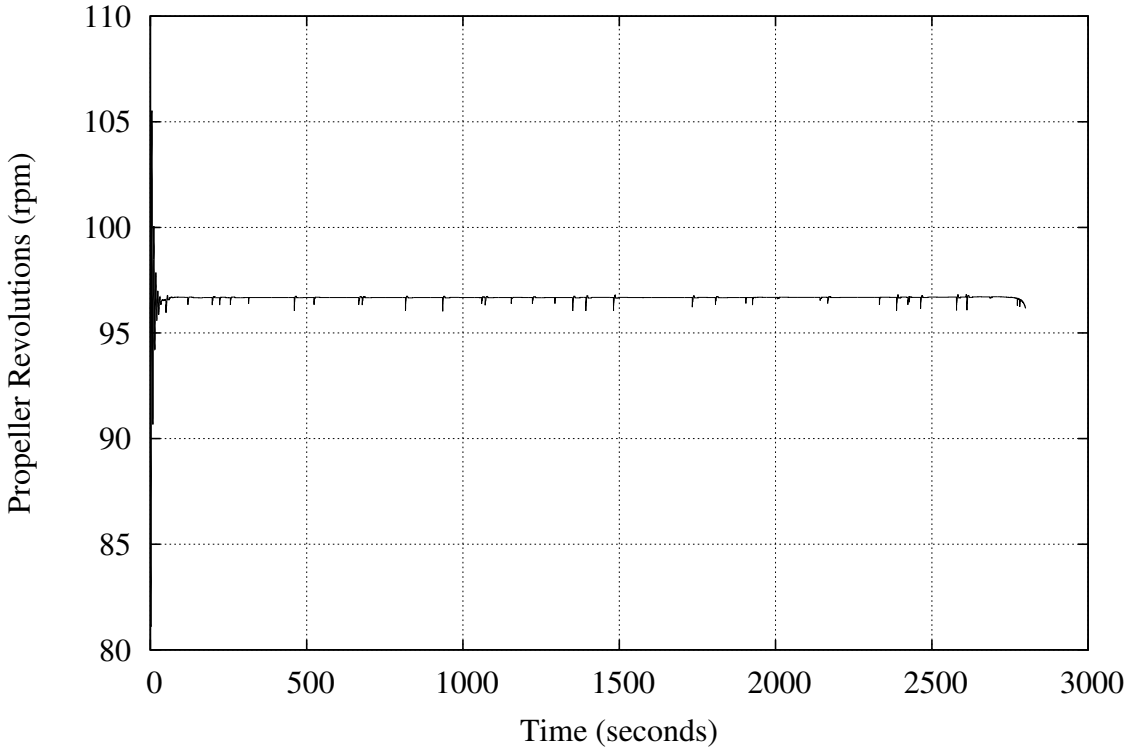

Figure C.110: *KCS* in Calm Water: Propeller Revolutions vs. Time

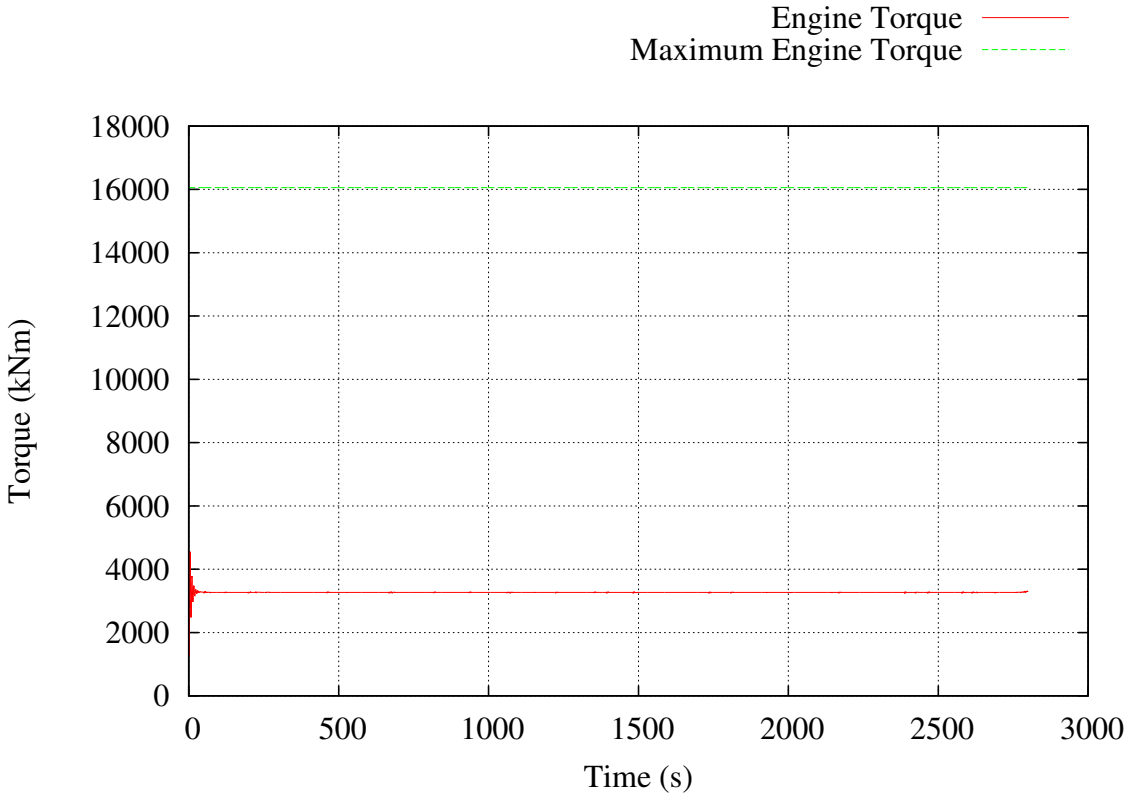

Figure C.111: *KCS* in Calm Water: Engine Torque vs. Time

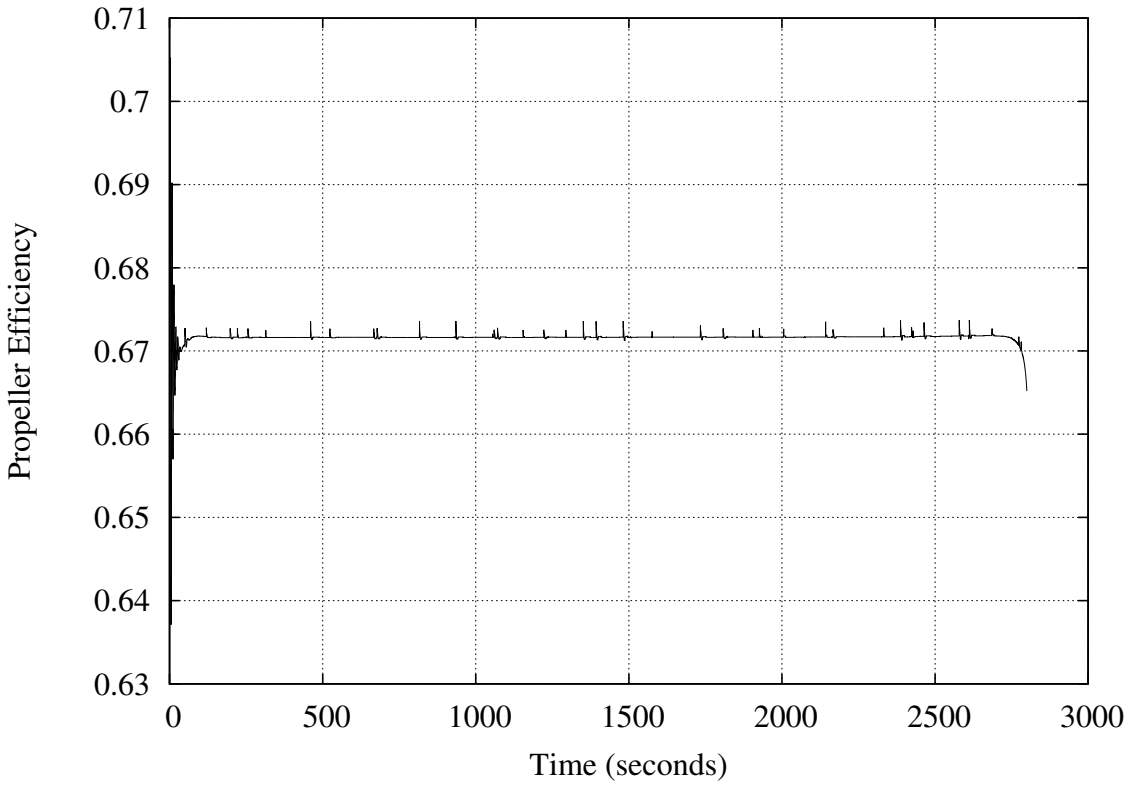

Figure C.112: *KCS* in Calm Water: Open Water Propeller Efficiency vs. Time